



You are cordially invited to attend

MinWien2023

17 to 21 September 2023

A joint meeting of the three Mineralogical Societies



Topics: Mineralogical, Petrological, Geochemical Sciences, deposits & related disciplines (basic, applied & industrial topics)

Programme

Sunday, 17 September 2023

Mineralogy for the public

Young Scientists meet each other

Opening Ceremony

After Party

Pre-conference

Male K...

16-17 S...

Guides: P. Bačík I. Bros...

Abstracts

Thursday,

September 2023

Scientific sessions

Poster presentations

Industrial exhibition

Conference dinner

Wednesday 20 September 2023

Festival Hall, Vienna's City Hall

Half-day tours

18-21 September, 2023

Poster Prizes for young scientists

DMG - General Assembly

Public lecture



Conference Site: Alma Mater Rudolfina - University of Vienna
Geozentrum - UZAI, Josef-Holaubek-Platz 2, 1090 Vienna

Organisation: Institut für Mineralogie und Kristallographie

Further information: <https://minwien2023.univie.ac.at>

e-mail: minwien2023.mineralogie@univie.ac.at

Photo on courtesy of Stephan Wolfsried

Zusammenstellung: Herta Effenberger
Christian Lengauer
(Universität Wien)

DOI: <https://doi.org/10.23689/fidgeo-6024>

Experimental study of hydrothermal alteration of volcanic rocks from the Volcanic Eifel

A. Abel¹, D. Sorger¹, T. Müller¹

¹*Geoscience Centre Göttingen, Georg-August-University, Germany
e-mail: angelina.abel@stud.uni-goettingen.de*

Hydrothermal alteration is known to cause intensive chemical and mineralogical changes in rocks driven by element fluxes between rock and infiltrating fluid depending on alteration conditions. Volume changes are commonly the result of mineral reactions associated with hydrothermal alteration and can lead to reaction-induced fracturing. In this experimental study we investigate the replacement of leucite by analcime in mafic rocks at near-surface hydrothermal conditions. The mineral reactions are shown to generate sufficient stresses to trigger fractures and even complete disintegration of the host rock depending on starting porosity and initial mineral modes. Tephritic and phonolitic foidites were collected in the Eifel Volcanic Fields in Western Germany. Both samples exhibit a porphyritic texture with clinopyroxene as dominant phenocrysts and a matrix consisting of clinopyroxene, feldspathoids and feldspar. The samples were reacted with a Na-K-Ca-Cl solution similar to seawater composition at 200 °C and 16 bars for intervals ranging from 1 to 8 weeks. Intact rock cores were placed into a batch reactor with fluid amounts twice their mass ($W/R = 2$). After the experiments, BSE and EDS measurements were used to identify and characterize reaction products and textures using a W-SEM. Samples were powdered and subsequently analysed with XRD including a Rietveld refinement for quantification. The cation concentrations in the reacted fluid were analysed by ICP-OES measurements. A replacement reaction of leucite by analcime was confirmed by both, SEM and XRD measurements. ICP-OES analyses reveal an increasing K^+ concentration in the fluid while Na^+ and Ca^{2+} concentrations decreased in contrast to the starting fluid. After 2 weeks of reaction, a steady state was reached for Na^+ , K^+ , and Ca^{2+} concentrations. No significant difference between the two starting materials could be measured for element fluxes between rock and fluid, but a variation in porosity increase was observed. In the phonolithic foidite, starting with lower porosity, complete disintegration of the rock formation was observed, while the tephritic foidite only showed reaction-induced fracturing. As the replacement reaction is associated with a 10 % increase in volume, crystallisation pressure lead to stresses that are potentially high enough for fracturing.

Uranium incorporation in andraditic garnet

C. Ackermann^{1,2}, H.R. Marschall^{1,2}, M. Kutzschbach³, D.C. Hezel^{1,2}, A.B. Woodland^{1,2},
L.J. Millonig^{1,2}, J.B. Walters^{1,2}, A. Schmidt^{1,2}

¹*Institut für Geowissenschaften, Goethe Universität, Altenhöferallee 1, 60438 Frankfurt am Main, Germany*

²*Frankfurt Isotope and Element Research Center (FIERCE), Goethe Universität, 60438 Frankfurt am Main*

³*Institut für Angewandte Geowissenschaften, Technische Universität Berlin,*

Ernst-Reuter-Platz 1, 10587 Berlin, Germany

e-mail: cl.ackermann@gmx.de

Minerals of the garnet supergroup are widespread in, e.g., medium- to high-pressure metamorphic rocks, where they form an integral part of many well-established geobarometers and -thermometers. Since a few years, garnet U-Pb dating by (in-situ) LA-ICPMS is being developed. This method offers rapid analysis of a large set of samples with high spatial resolution and an age precision comparable to other geochronometers. However, the success rate of the method is hampered by our limited ability to predict the suitability of a particular sample for U-Pb dating. This limitation is due to current ambiguities regarding the incorporation of uranium (and Pb) in garnet.

In this study we investigate the incorporation of Uranium in (Ti-bearing) andraditic garnet, from alkaline igneous rocks and skarns. Previous studies on the incorporation of U into the garnet structure were restricted to elbrusite that contains U as a major component (up to 27 wt.%) in conjunction with Zr (Galuskina et al., 2010). Most natural andradite, however, contains only trace levels of U (typically 1–50 µg/g) and the substitution and incorporation mechanisms at this concentration level are unknown. Furthermore, previous studies even have claimed that U is not incorporated in garnet at all, and that the analysed U content is due to U-bearing inclusions (e.g., Lima et al., 2014). On our suite of five andradites, two of which originated from alkaline igneous rocks and three from skarn deposits, we completed a full chemical characterization. This included major and trace-element analyses and mapping by EPMA and LA-ICPMS, determination of the oxidation state of Fe by the EPMA flank method and by Mössbauer spectroscopy, and U-Pb dating by LA-ICPMS. Our results demonstrate that uranium concentrations strictly follow the oscillatory growth zoning of garnet, and one sample even exhibited sector zoning of U in garnet (Fig. 1). In general, U shows a positive correlation with Th and with Ce, and no correlation between U and Zr, showing that the elbrusite substitution vector does not (necessarily) operate at the trace-element level in andradite. Instead, U is likely incorporated in the dodecahedral site and charge compensated by octahedral divalent ions and/or tetrahedral Fe³⁺.

Our results show that U, together with Th and the LREE, is indeed incorporated into the structure of garnet, as opposed to U being present only in submicroscopic inclusions. Also, the LREE abundance can be used as a proxy for U-enriched zones. Garnet U–Pb geochronology by LA-ICPMS on andraditic garnet will, thus, be able to reveal the age of the garnet crystallization itself, if U-rich inclusions are avoided. This conclusion agrees with mass-balance estimates presented by Millonig et al. (2020) for metamorphic garnet.

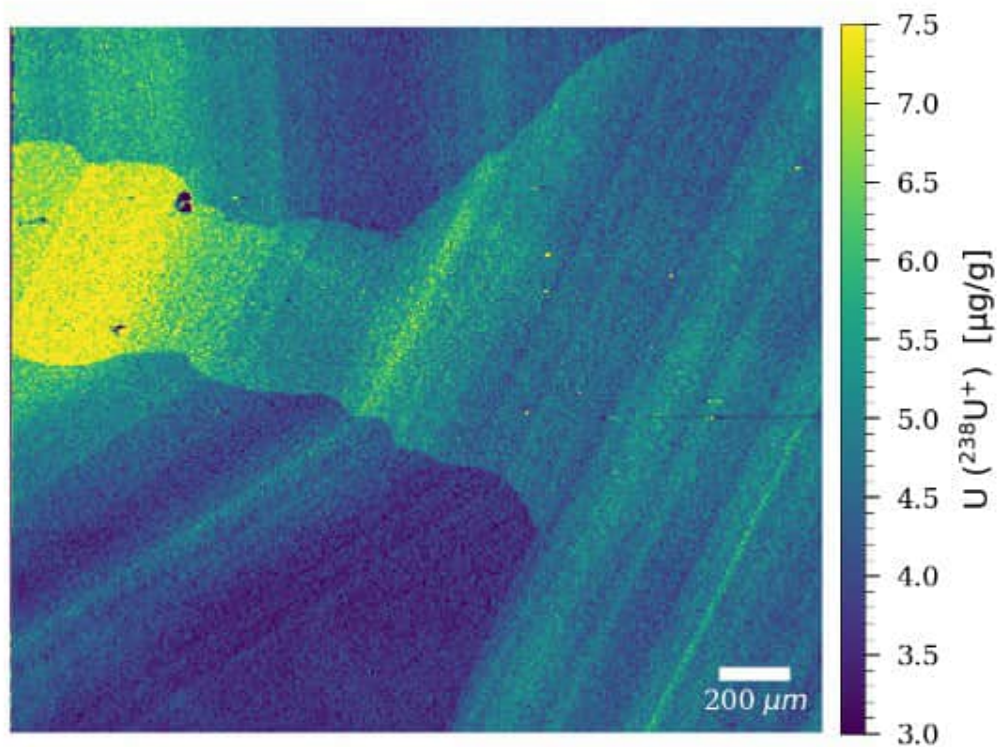


Figure 1. LA-ICP-MS mapping of ^{238}U in a Ti-rich andradite from Magnet Cove, Arkansas. Notice the very distinct oscillatory and sector zoning.

- Galuskina IO, Galuskin EV, Armbruster T, Lazic B, Kusz J, Dzierzanowski P, Gazeev VM, Pertsev NN, Prusik K, Zadov AE, Winiarski A, Wrzalik R, Gurbanov AG (2010): Elbrusite-(Zr)—A new uranian garnet from the Upper Chegem caldera, Kabardino-Balkaria, Northern Caucasus, Russia. - *Amer Mineral* 95, 1172-1181
- Lima SM, Corfu F, Neiva AMR, Ramos JMF (2012): U-Pb ID-TIMS dating applied to U-rich inclusions in garnet. - *Amer Mineral* 97, 800-806
- Millonig LJ, Albert R, Gerdes A, Avigad D, Dietsch C (2020): Exploring laser ablation U-Pb dating of regional metamorphic garnet The Straits Schist, Connecticut, USA. - *EPSL* 552, 116589

Plagioclase hosted magnetite micro-inclusions from oceanic gabbro: shape orientation and implication for bulk magnetic properties

O. Ageeva¹, G. Bian¹, G. Habler¹, R. Abart¹

¹University of Vienna, Department of Lithospheric Research
e-mail: olga.ageeva@univie.ac.at

In gabbro, fine-grained magnetite (MT) micro-inclusions hosted by rock-forming silicates contribute to bulk-rock magnetism. Specific crystal orientations of micro-inclusions relative to the silicate host may dramatically affect the direction and/or intensity of natural remanent magnetization (NRM) of the rock. Understanding the influence of oriented silicate-hosted magnetite micro-inclusions on rock-magnetism is important for obtaining reliable paleomagnetic data and for revealing rock magnetic fabrics, which may shed light on the mechanisms of rock formation or the tectonic evolution. We studied needle- and lath-shaped magnetite micro-inclusions in plagioclase of oceanic gabbro from the slow-spreading Mid Atlantic Ridge (11-17°N), aiming to reveal the genesis and ferromagnetic contribution of the MT inclusions to the magnetic properties of grains of host plagioclase. To this end, we combined a detailed petrographic study on magnetite-bearing plagioclase with crystal orientation analysis by electron backscatter diffraction (EBSD), measurements of the anisotropy of magnetic remanence (AMR) and alternating field (AF) demagnetization. The results show that:

(i) Needle and lath shaped MT inclusions have systematic shape orientations following eight specific crystallographic directions that coincide with the poles of low-index crystal planes/directions of the plagioclase host.

(ii) Statistically, the MT inclusions show two types of shape orientation distribution (Ageeva et al., 2022): One type is characterized by a predominantly oblate shape orientation distribution, due to a high fraction of needle-shaped inclusions oriented sub-parallel to the (010) plane of plagioclase and forming an about 30° wide “(010)-girdle”. These inclusions are considered to be of primary magmatic origin (Bian et al. 2023a). The other type of shape distribution features a high fraction of inclusions oriented parallel to the c-axis of the plagioclase-host. These inclusions are interpreted as secondary (Bian et al. 2023b), replacing primary inclusions in domains where high-temperature hydrothermal alteration of plagioclase was effective.

(iii) Twinning of plagioclase following the Albite, Pericline, Carlsbad and Manebach twin laws increases the dispersion of inclusion orientations within the (010)-girdle, and strengthens the lineation caused by the presence of inclusions oriented parallel to [001] of plagioclase.

(iv) The anisotropic shape orientation distribution of the MT-inclusions causes anisotropy of magnetic remanence (AMR) in the plagioclase grains (Ageeva et al., 2022). A good correspondence between the shape orientation distribution of the MT-inclusions and AMR is established in the majority of the studied plagioclase grains: The direction of minimum magnetic remanence R_{\min} is sub-perpendicular to the (010)-girdle. The direction of maximum magnetic remanence R_{\max} lies in the (010)-girdle and often is close to parallel to the PL [001] direction, which often corresponds to a maximum in the shape orientation distribution of MT-inclusions in twinned plagioclase.

(v) The vector of natural remanent magnetism (NRM) tends to lay in the (010)-girdle, often parallel to the maximum in the elongation orientation distribution of inclusions or/and parallel to the direction of maximum magnetic remanence.

The results indicate that oriented needle- and lath-shaped MT micro-inclusions in plagioclase endow the grains of host plagioclase with anisotropic ferromagnetism. Consequently, in case of preferred orientation of grains of magnetite-bearing plagioclase, which is typical for many geological settings including mid-ocean ridges and layered intrusions, a magnetic fabric may form. The identified characteristics of the plagioclase magnetic anisotropy are highly relevant for petrological and paleomagnetic studies of oceanic gabbro.

Ageeva O, Habler G, Gilder SA, Schuster R, Pertsev A, Pilipenko O, Bian G, Abart R (2022): Oriented magnetite inclusions in plagioclase: Implications for the anisotropy of magnetic remanence. – *Geochem Geophys Geosystems* 23, e2021GC010272

Bian G, Ageeva O, Roddatis V, Li C, Pennycook TJ, Habler G, Abart R (2023a): Crystal structure controls on oriented primary magnetite micro-inclusions in plagioclase from oceanic gabbro. - *J Petrol* 64, egad008

Bian G, Ageeva O, Roddatis V, Habler G, Schreiber A, Abart R (2023b): Oriented secondary magnetite micro-inclusions in plagioclase from oceanic gabbro. - *Amer Miner*, doi: 10.2138/am-2022-8784

Magmatic-hydrothermal versus metamorphogenic origin of tungsten mineralization: Examples from the Eastern Alps

F. Altenberger¹, J.G. Raith¹, J. Krause², C. Auer³, J. Weilbold³, H. Paulick³

¹Montanuniversität Leoben, Chair of Resource Mineralogy, Peter-Tunner-Straße 5, 8700 Leoben Austria

²Helmholtz Institute Freiberg for Resource Technology, Chemnitz Straße. 40, 09599 Freiberg, Germany

³GeoSphere Austria, Department of Mineral Resources, Neulinggasse 38, 1030 Wien, Austria,
e-mail: florian.altenberger@unileoben.ac.at

The increasing demand for tungsten in the European high-tech industry is offset by an increased supply risk. Hence, this metal has been on the list of critical raw materials for the EU since 2011. Global tungsten production is primarily from ore deposit types genetically related to granitic intrusions (e.g., skarn-type, vein-type, porphyry deposits etc.) and linked with magmatic-hydrothermal processes.

Europe's largest tungsten mine is located at Felbertal in Austria in (pre-)Variscan units of the Tauern Window in the Eastern Alps. Recent studies also support a magmatic-hydrothermal model and re-interpreted the Felbertal deposit as a metamorphosed vein-stockwork scheelite deposit associated with chemically evolved, W-rich granitic melts emplaced during the Variscan orogeny (Kozlik & Raith 2017). In the Eastern Alps, however, there are still numerous smaller (sub-economic) tungsten showings that differ significantly from the Felbertal deposit in terms of their geological and mineralogical characteristics. Most of them lack a direct relation to igneous intrusions but occur proximal to large-scale tectonic structures in Paleozoic strata with metacarbonate rocks (e.g., Tux-Lanersbach, Mallnock) of the low-grade metamorphic Austroalpine units. Syngenetic/syndiagenetic sedimentary-exhalative models were suggested in the past but a metamorphogenic origin as discussed by Palmer et al. (2022) for the formation of this style of mineralization elsewhere is also plausible.

Scheelite (CaWO₄) is the most common tungsten mineral in the Eastern Alps and was analyzed by the combined use of cathodoluminescence, electron probe microanalysis and in-situ LA-ICP-MS analysis to determine the mineralogical-chemical signature of scheelite from different styles of tungsten mineralization. The combination of geological-mineralogical information and trace element analysis of scheelite allows to distinguish three generic mineralization styles in the Eastern Alps, i.e., 1) *intrusion-related*, 2) *polymetallic* (As, Sb, Au), and 3) *carbonate-hosted stratabound* scheelite mineralization. Mineral chemistry shows that the trace elements Na, Sr, Nb, Mo and REE+Y in particular are suitable for differentiating scheelites from these different ore forming environments.

We demonstrate that the “Felbertal” magmatic-hydrothermal signature of scheelite is distinctly different from other styles of mineralization and that these findings can be used as an indicator in future exploration to evaluate the regional tungsten potential.

Kozlik M, Raith JG (2017): Variscan metagranitoids in the central Tauern Window (Eastern Alps, Austria) and their role in the formation of the Felbertal scheelite deposit. - *Lithos* 278-281, 303-320

Palmer MC, Scanlan EJ, Scott JM, Farmer L, Pickering D, Wilson VJ, Oelze M, Craw D, le Roux PJ, Luo Y, Graham Pearson D, Reid MR, Stirling CH (2022): Distinct scheelite REE geochemistry and ⁸⁷Sr/⁸⁶Sr isotopes in proximally- and distally-sourced metamorphogenic hydrothermal systems, Otago Schist, New Zealand. - *Ore Geology Reviews* 144, 104800

G.O.Joe: A new software for the evaluation and correction of LA-ICP-MS concentration data

F. Altenberger¹, T. Auer², J. Krause³, A. Auer², J. Berndt⁴

¹Montanuniversität Leoben, Chair of Resource Mineralogy, Peter-Tunner-Straße 5, 8700 Leoben Austria

²Moonshot Pioneers GmbH, Dorfbeuern 35, 5152 Dorfbeuern, Salzburg, Austria

³Helmholtz Institute Freiberg for Resource Technology, Chemnitz Straße 40, 09599 Freiberg, Germany

⁴Westfälische Wilhelms-Universität Münster, Corrensstraße 24, 48149 Münster, Germany
e-mail: florian.altenberger@unileoben.ac.at

Laser ablation-inductively coupled plasma-mass spectrometry (LA-ICP-MS) is widely used for spatially resolved measurements of the elemental and isotopic composition of solid materials. One of the problems of trace element analyses by LA-ICP-MS is the existence of interferences that cannot be resolved instrumentally. The software G.O.Joe was developed to calculate trace element concentrations in solid samples obtained by LA-ICP-MS analysis, offering several types of interference corrections. The software's algorithms are written in the Dart programming language within the Flutter programming environment and follow the procedure described in Jochum et al. (2006 and 2007). G.O.Joe operates online, allowing for immediate data evaluation. It efficiently processes large datasets, offering the flexibility to change parameters at any stage of the workflow. The software also includes features for uploading and storing multiple recovery files (.gojoe), thereby preserving the information from previously evaluated datasets.

A series of three self-instructive interfaces guide the user through a straightforward process of data evaluation. Clear visualization of raw data aids the evaluation of each measurement, facilitating the selection of background and sample signals. Concurrently, inclusions or mixed analyses can be excluded. The input of instrument settings and information about the reference material follows the data processing and is used to convert the isotope count rates to element concentrations. Importantly, advanced calculations can be applied to correct the measurements for isobaric or molecular interferences and abundance sensitivity. These essential advantages of G.O.Joe are demonstrated in different case studies that focus on the mineral chemistry of tungstates (i.e., scheelite) and silicates (e.g., garnet) including the relevant correction methods.

The exported result file (.xlsx) includes the calculated element concentrations, relevant statistical parameters, input data, and instrument settings, ensuring a transparent data processing. While G.O.Joe serves as a time-efficient, transparent, and easy-to-use tool for trace element analysis for experienced LA-ICP-MS users, it is also particularly appealing to newcomers to LA-ICP-MS data analysis. Notably, it is planned as non-commercial software and does not require installation. A first version of G.O.Joe is currently in the final stages of development and will be made available with further information at <https://www.gojoe.software>.

Jochum KP, Stoll B, Herwig K, Willbold M (2006): Improvement of in situ Pb isotope analysis by LA-ICP-MS using a 193 nm Nd:YAG laser. - J Analyt Atomic Spectrom 21, 666-675

Jochum KP, Stoll B, Herwig K, Willbold M (2007): Validation of LA-ICP-MS trace element analysis of geological glasses using a new solid-state 193 nm Nd:YAG laser and matrix-matched calibration. - J Analyt Atomic Spectrom 22, 112-121

Crystal structure and Li-ion conductivity in $\text{Li}_7\text{La}_3\text{Zr}_{12}\text{O}_{24}$ garnets: a review

G. Amthauer¹, D. Rettenwander², R. Wagner¹, G.J. Redhammer¹

¹University of Salzburg

²Norwegian University of Science and Technology Trondheim
e-mail: Georg.amthauer@plus.ac.at

Recent research has shown that certain Li-oxide garnets with more than 3 Li atoms per formula unit, such as $\text{Li}_7\text{La}_3\text{Zr}_{12}\text{O}_{24}$, have high ionic conductivities, as well as good chemical and physical properties for use in solid-state batteries (Murugan et al. 2007).

“Garnet” is the common name for a large number of natural and synthetic metal-oxide phases. Conventional oxide garnets have the general formula $\text{A}_3\text{B}_2\text{C}_3\text{O}_{12}$ and crystallize in the cubic space group $Ia\bar{3}d$. The O^{2-} ions, in the general crystallographic positions $96h$, form a framework with interstices occupied by the A cations, such as Ca^{2+} , Fe^{2+} , Y^{3+} , La^{3+} in the 8-fold coordinated position $24c$ (point symmetry 222), the B cations, such as Al^{3+} , Fe^{3+} , Zr^{4+} , Sn^{4+} , Sb^{5+} , etc. in the 6-fold coordinated position $16a$ (point symmetry $\bar{3}$), and the C cations, such as Li^+ , Al^{3+} , Fe^{3+} , Ga^{3+} , Ti^{4+} , Si^{4+} , etc. in the 4-fold coordinated $24d$ position (point symmetry $\bar{4}$). In addition to these cation sites, there are other interstices within the oxygen framework, which are empty in the conventional garnet structure, e.g. (i) the 6-fold coordinated $16b$ positions with point symmetry 32 , (ii) the 6-fold coordinated $48g$ positions with point symmetry 2 , and (iii) an additional 4-fold coordinated $96h$ position with point symmetry 1 . In “ $\text{Li}_7\text{La}_3\text{Zr}_{12}\text{O}_{24}$ ” garnet (LLZO), these interstices are filled by “excess” Li^+ ions giving rise to the excellent ionic conductivity.

There is a low temperature tetragonal modification of pure LLZO (SG: $I4_1/acd$) and a high temperature non quenchable cubic phase of LLZO (SG: $Ia\bar{3}d$). The tetragonal phase has distinctly lower ion conductivity than the cubic phase. Fortunately, the cubic phase can be stabilized at low temperatures by doping with low amounts of Al, Ga, and Fe (Buschmann et al. 2011; Rettenwander et al. 2016). In our contribution the results of single crystal X-ray diffraction studies will be presented. While Al-doped LLZO garnets always crystallize within the space group $Ia\bar{3}d$, Ga and Fe-doped LLZO garnets crystallize within the space group $I\bar{4}3d$ (Wagner et al. 2016). This symmetry change is combined with an increase in ionic conductivity up to $10^{-3} \text{ S cm}^{-1}$ which is very high for those kind of solid state electrolytes used in Li-ion batteries. These results will be discussed on the basis of the slightly different topologies of both space groups, respectively. Similar structural changes are observed by the incorporation of Co (Mir et al. 2023).

Buschmann H, Dölle J, Berendts S, Kuhn A, Bottke P, Wilkening M, Heitjans P, Senyshyn A, Ehrenberg H, Lotnyk A (2011): Structure and dynamics of the fast lithium ion conductor “ $\text{Li}_7\text{La}_3\text{Zr}_{12}\text{O}_{24}$ ”. - Phys Chem Chem Phys 13, 19378-19392

Murugan R, Thangadurai V, Weppner W. (2007): Fast lithium ion conduction in garnet-type $\text{Li}_7\text{La}_3\text{Zr}_{12}\text{O}_{24}$. - Angew Chem Int Ed 46, 7778-7781

- Mir MUD, Ladenstein L, Ring J, Knez D, Smetaczek S, Kubicek M, Sadeqi-Moqadam M, Ganschow S, Salagre E, Enrique G. Michel, Stefanie Lode, Gerald Kothleitner, Iulian Dugulan, Jeffrey G. Smith, Limbeck A, Fleig J, Donald J. DJ, Redhammer GJ, Daniel Rettenwander D (2023): A guideline to mitigate interfacial degradation processes in solid-state batteries caused by cross diffusion. - *Adv. Funct Mater* 2023, 2303680
- Wagner R, Redhammer GJ, Rettenwander D, Senyshyn A, Schmidt W, Wilkening M, Amthauer G (2016): Crystal structure of garnet-related Li-ion conductor $\text{Li}_{7-3x}\text{Ga}_x\text{La}_3\text{Zr}_2\text{O}_{12}$: Fast Li-ion conduction caused by a different cubic modification? - *Chem Mater* 28, 1861-1871
- Rettenwander D, Redhammer G, Preishuber-Pflügl F, Cheng L, Miara L, Wagner R, Welzl A, Suard E, Doeff MM, Wilkening M, Fleig J, Amthauer G (2016): Structural and Electrochemical Consequences of Al and Ga cosubstitution in $\text{Li}_7\text{La}_3\text{Zr}_2\text{O}_{12}$ solid electrolytes. - *Chem Mater* 28, 2384-2392

Trace metals in hydrothermal magnetite – current knowledge, application, and experimental approaches

T. Angerer¹, R. Bakker², F. Melcher³

¹GeoSphere Austria, Department of Mineral Resources and Geoenergy, Vienna

²Montanuniversität Leoben, Chair of Resource Mineralogy

³Montanuniversität Leoben, Chair of Geology and Economic Geology

e-mail: thomas.angerer@geosphere.at

Hydrothermal ore deposits host significant resources of iron and base, precious, and critical metals. In order to understand ore-forming hydrous fluid-rock interaction geoscientists analyse co-genetic mineral assemblages, fluid inclusions, elemental and isotopic geochemistry to approximate temperature, fO_2 , pH, and metal and ligand composition of hydrothermal fluids. Because the accessibility or applicability of measurable proxies is often limited in a given ore deposit, there is the need for other “recorders” of fluid-rock-interaction, preferentially ubiquitous, robust, and comfortably to analyse. In recent years, trace element abundances in magnetite have become a favourite study object due to its ability to robustly record complex fluid-rock interaction (Dupuis & Beaudoin 2011; Nadoll et al. 2014; Dare et al. 2014; Canil et al. 2016; Huang et al. 2018). The understanding of trace metal signatures has grown steadily, yet is far from being satisfactory. Here, the quantification of trace metal partitioning coefficients D between mineral and fluid as functions of system variables is a crucial requirement. For magnetite, empirical D' have been determined in numerous crystal/melt experimental studies, however, only a hand full of studies have dealt with trace metal partitioning in hydrothermal systems (e.g., Ilton & Eugster 1989; Lipko et al. 2020; Simon et al. 2006; Smagunov et al. 2021). In most published setups, experimental fluids were far away from representing natural ore-forming fluids, but designed to synthesise magnetite most efficiently. Metastudies for melt, metamorphic, or aqueous fluid systems reveal that magnetite D' values for given cations vary significantly (Dare et al. 2012; Dare et al. 2014; Nadoll et al. 2014; Nadoll et al. 2017). The present contribution provides an update on the use of magnetite chemistry, the present knowledge and experimental approaches, and introduces a new joint initiative to investigate hydrothermal magnetite.

In an FWF-funded 3-year postdoctoral project at GeoSphere Austria and Montanuniversität Leoben we are going to study systematically metal cation partitioning and fractionation in magnetite-rich high-T hydrothermal mineralisations. A multi-analytical approach will enable us to obtain and compare D' from hydrothermal magnetite from supercritical natural and synthetic samples. Magnetite synthesis from Fe-Si rich and trace metal doped chloride solutions can be archived in cold-seal Ni-steel autoclaves (Figure 1). Investigated systems comprise setups at ~ 1.5 kbar, 500–750 °C and various O_2 buffers (IM, MW, CCO, and MMO in outer capsules). Ore samples from similar systems will be selected to obtain complementary natural D' from magnetite and fluid inclusion chemistry in co-genetic transparent phases. To enhance the robustness of data, the competition for trace metals between magnetite and co-genetic phases such as silicates, sulfides, phosphates, and oxides will be considered, as well as any inter- and intra-grain chemical heterogeneity and solid inclusions at the micro- to nano-scale (Deditius et al. 2019, Verdugo-Ihl et al. 2021).

Building on the characterisation of co-existing mineral assemblages and fluid inclusions by petrography, EPMA, laser ablation ICPMS, microthermometry, and Raman spectroscopy, we plan following collaborative analyses: TEM petrography and ELNES with Liane Benning and Vladimir Roddatis from GFZ and Max Wilke from Uni Potsdam, SIMS O

isotopes with Etienne Deloule at CRPG-CNRS Nancy, fluid inclusion LA-ICPMS with Tobias Fußwinkel at RWTH Aachen, and alternative experimental setups with Bastian Joachim-Mrosko, Uni Innsbruck. We will select samples from own collections and from Robert Marschik, LMU Munich, and Christin Kehler, TU Freiberg.

Datasets from our holistic approach will provide an unprecedented, cross-validated, reservoir of quantitative information on the behaviour of cations in magnetite under distinct high-T hydrothermal conditions. New D' datasets may allow calibrating thermometers and O₂-barometers and approximating hydrothermal fluid chemistries from mineral chemistry.

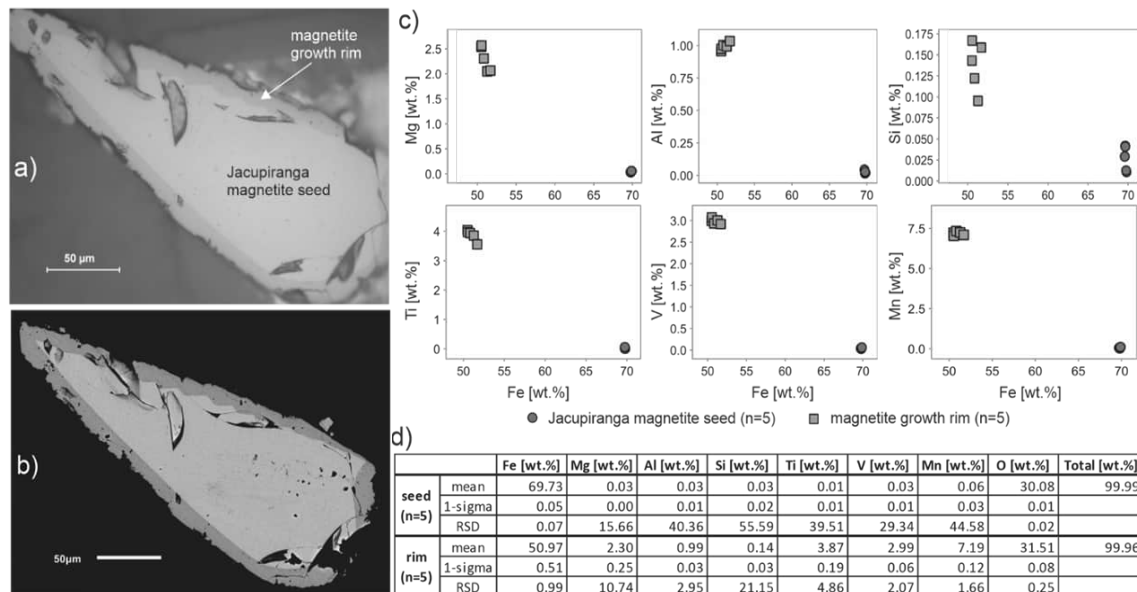


Figure 1. Magnetite seed with growth rim from a trial experimental run of 14 days at 600 °C and 1 kbar: (a) a plain polarized reflected light micrograph and (b) SEM backscatter image, both exposing a growth rim. (c, d) EPMA elemental analyses data show the distinct chemistry between seed and rim.

- Canil D, Grondahl C, Lacourse T, Pisiak LK (2016): Trace elements in magnetite from porphyry Cu–Mo–Au deposits in British Columbia, Canada. - *Ore Geol Rev* 72, 1116-1128
- Dare SA, Barnes S-J, Beaudoin G, Méric J, Boutroy E, Potvin-Doucet C (2014): Trace elements in magnetite as petrogenetic indicators. - *Mineral Deposita* 49, 785-796
- Dupuis C, Beaudoin G (2011): Discriminant diagrams for iron oxide trace element fingerprinting of mineral deposit types. - *Mineral Deposita* 46, 319-335
- Huang X-W, Boutroy É, Makvandi S, Beaudoin G, Corriveau L, De Toni AF (2018): Trace element composition of iron oxides from IOCG and IOA deposits: relationship to hydrothermal alteration and deposit subtypes. - *Mineral Deposita* 1-28
- Ilton ES, Eugster HP (1989): Base metal exchange between magnetite and a chloride-rich hydrothermal fluid. - *Geochim Cosmochim Acta* 53, 291-301
- Lipko S, Tauson V, Bychinskii V (2020): Gold partitioning in a model multiphase mineral-hydrothermal fluid system: Distribution coefficients, speciation and segregation. - *Minerals* 10, 890
- Nadoll P, Angerer T, Mauk JL, French D, Walshe J (2014): The chemistry of hydrothermal magnetite: A review. - *Ore Geol Rev* 61, 1-32
- Nadoll P, Mauk JL, Hayes TS, Koenig AE, Box SE (2017): Element partitioning in magnetite under low-grade metamorphic conditions – a case study from the Proterozoic Belt Supergroup, USA. - *Eur J Mineral* 29, 795-805
- Simon AC, Pettke T, Candela PA, Piccoli PM, Heinrich CA (2006): Copper partitioning in a melt–vapor–brine–magnetite–pyrrhotite assemblage. - *Geochim Cosmochim Acta* 70, 5583-5600
- Smagunov, N., Tauson, V., Lipko, S., Babkin, D., Pastushkova, T., Belozerova, O. and Bryansky, N. (2021) Partitioning and Surficial Segregation of Trace Elements in Iron Oxides in Hydrothermal Fluid Systems. *Minerals* 11, 57
- Deditius AP, Reich M, Simon AC, Suvorova A, Knipping J, Roberts MP, Rubanov S, Dodd A, Saunders M (2018): Nanogeochemistry of hydrothermal magnetite. - *Contrib Mineral Petrol* 173, 46
- Verdugo-Ihl MR, Ciobanu CL, Cook NJ, Ehrig K, Slattery A, Courtney-Davies L, Dmitrijeva M (2021): Nanomineralogy of hydrothermal magnetite from Acropolis, South Australia: Genetic implications for iron-oxide copper gold mineralization. - *Amer Mineral* 106, 1273-1293

Decompression of high-grade metamorphic mafic rocks constrained by small-scale compositional layering, Gföhl Unit, Moldanubian Zone

R. Asenbaum¹, M. Racek², R. Abart¹

¹*Department of Lithospheric Research, University of Vienna, Austria*

²*Institute of Petrology and Structural Geology, Faculty of Science, Charles University Prague, Czech Republic
e-mail: rene.asenbaum@univie.ac.at*

Mafic–ultramafic lenses embedded in felsic granulites of the Gföhl Unit, Moldanubian Zone, are considered as mantle fragments incorporated into mid-crustal levels of the Variscan orogenic crust. We investigated a several 100 m sized mafic lens mainly formed by eclogites. Several samples were collected from loose boulders. Petrographic features provide evidence for an early HP-HT eclogite-facies peak metamorphism overprinted to variable degrees by HT granulite-facies metamorphism at lower pressures.

The primary eclogite facies mineral assemblage comprises garnet, sodium-rich clinopyroxene (up to $X_{\text{Na}_M2} = 0.29$), kyanite, rutile and quartz. The rocks are characterized by compositional layering on the mm-scale, which is reflected by corresponding systematic variation of the compositions of garnet porphyroblasts. The garnets show homogeneous compositions in their internal domains defining plateaus, the compositional characteristics of which correlate with the compositional layering of the rocks and vary from $\text{Alm}_{19} \text{Prp}_{55} \text{Grs}_{27}$ to $\text{Alm}_{15-18} \text{Prp}_{42-50} \text{Grs}_{32-43}$. The systematic variation of garnet compositions with the bulk rock compositional layering testifies to lack of equilibration on the mm scale during HP-HT eclogite-facies metamorphism.

The HT-granulite-facies overprint is evident from the breakdown of the eclogite facies mineral assemblage. This is evident, for example, from the formation of sapphirine–spinel–an-rich plagioclase symplectites in garnet supposedly replacing garnet-hosted kyanite and clinopyroxene inclusion. Another peculiar feature is represented by the partial resorption of garnet by plagioclase and clinopyroxene in the form of corrosion tubes penetrating the garnet in a worm-like fashion. Finally, garnet is partially or entirely replaced by plagioclase–spinel–orthopyroxene—clinopyroxene symplectite, where Grs-rich garnets are systematically more strongly affected by this replacement than Grs-poor garnets. Quartz is consumed during the decompression reactions and can only be found as rare relic grains. When relic quartz is surrounded by a clinopyroxene matrix, the clinopyroxene becomes successively more Si-rich due to inverse Tschermak substitution towards the relic quartz grain.

Throughout the samples and irrespective of the layer they pertain to, the garnets show similar pronounced secondary compositional zoning in the outermost 200 μm . The zoning is characterized by a strong decrease of the Grs content accompanied by an increase of the Alm and Prp contents towards the rim. The compositional changes in garnet are gradual suggesting diffusion-mediated re-equilibration at decreasing pressures, and the composition of the garnet at the interface to the rock matrix is the same throughout the specimen indicating that the rock equilibrated on the cm scale during the HT overprint.

Pressure and temperature were estimated on the basis of equilibrium phase diagrams. They indicate peak pressures above 1.8 GPa and temperatures of around 1000 °C for the primary mineral assemblages and the different garnet cores. In accordance with peak P-T, the garnet rims indicate pressures of around 1.2 GPa with the same temperature.

Considering the regional metamorphic setting of the Moldanubian Zone, the relatively localized secondary chemical zoning of garnet at its rim indicates that the granulite-facies metamorphism was remarkably short-lived and suggests rapid transport of the mafic–ultramafic lithologies from mantle depths to the mid-crustal level. Very likely incorporation of the relatively hot mafic lens into a supposedly cooler dominantly felsic environment led to immediate cooling of the mafic lens.

The position of vanadium in the crystal structure of zoisite, a variety tanzanite

P. Bačík^{1,2}, M. Wildner³, J. Cempírek⁴, R. Škoda⁴, P. Cibula¹, T. Vaculovič⁵

¹Comenius University in Bratislava, Faculty of Natural Sciences,
Department of Mineralogy, Petrology and Economic Geology, Ilkovičova 6, 842 15 Bratislava, Slovak Republic

²Earth Science Institute of the Slovak Academy of Science,
Dúbravská cesta 9, 84005 Bratislava, Slovak Republic

³Institut für Mineralogie und Kristallographie, Geozentrum, Universität Wien,
Josef-Holaubek-Platz 2, 1090 Wien, Austria

⁴Masaryk University, Department of Geological Sciences, Kotlářská 2, 61137 Brno, Czech Republic

⁵Department of Chemistry, Faculty of Science, Masaryk University, Kamenice 5, Brno 62500, Czech Republic
e-mail: peter.bacik@uniba.sk

Tanzanite is the most valued gemmological variety of zoisite in which V is the dominant trace element and chromophore. However, the exact position and state of V in the zoisite structure are quite enigmatic and subject to many hypotheses based mainly on spectroscopic evidence but lacking any definite structural proof. Therefore, we combined a structure refinement with optical absorption spectroscopy and used two separate theoretical approaches to shed some light on this enigma.

Structure refinement of the zoisite–tanzanite structure did not provide sufficient evidence of the V location in the zoisite structure due to the small V content in tanzanite as evidenced by Electron-Probe Micro-Analysis and Laser-Ablation Inductively Coupled Plasma Mass Spectrometry. Structure refinement of the studied sample revealed an average bond length of the less distorted $M1,2O_6$ octahedron lower than 1.90 Å. At the same time, $M3O_6$ has slightly longer bonds with an average of ca. 1.96 Å. The $M1,2$ site has a slightly higher bond valence sum (BVS) of 3.03 vu, whereas BVS of $M3$ is significantly lower (2.78 vu).

Optical absorption spectra of the studied sample with measured bands at 13 160, ~15 500, 16 350, 16 700, 18 800, 26 120, 26 650, and 34 000 (?) cm^{-1} revealed that most V is trivalent with only a small portion likely in a four-valent state. Therefore, a crystal-field superposition-model and bond-valence model calculations were applied here with two necessary basic assumptions: (1) V is at octahedral sites; (2) it can be present in two oxidation states, V^{3+} or V^{4+} . Crystal field superposition model calculations made to interpret the optical spectra indicated that V^{3+} prefers occupying the $M1,2$ site; the preference of V^{4+} was impossible to determine from the present data.

Bond-valence model calculations showed no unambiguous preference for V^{3+} , although based on the simple bond-length calculation, the preference of the $M3$ -site could be suggested. In contrast, it is quite straightforward to assume that the $M1,2$ site has a more natural environment for V^{4+} . However, if the calculated octahedral distortions are taken into account, the $M1,2O_6$ octahedron shows a smaller change in distortion if occupied by V^{3+} than the $M3O_6$ octahedron.

Consequently, based on both the crystal field superposition model and bond-valence model calculations, it can be concluded that both V^{3+} and V^{4+} prefer the $M1,2$ site.

”Gold” hydrogen in natural fluid inclusions

R. J. Bakker

*Resource Mineralogy, Department Applied Geoscience and Geophysics, Montanuniversität Leoben, Austria
e-mail: bakker@unileoben.ac.at*

Fluid inclusions in minerals are natural storage vessels of fluids. The most common fluids that are preserved in inclusions are mixtures of water, carbon-dioxide and salts. In reduced geological environments gases such as methane (and other thermogenic alkanes, also known as “abiotic”), nitrogen, and hydrogen may be included. The present study gives some new results on the occurrence of hydrogen in natural fluid inclusions in specific geological settings.

Hydrogen is a highly volatile gas component that is not assumed to retain within the crust and mantle for a long period, but is continuously outgassed. Several natural seeps of hydrogen-rich fluids are already considered for exploration (so-called “gold” hydrogen). This hydrogen may be captured within fluid inclusions in environments with sufficient concentrations. Both seeps and fluid inclusions are aspects of the existence of a hydrogen-rich fluid that may circulate in rock. The latter may also provide information on hydrogen-rich flows in the geological past, because inclusions may preserve paleo fluid properties.

There are only few studies that mention the existence of hydrogen within fluid inclusions, that provide abundant speculative models of the origin of hydrogen within rock, usually with a lack of sufficient and relevant data. For example, both serpentinization and deserpentinization were considered as formation processes of hydrogen. Redox conditions in rock are the main factors that define the composition of a fluid phase in deep rock, that only occupy a minor volume fraction of the system. This fluid is buffered by the coexistence of solid phases within the rock. Highly reduced conditions are common within mantle rock. Methane is closely related to the occurrence of hydrogen as both represent these reduced conditions. Similar conditions exist in Si-undersaturated igneous environments (e.g. nepheline syenite). An alternative source of hydrogen is radiolysis, but this is not sufficiently supported by fluid inclusion studies.

Hydrogen-rich fluid inclusions are analysed in three different geological settings: 1. In Upper Cretaceous strongly serpentinized mantle rock (Troodos, Cyprus); 2. In Neogene pegmatites closely related to serpentinite host-rock from metamorphosed ophiolitic-sedimentary tectonic units (Elba, Italy) (Bakker & Schilli, 2016); 3. In Mesoproterozoic metasediments of the Mt Painter Inlier, Arkaroola (Australia) (Bakker & Elburg, 2006)

Inclusions in pyroxene in strongly serpentinized areas in Troodos contain mixtures of CH₄, H₂ and H₂O (Fig. 1). Similar fluids are observed in chromite in mantle rock that is hardly affected by serpentinization (McElduff, 1989).

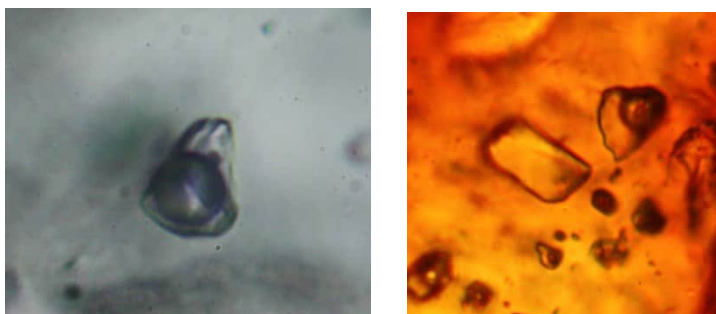


Figure 1. Fluid inclusions (ca. 10 μm) in pyroxene (left) and chromite (right). The vapour phase is highly enriched in H₂.

Fluid inclusions in pegmatites from Elba represent a complex interaction between magmatic and metamorphic fluids. Multiple pulses of low salinity H₂O-rich magmatic and reduced metamorphic fluid stages are recorded. Magmatic fluids are characterized by the presence of minor amounts of CO₂ and H₃BO₃, whereas the metamorphic fluids contain CH₄ and H₂ (minor N₂, H₂S, and C₂H₆) that may originate from the input of more reduced fluids from serpentinites, that may completely replace the magmatic fluid. H₂-rich fluid inclusions were observed in andalusite, quartz, plagioclase, and tourmaline.

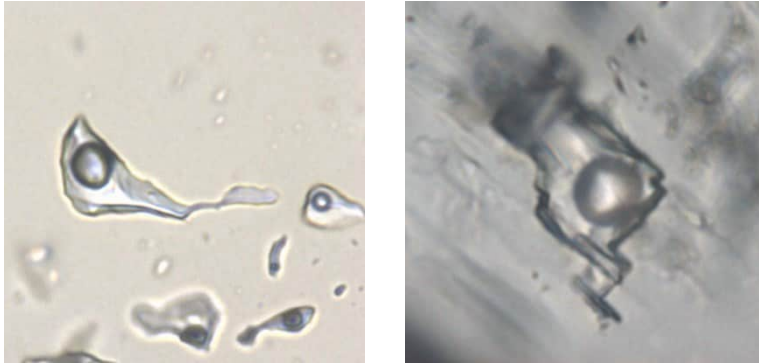


Figure 2. Fluid inclusions (ca. 20 µm) in quartz (left) and plagioclase (right) (Bakker & Schilli, 2016). The vapour phase is a mixture of mainly H₂ and CH₄.

A massive hydrothermal event in Arkaroola is demonstrated by an epithermal hematite-quartz assemblage, bladed calcite, and fluorite (Fig. 3). Fluid inclusions in fluorite contain a mixture of H₂O and H₂. The hydrogen occurs preferentially within the purple fluorite, which also includes some uranium mineralizations (radiation damage centres). These mineralizations are also proposed to be responsible for defining the colour of fluorite from green to purple that grew contemporaneously with the late hydrothermal quartz–hematite mineralization. The origin of hydrogen in fluid inclusions in fluorite is suggested to be radiolysis.

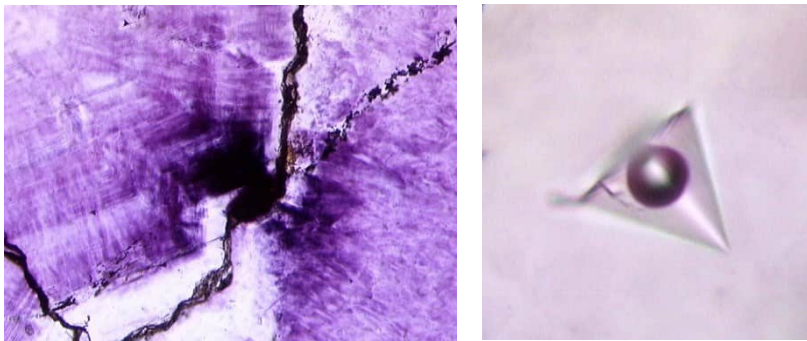


Figure 3. Purple fluorite with radiation damage centres (left), and H₂-rich fluid inclusions, ca. 10 µm (right) (Bakker & Elburg, 2006). Left image has a length of 200 µm.

Diffusion of hydrogen is a common aspect to explain the absence of hydrogen in most rock, even in environments where hydrogen is assumed to be a major fluid component. The examples illustrate that hydrogen may be preserved within fluid inclusions, similar to most fluid components.

Bakker RJ, Elburg MA (2006): A magmatic-hydrothermal transition in Arkaroola (northern Flinders Ranges, South Australia): from diopside-titanite pegmatites to hematite-quartz growth. - *Contrib Mineral Petrol* 152, 541

Bakker RJ, Schilli SE (2016): Formation conditions of leucogranite dykes and aplite-pegmatite dykes in the eastern Mt. Capanne plutonic complex (Elba, Italy): fluid inclusion studies in quartz, tourmaline, andalusite and plagioclase. - *Mineral Petrol* 110, 43

McElduff, B (1989): Inclusions in chromite from Troodos (Cyprus) and their petrological significance. - Ph.D. Thesis, Montanuniversität Leoben, Austria

The role of mineralogy: Case studies from Austr(al)ia

A. Baldermann¹

¹*Institute of Applied Geosciences, Graz University of Technology, NAWI Graz Geocenter, Rechbauerstraße 12, 8010 Graz, Austria*

The role and value of mineralogy in geosciences and material sciences have recently been hotly debated. In particular, the contribution of this long-established discipline in modern science and academic education has been questioned. So, what will mineralogy be focused on in the future, especially in the light of fundamental vs more applied perspectives? A closer look on mineralogy and the linked fields of crystallography, geochemistry and petrology, indicates interdisciplinary knowledge among the highly diverse fields of expertise to be key to an advanced process understanding in the various facets of human kind, climate change, resource scarcity, and technical challenges (Fig. 1).

In this contribution, various aspects of kinetic and equilibrium water-rock/mineral-gas interactions in low temperature settings are discussed, which are of high relevance for geo- and material scientist's present and future works. Focus is given on the assessment, identification and quantification of fundamental reaction mechanisms of mineral formation, dissolution, and transformation, tailoring/conditioning of (geo-)materials, and advanced understanding of the Earth system evolution throughout space and time. Case studies presented herein comprise of (i) carbonate vein infillings of vertical fractures (Erzberg), (ii) carbonation and external sulphate attack on concrete/shotcrete (Bosruck), (iii) (de)contamination/stabilization of soils using novel nZVI-bentonite nano-composites (Stadtschlaining), and (iv) environmental reconstruction of seawater chemistry by previously unrecognized archives (glauconites from the Arrowie and Amadeus basins, Australia). Recent advances in the analytical toolbox of mineralogists and (isotope) geochemists, such as in-situ Rb-Sr dating via LA-ICP-MS/MS, high-resolution optical imaging, and SEM-based automated mineral mapping, are highlighted, which offer new perspectives in geosciences and material sciences.

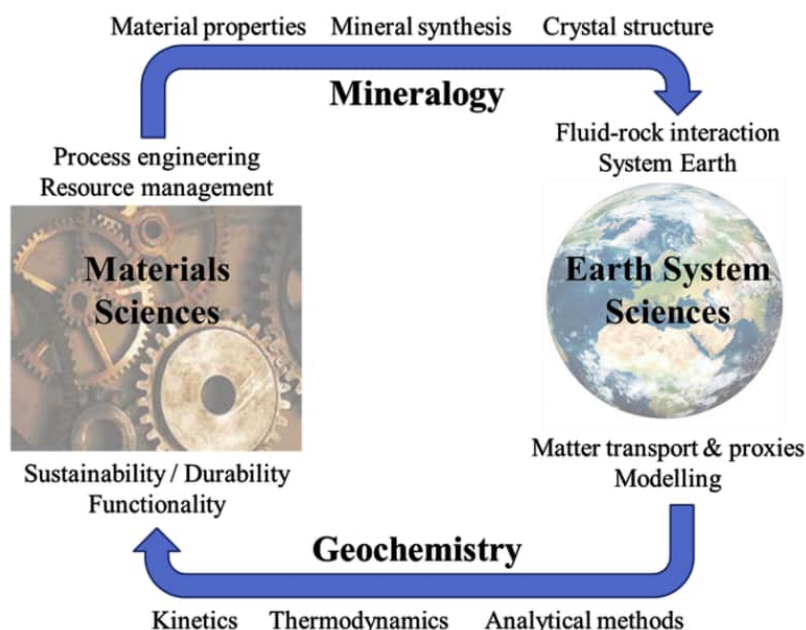


Figure 1. The role of mineralogy/geochemistry in geosciences and material sciences.

Zircon uses baddeleyite nanoparticles as fundamental building blocks

C. Ballhaus¹, H. Helmy², R. Wirth³, V. Roddatis³, T. Nagel⁴, A. Schreiber³

¹Universität Bonn, Germany

²Minia University, Egypt

³GFZ Potsdam, Germany

⁴Bergakademie Freiberg, Germany

e-mail: ballhaus@uni-bonn.de

Numerous experiments have been performed in the past to determine the crystallization temperature of zircon from silicate melts (Watson & Harrison 1983; Boehnke et al. 2013; Gervasoni et al. 2016; Borisov & Aranovich 2019; Marxer & Ulmer 2019). In designing those experiments, the implicit assumption was that zircon is a primary magmatic phase that crystallizes directly from the melt. Factors that determine the saturation of zircon are the Zr^{4+} (or ZrO_2) content of the melt, its silica activity (a_{SiO_2}), and the cation ratio $M = (Na + K + 2Ca) / (Al * Si)$ (Watson & Harrison 1983). The latter parameter roughly reflects the polymerization degree of a melt.

Our experiments give a somewhat different picture. We performed experiments with a phonolite composition that is modeled on a ne-normative pumice of the Laacher See, Eifel. The composition contains 60.6 SiO_2 , 20.1 Al_2O_3 , 2.5 FeO and CaO each, MgO 0.5, and total alkalis of 12.5 (all in wt.%). It is just corundum-normative. To prevent the introduction of zircon seeds, a synthetic aliquot of oxides and carbonates (Ca, alkalis) was synthesized. After the sample was sintered at 950 °C and CO_2 was expelled, Zr was added as $ZrCl_2O$ ICP standard solution. The mixture was then equilibrated at 1200 °C and 300 MPa in a piston cylinder press for 2 to 24 hours. After completion of the experiments, the Zr contents of the glasses were 1300 ± 160 ppm (average $\pm 1\sigma$ of 20 EPMA analyses).

Liquidus phases at 1200 °C were silicate melt and corundum (crn). Zircon did not crystallize because the composition is undersaturated with respect to zircon by factor of 10 (Fig. 1). Four Focussed Ion Beam (FIB) sections cut from experimental glasses showed that all charges crystallized at 1200 °C crystalline (and possibly amorphous) ZrO_2 nanophases (baddeleyite) (Fig. 2). The smallest and earliest ZrO_2 nanoparticles are found as inclusions in crn. These nanophases are as small as 3 to 4 nm and comprise perhaps 500 unit cells. They are so small because their growth was arrested after they were trapped by crn.

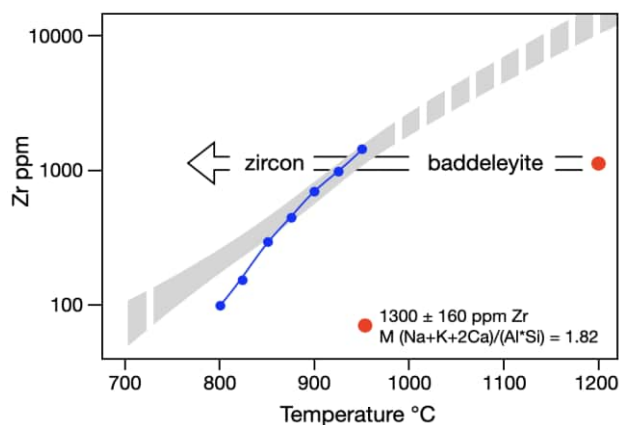


Figure 1. Starting mix with 1300 ± 160 ppm Zr - red circle. Grey - region in Zr-temperature space where magmatic zircon is stabilised (Watson & Harrison 1983; Boehnke et al. 2013; Gervasoni et al. 2016; Borisov & Aranovich, 2019). Blue symbols - zircon saturation experiments by Marxer & Ulmer (2019). For our composition zircon is expected to become stable at ~ 900 °C.

The results imply that zircon uses nanometer-sized ZrO_2 particles as building blocks when it nucleates from silicate melt. Zircon is stabilized by the reaction ZrO_2 (nanoparticle) + SiO_2 (melt) \rightarrow ZrSiO_4 (crystal). We think that in nature this reaction is a solution-precipitation reaction. Direct crystallization of zircon from Zr^{4+} and SiO_2 , if it indeed occurs, may be the exception rather than the rule. We assume that the ZrO_2 nanoparticles illustrated in Fig. 2 are stable, that they nucleated in local ΔG minima.

Many igneous rocks undersaturated with zircon may carry baddeleyite (e.g., Heaman & LeCheminant 1993). However, because baddeleyite tends to be extremely small, its presence is easily overlooked.

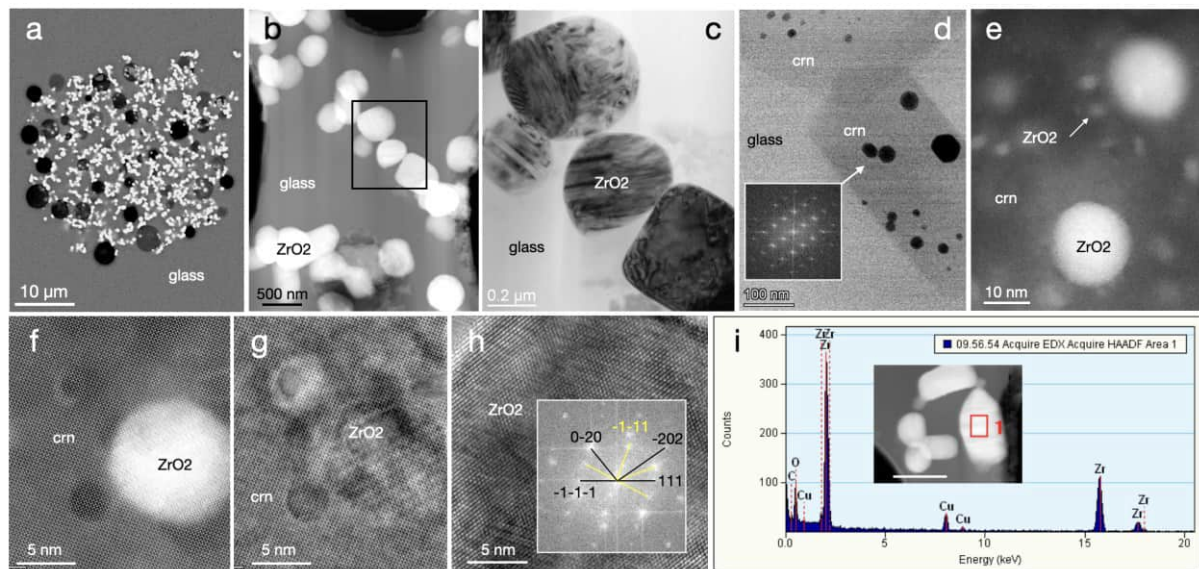


Fig. 2. ZrO_2 nanoparticles. (a) Baddeleyite (bdy) cluster in glass, after 10 hours at 1200 °C, in (b) TEM image at higher magnification; note tendency of bdy to attach and align to clusters and chains. (c) Brightfield (BF) image of twinned bdy in glass. (d) ZrO_2 nanoparticles trapped by liquidus corundum (crn). (e) HAADF image of ZrO_2 nanoparticles < 4 nm, in crn. (f) and (g) HAADF images, ZrO_2 nanoparticles in crn. (h) FFT of HREM, ZrO_2 in crn (crn in yellow). (i) Energy-dispersive spectrum to illustrate composition of bdy.

Boehnke P, Watson EB, Trail D, Harrison TM, Schmitt AK (2013): Zircon saturation re-revisited. - Chem Geol 351, 324–334

Borisov A, Aranovich L (2019): Zircon solubility in silicate melts: New experiments and probability of zircon crystallization in deeply evolved basic melts. - Chem Geol 510, 103-112

Gervasoni F, Klemme S, Rocha-Júnior ERV, Berndt J (2016): Contr Mineral Petrol 171, 21, DOI 10.1007/s00410-016-1227-y

Heaman LM, LeCheminant AN (1993): Paragenesis and U-Pb systematics of baddeleyite (ZrO_2). - Chem Geol 110, 95-126

Marxer F, Ulmer P (2019): Crystallisation and zircon saturation of calc-alkaline tonalite from the Adamello Batholith at upper crustal conditions: an experimental study. - Contr Mineral Petrol, <https://doi.org/10.1007/s00410-019-1619-x>

Watson EB, Harrison TM (1983): Zircon saturation revisited: temperature and composition effects in a variety of crustal magma types. - Earth Planet Sci Letters 64, 295-304

What does tourmaline reveal about the polymetamorphic evolution of the Matsch unit (Vinschgau, S-Tyrol, Italy)?

E. Bernabe¹, P. Tropper¹, C. Morelli², V. Mair²

¹University of Innsbruck, Institute of Mineralogy and Petrography, 6020 Innsbruck, Austria

²Amt für Geologie und Baustoffprüfung, Autonome Provinz Bozen - Südtirol

e-mail: peter.tropper@uibk.ac.at

The currently mapped sheet Schlanders (Project CARG F012) offers the chance to carefully investigate the Austroalpine units in the Vinschgau and their tectonic contacts and to implement them into a tectonic model based on new petrological, geochronological and structural data. The Austroalpine nappe stack in the investigated area, located in the Vinschgau area (South Tyrol), comprises from bottom to top the Campo-Ortler-nappe, the Texel-unit, the Ötztal-nappe and the Matsch unit. The Matsch unit in the northern flank of the Vinschgau valley shows a clear polymetamorphic evolution history which can be well reconstructed using the spatial distribution of the alumosilicates, the chloritoid-isograd and the observation of chemical zoning patterns in garnets, which, depending on the geographical position and the geological setting, exhibit single-phase, two-phase or even three-phase compositions. Geothermobarometry yielded a strong increase in eo-Alpine temperature conditions of 500 °C and 0.8 GPa to 650 °C and 1-1.2 GPa.

Tourmaline is especially well-suited as petrogenetic indicator owing to its expansive P - T stability, occurrence in rocks of widely varying composition, and settings ranging from sedimentary, to hydrothermal, metamorphic, and magmatic. Tourmaline composition varies systematically with changing P - T conditions in its host environment. A gradual increase in Al on the Y-site, the Mg/Fe-ratio, the vacancy content at the X site, accompanied by increasing Ca correlates with increasing metamorphic grade for metapelitic tourmalines.

Chemically the tourmalines are dravites. The tourmalines west of the chloritoid-isograd show a complex chemical zoning pattern with 3-5 zones, whereas east of the isograd only tourmalines with 2-4 zones occur. Chemical zoning within these western tourmalines reveals in the outermost rims a sharp increase in Ca(X), Al(Y), and the vacancy on X. The inner zones most likely represent stages of the pre-Alpine metamorphic evolution since the cores contain quite high Ca(X). The 3-zone eastern tourmalines show a clear prograde evolution with increasing Ca(X), Al(Y) and Mg/Fe. Overall, the Ca-content of tourmaline as indicator of increasing Eoalpine metamorphic conditions increases from the west (0.113 apfu) to the east (0.171 apfu).

The data show that most tourmalines in the western part of the Matsch nappe record mostly zones of pre-Alpine growth and only the outermost zone with sharp increases in Al, Ca and vacancy contents represents the Eoalpine growth stage. The eastern tourmalines on the other hand show almost no pre-Alpine growth stages (e.g., Ca-rich cores) and their zoning clearly shows the Eoalpine prograde metamorphic evolution.

Unearthing genetic insights through a multi-method geochemical approach of the sediment-hosted Cu-Co Dolostone Ore Formation deposit, Namibia

V. Bertrandsson Erlandsson^{1*}, R. Ellmies², F. Melcher¹

¹Montanuniversität Leoben, Leoben, Austria

²Gecko Namibia, Swakopmund, Namibia

e-mail: of communicating viktor.erlandsson@unileoben.ac.at

The sediment-hosted Cu-Co-Zn Dolostone Ore Formation (DOF) deposit is a recently discovered Cu-Co-Zn mineralization in the Kunene region of northwestern Namibia and is the first recognized Co mineralization in Namibia (Ellmies 2018). Understanding the geological formation processes responsible for Co deposits is vital due to the ever-increasing demand of Co for modern high-tech and green technologies (Alves Dias et al. 2018). As sediment-hosted Cu-Co deposits from the Central African Copperbelt are responsible for ca. 70% of global Co supplies (USGS 2020), the DOF deposit could prove to be a valuable asset for future Co production, especially as the DOF is situated in analogous stratigraphic and tectonic settings to the Co deposits of the Central African Copperbelt (Miller 2013; Bertrandsson Erlandsson et al. 2022). This study applies an array of geochemical methods to constrain genetic aspects of the DOF deposit, with the aim of better the understanding of sediment-hosted Cu-Co deposits.

Hosted in calcareous siltstones and argillites of the Ombombo Subgroup, which is part of the Neoproterozoic Damara Supergroup, the DOF is expressed as a horizon with a bell curve-like Cu-Co-Zn distribution. The highest metal (in particular Co) enrichment is referred to as the “Main DOF horizon”, whilst the extended Cu-Zn enrichment is called the “Wider DOF horizon” (Fig. 1). The sulfide mineralogy is relatively simple, with predominantly pyrite, pyrrhotite, chalcopyrite, sphalerite, linnaeite, and subordinate amounts of cobaltpentlandite and galena. Sulfides occur in six types of mineralization styles: disseminated, nodules, clusters, veins, pressure shadows, and “Events”. Events are a term coined by the exploration company Gecko Namibia and refer to vein-like structures that portray both ductile and brittle deformation. (Bertrandsson Erlandsson et al. 2022).

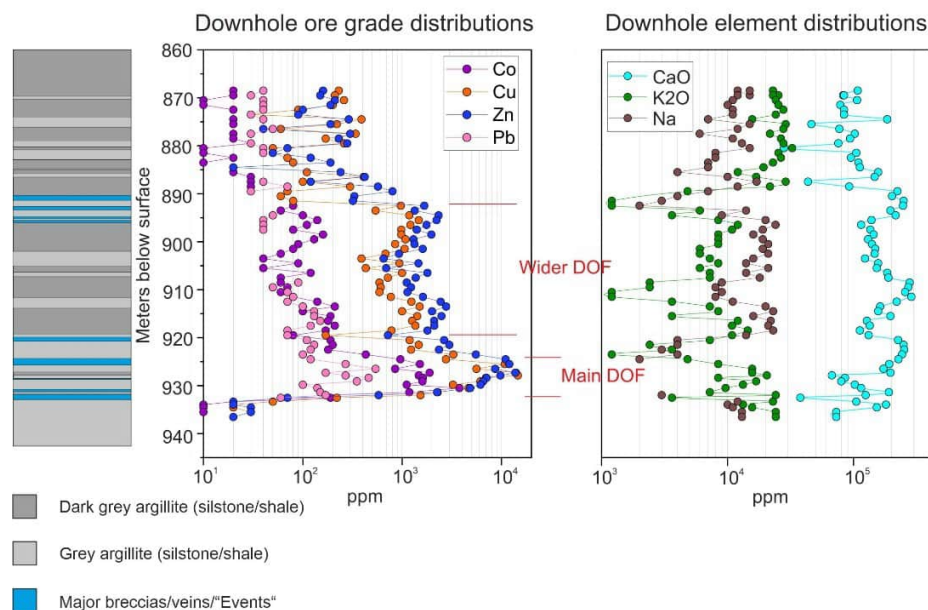


Figure 1. Simple drill core log from one of the studied DOF boreholes, with additional exploration assay data of selected elements, shown besides the drill core log.

Laser ablation inductively coupled mass spectrometry (LA-ICP-MS) analyses of sulfides from the six different mineralization styles reveal two main populations; disseminated, nodule, cluster, and Event sulfides group together (Group 1), whilst Group 2 comprises vein- and pressure shadow-hosted sulfides (Bertrandsson Erlandsson et al. 2022). The Ga-Ge-In-Mn-Fe in sphalerite geothermometer (Frenzel et al. 2016) indicates that the DOF mineralization formed at temperatures >310 °C, which suggests that they formed during regional metamorphism of the Damara Orogeny. Group 2 sulfides seem to have formed at relatively lower temperatures. This together with petrographic observations indicates that Group 2 sulfides (veins and pressure shadows) formed during a late orogenic stage of the Damara Orogeny (Bertrandsson Erlandsson et al. 2022). This interpretation is also supported by ore-associated hydrothermal monazite ages.

Petrographic evidence shows that Group 1 sulfides did not all form at once, but rather through several progressive stages. Cobalt is believed to have been initially hosted in pyrite, which was later remobilized due to changes in oxygen and/or sulfur fugacity to first form cobaltpentlandite and eventually linnæite. It was after this that Group 1 sphalerite and chalcopyrite precipitated, partially overgrowing the preexisting sulfides. This resulted in extremely Co-rich sphalerite (>1 wt%). Atom probe tomography of this extremely Co-rich sphalerite revealed that the Co^{2+} occurs through direct substitution of Zn^{2+} (Bertrandsson Erlandsson et al. 2023).

Trace element comparison of DOF sulfides to other sediment-hosted Cu(-Co) metallogenic districts (i.e., the Polish Kupferschiefer and the Central African Copperbelt) by Random Forest and Factor analyses indicate that sulfide trace element composition is heavily host basin dependent and that local metal sources dictate the sulfide composition (Bertrandsson Erlandsson et al. *in review*).

- Alves Dias P, Blagoeva D, Pavel C, Arvanitidis N (2018): Cobalt: demand-supply balances in the transition to electric mobility. - Publications Office of the EU 10, p. 97710
- Bertrandsson Erlandsson V, Foltyn, K, Muech P, Rantitsch G, Ellmies R, Melcher F (in review). Sulfide geochemistry in sediment-hosted Cu(-Co) metallogenic districts: LA-ICP-MS analyses of chalcopyrite, sphalerite, and pyrite. - Mineral Dep (*in review*)
- Bertrandsson Erlandsson V, Gopon P, Waldl H, Misch D, Ellmies R, Melcher F (2023): Sphalerite as a non-traditional critical metal source: Correlative microscopy (EPMA, EBSD, and APT) of cobalt-enriched sulfides from the sediment-hosted copper-cobalt Dolostone Ore Formation deposit, Namibia. - Front Earth Sci, 10.3389/feart.2023.1171859
- Bertrandsson Erlandsson V, Wallner D, Ellmies R, Raith JG, Melcher F (2022): Trace element composition of base metal sulfides from the sediment-hosted Dolostone Ore Formation (DOF) Cu-Co deposit in northwestern Namibia: Implications for ore genesis. - Jour Geoch Expl 243, 107105
- Ellmies R (2018): Extensive stratiform Cu-Co-mineralisation at Okondaurie, Kunene Region. - Internal Report, Kunene Resources (Pty) Ltd. (unpublished)
- Frenzel M, Hirsch T, Gutzmer J (2016): Gallium, germanium, indium, and other trace and minor elements in sphalerite as a function of deposit type—A meta-analysis. - Ore Geo Revs 76, 52–78
- Miller R (2013): Comparative Stratigraphic and Geochronological Evolution of the Northern Damara Supergroup in Namibia and the Katanga Supergroup in the Lufilian Arc of Central Africa. - Geosci Canad 40, Article 2, 118–140
- USGS (2020): Mineral commodity summaries 2020, DOI: 10.3133/mcs2020

Influence of deformation and fluids on Ti exchange in natural quartz

M. Bestmann¹, G. Pennacchioni², B. Grasemann¹, B. Huet², M.W.M Jones³, C.M Kewish⁴

¹Department of Geology, University of Vienna, 1090 Vienna, Austria

²Department of Geosciences, University of Padova, 35131 Padova, Italy

³Department of Hard Rock Geology, Geological Survey of Austria, 1030 Vienna, Austria

⁴Central Analytical Research Facility, Queensland University of Technology, Brisbane, 4000, QLD, Australia

⁵Australian Synchrotron, ANSTO, Clayton, 3186, Vic, Australia

e-mail: michel.bestmann@univie.ac.at

For over 10 years, the TitaniQ geothermometer has been used to constrain deformation temperatures in quartz-rich rocks. The calibration of the thermometer rests on the direct correlation of the titanium trace element concentration in quartz with respect to the ambient temperature. However, the processes and parameters which lead to re-equilibration of the Ti-in-quartz system during deformation are not yet fully understood. Here we analysed deformed quartz veins from the Eastern Alps (Prijakt Nappe) applying a combination of microstructural, spectroscopic, and geochemical analyses. In contrast to recent studies which highlight the importance of strain, we show that the availability of free grain boundaries, fluids, and their partitioning play the dominant role in Ti resetting towards lower concentrations in our studied case of retrograde deformation. We employ a robust analytical approach to investigate the interplay between grain-scale deformation, fluid-rock interactions, and geochemical exchange during increasing strain in the quartz mylonites. With this approach, the microstructures representing most re-equilibrated sites for the application of the titanium-in-quartz geothermometer can be readily identified, even at lower greenschist facies deformation conditions and a recrystallization regime dominated by subgrain rotation.

These coarse-grained quartz veins, that formed at amphibolite facies conditions, were overprinted by lower greenschist facies deformation to different degrees. During the overprint, subgrain rotation recrystallization was dominant during progressive deformation to ultramylonitic stages. The initial [Ti] (3.0-4.7 ppm) and cathodo-luminescence (CL) signature of the vein crystals decrease during deformation mainly depending on the availability of fluids across the microstructure. The amount of strain played a subordinate role in resetting to lower [Ti] and corresponding darker CL shades. Using a microstructurally-controlled analysis we find that the most complete re-equilibration in recrystallized aggregates ([Ti] of 0.2-0.6 ppm) occurred (i) in strain shadows around quartz porphyroclasts, acting as fluid sinks, and (ii) in localized microshear zones that channelized fluid percolation. [Ti] resetting is mainly observed along wetted high angle boundaries (misorientation angle >10-15°), with partial [Ti] resetting observed along dry low angle boundaries (<10-15°). This study shows for the first time that pure subgrain rotation recrystallization in combination with dissolution-precipitation under retrograde condition provide microstructural domains suitable for the application of titanium-in-quartz geothermobarometry at deformation temperatures down to 300-350 °C.

Evolution history of plagioclase hosted Fe-Ti oxides micro-inclusions from oceanic gabbros

G. Bian¹, O. Ageeva¹, A. Kovacs², G. Habler¹, R. Abart¹

¹University of Vienna, Department of Lithospheric Research

²Forschungszentrum Jülich, Ernst Ruska-Centrum für Mikroskopie und Spektroskopie mit Elektronen (ER-C)
e-mail: biang92@univie.ac.at

Fe-Ti oxides are commonly observed as oriented needle- and lath-shaped micro-inclusions in plagioclase. Our study focused on these inclusions in plagioclase from oceanic gabbros in the Mid-Atlantic ridge with distinct petrogenetic histories. Previous research indicates that the inclusions formed through precipitation from Fe-bearing plagioclase at temperatures ≥ 600 °C and low oxygen fugacity (Bian et al. 2021). They subsequently undergo a complex evolution, as determined through correlated polarisation microscopy, mineral chemical analysis by electron microprobe analyzer, scanning transmission electron microscopy and crystal orientation analyses.

Two evolutionary pathways are discerned. For both pathways, the Fe-Ti oxide micro-inclusions first formed as homogeneous titanomagnetite at ≥ 600 °C upon slow cooling and/or oxygen fugacity change. Such homogeneous titanomagnetite inclusions are rarely preserved.

Along pathway A, the inclusions experienced high temperature oxidation leading to formation of ilmenite-magnetite intergrowth. Ilmenite (Ilm) is typically present as lamellae in a matrix of magnetite (Mt) with $Mt\{111\} \parallel Ilm(0001)$. The magnetite still contains a small amount of Ti. As temperature decreases $< \sim 600$ °C, the Ti-bearing magnetite exsolves into ulvospinel (Usp) and magnetite. These inclusions thus contain ilmenite lamellae and extremely fine ulvospinel lamellae within a matrix of Ti-poor magnetite.

Along pathway B, high temperature oxidation did not occur, and the inclusions are devoid of ilmenite lamellae. This indicates comparatively low fO_2 at the early stage. When cooling below ~ 600 °C, titanomagnetite exsolves forming magnetite-ulvospinel intergrowth with a significant proportion of ulvospinel. At a later stage, ulvospinel may be oxidised into secondary magnetite (Mt_s) and ilmenite (Ilm_s) which tend to form aggregates along the contacts between exsolved ulvospinel and magnetite. The oxidation is likely linked to relatively low-temperature hydrothermal activity.

Inclusions in both pathways may form plate shaped Ilm or relics of ilmenite particles due to preferential dissolution of magnetite. The crystallographic orientation relationships (COR) of ilmenite inclusions to the plagioclase are determined by the COR between ilmenite lamellae and the dissolved magnetite hosting the ilmenite in the first place.

Two pathways represent different cooling conditions, with the key distinction being high-temperature oxidation during early hydrothermal alteration in A, which is absent in B. Path A is typical for non-altered oceanic gabbros (Ageeva et al. 2020; Bian et al. 2021), but was also revealed in the oceanic gabbro that was affected by felsic magmatism and high temperature hydrothermal overprint (Ageeva et al. 2016).

Path B was revealed in the plagioclase of gabbroic rocks from the Vema lithospheric section, the petrogenetic history of which shows several stages (Pertsev et al. 2015). Stage I: early magmatic crystallization of coarse-grained pyroxene-plagioclase assemblage. Stage II: late magmatic syn-deformation interaction between the crystal aggregate and residual melt with local magmatic-aqueous fluid at 800-900 °C. Stage III: local high temperature (about 600 °C) reducing hydrothermal alterations as a result of interaction with brine (20-21 % NaCl) remained after low temperature (< 500 °C) interaction of seawater with mantle peridotites. Stage IV: low temperature hydrothermal alteration associated with the infiltration of seawater derivatives with salinity (< 7 wt% NaCl) during tectonic exhumation of the lithospheric section.

The microstructural and textural evolution of the Fe-Ti oxide micro-inclusions can be linked to the main events in the petrogenetic history of the gabbro. In particular, the late magmatic stage with magmatic-aqueous fluid at the Stage II catalysed precipitation of Fe-Ti oxides from plagioclase forming the micro-inclusions. The ulvospinel-magnetite inclusions appeared as a result of exsolution of titanomagnetite during the reducing hydrothermal alterations (Stage III). Likely, this process was preceded by recrystallization of primary inclusions, because in these gabbros only micro-inclusions elongated parallel to the [001] direction of plagioclase are present, which is typical for recrystallized inclusions (Bian et al. 2023). The $\text{Ilm}_s\text{-Mt}_s$ micro-inclusions are related to water-rock interaction during the low temperature hydrothermal stage (Stage IV).

The magnetic signals recorded by plagioclase with oriented Fe-Ti oxide micro-inclusions may exhibit differing biases for pathway A and B. Consequently, comprehending the evolution of these micro-inclusions is crucial for paleomagnetic reconstructions.

- Ageeva O, Habler G, Pertsev A, Abart R (2016): Orientation relationships of Fe-Ti-oxide micro-inclusions and their hosts in the oceanic gabbro. - EMC-2016. Minerals, rocks and fluids: alphabet and words of planet Earth. Book of Abstract. p. 218
- Ageeva O, Bian G, Habler G, Pertsev A, Abart R (2020): Crystallographic and shape orientations of magnetite micro-inclusions in plagioclase. - *Contrib Mineral Petrol* 175, 95
- Bian G, Ageeva O, Recnik A, Habler G, Abart R (2021): Formation pathways of oriented magnetite micro-inclusions in plagioclase from oceanic gabbro. - *Contrib Mineral Petrol* 176, 1–21
- Bian G, Ageeva O, Roddatis V, Habler G, Schreiber A, Abart R (2023): Oriented secondary magnetite micro-inclusions in plagioclase from oceanic gabbro. - *Amer Mineral*, doi: 10.2138/am-2022-8784
- Pertsev AN, Aranovich LY, Prokofiev VY, Bortnikov NS, Cipriani A, Simakin SS, Borisovskiy SE (2015): Signatures of Residual Melts, Magmatic and Seawater-Derived Fluids in Oceanic Lower-Crust Gabbro from the Vema Lithospheric Section, Central Atlantic. - *J Petrol* 56, 1069-1088

Matching crystal structure plots to “atomic-resolution” HR-TEM images

J. Birkenstock¹, S. Pokhrel^{2,3,4}, L. Mädler^{2,3,4}

¹University of Bremen, FB5-GEO/Crystallography & Geomaterials, Klagenfurter Straße 2-4, 28359 Bremen

²Faculty of Production Engineering, University of Bremen, Badgasteiner Straße 1, 28359 Bremen

³Leibniz Institute for Materials Engineering IWT, Badgasteiner Straße 3, 28359 Bremen

⁴MAPEX Center for Materials and Processes, University of Bremen, 28359 Bremen

e-mail: jbirken@uni-bremen.de

High-resolution TEM images of single crystals, oriented with a prominent zone axis [uvw] parallel to the electron beam, display periodic arrangements of light and dark contrast. Considering that modern TEM instruments are claimed to supply sub-Ångström ($< 10^{-10}$ m) resolution one would expect that the interpretation should be easy, assuming that the light or dark contrast represent single atoms or voids. However, only in rare cases, e.g., using deep learning algorithms, automatic recognition has been applied to simple structures like graphene layers (Madsen et al. 2018) where the orientation of the layer with respect to the beam is previously known. If certain features like open, void channels exist and the channels are oriented parallel to the beam, recognizing the orientation of the crystal structure from its observed pattern is also quite easy, as e.g., shown by MacLaren & Ramasse (2014).

For complex structures without such features, determining the orientation of the crystal structure for an observed periodic pattern of dark and light contrasts presents a more difficult task. The reasons for this are manifold: It starts with noting that the observed image usually does not represent an atomic monolayer but results from transmission through a more or less thick stack of material. Accordingly, the observed pattern is a projection of the crystal structure, which can be more or less complex in terms of the number of independent crystallographic sites, involving chemical complexes in different orientations, solid solution sites etc. Thus, a single light or dark feature in the resulting HR-TEM image may represent any of these stacked on top of each other along the viewing direction, perfectly aligned or offset by fractions of an atomic diameter. On the other hand, some atoms may “invisible” in the respective image. Furthermore, light and dark contrast may be interchanged depending on the actual settings of the microscope, e.g., with respect to focus. Accordingly, even if the crystal structure is comprehensively known, interpretation of the observed dark and light contrast in the HR-TEM image in terms of a given crystal structure can be a major challenge.

The procedure presented here for matching a certain crystal structure to an observed periodic HR-TEM pattern relies on these steps:

- 1) Measurements of d-spacings d_{obs} via normal distances between parallel “rows” of either light or dark contrast in several directions in the observed patterns and determination of the angle(s) between pairs of normal distance directions (i.e., between their d-spacing vectors \mathbf{d}_{obs}). Notes: 1. Two directions will usually be sufficient since they define a plane in space, 2. d-spacings from HR-TEM images may suffer from systematic errors (often several percent) which should be considered by a standard uncertainty (of several percent) in observed d-spacings.
- 2) Comparison of observed d-spacings with a list of d-spacings calculated from the crystal structure and identification of potential hkl planes matching them.
- 3) Calculation of angles between the \mathbf{d}_{hkl} vectors of the identified lattice planes to find matches for the angles, too. Notes: 1. To find matches in the angles symmetrically equivalent hkl planes may have to be considered, too, 2. one pair of two lattice planes matching a single observed angle is usually sufficient.

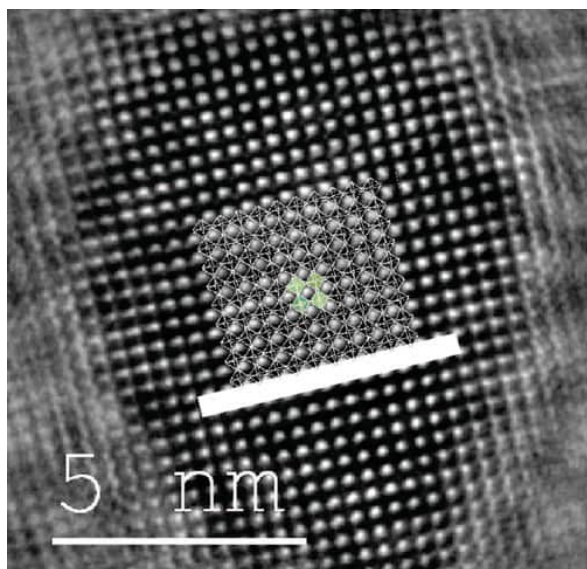


Figure 1. Crystal structure of WO_3 (monoclinic) matched onto the HR-TEM of nanoparticles of WO_3 which displays a pseudo-cubic arrangement when projected along $[001]$ direction ($[010]$ and $[100]$ similar). The scale bar in the crystal structure is 5 nm, too.

periodic dark and light contrast may be left unmatched. As a result, modifications in the crystal structure plot may have to be considered: 1) small scaling of the plot (a few percent only!), 2) display of selected crystallographic sites only since some (groups of) atoms may be missing in the contrast details, 3) as noted above, a single light or dark contrast may represent a single atom or groups of atoms from different crystallographic sites, potentially offset by fractions of an atomic diameter. Accordingly, highlighting groups of atoms, e.g., via polyhedral representation, may be indicated as well.

In this contribution we will show some well-documented, previously published examples which were taken from Pokhrel et al. (2023), Li et al. (2021), Dreyer et al. (2016), Kemmler et al. (2012), Pokhrel et al. (2009, see Figure 1).

- 4) If a match of two hkl planes and their angle is found, calculate the zone axis to identify the crystallographic direction $[uvw]$ that was parallel to the beam on measurement.
- 5) In the software used for displaying the crystal structure (e.g. VESTA, Momma & Izumi, 2011), create a structure model with a sufficiently large number of unit cells, set the viewing direction to $[uvw]$ from step 5. Add a scale bar matching that of the HR-TEM image.
- 6) Copy the crystal structure plot in semi-transparent mode onto the HR-TEM image, resize the crystal structure image to match the two scale bars.
- 7) Match the crystal structure to the dark and light contrast by translations and rotations of the crystal structure image on top of the HR-TEM image.

Further notes: If the identification of hkl was correct some details in the periodic motifs of the crystal structure or in the observed

- Momma K, Izumi F (2011): VESTA3 for three-dimensional visualization of crystal, volumetric and morphology data. – J Appl Cryst 44, 1272-1276
- Madsen J, Liu P, Kling J, Wagner JB, Hansen TW, Winther O, Schiøtz J (2018): A deep learning approach to identify local structures in atomic-resolution transmission electron microscopy images. - Adv Theory Simul 1, 1800037
- MacLaren I, Ramasse QM (2014): Aberration-corrected scanning transmission electron microscopy for atomic-resolution studies of functional oxides. – Int Mater Rev 59, 115-131
- Dreyer JAH, Pokhrel S, Birkenstock J, Hevia MG, Schowalter M, Rosenauer A, Urakawa A, Teoh WY, Mädler L (2016): Decrease of the required dopant concentration for $\delta\text{-Bi}_2\text{O}_3$ crystal stabilization through thermal quenching during single-step flame spray pyrolysis. – Cryst Eng Comm 18, 2046-2056
- Kemmler JA, Pokhrel S, Birkenstock J, Schowalter M, Rosenauer A, Bársan N, Weimar U, Mädler L (2012): Quenched, nanocrystalline $\text{In}_4\text{Sn}_3\text{O}_{12}$ high temperature phase for gas sensing applications. – Sens Actuators B Chem 161, 740-747
- Li H, Erinmwingbovo C, Birkenstock J, Schowalter M, Rosenauer A, La Mantia F, Mädler L, Pokhrel S (2021): Double flame-fabricated high-performance $\text{AlPO}_4/\text{LiMn}_2\text{O}_4$ cathode material for Li-ion batteries. – ACS Appl Energy Mater 4, 4428-4443
- Pokhrel S, Birkenstock J, Schowalter M, Rosenauer A, Mädler L (2009): Growth of ultrafine single crystalline WO_3 nanoparticles using flame spray pyrolysis. – Cryst Growth Des 10, 632-639
- Pokhrel S, Stahl J, Groeneveld JD, Schowalter M, Rosenauer A, Birkenstock J, Mädler L (2023): Flame aerosol synthesis of metal sulfides at high temperature in oxygen-lean atmosphere. – Adv Mater 2023, 2211104

CaCO₃ precipitation in drainage systems of subsurface infrastructure – Monitoring approaches and crystal growth control

R. Boch¹, M. Pettau¹, S. Eichinger², A. Leis³, H. Wagner², M. Dietzel¹

¹Graz University of Technology, Institute of Applied Geosciences

²ÖBB Infrastruktur AG, SAE, FB Bautechnik-Tunnelbau

³JR-AquaConSol GmbH

e-mail: ronny.boch@tugraz.at

Methodological approaches and enhanced process understanding interconnecting fundamental research with (geo)technical settings and problems benefit from each other regarding the calcium carbonate chemical system (cf. Boch 2020). The effective draining of subsurface infrastructure is frequently faced with unwanted mineral precipitation (Fig. 1A) based on elevated mineral and gas contents of the discharging groundwater being of high relevance for cleaning downtimes and maintenance of the infrastructure (Eichinger et al. 2020). Owing to regional geology in Austria (limestones, calcareous contents) and construction materials used in subsurface infrastructure (concrete, mortar), carbonate deposits consisting of various CaCO₃ polymorphs and accessory constituents are most abundant in the drainage systems (Fig. 1B) next to iron precipitates and interacting biomass (bacterial biofilms).

In the context of existing subsurface infrastructure (e.g. Semmering highway tunnels) and new excavations (e.g. Koralmtunnel) the recent years strongly increased the understanding of critical processes based on in-situ monitoring campaigns as well as related laboratory analyses and computer modelling. The drainage system and maintenance strategies were adapted based on the implementation of an underground “sinter test track” (Fig. 1C) and local test fields with typical construction materials but different constructive designs (Wedenig et al. 2022). The on-site and online application of sensors/data loggers and mobile instrumentation in combination with sample analyses provided new insights to water-gas-mineral-biology-substrate interaction and to the major controls of calcium carbonate precipitation.

An approach to systematically influence the nucleation and crystal growth of the unwanted deposits consists in the application of specific chemical additives (“green inhibitors”) to the ground-/drainage waters. In laboratory and field tests various substances (e.g. polyaspartic acid) and concentrations were investigated and a new test procedure was developed (Wedenig et al. 2021). This resulted in new insights concerning relevant parameters such as CaCO₃ supersaturation, pCO₂, Mg/Ca and water flow conditions in relation to mineralogy (polymorphism; Fig. 1D), crystal shapes/sizes, substrate effects (e.g. different plastic types) and further regarding proactive controls on fabrics and material consistency (hardness) of the deposits.



Figure 1. Diverse mineral precipitates (A) in the course of continuous groundwater discharge underground can block a tunnel drainage system (B) and were investigated by in-situ field tests (C) targeting an increased process understanding of the precipitation conditions (e.g. D: CaCO_3 polymorphism) as well as efficient countermeasures (e.g. optimized drainage design, addition of inhibitors).

Boch R (2020): Carbonates in natural and geotechnical settings – Chemical sediments as environmental archives. – *Jb Geol.-BA* 159, 67-130

Eichinger S, Boch R, Leis A, Koraimann G, Grengg C, Domberger G, Nachtnebel M, Schwab C, Dietzel M (2020): Scale deposits in tunnel drainage systems – A study on fabrics and formation mechanisms. – *Science of the Total Environment* 718, 137140

Wednig M, Boch R, Leis A, Wagner H, Dietzel M (2021): Green inhibitor performance against CaCO_3 scaling: Rate-modeling aided test procedure. – *Crystal Growth and Design* 21, 4, 1959-1971

Wednig M, Eichinger S, Boch R, Leis A, Wagner H, Dietzel M (2022): Understanding of tunnel drainage scale formation by in-situ monitoring. – *Tunnelling and Underground Space Technology*, 131(A43), 104853

Assessing enrichment efficiency: A study of mineralogical and physical characteristics of Pb-Zn ore from Erzgebirge, Germany

A. Bravo¹, O. Popov¹, H. Lieberwirth¹

*¹Institute for Minerals Processing Machines and Recycling Systems Technology (IART),
Technische Universität Bergakademie Freiberg, Germany
e-mail: bravo@iart.tu-freiberg.de*

The mineralogical and physical properties of minerals play a crucial role in understanding their behaviour during the comminution process, where materials are reduced into different sizes. Accurate determination of the characteristics of mineral phases present in the materials is essential to assess their potential selectivity during comminution. Then differences in the physical properties of gangue and ore minerals can be exploited. As a result, the valuable minerals appear in a different particle size than the gangue material and can be separated by classifying techniques.

In this study, an integrated assessment was conducted on samples of Pb-Zn ore from Reiche Zeche, located in Saxony's prominent mining district in Germany, the Ore Mountains, Erzgebirge Region. The Ore Mountains are mainly composed of metasediments (grey gneisses) and metamagmatites (red and grey gneisses) and exhibit hydrothermal polymetallic mineralisation including lead, zinc and silver. The veins are commonly categorised based on their orientation and mineral associations.

Smaller vein-like deposits along with the typical host rock gneiss from Freiberg, have been chosen as research environment for evaluating the enrichment of different sieve classes before and after undergoing jaw crusher and cross Beater mill processes. The mineralogical characterisation was performed using automated mineralogy through Mineral Liberation Analysis (MLA). The material's properties, such as the Point Load strength index, Vickers Hardness Number, and fracture toughness, were determined. MLA provided information on particle size distribution, liberation degree, association, and modal mineralogy for each fraction. The preliminary results showed an enrichment of smaller sieve classes for specific phases, including chalcopyrite, galena, sphalerite, and pyrite. These results were correlated with the rock's physical properties, including textural observations, as well as the behaviour of grains and grain boundaries within the rock.

Reviewing the formation and transformation behaviour of amorphous calcium carbonate: implications for environmental proxies

J.-M. Brazier^{1,2}, M. Pettau¹, K.E. Goetsch¹, M. Dietzel¹

¹*Graz University of Technology, Institute of Applied Geosciences, Rechbauerstraße 12, 8010 Graz, Austria*

²*Current address: University of Bern, Institute of Geological Sciences, Baltzerstraße 1+3, 3012 Bern, Switzerland*

e-mail: michael.wedenig@tugraz.at

The elemental and isotopic compositions of CaCO₃ minerals are commonly used as proxies to reconstruct the (paleo)environmental conditions that existed during their formation. Amorphous calcium carbonate (ACC) is known to be a metastable phase and a precursor to crystalline phases within the so-called "non-classical" nucleation pathway. Various factors can influence its formation, lifespan, structure, and transformation pathways, raising questions regarding the reliability of the crystalline phase resulting from precursor transformation as an archive for (paleo)environmental conditions. Evaluating the elemental and isotopic composition of such crystalline phases requires considerations of the specific pathways of CaCO₃ formation and transformation, as well as the system conditions, such as reaction kinetics versus equilibrium. In this review, we discuss the elemental and isotopic fractionations between ACC/crystalline CaCO₃ and the precipitating solution, focusing on structural characterization, ion exchange behaviour, precipitation kinetics, and transformation behaviour in open versus closed systems.

Monazite stability as a tool used for identification of granite stacking (a case study from the Western Carpathians)

Igor Broska¹, Igor Petrik¹

¹Earth Science Institute Slovak Academy of Sciences, 840 05 Bratislava
e-mail: Igor.Broska@savba.sk

The presence of monazite or allanite in granites is not only an important aspect of assessing their parental rocks to the I- or S-type, but their mutual relationship can also help to estimate PTX conditions in a given magmatic system. In the Western Carpathians, allanite and monazite became an effective tool for discrimination Variscan granites in terms of their I- or S-types affinity, in addition to the bulk-rock granite composition (Petrik & Broska 1994). For the S-type granites, typical is a reduction paragenesis of accessory ilmenite, monazite and apatite with higher content of Mn (Mn in reduced bivalent form easily replaces Ca). On the other hand, the I-type granites were identified by the presence of allanite, higher content of apatite with a low Mn and Fe, titanomagnetite, phlogopite (Mg-biotite), titanite, late pure magnetite, and locally also amphibole indicating a higher oxidation stage in this magmatic system compared to the S-type. It probably reflects initially a higher water content manifested also by late or post-magmatic oxidation of titanomagnetite, biotite and allanite.

Primary magmatic monazite and allanite: In arc orogenic granites, such as the Western Carpathian granites the presence of monazite is determined by PTX conditions, where parameter X represents the content of CaO and the REE's. At a higher ratio of CaO/REE in granite the allanite is stable (Gieré & Sorensen 2004; Janots et al. 2008; Spear 2010). The S-type granites, where the whole-rock CaO content greater than 2.5 wt % stabilises allanite can also produce a monazite due to local decrease of CaO activity, e.g. after massive crystallization of plagioclase which was at the beginning suppressed by higher water contents (Johannes and Holtz 1996). A relict allanite in such case, as a precursor of monazite, was documented in accessory paragenesis of granites from the Tribeč and the Malé Karpaty Mts. Alternatively, some Western Carpathian S-type granites, rich in the REEs, may also have changed early allanite for monazite due to a pressure drop whereby their PT path crosses the Aln/Mnz boundary and the parent granites were emplaced into upper part of the crust. Monazite in this sense represents a mineral whose dating can records the cooling time of the parental granite system.

Monazite breakdown to allanite and REE epidote: In the granites of the Alpine Tatric Unit, monazite is typically stable or only weakly altered, on the other hand (Fig. 1A), the granites from the higher Alpine nappes as the Fatric and Veporic units, show monazite breakdown forming coronas of the apatite and allanite (Fig. 1B). The monazite breakdown into apatite-allanite coronas is facilitated by the higher content of CaO, Al₂O₃, and LREE, and alkali-rich fluids (Budzyń et al. 2011). The monazite breakdown in metamorphic granites is illustrated by stability diagrams of monazite – allanite (Spear, 2010). In the case of the Western Carpathians in the Tribeč crystalline basement, the monazite breakdown in high CaO granites is predicted for the estimated pressure of ca 4 kbar at the temperature of about 450 °C due to crossing the monazite/allanite stability boundary by cooling along a near-isobaric PT trajectory (Broska et al. in prep.). Since an Alpine monazite has not been detected in these granites, the

breakdown of monazite has occurred due to prolonged residence in deeper parts of the Earth's crust achieving the isobaric trajectory. On the other hand, the non-altered monazite presented in the underlying Tatric granites in this Tribeč granite nappe system was preserved by the rapid ascent of granite into the upper crust, where the PT trajectory is close to isothermal. The rapid cooling here in the Tribeč field documents the shallow intrusion of the granites into phyllites.

Granite duplex: The undeformed S-type granites with unaltered monazite in the Tribeč Mts are found at deep part of the crystalline basement, i.e. these underlying granites are attributed to the Tatric Unit where unaltered monazite typically occurred. On the other hand, the granites from the higher, crest part of the mountain range, are metamorphosed and hydrothermally affected (altered) and contain monazite with breakdown coronas (Fig. 1B). Since both granite blocks, the upper metamorphic and the lower non-metamorphic, are similar in the age, the different monazite behaviour indicates existence of two different granite blocks. They had been originally at the time of generation during Variscan orogen at different crustal positions because otherwise they would not have shown different monazite responses. Moreover, the overlying granites with altered monazite are Alpine metamorphosed in PT conditions close to those known in the Veporic or Fatric unit but not high enough to produce a new Alpine monazite. Thus, in the present position of the Tribeč basement, there are two granite blocks one above the other, metamorphic block thrust on the non-metamorphic one. The stacking of the metamorphosed over non-metamorphosed block was flat and inclined to the northwest at an angle of about 20°, and in the present position represents an Alpine granite duplex. With altered granites Lower Triassic quartzites of the Lúžna formation were probably also moved, from which Uher et al. (2009) described a hydrothermal vein mineralization associated with fluids from the underlying granites forming in quartzites spectacular lazulite. The age of granite stacking is indicated by Ar/Ar age from muscovite of the overlying granites and it gives the age of 78 Ma. It postdates the stacking, since the dated muscovites have not been deformed. The identification of Tribeč granite alpine duplex can be considered as an example of the use of monazite stability for solving of geodynamic events.



Fig 1A Stable monazite from low CaO S-type granite; Nízke Tatry Mts, Tatric Unit. (Photo: I. Petrik, polarised light, lengths of monazite crystal is ca 300 μm).

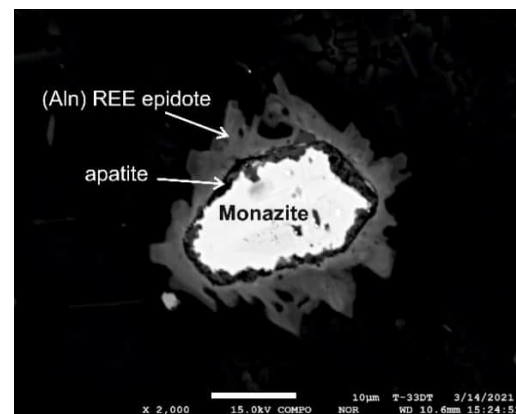


Fig. 1B Monazite breakdown into coronas of apatite and allanite in the S-type granite (Tribeč Mts. Fatric Unit). BSE image.

Acknowledgement: Authors thank to project VEGA 75/20 for financial support.

- Budzyn B, Harlov D, Williams ML, Jercinovic MJ (2011): Experimental determination of stability relations between monazite, fluorapatite, allanite, and REE-epidote as a function of pressure, temperature, and fluid composition. - *Amer Miner* 96, 1547–1567
- Giiéré R, Sorensen SS (2004): Allanite and other REE-rich epidote-group minerals. In: Liebscher A, Franz G (eds): *Epidotes*. - *Rev Miner Geochem* 56, 431-493, <http://dx.doi.org/10.2138/gsrng.56.1.431>
- Janots E, Engi M, Berger A, Allanz J, Schwarz J-O, Spandler C. (2008): Prograde metamorphic sequence of REE-minerals in pelitic rocks of the Central Alps: implications for allanite-monazite-xenotime phase relations from 250 to 610 °C. - *J Metamorphic Geol* 26, 509-526
- Petrík I, Broska I (1994): Petrology of two granite types from the Tribeč Mts., Western Carpathians: an example of allanite-magnetite vs. monazite-ilmenite dichotomy. - *Geol J* 29, 59-78, <https://doi.org/10.1002/gj.3350290106>.
- Uher P, Mikuš T, Milovský R, Biroň A, Spišiak J, Lipka J, Jahn J (2009): Lazulite and Ba, Sr, Ca, K-rich phosphates-sulphates in quartz veins from metaquartzites of Tribeč Mountains, Western Carpathians, Slovakia: Compositional variations and evolution. - *Lithos* 112, 447-460
- Spear FS (2010): Monazite-allanite phase relations in metapelites. - *Chem Geol* 279, 55-62

Accessory minerals in the Isua Supracrustal Belt

H. Brüschke¹, D. Sorger¹, A. Kronz¹, A.A.G. Webb², T. Müller¹

¹*Geoscience Center Göttingen, Georg-August-University Göttingen, Germany*

²*Department of Earth Sciences, The University of Hong Kong, Hong Kong, China
email: h.brueschke@stud.uni-goettingen.de*

The Isua supracrustal belt (ISB) is an example of Archean crustal evolution and well-known as it hosts Earth's oldest 10s-of-km scale supracrustal rocks. However, the conditions and timing of its metamorphic evolution are controversially debated. Most importantly, this knowledge is underpinning the different existing hypothesis of Eoarchean vs. Neoproterozoic tectono-metamorphic events and geodynamic models of horizontal vs. vertical tectonic evolution. Recent studies have shed light on the metamorphic conditions based on geothermobarometry and phase equilibria modeling of major rock forming minerals. However, data from accessory minerals in the ISB have only been sparsely studied despite their potential to better constrain the metamorphic evolution of the belt. In this work, we study structure, composition, and its spatial variation of the accessory phases, especially their rare earth element (REE) contents.

A total of 5 samples with bulk composition resembling so-called "mafic pelites" have been investigated. The typical mineral assemblage comprises garnet porphyroblasts, biotite, quartz and chlorite being the major rock forming phases. Garnet porphyroblasts indicate two stages of garnet growth marked by an inclusion-rich core (M1) and inclusion-poor overgrowth rim (M2). Zircon, monazite, rutile and ilmenite are the most prominent accessory minerals present in the studied lithology.

Backscattered electron images and polarization microscopy were used to petrographically describe the textural context. Major and trace elements have been analyzed using an electron microprobe.

Preliminary results reveal that zircons occur as 5 to 10 microns inclusions within garnet (both core and rim), biotite and chlorite. No visible CL pattern could be found in any of the studied grains indicating substantial metamictization. Despite the presence of zircons in the rocks, Zr-in-Rutile measurements of matrix grains are often below or around detection limit of the electron microprobe, resulting in unresolvable low temperature estimates.

Monazite grains occur as individual grains in the matrix and as inclusions in both, rim and core of garnet porphyroblasts. Rare earth element analysis indicates the absence of an Eu-anomaly in all types of monazites, suggesting growth in the absence of feldspar. Monazite inclusions in garnet cores exhibit slightly higher Sm, Gd and Y contents compared to monazite grains in garnet rims and matrix. One possible reason for the higher content of MREE is that this type of monazite was formed in absence of a competitor phase such as garnet or apatite. If true, this possibly indicates a monazite formation either before the first M1 garnet growth stage or in a different environment.

The preliminary results highlight the potential to reconstruct the metamorphic evolution of the belt in more detail. For example, variations in the REE content of accessory phases potentially shed light on the presence or absence of metamorphic index minerals during formation of accessory phases. Such knowledge provides additional information on the timing of the major tectonometamorphic event (M1) and thus feeds into the interpretation of the geodynamic evolution of the ISB.

Do chromium isotope compositions record signs of oxygenation in the Campbellrand-Malmani Platform (2.56 to 2.52 Ga, South Africa)?

S. Bruggmann¹, C. Thomazo², J. Marin Carbonne¹, S. Jaccard¹

¹University of Lausanne

²University of Burgundy

e-mail: sylvie.bruggmann@unil.ch

The oxygenation history of Earth's surface remains a highly investigated topic, with an increasing number of studies indicating a dynamic change from anoxic to oxic conditions in the Precambrian. The Campbellrand-Malmani platform (Transvaal Supergroup, South Africa) was deposited in a shallow marine environment between 2.56 and 2.52 Ga (Sumner and Grotzinger 2004), just before the Great Oxidation Event. The sedimentary rocks hold a large variety of stromatolites, which can produce oxygen through photosynthetic cyanobacteria. While some studies find indications of oxygen production (e.g., Czaja et al. 2012), post-depositional alteration can challenge interpretations of data from non-traditional isotope systems.

We present Cr isotope compositions ($\delta^{53}\text{Cr}$) and concentration data (trace metals) in sedimentary rocks from the Campbellrand-Malmani platform to better constrain the robustness of the Cr isotope system to post-depositional changes. Preliminary results show that even though the detrital contribution is low, most dolostone and chert samples show $\delta^{53}\text{Cr}$ values of around -0.12 ± 0.10 ‰ (2SD, $n = 14$) and are thus similar to the detrital $\delta^{53}\text{Cr}$ value. Only two samples fall off the detrital value, with one dolostones sample showing a positive $\delta^{53}\text{Cr}$ value of 0.26 ± 0.05 ‰ (2SE).

Our preliminary results indicate that many of the $\delta^{53}\text{Cr}$ values in the studied dolostones and cherts were overprinted by post-depositional processes. With the aid of additional isotope (S, N isotope compositions) and auxiliary data (trace metals), we seek to characterise the drivers of the observed $\delta^{53}\text{Cr}$ values.

Czaja A, Johnson M, Roden E, Beard B, Voegelin A, Nägler T, Beukes N, Wille M (2012): Evidence from free oxygen in the Neoproterozoic ocean based on coupled iron-molybdenum isotope fractionation. – *Geochim Cosmochim Acta* 86, 118-137

Sumner D, Grotzinger J (2004): Implications for Neoproterozoic ocean chemistry from primary carbonate mineralogy of the Campbellrand-Malmani Platform, South Africa. – *Sedimentology* 51, 1273-1299

Pressure-Temperature structure of the Makbal UHP complex (NW Kyrgyzstan)

D. Brunner¹, E. Skrzypek¹, S. Schorn¹, C. Hauzenberger¹, K. Stüwe¹, R. Orozbaev²

¹*Institute of Earth Sciences, University of Graz*

²*Institute of Geology, Kyrgyz National Academy of Sciences*
e-mail: danie.brunner@edu.uni-graz.at

The Makbal ultra-high-pressure (UHP) complex in NW Kyrgyzstan is one of several (ultra-)high-pressure [(U)HP] – low temperature (LT) complexes in the western part of the Tianshan mountain range. It is mainly composed of continental material and can be divided into a ultra-high, high (HP) and medium pressure (MP) unit. The UHP unit is located in the core of the complex and consists of quartzite, garnet-quartz-phengite schist and garnet-chloritoid-talc schist. UHP conditions were inferred from coesite inclusions in garnet from garnet-chloritoid-talc schist (Tagiri et al. 2010). The UHP unit is surrounded by the HP unit, which consists mainly of garnet-phengite±chloritoid schist. The outermost MP unit comprises greenschist facies phyllite and marble.

For HP and UHP unit samples, a maximum temperature of 510-530 °C ± 30 °C was determined using graphite thermometry. Thermodynamic modelling based on garnet and phengite composition yields a prograde P-T path leading from ~15 kbar and ~450 °C to peak conditions of ~18.5 kbar and ~510 °C for a HP sample located close to the MP unit. The HP sample collected at the boundary to the UHP unit indicates P-T conditions of ~19 kbar at ~470 °C for garnet core and ~23 kbar at ~510 °C for peak metamorphism. Electron probe microanalyzer monazite dating in the HP sample near the MP unit yields 488 ± 5.76 Ma (n = 34; MSWD = 0.48) and is interpreted as recording retrograde metamorphism. A garnet-chloritoid-talc schist sample from the UHP unit indicates P-T conditions of ~23.5 kbar and ~520 °C for garnet core and peak conditions of ~29 kbar and ~580 °C.

Our data reveal a continuous increase in P-T conditions towards the core of the UHP complex. This suggests that at least the UHP and HP unit could represent a continuous continental section that was subducted and also exhumed “en masse” as a single block.

Tagiri M, Takiguchi S, Ishida C, Noguchi T, Kimura M, Bakirov A, Sakiev K, Takahashi M, Takasu A, Bakirov A, Togonbaeva A, Suzuki A (2010): Intrusion of UHP metamorphic rocks into the upper crust of Kyrgyzian Tien-Shan: P-T path and metamorphic age of the Makbal Complex. - J Mineral Petrol Sci, 105, 233-250

Annealing of metamict minerals – spectroscopic study

C. Chanmuang N.¹, M. Zeug^{1,2}, A. Erlacher¹, K.A.G. Sameera^{3,4}, L. Nasdala¹

¹Institut für Mineralogie und Kristallographie, Universität Wien, 1090 Vienna, Austria

²Landesamt für Geologie und Bergwesen Sachsen-Anhalt,
An der Fliederwegkaserne 13, 06130 Halle (Saale), Germany

³Postgraduate Institute of Science, University of Peradeniya, P.O. Box 25, Peradeniya 20400, Sri Lanka

⁴Geological Survey and Mines Bureau, 569 B120, Sri Jayawardenepura Kotte 10100, Sri Lanka
e-mail: lutz.nasdala@univie.ac.at

In the country of Sri Lanka, efforts were recently undertaken to survey the occurrence of radioactive phases (Kuruppu et al. 2020; Sameera et al. 2020), among others as potential Th sources. However, phase identification is hampered in many cases because corpuscular self-irradiation over geologic periods of time, caused by the radioactive decay of Th and U and their instable daughter products, may cause these phases to undergo crystalline-to-aperiodic transition. The final, glassy state is referred to as *metamict* (Brøgger 1893).

Metamict minerals are difficult to identify, as structural analysis techniques cannot yield specific information. For instance, X-ray powder diffraction patterns of metamict aeschynite–(Y), euxenite–(Y), fergusonite–(Y), polycrase–(Y), pyrochlore, and samarskite–(Y) are widely similar (Erlacher 2021; and references therein). Similarly, Raman spectra of metamict minerals are extremely broadened and hence cannot be reliably distinguished from each other. The initial, crystalline mineral phase may in some cases be identified using annealing experiments. This, however, is only possible if upon dry annealing, the phase under discussion undergoes structural reconstitution but does not decompose. An example for the latter are allanite-group minerals: Already at temperatures as low as ca. 300 °C, potential dehydrogenation and Fe²⁺ oxidation need to be considered (Sobek et al. 2023; and references therein).

The heating-induced recovery of radiation-damaged minerals may be vastly different, depending on the degree of damage. If a specimen consists of aperiodic and remnant crystalline domains, moderate-T growth of the latter may contribute substantially to the reconstitution. In contrast, the recovery of metamict (that is, fully radiation-damaged) phases requires random nucleation in the glassy bulk and, therefore, typically requires more elevated T.

We present herein the identification of two metamict mineral species whose occurrence on the island of Sri Lanka was hitherto unconfirmed, gadolinite–(Y) (Y₂Fe²⁺Be₂Si₂O₁₀) and fergusonite–(Y) (YNbO₄). Stepwise annealings of multiple chips of samples was undertaken to study the recovery processes. Metamict gadolinite–(Y) recovers its initially monoclinic structure at above ca. 800 °C. Our Raman spectrum (Fig. 1), obtained after oxidising heating at 1150 °C, matches well with spectra of natural non-metamict (Allaz et al., 2020) and heated gadolinite–(Y) (Gorelova et al. 2021). Annealing of fergusonite–(Y) involves an α→β transition: At ca. 550–600 °C, tetragonal fergusonite–(Y) forms and at ca. 750 °C and above, monoclinic clinofergusonite–(Y) is present. The Raman spectrum in Fig. 1 was obtained after oxidising annealing at 1000 °C (Erlacher et al. 2021); it matches well the reference spectrum of Ruschel et al. (2010). We can of course not retrace whether fergusonite–(Y) or clinofergusonite–(Y) were initially present. Independent from that, further Raman analysis of annealed heavy minerals from “*katta*” (local name for the dark and radioactive fraction of heavy mineral concentrates) may help to widen our knowledge of metamict phases occurring in Sri Lanka. Photoluminescence spectroscopy might have similar potential; however, it is currently less suitable, because of the lack of a database of reference spectra.

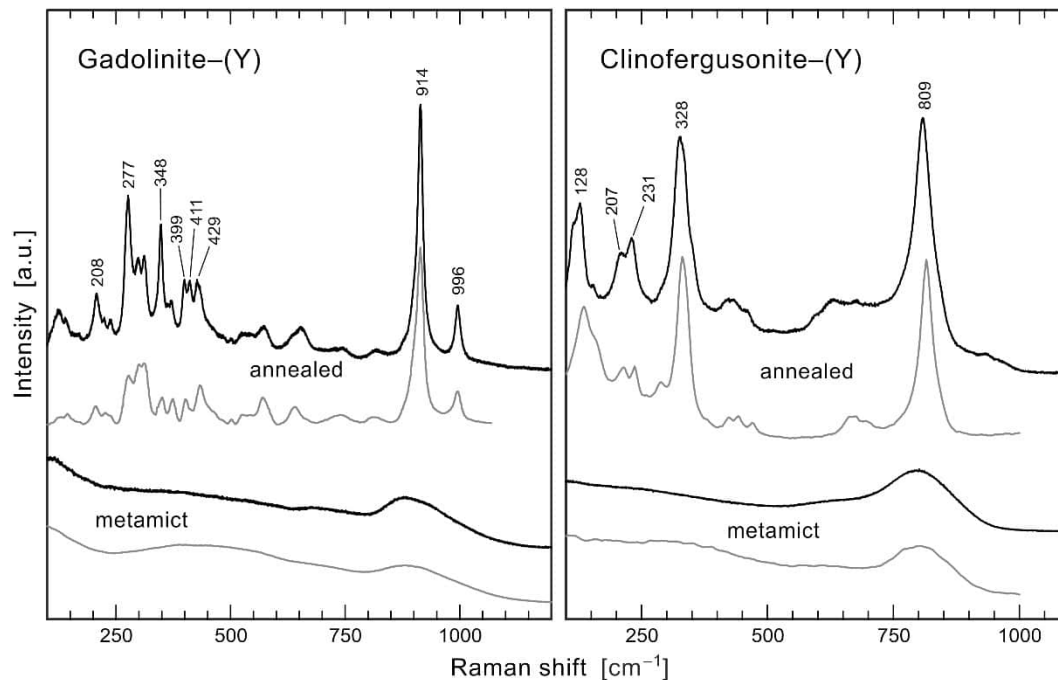


Figure 1. Raman spectra of metamict gadolinite-(Y) and metamict fergusonite-(Y) and their annealed analogues (black), in comparison with reference spectra (grey). Reference spectrum of metamict gadolinite-(Y) extracted from Tomašić et al. (2020); reference spectrum of annealed gadolinite-(Y) extracted from Gorelova et al. (2021); reference spectra of metamict and annealed clinofergusonite-(Y) extracted from Ruschel et al. (2010).

- Allaz JM, Smyth JR, Henry RE, Stern CR (2020): Beryllium-silicon disorder and rare earth crystal chemistry in gadolinite from the White Cloud pegmatite, Colorado, USA. - *Canad Miner* 58, 829-845
- Brogger WCA (1893): *Salmonsens Store Illustrerede Konversationsleksikon* 1. - Brødrene Salmonsens, København, 742
- Erlacher A, Zeug M, Škoda R, Sameera KAG, Nasdala L (2021): Metamict fergusonite from Kolonna and Masimbula, Sri Lanka. - *J Geol Soc Sri Lanka* 22, 1-14
- Gorelova LA, Panikorovskii TL, Pautov LA, Vereshchagin OS, Krzhizhanovskaya MG, Spiridonova DV (2021): Temperature-versus compositional-induced structural deformations of gadolinite group minerals with various Be/B ratio. - *J Solid State Chem* 299, 122187
- Kuruppu KADDN, Hewathilake HPTS, Illangasinghe IKMSCK, Ranasinghe RANC, Jayasinghe N, Dharmaratne TS (2020): Radioactivity survey on Godakawela gem field in Sri Lanka; to identify the origin of the unknown radioactive mineral. - *J Geol Soc Sri Lanka* 21, 57-65
- Ruschel K, Nasdala L, Rhede D, Wirth R, Lengauer CL, Libowitzky E (2010): Chemical alteration patterns in metamict fergusonite. - *Eur J Mineral* 22, 425-433
- Sameera KAG, Wickramasinghe WAGK, Harankahawa SB, Welikanna CR, de Silva KTUS (2020): Radiometric surveying for Th and U mineralization in southwestern, Sri Lanka: radiological, mineralogical and geochemical characteristics of the radioactive anomalies. - *J Geol Soc Sri Lanka* 21, 57-80
- Sobek K, Losos Z, Škoda R, Hola M, Nasdala L (2023): Crystal chemistry of ferriallanite-(Ce) from Nya Bastnäs, Sweden: Chemical and spectroscopic study. - *Mineral Petrol* 117, 345-357
- Tomašić N, Škoda R, Bermanec V, Šoufek M (2020): Crystal chemistry and microfeatures of gadolinite imprinted by pegmatite formation and alteration evolution. - *Amer Mineral* 105, 1647-1655

Speciation of La^{3+} in Cl-bearing hydrothermal fluids: Development of a new polarizable force field

R. Chattopadhyay¹, S. Jahn¹

¹*Institute of Geology and Mineralogy, University of Cologne, Zùlpicher StraÙe 49b, Cologne, Germany
e-mail: rchattop@uni-koeln.de*

The Rare Earth Elements (REEs) are an important group of elements both geologically as well as economically. REEs find important applications in the fields of green energy, electric vehicles and electronics. They are also important tracers for geological processes under hydrothermal /high grade metamorphic conditions. The ability of fluids to mobilize the REEs depend on the chemical composition and the presence of suitable ligands such as chloride and fluoride. *Ab initio* molecular dynamics simulations (AIMD) have been used to predict stability constants of various REE complexes and REE speciation under hydrothermal conditions (Stefanski & Jahn 2020; Guan et al. 2022). However, AIMD simulations often suffer from significant finite time and size effects.

The development of classical force fields for ions in aqueous solutions is essential in the field of hydrothermal geochemistry. The reliability and accuracy of classical force fields not only depends on its representation of effects of ionic size but also on polarization of solvent and solute charge densities. The latter many-body term becomes important particularly when dealing with highly charged ions (Piquemal et al. 2009) in concentrated solutions (Tribello et al. 2009) and in interfacial environments (Jungwirth & Tobias 2006). Many different polarizable force fields exist, each having a different representation of polarizability. Here, we choose the point polarizability model of Dang & Chang (1997) for H_2O , which was specifically parameterized to describe gas-liquid interface (Dang & Chang 1997).

We develop a new polarizable forcefield for La^{3+} in Cl-bearing hydrothermal fluids. The forcefield has been fitted to snapshots of AIMD simulations of La^{3+} and Cl^- ions in water at hydrothermal conditions (773 K, 5 kbar). We used Maximally Localized Wannier Functions (MLWFs) along with force and dipole matching techniques to fit the parameters of the potential (Tazi et al. 2012). We used the technique of Madden and co-workers to calculate the ionic polarizabilities of the charged ions (Salanne et al. 2012). Experimental and AIMD data (wherever available) were used to test the validity of this new potential by comparing structural and thermodynamic properties. We also investigate the speciation of La^{3+} in highly concentrated hydrothermal brines for which no experimental/AIMD data exists.

Stefanski J, Jahn S (2020): Yttrium speciation in subduction-zone fluids from *ab initio* molecular dynamics simulations. - Solid Earth 11, 767–789

Guan Q, Mei Y, Etschmann B, Louvel M, Testemale D, Spezia R, Brugger J (2022): Speciation and thermodynamic properties of La(III)-Cl complexes in hydrothermal fluids: A combined molecular dynamics and in situ X-ray absorption spectroscopy study. - Geochim Cosmochim Acta 330, 27–46

Piquemal J-P, Perera L, Cisneros GA, Ren P, Pedersen LG, Darden TA (2006): Towards accurate solvation dynamics of divalent cations in water using the polarizable amoeba force field: From energetics to structure. - J Chem Phys 125, 054511

Tribello GA, Bruneval F, Liew C, Parrinello M (2009): A molecular dynamics study of the early stages of calcium carbonate growth. - J Phys Chem B 113(34), 11680–11687, PMID: 19650654

- Jungwirth, P. and Tobias, D. J. (2006). Specific ion effects at the air/water interface. - Chem Rev 106(4), 1259–1281. PMID: 16608180
- Dang LX, Chang T-M (1997): Molecular dynamics study of water clusters, liquid, and liquid–vapor interface of water with many-body potentials. - J Chem Phys 106(19), 8149–8159
- Tazi S, Molina JJ, Rotenberg B, Turq P, Vuilleumier R, Salanne M (2012): A transferable *ab initio* based force field for aqueous ions. – J Chem Phys 136(11), 114507
- Salanne M, Rotenberg B, Jahn S, Vuilleumier R, Simon C, Madden PA (2012): Including many-body effects in models for ionic liquids. - Theoret Chem Accounts 131, 1143

Al, Si interdiffusion under lower mantle conditions

L. Czekay¹, N. Miyajima¹, C. McCammon¹, D. Frost¹

¹ Bayerisches Geoinstitut, University of Bayreuth
e-mail: laura.czekay@uni-bayreuth.de

The diffusion of atoms in minerals at high temperatures and pressures influences Earth's lower mantle dynamic processes. This study aims to better understand the physical behaviour of Earth's most abundant mineral with implications for lower mantle viscosity. Previous studies that measured Si-self diffusion coefficients in bridgmanite (Brg) showed a value at 25 ± 1 GPa and 1800 °C of $\text{Log}_{10}(D_{\text{Si}}) = -18 \pm 0.5$ (based on units of m^2/s ; relevant information can be found by Yamazaki et al. 2000; Dobson et al. 2008; Xu et al. 2011). Our study revealed a significantly slower diffusion coefficient that may challenge previous calculations of lower mantle viscosity. We investigated Al, Si interdiffusion in Brg experimentally at 24 GPa and 1750 to 2000 °C using a multi-anvil apparatus using diffusion couples composed of bridgmanites that were pre-synthesised from 0-5 mol.% Al_2O_3 -bearing MgSiO_3 enstatite. The Al diffusion profiles were analysed across the diffusion interface in the recovered samples using a scanning transmission electron microscope equipped with an energy-dispersive X-ray spectrometer. The obtained diffusion coefficient for interdiffusion (volume diffusion) at 24 GPa and 1800 °C was $\text{Log}_{10}(D_{\text{Al,Si}}) = -20.1 \pm 0.7$. The resulting data can be used to estimate deformational strain rates of Brg in the lower mantle from viscosity based on different creep mechanisms.

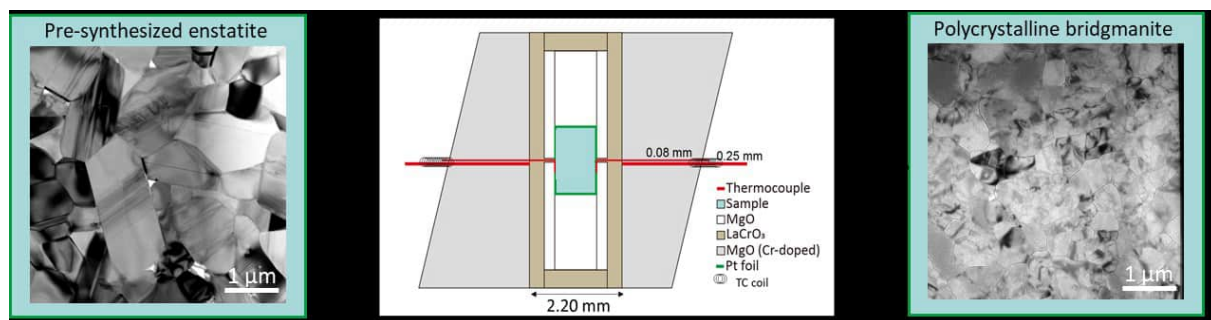


Fig. 1: Experimental setup of the 7/3 assembly and schematic drawing of the experimental path from the pre-synthesized enstatite to the polycrystalline bridgmanite for the diffusion experiments.

- Dobson DP, Dohmen R, Wiedenbeck M (2008): Self-diffusion of oxygen and silicon in MgSiO_3 perovskite. - Earth Planet Sci Lett 270, 125-129
- Xu J, Yamazaki D, Katsura T, Wu X, Remmert P, Yurimoto H, Chakraborty S (2011): Silicon and magnesium diffusion in a single crystal of MgSiO_3 perovskite. - J Geophys Res: Solid Earth 116(B12)
- Yamazaki D, Kato T, Yurimoto H, Ohtani E, Toriumi M (2000): Silicon self-diffusion in MgSiO_3 perovskite at 25 GPa. - Phys Earth Planet Inter [Internet] 119, 299–309

The lower Permian basalt - rhyolite - carbonatite magmatic activity in the Kvetnica volcanic area, Western Carpathians

R. Demko

*Turzovka, Stred 373, 023 54, Slovakia
rastislav.demko@geology.sk*

The Western Carpathians crystalline basement is built by granite–metamorphic rock complexes, covered by sedimentary sequences tectonically arranged into Alpine nappe structures. The Hronic Unit is one of the most spatially extended tectonic upper Alpine nappe structure in the Western Carpathians. The lithology of the Hronic Unit represents a record of volcanic and sedimentary rocks from the Upper Carboniferous to Upper Triassic and Jurassic period. The volcanism operated in parental Hronic area forming two main volcanic phases in the Lower and the Upper Permian with massive production of basalts, basaltic andesites, basaltic trachyandesites and their pyroclastics.

The presented results focus on news from the Kvetnica quarry near Poprad city in the Low Tatras, which belongs to the well-known locality of Maluzina Fm. During field research, I have identified intrusions of younger basalt accompanied by rhyolite, penetrating a set of older horizontally layered older basaltic lavas.

Based on the TAS classification, it is an intrusion of alkaline basaltic trachyandesite BTA and subalkaline rhyolite with a high SiO₂ content (76.5 wt.%). BTA has a porphyric amygdaloid texture dominated by zonal plagioclases and quartz-calcite amygdales. The rhyolite rock is black, aphanitic, with an association of small phenocrysts: quartz, albite, plagioclase, biotite, garnet, Fe-Ti oxides with accessory zircon and monazite. Garnet contains inclusions of orthopyroxene and ilmenite. The rhyolite rock itself is combined by inserted / mingled rhyolite and carbonatite magma, the relationship of which is determined by their mutual immiscibility, see Figure 1.

This is the first detection of rhyolite rock in the Hronicum unit, directly intruding a thick cover of basaltic effusions. The special composition of the rhyolite rock, made it possible to determine magmatic age of rhyolite as the Lower Permian (Kungurian) 278±6.2 Ma., using U-Th-Pb EPMA of monazites. The identified age is the first analytical geochronological data that assigns age of the Kvetnica paleovolcanic activity to the Lower Permian!

Thermobarometric study of Qtz+Pl+Bt+Grt phenocryst association of rhyolite provides PT data 800-750 °C at 135-200 MPa, indicating the depth of magma chamber emplacement, where BTA magma had differentiated to form rhyolite.

The K₂O (1.5 wt.%) and Fe₂O₃/FeO (0.51) content of the rhyolite rock is very similar to the host alkaline BT-andesite with K₂O (1.74 wt.%) and Fe₂O₃/FeO (0.63). Geochemical analyzes show significant REE fractionate during differentiation of basaltic parental magma, whose La/Yb_{C1} (4.64) and Eu/Eu*(0.82) fractionate toward rhyolitic magma with La/Yb_{C1} (18.43) and Eu/Eu*(0.58). REE modelling of basaltic rocks from the Hronic Unit shows that the first volcanic products (lower Permian) are result of lower melting degree 1.1% melt grt-peridotite & 14% melt of sp-peridotite mixed in mass (1/1.7) with continuous increase to melting of 1.9% melt Grt-peridotite & 13% melt of sp-peridotite mixed in mass 1/2.8 (fractional cumulated melting, McKenzie & O'Nions 1991). BTA composition from Kvetnica, as a parental analogue of rhyolite magma, shows a similarity with other Lower Permian basalts generated by lower degree of melting, which agrees with obtained magmatic age.

Petrographic observations and EPMA study showed existence of interstitial or droplet calcite, which represent a carbonatite melt in the host silicate magma. Their mutual spatial relationships indicate interaction of two immiscible liquids. For the first time in the evolution of BTA-rhyolite differentiation, a carbonatite melt is observed in a sample of BTandesite in form of spirally shaped carbonate globules, inclusions in plagioclase, and thin bounded zones of albite enclosed in intermediate plagioclases (56-54 anorthite mol.%). Thermodynamic MELTS modelling (Gualda et al., 2012; Ghiorso & Gualda 2015), focused on BTA fractionation and composition of feldspars, suggest highly oxidizing conditions in magma chamber. Observed composition of feldspars phenocrysts were reached in 1060-1050 °C and $\Delta QFM = +2$ or 1040-1030 °C and $\Delta QFM = +3$. The evolution of observed carbonatite melts is connected with degassing of released CO₂, which interacted with host silicate melt to form carbonatite.

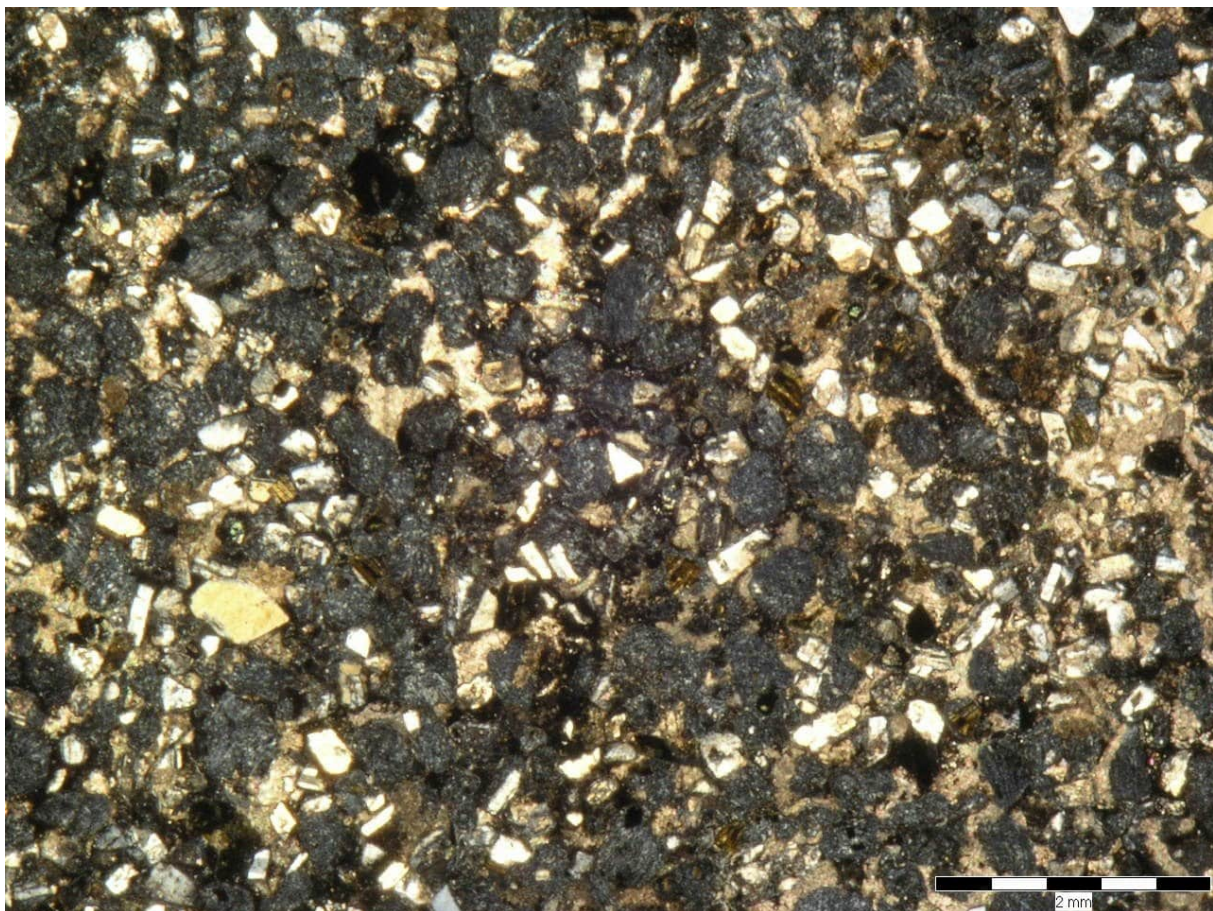


Figure 1: Fragments of rhyolite melt "frozen" between carbonatite immiscible liquid and phenocrysts of quartz, plagioclases, biotite, Fe-Ti oxides and garnet. Photography in polarized light.

- Ghiorso MS, Gualda GAR (2015): An H₂O - CO₂ mixed fluid saturation model compatible with rhyolite-MELTS. - *Contr Miner Petrol*, doi:10.1007/s00410-015-1141-8
- Gualda GAR, Ghiorso MS, Lemons RV, Carley TL (2012): RhyoliteMELTS: A modified calibration of MELTS optimized for silica-rich, fluid-bearing magmatic systems. - *J Petrol* 53, 875-890
- McKenzie D, O'Nions RK (1991): Partial Melt Distributions from Inversion of Rare Earth Element Concentrations. - *J Petrol* 32, 1021-1091

Fingerprinting graphite: The development of a three-step approach to differentiate between natural graphite deposits

V. Dietrich¹, R. Arató¹, F. Melcher¹

*¹Montanuniversität Leoben, Department of Applied Geosciences and Geophysics,
Peter-Tunner-Straße 5, 8700 Leoben
e-mail:valentina.dietrich@unileoben.ac.at*

Graphite is considered as a critical raw material due to its significant importance in various industrial applications, such as the steel and refractories industry, but energy storage being the most important industrial sector. Graphite is a vital component in lithium-ion batteries, which are widely used in electric vehicles and other electronic devices. The demand for lithium-ion batteries has been rapidly increasing, driving the demand for graphite and therefore also the interest in the origin of this raw material. Embedded in a framework project aimed at traceability of battery raw materials, this project aims to reinforce transparency, reliability and sustainability of complex critical raw material supply chains.

This study shows an innovative multi-parameter analytical approach in order to differentiate between graphite samples from different locations. Stable carbon isotopes offer a parameter to differentiate between different sources of carbon. The initial carbon in flake and amorphous graphite is of organic origin, whereas carbon in hydrothermal graphite deposits is inorganic and mostly originates from CO₂ or CH₄ rich fluids (Luque 2013). This distinction can be constrained via carbon isotopy and serves as the first step in distinguishing natural graphite deposits. The Raman spectrum of graphite is characteristic for its microstructural state and serves as a basis for estimating peak metamorphic temperatures during graphite formation (Lünsdorf et al. 2016; Rantitsch et al. 2016). As such, it provides a further means to distinguish different deposits. The third part for proving the origin of graphite is provided by trace element analysis. Given that the formation temperature of many flake graphite deposits is similar within error, the geographical origin of individual deposits can be traced only by means of characteristic trace elements. Research is still underway to find a suitable analytical method for this purpose (e.g., ICP-MS, LIBS, XRF). Solution-based analysis (e.g. via ICP-MS), however, proved to be unsuitable, as the complete dissolution of graphite is notoriously difficult, due to the carbon layers being very challenging or even impossible to break up. The digestions and their analytical results are therefore not consistently reproducible and also too costly to withstand routine application as a fingerprinting technology for industry purposes. LA-ICP-MS proved to be much more suitable also due to simpler sample preparation. Although the ablation of very fine-grained material in compressed form also poses challenges, pathfinder elements that allow a geographical differentiation of origins, could be found by LA-ICP-MS. ETV-ICP-OES serves as another potential methodology for discrimination of graphite deposits, especially as an approved methodology for analysis of trace elements in carbon-rich materials (Vogt et al. 2015). However, this methodology for graphite must first be evaluated to prove its suitability. Analytical proof of origin (APO) methods in general are regarded as the least corruptible methods, as they directly relate to the chemical composition of the raw material (Melcher et al. 2021). Other methods such as conventional documents, tracers, QR codes and barcodes can be outmanoeuvred in one way or another.

- Lünsdorf NK, Lünsdorf JO (2016): Evaluating Raman spectra of carbonaceous matter by automated, iterative curve-fitting. - *Int Jour Coal Geol* 160-161, 51-62
- Luque FJ, Huizenga JM, Crespo-Feo E, Wada H, Ortega L, Barrenechea JF (2014): Vein graphite deposits: geological settings, origin, and economic significance. - *Miner Deposita* 49, 261-277
- Melcher, F., Dietrich, V., Gäbler, H.-E. (2021): Analytical Proof of Origin for Raw Materials. - *Minerals* 11, 461
- Rantitsch G, Lämmerer W, Fisslthaler E, Mitsche S, Kaltenböck H (2016): On the discrimination of semi-graphite and graphite by Raman spectroscopy. - *Int Jour Coal Geol* 159, 48-56
- Vogt T, Bauer D, Neuroth M, Otto M (2015): Quantitative multi-element analysis of Argonne Premium Coal samples by ETV-ICP OES – A highly efficient direct analytical technique for inorganics in coal. – *Fuel* 152, 96-102

Mineralogical control of synergetic thallium and antimony weathering

T. Đorđević^{1,2}, M. Stöger-Pollach¹

¹University Service Centre for TEM, Technische Universität Wien, Wiedner Hauptstraße 8-10, Wien, Austria

²Institut für Mineralogie und Kristallographie, Universität Wien, Josef-Holaubek-Platz 2, Wien, Austria
e-mail: tamara.dordevic@tuwien.ac.at

As metals and metalloids have a strong impact on the environment, methods for their detection and speciation have received a particular attention in the last few years. Thallium (Tl), antimony (Sb) and arsenic (As) are important examples of such toxic elements. Their speciation is of the particular interest owing to their toxicity, bioavailability and reactivity. One of the world most famous deposit hosting all these three elements is Sb-As-Tl-Au Allchar deposit in North Macedonia, which mining waste dumps and technosoils served us as an ideal natural laboratory for the investigations of the oxidative processes on the primary sulfide and sulfosalt minerals. Of the particular interest were the weathering processes in the Sb-rich (Sb: 1000–16500 ppm) central part of the deposit, where Tl-concentrations have been measured in the range between 120-840 ppm (Đorđević et al. 2021).

In the scope of our previous study (Đorđević et al. 2021) we have identified primary and secondary mineralogy of the technosoils in the central part of Allchar deposit. As the main primary Tl-sources we have identified sulfosalts fangite, lorándite and pierrotite. Tl dissolved during weathering under circumneutral conditions is reprecipitated as avicennite and as tiny, fibrous Tl-bearing Mn oxides (up to 8.5 at.% of Tl). Furthermore, tiny spherulitic aggregates (up to 3 µm) of a Tl-Sb-oxide (unknown mineral species) have been found intergrown with quartz, muscovite and minor dolomite. Due to their small aggregate size, we have not been able to closer identify these oxides. Therefore, we have decided to take a closer look at these phases using transmission electron microscopy (TEM). The TEM-lamellae were prepared by means of focused ion beam (FIB) and were investigated under cryogenic condition (–184 °C) using high-resolution scanning transmission microscopy (HR-STEM) coupled with electron dispersive spectroscopy (EDS) and electron backscatter diffraction (EBSD). Just after a short electron exposure, Tl₂O₃ crystals in the size up to 100 nm formed on the surfaces of the Tl-Sb-oxides. EBSD on Tl-Sb-oxide particles confirmed that the Tl-Sb-oxide is crystalline and the EDS-line and area scans confirmed Tl:Sb ratio of 2.5, meaning that Tl enters the crystal structure of the new Tl-Sb oxides and is not hosted as the nanophase.

Both nano- and microcrystalline Tl-minerals are important products of oxidative weathering of Tl-bearing metal-sulphides. Our future study focused on the formation and dissolution of these phases will provide a much deeper insight into the mechanisms of formation of specific mineral association and will help to interpret common features in the alteration paths in general.

This work was supported by the Austrian Science Fund (FWF) [grant number P 36828-N to T. Đorđević]

Đorđević T, Kolitsch U, Drahota P, Majzlan J, Peřestá M, Serafimovski T, Tasev G, Boev I, Boev B (2021): Tl sequestration in the middle part of the Allchar Sb–As–Tl–Au deposit, North Macedonia. - Goldschmidt Virtual Conference, Abstracts, Lyon, France, 4–9 July 2021

New applications for digitised historical collections as teaching materials for special mineralogy and petrography

A. Duriagina¹, C. Kehr², G. Heide¹

¹*TU Bergakademie Freiberg, Institute for Mineralogy, Brennhausgasse 14, 09599 Freiberg*

²*TU Bergakademie Freiberg, Geoscientific Collections, Brennhausgasse 14, 09599 Freiberg*
e-mail: Asia.Duriagina@mineral.tu-freiberg.de

The Geoscientific Collections of the TU Bergakademie Freiberg are among the most extensive and diverse of their kind. Since the founding of the Bergakademie, they have been created in the context of teaching and further education of students as well as for research purposes and have been continuously expanded ever since. Today, the collections still form an important cornerstone within the education of students and specialist staff. In the emerging age of digital media and virtual realities, as well as against the background of an ever-increasing pool of historical collection material, the aim is to present, archive and use these objects appropriately.

Since the teaching collections and their objects are only accessible to a limited extent within the framework of courses, it is necessary, among other things, to digitise them so that they can be made available in interactive teaching formats. Especially in the field of mineralogy, crystallography and petrology, it is particularly important for students to deal with the greatest possible variety of different objects within the teaching collections. This can be optimally realised through the additional digitised content and thus complement conventional teaching. The digital and visualised collection recording is thus indispensable for a location-independent and cross-thematic use in teaching. Through digital recording, background knowledge on the exhibits is prepared in multimedia form, thus making a greater variety of knowledge accessible to the student in addition to classroom studies.

Digitisation also allows us to use other very interesting objects as teaching aids. For example, historical collection of decorative stones from the Altai Mountains (stone-cutting workshop in Kolywan) is usually not suitable for student work due to its rarity and uniqueness, but once it is digitised, it offers enormous potential for study.

The collection, compiled by Bernhard von Cotta (1808-1879) during his journey to Altai (Cotta et al. 1871), comprises 70 hand specimens and 40 thin sections and is housed in the Geosciences Collections of the TU Bergakademie Freiberg. Each rock slab is 8 x 4.5 cm, ground and polished on one side as well as on the edges, the other main side has a fresh fracture. They are mainly granites, felsic igneous rocks with porphyritic structure, marbles and various schists, as evidenced by a post-determination (Weber, 2019). In 2021, the samples were also digitally recorded using multi- and hyperspectral photography to provide reference data for the non-destructive analysis of museum objects. Furthermore, the historical thin sections were microscopically scanned with linear and cross polarised light and matched with the historical images.

Acknowledgements: We would like to thank the foundation "Innovation in der Hochschullehre" for the financial support and Mr. G. Sacher from "Fokus GmbH" for the discussions and talks.

Cotta B von, Teplouchow TA, Geinitz HB, Stelzner AW (1871): Der Altai: Sein geologischer Bau und seine Erzlagerstätten. - Leipzig: Weber JJ

Weber A (2021): Bernhard von Cottas historische Sammlung polierter Gesteinstafeln aus der russischen kaiserlichen Steinschleiferei zu Kolywan' im Altai. - Perspektive des Sammlungswissens, Humboldt-Universität zu Berlin 48-56, doi.org/10.18452/23914

Fused beads for the analysis of Li bearing samples by LIBS and XRF

D. Ebert¹, R. Möckel¹, A.D. Renno¹, A. Schneider^{1,2}, T. Dittrich³

¹Helmholtz-Zentrum Dresden-Rossendorf; Helmholtz-Institute Freiberg for Resource Technology, Chemnitzer Straße 40, 09599 Freiberg

²TU Bergakademie Freiberg, Institut für Organische Chemie, Leipziger Straße 29, 09599 Freiberg

³Deutsche Lithium GmbH, Am Junger-Löwe-Schacht 10, 09599 Freiberg
e-mail: d.ebert@hzdr.de

In recent decades, it has become apparent that due to the increasing complexity of deposits, the complexity of ore samples is also increasing. At the same time, the need for detailed geological and mineralogical information also increased. Therefore, it is important to combine methods in order to obtain more comprehensive conclusions.

We present a method of combining WDXRF (wavelength dispersive X-ray fluorescence) analyses with a wide spectrum of elements and pLIBS (portable laser induced breakdown spectroscopy, see Fig. 1) with a likewise spectrum and the additional possibility to detect light elements such as Li. Nevertheless, the representativeness of LIBS analyses is significantly smaller compared to XRF. To overcome this and effectively combine both methods, we designed and produced fused beads using $\text{Na}_2\text{B}_4\text{O}_7$ as flux. Unfortunately, such beads are transparent to the laser which makes LIBS analysis almost impossible, therefore, we tested two different approaches: 1) dying the bead by adding CuO to the flux and 2) roughen the beads surface. We used a mixture of $\text{Na}_2\text{B}_4\text{O}_7$ (+ CuO) + KI as matrix. Potassium iodide (KI) was added as a releasing agent. We used Greisen rocks from the Altenberg-Zinnwald district with known composition – including Li – and LiBO_2 in different concentration ratios to adjust the Li content.

To produce crack-free beads, we had to adapt the melting process in the fully automatic melting furnace TheOx (CLAISSE). For the analytical work, we use a portable LIBS instrument manufactured by SciAps (Z-300, laser wavelength 1064 nm) and a PANalytical Axiosmax minerals XRF spectrometer.

The fused beads will now serve as calibration samples for both XRF and LIBS measurements (see Fig. 2). Samples with unknown composition will be analysed by XRF first. It turned out that roughening the beads has no significant influence on the XRF-spectra as revealed in before and after scan measurements. In a second step the LIBS analysis is performed in particular for light element determination such as Li. Furthermore, adding a dying component such as Cu might be suitable as a robust internal standard for both LIBS and XRF.



Fig. 1: pLIBS measurement on a fused bead containing Cu as dying agent.

The obvious disadvantage of the method is that neither Cu, K nor Na can be included in the quantitative analysis. De-pending on the analytical problem, they would have to be determined in a preceding step (e.g. via a conventional Li-borate melt and XRF).

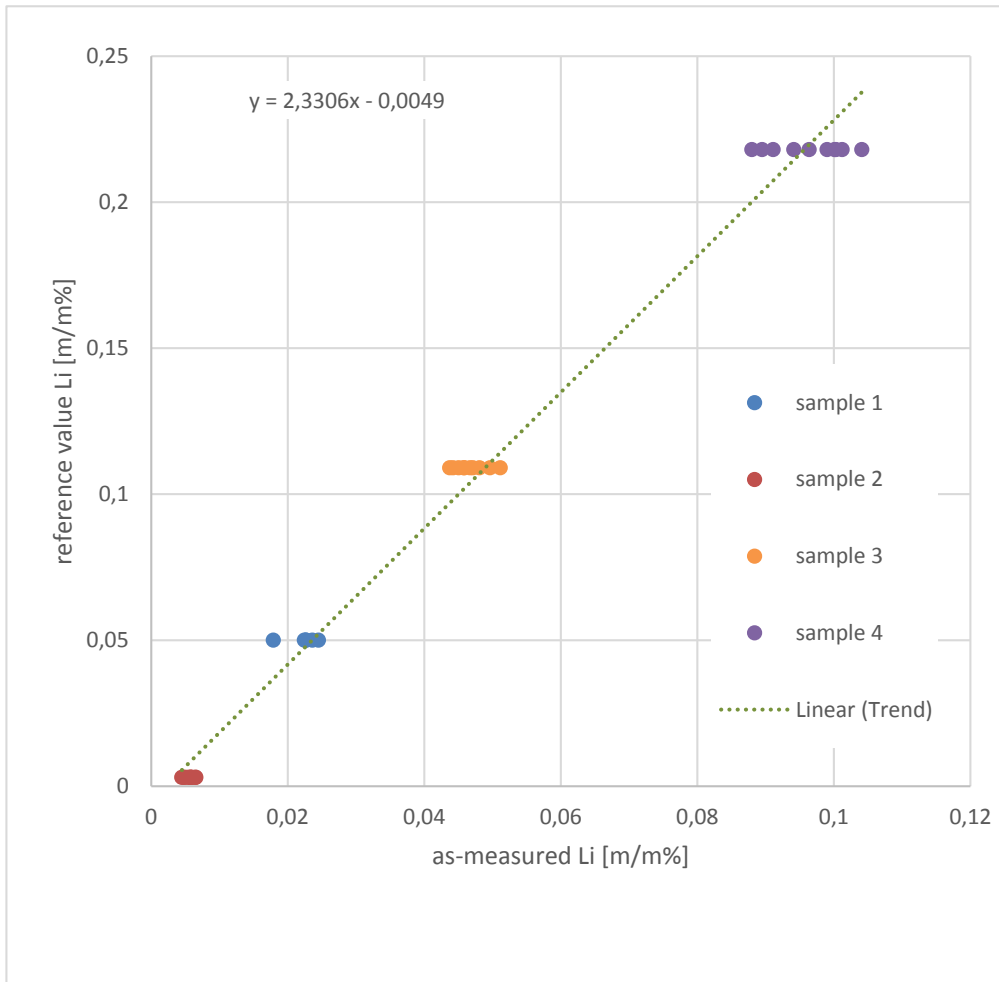


Fig. 2: Calibration factor derived from the initial fused beads, showing robust data on each sample.

Structural diversity in new, synthetic zemannite-type phases

F. Eder¹, A. Marsollier², M. Weil¹

¹TU Wien, Institute for Chemical Technologies and Analytics, Structural Chemistry

²IUT Bordeaux-Gradignan

e-mail: felix.eder@tuwien.ac.at

The mineral zemannite (Matzat 1967; Fig. 1), named in honor of Prof. Josef Zemann (1923–2022), has a composition of $[\text{Zn}^{2+}\text{Fe}^{3+}(\text{TeO}_3)_3]_2[\text{Mg}(\text{H}_2\text{O})_6] \cdot n\text{H}_2\text{O}$ ($n \leq 3$), and is the mineral of the MinWien2023 conference. Synthetic zemannite-type phases can be obtained from hydrothermal reactions between transition metal oxides, tellurium dioxide and alkali metal carbonates. In comparison with the usual set-up for a hydrothermal experiment, the drastic reduction of the water content changes the role of water from a typical solvent to a mineralizer. Under these conditions, the formation of numerous new phases with zemannite-type structures was observed (Eder et al. 2023).

The crystal structures of the new zemannite-type phases were determined on basis of single-crystal X-ray diffraction. Like the mineral zemannite itself, the crystal structures of $\text{Fe}_2(\text{TeO}_3)_3$, $\text{Na}_2[\text{Ni}_2(\text{TeO}_3)_3](\text{H}_2\text{O})_{2.5}$, $\text{K}_2[\text{Ni}_2(\text{TeO}_3)_3](\text{H}_2\text{O})$, $\text{K}_2[\text{Zn}_2(\text{TeO}_3)_3](\text{H}_2\text{O})_2$, $\text{Rb}_{1.25}[\text{Co}_2(\text{TeO}_3)_3](\text{H}_2\text{O})_{1.5}$, $\text{Rb}_{1.24}[\text{Mn}_2(\text{TeO}_3)_3](\text{H}_2\text{O})_2$, and $\text{Na}_{1.79}\text{Mg}_{0.11}[\text{Mg}_2(\text{TeO}_3)_3](\text{H}_2\text{O})_{3.86}$ show hexagonal metrics, with $a \approx 9.3 \text{ \AA}$ and $c \approx 7.7 \text{ \AA}$. Relative to this unit-cell, different kinds of superstructures are realized for $\text{Na}_2[\text{Cu}_2(\text{TeO}_3)_3](\text{H}_2\text{O})_{1.5}$ (threefold), $\text{K}_2[\text{Cu}_2(\text{TeO}_3)_3](\text{H}_2\text{O})_2$ (twofold), $\text{K}_2[\text{Co}_2(\text{TeO}_3)_3](\text{H}_2\text{O})_{2.5}$ (twofold and incommensurately modulated), $\text{Rb}_{1.5}[\text{Mn}_2(\text{TeO}_3)_3](\text{H}_2\text{O})_{1.25}$ (fourfold), and $\text{Cs}[\text{Mn}_2(\text{TeO}_3)_3](\text{H}_2\text{O})$ (fourfold).

The formation of these superstructures can be attributed to several influences. Variable water contents (compounds with zemannite-type structures are known for their zeolitic properties (Miletich 1995)), the space requirements of large alkali metal cations like Rb^+ or Cs^+ , and Jahn–Teller distortions of the coordination polyhedra of certain framework atoms like Cu^{II} or Mn^{III} play crucial roles in this respect.

Another aspect of zemannite-type crystal structures is the nature and distribution of the contents inside the large hexagonal channels perforating the framework. For most of the investigated phases, alkali metal cations and crystal water molecules are displaced up to 2 \AA from the channel center and are disordered around the 6_3 axis (or other symmetry elements containing a threefold rotation axis). In the superstructures of $\text{Rb}_{1.5}[\text{Mn}_2(\text{TeO}_3)_3](\text{H}_2\text{O})_{1.25}$ and $\text{Cs}[\text{Mn}_2(\text{TeO}_3)_3](\text{H}_2\text{O})$, ordered channel-contents were observed. $\text{Fe}_2(\text{TeO}_3)_3$ has empty channels, which causes some Te^{IV} atoms of the framework to “tilt” towards the channel center. In $\text{Na}_{1.79}\text{Mg}_{0.11}[\text{Mg}_2(\text{TeO}_3)_3](\text{H}_2\text{O})_{3.86}$, both Na^+ and Mg^{2+} cations inhabit the channels together with H_2O molecules, and the superposition of their respective environments can be noticed in the crystal structure refinement.



Figure 1. Zemannite—the mineral of the meeting. Photo: S. Wolfsried

Eder F, Marsollier A, Weil M (2023): Structural studies on synthetic $A_{2-x}[M_2(\text{TeO}_3)_3] \cdot n\text{H}_2\text{O}$ phases ($A = \text{Na}, \text{K}, \text{Rb}, \text{Cs}$; $M = \text{Mn}, \text{Co}, \text{Ni}, \text{Cu}, \text{Zn}$) with zemannite-type structures. - Mineral Petrol <https://doi.org/10.1007/s00710-023-00814-5>

Matzat E (1967): Die Kristallstruktur eines unbenannten zeolithartigen Tellurminerals, $\{(\text{Zn}, \text{Fe})_2[\text{TeO}_3]_3\} \text{Na}_x\text{H}_{2-x} \cdot y\text{H}_2\text{O}$. - Tschermaks Mineral Petrogr Mitt 12, 108–117

Miletich R (1995): The synthetic microporous tellurites $\text{Na}_2[\text{Me}_2(\text{TeO}_3)_3] \cdot 3\text{H}_2\text{O}$ ($\text{Me} = \text{Zn}, \text{Co}$): crystal structure, de- and rehydration, and ion exchange properties. - Monatsh Chem 126, 417–430

CuSeO₄ and Cu(SeO₃OH)₂·6H₂O: A tribute to the enlightenment of the stereochemistry of Cu²⁺ ions by Josef Zemann (1923–2022)

H.S. Effenberger¹, G. Giester¹, M. Wildner¹

¹Institut für Mineralogie und Kristallographie, Universität Wien
herta.silvia.effenberger@univie.ac.at

In the middle of the last century the stereochemistry of divalent copper atoms was mostly unknown. Crystal structure investigations of trippkeite, azurite, linarite, or teinite led Josef Zemann (1923–2022) to understand the coordination figures controlled by the Jahn-Teller-effect. In contrast to the earlier thought CuO₆ octahedra, he described the coordination figures as planar [4], tetragonal pyramidal [4+1], and tetragonal *dipyramidal* [4+2] (Zemann 1961; 1972). The additional ligands have none or only a minor influence on the geometry of the CuO₄ square. In honour to these pioneering investigations, two further compounds with Cu²⁺ ions are presented here: Cu(SeO₄) and Cu(SeO₃OH)₂·6H₂O. They were synthesized at low-temperature hydrothermal conditions (220 °C) and room temperature, respectively.

Snyman & Pistorius (1964) described two modifications of CuSeO₄: one crystallises in the structure type of ZnSO₄ (mineral name zincosite, space group *Pnma*), the high-pressure form in the NiSO₄-structure type (space group *Cmcm*). The new Cu(SeO₄) modification presented here adopts the MnAsO₄-structure type (space group *P2₁/n*), it represents a monoclinic distortion form the *Pnma* modification.

Mn³⁺ ions exhibit a pronounced [4+2] coordination due to the Jahn-Teller effect. Therefore, the substitution Cu²⁺ ↔ Mn³⁺ is not surprising. The coupled substitution Mn³⁺ + As⁵⁺ ↔ Cu²⁺ + Se⁶⁺ enables isotypy between CuSeO₄-*P2₁/n* and MnAsO₄.

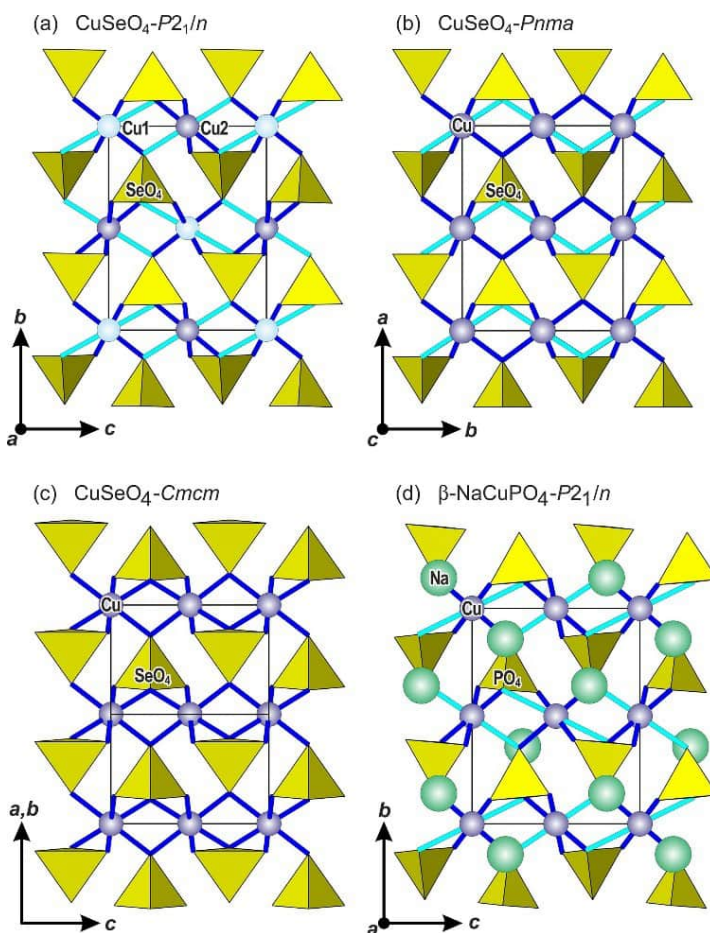


Fig. 1 The crystal structures of (a) Cu(SeO₄)-*P2₁/n* (structure type MnAsO₄), (b) Cu(SeO₄)-*Pnma* (structure type ZnSO₄), (c) Cu(SeO₄)-*Cmcm* (structure type NiSO₄), and (d) β-NaCuPO₄-*P2₁/n* (Kawahara et al. 1993).

The crystal structure of $\text{Cu}(\text{SeO}_3\text{OH})_2 \cdot 6\text{H}_2\text{O}$ crystallizes in a new structure type. It is characterized by three structural units (i.e., $[\text{Cu}^{4+2}(\text{H}_2\text{O}_w)_4\text{O}_2]$, $[\text{SeO}_3(\text{O}_h\text{H})]$, and $[\text{H}_2\text{O}_w7]$). They are connected mainly by hydrogen bonds (Fig. 2). The $\text{Cu}^{4+2}\text{O}_6$ polyhedron forms a quite regular tetragonal *dipyramid* with site symmetry $\bar{1}$. The two pairs of independent $\text{Cu}-\text{O}_w$ bonds within the CuO_4 square are nearly identical and vary only by 0.0016 Å; $\text{O}-\text{Cu}-\text{O}$ bond angles deviate up to 2° from the ideal value. Hence, the $\text{Cu}^{4+2}\text{O}_6$ *dipyramid* adopts a nearly regular shape, obviously due to the rather soft connection among the structural units. The bond valence sum calculated for the Cu atom is unexpectedly large (2.26 v.u.). It is a general experience that for coordination polyhedra loosely bound to further structural units the cation–anion distances are shortened to compensate for the under-saturation of the anions. Consequently, the bond valence sums are over-estimated. Blocksatz

During the final refinement cycles, anisotropic displacement parameters of the Se, Cu, and O atoms as well as isotropic ones for the H atoms were refined. Only for the atom $\text{Ow}7$ the displacement parameters of the two H ligands were constrained to equal values during the structure refinement. The protonated selenate(VI) group exhibits $\text{Se}-\text{O}$ bonds of 1.614 to 1.626 Å (to the atoms $\text{O}1$, $\text{O}2$, and $\text{O}3$) whereas the $\text{Se}-\text{O}_h$ bond is extended to 1.695 Å. This environment is in agreement with the average $\text{Se}-\text{O}_h$ value in *monoprotonated selenate(VI)* groups of 1.71 Å as compiled by Ferraris and Ivaldi (1984).

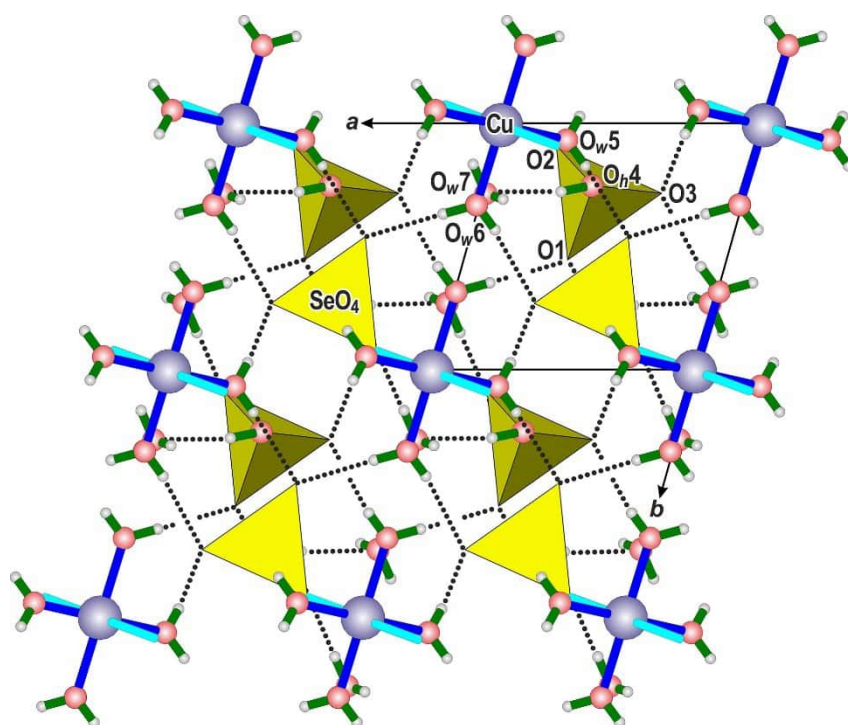


Fig. 2 The crystal structure of $\text{Cu}[\text{SeO}_3(\text{OH})]_2 \cdot 6\text{H}_2\text{O}$ in a projection parallel to $[001]$ on (110) . "Short" and "long" $\text{Cu}-\text{O}$ bond lengths are indicated in dark blue respectively turquoise colour.

- Ferraris G, Ivaldi G (1984): X–OH and O–H···O bond lengths in protonated oxoanions. – Acta Cryst B40, 1–6
 Kawahara A, Kageyama T, Watanabe I, Yamakawa J (1993): Structure du monophosphate synthétique de cuivre et de sodium. – Acta Cryst C49, 1275–1277
 Snyman HC, Pistorius CWFT (1964): Polymorphism in the selenates of Mg, Mn, Co and Cu at high pressures. – Z Krist 120, 317–322
 Zemann J (1961): Die Kristallchemie des Kupfers. – Fortschr Miner 39, 59–68
 Zemann J (1972): Copper. 29-A, Crystal chemistry. – Handbook of Geochemistry, Vol. 11/3, Berlin-Heidelberg-New York: Springer

Josef Zemann (25. Mai 1923 – 16. Oktober 2022)**H.S. Effenberger¹, R. Miletich¹**¹*Institut für Mineralogie und Kristallographie, Universität Wien
herta.silvia.effenberger@univie.ac.at*

The MinWien2023 meeting is dedicated to Josef Zemann. He was teacher, mentor, colleague, and friend to many colleagues in Vienna but also all over the world. Josef Zemann was born in Vienna on 25 May, 1923, a time of economic uncertainties and social instabilities. His scientific career started with the doctoral thesis entitled “*Über die Struktur des Pharmakosiderits*”, for which he received the academic degree *doctor philosophiae* on 17 July, 1946.

Inspired by crystallography, Josef Zemann stayed for one year at the Massachusetts Institute of Technology in Boston with Martin J. Bürger, one of the pioneers of X-ray crystallography. Quite shortly after his return to Vienna, he became associate professor and some years later full professor at the “Mineralogisch-Kristallographisches Institut” at the Georg-August-Universität in Göttingen. During this time Josef Zemann focussed primarily on topics in crystal chemistry, such as the stereochemistry of Li, Cu and Te atoms, electrostatic lattice energies, as well as crystal absorption spectra in the infrared range. His years in Göttingen constituted a fulfilled time, thanks to the great working conditions and an academically inspiring atmosphere. In 1967 he responded to the call to move to the University of Vienna and succeeded his former teacher Prof. Dr. Karl Ludwig Felix Machatschki. As the head the Institut für Mineralogie und Kristallographie at the Alma Mater Rudolphina - Universität Wien for 22 years until his retirement in 1989 he was scientifically active and an internationally recognised expert in the field of mineralogical crystallography.

Josef Zemann’s early work in Vienna, Bosten, and Göttingen was dedicated to the determination of crystal structures by X-ray diffraction. His interest was the recognition of the stereochemistry of cations, especially of Cu²⁺ and Te⁴⁺ ions that were basically unexplored at that time. In recognition of his research on the stereochemistry of Te⁴⁺ ions, a novel tellurite mineral was named after him, i.e. zemannite, [Zn²⁺Fe³⁺(TeO₃)₃]₂[Mg(H₂O)₆·nH₂O], *n* ≤ 3. (Fig. 1).

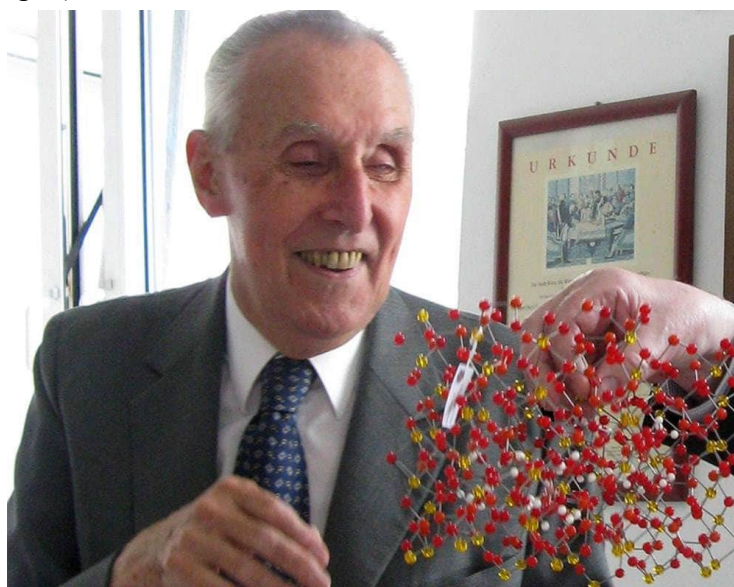


Figure 1. On the occasion of his 85th birthday in 2008 Josef Zemann receives a ball-and-stick model of the crystal structure of his mineral zemannite.

Foto: Kurt Mereiter

Among the milestones of his scientific work were infrared spectroscopic studies, where he tread new conceptual and methodological ground. At one hand he used polarized IR radiation and crystallographically oriented crystal platelets to localize hydrogen bonds associated with OH⁻ groups or H₂O molecules. At that time, it was practically impossible to localize H atom positions by means of X-ray diffraction techniques. Achievements in applying IR spectroscopy were groundbreaking as he recognized for the first time small amounts of hydroxyl groups to be detectable even in nominally anhydrous rock-forming silicates such as in olivine, andalusite, the three TiO₂ modifications, or in enstatite. Even here he was able to localise the orientation of the OH⁻ dipoles in relation to the crystallographic orientation of the mineral samples and consequently to the atomic arrangement. In addition, it was also possible to discriminate between liquid inclusions and structurally oriented hydroxyl groups incorporated in the crystal lattice. The strong interaction between the IR radiation and the OH⁻-dipoles allow to detect concentrations in the tenth weight-percent range. In the 1960s it was doubtless assumed that the Earth's mantle does not contain any OH⁻ or H₂O contents. Today, it is estimated that due to the solubility in the above-mentioned minerals large quantities of OH⁻ and H₂O are stored in the upper 660 km of the Earth's mantle corresponding to the volume to the Earth's oceans.

Josef Zemann's broad scientific oeuvre is supplemented by a series of papers dealing with the crystal chemistry of carbonates, focussing on both the structure types, their topological relations, as well as on the aplanarity of carbonate groups. The calculation of electrostatic lattice energies was a first step towards a modern atomistic modelling and the stability of structure types.

The significance of Josef Zemann's academic work and his reputation within the scientific community was honoured by a large number of honours and awards. He became honorary member of six National Mineralogical Societies (America, Austria, Soviet Union, Poland, Germany, and Romania). The ÖMG appointed him to their Honorary President. He received also numerous awards and medals: the Gustav-von-Tschermak-Seysenegg and the Erwin-Schrödinger medals (both from the Austrian Academy of Science), silver medals (the Abraham-Gottlob-Werner-Medal from the DMG and from the Masaryk University Bruno), a gold medal (Comenius University Bratislava), the Emanuel Bořický Medal (Karlsuniversität Praha), and he became correspondent of the Geologische Bundesanstalt Wien.

Furthermore, his remarkable contribution to crystal chemistry and his input to the knowledge in mineralogical and crystallographic sciences was honoured by various scientific academic memberships. On leave from Göttingen and as a welcome to Vienna he became Corresponding Member of the Akademie der Wissenschaften zu Göttingen in 1967 and the Österreichische Akademie der Wissenschaften (the latter elected him 1972 as a Full Member). A further membership was awarded by the Academia Mediterranea delle Scienze (Catania, Italy) and a Honorary Membership by the Hungarian Academy of Sciences. He was elected as a Corresponding Member by the Kroatische Akademie der Wissenschaften und Künste and the Polish as well as the Croatian Academies of Sciences. He was particularly pleased, in fact he was proud to become a Member and Senator of the Deutsche Akademie der Naturforscher Leopoldina, which had already founded in 1652.

On the evening of 16 October 2022 Josef Zemann passed away gently and peacefully only a few months ahead of his 100th birthday. His person, his tireless commitment and enthusiasm, his keen sense of observation, but also his kindness and humour remain unforgettable. We will remember Josef Zemann as our teacher, mentor, and an outstanding scientist.

Mechanisms of calcium carbonate mineral formation in a roman aqueduct near Cologne (Germany) - A microstructural and geochemical approach

I. Egartner¹, R. Boch¹, K. Grewe², M. Dietzel¹, D. Hippler¹

¹*Graz University of Technology, Institute of Applied Geosciences, Rechbauerstraße 12, Graz, 8010, Austria*

²*Tannenstraße 18, 53913 Swisttal-Morenhoven, Germany*

e-mail: egartner@student.tugraz.at

A special case of freshwater carbonate deposits in man-made settings are calcium carbonate (CaCO₃) scale deposits in aqueducts and water conduits of the roman times. They occur across the ancient expansion of the roman empire and therefore in different climate zones, from maritime to continental mid-latitude regions. Such scale deposits can serve as an archive, for the reconstruction of the physico-chemical environmental conditions, the palaeoclimate and the hydrogeology of the catchment and the aquifer. This study therefore aimed to investigate the ancient environmental physico-chemical conditions of the scale deposits of a roman aqueduct channel, the so called „Eifel-Wasserleitung“, that supplied water from the Eifel mountains to the roman city of Cologne, Germany by microstructural and geochemical proxies. In order to reveal the meso- and microstructural fabric as well as geochemical and stable isotope compositions of the CaCO₃ scale deposits, petrographic, mineralogical and geochemical analyses have been applied (e.g. light microscopy, XRD, Raman spectroscopy and LA-ICP-MS).

First results revealed differences in carbonate mineral nucleation and growth dynamics that are indicated by individual crystal shapes, arrangements and scale textures. The polished hand specimen of the investigated CaCO₃ scale deposit shows mesofabric characteristics of individual horizons ranging from 1 to 5 mm in size and low porosity. At the microfabric level, the calcite, which forms the individual laminae, shows different growth types, occurring as microsparit, elongated columnar calcite crystals and thin micritic layers. These growth types are well comparable to other investigations of CaCO₃ scale deposits in aqueducts of the roman empire, but they are also frequently found in freshwater carbonate deposits in man-made settings as well as in natural environments, like speleothems. The results of the macro- and microstructural characterization, major/trace element distributions (e.g., Mg, Ca, Sr, Ba) will be discussed in respect to reaction mechanisms and mineral growth rates, potential microorganic influence, and (water) discharge.

The incorporation of Li in the tourmaline structure

A. Ertl^{1,2}

¹Mineralogisch-Petrographische Abt., Naturhistorisches Museum, Austria,

²Institut für Mineralogie und Kristallographie, Universität Wien, Austria.

e-mail: andreas.ertl@a1.net

Using natural and synthetic samples, it was investigated which Li-containing short-range orders can occur in Li-bearing Al-rich tourmalines. The investigated samples have lattice parameters from $a = 15.72$, $c = 7.07$ Å to $a = 15.84$, $c = 7.10$ Å. The general tourmaline formula is $XY_3Z_6(BO_3)_3[T_6O_{18}]V_3W$, where the X site is usually occupied by Na, Ca or is vacant. The Y site is in such tourmalines usually occupied by Al and Li, and the Z site is only occupied by Al. The T site can be occupied by Si and by minor amounts of B and Al. The V site is usually occupied by OH and the W site by OH, O or F.

It is still not clear how Li enters the Y site in Li-rich tourmalines. Until now, syntheses have not been successful in producing Li-rich tourmalines (>0.5 apfu ^YLi). It therefore makes sense to take a closer look at which short-range orders Li can be built into. Synthetic Al-rich and Li-bearing tourmalines with no F, but with $^{[4]}\text{B}$ and $^{[4]}\text{Al}$ are of special interest, because they contain no Ca, only Na and vacancies (\square) at the X site and mainly Al and Li at the Y site (Ertl et al., 2012). Since these tourmalines (synthesized by David London) do not have such a complex composition, relationships are easier to recognize. In Tab. 1 all short-range orders are listed which can contribute to these synthetic samples (Z site is always occupied by Al).

Table 1. Short-range orders in synthetic tourmaline

Number	X site	Y site	T site	W site
1.1	Na	Al_2Li	Si_5B	OH
1.2	Na	Al_2Li	Si_5Al	OH
1.3	Na	Al_3	Si_4B_2	O
2.1	\square	Al_2Li	Si_6	OH
2.2	\square	Al_3	Si_5B	O
2.3	\square	Al_3	Si_5Al	O

Short-range order 2.1 is related to the rossmanite end-member. Short-range order 2.3 is related to the alumino-oxy-rossmanite end-member (Ertl et al., 2022), while 2.2 is related to the B-analogue of this tourmaline. It seems confirmed that the short-range order 1.3 is an essential component. Without it, it is not possible to explain the crystal chemical formulae of these synthetic tourmaline samples. The combination of these different short-range orders makes it clear that the Li content in such a tourmaline containing only Na and vacancies at the X site will be in the range of 0–1 apfu Li. When correlating the component of the different short-range orders in the examined tourmalines, which were synthesized at different temperatures, it can be recognized that with decreasing temperature the component of 2.1 increases, while it decreases with increasing temperature. This explains why the content of the tetrahedrally coordinated B towards lower temperatures significantly increases. There is no evidence that in these synthetic tourmalines a short-range order occurs, where the X and Y sites are occupied as in 1.1, but exclusively Si occupies the T site and only O occupies the W site. Such a short-range order may not be favourable at such pressure/temperature conditions or perhaps even unstable.

A natural Al-rich and Li-bearing tourmaline sample with a vacancy-dominant *X* site (rossmanite; Selway et al., 1998) with the updated crystal chemical formula $X(\square_{0.6}\text{Na}_{0.4})Y(\text{Al}_{2.2}\text{Li}_{0.7}\square_{0.1})Z\text{Al}_6(\text{BO}_3)_3[\text{Si}_{5.6}\text{B}_{0.4}\text{O}_{18}]V(\text{OH})_3W[(\text{OH})_{0.6}\text{O}_{0.3}\text{F}_{0.1}]$ seems to consist of the same short-range orders. A minor component may occur additionally: a short-range order with $X\text{Na}$, $Y(\text{Al}_2\square)$, $T\text{Si}$ and $W(\text{OH})$ (see also Ertl, 2023). However, the dominant component is short-range order 2.2 (Tab. 1), which is not surprising.

There occur natural Al- and Li-rich tourmalines with Li >1.0 apfu. Such tourmalines contain additionally some Ca and significant amounts of F (e.g., Ertl et al., 2006, 2010). The short-range orders occurring in such samples are already listed in Tab. 1, but additional short-range orders might also occur, which are listed in Tab. 2.

Table 2. Additional theoretical short-range orders in natural Al- and Li-rich samples

Number	<i>X</i> site	<i>Y</i> site	<i>T</i> site	<i>W</i> site
1.4	Na	Al ₂ Li	Si ₅ B	F
1.5	Na	Al ₂ Li	Si ₅ Al	F
2.4	□	Al ₂ Li	Si ₆	F
3.1	Ca	Li ₂ Al	Si ₆	F
3.2	Ca	Li ₂ Al	Si ₆	OH
3.3	Ca	Al ₂ □	Si ₅ Al	OH
3.4	Ca	Al ₂ □	Si ₅ B	OH

Short-range orders 3.1 and 3.2 have (Li₂Al) at the *Y* site. The combination of these components together with short-range orders 1.1, 1.2, 1.4, 1.5, 2.1 and 2.4 produces Li contents in the range 1-2 apfu Li. However, the 2.4 short-range order does not appear to occur, as a summary of approximately 9000 tourmaline analyses from different lithological environments show that for tourmaline with an average *X*-site charge of <+0.5, the maximum F amounts are <0.2 apfu (Henry & Dutrow, 2011). These chemical data of natural tourmalines indicate crystallographic influences. Natural tourmaline with relatively high Li contents always contains relatively high F contents. It seems that the contents of Li and the F are positively correlated (Ertl, 2021). It is therefore possible that short-range orders with Li and F (1.4, 1.5, 3.1; Table 2) are crystal-chemically more favourable than orders with Li and OH (1.1, 1.2, 2.1; Tab. 1; 3.2; Tab. 2). However, further investigations seem to be necessary.

This research was funded by the Austrian Science Fund (FWF) project P 35585.

Ertl A (2021): Why was it not possible to synthesize Li-rich tourmaline? - NATURA 111, 31–32

Ertl A (2023): Are the [6]-coordinated sites in tourmaline in certain cases partially vacant? Mineral Petrol 117, DOI: 10.1007/s00710-023-00815-4

Ertl A, Hughes JM, Prowatke S, Ludwig T, Prasad PSR, Brandstätter F, Körner W, Schuster R, Pertlik F, Marschall H (2006): Tetrahedrally coordinated boron in tourmalines from the liddicoatite-elbaite series from Madagascar: Structure, chemistry, and infrared spectroscopic studies. - Amer Mineral 91, 1847–1856

Ertl A, Rossman G, Hughes JM, London D, Wang Y, O'Leary JA, Darby MD, Prowatke S, Ludwig T, Tillmanns E (2010): Tourmaline of the elbaite-schorl series from the Himalaya Mine, Mesa Grande, California: A detailed investigation. - Amer Mineral 95, 24–40

Ertl A, Giester G, Ludwig T, Meyer H-P, Rossman GR (2012): Synthetic B-rich olenite: Correlations of single-crystal structural data. - Amer Mineral 97, 1591–1597

Ertl A, Hughes JM, Prowatke S, Ludwig T, Lengauer CL, Meyer H-P, Giester G, Kolitsch U, Prayer A (2022): Alumino-oxy-rossmanite from pegmatites in Variscan metamorphic rocks from Eibenstein an der Thaya, Lower Austria, Austria. - Amer Mineral 107, 157–166

Henry DJ, Dutrow BL (2011): The incorporation of fluorine in tourmaline: internal crystallographic controls or external environmental influences? - Canad Mineral 49, 41–56

Selway JB, Novák M, Hawthorne FC, Černý P, Ottolini L, Kyser TK (1998): Rossmanite, $\square(\text{LiAl}_2)\text{Al}_6\text{Si}_6\text{O}_{18}(\text{BO}_3)_3(\text{OH})_4$, a new alkali-deficient tourmaline: description and crystal structure. - Amer Mineral 83, 896–900

Ammonium-iron-sulfites from a burning coal-mine dump

B. Fehér¹, S. Szakáll², M. Ende³, H.S. Effenberger³, J. Mihály⁴, I. Sajó⁵,
L. Kótai⁴, D. Szabó⁶

¹Department of Mineralogy, Herman Ottó Museum, Miskolc, Hungary

²Institute of Mineralogy and Geology, University of Miskolc, Hungary

³Institut für Mineralogie und Kristallographie, Universität Wien, Austria

⁴Institute of Materials and Environmental Chemistry, Research Centre for Natural Sciences, Budapest, Hungary

⁵Szentágotthai Research Centre, University of Pécs, Hungary

⁶Department of Mineralogy, Eötvös Loránd University, Budapest, Hungary

e-mail: herta.silvia.effenberger@univie.ac.at

Three ammonium-iron-sulfites from a burning coal dump in an abandoned open coal pit at Pécs-Vasas (Mecsek Mountains, South Hungary) were identified. They were formed by the interaction of decomposing iron sulfides and ammonia released from organic matter. For synthetic analogues to these natural phases see Erämetsä (1943); Erämetsä & Valkonen (1972); Kocsis et al. (2018).

$(\text{NH}_4)_9\text{Fe}^{3+}(\text{SO}_3)_6$ is metastable and decomposes quickly. Larsson & Niinistö (1973) performed a crystal-structure investigation in space group $P\bar{3}$ from powder X-ray data. Identity with the natural samples was proved. Isolated Fe^{2+}O_6 polyhedra are corner-connected to sulfite anions. Each corner is shared with an O atom of a $(\text{SO}_3)^{2-}$ group forming $[\text{Fe}^{3+}(\text{SO}_3)_6]^{9-}$ clusters (Fig. 1). Thus, only one O atom of the sulfite group links to a FeO_6 octahedron; the others are acceptor atoms of the hydrogen bonds.

$(\text{NH}_4)_2\text{Fe}^{2+}(\text{SO}_3)_2$ (AIS-2) crystallizes in space group $R\bar{3}m$ and is characterized by a 2D net with composition $[\text{Fe}^{2+}(\text{SO}_3)_2]^{2-}$ (Fig. 2). All three O atoms belonging to the sulfite group represent corners in FeO_6 octahedra. Thereby two layers of O atoms are parallel to (0001) and in a close packed arrangement. 1/4 of the octahedral voids in this double layer are filled by Fe^{2+} ions.

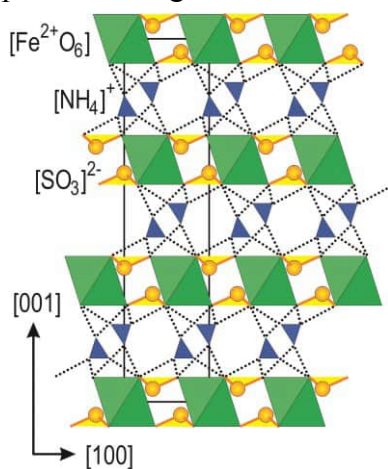


Figure 2. The crystal structure of $(\text{NH}_4)_2\text{Fe}^{2+}(\text{SO}_3)_2$

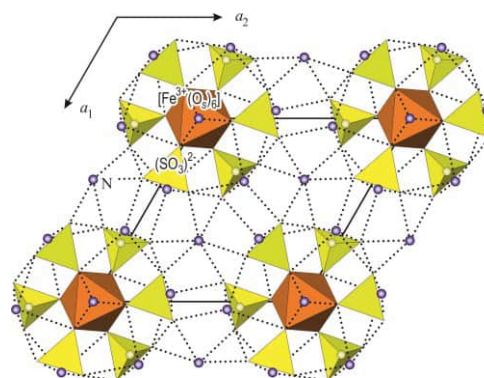


Figure 1. The crystal structure of $(\text{NH}_4)_9\text{Fe}^{3+}(\text{SO}_3)_6$

The apical S atom points into the 2D net, the lone-electron pairs are centred in the $[\text{Fe}(\text{SO}_3)_2]^{2-}$ layer.

The crystal structure is topologically equivalent to the buetschliite-type selenites $\text{K}_2\text{Mn}(\text{SeO}_3)_2$ and $\text{K}_2\text{Co}(\text{SeO}_3)_2$ (Wildner 1992a,b). Also carbonates like eitelite and buetschliite $[\text{Na}_2\text{Mg}(\text{CO}_3)_2, \text{K}_2\text{Ca}(\text{CO}_3)_2]$, are representatives belonging to this connection schema; here the C atom of the CO_3 triangles are close to the O atom layers as only minor but significant aplanarities of the carbonate groups are verified (Knobloch et al. 1980; Effenberger & Langhof 1984). Like for in the sulfites and selenites, the apex of the carbonate points towards the octahedral layer; as pointed out by Zemmann (1981) towards the smaller and higher charged cations where one expects stronger covalent contributions to the chemical bonds between the cations and oxygen atoms.

$(\text{NH}_4)_2\text{Fe}^{3+}(\text{OH})(\text{SO}_3)_2 \cdot \text{H}_2\text{O}$ (Fig. 3) crystallizes in space group $Cmcm$ and exhibits $[\text{Fe}^{3+}(\text{OH})(\text{SO}_3)_2]^{2-}$ chains. The Fe^{3+} ions are octahedrally coordinated to four O atoms belonging to sulfite groups (O_s atoms) and to two oxygen atoms belonging to hydroxyl groups (O_h atoms). These FeO_6 octahedra are corner linked to buckled chains; each two *trans*-arranged O_h atoms are shared and represent the backbone of the $[\text{Fe}^{3+}(\text{OH})(\text{SO}_3)_2]^{2-}$ chains. The shape of these chains is related to a wind wheel with the selenite groups pointing off the $[\text{Fe}(\text{O}_s)_4\text{O}_h]^{7-}$ columns. About 8 % of the Fe^{2+} ions are displaced along the c axis (the Fe' position is 0.64 Å apart from the Fe atom).

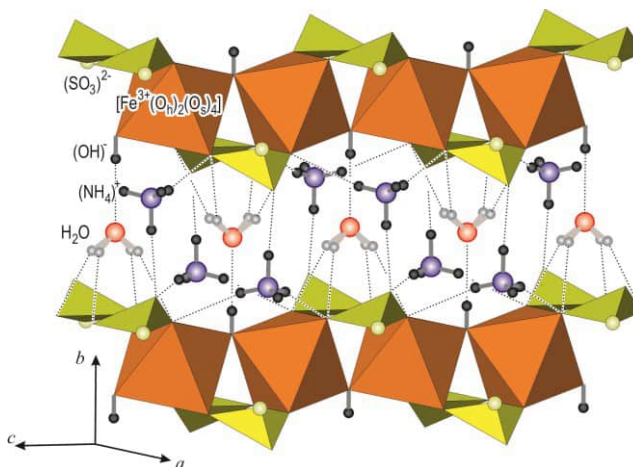


Figure 3. The crystal structure of the new mineral kollerite, $(\text{NH}_4)_2\text{Fe}^{3+}(\text{OH})(\text{SO}_3)_2 \cdot \text{H}_2\text{O}$

Intercalated between the $[\text{Fe}^{3+}(\text{OH})(\text{SO}_3)_2]^{2-}$ chains are the water molecules and the ammonium cations. Linkage is achieved by hydrogen bonds only. Despite this loose connection, the $(\text{NH}_4)^+$ group is ordered and forms clearly defined hydrogen bonds. As the O_w atom has site symmetry $m2m$, the water molecules exhibit a site disorder with respect to the H atoms at least for the structure model in space group $Cmcm$. As only two H atoms per formula unit are affected, order (neither by a reduction of symmetry nor by an enlargement of the unit cell) could be proved.

It is remarkable that for a crystal size of $6 \times 7 \times 65 \mu\text{m}^3$ it was possible to refine the half occupied H atom position without any restrictions (*i.e.*, with variable atomic coordinates and a variable isotropic displacement parameter). The H_2O molecules – like the Fe' atoms – exhibit an orientational disorder violating at least locally the *centro*-symmetry. X-ray data were collected at 220 K using a Stoe-StadiVari diffractometer equipped with a Dectris Pilatus 300 K pixel detector. It was operated with monochromatized $\text{MoK}\alpha$ radiation from a 100 W air-cooled Incoatec $\text{I}\mu\text{S}$ micro-focus X-ray tube (50 kV, 1 mA).

- Effenberg H, Langhof H (1984): On the aplanarity of the CO_3 group in buetschliite, dipotassium calcium dicarbonate, $\text{K}_2\text{Ca}(\text{CO}_3)_2$. A further refinement of the atomic arrangement. - Acta Cryst C40, 1299-1300
- Erämetsä O (1943): Über Ammonisulfitferriate. - Ann Acad Sci Fenn Ser A LIX, 5-30
- Erämetsä O, Valkonen J (1972): Ammonium ferric sulfites. Suomen Kemistilehti 45, 91–94
- Knobloch D, Pertlik F, Zemann J (1980): Crystal structure refinements of buetschliite and eitelite: a contribution to the stereochemistry of trigonal carbonate minerals. N Jb Mineral Mh 1980 230-236
- Kocsis T, Magyari J, Sajó IE, Pasinszki T, Homonnay Z, Szilágyi IM, Farkas A, May Z, Effenberg H, Szakáll S, Pawar RP, Kótai L (2018): Evidence of quasi-intramolecular redox reactions during thermal decomposition of ammonium hydroxodisulfiteferriate(III), $(\text{NH}_4)_2[\text{Fe}(\text{OH})(\text{SO}_3)_2] \cdot \text{H}_2\text{O}$. - J Therm Anal Calorim 132, 493–502
- Larsson LO, Niinistö L (1973): The crystal structure of ammonium hexasulphite-ferrate(III), $(\text{NH}_4)_9[\text{Fe}(\text{SO}_3)_6]$. - Acta Chem Scand 27, 859–867
- Wildner M (1992a): Structure of $\text{K}_2\text{Mn}(\text{SeO}_3)_2$, a further buetschliite-type selenite. - Acta Cryst C48, 595
- Wildner M (1992b): Isotypism of a selenite with a carbonate: structure of the buetschliite-type compound $\text{K}_2\text{Co}(\text{SeO}_3)_2$, a further selenite. - Acta Cryst C48, 410-412
- Zemann J (1981): Zur Stereochemie der Karbonate. - Fortschr Mineral 59 95–116

Petrology and geochemistry of the Haddo House – Arnage district contact aureole, Aberdeenshire / Scotland

A. Fehleisen¹, C.A. Hauzenberger¹, J. Booth¹

*¹University of Graz, Department of Earth Sciences, Universitätsplatz 2, 8010 Graz
e-mail: anna.fehleisen@edu.uni-graz.at*

In Aberdeenshire, NE Scotland, a suite of gabbroic intrusions was intruded roughly contemporaneous to peak regional metamorphism during the middle Ordovician Grampian orogenic event. This study is based on samples collected from the Belhelvie, Haddo House, Arnage and Huntly gabbro intrusions, their metamorphic aureoles and zones of contact anatexis. The intrusions are classified as various types of gabbro and norite, composed of anorthite-rich plagioclase, olivine (usually partially or completely altered) and pyroxenes. Many samples collected at the boundary of the intrusions are norites, with significant amounts of cordierite and biotite, indicating they probably formed from magma mixing with partial melts produced by anatexis of the country rocks. The parageneses of the overprinted metapelites of the country rock range from high grade hornfels within a few meters of the gabbro contact, with Opx+Grt+Sp+Plg+Bt+Crd+Cor assemblages, transitioning further out into middle-high grade Sill+Grt+Bt and calc-silicate rich assemblages, overprinting previous regional metamorphic assemblages that contained And+Cor. The high grade hornfels often contain thin, wispy, more leucocratic veinlets thought to be produced by partial melting. These mineral paragenesis, whole rock and mineral chemistry have been used to reconstruct PT-conditions. Preliminary geothermobarometric calculations indicate that the highest grade hornfels experienced peak conditions of around 900 °C and 4-6 kbar. Further studies are being conducted using trace elements distribution help to understand the role and origins of fluids involved in the metamorphism of the aureole and related anatexis. U-Pb age dating on zircons and monazites extracted from many samples will help constrain the absolute ages of both the gabbro intrusions and the adjacent regionally metamorphosed rocks. This range of methods should deliver new insights on the causal and temporal relationship between these intrusions and the regional metamorphic events (see Droop et al. 2003; Pattison et al. 2022).

Droop GTR, Clemens JD, Dalrymple DJ (2003): Processes and conditions during contact anatexis, melt escape and restite formation: the Huntly Gabbro Complex, NE Scotland. - *J Petrol* 44, 995-1029

Pattison DR, Goldsmith SA (2022): Metamorphism of the Buchan type-area, NE Scotland and its relation to the adjacent Barrovian domain. - *J Geol Soc* 179, <https://doi.org/10.1144/jgs2021-040>

P-T-t evolution of the Pulkau and Pleißing Nappes from the Moravo-Silesian Thaya Window, Lower Austria

M.J. Findl¹, C.A. Hauzenberger¹, E. Skrzypek¹, D. Gallhofer¹, M. Linner²

¹Department of Earth Sciences - NAWI Graz Geocenter,
University of Graz, Universitätsplatz 2, 8010 Graz, Austria

²Department of Hard Rock Geology, GeoSphere Austria, Neulinggasse 38, 1030 Vienna, Austria
e-mail: martin.findl@edu.uni-graz.at

The Moravo-Silesian Zone in the Bohemian Massif is a ~300 km long deformation zone that formed through underthrusting of the Brunia microcontinent beneath the Moldanubian–Lugian domain. The Moravo-Silesian zone crops out in three tectonic windows which are from north to south: (1) the Silesian zone, (2) the Svatka and (3) the Thaya windows, the last two being known as the Moravian zone sensu stricto. The Svatka and Thaya windows consist of a parautochthonous basement, a ~7 km thick pile of two nappes (the Lower and Upper Moravian Nappes) (Štípská et al. 2015). In relation to local ductile and brittle-ductile shear zones, only one major regional thrust runs through the Thaya Window, which separates the tectonically upper Pleißing (Lower and Upper Moravian Nappes) from the tectonically lower Pulkau Nappe (basement) (Linner et al. 2021). The research area is located in the Austrian part of the Thaya Window.

Samples taken along two SE-NW trending profiles (A and B) were used to constrain the P-T-t evolution of the Thaya Window using petrological modelling together with U-Pb zircon and Th-U-Pb monazite dating. Profile A, northern Thaya window: P-T estimates for the Pulkau Nappe are ~600 °C and 6.5-7.5 kbar and for the Pleißing Nappe slightly higher conditions of 550 °C up to 630 °C and 11 kbar. Graphite thermometry indicates 550±30 °C for the Pleißing Nappe. Two phase garnets can be clearly recognised in one sample. Inner garnet cores indicate P-T conditions of ca. 550 °C/5 kbar and inner garnet rims ca. 630 °C and 6 kbar.

Profile B, central Thaya Window: P-T estimates for the Pulkau Nappe are 600 °C and 8 kbar. Temperature is estimated to 603±30 °C (graphite thermometry) and 606±15 °C (Zr in rutile thermometry). The Pleißing Nappe exhibits 650-660 °C and 10.5-11 kbar, while graphite thermometry points to lower temperatures of 570±30 °C and 530±30 °C.

The Ky-Grt micaschists from Meiseldorf (Upper Moravian Nappe after Štípská et al. (2015); northwestern part of the Pleißing Nappe after Linner et al. (2021)) indicate 680-720 °C and 8-8.5 kbar based on petrological modelling and Zr in rutile thermometry.

Zircon dating by LA-MC-ICP-MS yields a weighted mean protolith ²⁰⁶Pb/²³⁸U age of 588±7.8 Ma for a metatuffite belonging to the Pleißing Nappe (profile A) and 592±7.8 Ma for a metatuffite from the Pulkau Nappe (profile B). Monazite commonly occurs in metapelite with grain sizes from 10-50 µm. In rare cases monazite can reach up to 100 µm. Th-U- total Pb chemical dating of monazite by EPMA yields 301-344 Ma in the Pleißing Nappe. ²⁰⁶Pb/²³⁸U monazite dates by LA-MC-ICP-MS range from 312 to 356 Ma.

We provide the first evidence for Ediacarian magmatism and coeval sedimentation for the protoliths of the Moravian zone. We confirm the occurrence of regional metamorphism from lower amphibolite to lower granulite facies conditions in the Austrian part of the Moravian zone and propose that peak P-T conditions were attained between 312 and 356 Ma based on monazite dating.

- Linner M, Rötzel R, Huet B, Hintersberger E (2021): A new subdivision for the Moravian Superunit - The redefined Pleißing and the newly defined Pulkau nappe. – In: Proceedings of the 4th Friends of the Bohemian Massif Meeting, October 7-10, Freistadt, Austria, 10
- Štípská P, Hacker BR, Racek M, Holder R, Kylander-Clark ARC, Schulmann K, Hasalová P (2015): Monazite dating of prograde and retrograde P–T–d paths in the Barrovian Terrane of the Thaya Window, Bohemian Massif. - J Petrol 56, 1007–1035, url: <https://doi.org/10.1093/petrology/egv026>

Computational studies of zeolites as adsorbents for the removal of pharmaceuticals and personal care products

M. Fischer^{1,2}, J. Brauer^{1,2}

¹*Crystallography & Geomaterials Research, Faculty of Geosciences, University of Bremen, Germany*

²*Bremen Center for Computational Materials Science and MAPEX Center for Materials and Processes,*

University of Bremen, Germany

e-mail: michael.fischer@uni-bremen.de

Pharmaceuticals and personal care products (PPCPs) have received considerable attention as emerging organic contaminants, with some members of this diverse group of compounds possessing a significant environmental hazard potential (Patel et al. 2019). Conventional wastewater treatment plants are not designed for the removal of these species, and a number of PPCPs show recalcitrant behaviour, entering water bodies and other environmental compartments. Adsorption-based processes constitute one possible technology that can improve the PPCP removal efficiency of wastewater treatment facilities. While carbon-based adsorbents are the most widely studied option, hydrophobic high-silica zeolites could be attractive alternatives due to their good regenerability and reduced co-adsorption of natural organic matter (Jiang et al. 2018). In this contribution, it will be discussed how atomistic modelling methods at different levels of theory can be employed to predict and understand the PPCP adsorption behaviour of these materials.

Given the diversity of zeolite frameworks that are available in highly siliceous form and the even larger number of PPCPs of possible environmental relevance, it is evident that an experimental investigation of all zeolite-PPCP combinations of potential interest would be extremely laborious. In previous work, it could be shown that relatively simple force field simulations deliver host-guest interaction energies that are well correlated with experimental removal efficiencies, providing a pathway to determine zeolite-PPCP combinations of potential interest prior to an experimental characterisation (Fischer 2020). Expanding upon this work, the implementation of a multi-step screening procedure allowed the exploration of a large number of combinations (>10 zeolites, >50 PPCPs) at relatively modest computational cost. Additionally, the capabilities of more sophisticated molecular dynamics simulations to calculate free energies of adsorption were explored. Such simulations allow direct predictions whether a given contaminant will be adsorbed in the zeolite or remain in solution.

Whereas the force field simulations are primarily employed for predictive purposes, dispersion-corrected density functional theory (DFT) calculations enable a more detailed understanding of the interactions that govern PPCP adsorption. Two recent studies dealt with the adsorption of carbamazepine (CBZ, Fig. 1a), an anticonvulsant medication, and triclosan (TCS, Fig. 1a), a disinfectant and preservative agent that is widely used in various products, in different zeolites (Fischer 2023a, Fischer 2023b). It was observed that the topology of the zeolite framework has a significant impact on the CBZ adsorption energy, whereas the interaction with TCS is largely determined by the pore size. This qualitative difference can be explained with the higher flexibility of TCS, which can adjust more readily to different pore shapes than the fairly rigid CBZ molecule. In addition to analysing factors that determine the strength of host-guest interactions, guest-guest interactions between co-adsorbed CBZ molecules were investigated. The study of TCS adsorption also addressed the competitive adsorption of the organic contaminant and water in zeolites having different framework compositions (all-silica zeolites and highly siliceous aluminosilicates, see Fig. 1b), permitting insights into the role of adsorbent hydrophobicity.

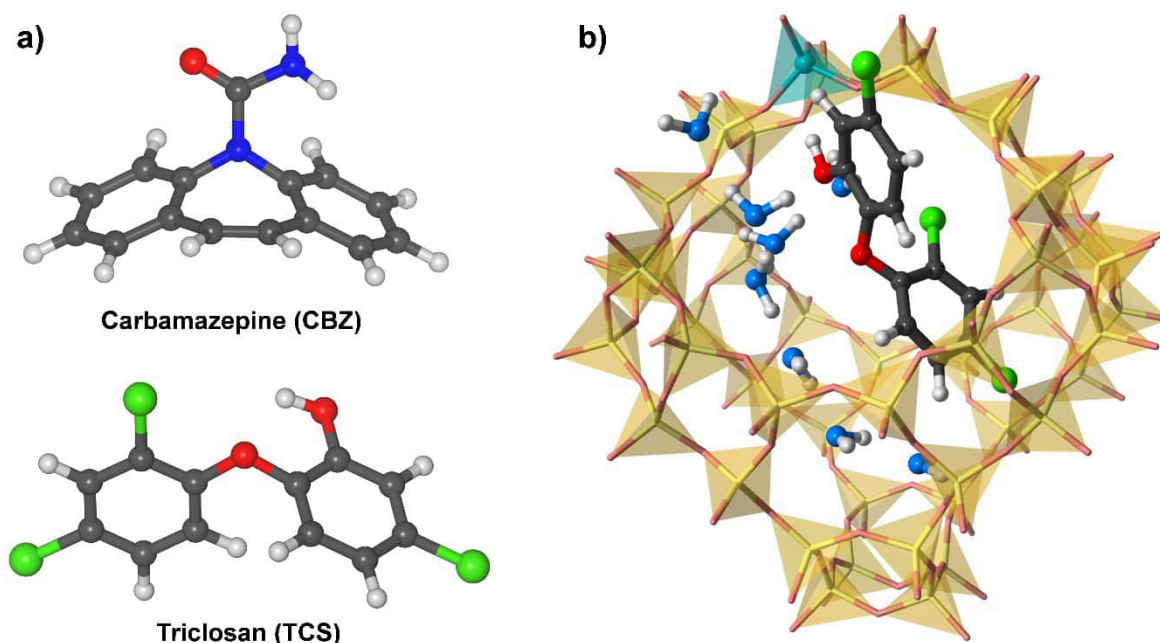


Figure 1. a) Molecular structures of carbamazepine and triclosan. b) Representative snapshot from a DFT-based molecular dynamics simulation addressing the co-adsorption of TCS and H₂O in protonated FAU-type zeolite.

Funding by the German Research Foundation (Deutsche Forschungsgemeinschaft) is gratefully acknowledged (projects 455871835 and 492604837).

Fischer M (2020): Simulation-based evaluation of zeolite adsorbents for the removal of emerging contaminants. – *Mater Adv* 1, 86

Fischer M (2023a): Adsorption of carbamazepine in all-silica zeolites studied with density functional theory calculations. – *Chem Phys Chem* 24, e202300022

Fischer M (2023b): Density functional theory study of hydrophobic zeolites for the removal of triclosan from aqueous solution. – *Environ Sci Adv* – accepted manuscript, DOI: 10.1039/D3VA00078H

Jiang N, Shang R, Heijman S G J, Rietveld, L C (2018): High-silica zeolites for adsorption of organic micro-pollutants in water treatment: A review. – *Water Res* 144, 145

Patel M, Kumar R, Kishor K, Mlsna T, Pittman C U, Mohan D (2019): Pharmaceuticals of Emerging Concern in Aquatic Systems: Chemistry, Occurrence, Effects, and Removal Methods. – *Chem Rev* 119, 3510

Twinning of götzenite and wöhlerite from the Fohberg phonolite, Kaiserstuhl

R.X. Fischer¹, J. Birkenstock¹, G. Biskup², L.A. Fischer³, W.-A. Kahl⁴, A. Klügel¹, S. Spürgin⁵

¹FB 5 Geowissenschaften, Universität Bremen, Klagenfurter Straße, 28359 Bremen, Germany

²Breslauer Straße 6a, 75181 Pforzheim, Germany

³Institut für Geo- und Umweltwissenschaften, Geochemie, Albert-Ludwigs-Universität Freiburg, Germany

⁴MAPEX Center for Materials and Processes, University of Bremen, 28359 Bremen, Germany

⁵Hans G. Hauri KG, Mineralstoffwerke, Bergstraße 114, 79268 Bötzingen, Germany

e-mail: rfischer@uni-bremen.de

Götzenite and wöhlerite were found as part of a fissure assemblage in the Fohberg phonolite (Kaiserstuhl, SW Germany), in close association with natrolite and clinopyroxene (aegirine-augite). Both minerals have a similar appearance with yellowish brown prismatic crystals as shown in Fig. 1. Single species were separated and investigated by single-crystal X-ray diffraction (SXR), electron probe microanalyzer (EPMA), laser ablation inductively coupled plasma mass spectrometry (LA-ICP-MS), and X-ray diffraction contrast tomography (DCT) showing the presence of two different phases, götzenite and wöhlerite.



Figure 1. Yellowish brown crystals of götzenite and wöhlerite in association with natrolite (white) and clinopyroxene (black). Widths of figures are 11 cm (top) and 5.7 mm (bottom), respectively.

Götzenite has a chemical composition of $\text{Na}_{1.5}\text{Ca}_{5.1}\text{Sr}_{0.1}\text{Zr}_{0.1}\text{Ti}_{0.8}\text{Nb}_{0.2}(\text{Si}_2\text{O}_7)_2\text{O}_{0.4}\text{F}_{3.7}$ with additional $\text{Fe}+\text{Mn}+\text{REE} < 0.3$. SXR D revealed rotation twinning on [001] (twin matrix -**a**-1/2**c**, -**b**, **c**; twin components 40:60) with lattice parameters $a = 9.6191(3) \text{ \AA}$, $b = 5.7342(2) \text{ \AA}$, $c = 7.3386(2) \text{ \AA}$, $\alpha = 89.986(1)^\circ$, $\beta = 101.040(1)^\circ$, $\gamma = 100.485(1)^\circ$, triclinic, space group $P\bar{1}$, refined to $R1 = 3.4 \%$.

Wöhlerite has a chemical composition of $\text{Na}_{1.6}\text{Ca}_{4.4}\text{Fe}_{0.2}\text{Mn}_{0.1}\text{Zr}_{0.6}\text{Ti}_{0.2}\text{Nb}_{0.8}(\text{Si}_2\text{O}_7)_2\text{O}_{2.4}\text{F}_{1.4}$ with additional $\text{Sr} + \text{REE} < 0.05$. SXR D revealed rotation twinning on [001] (twin matrix -**a**-**c**, -**b**, **c**; twin components 31:69) with lattice parameters $a = 10.842(1) \text{ \AA}$, $b = 10.249(1) \text{ \AA}$, $c = 7.2673(8) \text{ \AA}$, $\beta = 109.344(4)^\circ$, monoclinic, space group $P2_1$, refined to $R1 = 1.3 \%$.

The crystal structures closely resemble those of untwinned götzenite (Christiansen et al. 2003; Bellezza et al. 2004) and untwinned wöhlerite (Mellini et al. 1979; Biagoni et al. 2012), respectively.

Bellezza M, Merlino S, Perchiazzi N (2004): Chemical and structural study of the Zr,Ti-disilicates in the venanzite from Pian di Celle, Umbria, Italy. – *Europ J Mineral* 16, 957-969

Biagoni C, Merlino S, Parodi GC, Perchiazzi N (2012): Crystal chemistry of minerals of the wöhlerite group from the Los Archipelago, Guinea. – *Canad Mineral* 50, 593-609

Christiansen CC, Johnsen O, Makovicky E (2003): Crystal chemistry of the rosenbuschite group. – *Canad Mineral* 41, 1203-1224

Mellini M, Merlino S (1979): Refinement of the crystal structure of wöhlerite. – *Tschermaks Mineral Petrogr Mitt* 26, 109-125

Metamorphic reaction kinetics at anhydrous to water-saturated conditions

M. Franke¹, B.C. Schmidt², R. Stalder¹, B. Joachim-Mrosko¹

¹University of Innsbruck, Institute of Mineralogy and Petrography, Innrain 52, 6020 Innsbruck

²Department of Mineralogy and Petrology, Geoscience centre, Georg-August-University Göttingen,
Goldschmidtstraße 1, 37077 Göttingen
e-mail: bastian.joachim@uibk.ac.at

Metamorphic coronas and reaction rim structures are examples of a net-transfer reaction, where pre-existing mineral phases react to new phases. Growth of these metamorphic structures indicates a change in physical parameters such as pressure or temperature. One of the most important parameters that controls reaction rim growth is the presence of volatiles, which can affect rim thicknesses, phase stabilities or rim microstructures (e.g., Gardés et al. 2012). This implies that reaction rims have the potential to decipher the P-T-t-X history of a sample of interest.

In this study, reaction rim growth experiments were performed between periclase and quartz at nominally anhydrous to water-saturated conditions between 3 to 4 kbar and 1100 to 1300 °C for 66-168 h. Controlled minute amounts of water were added through OH-doped periclase, which allowed to perform experiments at controlled water-undersaturated conditions. For water-saturated experiments that contain wt% amounts of H₂O, controlled amounts of water were added in the form of brucite powder to the samples.

At anhydrous conditions, no reaction rim formed implying that water acts as a catalyst, and a minimum fluid threshold is needed to initiate metamorphic re-equilibration. In all experiments that used either water-doped periclase or brucite as source of water, the rim sequence Per | Fo | En | Qz developed. At water-undersaturated conditions, addition of minute amounts of water results in an increase in the overall reaction rim growth rate by more than 2 orders of magnitude while the relative forsterite/enstatite ratio increases from 0.6 to 2.4. At water-saturated conditions, growth rates reach a plateau value between 10⁻¹⁵ and 10⁻¹⁴ m²/s while forsterite/enstatite thickness ratios vary between 3 and 12.

This implies that reaction rim growth rates have the potential to monitor variations in water activity at those grain boundaries that serve as fast pathways for component transport at water-undersaturated conditions during metamorphic and metasomatic reactions in natural systems, allowing them to be used as sensitive “geohygrometers”. Additionally, the effect of water on relative layer thicknesses may provide an application for reaction rim microstructures to be used as new physico-chemical gauges that will allow us to discriminate between water-undersaturated and water-saturated conditions during metamorphic events.

Gardés E, Wunder B, Marquardt K, Heinrich W (2012): The effect of water on intergranular mass transport: New insights from diffusion-controlled reaction rims in the MgO-SiO₂ system. - Contr Mineral Petrol 164, 1–16

Bi-Te-S biomineralization in Precambrian Volyn biota (Ukraine)

G. Franz¹, R. Wirth², A. Schreiber², V. Khomenko^{1,3}

¹*Institut für Angewandte Geowissenschaften, Technische Universität Berlin*

²*Deutsches GeoForschungsZentrum Potsdam*

³*Institute of Geochemistry, Mineralogy and Ore Formation, Academy of Sciences, Kyiv*
e-mail: gefra548@gmail.com; gerhard.franz@tu-berlin.de

The Volyn biota represent an ancient subsurface lithoautotrophic microecosystem with a minimum age of ca. 1.5 Ga (Franz et al. 2023). The fossils are exceptionally well preserved in 3D due to their occurrence in cavities of pegmatites of the 1.8 to 1.7 Ga old Korosten Pluton in NW Ukraine, which experienced no diagenesis, metamorphism or deformation, which is very often the case in sediments. The fossilization occurred during influx of hot, HF-bearing fluids from the granitic source into the largemiarolitic cavities, producing a μm -wide rim of Al-silicate minerals (Franz et al., 2022). Some of the fossils were interpreted as biofilms (extracellular protein substance), others show similarities to filamentous fungi-like organisms, supported by the presence of chitosan, others are interpreted as methanogenic organisms.

In some of these filamentous and bulbous fossils we identified mineral inclusions with a size of approximately 50 to 100 nm. These nano-inclusions occur in the central part of the fossils, excluding their origin as post-mortem inclusions. Their composition is variable in the samples, but all are characterized by Bi-Te-S. In one sample they are randomly oriented in a distance of several micrometer. The composition is close to the minerals ingodite $\text{Bi}(\text{S},\text{Te})$ or joseite $\text{Bi}_4(\text{S},\text{Te})_3$.

In another sample, they occur in a central channel of the organisms, characteristic for some of the filamentous fossils. These nanoparticles are up to approximately 200 nm large, concentrated in aggregates, and their composition is dominantly Bi-Cu-S with Te and Pb as additional components. Electron diffraction patterns of these mosaic crystals indicate an orthorhombic phase with $a = 7.70 \text{ \AA}$, $b = 10.4 \text{ \AA}$, $c = 6.75 \text{ \AA}$, consistent with the phase Cu_3BiS_3 . Crystals away from the channel show the same composition Bi-Te-Pb-Cu.

In a bulbous fossil object, the nano-sized biominerals are arranged in groups of several crystals. Their composition is dominantly Bi-Te-S. These crystals are connected by a filament of amorphous material, a few nanometers wide, and similar filamentous extensions from the nanocrystals were observed (Fig. 1).

In modern fungi, Liang et al. (2019) observed the formation of Te- (and Se-) nanoparticles during growth experiments with different fungal species, and microbial reduction of Te (and Se) species shows the immobilization of these elements in intracellular and extracellular nanoparticles (Liang et al., 2020), supporting the interpretation of the fossils as fungi-like organisms.

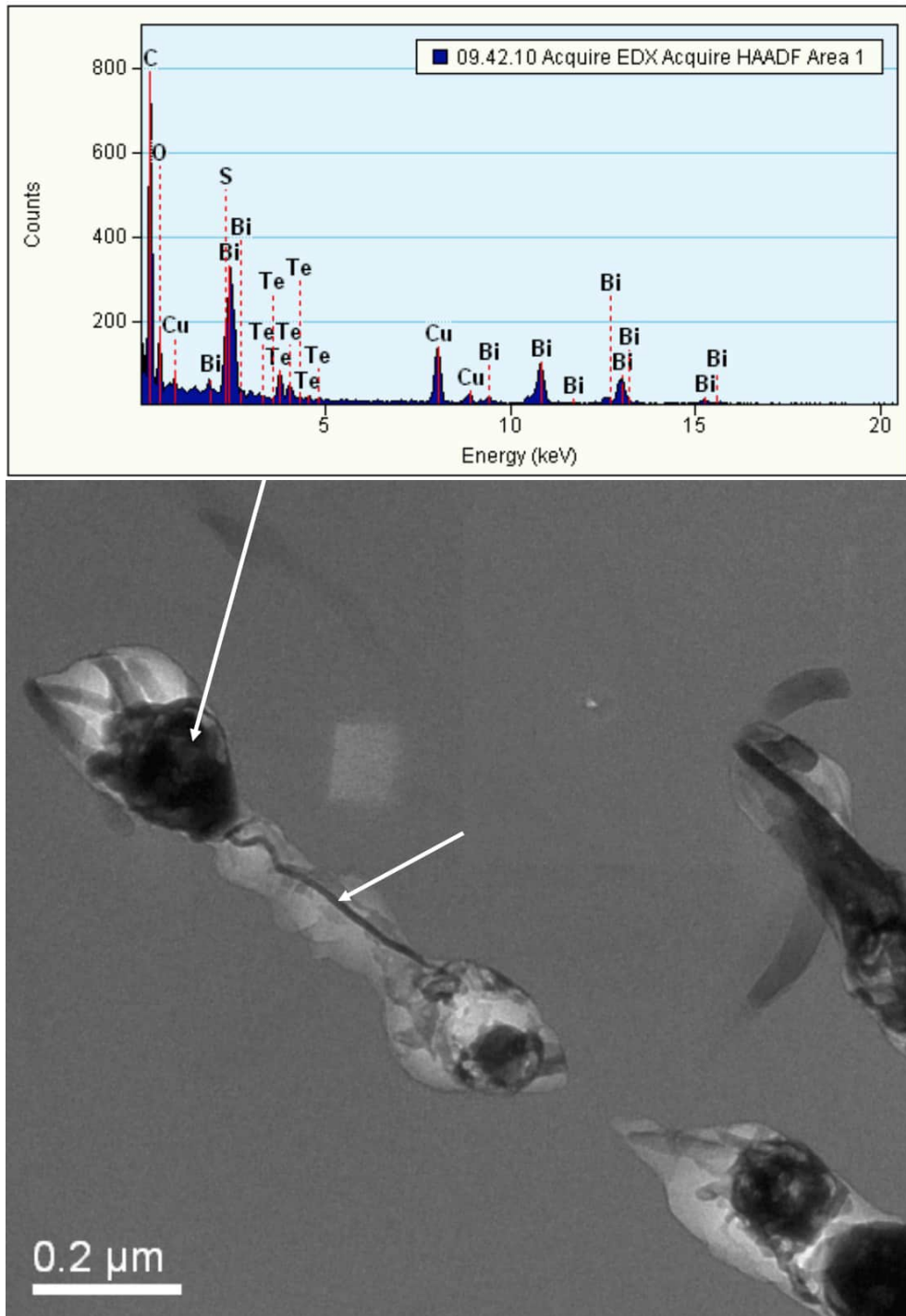


Fig. 1: TEM image and EDS analysis of biominerals in the Volyn biota. Arrows point to the location of the analysis and the thin connection of the nanoparticles.

Franz G, Lyckberg P, Khomenko V, Chournousenko V, Schulz H.-M, Mahlstedt N, Wirth R, Glodny J, Gernert U, Nissen J (2022): Fossilization of Precambrian organic matter (kerite) from the Volyn pegmatite, Ukraine. - *BioGeosciences* 19, 1795

Franz G, Khomenko V, Lyckberg P, Chernousenko V, Struck U, Wirth R, Gernert U, Nissen J (2023): The Volyn biota (Ukraine) – indications for 1.5 Gyr old eucaryotes in 3D-preservation, a spotlight on the ‘boring billion’. - *BioGeosciences* 20, 1901

Liang X, Perez MAM-J, Zhang S, Song W, Armstrong JG, Bullock LA, Feldman J, Parnell J, Csetenyi L, Gadd GM (2019): Fungal formation of selenium and tellurium nanoparticles. - *Appl Microbiol Biotech* 103, 7241

Liang X, Perez MAM-J, Zhang S, Song W, Armstrong JG, Bullock LA, Feldman J, Parnell J, Csetenyi L, Gadd GM (2020): Fungal transformation of selenium and tellurium located in a volcanogenic sulfide deposit. *Env Microbiol* 22, 2346

Extreme chemical disequilibrium patterns in hydrothermal vein minerals – a case study from Columbian emeralds

G. Franz¹, V. Khomenko^{1,2}, F. Schiperski¹, U. Gernert³, J. Nissen³

¹Institut für Angewandte Geowissenschaften, Technische Universität Berlin

²Institute of Geochemistry, Mineralogy and Ore Formation, Academy of Sciences, Kyiv

³Zentraleinrichtung Elektronenmikroskopie Technische Universität Berlin

e-mail: gefra548@gmail.com; gerhard.franz@tu-berlin.de

Chemical zoning in metamorphic and igneous minerals has been shown to be a very powerful tool for reconstruction of pressure-temperature-time condition of growth of minerals. Vein minerals have also been in the focus because of their common occurrence with economically interesting mineralizations. Columbian emeralds formed in veins in low-grade metamorphic black shales; they are known as highly-prized gemstones and have been studied extensively over the years (e.g., Pignatelli et al. 2015; Schmetzer & Martyan 2023). We present data about their growth phenomena, from combined element distribution mappings with μ -XRF and the electron microprobe EMPA in oriented thin sections, and from scanning electron microscopy SEM.

External growth phenomena are small indentations on the basal plane (0001), which are interpreted as an expression of skeletal growth along the c -axis of the beryl, and rare sceptre growth. Chemical zoning shows very unusual patterns with sector zoning, which is however variable for different elements in different crystals. Sector boundaries are in some instances straight, or curved, or serrate (Fig. 1). In addition to sector zoning, stripes in the a - and c -sector were observed with alternating chemical composition. Most unusual are chemical patterns produced by the substitution $\text{Al} + \square(\text{channel}) = \text{Mg} + \text{Na}$, with straight borders, but neither parallel nor perpendicular to the c -axis (Fig. 2). Another unusual feature was observed in the root zone of the crystals with cone-shaped structures extending in c -direction from a homogeneous zone.

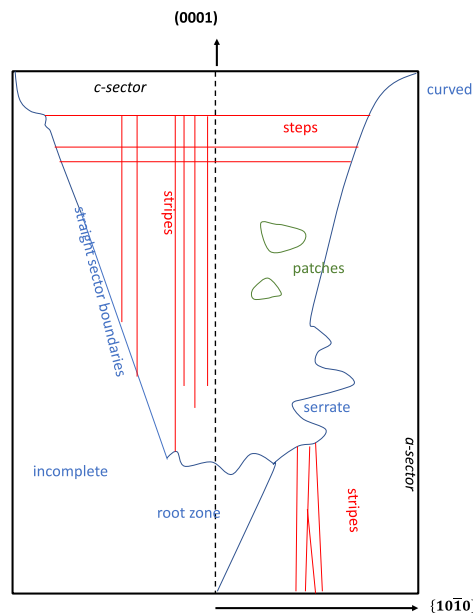


Fig. 1: Chemical zoning patterns in Columbian emerald

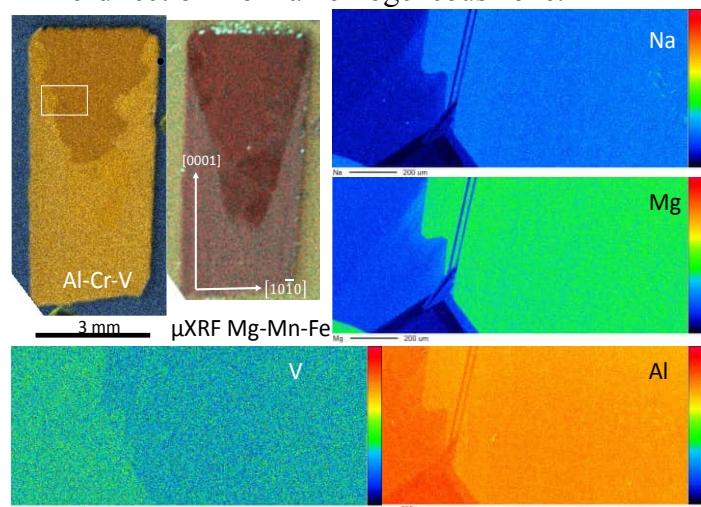


Fig. 2: Element distribution maps for crystal no. 2; left part shows combined intensities for μ XRF for the whole crystal, other images results from EMPA mapping of a selected area (white frame in Al-Cr-V-mapping).

Freely grown crystals, such as beryls in open veins are often characterized by dissolution-formed etch pits. The Columbian emeralds also show such etch pits, with different shapes (rectangular, diamond-shaped), originating from point- as well as line-defects. They are typically arranged in chains, parallel and oblique to the beryl's *c*-axis (Fig. 3), what has not been observed in pegmatitic beryls (Kurumathoor & Franz 2018). These chains of etch pits point to screw-dislocation arrays and are another indication for rapid growth of the crystals. In summary, both features of growth and dissolution phenomena point to extreme disequilibrium.

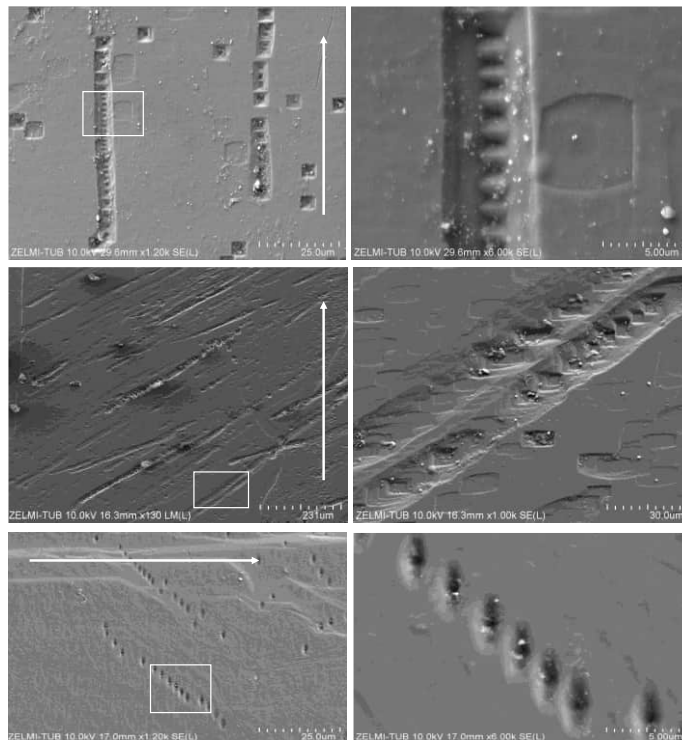


Fig. 3: SEM images of the first-order prism face of Columbian emeralds. Etch pits are arranged in chains, indicating dislocation arrays. Direction of *c*-axis is indicated by the arrow.

- Kurumathoor R, Franz G (2018): Etch pits in beryl as indicators for dissolution behaviour. – *Eur J Miner* 30, 107-124
- Pignatelli I, Giuliani G, Ohnenstetter D, Agrosi G, Mattheu S, Moriot C, Branquet Y (2015): Colombian trapiche emeralds: Recent advances in understanding their formation. - *Gems & Gemology* 51, 222-259
- Schmetzer K, Martayan G (2023): Morphology of Columbian emerald: some less-common cases and their growth and dissolution history. – *Gems & Gemology* 59, 46-71

High-Ti Paleozoic basalts in NE Bavaria

G. Franz¹, F. Lucassen², F. Schiperski¹, M. Kutzschbach¹

¹*Institut für Angewandte Geowissenschaften, Technische Universität Berlin*

²*MARUM-Center for Marine Environmental Sciences-Universität Bremen*

e-mail: gefra548@tu-berlin.de; gerhard.franz@tu-berlin.de

The Paleozoic sedimentary rocks, surrounding the Münchberg Massif with its relict high-pressure nappe pile in NE Bavaria, host Ordovician to Devonian mafic volcanic and subvolcanic rocks (commonly named diabase in the German literature) that formed timely close to the deposition of the sediments. In the W and SW of the Münchberg Massif, these rocks were previously studied for age, structure and chemical composition by Höhn et al. (2018); similar rocks can be found in the E of the Münchberg Massif. Late Carboniferous granites of the Fichtelgebirge represent the next magmatic pulse, and post-Variscan mafic dikes intruded these granites as well as the metamorphic series of the Münchberg Massif.

The focus of this study is the elemental composition of stratigraphically well-defined mafic volcanic rocks from the (meta)sedimentary Thuringian facies E of the Münchberg Massif (E-domain) and post-Variscan mafic dikes from this Massif, and the Sr, Nd, and Pb isotope compositions of these mafic volcanic rocks and comparison with previously studied mafic rocks from the W domain (Höhn et al. 2018). Of special interest are the unusually high Ti-contents.

The Ordovician diabase rocks from the E and the Devonian rocks from the W are characterized by high TiO₂-contents up to almost 6 wt%, accompanied by high Fe₂O_{3(tot)}-contents of up to almost 20 wt%. The initial ⁸⁷Sr/⁸⁶Sr_i of E Ordovician samples are variable (0.7031 to 0.7107) and most initial εNd_i (+2.8 to +6.3) closely scatter around +5 irrespective the locality and without covariation of Nd and Sr isotopes. The E post-Variscan dikes show a similar range of ⁸⁷Sr/⁸⁶Sr_i (0.7052 to 0.7081) but, compared with E Ordovician, much lower εNd_i between -1.3 and +0.9. The W Ordovician-Silurian samples show only a small variation ⁸⁷Sr/⁸⁶Sr_i (0.7033 to 0.7039) and εNd_i (+2.8 to +3.4). The ⁸⁷Sr/⁸⁶Sr_i (0.7042 to 0.7046) of the W Devonian rocks is rather uniform, but εNd_i is variable in two clusters, +4.8 to +6.1 and +2.3 to +2.5, that resemble the εNd_i of E and W Ordovician rocks. Initial uraniumogenic Pb isotope compositions of most Ordovician and Devonian samples from both domains plot in overlapping arrays above or near the crustal Pb-evolution line (Stacey and Kramers, 1975). The W Silurian rocks are different and show the highest ²⁰⁷Pb/²⁰⁴Pb_i and ²⁰⁶Pb/²⁰⁴Pb_i of the whole sample suite. The initial ²⁰⁸Pb/²⁰⁴Pb of all sample groups plot in a similar array except the Silurian samples with the two the highest and the lowest ²⁰⁸Pb/²⁰⁴Pb_i values. The E post Variscan dikes have a chemical signature which is clearly different from the Ordovician rocks.

The data are discussed in the context of the paleotectonic position of the rocks, the southern passive margin of the Rheic ocean bordering northern Gondwana or alternatively a separate Saxo-Thuringian Ocean between a Gondwana derived microcontinent and Gondwana.

Höhn S, Koglin N, Klopff L, Schüssler U, Tragelehn H, Frimmel H, Zeh A, Brätz H (2018): Geochronology, stratigraphy and geochemistry of Cambrian, Ordovician, Silurian and Devonian volcanic rocks of the Saxothuringian in NE Bavaria (Germany). – *Int J Earth Sci* 107, 359-377

Stacey JS and Kramers JD (1975): Approximation of terrestrial lead isotopic evolution by a two-stage model. – *Earth Planet Sci Lett* 26, 207-221

Enzymatically induced apatite formation as a key mechanism in fish fossilization – an experimental study

F. Gäb¹, S. Karačić², R. Wirth³, G. Bierbaum², C. Bultmann⁴

¹Institut für Geowissenschaften, University of Bonn,

²Institut für medizinische Mikrobiologie, University Hospital

³GFZ Potsdam

⁴Radiomed Gemeinschaftspraxis für Radiologie und Nuklearmedizin, Wiesbaden

e-mail: fgaeb@uni-bonn.de

Exceptionally preserved fish fossils are known from various locations and throughout most of Earth's history. They play an important role in understanding the history of life and process of evolution, yet the process that leads to their formation remains mostly unclear. Phosphorous is a scarce resource in the whole modern ocean and there is no evidence for this being different over the Phanerozoic. Nevertheless there are numerous examples for fish fossils preserved in apatite e.g. Solnhofen Plattenkalk (Jurassic of S' Germany), Gogo Fm. (Devonian of N' Australia) or Santana Fm. (Cretaceous of E' Brazil). Hence there is a need for a mechanism that provides exceptionally high amounts of P to facilitate the precipitation of large quantities of apatite.

In this study we investigate the role of microbially produced alkaline phosphatase (AP) as a source for the needed phosphate. AP is an ubiquitous enzyme throughout the world of bacteria and liberates phosphate from organic (macro)-molecules. It is known to provide phosphate for the formation of apatite *in vitro* (Cosmidis et al. 2015).

We conducted experiments, where AP was used to liberate phosphate from organic matter and, through oversaturation of the surrounding fluid, ultimately precipitated inorganically as apatite on fish scales. This might be the first step towards permineralization of the organic matter that is needed for fossilization. To strengthen the hypothesis the resulting apatite crystals were compared using TEM analysis with existing fossils. The result of these investigations showed a striking mineralogical similarity between the laboratory made and natural apatite crystals. This suggests that inorganic precipitation of apatite from an oversaturated solution indeed is a possible pathway for permineralization of a carcass which would ultimately lead to an exceptionally preserved fossil. Additionally this could mean that the fossil itself could be used as a geochemical and petrological indicator for the surrounding conditions, both of the sediment and the seawater, during its formation.

Cosmidis J, Benzerara K, Guyot F, Skouri-Panet F, Duprat E, Férard C, Guigner J-M, Babonneau F, Coelho C (2015): Calcium-phosphate biomineralization induced by alkaline phosphatase activity in *Escherichia coli*: localization, kinetics, and potential signatures in the fossil record. – *Frontiers in Earth Science* 3, 84

Relationships between fluid-flow, fluid-rock-interaction, and evolving microstructures in a polyphase system – results from experimental approaches using synthetic impure carbonates

J. Gätjen¹, B. Rose¹, D. Sorger¹, S. Piazzolo², T. Müller¹

¹*Geoscience Centre Göttingen, Georg-August-University, Germany*

²*School of Earth and Environment, The University of Leeds, United Kingdom*
e-mail: jochen.gaetjen@uni-goettingen.de

In polyphase materials (e.g., porous rocks), fluid-mineral-reactions typically result in complex microstructural changes – including a spatial and temporal evolution of fluid pathways. However, a full quantitative understanding of the accompanied processes governing the development of such microstructures remains elusive. In this experimental study, we focus on the wollastonite forming reaction in a synthetic impure carbonate system with two reactants (calcite + quartz) and two products (wollastonite + CO₂) phases. This decarbonation reaction causes a negative 33 % volume change of the solid phase.

The experiments were carried out using a rapid quench cold seal apparatus. In a first step, a CaCO₃-SiO₂-mixture (~ 7:3) was pressurized to 0.2 GPa together with a fluid phase (~ 5 wt% H₂O, initial $X(\text{CO}_2) = 0.5$) and heated to 600 °C for one week allowing the powder to recrystallize and anneal prior to overstepping of the reaction (initial porosity = ~ 13 vol%). In a second step, we increased the temperature (700 °C or 800 °C) to trigger the decarbonation reaction for an additional week.

Preliminary results indicate that variations in the reaction affinities govern the resulting microstructures. Experiments with conditions close to the equilibrium state (T = 700 °C, final $X(\text{CO}_2) = 0.56$, final porosity = ~ 20 vol%) exhibit low nucleation rates in combination with relative high growth rates resulting in a slightly more porous microstructure with a few idiomorphic wollastonite grains growing in the pore space. Here, only a small amount of SiO₂ and CaCO₃ reacted to form CaSiO₃ and CO₂ as the system reached the equilibrium state due to the evolving $X(\text{CO}_2)$ fluid composition in the internally buffered system. Experiments conducted at conditions far away from the equilibrium state (T = 800 °C, final $X(\text{CO}_2) = 0.86$) exhibit very high nucleation rates combined with comparatively low growth rates. Here, the reaction went to completion consuming all of the SiO₂ without reaching the equilibrium state. The remaining CaCO₃ grains are interconnected by a very porous (~ 35 vol%) nano- to microcrystalline mass of wollastonite.

Future experimental work will include piston cylinder experiments, fluid-flow experiments and time series. Quantitative orientation analysis using EBSD (Electron Backscatter Diffraction) will provide information about the micro/nano-structure of the material while serial sectioning within an SEM or NanoCT scanning will allow for porosity and permeability assessment. The experimental setup will be extended to include a mineral reaction with positive volume change (periclase + H₂O = brucite) – as well as a combination of both reaction types.

Mineral assemblage, geochemistry and geochronology of the Kawisigamuwa carbonatite, Sri Lanka

D. Gallhofer¹, E. Skrzypek¹, C.A. Hauzenberger¹, G. Auer¹, G.W.A.R. Fernando²

¹*Institute for Earth Sciences, University of Graz*

²*Department of Physics, The Open University of Sri Lanka*

e-mail: daniela.gallhofer@uni-graz.at

The Kawisigamuwa and Eppawala carbonatites in Sri Lanka are located within upper amphibolite to granulite facies metasedimentary and metaigneous rocks of the Wannu Complex. Both occurrences have previously been interpreted as mantle-derived carbonatites, however, a recent study has shown that the Eppawala carbonatite was derived from melting of a sedimentary carbonate protolith (Wang et al. 2021). Since the origin and formation of the Kawisigamuwa carbonatite is still unclear, this study investigates its mineral paragenesis, geochemistry (XRF, EPMA, IRMS), and geochronology (LA-ICPMS).

Textural relationships indicate the following sequence of mineral formation: 1) calcite, olivine, zircon 1, phlogopite, apatite, baryte, celestine, and spinel (?) form the primary mineral assemblage, 2) dolomite, monazite, zircon 2, baddeleyite, magnetite, spinel, ilmenite, and sulfides, 3) zirconolite, allanite, and Th-rich phases and a late stage of 4) serpentinization of olivine and weathering products of Fe-oxides and other minerals.

The Kawisigamuwa carbonatite is dominated by calcite (48-51.7 wt.% CaO), has low SiO₂ (<2.3 wt.%) and P₂O₅ (<0.14 wt%) and elevated Sr (4497-4930 µg/g), La (56-188 µg/g), and Ce (164-422 µg/g) contents. Olivine has moderately high x_{Mg} (0.85-0.91) and is surrounded by reaction coronae of tremolite and/or diopside and dolomite. Phlogopite has x_{Mg} ranging from 0.88 to 0.92, elevated Ba (0.04-0.19 apfu) and moderate F (0.35-0.56 apfu) contents. Oxygen ($\delta^{18}\text{O}_{\text{VSMOW}} = 13.75$ to 14.14) and carbon ($\delta^{13}\text{C}_{\text{VPDB}} = -2.73$ to -2.52) isotopes of calcite from Kawisigamuwa overlap those of Eppawala and are slightly lower than those of Sri Lankan marbles. Fractionation of oxygen isotopes between calcite and zircon indicate an equilibrium temperature of ~850 °C.

Geochronological data support a multi-stage evolution of the mineral assemblage at Kawisigamuwa: 1) oscillatory zoned zircon 1 yields the crystallisation age of 532.39 ± 0.66 Ma, 2) recrystallisation lead to partial resetting of U-Pb ages and formation of zircon 2 at 518 Ma or later and 3) a late stage of (re-)crystallisation is recorded by allanite (U-Pb ca.474 Ma).

While the Kawisigamuwa carbonatite shows mineral assemblages and some geochemical characteristics consistent with mantle-derived carbonatites, the mineral chemical and isotopic characteristics do not support a mantle origin. We suggest that the Kawisigamuwa carbonatite is another example of a crustal-derived anatectic carbonate body.

Zircon preservation in hybrid magmas from Mt. Hasan stratovolcano, Central Anatolia, and implications for magma mixing dynamics

G. Gencoglu Korkmaz^{1,2}, K.A. Cionoiu², A.K. Schmitt^{2,3}

¹Konya Technical University, Department of Geological Engineering, Konya, Turkey

²Heidelberg University, Institute of Earth Sciences, Heidelberg, Germany

³Curtin University, John de Laeter Centre, Perth, Australia

e-mail: Gulin.Gencoglu@geow.uni-heidelberg.de

Mt. Hasan, or Hasan Dağ, is a prominent stratovolcano within the Cappadocian Volcanic Province of central Anatolia. It experienced recurrent eruptions of mostly andesitic-dacitic lava flows from its main edifice on average every 5,000 to 15,000 years over the past 100 ka (Friedrichs et al. 2020). The northeastern flank of Mt. Hasan is dissected by a strand of the Tuz Gölü fault zone (TGFZ) with significant vertical and dextral offsets that in part have displaced lava coulees erupted from the eastern vent region of Mt. Hasan (little Mt. Hasan, or Küçük Hasan Dağ) from their respective source vents (Krystopowicz 2015). The volcano is underlain by a long-lived evolved magma reservoir that has remained viable for producing explosive and effusive eruptions since at least 550 ka (Friedrichs et al. 2020). Mafic magma recharge as evident by the presence of abundant rounded enclaves in Mt. Hasan lavas and geochemical mixing trends (Aydar & Gourgaud 1998) plays an important role in maintaining the magma system viable for such protracted durations. Here, we report mineral and whole-rock geochemical results for a suite of five lava flows from the eastern part of Mt. Hasan which were sampled on both sides of the TGFZ to provide piercing points for fault reconstruction. All lava flows yielded zircon, despite whole-rock compositions and mineral temperatures being clearly outside zircon saturation conditions. The implications of this observation on the timescales and processes of magma mixing are discussed here; geochronological analysis of zircon using U-Th and (U-Th)/He methods to determine crystallization and eruptions ages, respectively, is ongoing.

The investigated lavas compositionally span from basaltic andesite to dacite. They show hypocrySTALLINE porphyritic textures with varying amounts of glass. Basaltic andesites primarily consist of plagioclase, olivine, pyroxene, Fe-Ti oxides, and additionally quartz, which based on embayments and ocellar textures is considered xenocrystic. In the andesites, plagioclase, pyroxene, and Fe-Ti oxide minerals are commonly present, along with amphibole (often with breakdown textures), and rare olivine. Dacites, on the other hand, contain plagioclase, amphibole, pyroxene, Fe-Ti oxides, and scarce quartz microphenocrysts. Apatite and zircon are present as accessory minerals in all lavas. Plagioclase pheno-microphenocrysts in almost all investigated rocks generally show inverse and oscillatory zoning with An-contents between 33 and 70 mol% and total FeO between 0.19 and 0.75 wt%. They typically display various types of sieve textures. Amphibole is ubiquitous in the lavas, and is mostly classified as Mg-rich hornblende. However, the degree of preservation in the basaltic andesite-andesite lavas is low as indicated by intense opacification and thick breakdown rims (4–8 µm). In the dacite lavas, amphibole represents the primary mafic phase and is mostly intact. Except in the most mafic lava flow, minor amounts of biotite are present in the groundmass, typically surrounded by breakdown reaction rims. Olivine with Fo = 89–86 mol% in basaltic andesite-andesite lavas is compositionally in disequilibrium with their host. In comparison, the andesitic lavas contain olivine with lower Fo contents ranging from 79 to 84 mol%. Diopsidic augite and enstatitic orthopyroxenes are commonly present, and they are variably zoned.

Mineralogical and petrographic features of Mt. Hasan lavas indicate a hybrid nature, where evolved magmas were reheated by mafic recharge. The evolved magma resided at comparatively low temperatures in an upper crustal magma reservoir ($T = 800\text{--}835\text{ }^{\circ}\text{C}$, $P = 110\text{--}150\text{ MPa}$, based on amphibole geothermobarometry using the calibration of Ridolfi (2021), whereas eruption temperatures based on Fe-Ti-oxide pairs are up to $910\text{ }^{\circ}\text{C}$. Taking new and published data for Mt. Hasan (e.g., Aydar & Gourgaud 1998) into account, kinked trends in major element oxides variation diagrams indicate a combination of magma mixing and fractional crystallization. Magma mixing between basaltic and dacitic endmembers can explain the hybrid basaltic andesites, whereby the basaltic endmember is more primitive than the erupted compositions of Mt. Hasan as indicated by the preservation of high-Fo (Fig. 1) and high-Ni olivine in the hybrid lavas. A compositional equivalent to the mafic endmembers in these mixing scenarios are basaltic scoria cones erupted in the vicinity of Mt. Hasan (Gencoglu Korkmaz et al. 2022; Reid et al. 2017). Zircon is preserved in even the most mafic hybrid lavas, where strong undersaturation and high Zr diffusivity in the melt would nominally dissolve zircon at rates of $\sim 10^{-11}\text{ m/s}$ ($900\text{ }^{\circ}\text{C}$), so that a zircon sphere $50\text{ }\mu\text{m}$ diameter would become completely resorbed by the melt within ca. 7 weeks. This implies that zircon was either shielded as inclusions in phenocrysts, or that mixing and hybridization occurred only briefly before eruption.

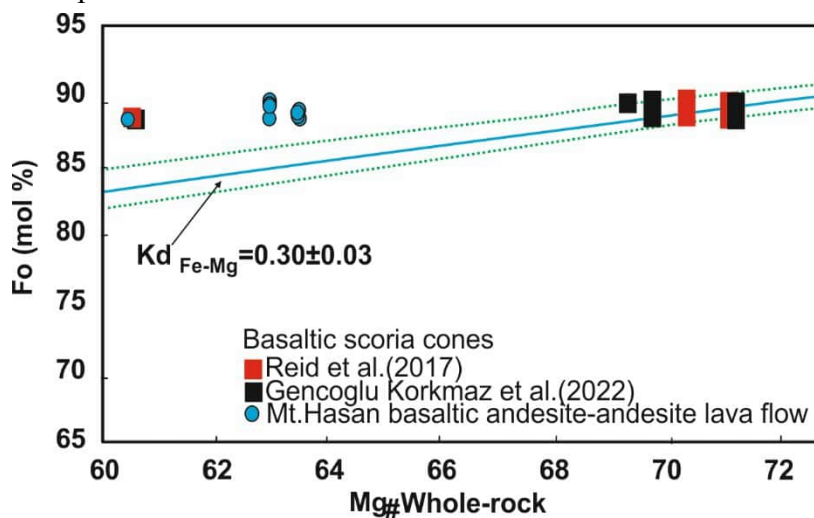


Figure 1. Whole-rock $\text{Mg}\#$ versus Fo (mol%) for olivine from northeastern Mt. Hasan basaltic andesite and andesite lava flows. Whole-rock and olivine compositions from scoria cones from the southwestern part of the Cappadocian Volcanic Province (Reid et al. 2017; Gencoglu Korkmaz et al. 2022) are shown for comparison.

Aydar E, Gourgaud A (1998): The Geology of Mount Hasan Stratovolcano, Central Anatolia, Turkey. - *J Volcanol Geotherm Res* 85, 129-152

Friedrichs B, Atıcı G, Danisik M.A, Çobankaya M, Harvey JC, Yurteri E, Schmitt AK (2020): Late Pleistocene eruptive recurrence in the post-collisional Mt. Hasan stratovolcanic complex (Central Anatolia) revealed by zircon double-dating. - *J Volcanol Geotherm Res* 404, 107007

Gencoglu Korkmaz G, Kurt H, Asan K, Petrelli M, Leybourne M (2022): The role of peridotite and pyroxenite melts in the origin of the Karapınar basalts, Cappadocia Volcanic Province, Central Anatolia. - *J Geosci* 67, 311-329

Krystopowicz NJ (2015): Constraining deformation, uplift, and activity along the Tuz Gölü fault zone, Central Anatolia, Turkey. - Master Thesis, Applied Science: University of Toronto

Reid MR, Schleiffarth WK, Cosca MA, Delph JR, Blichert-Toft J, Cooper KM (2017): Shallow melting of MORB-like mantle under hot continental lithosphere, Central Anatolia. - *Geochem Geophys Geosyst* 18, 1866-1888

Ridolfi F (2021): Amp-TB2: An updated model for calcic amphibole thermobarometry. - *Minerals* 11, 324

Eveslogite – Decoding the complexity of eveslogite through three-dimensional electron diffraction

E. Götz¹, M. Klementová², W. Depmeier³, S. V. Krivovichev^{4,5}, M. Czank³, M. Schowalter⁶, L. Palatinus², U. Kolb^{1,7}

¹*Institute of Applied Geosciences, Geomaterial Science, Technical University of Darmstadt, Germany*

²*Department of Structure Analysis, Institute of Physics of the Czech Academy of Sciences, Prague, Czech Republic*

³*Institute of Geosciences, Kiel University, Germany*

⁴*Kola Science Centre, Russian Academy of Sciences, Apatity, Russia*

⁵*Department of Crystallography, St. Petersburg State University, St. Petersburg, Russia*

⁶*Institute of Solid State Physics, University of Bremen, Germany*

⁷*Centre for High-Resolution Electron Microscopy, Johannes Gutenberg University, Mainz, Germany*

e-mail: Emilia.goetz@tu-darmstadt.de

Eveslogite is an exceptionally complex mineral, found exclusively at Mt. Eveslogchorr, located in the Khibiny alkaline massif, Kola peninsula, Russia. It occurs as a late-hydrothermal formation in veins breaching a poikilitic nepheline syenite, called rischorrite. Despite its discovery in 2003, the structure of eveslogite remained elusive due to its intricacies and the limitations of available methods and instruments at that time (Men'shikov et al. 2003). It was originally thought that the structure resembled that of a heterophyllosilicate (Ferraris & Gula, 2005), but doubts regarding the applicability of the modular approach arose after the crystal structure of a similar mineral, yuksporite, was determined (Krivovichev et al., 2004).

To overcome these challenges, advanced techniques such as three-dimensional electron diffraction (3DED; Gemmi et al., 2019) was used to determine the structure and high-angle annular dark-field scanning transmission electron microscopy (HAADF-STEM) was employed to verify it. These methods allowed the investigation of the eveslogite structure at the nanoscale, as the small crystal size and complex twinning prevented the use of traditional X-ray diffraction techniques. Additionally, energy dispersive X-ray spectroscopy (EDS) provided valuable insights into the elemental composition of the mineral.

Contradictory previous findings (Men'shikov et al., 2003) new cell parameters were proposed ($a = 14.2359 \text{ \AA}$, $b = 44.8242 \text{ \AA}$, $c = 15.9058 \text{ \AA}$, $\alpha = 90^\circ$, $\beta = 109.658^\circ$, $\gamma = 90^\circ$, with a cell volume of 9558.08 \AA^3) and the space group $P2_1$ was unambiguously assigned. This revised cell facilitated the structure determination of eveslogite, which comprises 345 symmetrically independent atom positions [see Figure 1(A)]. Based on the average elemental composition the sum formula of eveslogite is $\text{K}_{17.5}(\text{Ba},\text{Sr})_8(\text{Na},\text{Ca})_{40}[(\text{Ti},\text{Nb},\text{Fe},\text{Mn})_{11}\text{Si}_{62}\text{O}_{179}(\text{OH},\text{F})_{12}(\text{O},\text{OH})_{13}](\text{H}_2\text{O})$. The essential building blocks that make up the eveslogite structure are heterosilicate tubular chains (see Figure 1(B) and (C)) as well as double-tubes (see Figure 1(D) and (E)), extending along the a -axis. Zig-zag rows of the tubular building units are interconnected by ribbons of $(\text{Ca},\text{Na})\text{O}_x$ polyhedra likewise extending along $[100]$. The heterosilicate tubular building units of eveslogite show a certain degree of similarity with silicate-only modules occurring in charoite and denisovite (Rozhdestvenskaya et al., 2010; Rozhdestvenskaya et al., 2017). Additional diortho-silicate groups are always connected with the heteroatoms. The double-tubes consist of unbranched dreier double silicate chains connected via $(\text{Ti},\text{Nb},\text{Fe},\text{Mn})$ -heterocations (M) to diortho-silicate groups, resembling the structure of yuksporite. Notably, the M positions form MO_6 octahedra or MO_5 square pyramids within the double-tubes.

The findings of this research shed light on the complex structure of eveslogite, emphasizing the importance of avoiding twinning and acquiring data from single nm-sized crystals using 3DED. This study not only contributes to a deeper understanding of this remarkable mineral but also showcases the power of advanced electron microscopy techniques in unravelling the intricate structures of minerals.

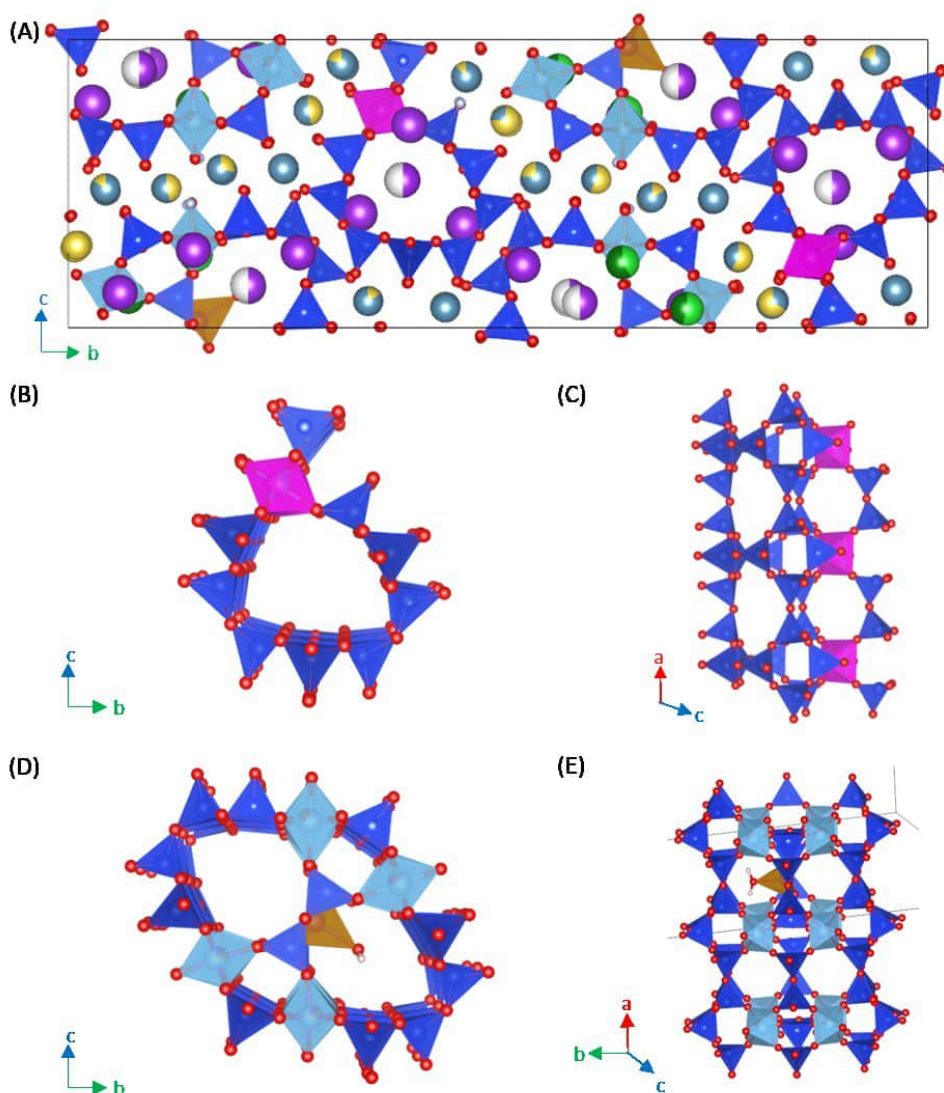


Figure 1: (A) Structure of eveslogite along [100]. The unit cell is marked by a black box. The heterosilicate tubular chains are shown along [100] in (B) and along the [010] in (C). (D) and (E) show the double-tube along [100] and along [329], respectively. Si is displayed in dark blue, M in light blue, (Ti, Nb) in pink, (Fe, Mn) in orange, Ba in light green, Sr in dark green, K in purple, Ca in blue-grey, Na in yellow, O in red, F in grey and H in white

- Ferraris G, Gula A (2005): Polysomatic aspects of microporous minerals – heterophyllosilicates, palysepioles and rhodesite-related structures. – *Rev Min Geochem* 57, 69-104
- Gemmi M, Mugnaioli E, Gorelik TE, Kolb U, Palatinus L, Boullay P, Hovmoller S, Abrahams JP (2019): 3D electron diffraction: The nanocrystallography revolution. – *ACS Central Science* 5, 1315-1329
- Krivovichev SV, Yakovenchuk VN, Armbruster T, Döbelin N, Pattinson P, Weber H-P, Depmeier W (2004): Porous titanosilicate nanorods in the structure of yuksporite, $(\text{Sr}, \text{Ba})_2\text{K}_4(\text{Ca}, \text{Na})_{14}(\text{Mn}, \text{Fe})\{(\text{Ti}, \text{Nb})_4(\text{O}, \text{OH})_4[\text{Si}_6\text{O}_{17}]_2[\text{Si}_2\text{O}_7]_3\}(\text{H}_2\text{O}, \text{OH})_n$, resolved using synchrotron radiation. – *Amer Min* 89, 1561-1565
- Men'shikov Y, Khomyakov A, Ferraris G, Belluso E, Gula A, Kulchitskaya E (2003): Eveslogite, $(\text{Ca}, \text{K}, \text{Na}, \text{Sr}, \text{Ba})_{24}[(\text{Ti}, \text{Nb}, \text{Fe}, \text{Mn})_6(\text{OH})_6\text{Si}_{24}\text{O}_{72}](\text{F}, \text{OH}, \text{Cl})_7$, a new mineral from the Khibina alkaline massif, Kola Peninsula, Russia. – *Zap Vseross Mineral Obshch* 132, 59-67
- Rozhdestvenskaya IV, Mugnaioli E, Czank M, Depmeier W, Kolb U, Reinholdt A, Weirich T (2010): The structure of charoite, $(\text{K}, \text{Sr}, \text{Ba}, \text{Mn})_{15-16}(\text{Ca}, \text{Na})_{32}[\text{Si}_{70}(\text{O}, \text{OH})_{180}](\text{OH}, \text{F})_4.n\text{H}_2\text{O}$, solved by conventional and automated electron diffraction. – *Min Mag* 74, 1, 159-177
- Rozhdestvenskaya IV, Mugnaioli E, Schowalter M, Schmidt MU, Czank M, Depmeier W, Rosenauer A (2017): The structure of denisovite, a fibrous nanocrystalline polytypic disordered 'very complex' silicate, studied by a synergistic multi-disciplinary approach employing methods of electron crystallography and X-ray powder diffraction. – *IUCrJ* 4, 3, 223-242

A machine learning force field for albite and the diffusion mechanisms of its defects

A. Gorfer^{1,2}, R. Abart², C. Dellago¹

¹Faculty of Physics, University of Vienna, Boltzmannngasse 5, 1090, Vienna, Austria

²Department of Lithospheric Research, University of Vienna, Josef-Holaubuek-Platz 2, 1090, Vienna, Austria
e-mail: alexander.gorfer@univie.ac.at

Feldspar is the most abundant mineral in the Earth's crust and the nature of its diffusive phase transformations are essential for reconstructing the thermal histories of magmatic and metamorphic rocks. Due to the large timescales over which these transformations proceed, the mechanism responsible for sodium diffusion and its possible anisotropy has remained a topic of debate. To elucidate the process, we have developed a machine learning force field (MLFF) (reviewed in Unke et al. 2022) trained on first-principle calculations of Albite (Na-feldspar) and its charged defects.

The MLFF has been trained to accurately predict a range of experimental macroscopic properties as well as defect formation energies, incorporating electrostatic corrections of the underlying first-principle calculation. Notably, we have discovered a new type of dumbbell interstitial defect, which is found to be the most favorable interstitial, and its formation free energy at finite temperature has been computed using thermodynamic integration.

Using the force field to drive molecular dynamics (MD) simulations allowed us to gain unprecedented insight into the diffusion mechanisms, as depicted in Figure 1. Through the analysis of jump rates, diffusion coefficients and tracer correlation factors we have determined that correlation plays a significant role, particularly in the $\perp(010)$ direction due to a distinct dumbbell/interstitialcy mechanism. Moreover, we have observed a high degree of anisotropy in diffusion, with variations up to 27-fold at 1000K, as illustrated in Figure 2. The strong agreement between our results and experimental diffusion coefficients leads us to conclude that MLFFs represent a mature and powerful methodology for investigating the dynamical properties of feldspar and other silicates.

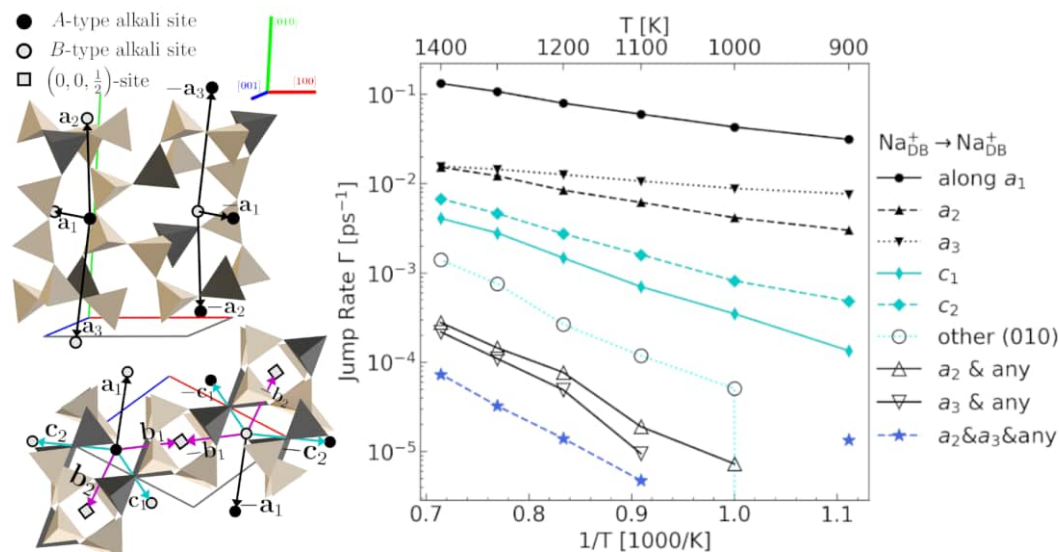


Figure 1. Left: diffusion pathways connecting the different sites. Right: jump rates for paths between alkali sites measured during an MD simulation using the MLFF. The dominance of diffusion along $a_{1,2,3}$ leads to the high anisotropy.

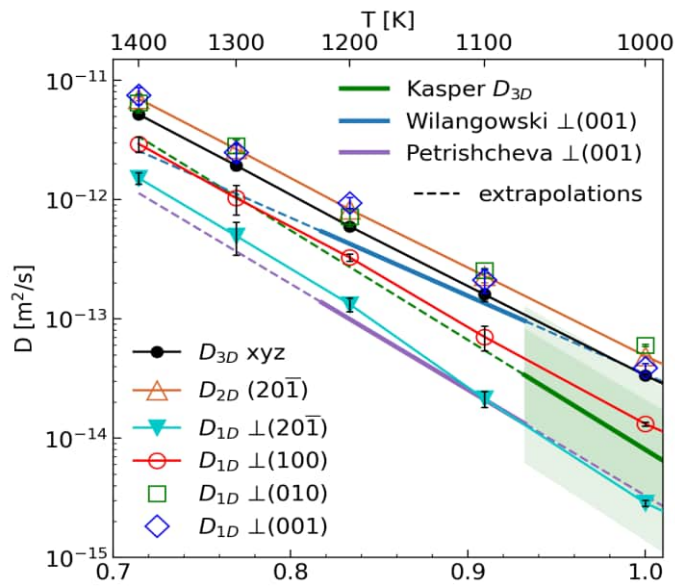


Figure 2. Diffusion coefficients for an interstitial defect measured over all dimensions D_{3D} and projected onto two D_{2D} or one dimension D_{1D} including experimental data of Kasper (1975), Wilangowski et al. (2015), and Petrishcheva et al. (2020)

- Unke O, Chmiela S, Saucedo E, Gastegger M, Poltavsky I, Schütt K, Tkatchenko A, Müller KR (2021): Machine Learning Force Fields. - Chem Rev 121 (16), 10142-10186
- Kasper RB (1975): Cation and Oxygen Diffusion in Albite - Ph.D. Thesis, Brown University.
- Wilangowski F, Divinski S, Abart R, Stolwijk NA (2015) (1962): Radiotracer experiments and Monte Carlo simulation of sodium diffusion in alkali feldspar: evidence against the vacancy mechanism. - Defects Diffus Forum 363, 79–84
- Petrishcheva E, Tiede L, Heuser D, Hutter H, Giester G, Abart R (2020): Multicomponent diffusion in ionic crystals: theoretical model and application to combined tracer- and interdiffusion in alkali feldspar. - Phys Chem Minerals 47, 35

Redox processes and metal sources recorded by Se and S isotopes of black smoker sulfides and host rocks

A. Grosche¹, M. Keith¹, R. Klemm¹, H. Strauss², S. König³

¹GeoZentrum Nordbayern, Friedrich-Alexander-Universität Erlangen-Nürnberg, Schlossgarten 5, 91054 Erlangen, Germany

²Institut für Geologie und Paläontologie, Westfälische Wilhelms-Universität Münster, 48149 Münster, Germany

³Instituto Andaluz de Ciencias de la Tierra (IACT), Consejo Superior de Investigaciones Científicas (CSIC) and Universidad de Granada (UGR), Avenida las Palmeras 4, Armilla, 18100 Granada, Spain
e-mail: anna.grosche@fau.de

Black smoker chimneys are products of submarine hydrothermal venting and have a complex internal zoning that is the result of mineral precipitation and maturation at evolving fluid conditions. The composition of the hydrothermal sulfides is thereby controlled by the fluid composition (e.g., temperature, pH, salinity), processes like fluid boiling, and the potential input of magmatic fluids. Advances in analytical techniques allow the quantitative analysis of stable isotope ratios of heavy elements, such as Se, which can provide new insights into the cycling of chalcophile elements in magmatic-hydrothermal systems (König et al. 2019; Rosca et al. 2022).

We sampled different zones of black smoker chimneys from the Nifonea vent field (New Hebrides Arc, W Pacific) from the inner chalcopyrite lining towards the outer rim. Homogeneous sulfide powders were analyzed for high-precision Se isotopes using a double spike and hydride generation sample introduction system attached to a ThermoFisher Scientific® NeptuneXT™ MC-ICP-MS at the IACT, Granada. Fractions of the same powders were also analyzed for S isotopes and the resulting data was combined with in-situ trace element data of genetically related sulfides.

The $\delta^{82/76}\text{Se}$ values (relative to NIST-3149) of chimney sulfides range from -3.7 ‰ to 0.6 ‰ \pm 0.2 ‰ (2SD) (Fig. 1), in accordance with previously reported values of seafloor hydrothermal sulfides (Rouxel et al. 2004). The $\delta^{34}\text{S}$ values (relative to VCDT) range between 2.1 ‰ and 4.0 ‰ reflecting typical mixing of H₂S derived from the host rocks and from thermochemical seawater sulfate reduction lacking any evidence for magmatic fluid input. The highest $\delta^{82/76}\text{Se}$ values occur in chalcopyrite that precipitated from high temperature fluids (370 °C) and overlap with $\delta^{82/76}\text{Se}$ values of fresh basaltic glass from the surrounding Nifonea caldera (Fig. 1). This suggests that metals were leached from the host rocks and that no significant isotope fractionation occurred during high temperature precipitation of chalcopyrite.

Decreasing Se/Tl and Co/Tl ratios of pyrite from the inner to the outer chimney wall record a temperature decrease. A coupled decrease of $\delta^{82/76}\text{Se}$ and $\delta^{34}\text{S}$ values towards the outer and low temperature zones (Fig. 1) can be related to local temperature-dependent isotope fractionation during redox reactions induced by mixing of the hydrothermal fluid with seawater. Understanding Se isotope fractionation during hydrothermal sulfide precipitation is crucial to subsequently identify the metal sources and the effect of fractionation processes in the upflow zone of submarine hydrothermal systems.

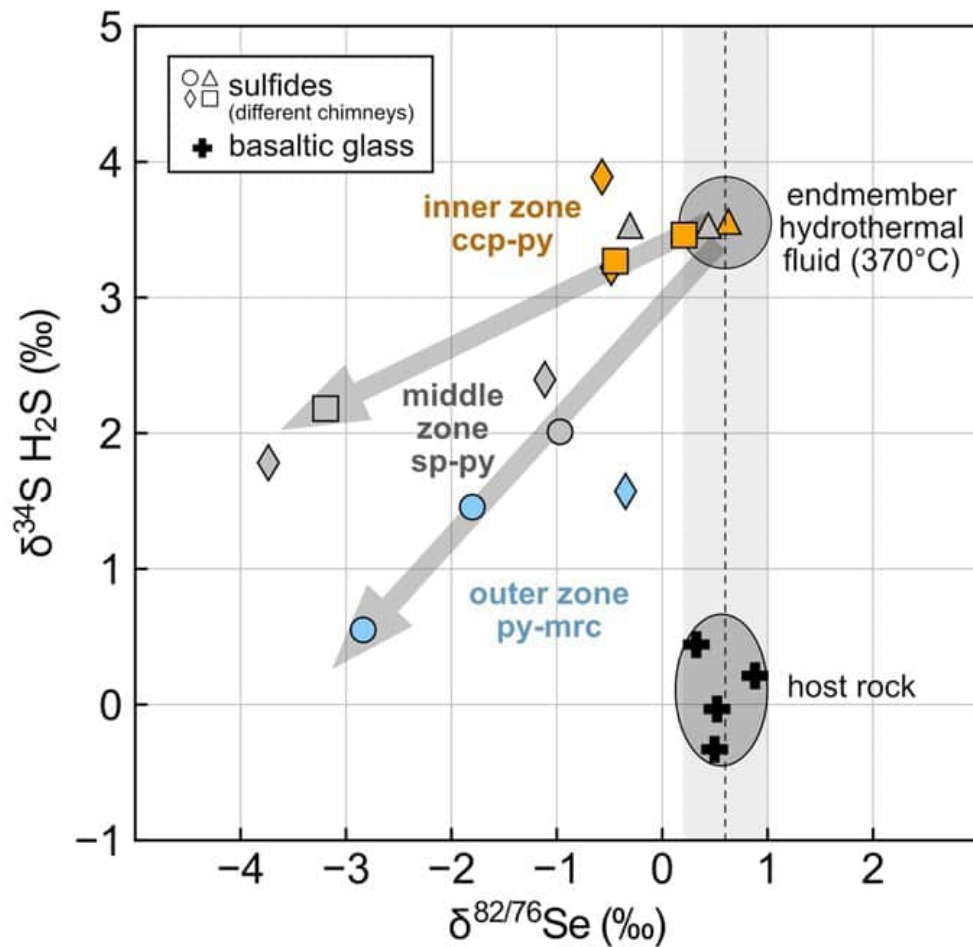


Figure 1. $\delta^{82/76}\text{Se}$ (relative to NIST-3149) versus $\delta^{34}\text{S}$ (relative to VCTD) values of black smoker sulfides and volcanic glass from Nifonea. The colors indicate whether the sulfide powder was derived from the inner, middle, or outer chimney zone. The symbols mark different vent sites. The $\delta^{34}\text{S}$ values of H_2S were calculated from the $\delta^{34}\text{S}$ value of the sulfide powder using the equilibrium isotopic fractionation factors by Ohmoto & Rye (1979) for the dominant sulfide phase at estimated fluid temperatures of 370°C (inner zone), 270 °C (middle zone), and 200 °C (outer zone). ccp = chalcopyrite, py = pyrite, sp = sphalerite, mrc = marcasite.

- König S, Eickmann B, Zack T, Yierpan A, Wille M, Taubald H, Schoenberg R (2019): Redox induced sulfur-selenium isotope decoupling recorded in pyrite. - *Geochim Cosmochim Acta* 244, 24–39
- Ohmoto H, Rye RO (1979): Isotopes of sulfur and carbon. - In: Barnes HL (ed) *Geochemistry of Hydrothermal Ore Deposits*. J Wiley and Sons, 509-567
- Rouxel O, Fouquet Y, Ludden JN (2004): Subsurface processes at the Lucky Strike hydrothermal field, Mid-Atlantic Ridge: Evidence from sulfur, selenium, and iron isotopes. - *Geochim Cosmochim Acta*, 68, 2295–2311
- Rosca C, Vlastélic I, Varas-Reus MI, König S (2022): Isotopic constraints on selenium degassing from basaltic magma and near-surface capture by fumarolic deposits: Implications for Se redistribution onto the Earth's surface. - *Chem Geol* 596, 120796

Real structure of mineral kenyaite, $\text{Na}_2\text{Si}_{20}\text{O}_{40}(\text{OH})_2 \cdot 8 \text{H}_2\text{O}$

I. Grosskreuz¹, B. Marler¹

¹*Dept. of Geology, Minerology and Geophysics, Ruhr University Bochum; Germany
e-mail: isabel.grosskreuz@rub.de*

Only very few natural occurrences of the rare mineral kenyaite are known. Named after Kenya, the country where the first sample had been discovered, kenyaite is known since 1967 with a composition of the type material $\text{NaSi}_{11}\text{O}_{20.5}(\text{OH})_4 \cdot \text{H}_2\text{O}$ according to Hans Eugster [1]. Different compositions, however, have been determined due to the fact that i) a part of the sodium cations can easily be leached from the structure with water and ii) the content of structural water seems to depend on the relative humidity and temperature of the environment and/or the pre-treatment of the sample prior to chemical analysis. The structure of kenyaite remained hidden for a long time because of very small crystals, a complex structure and a certain degree of structural disorder. Only in 2021, the crystal structure of synthetic kenyaite was published [2]. Kenyaite is a layered silicate and belongs to the group of Hydrated Layer Silicates (HLSs) [3] similar to minerals kanemite [4], $\text{Na}_4[\text{H}_4\text{Si}_8\text{O}_{20}] \cdot 12 \text{H}_2\text{O}$, magadiite [5], $\text{Na}_2[\text{Si}_{14}\text{O}_{26}(\text{OH})_6] \cdot 6 \text{H}_2\text{O}$, and makatite [6], $\text{Na}_8[\text{Si}_{16}\text{O}_{32}(\text{OH})_4] \cdot 16 \text{H}_2\text{O}$.

Experimental data: Natural kenyaite samples from Lake Magadi were kindly provided by K. Beneke and G. Lagaly, Kiel, Germany. In all samples, kenyaite was associated with either magadiite, quartz or both phases. For structure analysis, a fairly well crystalline sample (Fig. 1) was chosen which contained quartz as an impurity. Powder XRD data were recorded in modified Debye-Scherrer geometry using $\text{CuK}\alpha_1$ radiation. The average structure of kenyaite was refined using the FullProf 2K program [7].

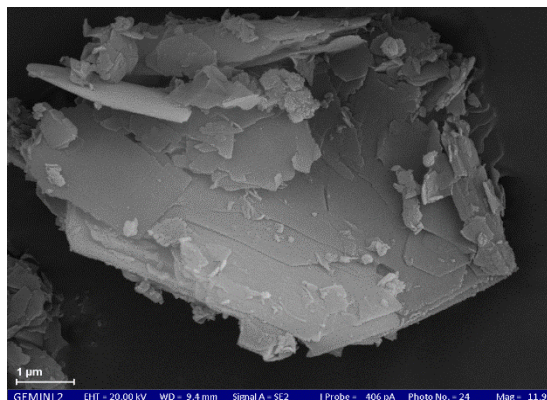


Fig. 1: Plate-like morphology of kenyaite crystals.

Subsequently, the disordered real structure was studied by comparing experimental powder XRD patterns with simulated ones calculated with the program DIFFaX [8]. In order to simulate the broadened reflections in the XRD powder diagram illustrating the disorder, various structure models were constructed based on a stacking disordered arrangement of layers.

The average structure

Nearly identical to synthetic kenyaite, the structure of the kenyaite mineral contains thick silicate layers (thickness: 15.9 Å) and bands of edge-sharing $[\text{Na}(\text{H}_2\text{O})_{6/1.5}]$ octahedra which are intercalated between these layers (Fig. 2). The dense layers (six layers [3]) have the same topology as the layers of RUB-6 [9] and synthetic kenyaite and possess a high silicon Q^4 to Q^3 ratio of 4.0. One half of the terminal $\equiv\text{Si}-\text{O}$ units form silanol groups ($\equiv\text{Si}-\text{OH}$) while the other half forms siloxy groups ($\equiv\text{Si}-\text{O}^-$) to compensate the charge of the sodium cations. Interestingly, quite strong hydrogen bonds ($d(\text{O}\cdots\text{O}) = \text{approx. } 2.5 \text{ \AA}$) exist (confirmed by ^1H MAS NMR spectroscopy) between the terminal silanol/siloxy groups themselves as intra-layer interactions, but also between the silanol/siloxy groups and water molecules of the octahedra. The kenyaite mineral crystallizes with space group symmetry $F2dd$ (No. 43, setting 3) and lattice parameters $a = 10.604(1) \text{ \AA}$, $b = 10.080(1) \text{ \AA}$, $c = 79.383(8) \text{ \AA}$.

Analysis of the real structure

The structure of kenyaite is slightly disordered typical for hydrous layer silicates which possess only weak ionic interactions between the alternating blocks of silicate layers and cations (in this case: $\text{Na}(\text{H}_2\text{O})_{6/1.5}$ octahedra). The silicate layers of kenyaite (six layers) and inter-layer regions containing the octahedra are stacked perpendicular to the *ab*-plane.

The type of stacking disorder was investigated in detail by calculating hypothetical powder diagrams corresponding to various stacking sequences. The regular (average) structure of kenyaite possesses an ordered ABCD... stacking sequence of identical six layers with a sequence of shift vectors of $0.5 a + 0.5 b \Rightarrow -0.5 a + 0.5 b \Rightarrow 0.5 a + -0.5 b \Rightarrow 0.5 a + 0.5 b$ between successive layers. In addition, successive layers are rotated by 90° against each other (Fig. 2). However, other shift vectors are also possible (e.g., $0.25 a + 0.25 b$ or $-0.25 a + 0.25 b$) without distortion of structural building blocks. Figure 3 shows a comparison between the experimental PXRD diagram and simulated diagrams.

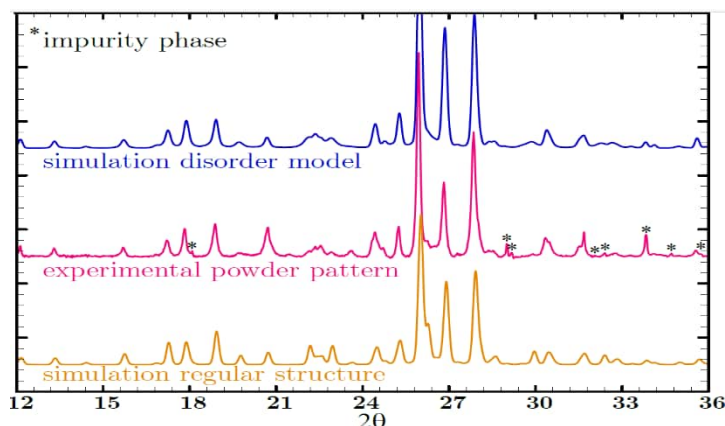


Fig. 3: Section of the experimental PXRD diagram of mineral kenyaite (quartz subtracted) and the simulated diagrams of the regular and disordered structure.

* indicate reflections of the impurity phase Trona.

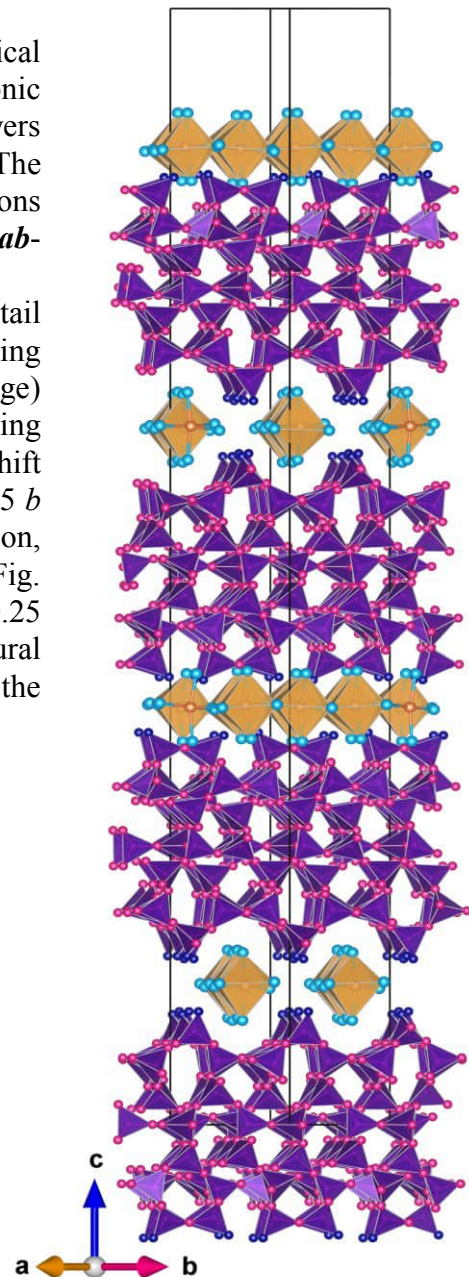


Fig. 2: Average structure of mineral kenyaite.

- [1] Eugster HP (1967): Hydrous sodium silicates from Lake Magadi, Kenya: precursors of bedded chert. - Science 157 (3793) 1177–1180
- [2] Marler B, Großkreuz I, Gies H (2021): The crystal structure of synthetic kenyaite, $\text{Na}_2\text{Si}_{20}\text{O}_{40}(\text{OH})_2 \cdot 8 \text{H}_2\text{O}$. - J Solid State Chem 300, Article No. 122215
- [3] Marler B, Grünewald-Lüke A, Ikeda T, Zuber P, Heimes H, Gies H: Database of hydrous layer silicates - <https://www.hls-database.com>
- [4] Vortmann S, Rius J, Marler B, Gies H (1999): Structure solution from powder data of the hydrous layer silicate kanemite, a precursor of the industrial ion exchanger SKS-6. - Eur J Mineral 11 125–134
- [5] Marler B, Krysiak Y, Grosskreuz I, Gies H, Kolb U (2022): The crystal structure of mineral magadiite, $\text{Na}_2\text{Si}_{14}\text{O}_{28}(\text{OH})_2 \cdot 8 \text{H}_2\text{O}$. - Amer Mineral 107, 211–2110
- [6] Annehed H, Faeth L, Lincoln LJ (1982): Crystal structure of synthetic makatite $\text{Na}_2\text{Si}_4\text{O}_8(\text{OH})_{2.4} \cdot \text{H}_2\text{O}$. - Z Kristallogr 159, 203–210
- [7] Rodríguez-Carvajal J (1993): Recent advances in magnetic structure determination by neutron powder diffraction. - Physica B: Condensed Matter 192, 55–69
- [8] Treacy MMJ, Deem MW, Newsam JM: *DIFFaX*, <https://www.public.asu.edu/~mtreacy/DIFFaX.html>
- [9] Krysiak Y, Marler B, Barton B, Plana-Ruiz S, Gies H, Neder RB, Kolb U (2020): New zeolite-like RUB-5 and its related hydrous layer silicate RUB-6 structurally characterized by electron microscopy. - IUCrJ 7, 522–534

Origin of ultramafic rocks associated with carbonatites and their bearing on the formation of HFSE-deposits

D. Gudelius^{1,2,3*}, M. W. Marks³, G. Markl³, T. F. D. Nielsen⁴, J. Kolb^{1,2}, B. Walter^{1,2}

¹Karlsruhe Institute of Technology, Chair of Geochemistry and Economic Geology, Institute for Applied Geosciences, Adenauerring 20b, 76131 Karlsruhe, Germany

²Laboratory for Environmental and Raw Materials Analysis (LERA), Adenauerring 20b, 76131 Karlsruhe, Germany

³Eberhard Karls University, Institute of Geosciences, Schnarrenbergstrasse 94-96, 72076 Tübingen, Germany

⁴Geological Survey of Denmark and Greenland, Department of Petrology and Economic, 16 Geology, Øster Voldgade 10, Copenhagen, Denmark
e-mail: b.walter@kit.edu

Many carbonatites occur together with large amounts of ultramafic rocks, melilitolites, foidolites and (foid)syenites. There is an ongoing debate if and how these contrasting lithologies were formed by differentiation of a common, mantle-derived silicate magma or rather by metasomatic processes between carbonatite and country rocks (Vasyukova & Williams-Jones, 2022). In order to find petrological evidence for one or the other, two key examples, the Gardiner (E Greenland) and Kovdor (Russia) complexes are compared in this study (Fig. 1). Despite their similar tectonic setting and succession of rock types, they show significant differences in the texture and mineral composition of ultramafic rocks.

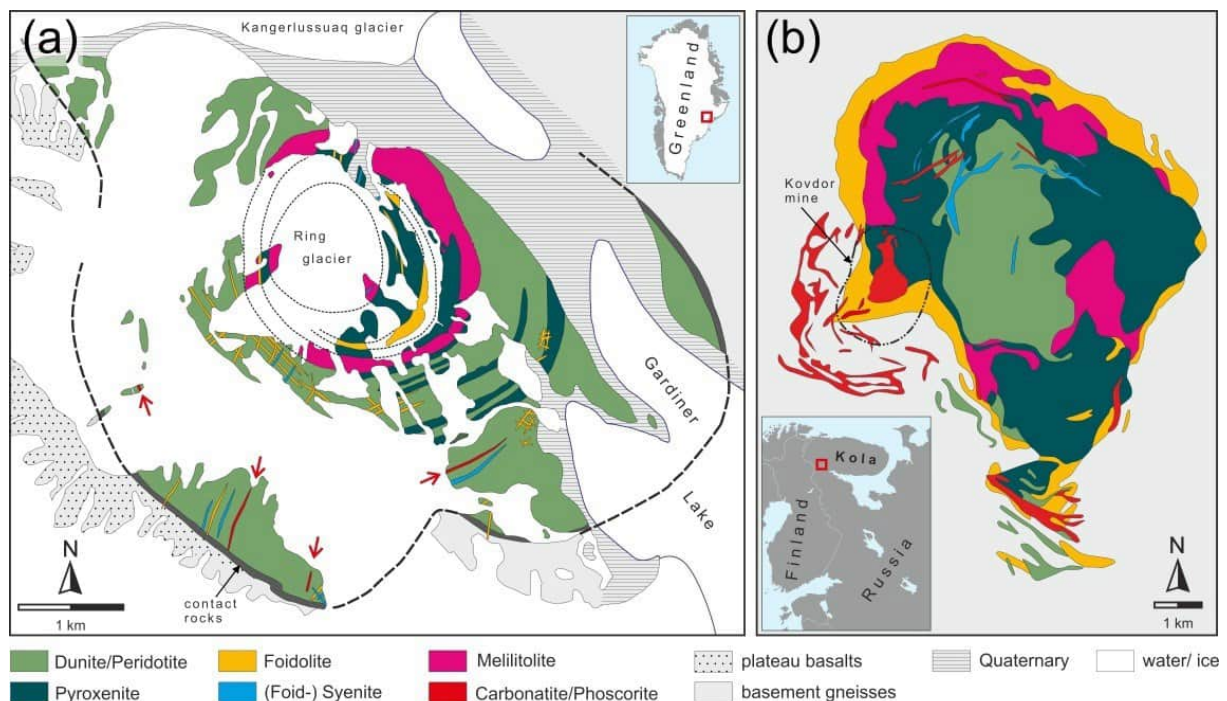


Figure 1: Geological maps of (a) Gardiner (E Greenland) and Kovdor (Russia), taken from Gudelius et al. (2023).

Ultramafic rocks from Kovdor include calcite- and biotite-rich dunites and pyroxenites without typical cumulate textures. They partly consist of Ni-poor forsterite (Fig. 2), Cr-poor diopside and Ni-Cr-poor spinel and are therefore interpreted as metasomatic reaction products between mantle-derived carbonatite melts and silicic host rocks. Similar ultramafic rocks are associated with carbonatites (e. g. at Palabora - South Africa, Afrikanda - Russia, and Salitre - Brazil). In contrast, the ultramafic rocks from Gardiner show well-preserved cumulate textures and consist

of Ni-rich forsterite, Cr-rich diopside as well as Cr-Ni-Ti-rich spinel and also contain F-Cl-rich apatite.

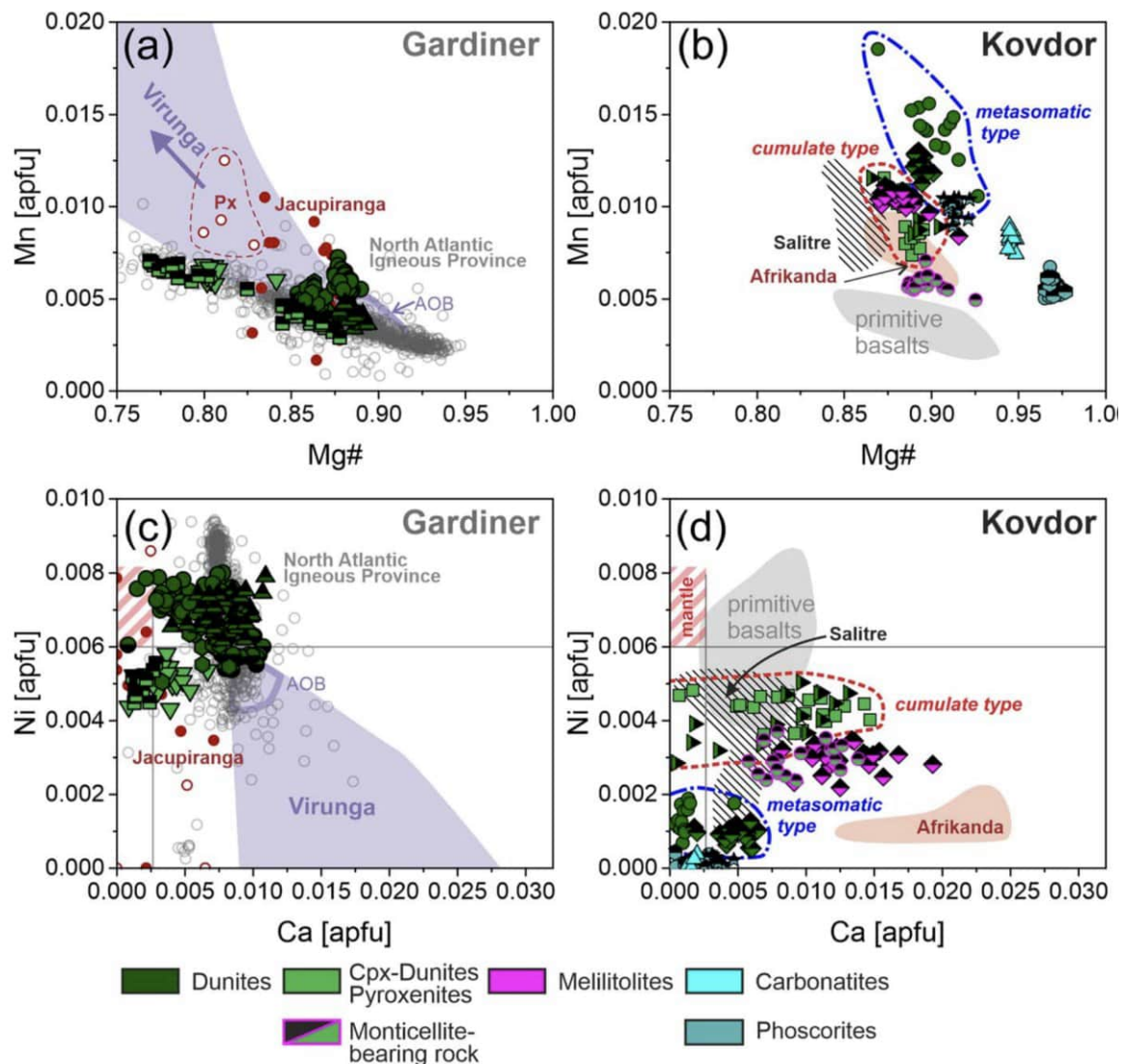


Figure 2: Comparison of olivine compositions from Gardiner (left column) and Kovdor (right column) with literature data (taken from Gudelius et al. 2023)

This indicates that these rocks represent cumulates of an evolving, mafic melt derived from Ti-rich mantle source, similar to other rocks of the North Atlantic igneous province (Fig. 2). In contrast to systems dominated by carbonatite metasomatism like Kovdor, Ti-rich parental silicate magmas can abundantly crystallize Ti phases, as recorded by massive perovskite cumulates in Gardiner melilitolites. This can effectively scavenge HFSE from the magmatic system early in its evolution and likely explains HFSE-barren carbonatites at Gardiner, while those from Kovdor are highly HFSE-enriched. In summary, ultramafic rocks in alkaline complexes can be of both cumulate and metasomatic origin; the specific type has an important bearing on their HFSE enrichment and on the types of ores present in such complexes.

Gudelius, D., Marks, M. W., Markl, G., Nielsen, T. F., Kolb, J., Walter, B. (2023): The origin of ultramafic complexes with melilitolites and carbonatites: a petrological comparison of the Gardiner (E Greenland) and Kovdor (Russia) intrusions. - *J Petrol*, egad036

Vasyukova, O.V. & Williams-Jones, A.E. (2022): Carbonatite metasomatism, the key to unlocking the carbonatite–phoscorite–ultramafic rock paradox. - *Chem Geol* 602, 120888

**“Nothing is more important than health” Eduard Suess (1831-1914)
Eduard Suess was a leading contributor to the
city of Vienna's projects of the century:
the 1st Vienna spring-water pipeline and the regulation of the Danube**

M. Hamilton¹

*¹Geological Archive, Department of Geology, University of Vienna
e-mail: margarete.hamilton@univie.ac.at*

E. Suess not only played an important role as a professor of paleontology and geology at the University of Vienna, but as a member of the Vienna City Council he also submitted his expertise on the two century projects of the city of Vienna.

In the Archive of the Geological Institute at the University of Vienna exist handwritten notes by E. Suess between 1861 and 1869 dealing with the meetings of the Vienna City Council with regard to the quality of the water for the city and, as a result, the health of the population.

In his memoirs, which were published posthumously in 1916, Suess points out in an essential conversation with the then mayor Cajetan Felder (1814-1894) that "nothing is more important than the health" of the population of Vienna. The rapid population increase, the infections with dysentery, typhus and cholera in 1855 were a significant problem, also poor water quality and a lack of sewerage.

Between 1869 and 1873 a 90 km long canal was built from the springs in the foothills of the Eastern Alps via tunnels and aqueducts to the water tanks of the city of Vienna. This first Vienna high spring water pipeline was officially opened on October 24, 1873 with the commissioning of the high jet fountain on Schwarzenbergplatz in the presence of Emperor Franz Josef I. There also exist a copy of the piano piece "Die Hochquelle" composed by Eduard Strauss (1835-1916) in 1911. The piece is dedicated to the initiator of the first Vienna spring-water pipeline Eduard Suess.

The second major project to improve water quality and thus improve the health of Vienna's population was the regulation of the Danube bed. With the Danube Regulation Commission created in 1868, not only should the devastating floods of the Danube river be prevented, but also new facilities for the creation of shipping and trade should be made possible. Work began on May 14, 1870 in the presence of Emperor Franz Josef I, and just 5 years later, on April 15 and 16, 1875, the two breakthroughs were made on the north and east of the Danube.

In the geological archive exist three soil maps of Vienna from the years 1873-1875 showing the course of the Danube in the old and new beds. A copy of a letter from the Emperor to E. Suess from 1911 has also survived, in which the Emperor praised E. Suess for his achievements for the benefit of the people of Vienna.



Figure 1. Stadler R Lithographie: Der neue Springbrunnen vor dem Schwarzenberg-Palais (1873)

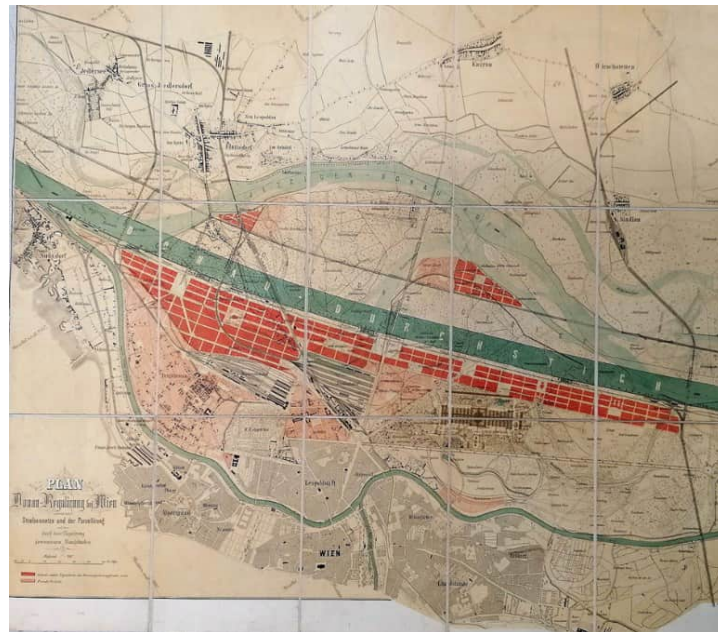


Figure 2. Plan der Donauregulierung in Wien. Donauregulierungskommission (1875). Geological Archive, KS ¼

Drenning A (1973): Die 1. Wiener Hochquellenleitung. - Festschrift aus Anlaß der 100-Jahr-Feier am 24. Oktober 1973

NN (1875): „Die Donau-Regulierung bei Wien“. - Herausgegeben aus Anlaß der feierlichen Eröffnung der Schifffahrt im neuen Strombette am 30. Mai 1875 von der Donau-Regulierungs-Commission in Wien

Stadler R (1873): Die Wasserversorgung der Stadt Wien in ihrer Vergangenheit und Gegenwart. Denkschrift zur Eröffnung der Hochquellenwasserleitung im Jahr 1873. 296 pp

Suess E (1916): Erinnerungen. 154 p

Geochemical patterns in karst bauxite of the Unterlaussa mining district (Upper Austria)

F.J. Hampl¹, F. Melcher¹, I. Dunkl², B. Schmidt³, V. Bertrandsson Erlandsson¹

¹*Chair of Geology and Economic Geology, Montanuniversität Leoben,
Peter-Tunner-Straße 5, 8700 Leoben, Austria*

²*Department of Sedimentology & Environmental Geology, Geoscience Center,
Georg-August-Universität Göttingen, Goldschmidtstraße 3, 37077 Göttingen, Germany*

³*Department of Mineralogy, Geoscience Center, Georg-August-Universität Göttingen,
Goldschmidtstraße 1, 37077 Göttingen, Germany
e-mail: ferdinand.j.hampl@gmx.at*

Numerous studies demonstrated the great potential of karst bauxites as sources of critical metals. The European karst bauxites may thus help to gain more independence from questionable non-European metal suppliers. Yet several European karst bauxites are untouched by modern scientific methods and the processes that are responsible for their element enrichment and depletion patterns are not fully understood. However, understanding the geochemical patterns in karst bauxites is not only fundamental for a prudent economic usage but can also facilitate reconstructions of paleo-environments and redox processes during weathering and diagenesis. To better understand the geochemical patterns, we investigated three profiles of Upper Cretaceous karst bauxite in the Unterlaussa mining district (Upper Austria) and used geochemical and mineralogical methods such as (micro-) X-ray fluorescence, (laser ablation-) inductively coupled plasma mass spectrometry, scanning electron microscopy, electron microprobe mapping and X-ray diffraction.

According to our results, the boehmitic karst bauxite was formed by intense weathering of a polygenetic sediment (parent material) that was deposited on karstified dolostone (Hampl & Melcher, 2023). The presence of detrital chromite in the karst bauxite suggests that sediments formed by weathering of ophiolitic material in the hinterland of the depositional site were also part of the parent material. (Sub)tropical weathering of the composite parent material caused the dissolution of aluminosilicates and the enrichment of weathering-resistant minerals. These weathering processes not only led to chemical depletion and enrichment patterns that are typical for karst bauxites (e.g., pronounced Al₂O₃, Fe₂O₃ and TiO₂ enrichment, and SiO₂, alkali and alkaline earth metal depletion) but also resulted in substantial enrichment of several critical metals compared to the upper continental crust: e.g., rare earth elements (REEs; La-Lu + Sc, Y) up to 2277 ppm, Li up to 900 ppm, or V up to 916 ppm. Most of the REEs and Li are enriched in the lowermost part of the bauxite and clay minerals are the most likely hosts. Moreover, the element distribution patterns also indicate reducing conditions in the lower part and redeposition in the upper part of the bauxite. Even though Cr- and U-mobility normally only plays a subordinate role in karst bauxites, we found a macroscopic, authigenic chromium oxyhydroxide mineralization and discrete U-minerals in reduction spheroids. Aside from U, some of these reduction spheroids are extremely rich in redox-sensitive elements such as V, Cr, or Mn. We discuss possible formation models for this unique U-mineralization.

Our results highlight the economic potential and the ample information content of karst bauxites and call for more European initiative to investigate them.

The inner beauty of Roman Egyptian blue: micro-CT and mineralogy

J. Heinemann¹, P. Tropper¹, G. Degenhart², B. Zerobin³, G. Goldenberg³, A. Rodler^{4,5}

¹University of Innsbruck, Institute of Mineralogy and Petrography, 6020 Innsbruck, Austria

²Medical University of Innsbruck, Institute of Radiology, 6020 Innsbruck, Austria

³University of Innsbruck, Institute of Archaeologies, 6020 Innsbruck, Austria

⁴Austrian Archaeological Institute of the Austrian Academy of Sciences, Franz-Klein Gasse 1, 1190 Vienna

⁵Department of Lithospheric Research, University of Vienna, Josef-Holaubek-Platz 2, 1090 Vienna

e-mail: peter.tropper@uibk.ac.at

Egyptian blue was the first synthetic pigment made by humankind. It mostly consists of the mineral cuprorivaite, which is a calcium-copper-silicate ($\text{CaCuSi}_4\text{O}_{10}$). This study reports the results of a mineralogical and computer tomographic study of Egyptian blue finds from the Roman sites of Aguntum in East Tyrol, as well as from Retznei and Wagna (formerly Flavia Solva) in southern Styria, Austria. The aim is to expand our understanding of the material processing and production technology of the artificial pigment Egyptian blue. Samples of Egyptian blue pellets were investigated with respect to their elemental composition and spatial distribution of the calcium-copper-silicate cuprorivaite $\text{CaCuSi}_4\text{O}_{10}$.

A thin section (with three cut layers) of an Egyptian blue pellet from Aguntum was examined using optical microscopy (OP), micro-X-ray fluorescence analysis (μ -XRF) and scanning electron microscopy coupled with energy dispersive X-ray spectroscopy (SEM-EDX). The pigment's initial composition as well as the manufacturing process seem to be the decisive factors for the quality of the final product. A relationship between the presence of trace iron (Fe), titanium (Ti), and sulfur (S) with the quartz and copper source of the initial raw material mixture is discussed.

In addition, micro-computed tomography (μ -CT) of three Egyptian blue finds (Aguntum, Retznei, Wagna-Flavia Solva) was performed, revealing several concise differences between the samples. The pellets from Aguntum and Retznei contained a significantly higher content of cuprorivaite and smaller crystals than the sample from Wagna-Flavia Solva. The spatial distribution of individual mineral phases was analysed with μ -CT-3D images. Here, the connective density, average particle size as well as spacing between individual particles of specific phases can be visualised. This confirms the semi-quantitative measurement of a phase's proportion to the total volume of a sample.

Concerning clues about the initial raw material mixture of the pellets, the results show that chalcosine and possibly quartz from beach sand were used as source for the Egyptian blue pellet from Aguntum. In addition, μ -CT data indicate that the pellet from Retznei contains the highest amount of cuprorivaite, followed by the sample from Aguntum, while that from Wagna-Flavia Solva contains the least amount of cuprorivaite.

Compressibility of pearceite-polybasite group minerals

C. Hejny¹

¹University of Innsbruck, Innrain52, 6020 Innsbruck, Austria
e-mail: Clivia.hejny@unibk.ac.at

Pearceite-polybasite group minerals (PPGM), $[(\text{Ag,Cu})_6(\text{As,Sb})_2\text{S}_7][\text{Ag}_9\text{CuS}_4]$, display Ag^+ fast ion conduction character. The crystal structure is described as being composed of two different layers: layer A with general composition $[(\text{Ag,Cu})_6(\text{As,Sb})_2\text{S}_7]^{2-}$ and layer B with general composition $[\text{Ag}_9\text{CuS}_4]^{2+}$. Ionic conductivity is observed in layer B (Bindi et al. 2007). The root-name *pearceite* is given to minerals where As is dominant over Sb and the root-name *polybasite* for Sb-dominant phases. A suffix attached to the root-name stands for the superstructure variant, the three most common ones are (1) trigonal with lattice parameters $a \approx 7.5$, $c \approx 12.0$ Å, PPG-*Tac*, trigonal with lattice parameters $a \approx 15.0$, $c \approx 12.0$ Å, PPG-*T2ac* and monoclinic with $a \approx 26.0$, $b \approx 15.0$, $c \approx 24.0$ Å, $\beta \approx 90^\circ$, PPG-*M2a2b2c*, although a number of different crystal structures and their temperature-induced phase transitions are known (e.g., Bindi et al. 2006).

In-situ single-crystal diffraction experiments of PPGMs in a diamond anvil cell were performed to test the possibility of using pressure as a switch for the ionic conductivity. Initial experiments have indeed shown that it is possible to induce phase transitions from the ionic conduction form with the aristotype crystal structure PPG-*Tac* to an ordered or partially ordered superstructure form with Ag ions “frozen-up” into fixed atomic positions. In this way a crystal of pearceite-*Tac* transformed to the -*T2ac* crystal structure at a pressure of 0.5(1) GPa and a crystal of polybasite-*T2ac* showed a phase transition to the -*M2a2b2c* superstructure variant at 4.5(2) GPa. In both cases the compressibility is significantly larger along the *c*-direction, i.e. perpendicular to the layered structure, which is in accordance with a reduction of the size for the ionic conductivity pathways. The limited number of datapoints within the small pressure range from AP to 5.4GPa and without considering phase transitions only allows for an estimation of the bulk modulus, which, with a value of $K = 48(1)$ GPa, is well in accordance of other sulphosalt materials.

Bindi L, Evain M, Pradel A, Albert S, Ribbs M, Menchetti S (2006): Fast ion conduction character and ionic phase-transitions in disordered crystals: the complex case of the minerals of the pearceite–polybasite group. - Phys Chem Miner 33, 677-690

Bindi L, Evain M, Stry PG, Menchetti S (2007): The pearceite-polybasite group of minerals: Crystal chemistry and new nomenclature rules. - Amer Miner 92, 918-925

Research insights based on documents from the Geological Archive of the University of Vienna

M. Heninger¹, B. Holly², P. Nagl³, R. Wohlschlägl¹, M. Hamilton⁴

¹*Institut für Geologie, Universität Wien*

²*Institut für Mineralogie und Kristallographie, Universität Wien*

³*Department für Lithosphärenforschung, Universität Wien*

⁴*Geologisches Archiv, Universität Wien*

e-mail: margarete.hamilton@univie.ac.at

The main task of the Geological Archive is the acquisition, evaluation, order, description, preservation, and utilization of written material, audiovisual material, and collections that are created in the institute and above all by the academic people working there. Of course, archiving is always linked to librarianship; nevertheless, in the present case, it is a special archive that deals with the preservation not of specialized library literature, but of documents and objects of geological research, whose historical significance is undisputed, but goes beyond literature.

In today's age of digitization and the new technical possibilities, an important aspect is making the holdings accessible via electronic media (Hamilton 2021). Furthermore, in accordance with the educational mandate of archiving, interested students are offered the opportunity to get to know the history of geosciences in detail in a special course and also to establish a connection to current research and to present it in seminars. The works presented here give an insight into specially selected documents from the Geological Archive and show their diversity.

Otto Ampferer (1875-1947) - The theory of the undercurrent: Plate tectonics and the name "Alfred Wegener" (1880-1930) are almost inextricably linked. Ships, research centers and asteroids have been named after the German explorer. Otto Ampferer and his undercurrent theory, which he presented as early as 1906, are less well known. He developed this theory in the course of his alpine research and mapping work. Remarkably, it comes very close to today's concept of "seafloor spreading".

Perhaps because his contributions were difficult for laypeople to read, the Austrian geologist is far less known as the godfather of institutions and sites than his German colleague. However, the interested reader soon notices his pictorial and skilful use of language as well as the high scientific quality of his contributions - reason enough to take a closer look at the researcher.

Historical personnel files of assistants and demonstrators: The present personnel files include documents from the period 1873 to 1945, which were first written in current, later in cursive handwriting and typewritten. In addition to letters that deal directly with the employment and salary of people, there are also ministerial decrees and documents that are directly or indirectly related to the military service of employees in the First and Second World Wars. The existing documents not only reflect the drastic change in correspondence, but also the special challenges for the University of Vienna in this very special time.

Historical geological maps - their origin and preservation: One of the oldest surviving maps in the Geological Archive of the Institute for Geology at the University of Vienna is the "Geognostic Map of the Areas of Krems and Manhardsberge" (1848). Based on this geological map, the author deals with the life and work of the map author Johann Baptist Cžjžek (1806-1855) and gives an overview of the creation and preservation of historical geological maps. Furthermore, the creation of geological maps in the past and present is examined.

Walter Medwenitsch - Expedition to East Africa in 1971: Walter Medwenitsch (1927-1992), whose numerous study trips took him halfway around the world, undertook a 15-day expedition to East Africa in February 1971. Driven by a broad interest in all natural sciences - but especially in geology (doctorate 1949 at the University of Vienna) - during these two weeks he visited cyanite and carbonatite deposits in Kenya, studied the young volcanism of the East African Rift Valley and dealt with the glaciology of the Kilimanjaro massif. His curiosity also led him to the extinct volcano Mount Kenya and its glaciers and to the Pleistocene fossils of Tanzania's Olduvai Gorge, considered part of the 'Cradle of Mankind'.

In the geological archive of the University of Vienna there is a comprehensive geological report by W. Medwenitsch ("Notes on the geological excursion to East Africa") on this wide-ranging expedition, as well as numerous maps and excerpts from reports that contain additional information on the areas visited.



Figure 1: Insights into the newly organized Geological Archive of the University of Vienna. Left: History of the Geological Institute, Box 1; Center top: geological maps, map box 1; Right: Walter Medwenitsch, box 5; center bottom: Otto Ampferer, Box 3 (Photos: M Hamilton)

Hamilton M (2021): The collections of the Archive of the History of Geology at the University of Vienna. - In: 15th International ERBE-Symposium, Eggenburg 2021. Proceedings, 58-74.

Glass transition temperatures and crystallization kinetics of a synthetic, anhydrous, amorphous calcium-magnesium carbonate

K.-U. Hess¹, J. Schawe², M. Wilding³, K.E. Goetschl⁴, S. Sturm⁵, K. Müller-Caspary⁵, E. Sturm¹, W. Schmahl¹, E. Griesshaber¹, T. Bissbort¹, D. Weidendorfer¹, M. Dietzel⁴, D.B. Dingwell¹

¹ Earth and Environmental Sciences, Ludwig-Maximilians-Universität München, Theresienstraße 41/III, 80333 Munich, Germany

² Mettler-Toledo GmbH, Analytical, Heuwinkelstrasse 3, 8603, Nänikon, Switzerland

³ School of Earth Sciences, Wills Memorial Building, Queens Road, Bristol, BS8 1RJ, United Kingdom

⁴ Institute of Applied Geosciences, Graz University of Technology, Rechbauerstraße 12, 8010 Graz, Austria

⁵ Fakultät für Chemie und Pharmazie, Physikalische Chemie, Ludwig-Maximilians-Universität München, Butenandtstraße 5-13, 81377, Munich, Germany
e-mail: hess@lmu.de

We report the first calorimetric observations of glass transition temperatures and crystallization rates of anhydrous, amorphous calcium-magnesium carbonate using fast scanning differential scanning calorimetry (FDSC). The hydrous amorphous $\text{Ca}_{0.95}\text{Mg}_{0.05}\text{CO}_3 \cdot 0.5\text{H}_2\text{O}$ (ACMC05) solid was precipitated from a $\text{MgCl}_2\text{-NaHCO}_3$ buffered solution, separated from the supernatant, and freeze-dried. Part of the freeze-dried samples were additionally dried at 250 °C for up to 6 hours in a furnace in a high purity nitrogen atmosphere to produce anhydrous ACMC. The limiting fictive temperature of the anhydrous $\text{Ca}_{0.95}\text{Mg}_{0.05}\text{CO}_3$ was determined (by applying different heating rates (2000-6000 K/s, see Fig. 1) and correcting for thermal lag) to be 376 °C and the intensity of the glass transition or relaxational heat capacity is $\Delta C_p = 0.16 \text{ J}/(\text{g K})$. Additionally, the heating rate dependence of the peak temperature of the corrected crystallization peaks is used to determine the activation energy of crystallization to be 275 kJ/mol. A high-resolution transmission electron microscopy study has been performed on the hydrous and anhydrous samples to provide further characterization of their compositional and structural states.

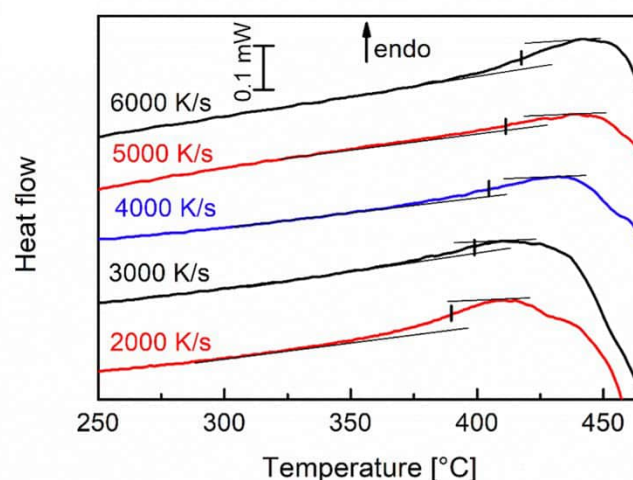


Figure 1. Heat flow curves of ACMC05.

The compositions of coherent exsolution lamellae in alkali feldspar measured with atom probe tomography

D. Heuser¹, R. Dubosq², G. Bian¹, G. Habler¹, E. Petrishcheva¹, B. Gault², C. Lengauer³, C. Rentenberger⁴, R. Abart¹

¹*Department of Lithospheric Research, University of Vienna*

²*Department Microstructure Physics and Alloy Design, Max Plank Institut für Eisenforschung GmbH, Düsseldorf*

³*Department of Mineralogy and Crystallography, University of Vienna*

⁴*Physics of Nanostructured Materials, University of Vienna
e-mail: david.heuser@univie.ac.at*

In the past, the compositions of experimentally produced coherent exsolution lamellae in alkali feldspars had to be determined indirectly from the “distorted” lattice parameters, because their small size prevented direct in-situ composition measurements. This indirect approach is based on strain models hinging on elastic constants, which are, however, subject to considerable uncertainties, especially for alkali feldspars with intermediate compositions (Robin 1974; Sipling & Yund 1976). In this study, we directly measured the compositions of experimentally produced exsolution lamellae using atom probe tomography (APT), a technique with near-atomic resolution which became available for non-conductive materials in the last decade.

At first, two K-rich gem quality alkali feldspars (Madagascar orthoclase and Volkesfeld sanidine) were shifted to intermediate Na-K-compositions by cation exchange with NaCl-KCl salt melt at 900 °C and subsequently annealed at ambient pressure and temperatures between 440 and 560 °C. Annealing conditions were within the miscibility gap of disordered alkali feldspar solid-solution and the initial compositionally homogeneous feldspars exsolved into a coherent lamellar intergrowth. Transmission electron microscopy (TEM) investigation of the exsolved feldspars revealed fully coherent exsolution lamellae subparallel to (-801) with lamellar widths of 5-30 nm. As the cell parameters of alkali feldspar exhibit considerable compositional dependence, the lattices of the more Na-rich and the more K-rich lamellae must be distorted in order to maintain coherency across the lamellar interfaces. In electron diffraction patterns this lattice distortion is evident from a splitting of the reflections corresponding to lattice planes sub-parallel to the lamellar interfaces.

APT revealed compositionally distinct domains corresponding to the expected Na-rich and K-rich lamellae. Time series experiments with different annealing durations were done at a given temperature to check when the lamellar compositions become stable, i.e. when thermodynamic equilibrium between the Na-rich and the K-rich lamella is reached. Even at the lowest applied temperatures equilibrium was reached within a few days, and lamellar compositions may be regarded as binodal points. The binodal points obtained at different temperatures delineate the coherent binodal curves. The results were compared to previously determined coherent solvi from the literature. Interestingly, Volkesfeld sanidine and Madagascar orthoclase show similar Na-K element partitioning and thus similar thermodynamic non-ideality of the alkali feldspar solid-solution in feldspar-salt melt cation exchange experiments at ambient pressure and temperatures between 800 and 1000 °C, but the coherent solvus of Volkesfeld sanidine lies well below the one of Madagascar orthoclase.

This apparent discrepancy may either be due to different degrees of thermodynamic non-ideality of the alkali feldspar solid-solution at the comparatively low temperatures of exsolution. Alternatively, this may be explained by different elastic properties of Volkesfeld sanidine and Madagascar orthoclase, which feed into the Gibbs energy of the solid-solution via the elastic energy associated with coherent lamellar intergrowth.

Robin PYF (1974): Stress and strain in cryptoperthite lamellae and coherent solvus of alkali feldspars. - Amer Mineral 59, 1299-1318

Sipling PJ, Yund RA (1976). Experimental determination of the coherent solvus for sanidine-high albite. - Amer Mineral 61, 897-906

On the existence of a new MgWO₄ polymorph

E. Hildebrandt¹, V. Kahlenberg¹, H. Krüger¹, S. Wagner¹

¹University of Innsbruck, Institute of Mineralogy and Petrography, Innrain 52, 6020 Innsbruck, Austria
e-mail: volker.kahlenberg@uibk.ac.at

Single-crystals of a quenchable high-temperature polymorph of magnesium tungstate (MgWO₄-II) have been grown using the flux method. Polycrystalline material of the same compound could be obtained from solid-state reactions performed at 1200 °C. Basic crystallographic data of the previously unknown modification are as follows: triclinic symmetry, space group $P\bar{1}$, $a = 6.5525(6)$ Å, $b = 7.5883(7)$ Å, $c = 7.6976(6)$ Å, $\alpha = 119.064(9)^\circ$, $\beta = 95.545(7)^\circ$, $\gamma = 107.645(8)^\circ$, $V = 304.84(5)$ Å³ and $Z = 4$. The crystal structure was solved from single-crystal diffraction data using direct methods and subsequently refined including fractional atomic coordinates and anisotropic displacement factors for all atoms to a residual value of $R1 = 2.16\%$ for 1517 independent observed reflections ($I > 2\sigma(I)$) and 110 parameters.

Both the divalent and hexavalent cations exhibit an octahedral oxygen coordination environment. The coordination spheres of the two symmetrically independent tungsten cations involve one very long W–O distance each and, therefore, one could also denote them as (5+1) coordinated. By sharing common edges and corners, the octahedra form a three-dimensional network, which can be built up from infinite rod-like elements running along [010] having a 2×2 octahedra wide cross section. Actually, a single rod can be imagined to be cut from the ReO₃-structure type and contains a total of four corner-sharing single-chains of octahedra. Within each single chain, strictly alternating cation sequences corresponding to ...Mg–W–Mg–W... can be observed. The [WO₆]-groups show a pronounced distortion due to second-order Jahn-Teller effects.

MgWO₄-II is topologically equivalent to the monoclinic so-called VO₂(HT) structure-type. A detailed analysis of the relationships with other ABO₄-compounds is presented based on concepts of group theory. Solid-state characterization has been supplemented by micro-Raman spectroscopy. Finally, the thermal expansion tensor of MgWO₄-II between ambient temperature and about 700 °C has been determined. The calculations indicate that the thermal expansion in MgWO₄-II is highly anisotropic and quasi two-dimensional with a very low value α_2 along the direction of the above-mentioned octahedral chains of the network.

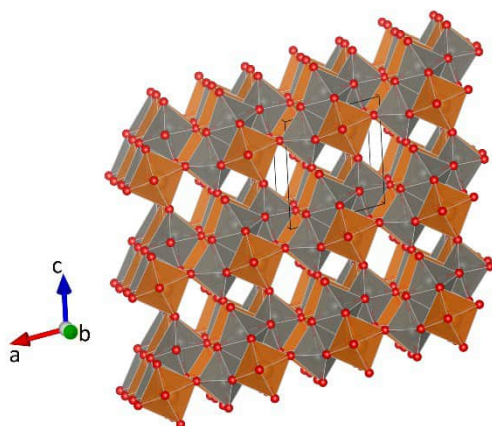


Figure 1. Side view of the crystal structure of MgWO₄-II. The MgO₆- and WO₆-octahedra are colored orange and grey, respectively. Small red spheres represent oxygen atoms. The outline of a single unit-cell is shown as well.

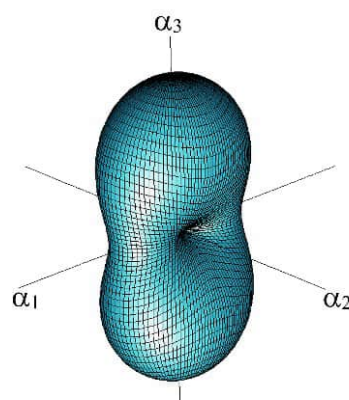


Figure 2. Three-dimensional representation surface of the thermal expansion tensor α_{ij} of MgWO₄-II at 500 °C.

Using combined C, Cd, Ba, and Ni isotopes as novel biomarkers to decipher Archean microbial metal cycling

S.V. Hohl¹, Y. Lv², S. Viehmann³, Yi-bo Lin⁴, Y. Zhang⁵, Y. Jiang¹

¹State Key Laboratory of Marine Geology, Tongji University, Shanghai; P.R. China

²State Key Laboratory of Geological Processes and Mineral Resources, China University of Geosciences, Beijing, P.R. China

³Department of Mineralogy, University of Hannover, Germany

⁴State Key Laboratory of Minerals Resources Research, Nanjing University, Nanjing, PR China

⁵Key State Laboratory of Palaeobiology and Stratigraphy (LBS)

Nanjing Institute of Geology and Palaeontology (NIGPAS)

e-mail: sv_hohl@tongji.edu.cn

Stromatolitic carbonates are geochemical archives that allow studying the long-term interplay of the biosphere, atmosphere, and hydrosphere through deep-time, with the unique potential to also investigate early life environments and the evolution of the metallome. Recently non-traditional stable isotopes of bioactive metals emerged as novel proxies to reconstruct the micronutrient cycling in stromatolitic microbial habitats.

In this study, we use stromatolites from the ~2.95 billion-year-old Pongola Supergroup (South Africa) as field laboratory for combined in-situ trace metal mapping and layer-specific novel stable metal isotope compositions to determine biogeochemical metal cycling in early Earth microbial habitats. LA ICP-MS maps reveal intrinsic bio-sedimentary enrichments of Ni and Cd in laminae; in contrast, Ba shows a more heterogeneous distribution throughout the stromatolite. Intra-laminae $\delta^{60}\text{Ni}$ and $\delta^{112}\text{Cd}$ follow typical kinetic isotopic fractionation, i.e., the isotopic composition of Cd and Ni evolves to heavier values with decreasing respective element concentrations arguing for carbonate precipitation from a fractionated Ni and Cd pool heavier than ambient silicate rocks. Further correlations with $\delta^{13}\text{C}$ and macronutrient P argue for co-existing methanogenetic, and photogenetic metal uptake responsible for pronounced isotopic fractionation. In contrast, $\delta^{138}\text{Ba}$ records isotope fractionation related to variable aragonite precipitation rates in the stromatolite, i.e., Ba evolves to isotopically heavier values with increasing concentrations under variable alkalinity in microbial habitats.

We show that the combination of Cd and Ni isotopes has a unique potential as novel isotope biomarker for early Earths bio-chemical sediment record of where traditional biomarkers are not applicable due to fragmentary preservation of organic material.

Deformation induced dissolution-precipitation of zircon in greenschist facies metasediments

M. S. Hollinetz¹, B. Grasemann¹, C. McFarlane², B. Huet³, D. Schneider⁴

¹ *Department of Geology, University of Vienna*

² *Department of Earth Sciences, University of New Brunswick*

³ *Department of Hard Rock Geology, GeoSphere Austria*

⁴ *Department of Earth and Environmental Sciences, University of Ottawa*

e-mail: marianne.sophie.hollinetz@univie.ac.at

Dissolution-precipitation coupled to mass transfer via an intergranular fluid is an essential mechanism to allow growth of metamorphic minerals and continuous equilibration during prograde metamorphism at greenschist facies conditions where the temperature is too low for allowing significant solid-state diffusion. As the prevailing stress field may control sites of preferred dissolution and precipitation, and mass transfer in the fluid may be highly anisotropic depending on the orientation and abundance of grain boundaries, all processes involved are inevitably linked with deformation. Although dissolution-precipitation and fluid-mediated mass transfer is well established for major components and growth metamorphic index minerals, little is known about the effects of these processes on accessory minerals that are considered nonreactive during metamorphism, consisting of elements that are considered as chemically immobile (e.g. Zr, Ti, Th). In this contribution, we present two case studies from the Staufen-Höllengebirge Nappe (Austroalpine Unit, Eastern Alps) which allow us to investigate the behaviour of Zr during greenschist facies prograde metamorphism in metasediments. At each locality we characterized detrital and metamorphic zircon populations with high-resolution SEM imaging and use a novel laser-ablation based strategy termed ‘bulk inclusion dating’ (Hollinetz et al. 2022) as a proxy for quantifying the extent of metamorphic zircon formation.

The first case study focuses on a chloritoid-bearing schist sampled at the base of the Staufen-Höllengebirge Nappe. Thermodynamic modelling predicts chloritoid growth in a P-T field between 450–490 °C and 0.5–0.7 GPa, indicating upper greenschist facies conditions. A conspicuous feature of this rock are numerous minute (0.1–3 µm), euhedral zircon crystals found both in chloritoid porphyroblasts and as matrix phases. From the zircon morphology, crystal size distribution, orientation and spatial distribution of different micro-zircon populations in the chloritoid core, its rim and the matrix, we interpret syntectonic zircon precipitation and progressive coarsening from a Zr-bearing fluid migrating along grain boundaries. Since no detrital zircon grains are observed in this sample, the Zr source is most likely a detrital Ti-phase that broke down during prograde metamorphism (e.g., titanite). Bulk inclusion dating of the chloritoid rim and its zircon inclusions yields a U-Pb age of 116.7 ± 9.1 Ma (MSWD: 1.5, n: 79), consistent with the Early Cretaceous timing of nappe stacking (Ortner et al. 2008). Systematic imaging of the targeted chloritoid domain combined with trace element data clarifies the abundance and size of different U-Pb bearing inclusions and unambiguously link the U-Pb age to micro-zircon inclusions. Our data therefore implies total mobilization of Zr during late prograde metamorphism.

The second case study focuses on metaconglomerates and -sandstones sampled in the Permian cover of the Staufen-Höllengebirge Nappe. In these lower greenschist facies samples, sedimentary features are preserved, but overgrown by a metamorphic mineral assemblage

consisting of chloritoid + pyrophyllite + muscovite + hematite + rutile + quartz that is consistent with P-T conditions of c. 350 °C and 0.2-0.6 GPa. Although all samples contain the same metamorphic mineral assemblage, they preserve significant differences regarding their primary sedimentological features (i.e., size of detrital clasts, layering) as well as secondary structural features (i.e. pressure solution cleavages). We investigated low-strain samples that exhibit a weakly developed fabric and high-strain samples with a pronounced spaced cleavage. Large, rounded detrital zircon grains that are occasionally fractured and/or porous are abundant in all samples. However, only in high-strain samples we find tiny zircon outgrowths on detrital grains and sparse submicron zircon (0.1–1 µm) in chloritoid. U-Pb ages of detrital zircon dominantly are between 700–400 Ma with the youngest concordant ages at c. 290 Ma. Bulk inclusion micro-zircon data in low-strain samples yield pre-Cretaceous dates younger than the detrital population, which indicates limited metamorphic zircon growth. In the “high-strain” samples, the bulk inclusion dates suggest significant micro-zircon crystallization in the Early Cretaceous. Combining microstructural observations and bulk-inclusion zircon data strongly suggests that Zr mobility and metamorphic zircon growth may be linked to intensity of deformation assisted by dissolution-precipitation.

We document deformation assisted Zr mobility in greenschist-facies metasediments and show that dissolution-precipitation coupled to mass transfer via an intergranular fluid is a process that is also relevant for elements reputed as immobile. As ongoing technological advances continuously shrink the limits imposed by instrumentation, the bulk-inclusion strategy can fill the gap in our understanding of the geological process leading to the precipitation of micro-zircon. This approach allows integration between metamorphic conditions, deformation and age constraints and opens up new applications in the investigation of low-grade metamorphic rocks, potentially including dating of deformation.

Hollinetz MS, Schneider DA, McFarlane CRM, Huet B, Rantitsch G, Grasmann B (2022): Bulk inclusion micro-zircon U–Pb geochronology: A new tool to date low- grade metamorphism. - *J Metamorphic Geol* 40, 207-227

Ortner H, Ustaszewski M, Rittner M (2008): Late Jurassic tectonics and sedimentation: breccias in the Unken syncline, central Northern Calcareous Alps. - *Swiss J Geosci* 101, 55-71

From allanite to monazite and back: a complex polymetamorphic REE-phase evolution

M. S. Hollinetz¹, B. Huet², C. McFarlane³, D. Schneider⁴, B. Grasemann¹

¹ Department of Geology, University of Vienna

² Department of Hard Rock Geology, GeoSphere Austria

³ Department of Earth and Environmental Sciences, University of Ottawa

⁴ Department of Earth Sciences, University of New Brunswick

e-mail: marianne.sophie.hollinetz@univie.ac.at

REE-bearing minerals (e.g. allanite / epidote, monazite, xenotime) are suitable targets for in-situ U-Th-Pb geochronology, thus it is essential to understand their stabilities during metamorphism for bringing the age data into any tectonic framework. At lower greenschist facies conditions, allanite / REE-rich epidote forms from the breakdown of detrital or low-grade metamorphic REE-bearing phosphates (e.g., monazite, xenotime). Depending on the bulk rock chemistry, the reverse reaction can occur at the greenschist – amphibolite facies transition or allanite remains stable at amphibolite facies conditions (e.g., Janots et al. 2008).

In this contribution, we present complex allanite – monazite – xenotime phase relations in chloritoid- and staurolite-bearing micaschist sampled at the base of the Schöckel Nappe (Austroalpine Unit, Eastern Alps). The samples contain large chloritoid, staurolite and retrogressed plagioclase porphyroblasts in a matrix of white mica, ilmenite, rutile and quartz. We distinguish two rock types that exhibit different REE-bearing minerals assemblages. Type 1 samples exhibit a simple REE-mineralogy that consist of a LREE-rich allanite core, which is overgrown by chemically zoned REE-rich epidote rim. U-Th-Pb dating using laser-ablation ICPMS yields an age of 275.2 ± 6.2 Ma (MSWD: 2.2, n: 45). In type 2 samples, the REE-phase relationships are much more complex. Few mm-scale LREE-rich allanite porphyroblasts possessing relicts of HREE-rich epidote rims are observed. Another generation of chemically zoned REE-epidote formed in fractures crosscutting both zones. Small (20–50 μm) REE-rich epidote blasts with a similar chemical composition occur in the vicinity of the large porphyroblasts. Additionally, up to 1 mm long aggregates consisting of small (10–20 μm) highly zoned, REE-rich epidote crystals intergrown with apatite are abundant. BSE imaging reveals highly irregular, micron-scale chemical zoning within the REE-epidote aggregate, resulting in a patchy appearance. In these aggregates small (<10 μm) monazite inclusions are typical. Small (<10 μm) xenotime crystals surrounding both the LREE-rich allanite and the REE-epidote aggregate also occur. U-Th-Pb dating that targeted the LREE-rich allanite was unsuccessful due to its high common Pb concentration. The zoned REE-rich epidote (overgrowth, blasts and aggregates) yield an age of 108.8 ± 6.2 Ma (MSWD: 3.1, n: 13).

Combining petrography, chemical composition and geochronological data from both sample types, we interpret LREE-rich allanite growth followed by formation of REE-rich epidote during prograde metamorphism in the Permian. Due to different bulk rock compositions, this assemblage remained stable at peak metamorphic conditions in type 1 samples, but was replaced by clusters of small monazite and xenotime crystals. During the Early Cretaceous metamorphic overprint in the allanite stability field, Permian monazite was destabilized and replaced by REE-rich epidote and apatite.

Janots, E, Engi, M, Berger, A, Allaz, J, Schwarz, JO, Spandler, C (2008): Prograde metamorphic sequence of REE minerals in pelitic rocks of the Central Alps: implications for allanite–monazite–xenotime phase relations from 250 to 610 °C. - J Metam Geol 26, 509-526

Raman spectroscopy of calcium oxalate hydrates from plant leaves

N. Horáková¹, J. Cempírek¹

¹Department of Geological Sciences, Masaryk University, Brno, Czech Republic
e-mail: nice.horak@gmail.com

There are several types of biominerals in plants; the most common are crystals and aggregates of calcium oxalate (CaOx), calcium carbonate (amorphous CaCO₃ or calcite) and amorphous silica. Ca-oxalates are represented by three hydrated forms of CaC₂O₄: whewellite (monohydrate; COM), weddellite (dihydrate; COD), and caoxite (trihydrate; COT). The most common mineral is COM whereas COD and COT are considered to be metastable phases; on the other hand, they are assumed to be precursor phases during COM or COD formation (Conti et al. 2015). Plant crystals are formed from endogenously synthesized oxalic acid which combines with calcium from the environment (Franceschi & Nakata, 2005).

We used synthetic analogues of CaOx hydrates to acquire high-resolution reference Raman spectra (Fig. 1). Consequently, we identified different CaOx hydrates in leaves of five different species of the *Araceae* family.

In the studied plants, the most common phase is COM in the form of needles (raphids), or crystalline sand; COD more commonly forms druses, dipramids or crystal twins, and COT is usually in the form of prisms or rounded aggregates. All three CaOx hydrates were found in 3 plant species, only COD in 4 plants and COM as the most common form in all five plants. COM is widespread, it is contained in all parts of the plant, mostly in the form of long needles stored in idioblasts, whereas the COD is in most cases in petiole in the form of druses. COT as the least stable phase is present only in rare cases in the leaves, its crystals were found in a large amount especially in *Alocasia macrorrhiza* Stingray.

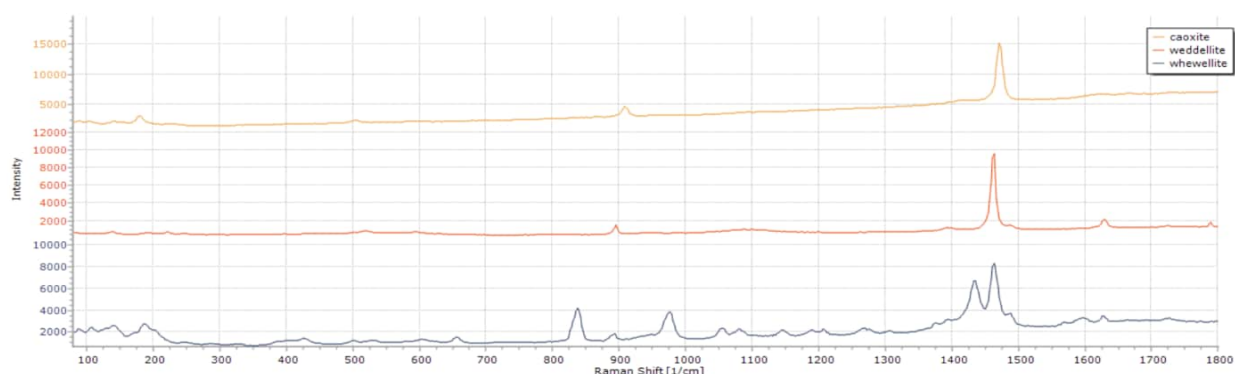


Figure 1 Raman spectra of COM, COD, and COT. - Foto: N. Horáková

Conti C, Casati M, Colombo C, Possenti E, Realini M, Gatta GD, Zerbi G (2015): Synthesis of calcium oxalate trihydrate: New data by vibrational spectroscopy and synchrotron X-ray diffraction. - *Spectrochimica Acta A, Molecular and Biomolecular Spectroscopy* 150, 721-730

Franceschi VR, Nakata PA (2005): Calcium oxalate in plants: formation and function. - *Annu Rev Plant Biol* 56, 41-71

Fluid “self-purification” – Insight from the particle attachment processes during the growth of three-dimensional mineral dendrites

Z. Hou¹, D. Woś², A. Rogowitz^{1,3}, C. Tschegg⁴, A.H.N. Rice¹, L. Nasdala¹,
F. Füsseis⁵, P. Szymczak², B. Grasmann¹

¹University of Vienna

²University of Warsaw

³University of Graz

⁴Glock Health, Science and Research GmbH, Deutsch-Wagram, Austria

⁵The University of Edinburgh

e-mail: zhaoliang.hou@univie.ac.at

Manganese (Mn) dendrites are a common type of mineral dendrites which can typically be found as two-dimensional branch-like patterns on rock surfaces, such as bedding planes and joints suggesting a fluid-rock interaction. Their three-dimensional (3D) counterpart has so far been massively overlooked, and thus little is known about 3D mineral dendrite growth processes and potential implications for fluid-rock interaction. Here, we combined high-resolution X-ray, electron-based micro-analyses with numerical modelling to show that the formation of natural 3D dendrites is an aggregation process of Mn-oxide nanoparticles in an aqueous environment. The dendrites form a < 15 mm high “forest” (Figure 1) in clinoptilolite-tuffs (zeolites), with trunks and branches, both having a core-rim structure and in the upper part of the forest, an alternating concentric core-rim layering. Secondary electron microscope (SEM) observations indicate dendrite growth reduced the rock’s original porosity from ~17% in the matrix to ~1% - 4% in the internal rims and 0% in the cores. High-resolution SEM shows dendrite-forming Mn oxides are built by sub-angular to rounded, several-nanometer- to 1- μ m-sized particles that have been aggregated forming larger clusters. Using the lattice Boltzmann method we modelled the formation and evolutionary processes of the 3D Mn dendrites. This allowed us to track the diffusing population of Mn ions and oxygen molecules as well as the reaction between them that led to the formation of Mn-oxide nanoparticles. The mobility and aggregation of nanoparticle populations were then tracked.

Our numerical models suggest sensitive feedback between dendrite morphology and the volume of infiltrating fluids, as well as the concentrations of Mn ions. Our work provides three important findings. First, 3D mineral dendrites can offer a simple system to investigate the affecting physical parameters of particle attachment processes in nature, such as the interplay of diffusion and surface energy effects between particles on dendrite growth dynamics. Second, the growth of the 3D dendrites, aggregating the particles in the surrounding fluids, can be seen as a fluid “self-purification” process. Third, the formation of the banding structures of the 3D dendrites, as well as the sensitive growth of dendrites in relation to the volume of infiltrating fluid and concentrations of Mn ion, strongly suggest the dendrites encode the hydrogeochemical history of the hosting rocks.

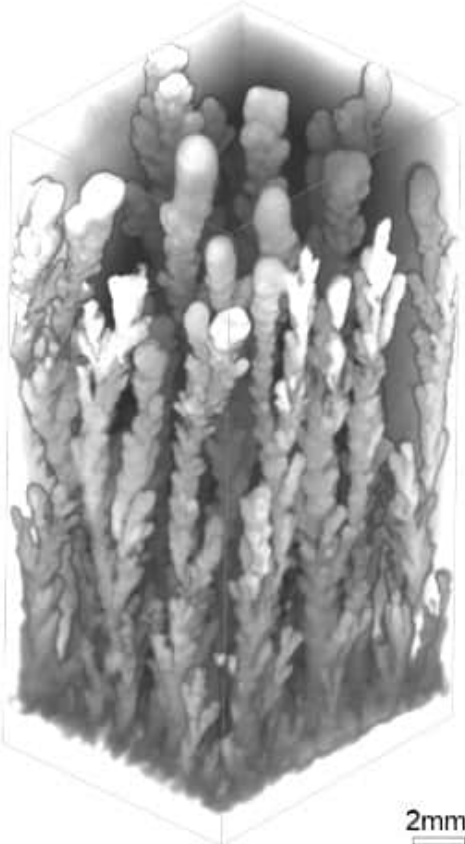


Figure 1. X-ray microtomography data show a 3D mineral dendrite forest.

**Creep, fail, and creep again at eclogite facies:
interactions between metamorphism and deformation at the
Hohl eclogite body (Koralpe, Eastern Alps, Austria)**

B. Huet¹, A. Rogowitz², S. Schorn²

¹GeoSphere Austria

²*Institute of Earth Sciences, University of Graz
e-mail: benjamin.huet@geosphere.at*

We present (micro)structural, petrographical, and chemical data from a series of low Mg – high Ti eclogite samples collected at the Hohl eclogite body (Koralpe, Eastern Alps, Austria). The eclogite mass is characterized by a pronounced foliation defined by the shape preferred orientation of the major minerals (average: 030/40) and mineral lineation defined by the shape preferred orientation of prismatic minerals (average: 324/18). In addition to omphacite, garnet, amphibole, epidote and rutile, minor euhedral quartz grains are present. Overall, grains show rather straight grain boundaries and uniform extinction. Thermodynamic forward modelling indicates that eclogitization occurred under fluid saturated conditions at about 1.8 GPa and 640 °C, which is slightly below the peak conditions.

The eclogite fabric is crosscut by a complex network of mineral veins characterized by coarse elongated crystals. These veins have a thickness comprised between a few millimeters and a few centimeters and contain the same assemblage as the host eclogite. In comparison to the host, they are enriched in quartz and epidote and depleted in garnet. Minerals composition is similar to the composition of the host eclogite indicating that veining occurred at eclogite facies conditions. One vein set is subperpendicular to the main foliation (average: 234/27) and the other is subparallel to it (average: 055/51). In both sets, the long axis of crystals is subparallel to the vein boundary and strikes NW-SE, which is compatible with crystal growth in the same tectonic regime as the eclogite fabric. Wing cracks indicate that the veins formed as shear fractures. Deflection of the eclogite fabric adjacent to the veins implies ductile reactivation of the veins as flanking structures and strain localization under top-to-the-W shearing. In consequence, the reactivated veins are characterized by undulatory extinction, twinning and subgrain formation in quartz, all being indicative of dislocation creep.

Our investigations document strong interactions between chemical (i.e., metamorphism) and mechanical (i.e., deformation) processes operating at eclogite facies and illustrate how metamorphic reactions dictate the deformation style of an eclogite. The microstructures of the eclogite host are interpreted as evidence of fluid-triggered syn-tectonic prograde eclogitization accommodated by diffusion and dissolution-precipitation processes. Ongoing prograde metamorphism resulted in progressive dehydration and minor melting of the already equilibrated eclogite. Subsequent increase in the pore-fluid pressure induced brittle failure and allowed precipitation of an eclogite facies assemblage in the vein. Finally, the quartz enriched veins localized ductile strain and deformed by dislocation creep. Hence, within the same tectonic event and without remarkable change of boundary conditions, eclogite can creep, fail and creep again.

Thermodynamic forward modelling of main and REE-bearing phases linking in situ U-Th-Pb REE-epidote ages and pressure-temperature conditions

B. Huet¹, D.A. Schneider², G. Rantitsch³

¹*GeoSphere Austria, Vienna*

²*Department of Earth and Environmental Sciences, University of Ottawa*

³*Department of Applied Geosciences and Geophysics, Montanuniversität Leoben
e-mail: benjamin.huet@geosphere.at*

REE-epidote is a solid solution of epidote-group minerals with rare earth elements plus yttrium that is a common phase of greenschist facies metapelites and a popular target for geochronology. Linking the time information to metamorphic conditions is however complicated by the diversity of reactions leading to the formation of REE-epidote as these involve REE- and/or Ca-bearing phases (e.g., monazite, apatite, calcite and plagioclase). We compiled a thermodynamic dataset for the system NaKCaFeMgAlSiTiHCOCeYPF from several sources (Berman, 1988; Connolly, 1995; Franzolin et al., 2011; Gaboreau et al., 2005; Hoschek, 2016; Pourteau et al., 2014; Spear, 2010; Spear & Pyle, 2010) in order to model equilibrium assemblages and phase chemistry for both main and REE-bearing phases in metapelites, especially in the greenschist facies.

We tested the dataset on a graphitic micaschist of the Schwarzkopf Formation collected at the foot of the Hochgamsburg (Fusch valley, Tauern Window). The sample shows relatively simple phase relationships and exhibits evidence for only one metamorphic event. The metamorphic assemblage consists of porphyroblasts of chloritoid, kyanite, REE-epidote and apatite in a matrix of muscovite, paragonite, margarite and quartz. Small rutile, graphite, xenotime and zircon are present as inclusions or in matrix. REE-epidote occurs as euhedral to subhedral, 250-1000 μm long grains and displays a microstructural and chemical core-mantle-rim zonation. The core has a patchy or oscillatory BSE pattern and is rich in inclusions of amoeboid quartz and minute graphite, as well as subordinate muscovite, chloritoid, rutile, xenotime and thorite. The mantle is discontinuous ($< 60 \mu\text{m}$ thick), inclusion-free and shows a bright smoother BSE pattern. The rim corresponds to dark and thin discontinuous overgrowths ($< 20 \mu\text{m}$ thick). Core, mantle and rim contain decreasing contents of REE+Th+U in the range 0.5–0.6, 0.4–0.6 and 0.1–0.3 a.p.f.u., respectively. The core and mantle are LREE-rich whereas the rim is HREE+Y-rich. LA-ICPMS analyses of REE-epidote mantle were carried out using a 20 μm laser spot diameter. All thirty-one analyses define a 27.5 ± 1.3 Ma U-Th-Pb isochron date (MSWD: 0.69) that is consistent with the conventional Tera-Wasserburg U-Pb date of 27.0 ± 2.3 Ma (MSWD: 0.36).

Thermodynamic forward modelling indicates that the observed assemblage chloritoid+kyanite+REE-epidote+muscovite+paragonite+margarite+apatite+rutile+xenotime+quartz is stable together with a graphite buffered COH-fluid in a narrow field centred at 12 kbar – 500 $^{\circ}\text{C}$, in agreement with results of Raman spectroscopy on carbonaceous material (511 ± 26 $^{\circ}\text{C}$). This field corresponds to the innermost part of the REE-epidote stability domain, in which the Ce-concentration progressively decreases from the margin to the centre. Modelling helps with interpreting the zonation of REE-epidote. The core grew from U-Th-rich monazite and most likely lawsonite once REE-epidote became stable. Xenotime inclusions represent products of this reaction. The mantle formed during continued growth further inside the REE-

epidote stability domain under increasing temperature. The HREE+Y-rich rim finally grew in an environment depleted in LREE, where xenotime was the main REE-source. Additionally the modelled compositions of chloritoid, white micas and apatite is compatible with the measured ones. Tests on the effect of unknown inputs (e.g., the bulk rock concentration of F) or poorly constrained thermodynamic data (e.g., the standard enthalpy of endmember allanite) indicate that these parameters have little impact on the results.

We could therefore acquire estimates for pressure and temperature and timing as well as coupling them tightly through thermodynamic modelling. The U-Th-Pb isochron date 27.5 ± 1.3 Ma represents the timing of the REE-epidote mantle growth and therefore corresponds to conditions close to peak metamorphism at 12 kbar – 500 °C. These P-T-t constraints are entirely consistent with the Barrovian metamorphic event that is widespread in the Tauern Window (“Tauernkristallisation”).

- Berman RG (1988): Internally-consistent thermodynamic data for minerals in the system Na₂O-K₂O-CaO-MgO-FeO-Fe₂O₃-Al₂O₃-SiO₂-TiO₂-H₂O-CO₂. - J Petrol 29, 445-522
- Connolly JAD (1995): Phase diagram methods for graphitic rocks and application to the system C-O-H-FeO-TiO₂-SiO₂. - Contr Miner Petrol 119, 94-116
- Franzolin E, Schmidt MW, Poli S (2011): Ternary Ca-Fe-Mg carbonates: subsolidus phase relations at 3.5 GPa and a thermodynamic solid solution model including order/disorder. - Contr Miner Petrol 161, 213-227
- Gaboreau S, Beaufort D, Vieillard P, Patrier P, Bruneton P (2005): Aluminum phosphate-sulfate minerals associated with Proterozoic unconformity-type uranium deposits in the East Alligator River Uranium Field, Northern Territories, Australia. - Canad Miner 43, 813-827
- Hoschek G (2016): Phase relations of the REE minerals florencite, allanite and monazite in quartzitic garnet-kyanite schist of the Eclogite Zone, Tauern Window, Austria. – Eur J Miner 28, 735-750
- Pourteau A, Bousquet R, Vidal O, Plunder A, Duesterhoeft E, Candan O, Oberhänsli R (2014): Multistage growth of Fe-Mg-carpholite and Fe-Mg-chloritoid, from field evidence to thermodynamic modelling. - Contr Miner Petrol 168, 25 pp
- Spear FS (2010): Monazite–allanite phase relations in metapelites. - Chem Geol 279, 55-62
- Spear FS, Pyle JM (2010): Theoretical modeling of monazite growth in a low-Ca metapelite. - Chem Geol 273, 111-119

Mineralogy and geochemistry of the Majala and Chacarilla Formations in Northern Chile (Atacama Desert): Implications for provenance, tectonic setting and paleoenvironmental conditions

N. Hurem¹, J. Méndez², V. Gesualdi³, M. Yurac⁴, M. Belvedere^{3,5}, C. Salazar², C. A. Meyer⁶, D. Hippler¹

¹*Graz University of Technology, Institute of Applied Geosciences, 8010 Graz, Austria*

²*Universidad Mayor, Escuela de Geología, 7500000 Providencia, Santiago de Chile, Chile*

³*Università degli Studi di Firenze, Dipartimento di Scienza della Terra, 50121 Firenze, Italy*

⁴*Unidad de Patrimonio Paleontológico, Consejo de Monumentos Nacionales 7500000 Providencia, Santiago de Chile, Chile*

⁵*NBFC, National Biodiversity Future Center, Piazza Marina 61, Palermo 90133, Italy*

⁶*University of Basel, Department of Environmental Sciences, 4056 Basel, Switzerland*

e-mail: nejla.hurem@student.tugraz.at

The Mesozoic sedimentary record of the northern Atacama and Tarapacá region in Chile is still to be fully explored. Mineralogical and geochemical studies as well as dating methods have never been carried out in this region, even though numerous and well-preserved Late Jurassic to Early Cretaceous dinosaur tracksites have been found recently. A pioneer field campaign was therefore carried out in 2022 in the Quebrada Huatacondo followed by a second campaign in 2023 in the Quebrada Arca. At both sites, Late Jurassic to Early Cretaceous sedimentary rocks of the Majala and Chacarilla Formations are well-exposed and constitute a promising geological archive. We sampled the sedimentary rocks, mainly fine-grained sandstones and siltstones, along the lithological sections in order to investigate the depositional and paleo-environmental conditions, provenance and tectonic setting as well as paleo-weathering and climate. In order to achieve our goals, we performed mineralogical and geochemical analysis using XRD and XRF in combination with high-resolution photogrammetry of the outcrops.

Preliminary results indicate that most of the fine-grained sandstones and siltstones can be classified as (sub-) litharenites mainly consisting of quartz and minor to accessory contributions of alkali feldspar, illite and chlorite. Finely-disseminated magnetite and pyrite produce the dark fresh-cut color and the reddish weathering color. Calcite and/or quartz constitute the main cementing phases. The geochemical composition of the sampled sedimentary rocks equals an almost upper crustal composition with distinct formation-specific differences between sand- and siltstones of the Majala and Chacarilla Formations: Rocks of the Majala Fm are slightly enriched in Cr, Ni and Cu, whereas rocks of the Chacarilla Fm show slight differences in elemental composition between the base and the top part. Summarizing the preliminary results, changes in the geochemistry between the two formations can already be clarified. With the complementary new data of the Quebrada Arca, the paleo-environmental conditions of the region can be reconstructed in a promising way. Additional U-Pb dating of the formations will provide desirable age constraints of deposition and provenance to set up an overall picture of the Late Jurassic to Early Cretaceous paleo-environment in Northern Chile.

The importance of volatiles in the formation of magmatic sulfide ore deposits: experimental constraints

G. Iacono-Marziano¹, M. Le Vaillant², S.J. Barnes², B. Godel²

¹ Institut des Sciences de la Terre d'Orléans, CNRS-Université d'Orléans-BRGM, Orleans, France

² CSIRO Mineral Resources, Perth, Australia
e-mail: giada.iacono@cnr-orleans.fr

Research studies provide growing evidence for the presence of fluids within magmatic mineral systems of mafic-ultramafic composition, although these ore-forming magmas are generally considered as volatile-poor. Here we summarize the results of two experimental studies that clarify the role of volatiles in the formation of magmatic sulfide ore deposits in mafic-ultramafic magmas: (i) interaction experiments simulating magmatic assimilation of sulfate and/or organic compounds (Iacono-Marziano et al. 2017); (ii) a more recent experimental study shedding light on previously unnoticed physical processes ensuing from the association between sulfide melt and fluid phase (Iacono-Marziano et al. 2022). The silicate melt composition used for both studies is similar to the parental melt of the Noril'sk-Talnakh ore bearing intrusions in Polar Siberia and all materials used in the experiments were sampled from the Noril'sk region. Moreover, the experiments were conducted at magmatic conditions relevant to the emplacement pressures and temperatures of the Noril'sk-Talnakh intrusions, so that experimental findings are directly applicable to these world-class ores.

The addition of external sulfur to the magma is one of the most common ore-forming processes invoked for magmatic sulfide deposits. Sulphur can be introduced into the magma by several process, our experiments at magmatic conditions (1200 °C, 80 MPa) show that anhydrite assimilation in the presence of a reducing agent, i.e. organic matter-rich rocks such as coal, is extremely efficient in producing high sulfide supersaturation in the magma.

The association between the sulfide melt and the fluid phase has been shown to allow the upward transfer of the sulfide melt (Mungall et al. 2015). Our recent experimental results illustrate another physical process that occurs when the proportion of fluid phase in the magma is low: the sulfide-fluid association favors the accumulation of sulfide liquid by facilitating the coalescence of the sulfide droplets that are attached to the same fluid bubble. This leads to the accumulation of the sulfide melt in the upper part of the experimental samples. Coalescence of sulfide droplets may be facilitated by the lowering of their interfacial tension induced by the bubble. However, the main driver for coalescence to occur is likely to be the fact that connection to the bubbles keeps the droplets in contact for long enough to allow drainage of the melt film between them, as opposed to the situation in a flowing magma where adjacent droplets are sheared apart before the melt film has time to drain (Robertson et al. 2015). This process may enable sulfide droplets coalescence and deposition in flowing magma, which otherwise have been shown to be unlikely processes (Robertson et al. 2015).

Experimental results indicate that sulfur degassing to the fluid phase increases with increasing proportion of fluid phase, concurrently reducing sulfide melt stability. Consequently, the sulfide melt is consumed and its metal content augments. Experimental samples with increasing fluid contents present increasingly Ni- and Cu-rich sulfide melts, illustrating how metal enrichment of sulfide melt can be attained by sulfur degassing. Magma degassing can therefore lead to sulfide upgrading.

Extensive sulfur degassing may completely consume the sulfide melt and form platinum-group minerals (PGMs) at relatively high temperatures (1150 °C in our experiments). Platinum-group mineral formation in the experimental samples occurs by desulfurisation of the

sulfide melt, while Ni and Cu are partitioned between the silicate melt and the fluid phase. This suggests an unconventional mechanism of PGM formation at temperatures higher than those typical of sulfide melt crystallization.

The experimental results presented above illustrate how the occurrence of a fluid phase in a mafic-ultramafic magma may represent a significant boost for magmatic sulfide ore forming processes: sulfide melt accumulation, tenor increase, and crystallization of PGMs are indeed key processes in the formation of magmatic Ni-Cu-Co-PGE ore deposits. We use the world-class Noril'sk-Talnakh ore deposits, in Polar Siberia as a case study.

Noril'sk-Talnakh ores are hosted in mafic-ultramafic subvolcanic ribbon-shaped intrusions. Extensive interaction of the ore-forming magmas with evaporitic and carbonaceous rocks has been proposed to be at the origin of the mineralization and the coexisting abundant fluid phase (e.g. Iacono-Marziano et al. 2017). The three main ore types are described in ore-bearing intrusions: (i) massive sulfides in the lower part of the intrusion and largely in the country rocks; (ii) disseminated sulfides (also called globular ores) inside picritic and taxitic rocks, also in the lower part of the intrusion; (iii) low-sulfide PGE ores in the upper part of the intrusion (e.g. Le Vaillant et al. 2017; Schoneveld et al. 2020). In the second and third ore-types subspherical structures within the crystalline framework have been interpreted as fluid bubbles filled with late magmatic phases (segregation vesicles) and/or hydrothermal minerals (e.g. Le Vaillant et al. 2017; Schoneveld et al. 2020). In the lower part of the intrusion, these structures are systematically associated with sulfide minerals suggesting they represent sulfide-fluid associations preserved in the olivine-rich magmatic rocks (Le Vaillant et al. 2017). In the upper part of the intrusion, these subspherical structures are even more common, typically associated with oxide mineral coatings, and generally containing lower amounts of sulfide minerals but abundant PGMs (Schoneveld et al. 2020), suggesting higher extents of sulfur degassing and sulfide dissolution. In contrast, massive sulfides are proposed to have experienced low extents of sulfur degassing, attested by the lower metal contents with respect to disseminated sulfides.

The distribution of ore types in Noril'sk-Talnakh intrusions therefore strongly suggests an increasing extent of degassing toward the top of the intrusions, implying increasing sulfide melt consumption and metal enrichment. Several other magmatic sulfide ores present evidence of the occurrence of a fluid phase during ore formation (relevant information can be found in Iacono-Marziano et al. 2022). Although a role for volatiles is less clear in other deposits, an increasing number of examples of sulfide-fluid associations is reported, suggesting that the mechanisms illustrated by the experiments may be more common than currently considered. We conclude that the role of volatiles in the formation of magmatic sulfide deposits should probably be re-evaluated.

Iacono-Marziano G, Ferraina C, Gaillard F, Di Carlo I, Arndt NT (2017): Assimilation of sulfate and carbonaceous rocks: experimental study, thermodynamic modeling and application to the Noril'sk-Talnakh region (Russia). - *Ore Geol Rev* 90, 399–413

Iacono-Marziano G, Le Vaillant M, Godel BM, Barnes SJ, Arbaret L (2022): The critical role of magma degassing in sulphide melt mobility and metal enrichment. - *Nature Communications* 13, 2359

Le Vaillant M, Barnes SJ, Mungall JE, Mungall EL (2017): Role of degassing of the Noril'sk nickel deposits in the Permian-Triassic mass extinction event. - *Proceedings of the National Academy of Sciences* 114, 2485–2490

Mungall JE, Brenan JM, Godel B, Barnes SJ, Gaillard F (2015): Transport of metals and sulphur in magmas by flotation of sulphide melt on vapor bubbles. - *Nature Geoscience* 8, 216–219

Robertson JC, Barnes SJ, Le Vaillant M (2015): Dynamics of magmatic sulphide droplets during transport in silicate melts and implications for magmatic sulphide ore formation. - *J Petrol* 56, 2445–2472

Schoneveld L, Barnes SJ, Godel B, Le Vaillant M, Yudovskaya MA, Kamenetsky V, Sluzhenikin SF (2020): Oxide-sulphide-melt-bubble interactions in spinel-rich taxitic rocks of the Noril'sk-Talnakh intrusions, polar Siberia. - *Econ Geol* 115, 1305–1320

Melting experiments reproducing early differentiation in primitive achondrites

S. Iannini Lelarge¹, M. Masotta^{1,2}, L. Folco^{1,2}, T. Ubide³, M.D. Suttle^{1,4}, W.N. Wegner⁵, L. Pittarello⁵

¹Università di Pisa, Italy

²Centro per l'Integrazione della Strumentazione Università di Pisa (CISUP), Pisa, Italy

³The University of Queensland, Brisbane, Australia

⁴The Open University, Milton Keynes, United Kingdom

⁵Naturhistorisches Museum, Vienna, Austria

e-mail: lidia.pittarello@nhm.at

Even small planetary bodies can have experienced internal differentiation, i.e., separation of the metal-sulphur components from the silicates forming a core and a mantle, respectively. In the meteorite record, primitive and anomalous achondrites represent a puzzle for scientists, as they seem to result from a differentiation process, but contain some primitive characteristics. Dedicated heating experiments in a piston-cylinder at 1 GPa and temperature steps from 1050 °C to 1400 °C, for 24h, have been performed to understand the uncomplete differentiation occurring on the parent body(ies) of such meteorites. As starting material, chondrites representative of specific early chemical settings were chosen: a) shocked L6 (DAV 01001), for intermediate redox state among the ordinary chondrites, b) carbonaceous chondrite (CM2, MCY12002), for oxidised parent bodies, and c) enstatite chondrite (EL6, MCY14005), for the reduced material in the Solar System. The resulting samples have been investigated with scanning electron microscope, electron microprobe analyser, laser ablation inductively coupled plasma mass spectrometry, Raman spectroscopy, and synchrotron radiation-micro computed tomography.

The experiments with the L6 chondrite resulted in non-eutectic melting of a small percent of the sample, with the metal and sulphide phases being mobilised first, already for the lowermost heating temperatures, and the silicates melting according to the sequence plagioclase-Ca-pyroxene-low Ca-pyroxene-olivine. This melting sequence affects the composition of the first melt produced, which evolves from trachyandesitic to more andesitic terms for increasing vol% of melting. Despite the fast quenching, crystallisation of olivine dendrites could not be avoided. The chemical composition of the produced melt shows similarities with that of some andesitic to trachyandesitic anomalous achondrites, such as NWA 11119, EC002, GRA 60128/9, Almahata Sitta clast ALM-A, NWA 6698, and NWA 11575. This suggests that these anomalous achondrites could have formed by incipient melting of chondritic material under fast heating conditions, like due to planetary collisions.

In the case of the CM2 carbonaceous chondrite as starting material, the obliteration of the initial texture is immediate. The melt produced has a composition ranging from picobasaltic to basaltic-andesite, but already at the “low” temperature experiments several phases crystallises from the melt, such as Ca-rich olivine, pyroxene, spinel, kirschsteinite, and Ca-phosphates. The composition of the newly formed phases and the melt closely recall those found in angrites, some rare and peculiar basaltic achondrites, which likely have an impact origin (Rider-Stokes et al., 2023), where one of the bodies had a carbonaceous composition.

The analyses of the experiments with the enstatite chondrite are still ongoing. However, this work shows the importance of an experimental petrologic approach in constraining magmatic processes in the early Solar System.

Deformation and reaction of crustal rocks under high-pressure, high-temperature conditions

S. Incel^{1,2}, L. K. Mohrbach^{1,3}, J. Renner¹

¹*Institute for Geology, Mineralogy and Geophysics, Ruhr Universität Bochum, 44801 Bochum, Germany*

²*Present address: Imperial College London, Department of Materials, South Kensington Campus, SW7 2AZ, London, United Kingdom*

³*Present address: WWU Münster, Institute for Mineralogy, 48149 Münster, Deutsches Elektronen Synchrotron, Beamline P02.2, 22607 Hamburg, Germany
e-mail: sincel@imperial.ac.uk*

In the plagioclase-rich lower continental crust, hydrous epidote-group minerals will, among other phases, replace plagioclase once minor amounts of fluids are available (Goldsmith 1981). It has previously been shown that reacting plagioclase aggregates are significantly weaker than their unreacted counterparts at otherwise identical conditions (Stünitz & Tullis 2001). Yet, it still remains unclear if the observed weakening is due to the nucleation and growth of inherently weaker product phase, e.g., epidote-group minerals, or due to inhibited grain growth in a polyphase aggregate as a result of Zener pinning. Our working hypothesis was the former: Epidote-group minerals are inherently weaker than plagioclase under the same experimental conditions. To test this hypothesis, we experimentally investigated the relative strength of pure epidote and pure plagioclase aggregates at a confining pressure of 1 GPa, two different temperatures (550 and 650 °C) and two different strain rates ($5 \cdot 10^{-5}$ and $5 \cdot 10^{-6}$ s⁻¹) using a Griggs apparatus. Furthermore, epidote-group minerals will be initially much smaller than plagioclase, they are replacing. Hence, we also investigated potential strength differences due to differences in grain size by deforming aggregates with a grain-size range of either ≈ 90 – 135 μm or <25 μm . Under identical conditions, epidote aggregates are significantly stronger than their plagioclase counterparts even when partially reacted. Furthermore, we observe that reaction can induce a change in deformation behavior from distributed cracking to faulting in our epidote aggregates.

Goldsmith JR (1981): The join $\text{CaAl}_2\text{Si}_2\text{O}_8$ – H_2O (anorthite–water) at elevated pressures and temperatures. - *Amer Mineral* 66, 1183–1188

Stünitz H, Tullis J (2001): Weakening and strain localization produced by syn-deformational reaction of plagioclase. - *Internat J Earth Sci* 90, 136–148. <https://doi.org/10.1007/s005310000148>

Calorimetric characterisation of the alkali feldspar binary

F. Ingegneri¹, E. Dachs², R. Abart¹

¹ Department of Lithospheric Research, University of Vienna

² Department of Chemistry and Physics of Materials

Section Materials Science and Mineralogy, Salzburg University

e-mail: flora.ingegneri@univie.ac.at

The thermodynamic study of materials is vital as thermodynamic data such as Gibbs energy are of pivotal importance for modelling phase equilibria and processes in both nature and industry. This work aims at contributing to the thermodynamic characterisation of the most common mineral group in Earth's crust, namely feldspar. The focus is on the alkali feldspar solid solution, the endmembers of which are Albite (NaAlSi₃O₈) and Orthoclase (KAlSi₃O₈), and on the quantification of its molar heat capacity c_p and vibrational entropy S^{vib} as functions of composition X_{Or} .

Gem quality sanidine from Volkesfeld, Germany, with a composition of $X_{\text{Or}} = 0.85$ was used as starting material for cation exchange with a (Na,K)Cl salt melt. A total of 14 feldspar samples together with different (Na,K)Cl salt mixtures were held at 900 °C for a duration of 30 to 45 days in order to reach equilibrium. The resulting series was analysed on the EPMA Cameca SX Five FE at the University of Vienna and represents the composition of the whole binary.

10 of these samples have already been analysed via heat pulse calorimetry using the Physical Property Measurement System (PPMS) by Quantum Design at Salzburg University. C_p data were obtained for the temperature range from 2 to 300 K. S^{vib} was subsequently calculated by numerical integration of c_p/T and is shown in Tab. 1. The corresponding plot can be found in Fig. 1. The relative error for S^{vib} is estimated at $\pm 0.7\%$ (Dachs & Bertoldi 2005).

These preliminary results yield a positive excess entropy with a maximum of $S^{\text{ex}} \approx 2 \text{ J mol}^{-1} \text{ K}^{-1}$. Further samples are being prepared for calorimetric analysis to close the current gap at $X_{\text{Or}} = [0.1, 0.3]$. As soon as the missing calorimetric data is available a Margules mixing model will be fitted to the data in order to obtain S^{vib} and S^{ex} as a function of X_{Or} .

Table 1. Vibrational entropy S^{vib}
at $T = 298.15 \text{ K}$

X_{Or} []	S^{vib} [$\text{J mol}^{-1} \text{ K}^{-1}$]
0.06	207.0
0.33	211.2
0.40	211.4
0.50	212.2
0.56	212.4
0.60	211.9
0.68	212.7
0.83	212.9
0.93	212.9
1.00	213.1

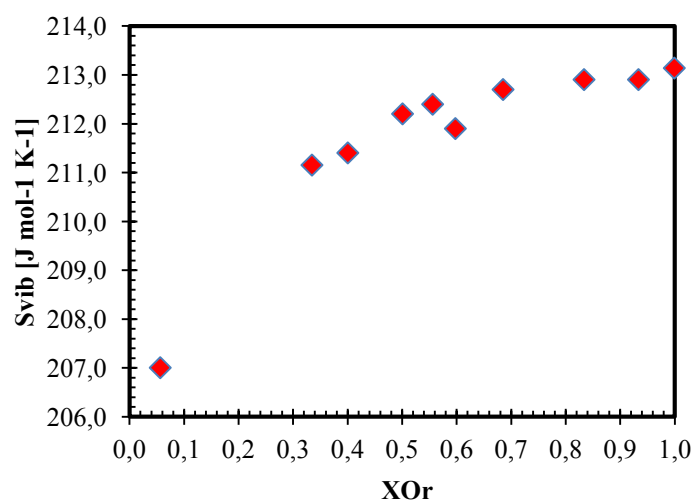


Figure 1. Vibrational entropy S^{vib} at $T = 298.15 \text{ K}$

Impurities in quartz from Amazon river sands

D. Jaeger¹, T. Ludwig², S. Andó³, E. Garzanti³, A.O. Sawakuchi⁴, C. Chiessi⁴,
M. Strasser¹, R. Stalder¹

¹University of Innsbruck

²Heidelberg University

³University of Milano

⁴University of São Paulo

e-mail: roland.stalder@uibk.ac.at

Incorporation of impurities in quartz is primarily controlled by (1) the availability of the respective impurity in the chemical system and (2) the crystallisation condition. Even if the concentration of some of the impurities (such as OH species) may later be affected by metamorphic overprint, the total impurity inventory of each individual grain reflects its geological history. As the impurities are rather stable throughout sedimentary processes, quartz from siliciclastic sediments may thus serve as archive for the crystallisation conditions of the rocks in the source area. As hydrous defects are usually charge balanced by trace metals, concentrations in the most important charge balancing elements (Al, Li, B) may be reflected in the IR spectra, unless the sample lost OH by diffusion during metamorphic dehydration.

In this study quartz from several sediment samples from the lower Amazon and from three major tributaries of the Amazonian river system were analysed by FTIR spectroscopy and secondary ion mass spectrometry (SIMS) in order to characterise individual grains with respect to hydrous defects and trace metal contents.

Differences between the four samples are subtle but discernable. Trace element contents relevant for hydrous defects (Al, Li, B) are in general lower in quartz from the rivers draining the old continental shields (Xingu and Rio Negro) compared to quartz from the lower Amazon River; grains from Solimões, partly drained from the Andean orogeny, exhibit in general the highest trace element concentrations. The trace element contents are partly reflected in the OH signatures of quartz: samples from Solimões and lower Amazon exhibit a larger fraction of OH-rich grains, and the Li- and Al-specific absorption bands is less evolved in grains from Xingu and Rio Negro.

Taking into account trace element contents and OH signatures in quartz, quartz grains from the lower Amazon sample represent a mixture with significant contributions from Andean and shield sources. Conversely, heavy-mineral analysis indicates the Solimões River as the dominant source of sediment. This apparent discrepancy is reconciled considering that Andean detritus has a much higher heavy-mineral concentration than detritus recycled from siliciclastic rocks exposed in the Andean foothills, siliciclastic covers of the Brazilian-Guiana Shield, and quartz-rich sediments incised all across the retroarc basin and Amazonian lowlands.

Structure and vibrational properties of hydrous and anhydrous amorphous SiO₂ at high pressures

S. Jahn¹, M. Herrmann¹, M. Schulze¹, J. Dreschmann¹, W. Morgenroth², G. Garbarino³,
M. Mezouar³, M. Wilke²

¹ Institut für Geologie und Mineralogie, Universität zu Köln, Zùlpicher Straße 49b, 50674 Köln, Germany

² Institut für Geowissenschaften, Universität Potsdam, Karl-Liebknecht-Str. 24, 14476 Potsdam, Germany

³ ESRF, CS 40220, 38043 Grenoble Cedex 9, France

e-mail: s.jahn@uni-koeln.de

Volatiles such as H₂O are important components in natural silicate glasses and melts. Their solubility and structural incorporation mechanisms depend on many parameters, and they change continuously with pressure and temperature. For a systematic understanding of those changes, in situ measurements are required. Here, we study the pressure-induced structural evolution of hydrous amorphous SiO₂ in diamond and moissanite anvil cells up to 40 GPa by Raman spectroscopy and X-ray diffraction, and compare the results to those from the respective anhydrous samples. The hydrous sample contains 10 wt% H₂O. Both hydrous and anhydrous samples show the characteristic features of the 4-fold to 6-fold Si coordination transition, which is essentially completed at the highest pressures of this study. Raman spectra indicate the predominance of molecular H₂O species over hydroxyl groups in the whole pressure range. However, the spectra change significantly at wavenumbers in the range of the O-H stretching vibrations. By analogy to spectra of pure liquid and crystalline H₂O, a transition from water-like to ice-VI-like behavior is observed, before the spectra become very broad at the highest pressures. The interpretation of the experimental data is supported by *ab initio* molecular dynamics simulations.

This work was supported by BMBF project 05K19PK2. Simulations were performed on the JUWELS supercomputer at Jùlich Supercomputing Centre (JSC).

Ca₂(Mn,Ti)O₄, a potentially new mineral with the Ruddlesden-Popper structure

R. Juroszek¹, B. Krüger², G. Cametti³

¹ Institute of Earth Sciences, University of Silesia, Katowice, Poland

² Institute of Mineralogy and Petrography, University of Innsbruck, Innsbruck, Austria

³ Institute of Geological Science, University of Bern, Bern, Switzerland

e-mail: rafal.juroszek@us.edu.pl

A potentially new mineral Ca₂(Mn,Ti)O₄, was found within the xenolith sample from the Bellerberg volcano in Germany. It is an accessory phase in partially altered xenolith composed mainly of cuspidine, fluorapatite, and gehlenite. It forms flat plate dark-brown crystals up to 100 μm in size. The empirical formula, established by electron microprobe analyses, is (Ca_{1.98}Ce_{0.06})_{Σ2.04}(Mn⁴⁺_{0.36}Ti_{0.35}Fe³⁺_{0.19}Al_{0.09})_{Σ0.99}O₄.

This mineral exhibits a Ruddlesden-Popper type structure characteristic for perovskite-like layered oxides of general formula $A_{n+1}M_nO_{3n+1}$, where A is typically an alkaline or rare earth ion, and M is a transition or post-transition metal ion (Ruddlesden and Popper, 1957). The diffraction pattern of the analysed crystal reveals a tetragonal lattice with unit cell parameters $a = 3.7666(2)$ Å, $c = 11.9861(8)$ Å, and volume $V = 170.050(17)$ Å³. The A site was refined with Ca²⁺ and Ce³⁺ scattering factors, whereas for the M site, a mixed scattering curve was used (0.55 Mn/Fe + 0.36 Ti + 0.09 Al) according to the chemical analyses. The final structure refinement converged to $R = 2.74\%$. The crystal structure of Ca₂(Mn,Ti)O₄ exhibits a modular nature and consists of Ca(Mn,Ti)O₃ perovskite layers, which are packed between CaO rock-salt layers arranged along the c -axis (Fig. 1).

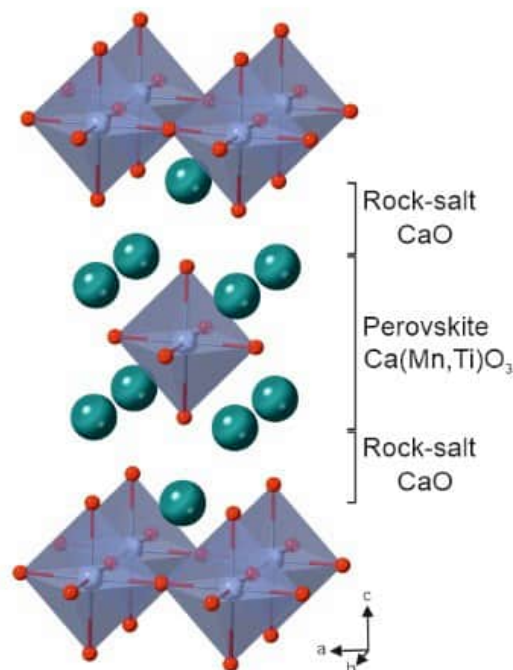


Figure 1. The Ca₂(Mn,Ti)O₄ phase with Ruddlesden-Popper structure, comprising rock-salt (CaO) and perovskite layers Ca(Mn,Ti)O₃ build by Ca-green spheres and (Mn,Ti)O₆ octahedra.

Previous reports indicate that Ruddlesden-Popper calcium manganates exhibit functional electronic properties and are interesting for various electronic phenomena, such as insulator-to-metal transitions, charge-ordering, and colossal magnetoresistance effect (Fawcett et al. 1998; Autret et al. 2004).

The investigation was partially supported by the National Science Center of Poland Grant (grant number 2021/41/B/ST10/00130).

Autret C, Martin C, Hervieu M, Retoux R, Raveau B, André G, Bourée F (2004): Structural investigation of Ca_2MnO_4 by neutron powder diffraction and electron microscopy. – J Solid State Chem 177, 2044-2052

Fawcett I.D, Sunstrom J.E, Greenblatt M, Croft M, Ramanujachary K.V (1998): Structure, magnetism, and properties of Ruddlesden-Popper calcium manganates prepared from citrate gels. – Chem Mater 10, 3643-3651

Ruddlesden S, Popper P (1957): New compounds of the K_2NiF_4 type. – Acta Crystallogr 10, 538-539

Interstitial diamonds reveal dry exhumation of UHP metamorphic rocks - insights from 3-D spatially resolved X-ray microtomography data

W.-A. Kahl¹, H.-P. Schertl²

¹MAPEX Center of Materials and Processing, Universität Bremen, 28359 Bremen, Germany,

*²Institute of Geology, Mineralogy and Geophysics, Ruhr-University Bochum, 44780 Bochum, Germany
e-mail of communicating author: wakahl@uni-bremen.de*

The Kokchetav Massif of northern Kazakhstan is part of one of the largest suture zones in Central Asia and contains slices of HP and UHP metamorphic rocks. The Kumdy Kol area is the first recorded locality of diamondiferous UHP rocks (Sobolev & Shatsky 1990) that were formed due to subduction processes at mantle depths. The diamond grains in these rocks are exceptionally large for such an environment reaching 200 µm. In a calcsilicate rock studied they form inclusions within Grt or Cpx, or occur as interstitial grains along Grt-Cpx boundaries. Such diamonds were reported to have formed by C-O-H fluids, but is it possible to identify potential fluid pathways? Our true spatially resolved tomography data of a piece of rock indicate, that the location of diamonds is related to a network of deformational microcracks. Local hydrothermal alteration in parts accompanied by Hbl-formation refers to a late event. Our data corroborate a diamond formation by fluids and an early dry exhumation history after peak metamorphic conditions were reached.

Sobolev NV, Shatsky VS (1990): - Nature 343, 742–746

Please add – many thanks:

----- Name of the abstract file: **Kahl_W-A_InterstitialDiamonds_AbsForm2**

The abstract file should be named according to the first author's last name (e.g., Zemmann.docx). Only doc or docx formats are accepted. The abstract should be sent as an attachment to an e-mail to minwien2023.mineralogie@univie.ac.at

----- Presenting author: **Wolf-Achim Kahl**

Please indicate your preferences for the presentation of your contribution:

----- Preferred presentation: Oral Poster

----- Preferred session of the contribution

	first - second choice	
Young Scientist Session. Chairs: L. Czekay (Bayreuth), R. Volkmann (Potsdam)	<input type="checkbox"/>	<input type="checkbox"/>
Metal enrichment processes - latest advances in the understanding of ore formation. Chairs: M. Wilke (Potsdam), J. Michaud (Hannover), M. Korges (Potsdam)	<input type="checkbox"/>	<input type="checkbox"/>
The co-evolution of Earth's atmosphere, oceans, continents, and life from the early Archean until today. Chairs: S. Viehmann (Hannover), A.S. Rodler (Vienna), S.V. Hohl (Shanghai, China)	<input type="checkbox"/>	<input type="checkbox"/>
Carbonates in natural and technical environments – Precipitation mechanisms, monitoring and applications. Chairs: R. Boch (Graz), P. Németh (Budapest, Veszprém), M. Dietzel (Graz)	<input type="checkbox"/>	<input type="checkbox"/>
Interplay of chemical and mechanical processes across scales. Chairs: S. Schorn (Graz), A. Rogowitz (Graz)	<input type="checkbox"/>	<input type="checkbox"/>
Chronology of geological processes: past, present, future. Chairs: D. Gallhofer (Graz), E. Skrzypek (Graz)	<input type="checkbox"/>	<input type="checkbox"/>
Spectroscopic methods in modern geosciences. Chairs: M. Kaliwoda (Munich), J. Göttlicher (Eggenstein-Leopoldshafen)	<input type="checkbox"/>	<input type="checkbox"/>
Linking microstructures, crystallographic textures, and the nature of interfaces. Chairs: T. Griffiths (Wien), G. Habler (Wien)	<input type="checkbox"/>	<input type="checkbox"/>
Crystallographic Materials Science: from basics to application. Chairs: S. Schorr (Berlin), C. Weidenthaler (Duisburg-Essen)	<input type="checkbox"/>	<input type="checkbox"/>
Structure-property relationships of minerals and beyond - Minerals as advanced materials. Chairs: M. Münchhalfen (Bochum), J. Schreuer (Bochum)	<input type="checkbox"/>	<input type="checkbox"/>
"Early Earth – Crustal evolution, metamorphism and tectonics" Chairs: Thomas Müller (Göttingen), Dominik Sorger (Göttingen), Matthias Willbold (Göttingen)	<input type="checkbox"/>	<input type="checkbox"/>

Stable and radiogenic isotopes as fingerprints of processes in natural materials
Chairs: Johannes Pohlner (Frankfurt) & Chunhui Li (Cologne/Chengdu)

Mineral history & teaching - Geoscientific collections & museums
Chairs: Vera Hammer (Wien), Christin Kehler (Freiberg),
Dorothee Kleinschrot (Würzburg), Birgit Kreher-Hartmann (Jena)

Oral contribution & panel discussion

Turning toolboxes into an ecosystem: How to make research software interoperable?
Chairs: T. Rose (Frankfurt), D.C. Hezel (Frankfurt)

You do not find a suitable session for your abstract here - please suggest an additional symposium. The list of sessions is completed regularly at <https://minwien2023.univie.ac.at/abstracts.html>

**---- Further session topics - please mark your preferences
(first and second choice)**

Mineralogy and Crystallography

Properties of minerals & materials - Physics and chemistry of minerals
Crystal structures of minerals and related compounds
Topology and modular aspects of crystal structures - Aperiodic & quasi-crystals
(New) minerals and mineral classification
Phase transitions and high-pressure / high-temperature mineralogy
Neutron and electron scattering – Microstructures & textures of minerals
Recent analytical developments used in the Earth sciences

Applied and Technical Mineralogy

Environmental mineralogy and technical applications
Forensic mineralogy - archeometry and cultural heritage
Cements, ceramics, glasses and building stones
Biomineralogy and biomineralization
Mineralogical aspects related to climate change (carbon cycle)

Environmental and medical mineralogy

Biosphere-geosphere interactions: environmental aspects
Weathering, dissolution, adsorption, and transport processes
Developments and applications of analytical methods
Stable isotopes in biogeochemistry: experiment and theory
Biogenic substances - CO₂ cycle and storage - anthropogenic environments
Biogeochemical interfaces and environmental mineralogy

Petrology and Geochemistry

From melts to rocks and P-T evolution of rocks
Timing and duration of metamorphic events and reactions
Transport reactions, fluid—mineral—rock interactions and interfaces

Stable and radioactive isotopes: clocks & tracers of rock formation/evolution
Geochronology and petrochronology - fluid processes in the crust and mantle
Sedimentology and weathering of rocks - thermodynamics and phase equilibria
Experimental mineralogy, petrology and geochemistry - the deep Earth and beyond
Astro-mineralogy, early solar system and the mineral record of impact events

Economic Geology and Ore Deposits

Raw materials & metals - Industrial, economic and ore minerals
Critical geosystems - (Deposit) modelling and mapping
Geometallurgical aspects in the beneficiation of metallic ore deposits
Genesis of ore & mineral deposits - Field studies - Supergene enrichments

Open Sessions

Computer programmes - gemmology and gemstones
Mineral history & teaching - mineralogical museums and collections
Other general aspects of mineralogy, petrology, and geochemistry

Amphibole megacrysts with cavities reveal rapid crystal growth at mantle depth during the 1951 eruption of Fogo (Cape Verdes)

W.-A. Kahl¹, A. Klügel²

¹*MAPEX Center of Materials and Processing, Universität Bremen, 28359 Bremen, Germany*

²*Faculty of Geosciences, Universität Bremen, 28359 Bremen, Germany*

e-mail: wakahl@uni-bremen.de, aklugel@uni-bremen.de

The late basaltic deposits of the 1951 Fogo eruption contain peridotite xenoliths, ultramafic cumulate xenoliths, and euhedral kaersutite megacrysts up to 12 cm in size. The megacrysts contain abundant of cavities that locally contain vesicular basaltic glass with small clinopyroxene phenocrysts, with compositions more primitive than the host magma. Some of these cavities remind of hopper textures. Micro-CT analyses reveal that the cavities are only in part interconnected and in some cases form funnel-like openings to the crystal surface. In addition to some spinel and clinopyroxene inclusions, the kaersutite contain numerous pyrrhotite rods aligned perpendicular to the crystal surface, and some pyrrhotite blebs. We interpret these structures to result from rapid crystal growth in a volatile-rich silicate melt with abundant droplets of exsolved sulfide melt. Barometric data indicate that this rapid growth occurred in the uppermost mantle. Possible causes for the rapid growth event include magma mixing or sudden H₂O loss to raise the liquidus.

Structural news from the quaternary system Na₂O-K₂O-CaO-SiO₂

V. Kahlenberg¹, H. Krüger¹, S. Garber¹, J. Aschauer¹

¹University of Innsbruck, Institute of Mineralogy and Petrography, Innrain 52, 6020 Innsbruck, Austria
e-mail: volker.kahlenberg@uibk.ac.at

The crystalline compounds and sub-solidus equilibria in the ternary subsystems Na₂O-CaO-SiO₂ and K₂O-CaO-SiO₂ have been studied frequently in the past. On the contrary, the quaternary system containing both alkali oxides is rather uncharted territory and no thermodynamic or detailed phase-analytical data are available. So far, only a few potassium-sodium-calcium silicates such as K_{1.08}Na_{0.92}Ca₆Si₄O₁₅ (Kahlenberg et al. 2018a) or Na_{1.5}K_{0.5}Ca₆Si₄O₁₅ (Kahlenberg et al. 2018b) or NaKCa₄[Si₉O₂₃] (Kasatkin et al. 2019) have been structurally characterized. While the first two members are mixed-anion silicates and isostructural with ternary phases, the latter compound corresponding to the mineral patynite represents a previously unknown structure type and belongs to the group of tubular inosilicates.

Our own recent synthesis experiments in the quaternary system K₂O-Na₂O-CaO-SiO₂ proved that there exists a complete solid-solution series between Na₄CaSi₃O₉ and its K-counterpart: Na_{4-x}K_xSi₃O₉. Lattice parameters of the cubic materials (space group $Pa\bar{3}$) obtained in polycrystalline form from solid-state reactions vary between 15.0998 (x = 0) and 15.9472 (x=4) Å. The silicate anions form strongly corrugated 12-membered tetrahedral rings.

Furthermore, we were able to prepare a previously unknown compound with composition K_{0.72}Na_{1.71}Ca_{5.79}Si₆O₁₉. Single-crystals of sufficient size and quality could be retrieved from a starting mixture with a K₂O:Na₂O:CaO:SiO₂ ratio of 1.5:0.5:2:3. The crystal structure was determined by direct methods at 25 °C from single crystal X-ray diffraction data (tetragonal symmetry, space group $P4_122$, $a = 7.3659(2)$ Å, $c = 32.2318(18)$ Å, $V = 1748.78(12)$ Å³, $Z = 4$, $R_1 = 0.026$, $wR_2 = 0.063$, for 1690 observed reflections with $I > 2\sigma(I)$). The silicate anion consists of highly puckered unbranched six-membered oligogroups of composition [Si₆O₁₉] having point-group symmetry 2 (C₂). Even though several thousands of natural and synthetic oxidosilicates have been structurally characterized, the present compound is the first representative for this type of catena-hexasilicate anion - at least to the best of our knowledge.

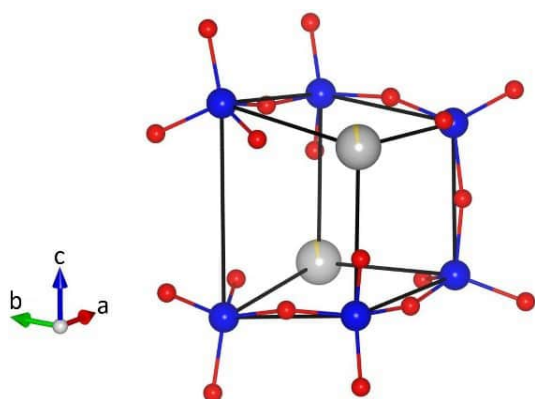


Figure 1. Conformation of a single [Si₆O₁₉] group in K_{0.72}Na_{1.71}Ca_{5.79}Si₆O₁₉. The six Si atoms (blue) can be thought of as being located at the corners of an imaginary distorted cube with edge lengths between 3.22 and 4.60 Å. The remaining two corners are occupied by Na/Ca cations (grey/yellow). Oxygen atoms are shown in red.

- Kahlenberg V, Mayerl MJP, Schmidmair D, Krüger, H (2018a): First investigations on the quaternary system Na₂O-K₂O-CaO-SiO₂: synthesis and crystal structure of K_{1.08}Na_{0.92}Ca₆Si₄O₁₅. - *Miner Petrol* 112, 219-228
- Kahlenberg V, Mayerl, MJP, Schmidmair D, Krüger H, Tribus M (2018b): Preparation and characterization of Na_{1.5}K_{0.5}Ca₆Si₄O₁₅ and Na_{1.41}K_{0.19}Ca_{2.20}Si₂O₇: two new phases in the system Na₂O-K₂O-CaO-SiO₂. - *Eur J Mineral* 30, 957-966
- Kasatkin AV, Cámara F, Chukanov NV, R. Škoda, F. Nestola, AA Agakhanov, DI Belakovskiy, V.S Lednyov (2019): Patynite; NaKCa₄[Si₉O₂₃], a new mineral from the Patynsky massif. - *Minerals* 6, 611, 18 pp

3D electron and powder X-ray diffraction: the best of both worlds to study the crystal structure of γ - $\text{Na}_2\text{Ca}_6\text{Si}_4\text{O}_{15}$

V. Kahlenberg¹, H. Krüger¹, J. Vinke¹, S. Ito², C.J. Schürmann³

¹Institute of Mineralogy and Petrography, University of Innsbruck, Innrain 52, 6020 Innsbruck, Austria

²Rigaku Corporation, 3-9-12 Matsubaru-cho, Akishima, Tokyo 196-8666, Japan

³Rigaku Europe SE, Hugenottenallee 167, 63263 Neu Isenburg, Germany

e-mail: volker.kahlenberg@uibk.ac.at

Phase assemblages of mixtures containing Na_2CO_3 , CaCO_3 , and SiO_2 in the molar ratio 1:3:2 have been studied at elevated temperatures. Synthesis experiments have been performed at 1000, 1100 and 1200 °C within a DTA-TGA apparatus. Mass losses during heating and annealing periods of the high-temperature treatment have been studied *in-situ* using thermogravimetry. For the run at 1200 °C, the solid-state reactions resulted in almost phase pure polycrystalline material of a previously unknown high-temperature polymorph of $\text{Na}_2\text{Ca}_6\text{Si}_4\text{O}_{15}$, whose formation was triggered by significant Na_2O losses at the reaction temperature. The new so-called γ -phase has been structurally characterized by a combination of 3D single-crystal electron and powder X-ray diffraction.

Basic crystallographic data at ambient conditions are as follows: monoclinic symmetry, space group $C2$, $a = 17.2066(1)$ Å, $b = 5.47863(3)$ Å, $c = 7.32583(4)$ Å, $\beta = 91.435(4)^\circ$, $V = 690.38(1)$ Å³, $Z = 2$. Structure solution was accomplished by electron diffraction, whereas the subsequent refinement calculations were based on the Rietveld method using high-resolution data from a laboratory powder diffractometer. Similarly to the two already known $\text{Na}_2\text{Ca}_6\text{Si}_4\text{O}_{15}$ modifications, the crystal structure of the γ -phase contains both $[\text{Si}_2\text{O}_7]$ dimers and insular $[\text{SiO}_4]$ moieties. Tetrahedra and $[\text{CaO}_6]$ octahedra form a three-dimensional framework whose topological characteristics have been studied. The remaining Ca and Na cations are located on five symmetrically independent positions in the cavities of the network.

There are sufficiently strong arguments that previously described “triclinic $\text{Na}_2\text{Ca}_3\text{Si}_2\text{O}_8$ ” is actually misinterpreted γ - $\text{Na}_2\text{Ca}_6\text{Si}_4\text{O}_{15}$ and that a sodium calcium silicate with a molar ratio of $\text{Na}_2\text{O}:\text{CaO}:\text{SiO}_2 = 1:3:2$ probably does not exist. Our investigation is an excellent example that 3D electron diffraction has transformed from an exotic technique for crystal-structure determination into an indispensable method for problems where small sizes of the crystallites is an issue.

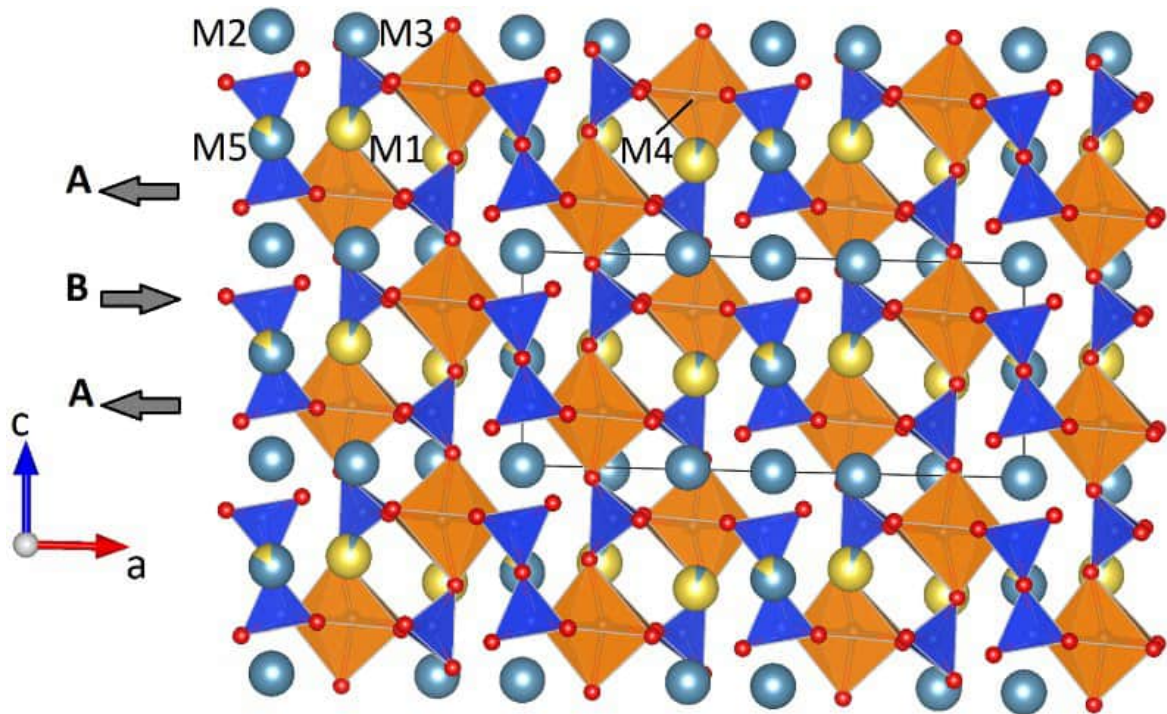


Figure 1. Projection of the whole crystal structure of $\gamma\text{-Na}_2\text{Ca}_6\text{Si}_4\text{O}_{15}$ (monoclinic) along $[0\bar{1}0]$. $[\text{SiO}_4]$ tetrahedra and calcium dominated $[\text{M}_4\text{O}_6]$ octahedra are shown in dark blue and orange, respectively. Small red spheres represent oxygen atoms. Interstitial Ca and Na atoms are given in light blue and yellow. Bi-colored spheres indicate mixed Ca-Na positions. The alternating ...ABA... stacking sequence of adjacent layers building up the network as well as the relative shift vectors are indicated.

Children's and teenagers' geoscience projects at the Mineralogical State Collection Munich (MSM)

M. Kaliwoda^{1,2}, M. Junge^{1,2}, F. Hentschel¹, F. Joseph¹, W.W.Schamahl^{1,2}

¹Mineralogical State Collection Munich, SNSB

*² Department of Earth and Environmental Sciences, LMU, Ludwig Maximilians University, Munich
e-mail: kaliwoda@snsb.de*

The Museum Mineralogia München is the publicly accessible part of the Mineralogical State Collection Munich (MSM), which belongs to the Bavarian State Natural Science Collections (SNSB). The aim of the State Collection is to impart knowledge in the STEM subjects, i.e. especially in the field of geosciences. The MSM has been trying to fulfil this task for more than 16 years and has thus gained a great amount of experience in the teaching-learning field.

Since the geosciences are unfortunately not a school subject, but geoscientific topics are becoming more and more relevant for socio-political concerns, it is important to sensitize and inspire children and young people for the geosciences at an early age.

The Museum Mineralogia therefore offers a variety of activities on topics such as (1) volcanism, (2) the cycle of rocks, (3) meteorites, (4) the construction of a smartphone and critical raw materials. In addition, there are special exhibits each year on a variety of earth science topics that are incorporated into the student projects and tours. All projects offered can also be booked as school and kindergarten projects, if there is capacity. In addition, there is a network with other science laboratories for schoolchildren both in Munich (Muc-Labs) and throughout Germany (LeLa). Participation (e.g., in Girls' Day, Science Days (Forscha), or the Children's Culture Summer) as well as many different projects in Munich and the surrounding area with other museums and research institutes also strengthen the reach. In addition to national projects, international projects (e.g. with Austria, Italy, Norway) are carried out.

As a further concept, internships are also offered for school students from the age of 14. In addition, the Mineralogische Staatssammlung Munich has successfully participated in two funded programs on ease-Corona (BMBF - catching up after Corona). Here, especially children and teenagers who show Corona and Lock-down induced learning deficits should be supported.

Raman spectroscopy as an important tool for the petrological study of different meteorite samples

M. Kaliwoda^{1,2}, I. Drozdovsky³, F. Joseph¹, F. Dellefant², W.W. Schmahl^{1,2}

¹Mineralogical State Collection Munich, SNSB, Munich, Germany

²Department of Earth and Environmental Sciences, LMU, Ludwig Maximilians University, Munich, Germany

³European Astronaut Centre (EAC) - European Space Agency, Cologne, Germany

e-mail: kaliwoda@snsb.de

Spectroscopic methods with their capability to gain information on different rocks and minerals as well as on fluids and other types of inclusions are becoming more and more relevant in earth sciences in order to open up new fields of research and providing solutions to problems in various scientific disciplines.

Raman spectroscopy represents a fast and at the same time precise method to characterize materials in different types of environments. Furthermore, Raman spectroscopy can be an important tool to investigate extraterrestrial bodies, because the measurements are more or less independent of the surrounding environmental effects including the temperatures. Therefore, it will be an important goal to gain as much experience as possible by Raman measurements of meteorites in order to be able to apply this experience to extraterrestrial bodies.

At the mineralogical state collection Munich (MSM) Raman spectroscopy is used to characterize different meteorites, with main focus to mars, moon and vesta, in order to find out the composition of the various minerals, the high pressure phases, the possible glass components and the inclusions. All the measured phases are collected in an in-house Raman database (Kaliwoda et al. 2013, 2021; Drozdovsky et al. 2020).

Raman spectroscopy make it possible to gain more information about the mineral composition and the original pressure and temperature conditions on these extraterrestrial bodies. In addition, it is possible to draw parallels to the composition and to the formation history of the early earth. In another Raman study we aim at getting more detailed information about the earth mantle and investigate therefore mantle-xenoliths and ophiolitic mantle sections.

One examples of our research targets is NWA11266 meteorite, discovered in 2017, that has already been classified as lunar feldspar breccia (Gattacceca et al., 2019). In the MSM we did further investigations with Raman spectroscopy. The main minerals are mafic olivines and pyroxenes, beside anorthitic feldspar minor graphite and tiny little glass patches. Furthermore, metallic components and accessory phases like apatite and zircon could be identified. In addition, we like to compare brecciated meteorites with other terrestrial Breccias, like those from the Nördlinger Ries.

Drozdovskiy I, Ligeza G, Jahoda P, Franke M, Lennert P, Vodnik P, Payler SJ, Kaliwoda M, Pozzobon R, Massironi M, Turchi L, Bessone L, Sauro F (2020): The PANGAEA Mineralogical Database. - Data in Brief 31, S2352-3409(20), 30879-9, <https://doi.org/10.1016/j.dib.2020.105985>

Gattacceca J, Bouvier A, Grossman J, Metzler K, Uehara M (2019): The meteoritical bulletin, no. 106. -Meteorit Planet Sci 54, 469–471

Kaliwoda M, Giordano D, Krüger ME, Uysal I, Akmaz MR, Hoffman V, Hochleitner R, Schmahl WW (2021): Raman spectroscopy as a tool for the quantitative estimate of chromium aluminium oxide content in chromite. - Spectroscopy 36, 17-23

Kaliwoda M, Hochleitner R, Hoffmann VH, Mikouchi T, Gigler AM, Schmahl WW (2013): New Raman spectroscopic data of the Almahata Sitta Meteorite. - Spectroscopy letters 46, 141-146

Investigation of Martian and other meteorites using Raman spectroscopy

M. Kaliwoda^{1,2}, F. Joseph^{1,2}, V. Helmbrecht², J. Zuncke^{1,2}, A. Nömer², L. Eckle²,
I. Drozdovsky³

¹*Mineralogical State Collection Munich (SNSB)*

²*Department of earth and environmental sciences, LMU, Ludwig-Maximilians University*

³*European Astronaut Centre (EAC) - European Space Agency (Linder Höhe, D-51147 Cologne, Germany
e-mail: kaliwoda@snsb.de*

Our solar system consists of a wide range of different objects. Planet Mars is one of them, and its proximity to Earth makes it an important place to study. Investigations are currently related to rover missions; human missions are planned, and, in addition, the study of meteorites provides us with a lot of new data. Martian meteorites deliver us a sample in a "nutshell" that can tell us about (1) the composition of the Martian surface, (2) the chemical composition of minerals, (3) rock temperatures and pressures during formation, (4) and possible melting processes.

In the Mineralogical state collection Munich (MSM) there are several Martian but also other meteorites, i.e. from the Moon, Vesta or other extraterrestrial bodies for investigation with Raman-Spectroscopy, SEM and electron microprobe. In the following context, we want to present two Martian meteorites NWA13366 and NWA7032. Our first investigations belong to NWA13366, this meteorite is composed of olivine with 55 vol.-% and pyroxene with 35 vol.-%. Olivine is generally Mg-rich and pyroxenes have an enstatitic composition. Another present phase is maskelynite with 5 vol.-% next to older feldspar grains. Maskelynite is a plagioclase glass that possibly formed during a high-pressure impact. Minor amounts of ilmenite, chromite, hematite, iron sulfide (possibly troilite), calcite, and calcium phosphate (possibly merrillite) also occur in the NWA 13366, the meteorite belongs furthermore to the shergottite group of Martian meteorites. NWA 13366 has a bimodal texture of poikilitic and non-poikilitic areas. Poikilitic domains consist of mm-sized anhedral magnesian low-Ca pyroxene crystals (oikocrysts) and smaller interlocked subhedral to euhedral Mg-rich olivine crystals (chadacrysts). Cr-rich chromite is also present. Olivine grains show chemical zoning from Fe-rich rims to Mg-rich cores in poikilitic domains. Pyroxene in poikilitic areas might be zoned as well. Non-poikilitic domains contain smaller olivine and pyroxene grains, that are chemically more evolved with higher Fe- and Ca-contents. Calcium carbonate (calcite) is present in fracture zones. It could originate from primary Martian aqueous or hydrothermal alteration or due to secondary alteration on Earth. The meteorite shows many features indicative of high shock stages. The chemical differences and the bimodal texture in the shergottite indicate a complex crystallization history of the meteorite. NWA7032 belongs also to the Martian group of meteorites and shows gabbroitic compositions. The rock is at the moment under investigation, more details will be shown later on. The detailed investigation of meteorites helps us to understand the composition of the Martian surface and besides this gives us important data for the in-house Raman database (MSM-MRD), which also takes part in the Raman database of the ESA [1].

Crystal-chemical effects of high-temperature treatment on Mg-dominant tourmalines

P. Kardošová¹, P. Bačík^{1,2}, J. Fridrichová¹, O. Rybnikova¹, M. Miglierini³, T. Mikuš⁴

¹Comenius University in Bratislava, Faculty of Natural Sciences,

Department of Mineralogy, Petrology and Economic Geology, Bratislava, Slovak Republic

²Earth Science Institute of the Slovak Academy of Science, Bratislava, Slovak Republic

³Slovak University of Technology, Faculty of Electrical Engineering and Information Technology

Institute of Nuclear and Physical Engineering, Bratislava, Slovak Republic

⁴Earth Science Institute of the Slovak Academy of Science, Bratislava, Slovak Republic

e-mail: kardosova6@uniba.sk

We present a detailed study of oxidation-induced deprotonation and its influence on tourmaline breakdown. The crystal-chemical effects of high-temperature treatment on Mg-dominant tourmalines, the oxidation of Fe³⁺ associated with the deprotonation of OH⁻ groups and its subsequent effect on the breakdown of tourmaline. Tourmaline samples were studied using a wide range of analytical methods. The chemical composition of all samples is Mg dominant, but with variable X_{Mg} [Mg/(Mg+Fe)]: TSCH – schorlitic dravite from Tanzania with X_{Mg} of 0.5-0.8; CHD – Mg-dominant dravite from China with X_{Mg} > 0.9; TUV – Cr-bearing uvite from Tanzania with X_{Mg} > 0.98). Tourmaline samples were heat-treated in air at atmospheric pressure at temperatures from 700 to 1000 °C to obtain information on the effect of oxidation on the deprotonation of OH groups.

The majority of Fe was oxidized after heating at 800 °C which was observed in the Mössbauer spectrum of TSCH and optical spectrum of CHD. This CHD sample had insufficient Fe content for Mössbauer spectroscopy but changes in the optical spectrum indicated partial Fe oxidation – an increase in band intensity at 750 nm and the shift of the absorption edge to the green region due to electron interactions between Fe²⁺ and Fe³⁺ ions. The influence of the possible cation oxidation on the OH⁻ groups bonded at the edges of YO₆ octahedra was determined by IR spectroscopy. The TSCH sample shows a significant decrease in absorbance of OH⁻ bands which indicates deprotonation induced by Fe oxidation, the absorbance decrease in the CHD spectra is less pronounced, and TUV does not show any decrease in absorbance suggesting no oxidation could take place due to a very low Fe, Mn, and V content. This influenced the appearance of samples after the structural breakdown: TSCH heated at 1000 °C changed appearance and cracked but there were no volumetric changes; CHD and TUV samples expanded. This suggests that before the structural breakdown, TSCH released water gradually due to Fe oxidation but CHD and TUV samples kept a majority of water in the structure due to the low content of Fe and released at one moment causing the expansion of samples.

However, the CHD and TUV samples retained most of the water in the structure due to the low Fe content that could oxidize, so the OH⁻ groups were not significantly deprotonated. Deprotonation occurred in one sudden moment as the structure broke down, with the released water escaping rapidly in the form of steam in all directions, causing the samples to expand. The contents of chromophores in the samples were too low to colour the resulting products in the new forms.

Meta-igneous rocks from the Kaintaleck Metamorphic Complex as indicators of a Variscan Ocean within the Eastern Alps

K. Karner-Rühl¹, C.A. Hauzenberger¹, E. Skrzypek¹, H. Fritz¹

*¹University of Graz, Universitaetsplatz 2, 8010 Graz, Austria
e-mail: kevin.karner-ruehl@edu.uni-graz.at*

The Kaintaleck Metamorphic Complex is part of the Eastern Greywacke Zone, Eastern Alps. The Eastern Greywacke Zone is subdivided into three Alpine nappes, with the Veisch nappe being overlaid by the Silbersberg and Noric nappe. The Silbersberg nappe contains intercalated crystalline fragments of Variscan age, the Kaintaleck Metamorphic Complex. It is represented by a mafic suite, comprising amphibolite, garnet-amphibolite, greenschist and serpentinite, and a felsic suite, that consists mostly of gneiss and mica schist, some of them garnet-bearing. Petrological, geochemical and geochronological investigations were carried out to provide new insights into the metamorphic and tectonic evolution of the Kaintaleck Metamorphic Complex. Geochemical results indicate, that the mafic suite originates from tholeiitic basalts. Amphibolites from the locality of Frauenberg show an enrichment in LREE indicative for either an E-MORB or OIB affinity. Garnet-amphibolites, amphibolites, and greenschists from the localities of Prieselbauer, Oberdorf, Unteraich, Kalwang, Arzbach and Schlöglmühl show flat REE patterns with only a slight depletion in HREE and resemble T-MORB. Samples from the localities of Stübminggraben and Utschgraben are depleted in LREE, typical for N-MORB affinity. U-Pb zircon dating of a garnet-amphibolite sample from the locality of Prieselbauer yields an Early Devonian age of 414.2 ± 5.6 Ma, interpreted as the age of protolith formation. Garnets from these garnet-amphibolites show distinct plagioclase-epidote-rich symplectitic coronae, indicating decompression from former high-pressure metamorphic conditions. The evolution of the Kaintaleck Metamorphic Complex might be related to the opening and closure of the short-lived Balkan-Carpathian Ocean. The onset of rifting might be due to slab roll-back and back-arc spreading during Late Ordovician and Early Silurian. During the Late Devonian and Early Carboniferous, the Balkan-Carpathian Ocean was subducted. The mafic suite of the Kaintaleck Metamorphic Complex, comprising the oceanic crust of the Balkan-Carpathian Ocean, was dragged into the subduction channel and underwent HP metamorphism with conditions of $\sim 550^\circ\text{C}$ and $\sim 1.7\text{-}2.2$ GPa. Subsequent exhumation resulted in a near isothermal decompression. Further relics of Devonian age are exposed in the North-Gemeric Klatov and Rakovec Complexes in the Western Carpathians (Putiš et al. 2009). Neubauer et al. (2022) propose, that the Klatov and Rakovec Complexes are small remnants of the Balkan-Carpathian Ophiolite, dated with an age of 405.0 ± 2.6 Ma by Zakariadze et al. (2012). Similarities in their age, the affinity to MORBs, the presence of serpentinite and the general conception, that the Klatov Complex might be a continuation of the Kaintaleck Metamorphic Complex within the Western Carpathians, might relate the mafic suite of the Kaintaleck Metamorphic Complex to the Balkan-Carpathian Ocean.

- Putiš M, Ivan P, Kohút M, Spišiak J, Siman P, Radvanec M, Uher P, Sergeev S, Larionov A, Méres Š, Demko R, Ondrejka M (2009): Meta-igneous rocks of the West-Carpathian basement, Slovakia: indicators of Early Paleozoic extension and shortening events. - *Bull Soc Géol Fr* 180, 461–471
- Neubauer F, Liu Y, Dong Y, Chang R, Genser J, Yuan S (2022): Pre-Alpine tectonic evolution of the Eastern Alps: From Prototethys to Paleotethys. - *Earth-Science Reviews* 226, doi:10.1016/j.earscirev.2022.103923
- Zakariadze G, Karamata S, Korikovskiy S, Ariskin A, Adamia S, Chkhotua T, Sergeev S, Solov'eva N (2012): The Early–Middle Palaeozoic Oceanic events along the Southern European Margin : The Deli Jovan Ophiolite Massif (NE Serbia) and Palaeo-oceanic Zones of the Great Caucasus. - *Turkish J Earth Sci* 21, 635–668, doi:10.3906/yer-1011-2

Antimony isotope evolution during hydrothermal precipitation and during oxidative weathering of diverse antimony mineralization in the Western Carpathians (Slovakia)

A. Kaufmann^{1,2}, M. Lazarov^{1*}, S. Weyer¹, J. Majzlan²

¹ Institute of Mineralogy, Leibniz University Hannover, Germany

² Institute of Geosciences, Friedrich Schiller University Jena, Germany

*e-mail: m.lazarov@mineralogie.uni-hannover.de

Numerous hydrothermal Sb or Sb-Au mineralization and ore deposits are seated in a Variscan basement of the Western Carpathians (Slovakia). Stibnite is the most common mineral in all of them. However, each deposit has its specific mineralization association and Sb is found in a variety of sulfides, sulfosalts, or oxides, in combination with Cu, Pb, Fe, or Ag. All these minerals, on macro- or microscale, carry information about the ore-forming processes. In this study, a variety of Sb minerals from four ore deposits: Dve Vody, Magurka, Dúbrava and Pezinok, are investigated for their Sb isotope composition. Measurements were conducted *in-situ* by deep UV-fs laser ablation system coupled with MC-ICP-MS following the procedure of Kaufmann et al. (2021).

The $\delta^{123}\text{Sb}$ values of all investigated primary hydrothermal minerals show a range of -0.8 to +1.0 ‰. Variations of $\delta^{123}\text{Sb}$ for each deposit do not exceed 0.8 ‰. Combining information from textural relationships and Sb isotope compositions, in some cases also mineral trace-element contents, implies that mineral $\delta^{123}\text{Sb}$ can be correlated with the mineral precipitation sequence. This relationship can be observed on hand-specimen as well as on ore body and ore deposit scale. The systematic increase of $\delta^{123}\text{Sb}$ values during progressive precipitation of primary Sb minerals can be rationalized by a Rayleigh crystallization model, applying a uniform isotope fractionation factor for all minerals that was determined for stibnite by Zhai et al. (2021).

Each ore deposit has its own distinct mean of $\delta^{123}\text{Sb}$. Dúbrava displays the lowest values of around -0.11 ± 0.56 ‰, followed by Magurka and Pezinok with a mean of 0.08 ± 0.59 ‰ and 0.24 ± 0.48 ‰, respectively. The overall heaviest isotopic compositions are observed for Dve Vody $\sim 0.53 \pm 0.88$ ‰. These differences may indicate that either different sources or differently developed fluids, or both were responsible for each deposit formation.

A similar spread of $\delta^{123}\text{Sb}$ (-0.50 to +0.8 ‰) was observed for secondary Sb minerals formed near surface as the result of weathering. Depending on the amount of leached, primary mineral, and redox changes during transport and formation of secondary minerals, Sb isotope fractionation of more than 0.3 ‰ was observed. While the Sb oxides tend to become isotopically heavier, Sb hydroxides, Fe,Sb oxides or silicates prefer the ^{121}Sb isotope and display lower $\delta^{123}\text{Sb}$ signatures, compared to the coexisting primary minerals.

Thus, considering all studied deposits, mineral $\delta^{123}\text{Sb}$ may help to constrain the precipitation sequences in primary ore deposits, to decipher hydrothermal remobilization or near-surface weathering of primary ores and to constrain the potential source(s) of the metalloid.

Kaufmann AB, Lazarov M, Kiefer S, Majzlan J, Weyer S. (2021): In-situ determination of antimony isotope ratios in Sb minerals by femtosecond LA-MC-ICP-MS. - JAAS 36, 1554-1567

Zhai D, Mathur R, Liu SA, Liu J, Godfrey L, Wang K, Vervoort J. (2021): Antimony isotope fractionation in hydrothermal systems. - Geochim Cosmochim Acta 306, 84-97

Isotope fractionation of antimony during oxidative weathering of stibnite (Sb_2S_3)

A.B. Kaufmann^{1,2}, M. Lazarov², J. Majzlan¹, S. Weyer²

¹Friedrich-Schiller University Jena

²Leibniz University Hannover

e-mail: a.kaufmann@mineralogie.uni-hannover.de

Antimony (Sb) has two stable isotopes with almost equal abundances ($^{121}\text{Sb} = 57.213\%$, $^{123}\text{Sb} = 42.787\%$). Similar to Mo, V, Fe and U, Sb is redox-sensitive, however, with a higher redox potential (Eh value) than the aforementioned elements. It can occur in four formal (-I, 0, +III, +V) oxidation states with commonly +III and +V encountered in nature. Therefore, stable Sb isotope signatures could have great potential as a redox proxy in low-temperature surface studies to reconstruct the weathering conditions of recent and Early-Earth environments. The transport of Sb in the environment (including soils, water and sediment) was reviewed by Herath et al. (2017), however, only scarce experimental data exist, regarding the environmental release of Sb (e.g., Biver et al. 2012) under different Eh conditions.

In this study, we experimentally explored the leaching behaviour of stibnite (Sb_2S_3), the most common Sb mineral in nature, and associated isotope fractionation. For this, we performed leaching experiments with an isotopically homogeneous stibnite powder (0.14 g) and three different acids (0.05 M HCl, 0.5 M HNO_3 and 0.1 M oxalic acid) with a volume of 200 ml each. Antimony concentration, isotope composition, pH, and Eh values were determined at selected time steps in a time interval from 30 minutes to 13 days. During the leaching experiments, the pH value of oxalic acid and HCl solutions remained constant at 1.4 and 1.5, respectively, whereas that of HNO_3 rapidly increased from 0.7 to 1.2 and stabilized at 1. The Eh of the HCl solution was adjusted at 570 mV during the first 20 hours, whereas the Eh of HNO_3 and oxalic acid decreased to <630 mV till the end of the experiment. During the first 6 hours, with high Eh (>730 mV) for HNO_3 and oxalic acid, stibnite released almost 1% of Sb (>900 μg), resulting in $\sim 0.1\%$ heavier and $\sim 0.3\%$ lighter $\delta^{123}\text{Sb}$ for oxalic acid and HNO_3 , respectively. In comparison, HCl, without large Eh changes, preferentially mobilized the lighter Sb isotope, resulting in $\delta^{123}\text{Sb} \sim -0.4\%$ compared to the precursor material ($\delta^{123}\text{Sb} = -0.21\%$). In the HCl experiment, equilibrium was achieved after 20h with constant Sb concentration and $\delta^{123}\text{Sb}$. Conversely, progressive leaching with HNO_3 and oxalic acid, accompanied with a Eh drop, resulted in an increase of the Sb content (>2 %) with preferential mobilisation of the heavy Sb isotope.

The leachate for the first 20 hours of leaching is marked by <0 saturation indexes relative to Sb oxides, resulting into progressive dissolution of Sb. After a further slight decrease of Eh values (e.g. from 630 mV to down to 565 mV for oxalic acid) at >20 hours, the leachate became alternately over- and undersaturated relative to Sb oxides, resulting in the precipitation of Sb oxides along with additional Sb leaching. In comparison, natural secondary minerals show an isotopic variation of -0.5 to +0.3 ‰ with also preferentially enrichment of light Sb isotope compared to primary minerals (isotopic range: -0.4 to +0.8) that are consistent with our leaching results with weak acids of HNO_3 and HCl, which generates heavy isotopic Sb enriched residues. With this in mind, our first results indicate the potential of Sb isotopes as a new proxy to interpret modern and past weathering and hydrothermal alteration environments.

- Biver M, Shotyk W (2012): Stibnite (Sb_2S_3) oxidative dissolution kinetics from pH 1 to 11. – *Geochim Cosmochim Acta* 79, 127-139
- Herath I, Vithanage M, Bundschuh J (2017): Antimony as a global dilemma: Geochemistry, mobility, fate and transport. – *Environmental Pollution* 223, 545-559

Reconstruction of a 3.5-billion-year-old marine environment: Evidence from trace element data of iron formation from the Daitari Greenstone Belt, Singhbhum Craton, India

S. Kienle¹, S. Viehmann², J. Jodder^{3,4}, A. Hofmann⁴, T. Schulz¹, C. Koeberl¹

¹Department of Lithospheric Research, University of Vienna, Austria

²Institute of Mineralogy, Leibniz University Hanover, Germany

³Evolutionary Studies Institute, University of the Witwatersrand, South Africa

⁴Department of Geology, University of Johannesburg, South Africa

e-mail: a01616435@unet.univie.ac.at

Banded Iron Formations (BIF) are marine chemical sedimentary rocks common in Precambrian volcano-sedimentary sequences. BIFs serve as geochemical archive of the composition of Precambrian seawater, and their trace element composition aids to investigate the geochemical evolution of the early Earth.

The Daitari Greenstone Belt (DGB) in the Singhbhum Craton of India hosts a ca. 3.5–3.3 Ga old volcano-sedimentary sequence with BIFs preserved within the Tomka Formation (Jodder et al. 2023). The DGB has only experienced greenschist-facies metamorphic conditions (Hofmann et al. 2022) providing a unique record for marine chemical sediments from the early Archean. Here we studied the Tomka BIF, which might serve as an excellent geochemical archive to reconstruct physico-chemical conditions of the 3.5-billion-year-old marine environment in the Daitari area. It may provide unique insights into the state of Earth's oceans, continents, and atmosphere within this critical time window.

Trace element compositions of high pressure-high temperature digestions of individual chert-, Fe- and mixed Fe- and chert-microbands were determined via quadrupole ICP-MS following the protocol described in Viehmann et al. (2016). Trace element compositions of chemical sediments can be used to reconstruct the depositional environment and physico-chemical conditions of the ambient atmosphere and hydrosphere. The Tomka BIF samples have very low concentrations of incompatible elements such as Al, Hf, Th, and Zr. In addition, the concentrations of rare earth elements and yttrium (REY) show no correlations with fluid-mobile elements such as Sr. The chemical compositions thus highlight their usefulness as a geochemical archive of Paleoarchean seawater. Pure chert, Fe- and mixed layers of the Tomka BIF display typical REY distribution patterns of Archean seawater (e.g., Alexander et al., 2008) and shale-normalized (subscript SN) REY_{SN} patterns similar to modern seawater, i.e., enrichment of heavy to light REY_{SN} (Y_{SN}/Pr_{SN}: 2.67-20.4), positive La_{SN} (La_{SN}/La_{SN}*: 1.43-3.43) and Gd_{SN} (Gd_{SN}/Gd_{SN}*: 1.12-1.64) anomalies and super-chondritic Y/Ho ratios (41.2-66.7). The presence of positive Eu_{SN} (Eu_{SN}/Eu*_{SN}: 1.37-3.17) anomalies indicate REY contributions from high-temperature hydrothermal fluids in seawater of the Tomka depositional environment. The lack of negative Ce_{SN} (Ce_{SN}/Ce*_{SN}: 0.67-1.37) anomalies suggests anoxic atmospheric-hydrospheric conditions during BIF deposition.

The presence or absence of Eu anomalies in chondrite-normalized (subscript CN) REY patterns of BIFs can be used to distinguish between Archean and Post-Archean chemical sedimentary rocks. REY data of pure BIFs show that Eu_{CN}/Eu^*_{CN} ratios of Precambrian seawater follow a general global evolution curve with BIFs displaying strong positive Eu_{CN} anomalies in the Eoarchean, followed by decreasing Eu_{CN}/Eu^*_{CN} ratios until the Neoarchean (Viehmann et al. 2015). Eu data from BIFs in the time frame around 3.5 Ga, however, are lacking to date. Eu_{CN}/Eu^*_{CN} ratios of the Tomka BIF that fall into this time window do not follow the global seawater Eu curve but show significantly lower Eu_{CN}/Eu^*_{CN} values than expected. These values may indicate a less pronounced flux of high-temperature hydrothermal REY to the Archean ocean 3.5 Ga ago.

- Alexander BW, Bau M, Andersson P, Dulski P (2008): Continentally-derived solutes in shallow Archean seawater: Rare earth element and Nd isotope evidence in iron formation from the 2.9 Ga Pongola Supergroup, South Africa. - *Geochim Cosmochim Acta* 72(2), 378–394
- Hofmann A, Jodder J, Xie H, Bolhar R, Whitehouse M, Elburg M (2022): The Archaean geological history of the Singhbhum Craton, India – a proposal for a consistent framework of craton evolution. - *Earth-Science Reviews* 228, 103994
- Jodder J, Hofmann A, Xie H, Elburg MA, Wilson A 2023: Geochronology of the Daitari Greenstone Belt, Singhbhum Craton, India. - *Precamb Res* 388, 106997
- Viehmann S, Bau M, Böhn B, Dantas EL, Andrade FRD, Walde DHG (2016): Geochemical characterisation of Neoproterozoic marine habitats: Evidence from trace elements and Nd isotopes in the Urucum iron and manganese formations, Brazil. - *Precamb Res* 282, 74–96
- Viehmann S, Bau M, Hoffmann JE, Münker C (2015): Geochemistry of the Krivoy Rog Banded Iron Formation, Ukraine, and the impact of peak episodes of increased global magmatic activity on the trace element composition of Precambrian seawater. - *Precamb Res* 270, 165–180

Special exhibitions are suitable for knowledge transfer

D. Kleinschrot¹

*¹University of Wuerzburg
e-mail:kleinschrot@uni-wuerzburg.de*

The most beautiful exhibits are in the showcases of our museum and attract numerous visitors who want to see these original objects from locations all over the world. The permanent exhibition can be visited at any time during opening hours and gives visitors enough time and space to learn more about the objects or to deal with a specific topic. In the temporary exhibitions of the Mineralogical Museum, for example, current topics such as raw materials in smartphones are dealt with. Scientists take the opportunity to present their research results to a broad public and thus emphasize their importance for society. In 2007 we presented 25 years of Antarctic research. Mining in Namibia and the exploration of eclogite and gold were also themes of exhibitions. Collaborations with various artists attract visitors to the museum who previously had little or no interest in geosciences. Together with other institutions, museums, and students, we organized an interdisciplinary exhibition project that showed the different aspects of color. Today we are still showing a showcase from this exhibition. The formats of the respective exhibitions are different. We have the showcase that changes quarterly, showing a mineral's properties, its origin and use as a raw material. Every one to two years we create larger exhibitions lasting 6 to 12 months. The museum team conveys the complex content in easy-to-understand exhibition texts, organizes lectures, guided tours, action Sundays for families and hands-on stations in order to reach a broad target group and, above all, to introduce young people to science. The amount of work is enormous and a temporary exhibition is usually associated with high costs. In order to convince sponsors of our work, we carried out visitor statistics, among other things. We can thus show that the number of visitors is increasing during special exhibitions and that the accompanying program is being used for further training by school classes and individuals of different ages.

GEOROC 2.0: A globally connected geochemical database to facilitate interdisciplinary, data-driven research

M. Klöcking¹, A. Sturm², B. Sarbas¹, L. Kallas¹, S. Möller-McNett¹, K. Lehnert³, K. Elger⁴,
W. Horstmann², D. Kurzawe², M. Willbold¹, G. Wörner¹

¹Geoscience Centre, Universität Göttingen

²Göttingen State and University Library

³Columbia University, New York

⁴GFZ Data Services, Potsdam

e-mail: gwoerne@gwdg.de

The GEOROC database is one of the leading, open-access sources of geochemical and isotopic datasets that provides access to curated compilations of igneous and metamorphic rock and mineral compositions from >20,600 publications. It is an international data resource that supports hundreds of new research publications each year across multiple geoscientific and related disciplines (Chamberlain et al., 2021; Klöcking et al., 2023).

In this context, the Digital Geochemical Data Infrastructure (DIGIS) initiative is currently developing a new IT and data infrastructure for GEOROC 2.0 to facilitate modern solutions to data submission, discovery and access (Fig. 1). GEOROC data compilations are made accessible via a web search interface and through a dedicated API. DIGIS also maintains a direct data pipeline of GEOROC compilation data to the EarthChem Portal (Fig. 2), which enables combined searches across six distinct geochemical databases. The DIGIS infrastructure further includes a domain repository for direct submission of geochemical datasets by the community (Fig. 2). This repository is hosted and curated in partnership with the GFZ Data Services of the GFZ (German Research Centre for Geosciences) in Potsdam. In addition, this repository can also be used for archiving citeable database versions.



Fig. 1: Setup and IT-environment of the GEOROC database

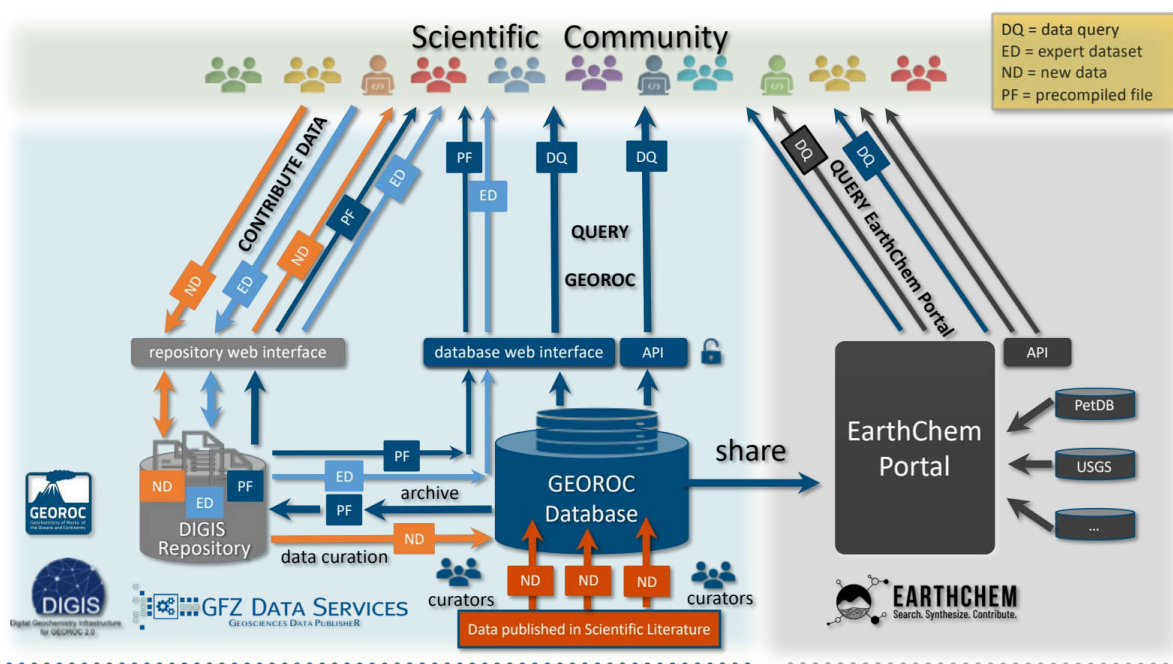


Fig. 2: The GEOROC data base and links to geochemical data services

In an effort to standardise geochemical data reporting, DIGIS collaborates with EarthChem, Astromat, and MetBase to develop common vocabularies that will enhance international interoperability of geo- and cosmochemical data systems. Part of this cooperation is the development of a joint, browser-based data entry tool for the GEOROC, PetDB and Astromat synthesis databases, which will avoid duplication of data and ensure consistent data and metadata quality through common curation policies. With these efforts, and as a participant of the “OneGeochemistry” initiative, DIGIS is working towards the goal of globally harmonised and FAIR geochemical data and support interdisciplinary, data-driven research.

Klöcking M, Wyborn L, Lehnert K, Ware B, Prent A, Profeta L, Kohlmann F et al. (2023) Community recommendations for geochemical data, services and analytical capabilities in the 21st century. - *Geochim Cosmochim Acta* 351, 192-205. DOI: <https://doi.org/10.1016/j.gca.2023.04.024>

Chamberlain KJ, Lehnert KA, McIntosh IM, Morgan DJ, Wörner G (2021) Time to change the data culture in geochemistry. - *Nat Rev Earth Environ* (2021), <https://doi.org/10.1038/s43017-021-00237-w>

The anatectic genesis of lithium pegmatite from the Austroalpine Unit Pegmatite Province

T. Knoll¹, B. Huet², R. Schuster¹, H. Mali³

¹ Division of Geophysical and Applied Geological Services, Geosphere Austria, Neulinggasse 38, 1030 Vienna, Austria

² Division of Basic Geological Services, Geosphere Austria, Neulinggasse 38, 1030 Vienna, Austria

³ Department of Applied Geosciences and Geophysics, Montanuniversität Leoben, Peter-Tunnerstraße 5, 8700 Leoben, Austria
e-mail: tanja.knoll@geosphere.at

Whether rare element pegmatites are always related to fractional crystallization of melts derived from large fertile granite bodies or they can also form directly from limited portions of enriched anatectic melt is since long a debated topic (e.g. Stewart 1978; Cerný 1991). We here present the results of a recent case study that documents continuous evolution from anatectic melt generated in staurolite-bearing micaschist to albite-spodumene pegmatite (Knoll et al., 2023). The investigated Austroalpine Unit Pegmatite Province (AUPP, Eastern Alps) formed in the Adria crust during Permian lithospheric extension (Figure 1a, Schuster & Stüwe 2008) and all levels of the Permian crust are now accessible in a Cretaceous nappe stack (Froitzheim et al. 2008).

It can be shown that the Permian pegmatites of the AUPP are neither spatially nor genetically related to large fertile granite bodies. Geochronological data proofs that emplacement of pegmatite and leucogranite is broadly contemporaneous with high temperature-low pressure metamorphism of the country rocks in a time range between 247 and 288 Ma (Knoll et al. 2023; and references therein). Permian albite-spodumene pegmatites are restricted to certain lithostratigraphic complexes (e.g. Rappold Complex, Strieden Complex or Silvretta Complex; Schuster et al. 2001; Knoll et al. 2018). Pegmatite-bearing units mainly consist of aluminosilicate-bearing partly migmatitic micaschist and paragneiss as well as staurolite-bearing micaschist. Field observations give clear evidence of a genetic link between simple pegmatite, leucogranite, evolved pegmatite and albite-spodumene pegmatite, on the one hand, and the subsolidus or suprasolidus metasediment hosting them on the other hand. These relationships are supported by geochemical investigations of major and trace elements in all mentioned rock types and the minerals they contain.

The Li source rock is found to be an Al-rich metapelite, richer in Li (70-270 ppm) than the average upper continental crust. The primary Li-carrier is staurolite with up to 3000 ppm Li. The pegmatite and leucogranite are derived from anatectic melts that formed at 0.6-0.8 GPa and 650-750 °C, corresponding to 18-26 km depth. During melt formation staurolite was consumed by sillimanite forming reactions. Subsequently, the melts were enriched in Li during their ascent to higher crustal levels by fractional crystallization of quartz and feldspar. While simple pegmatite and inhomogeneous leucogranite formed in lower and intermediate levels, evolved and albite-spodumene pegmatite crystallised at high levels at 0.3-0.4 GPa and 500-570 °C, corresponding to about 12 km depth.

On the basis of this data we developed a geochemical model showing that Li can be transferred from a metasediment into an anatectic melt if Li-bearing staurolite is stable or metastable at the onset of melting (Figure 1b). Such a melt can initially contain between 200

and 1000 ppm Li and be further enriched by fractional crystallization, with up to 5000-10000 ppm Li allowing crystallization of spodumene (Figure 1c). Estimated fractionation degrees vary between 81 and 99 %, depending on the protolith composition, the melting scenario and the partitioning coefficients. Li-Al-rich metasediments are therefore a significant source of Li when they first melt. This anatectic model provides an alternative explanation for the formation of Li-rich pegmatite if no fertile parent granite can be identified.

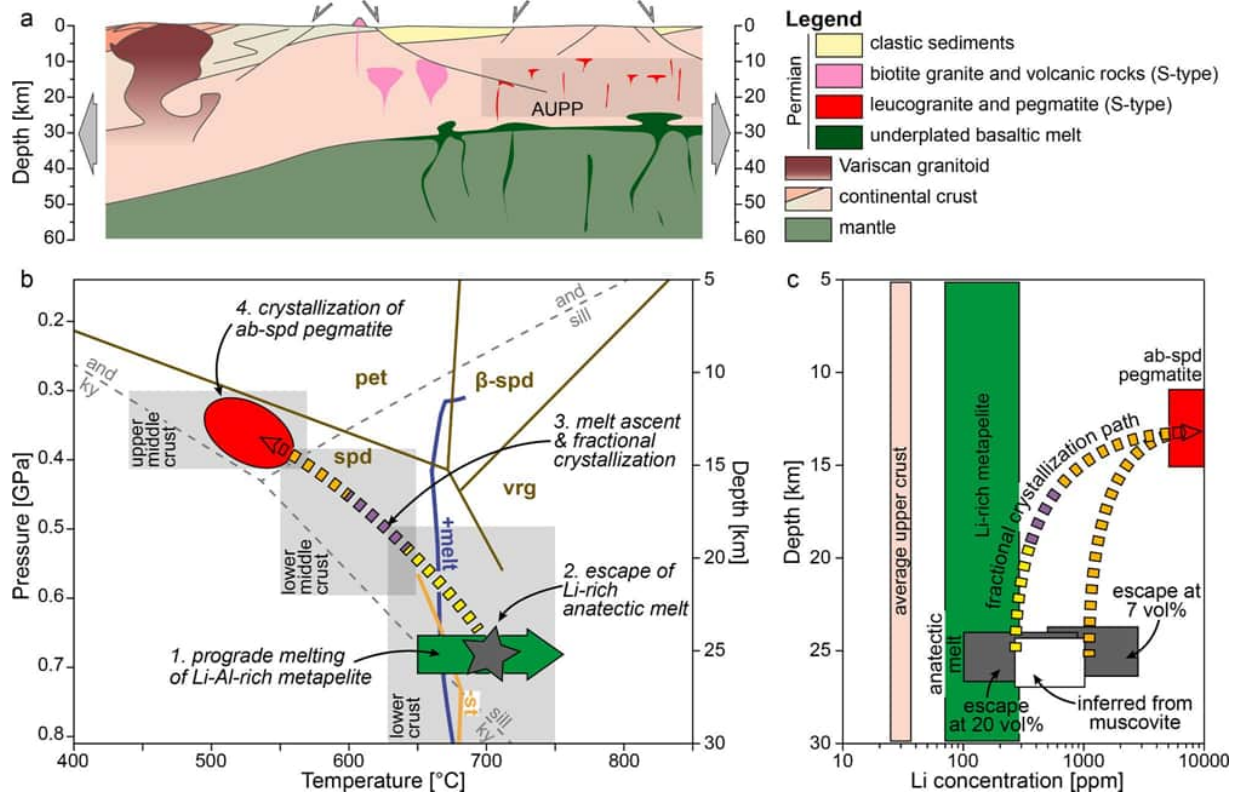


Figure 1. a. Position of the Austroalpine Unit Pegmatite Province (AUPP) within the Adria continental crust during Permian lithospheric extension. b. The main processes of the genetic model placed on a pressure–temperature diagram: 1. Prograde melting of Li-Al-rich metapelite in the lower crust. 2. Escape of Li-rich anatectic melt from the migmatite of the lower crust. 3. Ascent of the melt through the lower middle crust and progressive fractional crystallization. 4. Crystallization of residual melt as albite-spodumene pegmatite in the upper middle crust. c. Postulated evolution of Li concentration in anatectic melt during ascent (see also Knoll et al. 2023).

Cerný P (1991): Rare-element granitic pegmatites. Part I: Anatomy and internal evolution of pegmatite deposits. - *Geosci Canad* 18, 49–67

Froitzheim N, Plasienska D, Schuster R (2008): In: McCann, T. (Ed.), *The Geology of Central Europe, 2. Mesozoic and Cenozoic*. - *J Geol Soc* 1141–1232

Knoll T, Schuster R, Huet B, Mali H, Onuk P, Horschinegg M, Ertl A, Giester G (2018): Spodumene Pegmatite and Related Leucogranite from the Austroalpine Unit (Eastern Alps, Central Europe): Field Relations, Petrography, Geochemistry, and Geochronology. - *Canad Mineral* 56, 489–528

Knoll T, Huet B, Schuster R, Mali H, Ntaflos T, Hauzenberger C (2023): Lithium pegmatite of anatectic origin-A case study from the Austroalpine Unit Pegmatite Province (Eastern European Alps): geological data and geochemical model. - *Ore Geol Rev* 154, 105298

Schuster R, Scharbert S, Abart R, Frank W (2001): Permo-Triassic extension and related HT/LP metamorphism in the Austroalpine-Southalpine realm. - *Mitt Ges Geol Bergbaustud Österr* 45, 111–141

Schuster R, Stüwe K (2008): Permian metamorphic event in the Alps. - *Geology* 36, 603–606

Stewart D B (1978): Petrogenesis of lithium-rich pegmatites. - *Amer Mineral* 63, 970–980

Petrogenetic information stored in needle-shaped rutile inclusions in pegmatoid garnet

V. Kohn¹, T. Griffiths¹, E. Libowitzky¹, O. Ageeva¹, R. Abart¹, G. Habler¹

¹ University of Vienna, Josef-Holaubek-Platz 2, 1090, Wien, Austria
e-mail: victoria.kohn@univie.ac.at

We investigate the petrogenetic information stored in needle-shaped rutile inclusions hosted by garnet. For this purpose, microstructural and compositional zoning of almandine-spessartine garnet (Grt) in a pegmatoid from the Gföhl Unit (Bohemian massif, AT) is correlated with host-inclusion crystallographic and shape orientation relationships along the transition between microstructurally distinct garnet growth zones. The transition from the Grt core to the garnet rim (R1) is defined by a gradual increase in the aspect ratio of rutile (Rt) inclusions accompanied by a reduction in Grt colour intensity. The coloured outer core of Grt hosts equant rutile inclusions, whereas the uncoloured Grt zone R1 contains rutile needles of c. 100 – 150 μm length (Figure 1).

More than 11 different crystallographic orientation relationships (CORs) between Grt host and Rt inclusions are known (Hwang et al. 2016; Griffiths et al. 2016). The new dataset documents a systematic correlation of the shape preferred orientations (SPOs) of rutile inclusions in garnet, and the CORs between the two phases. This allows grouping specific CORs according to the particular crystallographic axes that coincide with the needle elongation directions: Group A $\text{Rt}\langle 103 \rangle \parallel \text{Grt}\langle 111 \rangle^*$, Group B $\text{Rt}\langle 001 \rangle \parallel \text{Grt}\langle 111 \rangle^{**}$ and Group C $\text{Rt}\langle 001 \rangle \parallel \langle 100 \rangle^{***}$. The two microstructural domains show remarkable differences in the frequencies of these COR groups. In the outer core of garnet Group A CORs are predominant (> 70%), while Grt zone R1 shows a predominance of Group B CORs, as well as a significantly higher abundance of CORs assigned to Group C, which are almost absent in the outer core.

As the major element profile of garnet along this microstructural transition is continuous, and the trace element distribution in Grt allows us to exclude significant re-equilibration by diffusion, we conclude that other factors than changes in the PT-conditions are responsible for the differences in the garnet microstructure and COR frequencies.

Growth zone R1 is characterized by the exclusive presence of Qtz inclusions and elevated Na_2O and OH^- content compared to the Grt core, implying an increase in the water activity during R1 growth. Hydrogen content in Alm-Sps garnet has been confirmed to increase from wall to core zones of pegmatites and to serve as tracer for their evolution (Arredondo et al. 2001). Consistently, we also observe an increase in anorthite content in matrix plagioclase (Pl). In analogy to basaltic systems, Pl crystallising from a melt at constant or decreasing temperature can be referred to an increase in water activity (Lange et al. 2009, Housh and Luhr, 1991). Therefore, change in Pl-composition caused by increasing water activity could represent the source of Si and Na during R1 garnet growth. In summary, the observed compositional zoning trends of garnet and plagioclase are consistent with an increase in H_2O concentration of the melt, without need for significant changes in PT-conditions during garnet core and R1 growth.

The comparison of the studied sample with a pegmatite garnet from the Koralpe (Eastern Alps, AT) shows remarkable similarities (Griffiths et al. 2014; 2016). There, the coloured garnet core comprises mostly equant rutile inclusions and corundum, while colourless garnet rim domains contain needle-shaped rutile inclusions and aluminosilicates, and are intergrown with Qtz. Most interestingly, the Koralpe pegmatite garnet rim also has a higher abundance of Group B CORs, compared to the garnet core domains of the same sample. We

conclude that the observed microstructural transition is possibly connected with an increase of Si and/or H₂O-concentration in the melt.

As the formation of dispersed needle-shaped rutile inclusions in garnet is often referred to exsolution from the host garnet (Griffin et al. 1971; Gou et al. 2014), the frequencies of shape preferred orientations (SPOs) of rutile in garnet zone R1 were studied on the basis of > 2500 rutile needles. We observe SPOs of rutile along particular garnet crystal directions, where rutile needle elongation parallel to $\langle 111 \rangle$ Grt by far exceeds Rt needle elongation direction parallel to $\langle 100 \rangle$ Grt. Based on the assumption that the exsolution of rutile inclusions from garnet would lead to equal abundance of SPOs in symmetrically equivalent directions, each individual needle orientation was counted in R1 zones of two $\{112\}$ Grt growth sectors corresponding to different crystallographically equivalent garnet facets. We find that those rutile needles parallel to $\langle 111 \rangle$ Grt with the lowest angle to the garnet growth direction have a higher abundance, whereas rutile needles with their elongation direction parallel to the particular Grt growth facet plane are absent in both studied growth sectors. Due to this growth-related effect on the SPO frequencies we conclude that the rutile needles originate from co-growth with their host crystal (Griffiths et al. 2020).

- * Group A contains the specific CORs with a common axial relationship: COR-1, 2, 2', 3, R3a and an undescribed COR defined by $Rt \{100\} \parallel Grt \{112\}$ and $Rt \{320\} \parallel Grt \{120\}$,
- ** Group B contains COR-4 and 4b,
- *** Group C contains COR-5 and 5a (Hwang et al 2016; Griffiths et al. 2016).

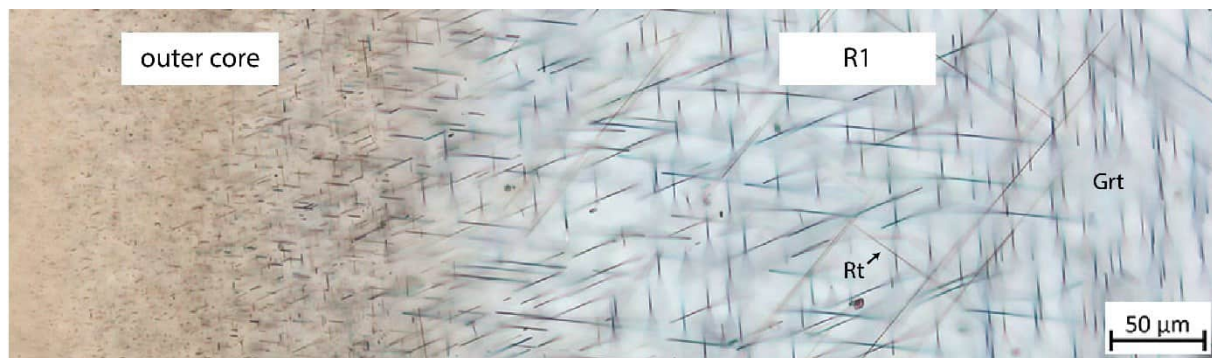


Figure 1. Optical micrograph (plane polarized light) of the microstructural transition from the outer garnet core to the garnet growth zone R1 in a $\{112\}$ Grt growth sector. Note the increasing aspect ratio of rutile (Rt) inclusions and the decrease in garnet (Grt) colour intensity from the outer core to R1.

- Arredondo E, Rossman G, Lumpkin G (2001): Hydrogen in spessartine-almandine garnets as a tracer of granitic pegmatite evolution. - *Amer Mineral* 86, 485
- Gou L, Zhang C, Zhang L, Wang Q (2014): Precipitation of rutile needles in garnet from sillimanite-bearing pelitic granulite from the Khondalite Belt, North China Craton. - *Chin Sci Bull* 59, 4359
- Griffin WL, Jensen BB, Misra SN (1971): Anomalously elongated rutile in eclogite-facies pyroxene and garnet. - *N J G* 51, 177
- Griffiths TA, Habler G, Rhede D, Wirth R, Ram F, Abart R (2014): Localization of submicron inclusion re-equilibration at healed fractures in host garnet. - *Contrib Mineral Petrol* 168, 1
- Griffiths TA, Habler G, Abart R (2016): Crystallographic orientation relationships in host-inclusion systems: New insights from large EBSD data sets. - *Amer Mineral* 101, 690
- Griffiths TA, Habler G, Abart R (2020): Determining the origin of inclusions in garnet: challenges and new diagnostic criteria. - *A J S* 320, 753
- Housh TB, Luhr JF (1991): Plagioclase-melt equilibria in hydrous systems. - *Amer Mineral* 76, 477
- Hwang SL, Shen P, Chu HT, Yui TF (2016): On the forbidden and the optimum crystallographic variant of rutile in garnet. - *J Appl Cryst* 49, 1922
- Lange RA, Frey HM, Hector J (2009): A thermodynamic model for the plagioclase-liquid hygrometer/thermometer. - *Am Mineral* 94, 494

**The crystal structure of a new natural
Na-(Sr,Ba,Ca,K)-Fe-tungstophosphate, a derivative of the
betpakdalite-group topology from Le Mazet, Échassières, Allier, France**

U. Kolitsch^{1,2}

¹*Mineralogisch-Petrographische Abteilung, Naturhistorisches Museum, Burgring 7, A-1010 Wien, Austria*
²*Institut für Mineralogie und Kristallographie, Universität Wien, Josef-Holaubek-Platz 2, A-1090 Wien, Austria*
e-mail: uwe.kolitsch@nhm.at

A new tungstophosphate mineral was found on dumps of the Le Mazet wolframite-bearing quartz vein of the Les Montmins mining district (Échassières, Allier, France). It was not yet found at the nearby, very mineral-rich Ste Barbe vein. The new mineral forms very small, bright yellow to orange-yellow, pseudo-octahedral crystals, indistinct corroded tabular crystals and anhedral grains. The mineral, which shows a vitreous lustre, sits in small voids of a dark pink-grey, fine-grained quartz matrix. The colour of the mineral is somewhat reminiscent of that cyrilovite which also occurs at the locality.

The complex crystal structure was solved from single-crystal intensity data (MoK α ; 293 K). The space group is $R\bar{3}m$ (no. 166), with $a = 10.874(2)$, $c = 28.243(6)$ Å, $V = 2892.1(1)$ Å³; $R(F) = 2.1\%$. The asymmetric unit contains one Na site with refined occupancy Na_{~0.54(3)}, one (Sr,Ba,Ca,K) site, two Fe sites, one (P,As) site (refined P:As ratio = 0.719(19):0.281), one W site and nine O sites, four of which represent H₂O molecules. The latter are all partially occupied. The new mineral has the following simplified (and presently tentative) formula: [Na_{~0.27}(Sr_{0.46}Ba_{0.31}Ca_{0.17}K_{0.08})(H₂O,OH)_{~9.02}][W₃(P,As)Fe³⁺₂O₁₆]. The (P,As)O₄ tetrahedron is, via its basal corners, connected to three Fe(2)O₆ octahedra. The remaining apex is shared with a cluster of three edge-sharing, strongly distorted WO₆ "octahedra". This cluster is connected via an Fe(1)O₆ octahedron to symmetrically equivalent clusters. Channels and voids in the resulting 3D framework extend along [100] and [110] and are filled with (Sr,Ba,Ca,K)O_{12-x} polyhedra and partially occupied NaO₆ octahedra.

The atomic arrangement is a derivative of that of the members of the betpakdalite group, a group of monoclinic heteropolymolybdates with a pseudo-hexagonal symmetry of their framework topology (Kampf et al. 2012). A comparison with betpakdalite-CaMg, [Ca₂(H₂O)₁₇Mg(H₂O)₆][Mo₈As₂Fe³⁺₃O₃₆(OH)], shows that the two corner-sharing Mo(3)O₆ octahedra, which link adjacent units, are replaced in the new mineral with a single Fe(1)O₆ octahedron. The Ca site is replaced with a (Sr,Ba,Ca,K) site, while the Mg site is a Na site in the new mineral.

Further SEM-EDS analyses and additional single-crystal determinations of unit-cell parameters of other samples show that some samples are As-free, and suggest that some may be As-dominant (i.e., a tungstoarsenate). The atomic ratio Sr:Ba:Ca:K is variable, but Sr is always clearly dominant. The Na content is also variable.

Heinz Förch and the late Hans Schmid are thanked for providing samples for study.

Kampf AR, Mills SJ, Rumsey MS, Dini M, Birch WD, Spratt J, Pluth JJ, Steele IM, Jenkins RA, Pinch WW (2012): The heteropolymolybdate family: structural relations, nomenclature scheme and new species. - Mineral Mag 76, 1175-1207

Crystal structure of anthropogenic $\text{Ca}_2(\text{OH})(\text{AsO}_4) \cdot 2\text{H}_2\text{O}$ found in the Clara mine, Black Forest, Germany

U. Kolitsch^{1,2}

¹*Mineralogisch-Petrographische Abteilung, Naturhistorisches Museum, Burgring 7, 1010 Wien, Austria*

²*Institut für Mineralogie und Kristallographie, Universität Wien, Josef-Holaubek-Platz 2, 1090 Wien, Austria
e-mail: uwe.kolitsch@nhm.at*

The arsenate compound $\text{Ca}_2(\text{OH})(\text{AsO}_4) \cdot 2\text{H}_2\text{O}$, known from studies of the system Ca-As-O-H and reported to be stable in the pH range 11-12 (Bothe & Brown 1999, 2002), had a previously unknown unit cell (unindexed powder diffraction pattern ICDD-PDF 18-289) and crystal structure. Its formula was given in the various literature as $4\text{CaO} \cdot \text{As}_2\text{O}_5 \cdot 5\text{H}_2\text{O}$, $\text{Ca}_3(\text{AsO}_4)_2 \cdot \text{Ca}(\text{OH})_2 \cdot 4\text{H}_2\text{O}$, or $\text{Ca}_4(\text{OH})_2(\text{AsO}_4)_2 \cdot 4\text{H}_2\text{O}$.

The anthropogenic occurrence of $\text{Ca}_2(\text{OH})(\text{AsO}_4) \cdot 2\text{H}_2\text{O}$ in the famous Clara baryte and fluorite mine, Black Forest, Germany, was reported by Blaß & Graf (1995), based on X-ray powder diffraction data. This occurrence is due to the use of concrete underground; several other Ca arsenates (both crystalline and amorphous) are known to occur in such assemblages (named „Beton-Paragenese“ among collectors). $\text{Ca}_2(\text{OH})(\text{AsO}_4) \cdot 2\text{H}_2\text{O}$ was also detected by the present author in 2017 on two samples from the Clara mine. The first sample shows white sprays of colourless, lath-shaped, glassy, transparent crystals up to ~0.3 mm in length. The second sample, erroneously labelled „Calcit, Svabite“, shows pale bluish, blocky, transparent to translucent crystals (up to ~0.5 mm) arranged to form sprays and rounded aggregates. SEM-EDS analyses of carbon-coated fragments showed, apart from Ca, As and O, very minor Si in the first sample, and traces to very minor amounts of Na, Cu, Si and Cl in the second sample.

The crystal structure of $\text{Ca}_2(\text{OH})(\text{AsO}_4) \cdot 2\text{H}_2\text{O}$ was solved from single-crystal intensity data (MoK α ; 293 K). The space group is $P2_1/c$ (no. 14), with $a = 6.178(1)$, $b = 15.688(3)$, $c = 6.876(1)$ Å, $\beta = 99.67(3)^\circ$, $V = 656.96(19)$ Å³; $R(F) = 2.1\%$. The asymmetric unit contains two Ca sites, one As site containing minor Si [refined As:Si ratio = 0.911(2):0.089], seven O sites, one of which represents an OH group and two of which represent water molecules, and five H sites (all detected and refined). The structure is built from an (As,Si)O₄ tetrahedron ($\langle \text{As-O} \rangle = 1.684$ Å) linked to a distorted ^[6]CaO₆ polyhedron and a ^[7]CaO₇ polyhedron. The Ca-O polyhedra share edges with themselves and corners with three of the O ligands of the As atom to form a heteropolyhedral layer parallel to {010}. Hydrogen bonds connect these layers; the “free” O ligand of the As site, O₂, is acceptor of three H-bonds of medium strength (2.660 - 2.703 Å).

Heinz Förch and Richard Bayerl are thanked for providing samples for study.

Blaß G, Graf HW (1995): Namibit, ein Neufund aus dem Schwarzwald. - Mineralien-Welt 6, 20-22

Bothe JV, Brown PW (1999): The stabilities of calcium arsenates at 23±1 °C. - J Hazard Mat 69, 197-207

Bothe JV, Brown PW (2002): CaO-As₂O₅-H₂O system at 23° ± 1 °C. - J Amer Ceram Soc 85, 221-224

**Litharge from El Centenillo and Fuente Espi:
A geochemical and mineralogical investigation of
Spanish silver processing in the Sierra Morena**

P. Krause^{1,2}, S. Klein^{2,3}, C. Domergue⁴, C. Berthold^{5,6}, N. Jöns¹

¹*Institut für Geologie, Mineralogie und Geophysik, Ruhr-Universität Bochum,
Universitätsstrasse 150, 44801 Bochum, Germany*

²*Forschungsbereich Archäometallurgie, Deutsches Bergbau-Museum Bochum,
Am Bergbaumuseum 31, 44791 Bochum, Germany*

³*Institut für Archäologische Wissenschaften, Ruhr-Universität Bochum,
Am Bergbaumuseum 31, 44791 Bochum, Germany*

⁴*Laboratoire TRACES (UMR 5608 CNRS), Université Toulouse-Jean Jaurès,
Allées Antonio Machado, 31058 Toulouse Cédex 9, France*

⁵*Competence Center Archaeometry, Baden-Wuerttemberg (CCA-BW), Eberhard Karls-Universität Tübingen,
Wilhelmstraße 56, 72074 Tübingen, Germany
e-mail: Paul.Krause@ruhr-uni-bochum.de*

Galena is treated as the most important silver ore in antiquity and especially in Roman mining history, but many other silver mineralisation and phases occur in the Earth's crust that also contain valuable amounts of silver for exploitation. This study addresses the silver-containing sulfosalts and how to decide between the alternative ores when only metallurgical remains are preserved and the mining context is not evident. Numerous samples of ore minerals, slags, lead metal and stones were collected by one of us (C. Domergue) over several years in the Spanish Sierra Morena, including two Roman foundry sites: Cerro del Plomo and Fuente Espi, both in the mining district of Linares-La Carolina. Cerro del Plomo is closely associated with lead-bearing ore veins near the foundry, while the mines that supplied Fuente Espi with lead ore have not yet been archaeologically explored. The metallurgical remains from the two foundries were analysed for their microstructure, mineralogy and phase composition using microscopy, electron microprobe analysis, and X-ray diffraction. It was hoped that the litharge in particular would provide information about the ores used. Metal inclusions of copper and lead were identified, both still containing some silver. The cooling history and stratigraphy of the litharge cakes were developed and parallels drawn with earlier cupellation models. The litharge cakes from Cerro del Plomo and Fuente Espi are comparable in terms of microstructure and phase composition. Chemical and isotope analysis will follow and be the subject of a separate publication.

The "Societät für die gesammte Mineralogie zu Jena" – Members and minerals from Austria, Slovakia, and Hungary

B. Kreher-Hartmann¹

¹*Friedrich-Schiller-University Jena, Mineralogical Collection
e-mail: Birgit.kreher@uni-jena.de*

The "Societät für die gesammte Mineralogie zu Jena" is the first purely geoscientific society in the world. It was founded in 1797 by Johann Georg Lenz (Fig. 1) at the University of Jena, Germany, and its members were scattered all over the globe. Of the more than 2,500 known members, particularly many members came from the then Hungarian region (i.e. today's Slovakia, Hungary, and Romania). These members sent minerals and rocks from their home countries from localities that are often no longer accessible today. The members established networks and in Hungary a Hungarian Mineralogical Society was founded following the Jena model. Famous contemporaries such as Johann Rudolf von Gersdorff, Daniel Mihályik, or Christian Andreas Zipser can be found among the members. Not all members were mineralogists, many teachers, also theologians, and pharmacists were among them. But the occupation with the formations, parageneses, and formation conditions of the minerals united them.



Figure 1. Johann Georg Lenz (1745-1832).

Domokos Teleki de Szék was elected the first president of the Society. He died unexpectedly already in his first year in office. A gift collection of opals from Červenica, Slovakia, among others, which he had initiated, reached Jena only after his death.

When they arrived at the Mineralogical Collection in Jena, the gift collections received were arranged chronologically, according to their arrival. So were for example K-Feldspars from Karlovy Vary area with pyromorphites from different European areas and granites from Silesia side by side on display. Over the many years and after several moves, these gift suites were torn apart and systematically sorted into the collection that has now existed for more than 240 years. With the help of the catalogs and member letters, more than 6,500 specimen could be reassigned to the original suites in recent years.

Kreher-Hartmann B (2014): Die Mineralogische Societät zu Jena – Beiträge aus den Sammlungen der Universität Jena, Bd. 3

Lenz G Schwabe (1823): Neue Schriften der Großherzoglich-S. - Societät für die Gesammte Mineralogie in Jena 1, Neustadt, O

Mechanical-thermochemical process combination for the recycling of fine fractions from waste treatment plants – A journey into waste mineralogy

T. Kremlicka¹, T. Sattler¹, S. Steiner², S. A. Viczek³, K. P. Sedlazeck¹

¹*Chair of Waste Processing Technology and Waste Management, Montanuniversitaet Leoben, Leoben, Austria*

²*Institute of Technology and Testing of Construction Materials, Graz University of Technology, Graz, Austria*

³*Holcim (Österreich) GmbH, Trabrennstraße 2A, 1020 Vienna, Austria*

e-mail: thomas.kremlicka@unileoben.ac.at

Austria produces approximately 1.5 million tons of municipal solid waste annually. Additionally, about 500,000 tons of slags and ashes from thermal waste treatment plants are generated. There are an estimated 1.9 million tons of fine fractions, which includes one million tons of rubble from construction waste, per year, most of which are landfilled (BMK, 2021).

These fine fractions often contain high amounts of metal and mineral contents, however, they may also include pollutants (Viczek et al. 2021b, Vollprecht et al. 2020). This poses a challenge for recycling, as it is essential to avoid keeping mobile pollutants in the material cycle. Recycling fine fractions can immobilize contaminants, like heavy metals, in stable phases (Sarmiento et al. 2019).

The “Meteor” project aims to close material cycles by reintegrating these fine fractions as resources and therefore to further develop the circular economy, reduce CO₂ emissions and increase the recycling quota in Austria. The following objectives are pursued:

1. Mineralogical and chemical characterization of fine fractions and mechanical processing.
2. Testing of different thermochemical treatment methods.
3. Investigation of the mineralogy and leachability of the slags resulting from the thermochemical treatment.
4. Removal/immobilization of contaminants in the fine fractions.
5. Life cycle assessment (LCA) of recycling routes and systemic evaluation of waste management.

An interdisciplinary consortium of universities and industrial partners (see Fig. 2) is dedicated to achieving the project's goals.

The first steps will be sampling selected waste streams, chemical and mineralogical analysis. The mineralogical analysis will consist of, but is not limited to, powder X-ray diffraction, X-ray fluorescence and electron probe microanalysis. Mechanical processing is then used to produce concentrates that are analyzed similarly to the sampled waste. These concentrates are then tested by the project partners for suitability for the various recycling routes. The project plan and the resulting dependencies are shown in Fig. 1

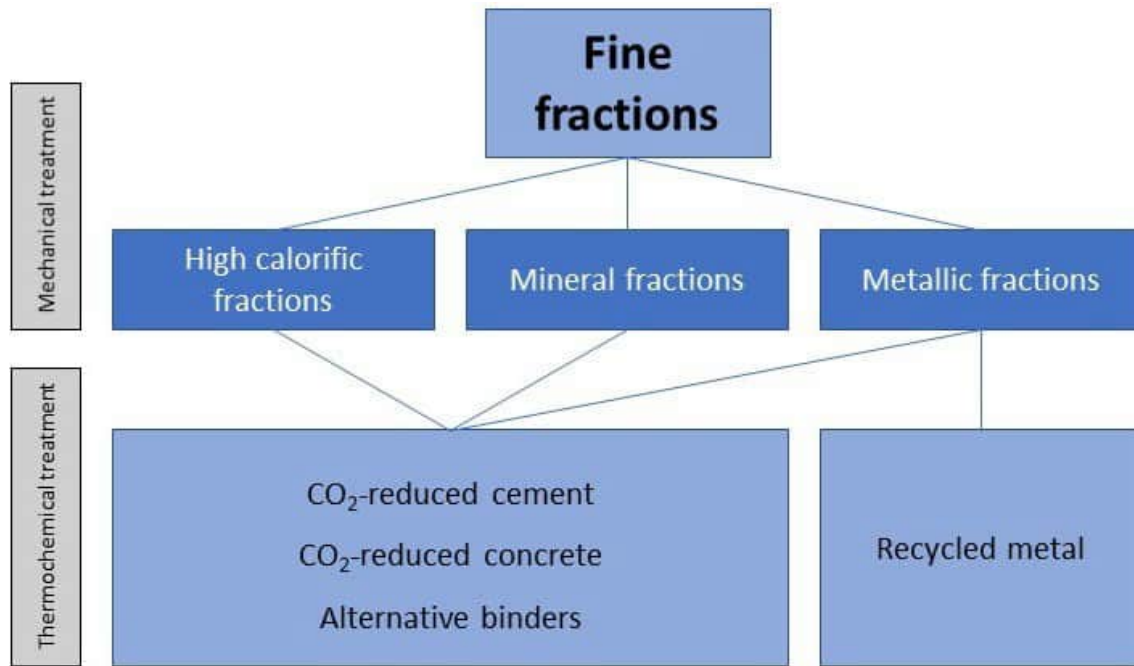


Figure 1. Scheme of the Meteor project

By achieving the project goals, unused waste fractions containing raw materials can be utilized. Applying waste mineralogy methods, the mineral fractions can be characterized and optimized for reuse. The project enables more efficient use of resources and reintegrating waste into production chains and recycling cycles. This project is funded by the Austrian Research Promotion Agency (FFG, www.ffg.at), grant number 889863.



Figure 2. Logos of the consortium partners, funding agency and ministry of climate action, environment, energy, mobility innovation and technology in random order

- Bundesministerium für Klimaschutz, Umwelt, Energie, Mobilität, Innovation und Technologie (BMK) (2021): Die Bestandsaufnahme der Abfallwirtschaft in Österreich – Statusbericht (Referenzjahr 2019)
- Sarmiento LM, Clavier KA, Paris JM, Ferraro CC, Townsend TG (2019): Critical examination of recycled municipal solid waste incineration ash as a mineral source for Portland cement manufacture – a case study. - Resour Conserv Recycl 148, 1-10
- Viczek SA, Khodier K, Kandlbauer L, Aldrian A, Redhammer G, Tippelt G, Sarc R (2021): The particle size-dependent distribution of chemical elements in mixed commercial waste and implications for enhancing SRF quality. - Sci Total Environ 776, 154343
- Vollprecht D, Hernández Parrodi JC, Lucas HI, Pomberger R (2020): Case study on enhanced landfill mining at Mont-Saint-Guibert landfill in Belgium: mechanical processing, physico-chemical and mineralogical characterization of fine fractions <4.5mm. - Detritus 10, 26-43

A potentially new mineral $\text{Ca}_2\text{Mg}_2\text{Fe}_{14}\text{O}_{25}$ from Hatrurim Basin, Israel

B. Krüger¹, I. Galuskina², M. Tribus¹, G. Cametti³, Ye. Vapnik⁴, E. Galuskin²

¹*Institute of Mineralogy and Petrography, University of Innsbruck, Innsbruck, Austria,*

²*Faculty of Natural Sciences, Institute of Earth Sciences, University of Silesia, Poland*

³*Institute of Geological Science, University of Bern, Bern, Switzerland*

⁴*Department of Geological and Environmental Sciences,*

Ben-Gurion University of the Negev Beer-Sheva, Israel

e-mail: biljana.krueger@uibk.ac.at

A potentially new mineral $\text{Ca}_2\text{Mg}_2\text{Fe}_{14}\text{O}_{25}$ was discovered in ferrite-rich veins of gehlenite-bearing hornfels, found near the east slope of Mount Ye'elim in the Hatrurim Basin, Israel (Vapnik et al., 2007; Galuskina et al., 2017). Xenomorphic aggregates of this natural ferrite are observed in association with hematite, magnesioferrite, franklinite, fluorapatite, and minerals of the khesinite-devilliersite series. The empirical formula, established by microprobe analysis is $\text{Ca}_2(\text{Mg}_{0.61}\text{Cu}_{0.48}\text{Zn}_{0.41}\text{Ca}_{0.32}\text{Ni}_{0.13}\text{Mn}^{2+}_{0.03}\text{Fe}^{2+}_{0.02})_{\Sigma 2}(\text{Fe}^{3+}_{13.78}\text{Al}_{0.22})_{\Sigma 14}\text{O}_{25}$.

The dimensions of the unit cell are $a = 5.932$ (1) and $c = 31.302(7)$ Å. The space group $P\bar{3}c1$ of natural $\text{Ca}_2\text{Mg}_2\text{Fe}_{14}\text{O}_{25}$ correspond to that of the synthetic β -CFF phase $\text{Ca}_{2.5}\text{Fe}_{15.5}\text{O}_{25}$ reported by Arakcheeva & Karpinskii (1983). Its crystalline structure is built by an alternating stacking of spinel blocks and F blocks along the c axis (Fig. 1). The spinel block contains two kagome-type layers with $(\text{Fe,Mg})\text{O}_6$ octahedra connected by mixed layers made of $(\text{Fe,Mg})\text{O}_6$ octahedra and FeO_4 tetrahedra. In block F, two layers with mixed polyhedra $(\text{Fe,Mg})\text{O}_6$, FeO_4 , and CaO_7 are connected by a central layer built by trigonal FeO_5 bipyramids.

There are a large number of minerals, in which the triple spinel module intercalates with additional modules, like M-type ferrites (e.g., $\text{BaFe}_{12}\text{O}_{19}$). However, structurally $\text{Ca}_2\text{Mg}_2\text{Fe}_{14}\text{O}_{25}$ is closely related to Y-ferrites, such as $\text{Ba}_2\text{Zn}_2\text{Fe}_{12}\text{O}_{22}$, whose natural analogues are still not found. So far, four polytypes of the CFF phase (α , β , γ , and δ) are known, exhibiting different numbers of spinel and F-blocks along the c axis (Arakcheeva & Karpinskii 1989).

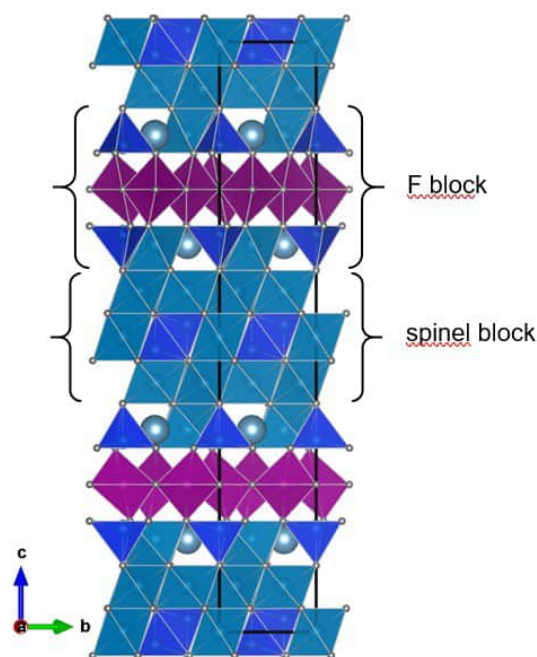


Figure 1. Structure of $\text{Ca}_2\text{Mg}_2\text{Fe}_{16}\text{O}_{25}$. $(\text{Fe,Mg})\text{O}_6$ in cyan, FeO_5 in magenta, FeO_4 in blue colour, and Ca as spheres

Arakcheeva AV, Karpinskii OG (1983): Crystal structure of hexagonal ferrite $\text{Ca}_{2.95}\text{Fe}_{14.85}\text{O}_{25}$. - Dokl Akad Nauk SSSR 273, 1127

Arakcheeva AV, Karpinskii OG (1983): Crystal chemical concept of formation of high-ferrous ferrites. - Kristallografiya 35, 1160-1166

Galuskina I, Vapnik Y, Lazic B, Armbruster T, Murashko M and Galuskin E (2014) Harmunite, CaFe_2O_4 – a new mineral from the Jabel Harmun, West Bank, Palestinian Autonomy, Israel. - Amer Mineral 99, 965-975

Vapnik, Y, Sharygin, VV., Sokol, EV and Shagam R (2007): Paralavas in a combustion metamorphic complex: Hatrurim Basin, Israel. - Rev Eng Geol 18, 1-21

Incommensurate structure and phase transition of cymrite

H. Krüger¹, K. Skrzyńska², R. Juroszek²

¹*Institute of Mineralogy and Petrography, University of Innsbruck, Innsbruck, Austria*

²*Institute of Earth Sciences, University of Silesia, Sosnowiec, Poland*
e-mail: Hannes.Krueger@uibk.ac.at

Cymrite, from a hydrothermally altered pyrometamorphic rock of the Hatrurim Complex, found on the east slopes of Mt. Yeelim (Israel), has been investigated using high-temperature single-crystal X-ray diffraction. The empirical formula, as established by electron microprobe analysis, is $\text{Ba}_{0.97}\text{Na}_{0.01}(\text{Al}_{2.00}\text{Si}_{2.01})\text{O}_8 \cdot 1.48 \text{H}_2\text{O}$.

The diffraction pattern of cymrite exhibits a pseudo-hexagonal lattice ($a = 5.3$ and $c = 7.67 \text{ \AA}$), with additional satellite reflections in the $\mathbf{a}^*\mathbf{b}^*$ -plane ($\mathbf{q} \approx 0.125\mathbf{a}^*$, Figure 1), however, the true symmetry is lower. Some crystals show obvious differences in the intensities of the satellites along the three twin-related directions. A more suitable interpretation of the diffraction pattern is obtained using a (pseudo-orthorhombic) C-centred monoclinic lattice ($a = 5.34$, $b = 9.24$, $c = 7.69 \text{ \AA}$). The satellite reflection can be indexed with $\mathbf{q} = 0.31\mathbf{b}^*$. A temperature-dependent series of diffraction experiments revealed that the \mathbf{q} -vector does not change significantly up to $160 \text{ }^\circ\text{C}$. Between 160 and $250 \text{ }^\circ\text{C}$, it decreases linearly from $0.31\mathbf{b}^*$ to $0.26\mathbf{b}^*$. Above $250 \text{ }^\circ\text{C}$, no significant changes are observed until the satellites disappear between 400 and $450 \text{ }^\circ\text{C}$ and a transformation to a hexagonal structure takes place. At $450 \text{ }^\circ\text{C}$, cymrite adopts space group $P6/mmm$.

Earlier studies on cymrite from the Baikal region (Drits 1975) and Alaska (Bolotina 2010) report fourfold superstructures ($4 \times b$, with respect to the given monoclinic lattice). The observed temperature-dependent change of the \mathbf{q} -vector proves that cymrite from Hatrurim exhibits an incommensurately modulated structure. Possibly, this is related to the water content.
Acknowledgements: KS acknowledges support from Federal Ministry of Education, Science and Research (BMBWF) OeAD – Austria's Agency for Education and Internationalisation (project-No MPC-2022-03371).

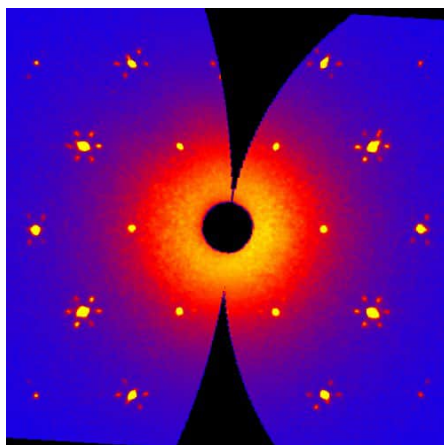


Figure 1. $hk0$ -layer (pseudo hexagonal setting) of the diffraction pattern of cymrite from Israel, exhibiting three pairs of satellite reflections for each Bragg spot as a result of twinning.

Oriented triphylite rods in apatite (Stankuvatske Li deposit, Ukraine): result of pegmatite–wall rock interaction

S. Kurylo¹, I. Broska¹, R. Gieré², N. Lyzhachenko³

¹Earth Science Institute, Slovak Academy of Sciences, 840 05 Bratislava

²Department of Earth and Environmental Science, University of Pennsylvania, Philadelphia, USA

³SI, "Institute of Environmental Geochemistry of the National Academy of Sciences of the Ukraine",
UK Kyiv

e-mail: kurylo.sergiy@savbb.sk

Introduction. Exomorphic haloes found around pegmatites in the Stankuvatske Li deposit (SLD) (Ukraine) are enriched in Rb, Cs, Li, Be, Nb and Ta, and such types of haloes around evolved magmatic systems are important for the concentration of critical mineral sources. Metasomatic processes in the SLD can be an example for the formation of apatite as a geochemical barrier with metallogenetic implications, which takes place at the contact between a rare-metal pegmatite and amphibolite. The aim of current report is to describe the unique occurrence at the SLD of oriented triphylite rods in green apatite, resulting from the interaction between pegmatite- and amphibolite-derived fluids. A genetic interpretation of a two-way directed element mobility in an evolved pegmatite are presented here for the first time.

Geological background. The petalite- and spodumene-pegmatite dykes of the SLD are located in the NW part of the Lypniashka Dome Structure in the western part of the Inhul Domain in the Ukrainian Shield. Pegmatite dykes intruded amphibolite and ultrabasic rocks and were subsequently overprinted by tectonic activity forming metapegmatites. According to the classification of Černý & Ercit (2005), the studied pegmatite dykes show affinity to the rare-element class, and the petalite or spodumene subtype of the LCT family. The general characteristics of the pegmatites have already been reported (Syomka et al. 2022; Kurylo et al. 2022).

Results and discussion. The contact zone was investigated by the drill core materials (No 61-89) on a complete cross section from the host amphibolite to the adjacent metapegmatite dyke. A parallel mineral layering in the metapegmatite endocontact with host amphibolite was formed in the contact zone.

The exocontact *biotite zone* (BT) in the host amphibolite was formed as a result of metasomatic alteration of rock-forming amphibolite by the intruded pegmatite; newly formed biotite (with up to 2.5 wt.% of Rb₂O) and holmquistite are characteristic minerals in this zone. The pegmatite endocontact has a width of ca 8 cm and consists of four thin zones: (1) *aplitic* (APL), (2) *fluorapatite* (AP), which contains apatite with tiny, needle-shaped and oriented parallel c-axis inclusions of triphylite (Figure 1), (3) *triphylite* (TR), and (4) *transitional zone* (TRN). Within of the endocontact, Nb-Ta-Sn oxides, ilmenite, gahnite, native bismuth, chrysoberyl, and relics of zircon rimmed by brabantite or thorite have been identified. The adjacent metapegmatite (PGM) represents petalite and spodumene bearing metapegmatite. A detailed description of all zones is currently in preparation.

Two stages of metasomatic alteration can be distinguished in the studied metapegmatite – wall-rock amphibolite system: (i) K-Rb-F metasomatism at low P activity, and (ii) the metasomatic Li-P precipitation. The analysis of the studied metasomatic contact zone provides evidence for a two-way directed interaction between host-amphibolite and pegmatite, whereby a fluid derived from the amphibolite infiltrated the adjacent pegmatite while a fluid derived from the pegmatite dykes migrated into the amphibolite.

The presence of TR, AP, and APL zones in the endocontact of the pegmatite offers an understanding of the mobility of Ca, P, and Li in a pegmatite-amphibolite geochemical system. The main source for Ca represents the host amphibolite, which released Ca by alteration of hornblende to biotite. The Ca-enriched fluid was driven towards the pegmatite, which was primarily enriched in P and Li as an evolved system. The interaction of these two fluid systems, one enriched in Ca, the second in P and Li led to the formation of apatite, which represent a geochemical barrier and preserved Li from further migration outside of pegmatite. In such terms, apatite became the main geochemical barrier for the Li flow from the pegmatite towards the host-rock amphibolite, which also indicates the formation of triphylite clusters at the contact with the apatite layer.

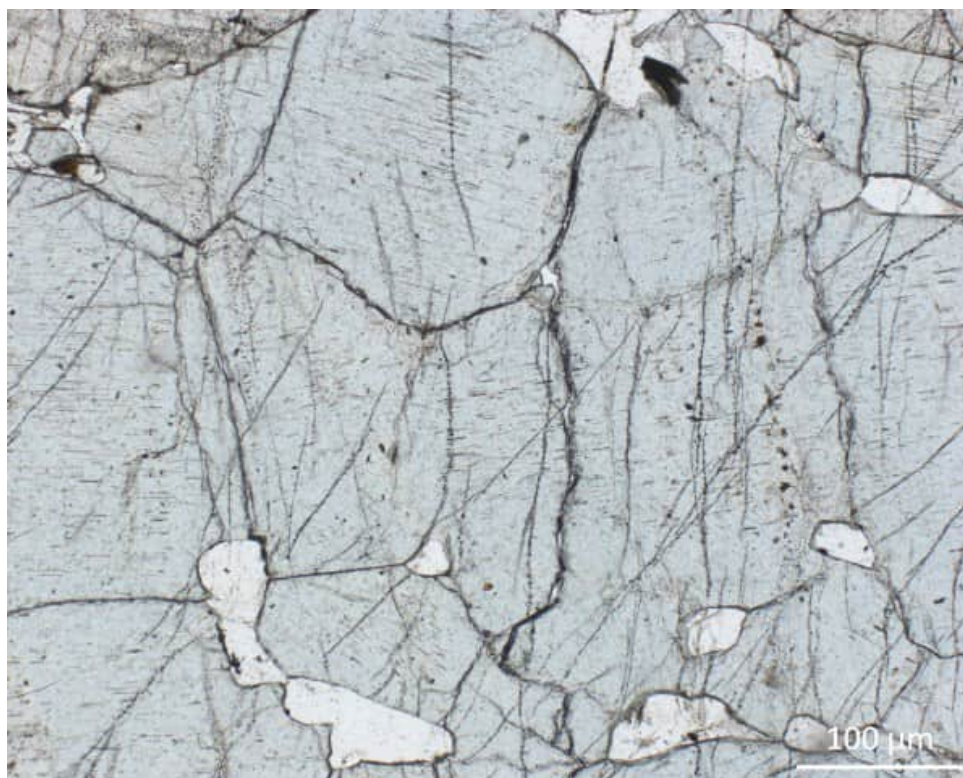


Figure 1. Apatite with needles of oriented triphylite (under plane-polarized light).

Acknowledgement: The authors are grateful for the financial support provided by grant PEGMAT within the ERA MIN2 framework.

- Černý P, Ercit S (2005): The classification of granitic pegmatites revisited. - *Canad Miner* 43, 2005–2026
- Kato S, Ikeda S, Saito K, Ogasawara M. (2018): Fe incorporation into hydroxyapatite channels by Fe loading and post-annealing. - *J Solid State Chem*, 265, 411–416
- Kurylo S, Uher P, Broska I, Lyzhachenko N, Bondarenko S, Gieré R. (2022): Fine-grained petalite and spodumene dykes in the Stankuvatske Li-deposit, Ukrainian Shield: products of tectono–metamorphic recrystallisation. - *Mineral Mag* 86, 863–882
- Syomka V, Ponomarenko O, Stepanyuk L, Bondarenko S, Sukach, V, Kurylo S, Donskyi M (2022): Lithium ores of Stankuvatka and Polokhivka ore fields (Ukrainian Shield). - *Mineral J* 44, 102–124

Tracing high-pressure metamorphism: The spatial evaluation of the Eoalpine metamorphic gradient in the Texel unit (S-Tyrol, Italy)

J. Lanziner-Oberrauch¹, P. Tropper¹, K. Fassmer², H. Pomella², G. Hoinkes³

¹*Institute of Mineralogy and Petrography, University of Innsbruck, Austria*

²*Institute of Geology, University of Innsbruck, Austria*

³*Institute of Earth Sciences, University of Graz, Austria*
e-mail: peter.tropper@uibk.ac.at

In the Austroalpine basement west of the Penninic Tauern Window there are four different units that can be attributed to the Upper Austroalpine, but can be distinguished on the basis of their different lithologies and metamorphic histories. These are 1) the Ötztal-Bundschuh nappe system, which includes the Ötztal unit, 2) the Koralpe-Wölz high pressure nappe system including the Schneeberg and Texel units, 3) the Silvretta-Seckau nappe system with the Ortler-Campo unit, and 4) the Drauzug-Gurktal nappe system, which includes the Matsch unit, the Tonale nappe, and the Meran-Mauls nappe stack.

The Texel unit consists of a metasedimentary sequence with intercalating orthogneisses, amphibolites, and eclogites. Previously, the so-called Laas unit was considered both as part of the Texel unit and as an independent unit. However, because of intense Permo-Triassic metamorphism, for which there is as yet no evidence in the rest of the Texel unit, it should be considered as a separate unit called the Lodner unit (Hoinkes et al. 2021). In their present position in the alpine nappe stack, these two units lie in the above of the Ortler-Campo unit and below the Schneeberg and Ötztal units. Based on the Eoalpine age of the eclogites, the Texel unit is considered to be part of the Koralpe-Wölz nappe system and thus an intracontinental subduction-related high-pressure area related to the Neotethys closure. Overall, the Texel unit has been significantly overprinted by Variscan and Eoalpine metamorphism. Only the so-called Lodner unit shows a Permo-Triassic overprint. The Texel unit reached eclogite-facies during subduction. P-T conditions reached 1.2 to 2.2 GPa and 540 to 620 °C or 680 to 730 °C and 2.7 to 2.9 GPa, depending on the author. The age of the pressure maximum of Eoalpine metamorphism in the Texel unit is 85 ± 5 Ma. The eclogites occur only locally in the Texel unit and the question arose whether this "high-pressure memory" is also detectable in the mica schists and paragneisses.

For this purpose 24 metapelite samples (garnet + biotite + plagioclase + muscovite + quartz \pm kyanite) were investigated geothermobarometrically (Thermocalc v.3.33, mode 1 and mode 2). It was found that the P-T data can be divided into three groups: P = 0.6-0.8 GPa, P = 0.8-1.2 GPa, and P = 1.2-1.6 GPa, and T = 570-600 °C, T = 600-700 °C, and T > 700 °C. Most pressures were in the range 0.8-1.2 GPa, but some samples taken in the vicinity the eclogites still show elevated P values of 1.2-1.6 GPa. Mineral chemically, a pressure-affected earlier stage of Eoalpine metamorphism can also be detected in the elevated Si contents (3.2-3.3 apfu) of muscovite cores. Regionally, a "central zone" with the highest pressure values in the Texel unit can currently be identified. This correlates spatially with the area in the Texel unit where the eclogites occur. Towards the edge of the Texel unit the pressures decrease again.

Characterization of NaOH gas attack on silica bricks by experimental alkali vapour tests and thermochemical modelling by FactSage™

N. Lechner¹

¹RHI Magnesita, Technology Center Leoben, Global R&D – Mineralogy,
Magnesitstraße 2, 8700, Leoben, Austria
e-mail: nikolaus.lechner@rhimagnesita.com

Silica bricks are used as refractory lining in the crown area of glass melting furnaces. During glass production the bricks are subjected to highly corrosive NaOH vapour evaporating from the subjacent glass bath. The interaction between NaOH gas and the refractory leads to a lowering of the melting point and the formation of alkali bearing SiO₂-rich melts within the product. A high volumetric amount and loss of the liquid phase appearing in the refractory could decrease the static stability and the lifetime of the glass furnace crown significantly. Thus, a detailed understanding about the atmospheric conditions favouring NaOH gas formation from the glass bath and its consequent interaction with the silica brick crown lining is of crucial importance to avoid lifetime shortening of the refractory. For that purpose, a mineralogical study by using a combination of experimental alkali vapour tests with thermochemical phase equilibrium modelling by FactSage™ and XRD-Rietveld analyses has been executed to evaluate the corrosive behaviour of a NaOH bearing glass furnace atmosphere on silica bricks. It is shown that a varying concentration of gaseous N₂, CO₂ and H₂O in the furnace atmosphere influences (1) the efficiency of Na₂O evaporation into NaOH gas and (2) the NaOH partial pressure that play a major role for the corrosive interaction with the silica bricks. Furthermore, the condensation behaviour of NaOH gas within the refractory and subsequent corrosion by liquid phase formation strongly depends on a temperature gradient developing in the product during operation.

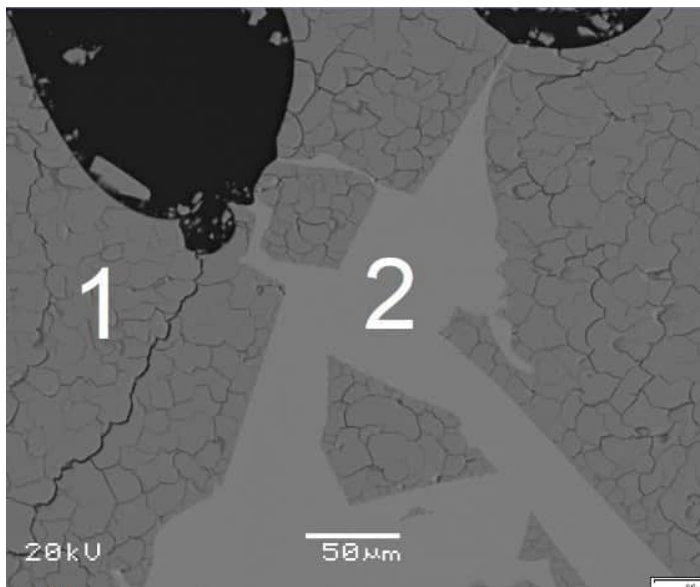


Figure 1. Micrograph of a typical silica brick after use in a glass melting furnace crown lining. Cristobalite (1). Glass phase (2).

Stable Ba isotopes of Alpine mantle peridotites

C. Li^{1,2,3}

¹*Research Centre for Planetary Science, Chengdu University of Technology, Chengdu, China*

²*School of Earth and Space Science, University of Science and Technology of China, Hefei, China*

³*Institut für Geologie und Mineralogie, Universität Köln, Germany*

email: lichunhui@cdu.edu.cn

Barium is a highly incompatible and fluid-mobile lithophile element. Previous studies on basalts and metamorphic rocks from subduction zones have shown that Ba isotopes can reveal more details of the recycling of surface materials into the mantle. However, to our knowledge, Ba isotopic data of mantle peridotites have not been investigated in detail. In this session, we report our new measurement of Ba isotope compositions of Alpine mantle peridotites. These samples include lherzolite, harburgite and pyroxenite which were not thought to contain crustal and surface materials. The Ba isotope compositions of the investigated samples show large variations which we interpret as results of modifications by subduction and contamination of continental crust during the up-welling of the mantle materials. Our data suggest mantle peridotites, even the most clean and pristine ones, may have recorded mantle-crust interaction.

Bismoclite BiOCl from the Jean Baptiste mine, Lavrion area, Greece

I. Liebhart¹, B. Rieck¹, M. Zeug^{1,2}, G. Giester¹

¹Department of Mineralogy and Crystallography, University of Vienna, Josef-Holaubek-Platz 2, 1090 Vienna

²Landesamt für Geologie und Bergwesen, An der Fliederwegskaserne 13, 06130 Halle (Saale), Germany

e-mail: gerald.giester@univie.ac.at

Bismoclite was first discovered and described from a museum specimen No 4465 in the McGregor Museum, Kimberly. The sample is from Jakkalswater, South Africa (Mountain, 1935). Chemical analysis resulted in Bi₂O₃ 89.41, Cl 13.67, less O=Cl₂ 3.08, sum 100 wt. % (Mountain, 1935). In the same year, Bannister & Hey (1935) synthesised the compound BiOCl and named it bismoclite. The crystal structure was solved on synthetic samples in space group *P4/nmm*, with unit cell data $a = 3.887(5)$, $c = 7.354(5)$ Å and refined to $R = 9.17\%$ (Keramidas et al. 1993). Furthermore, a sample from a Bi-Cu-Au deposit, Argentina was studied by infrared analysis, thermal analysis using DTA and TGA, chemical analysis using inductively coupled plasma mass spectrometry (ICP-MS) and an instrumental neutron activation analysis (INAA), microscopy analysis using scanning electron microscopy (SEM), and by pXRD (Testa et al. 2016).

Recently, rare bismoclite was discovered at the 2nd level of the Jean Baptiste Mine in the central part of the Agios Konstantinos area, Lavrion mining district, Attica, Greece. Natural bismoclite was investigated for the first time by single-crystal X-ray diffraction, confirming space group *P4/nmm* with unit cell parameters $a = 3.887(2)$, $c = 7.357(5)$ Å, $Z = 2$, $V = 111.16(14)$ Å³ and refined to final values $R1 = 0.0134$ and $wR2 = 0.0363$. Examined by Raman spectroscopy, the spectrum shows the most intense Raman band at 144 cm⁻¹, smaller bands were observed at 198 and 396 cm⁻¹.



Figure 1. White, in thin sections colourless bismoclite surrounded by ore minerals. FOV 2.9 mm. Foto: B. Rieck

Bannister FA, Hey MH (1935): The crystal-structure of the bismuth oxyhalides. - Mineral Mag 24, 49–58

Keramidas KG, Voutsas GP, Rentzeperis PI (1993): The crystalstructure of BiOCl. - Z Kristallogr 205, 35–40

Mountain ED (1935): Two new bismuth minerals from South Africa. - Mineral Mag 24, 59–64

Testa FJ, Cooke DR, Zhang L, Mas GR (2016): Bismoclite (BiOCl) in the San Francisco de los Andes Bi–Cu–Au Deposit, Argentina. First occurrence of a bismuth oxychloride in a magmatic–hydrothermal breccia pipe and its usefulness as an indicator phase in mineral exploration. - Minerals 6, 62

In-situ powder diffraction study on the formation and reaction pathways of potassium calcium silicates

H. Liu, V. Kahlenberg, C. Hejny, H. Krüger

*University of Innsbruck, Institute of Mineralogy and Petrography, Innrain 52, 6020 Innsbruck, Austria
e-mail: hang.liu@uibk.ac.at*

The K_2O - CaO - SiO_2 system is critically influential in several industrial sectors involving glasses, ceramics, pyrometallurgical processes, energy production, and biomass power. It is of particular interest due to the presence of potassium calcium silicates in the ashes from biomass combustion, modified electric arc furnace slag as well as fertilizers produced from the residues of oil-shale industry or from steelmaking slags. Understanding their high-temperature behaviour can i) contribute to avoid negative effects in the production process due to slagging, fouling or sintering and ii) facilitate the reutilization of residual materials.

In recent years, numerous potassium calcium silicates have been successively identified. $K_2Ca_2Si_2O_7$ and $K_2Ca_6Si_4O_{15}$, notable for their comparatively high melting points, are key contributors to slagging within the system (Santoso et al. 2020). They have been reported to remain in the solid state at temperatures reaching up to 1200 °C. $K_2Ca_3Si_3O_{10}$, located adjacent to $K_2Ca_2Si_2O_7$ within the phase diagram, has been reported to occur under ambient pressure at temperatures of 900 °C, but does not prevail as a primary phase (Schmidmair et al. 2015). While the crystal structures of these potassium calcium silicates have been deciphered, no information is available concerning the question how the complex solid-state reactions in this system proceed and if intermediate / metastable phases are involved.

In the present study, the reaction pathways during the formation of the aforementioned three compounds from silica and carbonate educts were reconstructed through a combination of in-situ powder X-ray diffraction, DTA/TG, and isothermal annealing experiments. Our current observations suggest that K_2CO_3 absorbs water and CO_2 from the air to form $KHCO_3$ at room temperature and reverts through a dehydration process when heated to around 120 °C. Potassium carbonate in the educts tends to combine with $CaCO_3$ to form $K_2Ca(CO_3)_2$ before the formation of the silicates, and undergoes a polymorphic transition from Bütschliite to Fairchildite at ~500 °C. Upon complete decarbonation (~730-800 °C), in all starting mixtures corresponding to the target compositions $K_2Ca_2Si_2O_7$ (E₁₂₂), $K_2Ca_6Si_4O_{15}$ (E₁₆₄), and $K_2Ca_3Si_3O_{10}$ (E₁₃₃) the same two crystalline silicate phases could be identified equivocally: $K_2Ca_2Si_2O_7$ and Ca_2SiO_4 . $K_2Ca_6Si_4O_{15}$ begins to form at ~890 °C, originating from the combination of Ca_2SiO_4 and probably potassium silicate. The temperature range between 920 and 1070 °C can be considered the dominant range for $K_2Ca_2Si_2O_7$, where the previously formed $K_2Ca_6Si_4O_{15}$ further reacts with potassium silicate to form $K_2Ca_2Si_2O_7$, and Ca_2SiO_4 undergoes complete resorption. Starting at 1070 °C, $K_2Ca_6Si_4O_{15}$ is the main phase. However, after further heating to 1150 °C, $K_2Ca_6Si_4O_{15}$ almost fully reacts into Ca_2SiO_4 which exhibits a notable potassium solubility. Above ~1150 °C, no crystalline phases were present for mixture E₁₃₃. In particular, $K_2Ca_3Si_3O_{10}$ is not observable in any stage of the heating process of the three educts.

- Schmidmair D, Kahlenberg V, Perfler L, Tribus M, Hildebrandt J, Töbrens DM (2015): On the ambient pressure polymorph of $K_2Ca_3Si_3O_{10}$ - An unusual mixed-anion silicate and its structural and spectroscopic characterization. - J Solid State Chem 228, 90-98
- Santoso I, Taskinen P, Jokilaakso A, Paek M-K, Lindberg D (2020): Phase equilibria and liquid phase behavior of the K_2O - CaO - SiO_2 system for entrained flow biomass gasification. - Fuel 265, 116894

H₂O degassing experiments of the lower Laacher See Phonolite – on the way to eruption

P. Marks¹, M. Nowak¹

¹Eberhard Karls University Tübingen, Germany
e-mail: patricia.marks@uni-tuebingen.de

The Laacher See volcano is one of the youngest volcanoes in Germany with its last eruption $13,006 \pm 9$ years BP (Reinig et al. 2021). About 6.3 km³ of phonolitic magma was explosively erupted by phreatomagmatic and plinian eruptions in less than 10 days (Wörner and Schmincke 1984). The eruption behavior of such volcanic systems is determined by the phase separation mechanism of H₂O fluid from the supersaturated hydrous silicate melt, caused by the pressure decrease of the magma. The number of fluid vesicles per unit volume of silicate melt (*VND*) is a standard parameter used to quantify the efficiency of fluid-melt separation and thus the acceleration of magma ascent. Two important homogeneous vesicle formation mechanisms are established in the investigation and evaluation of the degassing behavior of silicate melt systems. According to the classical nucleation theory, the *VND* increases strongly with decompression rate (Toramaru 2006) and is therefore a proper parameter for quantifying ascent rate. Recently and specifically for phonolitic melts, the process of spinodal decomposition has been demonstrated, which manifests in the independence of *VND* from the decompression rate (Allabar and Nowak 2018).

To characterize the degassing behavior of the lower Laacher See composition, systematic decompression experiments were conducted in the internally heated pressure vessel. The melts were hydrated with 5.7 or 5.0 wt% H₂O at 200 MPa and 1523 K for 96 h and then continuously decompressed at 1323 K with 0.064 – 1.7 MPa/s to final pressures between 110 MPa and 30 MPa. By reaching the final pressure, the samples were rapidly quenched to room temperature to preserve the vesicle textures and the residual H₂O contents in the melts and to minimize vesicle shrinkage until the glass transition temperature was reached. The *VND*s and the spatial distribution of the vesicles, as well as the H₂O contents in the decompressed melts were analyzed with quantitative image analysis, transmission light microscopy, and FTIR-spectroscopy.

Upon reaching sufficient supersaturation pressure of >100 MPa, all samples exhibit homogeneously dispersed vesicles in the sample center (Fig. 1). Vesicle sizes range from 2 to 13 μm in diameter. Preliminary results indicate that *VND* is independent of decompression rate at all decompression rates. Irrespective of the decompression rate, high log*VND*s of 4.1 to 5.6 mm⁻³ are observed. Further decompression of the degassed melts leads to the formation of coalescence, resulting in a significantly reduced *VND* of the melts.

These observations are consistent with that of Allabar and Nowak (2018), who determined a log*VND* of ~5.2 mm⁻³ for hydrous phonolitic melt of the AD79 Vesuvius white pumice composition. From this, a trend emerges that at least for hydrated phonolitic melt, spinodal decomposition plays a crucial role in the degassing behavior of the melt and thus in the explosive eruption behavior of the volcanic systems.

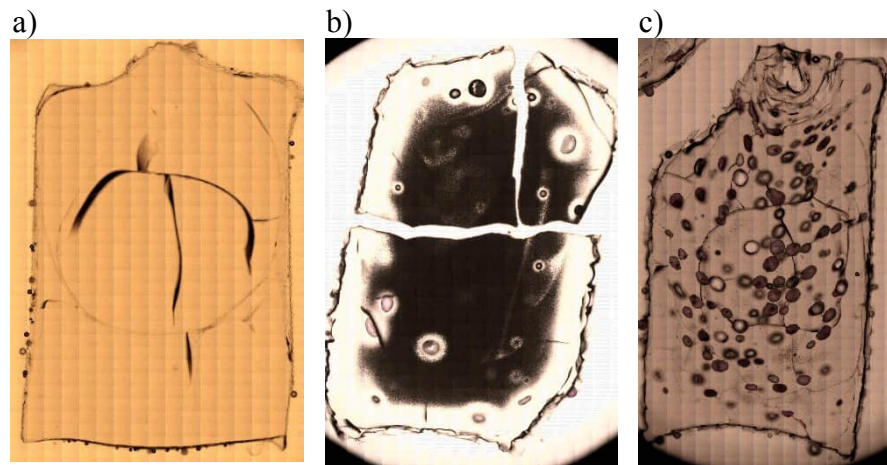


Figure 1. The three degassing steps of an ascending melt. a) No vesicle formation was initiated yet. b) Spontaneous phase separation was triggered by the extreme supersaturation of the melt. c) Further decompression leads to coalescence of the growing vesicles.

Allabar A, Nowak M (2018): Message in a bottle: Spontaneous phase separation of hydrous Vesuvius melt even at low decompression rates. - *EPSL*, 501, 192-201

Reinig F, Wacker L, Jöris O, Oppenheimer C, Guidobaldi G, Nlevergelt D, Adolphi F, Cherubini P, Engels S, Esper J, Land A, Lane C, Pfanzen H, Remmele S, Sigl M, Sookdeo A, Büntgen U (2021): Precise date for the Laacher See eruption synchronizes the Younger Dryas. - *Nature*, 595, 66-69

Toramaru A (2006): BND (bubble number density) decompression rate meter for explosive volcanic eruptions. - *J. Volcanol. Geotherm. Res.* 154, 303-316

Wörner G, Schmincke H-U (1984): Petrogenesis of the Zoned Laacher See Tephra. - *J. Petrol.*, 25, 805-835

Thermal expansion of SiO₂ polymorphs keatite, RUB-11 and silica-sodalite

B. Marler¹, I. Grosskreuz¹

¹*Department of Geology, Mineralogy, and Geophysics, Ruhr University Bochum, Germany
e-mail: bernd.marler@rub.de*

With very few exceptions, dense silica polymorphs like α -quartz or β -cristobalite exhibit a positive volume thermal expansion while microporous silica polymorphs (= guest free silica zeolites) like siliceous faujasite or siliceous chabasite show negative expansion (Lightfoot et al. 2001).

Here, we present the analysis of the thermal expansion coefficients of three silica polymorphs, which have, so far, not been investigated.

Keatite (tetragonal, $\rho = 2.50 \text{ gcm}^{-3}$) is a rare, metastable SiO₂ polymorph possessing a dense silica framework, synthetic keatite is known since 1954 (Keat et al. 1954) and has more recently been discovered as a mineral (Hill et al. 2013).

The all-silica form of sodalite (cubic above 412 K, $\rho = 1.67 \text{ gcm}^{-3}$) has the same microporous framework comprising cage-like voids (Werthmann et al. 2000) as the sodalite mineral, Na₈Cl₂[Si₆Al₆O₂₄].

RUB-11 (monoclinic, $\rho = 2.11 \text{ gcm}^{-3}$) can be regarded as an Interlayer Expanded Zeolite of the natural layer silicate magadiite, Na₂[Si₁₄O₂₈(OH)₂]·8H₂O, however, with additional SiO₄ tetrahedra interconnecting the silicate layers instead of intercalated sodium and water. RUB-11 possesses a silica framework with channel-like pores (Grosskreuz et al. 2023).

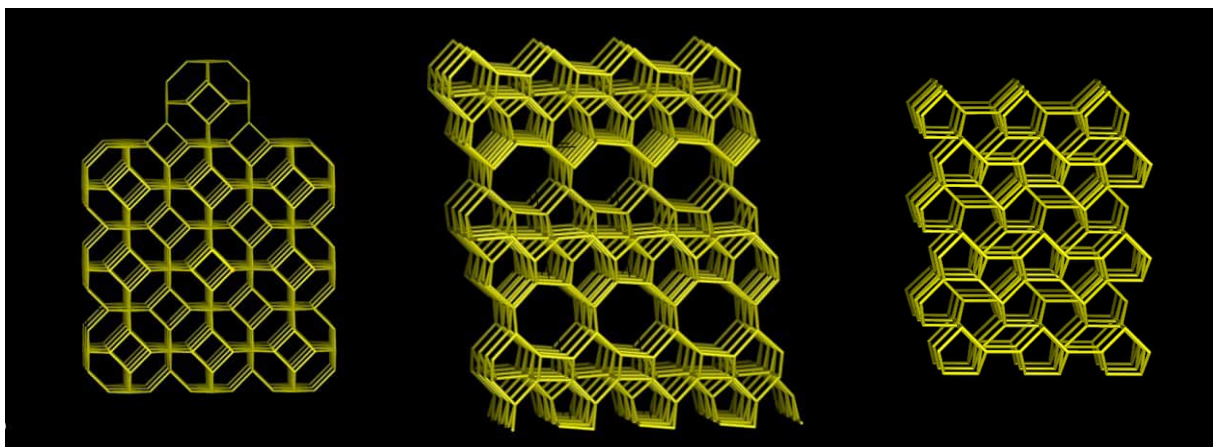


Figure 1. The framework structures of cubic silica sodalite (left), RUB-11 (middle), and keatite (right).

Experimental data: Keatite was synthesized heating a silicate gel prepared from Si(OC₂H₅)₄, LiNO₃, Cr(NO₃)₃ and water at 830 K. Trioxane-silica-sodalite and RUB-11 were hydrothermally synthesized from reaction mixtures of SiO₂/Trioxane/H₂O and SiO₂/ethylenediamine/H₂O/Xe, respectively. Trioxane-silica-sodalite was subsequently heated to remove all organic material from the cage-like pores producing pure silica-sodalite.

Powder XRD data (CuK α ₁) of all samples, kept in glass capillaries, were collected in Debye-Scherrer geometry. Silicon or quartz powder served as an internal standard. The samples were heated in steps of 50 K (silica-sodalite), 100 K (RUB-11) and 110 K (keatite) up to 729, 898 or 713K. Rietveld refinements revealed the lattice parameters and unit cell volumes.

The guest-free silica sodalite is trigonal at room temperature and transforms into a cubic symmetry at 412 K (Werthmann et al. 2000). The cubic silica sodalite exhibits isotropic (negative) expansion while RUB-11 and keatite show a pronounced anisotropic behaviour with negative and positive expansion in different directions. Linear expansion coefficients are

Silica-sodalite (454 – 729 K): $\alpha[100] = -3.7 \cdot 10^{-6}$

RUB-11 (298 – 898 K): $\alpha[100] = -10.2 \cdot 10^{-6}$, $\alpha[010] = +10.1 \cdot 10^{-6}$, $\alpha[001] = -2.1 \cdot 10^{-6}$

Keatite (293 – 713 K): $\alpha[100] = -6.1 \cdot 10^{-6}$, $\alpha[001] = +15.0 \cdot 10^{-6}$

Corresponding expansion coefficients of the volumes $\alpha(V)$ are:

cubic silica sodalite = $-11.2 \cdot 10^{-6}$; RUB-11 = $-6.4 \cdot 10^{-6}$ and keatite = $+2.9 \cdot 10^{-6}$

When listing microporous and dense silica polymorphs with densities ranging from 1.3 to 2.9 g cm^{-3} it appears that materials with intermediate densities (about 2.0 g cm^{-3}) have particular small (positive or negative) expansion coefficients (see Table 1). Considering this fact, it seems not impossible to discover or specifically synthesize a silica polymorph with nearly zero expansion. Since SiO_2 polymorphs are chemically, mechanically and thermally very stable when exposed to most chemicals, pressure and/or high temperature such a material might be useful for many purposes.

Table 1. Selection of SiO_2 polymorphs of intermediate density

SiO_2 polymorph	Density [g cm^{-3}]	Volume thermal expansion coefficient [ppm/K], (temperature range)	Reference
MFI-type zeolite	18.4	-7.6 (373-673 K)	Bhange et al. 2007
RWR-type zeolite	19.2	+3.7 (298-773 K)	Koike et al. 2023
High density zeolite RUB-11	21.1	-6.4 (298-898 K)	This study
High density zeolite RUB-5	22.0	-7.5 (293-743 K)	Marler et al. 2020
Silica glass	22.0	+0.5 (273-873 K)	Heraeus 2023
High density zeolite RWZ-1	22.1	-3.9 (298-773 K)	Koike et al. 2023

Bhange DS, Ramaswamy V (2007): High temperature thermal expansion behavior of silicalite-1 molecular sieve: in situ HTXRD study. - *Micropor Mesopor Mater* 103, 235-242

Grosskreuz I, Krysiak Y, Gies H, Mugnaioli E, Marler B (2023): Synthesis and real structure of RUB-11, a novel high-density silica zeolite based on magadiite layers. - Submitted.

Heraeus: Properties of fused silica (accessed April 27th 2023) - https://www.heraeus.com/en/hca/fused_silica_quartz_knowledge_base_1/properties_1/properties_hca.html#tabs-608478-5

Hill TR, Konish H, Huifang X (2013): Natural occurrence of keatite precipitates in UHP clinopyroxene from the Kokchetav Massif: A TEM investigation. - *Am Mineral* 98, 187-196

Koike M, Grosskreuz I, Asakura Y, Miyawaki R, Gies H, Wada H, Shimojima A, Marler B, Kuroda K. (2023): Bridging the gap between zeolites and dense silica polymorphs: Formation of all-silica zeolite with high framework density from natural layered silicate magadiite. - Submitted to *Angew Chem*

Keat PP (1954): A new crystalline silica. - *Science* 120, 328-330

Lightfoot P, Woodcock DA, Maple MJ, Villaescusa LA, Wright PA (2001): The widespread occurrence of negative thermal expansion in Zeolites. - *J Mater Chem* 11, 212-216

Marler B, Krysiak Y, Kolb U, Grafweg C, Gies H (2020): Two new members of the Silica-X family of materials: RUB-5, a silica zeolite with a very high framework density and RUB-6, a hydrous layer silicate, Micropor. - *Mesopor Mater* 296, 109981

Werthmann U, Marler B, Gies H (2000): Gastmolekülfreier Silica-Sodalith: Eine neue SiO_2 -Modifikation, *Z Kristallogr Supplement Issue*, 17, 188

Structural changes in *Ln*-monazites under swift heavy ion irradiation

J. Marquardt¹, T. Lender², L. Bayarjargal¹, E. Haussühl¹, C. Trautmann³,
L. Peters², B. Winkler¹

¹*Institute of Geoscience, Johann Wolfgang Goethe-University Frankfurt am Main*

²*Institute of Crystallography, RWTH Aachen*

³*GSI Helmholtz Centre for Heavy Ion Research, Darmstadt*

e-mail: marquardt@kristall.uni-frankfurt.de

The safe disposal of nuclear waste is one of the intergenerational issues which needs to be solved. A potential route to effectively immobilize radionuclides could be realized by their incorporation into crystalline solid phases in future radioactive waste repositories. In particular, the immobilization of specific waste streams containing minor actinides (Np, Am, Cm) or plutonium in crystalline solid phases may be advantageous compared to glass matrices, which may be less resistant to leaching and disintegration (Donald et al. 1997; Ewing 1999; Lumpkin et al. 2006). Due to their radiation stability and chemical and structural flexibility, monazite-type compounds are considered suitable matrix materials (Schlenz et al., 2013).

To better understand structural changes due to radiation damage, synthetic monazite single crystals with different chemical compositions (La, Nd, Pm, Sm)PO₄ were irradiated at the UNILAC beamline of GSI Helmholtz Centre Darmstadt using 1.7 GeV Au ions and fluences of up to 1e13 ions/cm². The irradiated single crystals were characterized by Raman spectroscopy, secondary electron microscopy and single crystal X-ray diffraction.

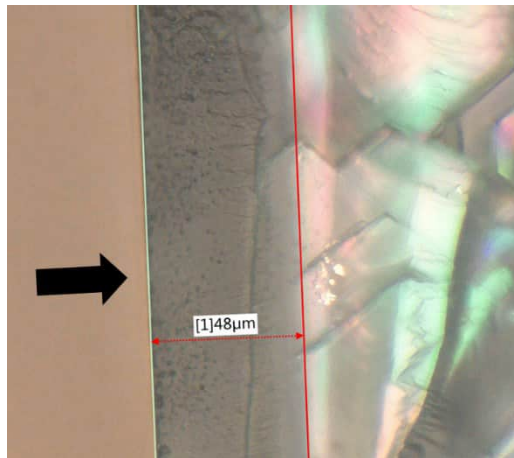


Figure 1. Cross section of a (Pr,Nd)PO₄ monazite crystal, prepared parallel to the direction of the irradiation indicated by the black arrow

The irradiation of monazite with 1.7 GeV Au ions results in an embrittlement of the crystals and the formation of a glassy surface layer of about ~48 μm thickness (Fig. 1), which correlates well with the projected range of ~44 μm according to SRIM-2013 calculations (Ziegler et al. 2010). The irradiation results in a significant broadening of all Raman modes up to the complete disappearance of the symmetric stretching mode ν_1 and further changes in the lattice dynamics. X-ray diffraction experiments revealed the amorphization of the surface layer.

Donald IW, Metcalfe BL, Taylor RNJ (1997): The immobilization of high level radioactive wastes using ceramics and glasses. - J Mater Sci 32, 5851-5887

Ewing RC (1999): Nuclear waste forms for actinides. - PNAS 96, 3432-3439

Lumpkin GR (2006): Ceramic waste forms for actinides. - Elements 2, 365-372

Schlenz H, Heuser J, Neumann A, Schmitz S, Bosbach D. (2013): Monazite as a suitable actinide waste form. - Z Kristallogr – Cryst Mater 228, 113-123

Ziegler JF, Ziegler MD, Biersack JP (2010): SRIM - The stopping and range of ions in matter. - Nucl Instrum Methods Phys Res B 268, 1818-1823

J.M & B.W. acknowledge the German Federal Ministry of Education and Research (BMBF) for financial support in the project No. 02NUK060E. T.L. & L.P. acknowledge support by BMBF under project number 02NUK060B.

High-pressure gneiss with pseudomorphs after jadeite from the Variscan Erzgebirge in Saxony

H.-J. Massonne¹

¹*School of Earth Sciences, China University of Geosciences, Wuhan, P.R. China
e-mail: h-j.massonne@mineralogie.uni-stuttgart.de*

The Erzgebirge in Saxony is known for occurrences of various ultrahigh-pressure (UHP) rocks (Massonne, 2001, 2003), but gneiss, the major rock type there, was rarely addressed in scientific studies (e.g., Willner et al. 1997). A paragneiss (sample E98-36), rich in quartz and white mica, was sampled very close to an eclogite body of the Gneiss-Eclogite Unit (GEU) c. 5 km north of the Saldenbach reservoir where UHP rocks were found.

Millimetre-sized garnet grains in this gneiss can be zoned with a relatively Ca-poor core ($X_{Ca} = Ca/(Ca+Fe^{2+}+Mg+Mg)$ around 0.04, $X_{Mg} = 0.16$, $X_{Mn} = 0.005$) surrounded by a mantle with $X_{Ca} = 0.07-0.09$, $X_{Mg} = 0.13-0.18$, and $X_{Mn} = 0.01$. The contact between these two garnet generations is sharp. Large oriented white mica flakes are phengite with Si contents around 3.42 per formula unit (pfu) in the core and slightly decreasing Si contents towards the rim. A new generation of potassic white mica with lower Si contents formed at the rim of these flakes. A peculiar feature of the studied paragneiss is the occurrence of mm-sized clusters of small albite grains with thin potassic white mica flakes in between. The Si contents of these flakes is between 3.23 and 3.31 pfu and, thus, similar to those of the rim generation of large flakes. The observed elongated clusters, being oriented in the same direction as the large mica flakes, are interpreted as former jadeite grains, which decomposed during exhumation of the rock under infiltration of K-bearing hydrous fluids.

Thermodynamic modelling with PERPLE_X (Connolly, 2005: version 6.6.6) was applied to decipher the metamorphic evolution of the paragneiss. According to the calculated pressure-temperature (P-T) pseudosection contoured with various isopleths for garnet and potassic white mica, an early metamorphic stage (Ca-poor garnet core) occurred at P-T conditions of 0.9 ± 0.1 GPa and 635 ± 25 °C (Fig. 1). The conditions of the high-pressure (HP) stage (garnet mantle) were difficult to determine precisely because compositions of the early garnet mantle and phengite can coexist over a wider P-T range. Thus, a temperature increase from 580-600 °C to 660 °C can be accompanied by a slight pressure decrease from 1.8 to 1.7 GPa, but also by a clear one from ca. 2.4 to 1.7 GPa. This not well determinable portion of the P-T path is compatible with the presence of jadeite and absence of primary biotite. Further decompression without deformation resulted in the formation of pseudomorphs after jadeite. The obtained conditions of 660 °C at 1.7 GPa are similar to those of 715 °C at 1.8 GPa determined for the adjacent eclogite (Massonne 2011).

In-situ U-Th-Pb dating of monazite with the electron microprobe (e.g., Rahimi & Massonne, 2018) yielded an average age of 338.4 ± 2.3 (2σ) Ma (40 of 44 monazite analyses). This age was assigned to the HP event according to previous studies of rocks from the GEU (e.g., Hallas et al. 2021). A small monazite grain enclosed in garnet yielded an age of 386.4 ± 10.5 (2σ) Ma, which was related to the garnet core-forming event (Fig. 1).

Based on the here presented data and those gathered from the literature, the following conclusions are drawn: (1) An Early Carboniferous continent-continent collisional scenario was responsible for the HP event in the GEU. Evidence for metamorphism at UHP is lacking in metasediments and metagranitoids. Diamondiferous rocks in the Erzgebirge in Saxony are crystallization products of melts, which ascended from great Earth's depths and intruded the

Early Carboniferous HP rocks. (2) These HP rocks of the GEU, including eclogites, originally experienced Late Devonian medium-pressure, medium-temperature metamorphism and were constituents of a medium to lower portion of the downgoing plate in the Early Carboniferous collisional scenario. (3) Jadeite should characterize medium-temperature metasediments and metagranitoids that had experienced lithostatic pressure in excess of 1.6 GPa. This study demonstrates that jadeite can be recognized in corresponding HP rocks even after complete decomposition. This means that previously suggested UHP terranes worldwide, lacking relics and pseudomorphs of jadeite and coesite, have never experienced UHP.

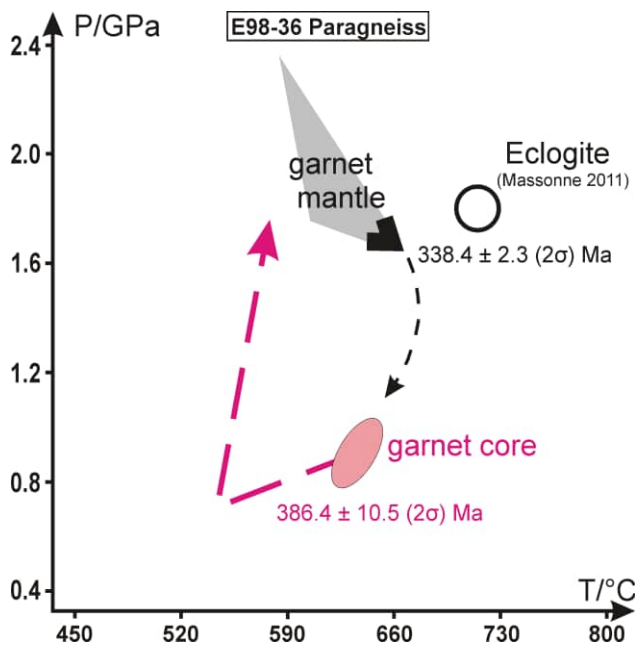


Figure 1. P-T evolution of paragneiss E98-36 developed by thermodynamic modelling. The broken paths were estimated. The given ages resulted from monazite dating using the electron microprobe. The open circle refers to P-T conditions derived by Massonne (2011) for eclogite adjacent to E98-36.

- Connolly JAD (2005): Computation of phase equilibria by linear programming: a tool for geodynamic modeling and its application to subduction zone decarbonation. - *Earth Planet Sci Lett* 236, 524-541
- Hallas P, Pfänder J A, Kroner U, Sperner B (2021): Microtectonic control of $^{40}\text{Ar}/^{39}\text{Ar}$ white mica age distributions in metamorphic rocks (Erzgebirge, N-Bohemian Massif): Constraints from combined step heating and multiple single grain total fusion experiments. - *Geochim Cosmochim Acta* 314, 178-208
- Massonne H-J (2001): First find of coesite in the ultrahigh-pressure metamorphic region of the Central Erzgebirge, Germany. - *Eur J Mineral* 13, 565-570
- Massonne H-J (2003): A comparison of the evolution of diamondiferous quartz-rich rocks from the Saxonian Erzgebirge and the Kokchetav Massif: are so-called diamondiferous gneisses magmatic rocks? - *Earth Planet Sci Lett* 216, 347-364
- Massonne H-J (2011): Pre-conference field trip: Erzgebirge (Ore Mountains), Germany and Czech Republic; German part of the Saxonian Erzgebirge. - *Geolines* 23, 29-59
- Massonne H-J (2023): A new type of saidenbachite with pseudomorphs after coesite phenocrysts from the north-western Bohemian Massif, Germany. - *Terra Nova* in press, <https://doi.org/10.1111/ter.12659>
- Rahimi G, Massonne H-J (2018): Pressure-temperature-time evolution of a Variscan garnet-bearing micaschist from the northern Fichtelgebirge, NW Bohemian Massif in central Europe. - *Lithos* 316-317, 366-384
- Willner A P, Rötzler K, Maresch WV (1997): Pressure-temperature and fluid evolution of quartzo-feldspathic metamorphic rocks with a relic high-pressure, granulite-facies history from the Central Erzgebirge (Saxony, Germany). - *J Petrol* 38, 307-336

The effects of anion and cation substitution on the crystal structure of Cu-based quaternary chalcogenides

D. Matzdorff^{1,2}, M. Avdeev³, D. Sheptiakov⁴, G. Gurieva¹, S. Schorr^{1,2}

¹Helmholtz-Zentrum Berlin für Materialien und Energie, Hahn-Meitner-Platz 1, 14109 Berlin, Germany

²Institut für Geologische Wissenschaften, FU Berlin, Malteserstraße 74-100, 12249 Berlin, Germany

³Australia's Nuclear Science and Technology Organisation, Sydney, Australia

⁴Paul Scherrer Institute, Villigen PSI, Switzerland

e-mail: david.matzdorff@helmholtz-berlin.de

The research of quaternary Cu-based chalcogenide semiconductors has caught a large interest for photovoltaic applications, as these materials consist of non-toxic and earth abundant elements. While being environmentally friendly and low cost and stable under environmental conditions, materials like $\text{Cu}_2\text{MnSnS}_4$ or $\text{Cu}_2\text{MnGeS}_4$ are very promising candidates for use as top cell absorbers in tandem solar cells, because they can cover a wide bandgap range of 1.52-1.72 eV (Beraich et al. 2020; Ramasamy et al. 2018). Compounds like $\text{Cu}_2\text{MnSnSe}_4$ could even be considered for the application in single junction solar cell with a band gap energy of 1.21 eV (Gurieva et al. 2022). This study presents new insight into the structural transformation mechanisms within the $\text{Cu}_2\text{Mn}(\text{Ge},\text{Sn})(\text{S},\text{Se})_4$ solid solution series via neutron powder diffraction.

Since Cu^+ and Ge^{4+} are isoelectronic cations and Mn^{2+} is electronic similar to Cu^+ and Ge^{4+} , they cannot be differentiated in a structural analysis based on X-ray powder diffraction data alone. However, their neutron scattering lengths are considerably different, that is why we apply neutron diffraction to analyze the crystal structure of $\text{Cu}_2\text{Mn}(\text{Ge},\text{Sn})(\text{S},\text{Se})_4$ mixed crystals. Moreover, the basis of our investigations is a careful determination of the chemical composition of the mixed crystals by WDX spectroscopy.

The endmembers of the $\text{Cu}_2\text{Mn}(\text{Ge},\text{Sn})(\text{S},\text{Se})_4$ solid solution series crystallize in different structure types: $\text{Cu}_2\text{MnSnS}_4$ and $\text{Cu}_2\text{MnSnSe}_4$ crystallize in the tetragonal stannite-type structure (space group $I\bar{4}2m$), whereas $\text{Cu}_2\text{MnGeS}_4$ and $\text{Cu}_2\text{MnGeSe}_4$ adopt the orthorhombic wurtz-stannite structure (space group $Pmn2_1$). Thus, within the solid solution series with mixed cations a structural transition from the tetragonal to the orthorhombic crystal structure can be expected.

For the presented study the compounds were synthesized by solid state reaction of pure elements in evacuated silica tubes at temperatures of 730 °C (Se-only compounds), 740-780 °C (mixed anion compounds) and 800 °C (S-only compounds). The chemical composition and homogeneity of the synthesized polycrystalline powder materials were investigated by WDX spectroscopy using an electron microprobe system. It was revealed that the synthesized powders contained the desired phase as a chemically single, homogeneous quaternary phase with slight shifts in the stoichiometric composition as well known in this type of materials (Schorr et al. 2020). LeBail refinement of the powder X-ray diffraction data was used to determine the lattice parameters of the mixed crystals. The cation distribution in the unit cell was defined by applying the average neutron scattering length analysis method (Schorr 2011) which is based on the site occupancy factors determined by Rietveld refinement of the neutron diffraction data. The derived cation distribution model is the basis to conclude on the crystal structure and structural disorder as well as to elucidate the mechanism of structural phase transition.

It will be shown that Sn-rich mixed crystals adopt the stannite type structure, whereas Ge-rich mixed crystals of the mixed cation solid solution series adopt the wurtz-stannite type structure. Within the intermediate range, two chemically identical but structurally different quaternary phases coexist, adopting the tetragonal and the orthorhombic structure respectively. It will also be shown that the respective anions influence the concentration of intrinsic point defects differently and independent to the off-stoichiometric composition.

The results of the chemical composition study in combination with structural characterization and optical bandgap evaluation from diffuse reflectance of $\text{Cu}_2\text{Mn}(\text{Ge},\text{Sn})(\text{S},\text{Se})_4$ mixed crystals will be presented. These investigations enabled us not only to determine the type and concentration of intrinsic point defects, but to show as well the structure type transformation from the stannite- to the wurtz-stannite-type structure.

- Beraich et al. (2020): Facile synthesis of the wurtz stannite (orthorhombic) $\text{Cu}_2\text{MnGeS}_4$ thin film via spray ultrasonic method: Structural, Raman, optical and electronic study. - J All Comp 845, 156216
- Gurieva G, Niedenzu S, Siminel N, Franz A, Schorr S (2022): The kesterite–stannite structural transition as a way to avoid Cu/Zn disorder in kesterites: the exemplary case of the $\text{Cu}_2(\text{Zn},\text{Mn})\text{SnSe}_4$. - Faraday Discussions 239, 51-69
- Ramasamy et al. (2018): Nanocrystals of CuMSnS_4 (M = In or Ga) for solar energy conversion applications. - Chemical Communications 54, 11757
- Schorr (2011): The crystal structure of kesterite type compounds: A neutron and X-ray diffraction study. - Sol. Energy Mat Solar Cells 95, 1482-1488
- Schorr et al. (2020): Point defects, compositional fluctuations, and secondary phases in non-stoichiometric kesterites. - J Phys Energy 2, 012002

The authors gratefully acknowledge the Australia's Nuclear Science and Technology Organisation (ANSTO) for providing us beamtime (proposal number 13403) at the ECHIDNA end station and the Paul Scherrer Institute and the Swiss Spallation Neutron Source (SINQ) for providing us beamtime (proposal number 20202094) at the HRPT diffractometer.

Trace element geochemistry and isotopic data of sulphides in Alpine-type Pb-Zn deposits in the Eastern and Southern Alps

F. Melcher¹, V. Bertrandsson Erlandsson¹, V. Gartner¹, E. Henjes-Kunst¹, P. Onuk¹, J. Raith¹, G. Rantitsch¹, F. Henjes-Kunst², B. Potočnik Krajnc³, A. Šoster³

¹Department of Applied Geosciences and Geophysics, Montanuniversität Leoben, Austria

²Federal Institute of Geosciences and Natural Resources (BGR), Hannover, Germany

³Faculty of Natural Sciences and Engineering, University of Ljubljana, Slovenia

e-mail: F.Melcher@unileoben.ac.at

More than 500 occurrences of Pb-Zn ores are documented in Mesozoic carbonate sequences of the Eastern and Southern Alps. They are invariably hosted by shallow lagoonal and reef carbonates of Middle and Upper Triassic (Anisian and Carnian) age and are collectively termed “Alpine-type” (APT) deposits. The district has a long mining history starting in Roman times and terminating in the early 1990ies when the last operations closed at Bleiberg (Austria), Cave del Predil/Raibl (Italy), and Mežica/Mies (Slovenia) (Schroll 2008). The Bleiberg deposit was closed in 1993 after more than 700 years of mining. It is regarded as a world-class deposit (Leach et al. 2005) and represents the type locality of APT Pb-Zn deposits. The historical total metal production from APT deposits exceeded 6×10^6 tons (Mt) Zn and Pb from a resource exceeding 110 Mt (Cerny 1989; Cerny & Schroll 1995; Leach et al. 2003; Spangenberg & Herlec, 2006). Renewed interest in base metals, and especially in their by-products such as Ge, Ga, In and Cd, has initiated modern exploration activities in some of the mining districts. Germanium and Cd have been recovered from ores in the past; about 200 tons Ge, mostly from Bleiberg and Raibl, were produced from APT deposits.

Although the deposits occur in a wide region, they share common features such as a simple mineralogical composition, complex ore textures, light sulphur isotopic compositions, Late Palaeozoic Pb model ages, and trace element compositions in sphalerite, galena and pyrite. Ore textures are complex and often equivocal. They include rare examples indicating syngenetic to early diagenetic origin, besides abundant epigenetic textures such as crosscutting veins and breccia ores. However, biogenic textures and relict bacteria colonies are present (Kucha et al. 2010). Therefore, some mineralization must have precipitated at shallow level at low temperature.

Sphalerite is low in Fe (commonly 0.01-0.5 %), Mn, Co, Ga and In, but commonly contains elevated Cd, Ge, As, Tl and Pb concentrations. Median concentrations of Ge determined by LA-ICP-MS are 846 ppm in the Fladung deposit, 229 ppm at Bleiberg and 222 ppm at Raibl where the highest contents of As and Tl have been determined. Sphalerite chemistry indicates that temperatures of formation range from 60 to 140 °C. This is lower than suggested by previous fluid inclusion data, but in line with results of thermal modelling. Metamorphosed sphalerite (>450 °C) in the Brenner and Stangalm Mesozoic reveals metal exchange to higher Fe and Mn, and lower Ga, Ge, As and Tl concentrations. Galena is Ag-poor, although Ag concentrations both in sphalerite and galena increase towards the north of the Austroalpine nappe system. Pyrite- and marcasite-rich ores display an As-Tl-(Hg) association, and are low in Co and Ni. Pyrite is stable to higher temperatures, keeping its original low-temperature trace element compositions.

The sulphur isotope composition of sulphides in APT deposits varies over a wide range and is often bimodally distributed, attaining a maximum at highly negative values ($\delta^{34}\text{S} \leq -20$ ‰) explained by bacteriogenic sulphate reduction, and a second maximum at $\delta^{34}\text{S} = -10$ to 0 ‰ explained by thermogenic sulphate reduction from a second source (Schroll & Rantitsch 2005). APT ores in general show lead isotopic compositions above the crustal lead growth curves. The variable enrichment in ^{207}Pb and ^{208}Pb originated from an isotopically enriched continental source (Köppel 1997). Local differences in the bedrock geology and/or its variable common Pb composition are responsible for the Pb isotopic variability of the individual APT deposits. A metal source from the Paleozoic basement and Triassic sedimentary rocks is most likely.

Rb-Sr isochrons of sphalerite from the Bleiberg deposit indicate two phases of ore deposition: a first one at about 229 Ma and a second at about 207-201 Ma. Initial $^{87}\text{Sr}/^{86}\text{Sr}$ of the early (229 Ma) sphalerite agrees with Carnian seawater composition. The Carnian Rb-Sr isochron age corresponds to U-Pb ages of calcite associated to ore minerals of the (Southalpine) Gorno deposit (Giorno et al. 2022). The younger (≈ 205 Ma) age reflects fluid flow within the carbonate sequence, probably due to fracturing of the platform during initial rifting of the Penninic Ocean. This process is probably related to ongoing tectonic instability following sedimentation of the Upper Hauptdolomit with formation of deep basins, where hydrocarbon source rocks were deposited. In a wider context of central and southern Europe, mineralizing processes during the Mesozoic have been explained as a response to the Pangaea breakup (Burisch et al. 2022). The oldest hydrothermal processes in the circum-Mediterranean are related to the initial rift axes. Mineralization spans a range from 230 to 160 Ma with a maximum at 230-200 Ma.

- Burisch M, Markl G, Gutzmer J (2022): Breakup with benefits - hydrothermal mineral systems related to the disintegration of a supercontinent. - *Earth Planet Sci Let* 580, 117373
- Cerny I (1989): Die karbonatgebundenen Blei-Zink-Lagerstätten des alpinen und außeralpinen Mesozoikums. Die Bedeutung ihrer Geologie, Stratigraphie und Faziesgebundenheit für Prospektion und Bewertung. - *Arch Lagerstförsch Geol Bundesanst* 11, 5-125
- Cerny I, Schroll E (1995): Heimische Vorräte an Spezialmetallen (Ga, In, Tl, Ge, Se, Te und Cd) in Blei-Zink- und anderen Erzen. - *Arch Lagerstförsch Geol Bundesanst* 18, 5-33
- Giorno M, Barale L, Bertok C, Frenzel M, Looser N, Guillong M, Bernasconi SM, Martire L (2022): Sulphide-associated hydrothermal dolomite and calcite reveal a shallow burial depth for Alpine-type Zn-(Pb) deposits. - *Geology* 50, 853-858
- Köppel V (1997): 3.5. Bleiisotope. - *Arch Lagerstförsch Geol Bundesanst* 19, 485-495
- Kucha H, Schroll E, Raith JG, Halas S (2010): Microbial sphalerite formation in carbonate-hosted Zn-Pb ores, Bleiberg, Austria: Micro- to nanotextural and sulphur isotope evidence. - *Econ Geol* 105, 1005-1023
- Leach DL, Bechstädth TH, Boni M, Zeeh S (2003): Triassic-hosted MVT Pb-Zn ores of Poland, Slovakia and Italy. - In: Kelly JG et al. (eds.): *Europe's major base metal deposits*. Irish Ass Econ Geol, 169-213
- Leach DL, Sangster DF, Kelley KD, Large RR, Garven G, Allen CR, Gutzmer J, Walters S (2005): Sediment-hosted Pb-Zn deposits: A global perspective. - *Econ Geol* 100th Anniv Vol, 561-607
- Schroll E (2008): Die Blei-Zink-Lagerstätte Bleiberg. Die Geschichte ihrer Erforschung. - *Carinthia* II 62, 287 pp
- Schroll E, Rantitsch G (2005): Sulphur isotope patterns from the Bleiberg deposit (Eastern Alps) and their implications for genetically affiliated lead-zinc deposits. - *Mineral Petrol* 84, 1-18
- Spangenberg JE, Herlec U (2006): Hydrocarbon biomarkers in the Topla-Mežica zinc-lead deposits, Northern Karavanke/Drau Range, Slovenia: paleoenvironment at the site of ore formation. - *Econ Geol* 101, 997-1021

Corundum-rich rocks in the Tauern Window, Austria

F. Melcher¹, M. Feichter¹, H. Mali¹, H. Grill², B. Huet³

¹*Department of Applied Geosciences and Geophysics, Montanuniversität Leoben, Austria,*

²*Birkenweg, Neumarkt, Austria*

³*Geosphere Austria, Vienna, Austria*

e-mail: F.Melcher@unileoben.ac.at

In the search for the origin of a 60 kg block of a dark grey corundum-rich rock that was found in the river bed of the Obersulzbach Valley near Hopffeldboden, Venediger Alps (Salzburg, Austria; Melcher et al. 2022), boulders of similar material were discovered underneath a cliff in the region named Bettlerscharte. In this area, Variscan granite gneisses of the Central Gneiss Supersuite are intercalated with metavolcanics (amphibolite, chlorite schist) and metasedimentary rocks (micaschist, graphitic phyllite, quartzite) attributed to the Habach Group. Corundum-bearing rocks with or without sulphide mineralization are associated with a diverse suite of metasedimentary and metavolcanic rocks that outcrop in the cliff northwest of the Bettlerscharte. Rocks comprise white, partly kyanite-bearing quartzite, garnet-bearing chloritoid-chlorite-muscovite schist, amphibolite, and epidote schist with massive bands of magnetite. The quartzites show strong foliation and disseminated sulphide mineralization comprising mainly pyrite, but in places also abundant molybdenite. The assemblage resembles the one described as type locality of the Habach Formation (Steyrer 1983).

Similar to the specimen found in the Obersulzbach valley investigated earlier (Melcher et al. 2022), microscopic examination of the corundum-bearing rocks reveals abundant magnetite, ilmenohematite, and variable pyrite in a very fine-grained non-foliated matrix, in which rare white mica flakes and aggregates are visible. The fine matrix consists mainly of anhedral corundum of 30-50 μm grain size intergrown with green-blue pleochroic Fe-rich chloritoid (#Mg = 15-27) and less abundant light green chlorite with #Mg ranging from 40-60. White mica aggregates consist of intergrown margarite and paragonite and are often surrounded by large chloritoid crystals. Apatite is present throughout the rock, although grain size and abundance vary. Accessory phases include diaspore, epidote/allanite, zircon, and monazite. Oxide minerals mainly consist of magnetite and ilmenohematite. Uraninite and Nb-rich rutile (4-6 wt% Nb₂O₅) are subordinate. Sulphides postdate the oxide-silicate assemblage and mainly consist of pyrite and chalcopyrite, with rare molybdenite. The corundum-rich assemblage is associated with rocks carrying relict garnet replaced by chloritoid, chlorite and white mica. These rocks also carry abundant magnetite, ilmenohematite and pyrite.

Chemical analysis of corundum-rich rocks by wavelength-dispersive X-ray fluorescence spectroscopy on fused discs reveals high contents of Al₂O₃ (36-55 wt%) and Fe₂O₃ (22-35 wt%), low SiO₂ (3.8-22 wt%), CaO (0.7-2.6 wt%), MgO (0.7-2.1 wt%), K₂O (<1.8 wt%) and Na₂O (<1.2 wt%). Sulphur contents in some samples reach up to 10 wt%. TiO₂ (2.2-4.2 wt%) and P₂O₅ (0.7-1.2 wt%) are severely enriched compared to typical crustal rocks. Among the trace elements, high contents of Zr (356-848 ppm), V (321-559 ppm), Nb (39-89 ppm), Cu (156-1550 ppm) and Ga (49-106 ppm) are noteworthy, along with low Cr, Ni, Y and REE.

Chemical composition and mineralogy both strongly argue in favour of a bauxitic origin of the samples, resembling Si-depleted, Fe-rich bauxite. Compared to other metabauxites, the P content is extraordinarily high. Apart from S, Fe, Cu and P, levels of minor and trace elements are within the ranges expected for bauxite. Trace element concentrations, especially low Ni-Cr contents favour an origin from acidic precursor rocks.

The association with both, rocks typical of the Habach Formation (amphibolite) and quartzitic metasediments is regarded as an indication for a situation where pre-Permian rocks have been weathered producing local bauxitic rocks associated with less Si-depleted, clay-rich material. These paleosoils have been covered by impure sandstone, probably in the Lower Triassic. Weathering horizons in similar stratigraphic and tectonic positions have been described from other areas within the Tauern Window (Barrientos & Selverstone 1987; Franz et al. 2021).

Preliminary metamorphic P-T conditions have been determined for the metabauxite using pseudosections calculated with the Theriak-Domino software package (de Capitani & Petrakakis 2010). The targeted sample is the one investigated in Melcher et al. (2022). The observed oxide-silicate assemblage with corundum, chloritoid, chlorite, margarite, paragonite, rutile, hematite, ilmenite and magnetite points to peak conditions at 500 ± 30 °C and 8.5 ± 1.5 kbar. In this range, the model predicts stability of corundum, chloritoid, chlorite, margarite, paragonite and rutile together with a complex topology between the fields containing one or two of the three Fe-Ti oxides hematite, ilmenite and magnetite. This explains the observed complex reaction features between those.

Barrientos X, Selverstone J (1987): Metamorphosed soils as stratigraphic indicators in deformed terranes: An example from the Eastern Alps. – *Geology* 15, 841-844

de Capitani C, Petrakakis K (2010): The computation of equilibrium assemblage diagrams with Theriak/Domino software. - *Amer Mineral* 95, 1006-1016

Franz G, Kutzschbach M, Berryman EJ, Meixner A, Loges A, Schultze D. (2021): Geochemistry and paleogeographic implications of Permo-Triassic metasedimentary cover from the Tauern Window (Eastern Alps). - *Eur J Mineral* 33, 401-423

Melcher F, Feichter M, Mali H, Grill H (2022): Ein ungewöhnliches Korundgestein im Tauernfenster: Metabauxite in der Habach-Gruppe? – *Mitt Österr Mineral Ges* 168, 89-99

Steyrer HP (1983): Die Habachformation der Typlokalität zwischen äußerem Habachtal und Untersulzbachtal (Pinzgau/Salzburg). – *Mitt Österr Geol Ges* 76, 69-100

Rohstoffe für den Green Deal: woher nehmen?

F. Melcher

*Lehrstuhl für Geologie und Lagerstättenlehre, Montanuniversität Leoben, Österreich
Frank.Melcher@unileoben.ac.at*

Die Europäische Union hat mit dem European Green Deal das ehrgeizigste Transformationsprogramm ihrer Geschichte initiiert. Die Reduktion der Treibhausgasemissionen sowie der Ausbau des Anteils erneuerbarer Energien werden gewaltige Mengen an mineralischen und metallischen Rohstoffen verbrauchen. Viele dieser Rohstoffe werden in der Union als kritisch klassifiziert und müssen daher zum überwiegenden Teil importiert werden. Hier ist vor allem die dominierende wertschöpfungsübergreifende Rolle Chinas in der Versorgung mit Rohstoffen und Zwischenprodukten zu nennen.

Trotz der Innovationen in Recyclingtechnologien und den Bemühungen zur Umsetzung einer Kreislaufwirtschaft werden primäre mineralische Rohstoffe weiterhin und sogar verstärkt genutzt werden müssen, um die Schlüsseltechnologien (Windkraft, Solarenergie, Batterien) und ihre Infrastruktur (Leitungen, Fundamente) zu versorgen. Es werden zusätzliche Mengen an strukturellen Materialien (Baurohstoffe, Stahl, Kupfer) und technologie-spezifischen Materialien benötigt. Letztere, beispielsweise Lithium, Kobalt, Seltene Erden, Indium und Germanium müssen derzeit zu nahezu 100% importiert werden.

Die Abhängigkeit der europäischen Industrie bezüglich der Rohstoffe für die Energiewende ist unumstritten und seit Jahren bekannt. Trotz intensiver Diskussion auf nationaler und europäischer Ebene hat sich die Situation für den Bergbau in Europa seit 30 Jahren nicht signifikant verbessert.

Der Vortrag wird besonders die Möglichkeiten der Versorgung mit mineralischen Rohstoffen aus europäischen Quellen beleuchten. Hier sind Potenziale für Lithium, Graphit, Seltene Erden und Kobalt, aber auch Baurohstoffe zu nennen. Die Eigenverantwortung der europäischen Länder impliziert, dass die Gewinnung zusätzlicher Rohstoffmengen genehmigt und geduldet werden muss, um größeren Schaden an Umwelt und Klima zu vermeiden. Erweiterungsverfahren oder Neuerschließungen sind jedoch mit erheblichen Problemen konfrontiert. Vielfältige konkurrierende Nutzungen müssen bedacht werden, und schließlich können Eingaben und Politik jedes Projekt kippen. Dies ist aus Sicht der Nachhaltigkeit der Versorgung mit den notwendigen Rohstoffen für die Energiewende nicht vereinbar. Somit ist der Ausbau der erneuerbaren Energien eine Herausforderung, die es an vielen Fronten zu meistern gilt.

On preventing Sn-loss in experimental studies

J. A.-S. Michaud¹, F. Holtz¹, T. Fusswinkel²

¹*Institute of Mineralogy, Leibniz University, Callinstr. 3, 30167 Hannover, Germany*

²*Institute of Applied Mineralogy and Economic Geology, RWTH Aachen University*

Willnerstraße 2, 52062 Aachen, Germany

e-mail: j.michaud@mineralogie.uni-hannover.de

Tin (Sn) transport and concentration are essentially controlled by a combination of melt- and fluid-driven processes and its cycle within the crust strongly depends on its partitioning. Given the complexity of natural systems, it is rather hard to evaluate the effect of individual parameters (e.g., pressure (P), temperature (T), proportion and composition of involved phases or redox conditions) on Sn behaviour.

As an alternative, natural processes can be simulated experimentally under a range of conditions relevant to natural systems. However, in experiments conducted at elevated P-T, samples containers are made of noble-metal capsules (e.g., Au, Pt, Au-Pd) and Sn alloys with all these materials especially under reducing conditions and when an aqueous phase is present. This often results in capsule failure and/or to problems for the accurate determination of Sn partitioning between phases due to partial Sn loss during the experiment. Several experimental studies have focused on Sn behaviour (e.g., Keppler & Wyllie 1991; Schmidt et al. 2020; Michaud et al. 2021; Pichavant 2022) but to our knowledge none of the methods proposed so far were completely satisfactory when it comes to preventing Sn loss and determining partition coefficients accurately and reproducibly.

Inspired from Lerchbaumer & Audétat (2012) and Derrey et al. (2017), we propose a new capsule setup (Fig.1) which has been tested on the example of Sn partitioning experiments

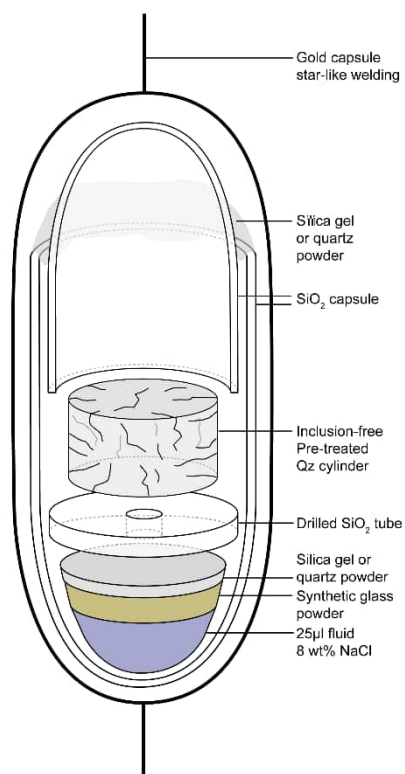


Fig.1: Capsule setup designed to prevent Sn-loss during HT-HP experiments.

between a strongly peraluminous melt and an aqueous phase. In order to avoid interactions with the noble-metal capsule and minimise Sn loss, 15 mg of glass powder containing *ca.* 600 ppm Sn, 25 µl of 8wt% NaCl fluid and a pre-cracked quartz cylinder are inserted in an inner silica capsule consisting of two fitting tubes. Silica gel or quartz powder is added to insure sealing of the silica tubes during heating.

Several experiments were run at 800°C, 150 MPa, under boiling conditions (i.e., phase separation resulting in coexisting brine and vapour-rich fluid inclusions), for 24 and 48h and under oxidising (QFM+3; fO_2 is 3 log units higher than fO_2 buffered by Quartz-Fayalite-Magnetite buffer) and reducing conditions (QFM -0.5).

Boiling assemblages were found in all samples, with brine and vapour-rich inclusions entrapped in quartz cylinders having generally a size in the range of 10 to >25 µm. Under reducing conditions, quenched glasses contain numerous albite crystals and few cassiterites. Under oxidising conditions, the glass is rather homogeneous and cassiterite has only been found within what was formerly a silica drilled tube separating the quartz cylinder from the rest (see Fig. 1).

Tin concentrations were measured in quenched glasses and brine and vapour-rich inclusions with electron microprobe and LA-ICP-MS. Under oxidising conditions, Sn concentrations are rather homogeneous in the quenched glass (i.e., ~ 200-250 ppm) and a bit more scattered in brine inclusions (i.e., 100-640 ppm; median 347 ppm) but all lower than the Sn concentration in the starting glass. Under reducing conditions, Sn concentrations in glass are more scattered in the 24h run (i.e., median 2631 ± 1464 ppm) than in the 48h one (i.e., median 1752 ± 699 ppm). This heterogeneity is probably related to the high crystallinity observed in these glasses. Concentrations in brine inclusions are rather clustered for both duration (i.e., median 107 ± 38 ppm and 84 ± 50 ppm for the 24 and 48h runs, respectively). Concentrations in vapour-rich inclusions could only be measured in the 48h run and are very low (i.e., median 0.6 ± 6 ppm).

Overall, Sn shows a contrasted behaviour depending on redox conditions, being preferentially partitioned to the fluid under oxidising and to the melt under reducing conditions. This result is supported by the presence of cassiterite crystallizing from the fluid at oxidizing conditions and of cassiterite crystallizing from the melt at reducing conditions. Our dataset and mass balance calculations indicate that the use of a silica capsule inserted in noble metal capsules is rather successful in preventing important Sn-loss during experiments.

- Derrey IT, Albretch M, Dupliy E, Botcharnikov RE, Horn I, Junge M, Weyer S, Holtz F (2017): Experimental tests on achieving equilibrium in synthetic fluid inclusions: Results for scheelite, molybdenite, and gold solubility at 800 °C and 200 Mpa. - *Amer Miner* 102, 275-283
- Keppler H, Wyllie PJ (1991): Partitioning of Cu, Sn, Mo, W, U and Th between melt and aqueous fluid in the systems haplogranite-H₂O-HCl and haplogranite-H₂O-HF. - *Contr Miner Petrol* 109, 139-150
- Lerchbaumer L, Audétat A (2012): The quartz capsule - a new method to avoid alloying problems with noble-metal capsules in hydrothermal experiments. - *Eur J Miner* 24, 683-693
- Michaud JA-S, Pichavant M, Villaros A (2021): Rare elements enrichment in crustal peraluminous magmas: insights from partial melting experiments. - *Contr Miner Petrol* 176, 96
- Pichavant M (2022): Experimental crystallisation of the Beauvoir granites as a model for the evolution of Variscan rare metal magmas. - *J Petrol* 63, 1-28
- Schmidt C, Romer R, Wohlgemuth-Ueberwasser CC, Appelt O (2020): Partitioning of Sn and W between granitic melt and aqueous fluid. - *Ore Geol Rev* 117, 103263

Atomistic processes in actinolite and tremolite at elevated temperatures

B. Mihailova¹, C. Rösche¹, N. Petrova², T. Malcherek¹, J. Schlüter³

¹FB Erdsystemwissenschaften, Universität Hamburg, Grindelallee 48, 20146 Hamburg, Germany

²Institute of Mineralogy and Crystallography "Acad. Ivan Kostov", Bulgarian Academy of Sciences, Acad. Georgi Bonchev Str. 107, 1113 Sofia, Bulgaria

³Mineralogisches Museum, Leibniz-Institut zur Analyse des Biodiversitätswandels, Grindelallee 48, 20146 Hamburg, Germany

e-mail: borianna.mihailova@uni-hamburg.de

Elucidating the atomistic mechanism of high-temperature transformations of iron-containing amphiboles ($AB_2C_5T_8O_{22}W_2$, with $C_5 = M(1)_2M(2)_2M(3)$) may have important implications in several fields, including metamorphic petrology, geophysics, and environmental sciences. Here the effect of octahedrally coordinated Fe^{2+} on the temperature-driven dehydrogenation/dehydroxylation in Mg-rich amphiboles is analysed by a comparative study of tremolite and actinolite via *in situ* high-temperature Raman spectroscopy, thermogravimetric/mass-spectrometry analyses, and X-ray diffraction (Rösche et al. 2022).

We show that similar to Fe-rich amphiboles (Mihailova et al. 2021, 2022, Bernardini et al. 2023) thermally activated delocalized e^- and H^+ are also formed in Fe-bearing magnesian amphiboles, but at much higher temperatures than in ferrous (e.g. grunerite) and mixed-valence iron-rich amphiboles (e.g. riebeckite). The delocalized electrons in actinolite couple with polar FeO_6 phonons to form polarons. However, the polaronic dipoles in actinolite are not mutually aligned as in the case of Fe-rich amphiboles, because iron cations are present in the actinolite structure as isolated octahedra or dimers of octahedra, while the majority of MO_6 octahedra in the strips are occupied by Mg. The final product of the thermally-induced decomposition of both actinolite and tremolite is a single phase of monoclinic pyroxene with an intermediate chemical composition between diopside and clinoenstatite, having vacancies at the octahedral sites and, for actinolite, also Fe^{3+} . Cristobalite occurs only as a minor phase in amounts less than 1% and ~5% for tremolite and actinolite, respectively. The dehydroxylation of tremolite causes immediate collapse of the silicate double chain into SiO_4 single chains, which is followed up by a rearrangement of the amphibole B-type and C-type cations into pyroxene octahedral sheets. The actinolite-to-pyroxene breakdown is preceded by a state of "oxo-actinolite" in which all Fe^{2+} are exchanged to Fe^{3+} , all ${}^W(OH)^-$ groups next to Fe-containing $M(1)M(1)M(3)$ configurations are exchanged to ${}^WO^{2-}$, and all H^+ , including those from W -site anions next to MgMgMg triads, are delocalized, but still in the bulk of the crystal grain.

Bernardini S, Della Ventura G, Schlüter J, Mihailova B (2023): Thermally activated electron hopping in Fe-rich amphiboles: implications for the high-conductivity anomalies in subduction zones. - *Geochem* 83, 125942

Mihailova B, Della Ventura G, Waesermann N, Xu W, Schlüter J, Galdenzi F, Marcelli A, Redhammer GJ, Boiocchi M, Oberti R (2021): Atomistic insight into lithospheric conductivity revealed by phonon-electron excitations in hydrous iron-bearing silicates. - *Commun Mater* 2, 57

Mihailova B, Della Ventura G, Waesermann N, Bernardini S, Xu Wei, Marcelli A (2022): Polarons in rock-forming minerals: physical implications. - *Condens Matter* 7, 68

Rösche C, Waesermann N, Petrova N, Malcherek T, Schlüter J, Mihailova B (2022): Oxidation processes and thermal stability of actinolite. - *Phys Chem Mineral* 49, 47

**Zemannite, $\text{Mg}(\text{H}_2\text{O})_6[\text{Zn}^{2+}\text{Fe}^{3+}(\text{TeO}_3)_3]_2 \cdot n\text{H}_2\text{O}$, $n \leq 3$:
Trigonal symmetry enables a fully ordered host-guest structure**

R. Miletich¹, H.S. Effenberger¹, M. Ende¹

*Institut für Mineralogie und Kristallographie, Universität Wien
ronald.miletich-pawliczek@univie.ac.at*

The microporous crystal structure of zemannite was originally described in space group $P6_3/m$ (Matzat 1967; Mandarino et al. 1967; Miletich 1995), later revised to $P6_3$ (Cametti et al. 2017; Missen et al. 2019). Most recently the diffraction pattern of a single-crystal sample was re-investigated using a high-sensitivity Dectris Pilatus pixel detector (Effenberger et al. 2023). Unexpectedly, several uneven low-order $00l$ reflections showed unequivocally verifiable weak intensities clearly violating the 6_3 screw-axis reflection conditions. These observations promoted detailed X-ray crystallographic investigation to be resumed.

The crystal-structure type of zemannite is characterised by a honey-comb like $[\text{Zn}^{2+}\text{Fe}^{3+}(\text{TeO}_3)_3]^{1-}$ framework building channels along $[001]$. It consists of $M_2\text{O}_9$ dimers formed by two face-sharing MO_6 octahedra, $M = (\text{Zn}^{2+}, \text{Fe}^{3+})$ with $\text{Zn}^{2+}:\text{Fe}^{3+} \sim 1:1$. These dimers are linked by $(\text{Te}^{4+}\text{O}_3)^{2-}$ figures and form the channel walls. The channels are filled by the extra-framework constituents, i.e. $0.5 [\text{Mg}(\text{H}_2\text{O})_6]^{2+}$ cations per formula unit in addition to up to 1.5 interstitial H_2O molecules. So far, none of the space-group symmetries $P6_3/m$ or $P6_3$ was compatible with a fully ordered atomic arrangement. In space group $P6_3/m$ there is one $M = (\text{Zn}^{2+}\text{Fe}^{3+})$ position, thus an order of the M atoms is impossible. However, the ionic radii of the two M cations differ suggesting a tentative order and, furthermore, $\text{Fe}^{3+}_2\text{O}_9$ dimers besides $\text{Zn}^{2+}_2\text{O}_9$ dimers are not likely. Ordering of the extra-framework atoms is impossible within the given symmetry constraints for both space groups mentioned above. In the acentric space group the M position splits into two sites, $M1$ and $M2$; an order between Zn^{2+} and Fe^{3+} might be possible but could not be proofed so far (Cametti et al. 2017).

For this work X-ray diffraction data were collected at 298 ± 0.5 K, 200 ± 1 K, and 100 ± 3 K ($2\theta_{\text{max}} = 101.4^\circ$, $\text{MoK}\alpha$ radiation). Careful inspections of the entire images did not show any evidence for satellite reflections in the surrounding of the Bragg-peak positions. Furthermore, there is no hint neither for diffuse scattering nor for the appearance of superstructure reflections. Thus, an incommensurately modulated atomic arrangement or disorder phenomena in neighbouring channels are not likely.

A series of comparative refinement models were performed in the space groups $P6_3/m$ and its subgroups $P6_3$, $P\bar{6}$, and $P3$. Order of the Fe and Zn atoms in the frame work is possible in all subgroups of $P6_3/m$. Due to mirror planes parallel to (0001) , space group $P\bar{6}$ allows Fe_2O_9 or Zn_2O_9 dimers, which contradicts the results of *ab initio* calculations (Cametti et al. 2017). A fully ordered atomic arrangement of the one-dimensional extra-framework atoms is possible in $P3$ only (Fig. 1). Refinements confirm the earlier postulated theoretical structure model with $[\text{Mg}(\text{H}_2\text{O})_6]^{2+}$ octahedra alternating with interstitial H_2O molecules along $[001]$ (Miletich, 1995). The interaction between these structural units as well as the bonding between the host and guest atoms is achieved solely by hydrogen bonds. The final refinements in space group $P3$ yield $R1 \sim 0.025$ for the entire data sets.

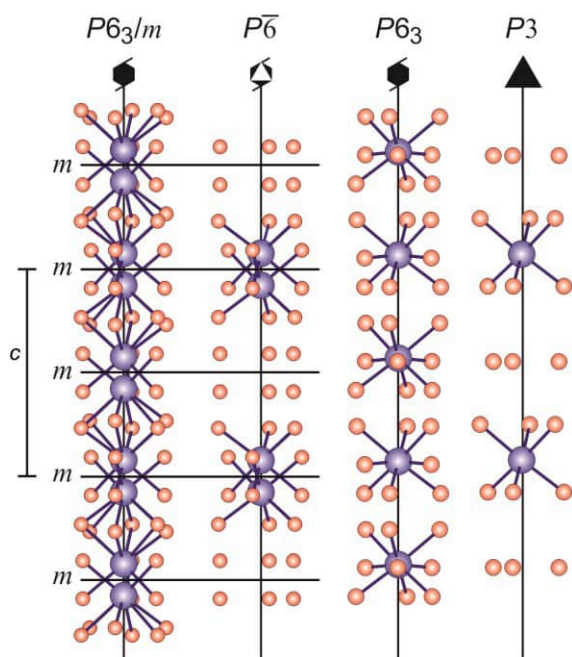


Figure 1. The extra-framework atoms and their distribution (full site multiplicity in the respective space group is shown). Mg and O atom position are shown as blue and red spheres, respectively. In $P3$ full order is achieved without the necessity of partial site occupations.

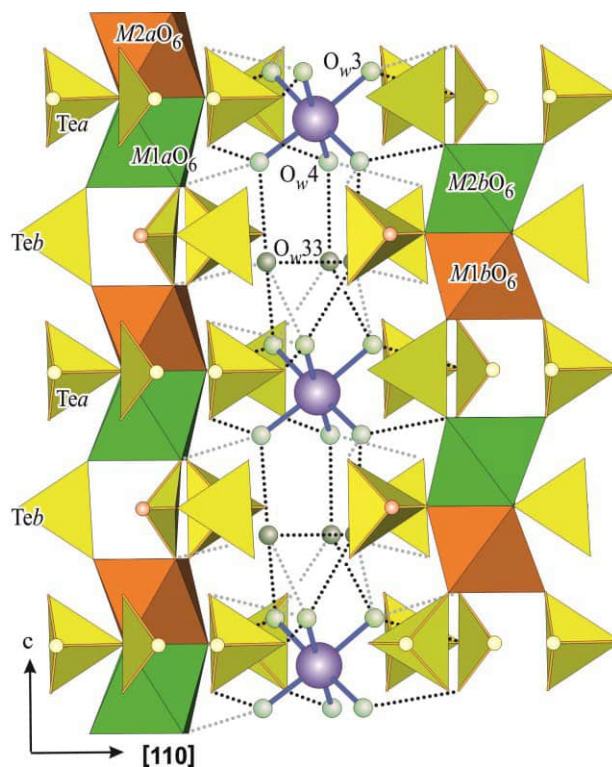


Figure 2. Detail of the atomic arrangement (space-group symmetry $P3$): the host structure consists of M_2O_9 dimers and TeO_3 groups. $M^{2+}O_6$ octahedra with $M = (Zn^{2+}, Fe^{3+})$ are shown in green and $M = (Fe^{3+}, Zn^{2+})$ in brown shades. – The channel is filled by $Mg^{[6]}$ atoms (blue) and H_2O molecules (O atoms in shades of green). Short and long O-H...O hydrogen bridges are indicated as dotted black and grey lines.

In accordance with the observed violation of the 6_3 screw axis, it is evident from crystal-structure refinements and crystal chemical considerations, that the atomic arrangement of zemannite is best described in space group $P3$. Zn^{2+} and Fe^{3+} ions are not fully ordered in the individual MO_6 octahedra but show a predominant occupation that explains the violation of the 6_3 screw axis. It is to be mentioned that neighbouring M_2O_9 dimers are differently orientated with Zn^{2+} respectively Fe^{3+} centred octahedra pointing upwards and downwards, respectively (Fig. 2). In contrast, symmetry $P6_3$ cause a parallel orientation of all dimers.

- Cametti G, Churakov S, Armbruster T (2017): Reinvestigation of the zemannite structure and its dehydration behavior: a single-crystal X-ray and atomistic simulation study. - Eur J Mineral 29, 53-61
- Mandarino JA, Matzat E, Williams SJ (1967): Zemannite, a zinc tellurite from Moctezuma, Sonora, Mexico. - Canad Mineral 14, 387-390
- Matzat, E (1967): Die Kristallstruktur eines unbenannten zeolithartigen Telluritminerals $\{(Zn,Fe)_2[TeO_3]_3\} N_xH_{2-x}yH_2O$. Tschermaks Mineral Petrogr Mitt 12, 108-117
- Miletich R (1995): Crystal chemistry of the microporous tellurite minerals zemannite and kinichilite, $Mg_{0.5}[Me^{2+}Fe^{3+}(TeO_3)_3] \cdot 4.5H_2O$, ($Me^{2+} = Zn, Mn$). - Eur J Mineral 7, 509-523
- Missen OP, Mills SJ, Spratt J, Birch WD, Brugger J (2019): Crystal chemistry of zemannite-type structures: I. A re-examination of zemannite from Moctezuma, Mexico. - Eur J Mineral 31, 519-527

LA-ICPMS U-Pb dating of garnet from the Adula nappe, Central Alps

L.J. Millonig¹, J. Pleuger², T. John², A. Gerdes¹

¹*FIERCE, Goethe University Frankfurt am Main*

²*Freie Universität Berlin*

e-mail: l.millonig@em.uni-frankfurt.de

The Adula nappe is located in the Lepontine Alps, Switzerland and Italy, and comprises crustal gneisses, metasediments and mica schists, as well as mafic and ultramafic units including eclogites, amphibolites and peridotites. Rocks from the Adula nappe show a gradual increase in pressure and temperature from north to south and record a high-pressure (HP) event followed low-pressure (LP)/high-temperature (HT) conditions, with the intensity of the overprint also increasing to the south. HP metamorphism and subsequent LP-HT overprint are considered to result from a single P–T evolution. However, geochronological data from the Adula nappe yielded partially inconsistent results and the timing and extent of HP metamorphism in the Adula nappe remains somewhat ambiguous. While eclogites from the southern part of the nappe yielded ages between 42 and 34 Ma (garnet Lu–Hf and Sm–Nd; zircon U–Pb), eclogites in the northeastern part of the nappe yielded only Palaeozoic ages of ~330–340 Ma (U–Pb zircon) and ~324 Ma (Lu–Hf garnet) for the HP stage. Eclogites from the central part of the Adula nappe gave both Alpine (~37–39 Ma) and Variscan (336 Ma) garnet Lu–Hf ages and zircon U–Pb ages (~31–33 and ~370 Ma). P–T conditions recorded by the Adula nappe are attributed to Variscan-Alpine polymetamorphism and a polyphase Alpine deformation history, which obscured the mineral equilibria developed during each high-grade metamorphic event. Polymetamorphism of the Adula nappe is reflected in compositionally and chronologically distinct garnet domains and generations. However, published ages from polymetamorphic garnet from the Adula nappe represent approximate maximum or minimum ages, because the mixing of different garnet age domains during hand picking cannot be ruled out when using conventional dating techniques. We therefore applied in-situ garnet U–Pb dating by LA-ICP-MS to spatially resolve different garnet growth zones, as revealed by major and trace element mapping.

Our preliminary results indicate that Variscan metamorphism in the northeastern Adula nappe also occurred at ~370 Ma, whereas lithologies from the central and southern Adula nappe yielded garnet U–Pb dates of ~40–35 Ma. Moreover, some samples from the central Adula nappe yielded single well-defined Alpine garnet growth ages, whereas others indicate ill-defined pre-Alpine garnet growth events. Such samples will be further investigated in greater detail to resolve the two growth events.

In-situ monitoring of ATP hydrolysis as a function of p-T-Mg²⁺: new insights into metabolic kinetics

C. Moeller¹, C. Schmidt², D. Testemale³, F. Guyot⁴, M. Kokh^{1,5}, M. Wilke¹

¹Institut für Geowissenschaften, Universität Potsdam, Germany

²Helmholtz-Zentrum Potsdam, Deutsches GeoForschungsZentrum GFZ, Germany

³Univ. Grenoble Alpes, CNRS, Institut Néel, Grenoble, France.

⁴IMPMC Muséum National d'Histoire Naturelle, Paris, France

⁵Institut für Mineralogie, Westfälische-Wilhelms-Universität, Münster, Germany

e-mail: chmoeller@uni-potsdam.de

The thriving exploration of geologically extreme environments has led to the discovery of new habitats of extremophiles. Fascinating biological communities were discovered at hot springs, in deep oceanic sediments, and hydrothermal vents. Biological-geological interaction enables life up to 120 °C and 300 MPa. Experimental studies, albeit controversial, expanded this T-P-range (Sharma et al. 2002, Takai et al. 2008). Stability of vital molecules like ATP can serve as proxies to determine physicochemical boundary conditions for life (Bains et al. 2015)

The exergonic enzymatic hydrolysis of adenosine triphosphate (ATP) to adenosine diphosphate (ADP) is a key reaction in all metabolic systems. It is counteracted by the abiotic hydrolysis of ATP; therefore, the rate constant and the related half-life can be used as a proxy for bioavailability. The abiotic hydrolysis is kinetically enhanced at elevated temperatures and low pH values (Leibrock et al. 1995; Moeller et al. 2022). The dependence on pressure of the rate constant of the hydrolysis can be best described by a power law and shows only a vanishingly low effect up to 500 MPa. Addition of Mg²⁺ and Ca²⁺ decelerate the hydrolysis; in contrast to Cu (II) and Co (III) complexes, which lead to an acceleration (Buisson and Sigel 1974, Suzuki et al. 1978).

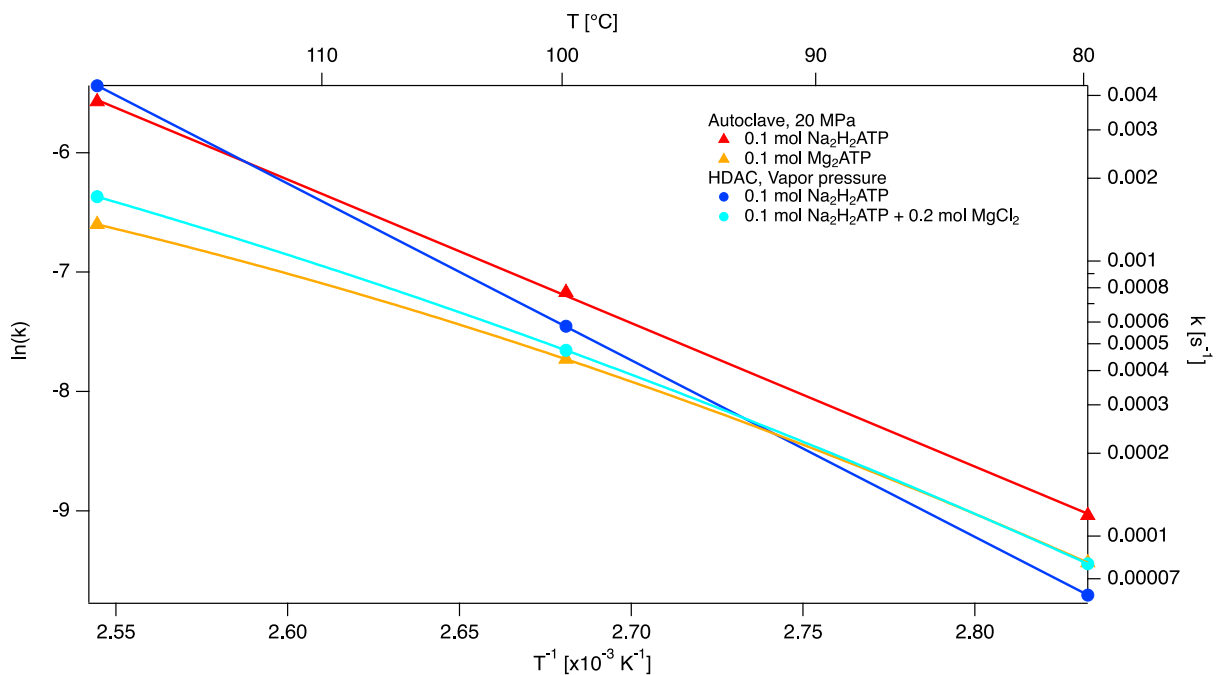


Figure 1: Arrhenius graph of the hydrolysis rate constants of ATP.

In biological systems, ATP is commonly found in a complexed form with Mg^{2+} . Earlier, experimental studies were performed on monovalent analogs of ATP like Na_2H_2ATP as commercial Mg_2ATP salts are rare and expensive. Effects of Mg^{2+} were simulated by addition of magnesium salts (e.g., in Leibrock et al. 1995). A novel in-situ protocol based on the combination of optical high-pressure cells and Raman spectrometry allowed us to determine the hydrolysis rate constants on small sample volumes without any artifacts due to quenching. The investigated temperature range was from 80 – 120 °C for sample solutions of $Na_2H_2ATP + MgCl_2$ and of Mg_2ATP . Our preliminary results verify a decrease of the hydrolysis rate constant by 30% at 80 °C. In contrast to studies on Na_2H_2ATP systems, our initial data suggest a significant deviation from the Arrhenius relation in the investigated T-interval (Fig. 1). This very new insight on the kinetic stability of Mg_2ATP suggests that the reaction mechanism changes at high temperature in the presence of magnesium. In terms of bioavailability, Mg^{2+} almost doubles the half-life of ATP at 120 °C which is 20% higher than previously assumed.

- Sharma A, Scot JH, Cody GD, Fogel ML (2002): Microbial Activity at Gigapascal Pressures. - *Science* 295, 5539, 1514-1516
- Takai K, Nakamura K, Toki T, Horikoshi K (2008): Cell proliferation at 122°C and isotopically heavy CH_4 production by a hyperthermophilic methanogen under high-pressure cultivation. - *PNAS* 10949-10954
- Bains W, Xiao Y, Yu C (2015): Prediction of the maximum temperature for life based on the stability of metabolites to decomposition in water. - *Life* 5, 1054-1100
- Leibrock E, Bayer P, Lüdemann HD (1995): Nonenzymatic hydrolysis of adenosinetriphosphate (ATP) at high temperatures and high pressures. - *Biophys Chem* 54, 175-180
- Moelle C, Schmidt C, Guyot F, Wilke M (2022): Hydrolysis rate constants of ATP determined in situ at. - *Biophys Chem* 290
- Buisson DH, Sigel H (1974): Significance of binary and ternary copper(II) complexes for the promotion and protection of adenosine 5'-di- and triphosphate toward hydrolysis. – *Biochim Biophys Acta (BBA) - General Subjects* 343, 45-63
- Suzuki S, Higashiyama T, Nakahara A (1978): Nonenzymatic hydrolysis reactions of adenosine 5'-triphosphate and its related compounds—III: Catalytic aspects of some cobalt(III) complexes in ATP-hydrolysis. - *Bioinorg Chem* 8, 277-289

Mineralogical characteristics of agates and their host rocks in Chihuahua, Mexico

M. Mrozik^{1,2}, J. Götze²

¹ Geowissenschaftliche Sammlungen, TU Bergakademie Freiberg, Brennhausgasse 14, 09599 Freiberg

²Institute of Mineralogy, TU Bergakademie Freiberg, Brennhausgasse 14, 09599 Freiberg

e-mail: Maximilian.mrozik@geosamm.tu-freiberg.de

Agates from the state of Chihuahua in Mexico are known worldwide among collectors and jewelry dealers because of their color variety and high quality. The single deposits are limited to different areas which are distributed in the whole federal state of Chihuahua. The agates of the different localities partly differ in their basic coloring as well as in their general appearance and the abundance of pseudomorphs. Despite the wide distribution and individual locality-typical characteristics, most of the best-known deposits can be assigned to the same volcanic unit, the so-called Rancho el Agate Andesite. This is an approximately 300 m thick unit of intermediate lava flows, which all have a strongly vesicular texture (Keller et al. 1982). The host rocks for most of the presently mined agate deposits in the main production area of the Sierra del Gallego can be classified almost exclusively as quartz-free latite (Mrozik et al. 2023). The intermediate chemism of the rocks can be explained by a mixing of magmas with different SiO₂ contents.

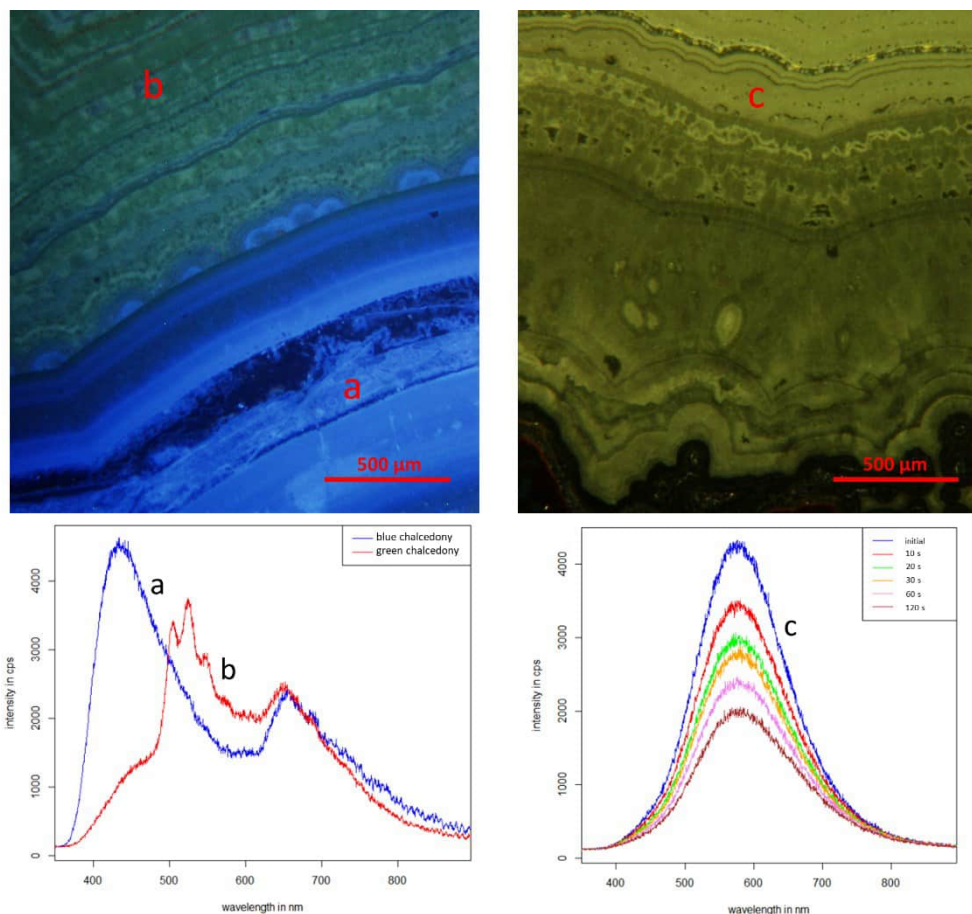


Figure 1. CL-micrographs with the associated CL-spectra. The CL-colors and spectra reveal different structural defects as well as the incorporation of trace elements and compounds like for example the uranyl-ion within the green luminescent parts of the chalcedony. (Figure from Mrozik et al. 2023)

Different reasons for the coloration of the agates could be determined by various spectroscopic methods as well as with trace element analyses and microscopic studies. While different structural defects can be detected in many areas of the mineralization (Fig. 1) the coloration of most of the bands in the agates is caused by inclusions, for example hematite and goethite. The different colors are not exclusively caused by the mineral phase but also by the particle size as well as the distribution of the coloring components within the matrix of the chalcedony. Some of these inclusions were incorporated within the agates during the initial crystallization of the chalcedony, others were later fixed within the matrix by secondary infiltration (Fig. 2) (Mrozik et al. 2023).

A mixture of near-surface weathering solutions with deep hydrothermal fluids from the Tertiary volcanism has led to the formation of the agates. The enrichment of differently mobile elements which were fixed during the formation of the agates in the structure of the chalcedony itself as well as in the paragenetic inclusions indicate the involvement of hydrothermal fluids. Due to the very different contents of under weathering conditions rather immobile elements like zirconium and chromium as well as almost exclusively hydrothermally accumulated elements like antimony and zinc a variable influence of deep hydrothermal fluids in the different agate occurrences can be assumed. Thus, the local differences in the agate formation are not caused by a basically different formation process but by a various influence of the respective fluids as well as slightly different local geochemical conditions. In the current studies different generations of chalcedony could be determined within the mineral formations (Fig. 2) which indicates that many of the agates were not formed by a single geochemical process but underwent a multiphase formation with partly different fluids under slightly differentiated conditions. (Mrozik et al. 2023)

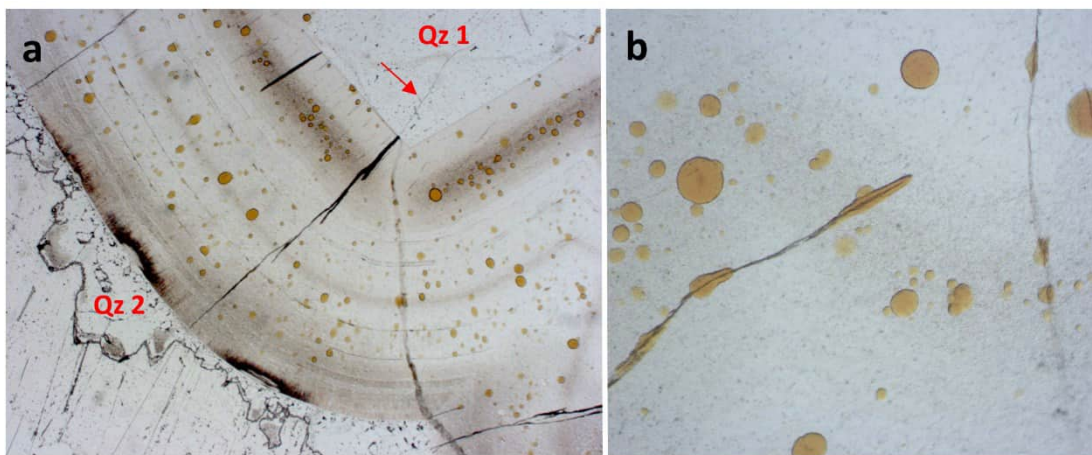


Figure 2. (a) The micrograph shows different generations of the SiO₂-mineralization with at least two generations of macrocrystalline quartz (Qz 1, Qz 2). The red arrow marks a secondary crack which can be followed within the first generation but ends at the second generation of quartz. (b) The micrograph shows a detailed view of the same agate which shows the distribution of different inclusions within the chalcedony matrix. Note that some of the inclusions are arranged along secondary cracks, which assigns a later formation of some of the coloring particles by infiltration. (Figure from Mrozik et al. 2023)

Mrozik M, Götze J, Pan Y, Möckel R (2023): Mineralogy, Geochemistry and Genesis of Agates from Chi-huahua, Northern Mexico. - *Minerals* 13, 687, <https://doi.org/10.3390/min13050687>

Keller PC, Bockoven NT, McDowell FW (1982): Tertiary volcanic history of the Sierra del Gallego area, Chihuahua, Mexico. - *Geol Soc Amer Bull* 93, 303-314

Special exhibition
Wonder world agate - fascination between legend and science

M. Mrozik¹, J. Götze², A. Massanek¹, M. Gäbelein¹

¹ *Geowissenschaftliche Sammlungen, TU Bergakademie Freiberg, Brennhausgasse 14, 09599 Freiberg*

² *Institute of Mineralogy, TU Bergakademie Freiberg, Brennhausgasse 14, 09599 Freiberg*

e-mail: Maximilian.mrozik@geosamm.tu-freiberg.de

Due to their variety of colours and shapes, agates belong to the most fascinating mineral formations of nature and have played an important role as jewellery and gemstones since ancient times. The name "agate" appears in literature as early as 350 B.C. (Theophrast) and was probably derived from deposits on the river Achates (now Drillo) in Sicily.

Agate deposits and agate processing are recorded worldwide in both historical and currently mined regions. Of particular interest are the almost inexhaustible deposits of agate in the province of Rio Grande do Sul in Brazil, which have been supplying the world markets with raw agates for centuries. In China there is a centuries-old tradition of agate processing as a stone-carving art (Fig. 1). In the city of Fuxin in the province of Liaoning, also known as the "world city of agate", 60,000 people currently work in the agate industry. In Saxony, the systematic search for agate and "precious stones" was promoted early on by Elector August (1553 - 1586) and later especially by the Saxonian King "August the Strong". Therefore, systematic collections and descriptions already exist from this time. The region around Idar-Oberstein is also famous in history as a supplier and processing centre for high-quality agates.

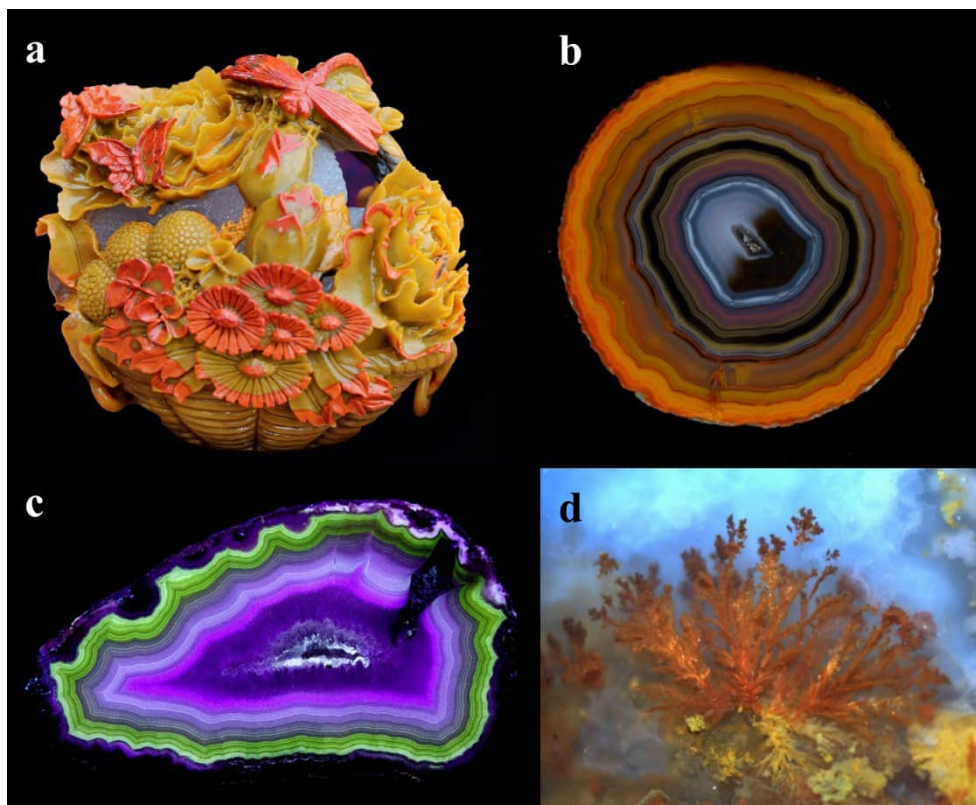


Figure 1. Different photographs and micrographs of agate samples. (a) stone carving art made from an agate from Xuanhua, China; (b) polished agate sample from Xuanhua, China; (c) luminescence colours under UV-light (254 nm) of an agate from Rancho Coyamito, Chihuahua, Mexico; (d) micrograph of an "Orpheus"-agate from Kardzhali, Bulgaria.

Besides their impressive aesthetics, agates also provide many clues for scientific research. This is mainly due to the fact that the formation of agate cannot be observed directly and also that until today no successful agate syntheses exist on a laboratory scale. One of the most discussed questions of the agate problem is probably the "secret" of agate formation, which has led to many speculations in the past and present. But the micro-world of agates also provides exciting insights into the complex processes of nature.

The exhibition gives an insight into the fascinating world of agates. With Wonder World Agate for the first time a combined special exhibition is housed in the three different collections in the city of Freiberg, which together form the largest mineralogical collection complex worldwide. The main part of the exhibition (Fig. 2), which presents impressive specimens from the most important agate deposits of the world, is displayed in the terra mineralia. You can find the different showcases arranged according to the different continents and most important agate deposits. Additionally, there are some thematic display cases (e.g. different types of agates, special agates or pictures in agates) as well as interactive elements explaining for example luminescence effects in agates or different microstructures. The whole exhibition is accompanied by numerous knowledge boards and art-like pictures of microstructures in agates to explain some exciting questions regarding the formation and properties of agates.

The Mineralogical Collection of Germany hosts agate samples from whole Germany. This part of the special exhibition shows the great variety and importance of German agate deposits.

The third part is housed in the Wernerbau framed by the historic mineralogical collection of the TU Bergakademie Freiberg. This exhibition part displays agates from some special localities in Saxony and shows the relation between primary and secondary agate deposits in one of the mineral richest states of Germany.

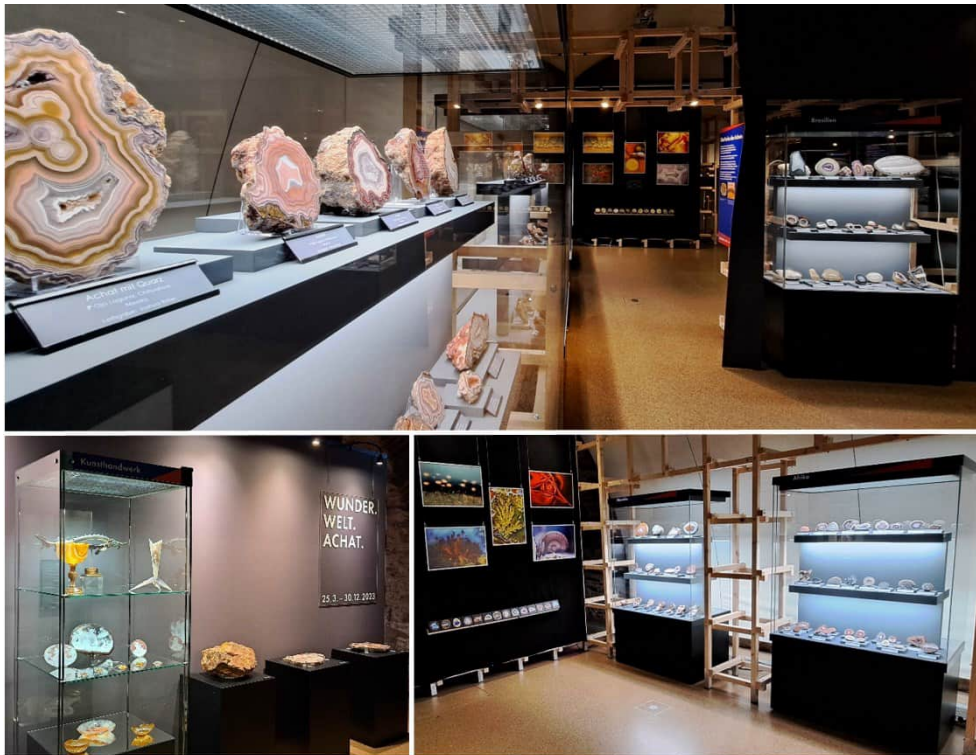


Figure 2. Some impressions of the actual special exhibition Wonder World Agate.

Minerals in a greenhouse environment: a cross-disciplinary exhibition

S.P. Mueller¹

*¹Mineralogical Museum, University of Marburg, Germany
e-mail: s.mueller@geo.uni-marburg.de*

During the winter months of 2023, the Mineralogical Museum Marburg was 'on tour' in the greenhouses of the Botanical Garden of the University of Marburg. In a collaborative, cross-disciplinary effort, we highlighted links between mineralogy and botany in a variety of display cases, in reference to the respective topical focus of the houses: e.g., which ore minerals are needed to build a smartphone, and how does their mining affect tropical rainforests? How do ferns turn into coal (and ultimately into diamonds)? Which minerals are typical for the Australian outback? How (and where) is amber formed?

The exhibition was open on a total of 9 Sundays during the winter months (a period the greenhouses are normally closed to the public) and attracted a large number of visitors to the botanical garden during this time. In particular, the interdisciplinary linking of what at first glance appear to be very different disciplines within natural sciences was positively highlighted in many of the visitors' feedbacks.

Thermoelastic properties of radiation-damaged zircon

M. Münchhalfen¹, J. Schreuer¹

¹*Ruhr-Universität Bochum, Institut für Geologie, Mineralogie und Geophysik,
Universitätsstraße 150, Bochum, 44801, Germany
e-mail: marie.muenchhalfen@rub.de*

Radioactive decay of unstable isotopes causes damage to zircon, which significantly reduces its elastic stiffnesses (e.g., Özkan, 1976). These damages can be partially healed by temperature treatment of the zircon crystal. In order to study in situ the recrystallization of radiation-damaged zircon, thermoelastic properties, and thermal expansion data were collected between 100 K and 1600 K utilizing resonant ultrasound spectroscopy, dilatometry, and high-temperature powder x-ray diffraction. The investigated samples of natural gem-quality zircon belong to the damage stage I introduced by Holland & Gottfried (1955), i.e., the damage in the crystal structure is mainly dominated by the accumulation of isolated point defects.

While non-metamict zircon samples display a linear decrease in elastic stiffnesses, the partial radiation-damaged zircon samples undergo strong irreversible effects detected in all utilized methods. The increase of elastic stiffnesses starts at about 700 K, while the thermal expansion decreases (Fig. 1). The severity of this effect becomes more pronounced with an increasing initial state of damage and thus can be related to the healing of defects induced by radioactive decay. A second effect sets in at about 1100 K, likely related to a transition from static to dynamic behavior. This supports the idea that reducing radiation damage is a multi-stage process, including point defect healing and recrystallization of an amorphous fraction.

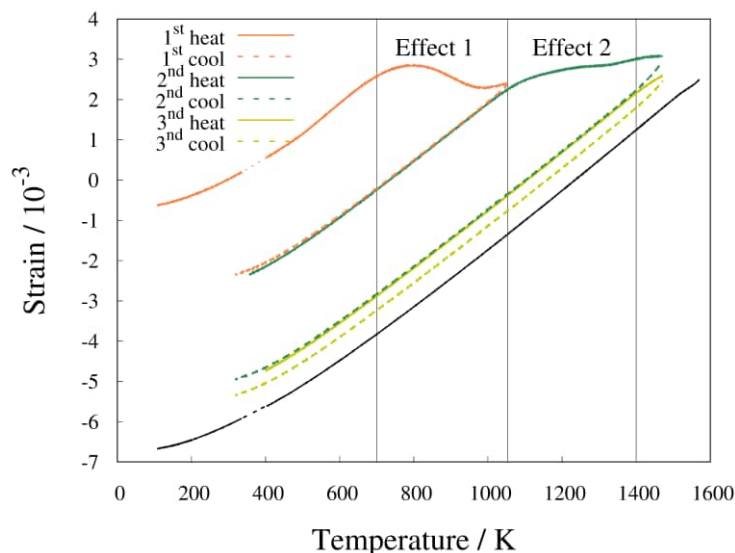


Figure 1. Different effects observed in thermal strain of radiation damaged zircon compared to non-metamict zircon (black line).

Özkan H (1976): Effect of nuclear radiation on the elastic moduli of zircon. - J Appl Phys 47, 4772-4779

Holland H, Gottfried D (1955): The effect of nuclear radiation on the structure of zircon. - Acta Cryst 8, 291-300

Rates, mechanisms and microstructures of transport-controlled reaction front propagation

T. Müller¹, S. Piazzo²

¹*Geoscience Centre Göttingen, Georg-August-University, Germany*

²*School of Earth and Environment, The University of Leeds, United Kingdom*
e-mail: thomas.mueller@geo.uni-goettingen.de

Fluid-mediated mineral reactions are governing the redistribution of elements and isotopes in the geosphere. Incomplete elemental redistribution is preserved in the rock record in the form of geochemical reaction fronts. Key features of such systems are reaction induced creation/destruction of porosity increasing/decreasing permeability and further focussing of fluid into/away from the zone of reaction; hence this results in a positive or negative feedback between reaction, fluid ingress and further reaction. To the same end, sluggish element mobility can lead to variations in fluid chemistry within the propagating reaction front controlling the stable mineral assemblage and its chemical/isotopic composition. Recent studies provided conclusive evidence for the presence of transport-controlled reaction fronts in mineral reactions such as the replacement of calcite single crystals by Mg-carbonates (Jonas et al. 2015; 2017). Here, we present a follow-up investigation providing detailed chemical and microstructural data as well as a model for the kinetically controlled evolution of the reaction rim.

The replacement reactions of single calcite cubes (2 mm) were carried out experimentally in batch reactor vessel at 200 °C using a 1 M MgCl₂ fluid and a water-to-rock-ratio of 10 for run durations of 2-30 days. Solid reaction products have been characterized using an FEG-SEM including EBSD and chemical variations have been measured using an electron microprobe.

Experimental results reveal the time-dependent formation of a layered, multiphase reaction rim by dissolution-precipitation forming Mg-carbonate phases of different composition and variable porosity. The initial reaction rim is formed of small, rhombic almost pure magnesite crystals which become more Ca-rich as the reaction progresses. Subsequently, a sharp interface marks the change to the precipitation of high magnesium calcite (HMC) instead of magnesite, albeit the HMC precipitates with a constant X_{Mg} of 0.4. With increasing run durations, the reaction does not progress but grains in the existing reaction rim exhibit grain coarsening and elimination of (interconnected) porosity. This grain growth is accompanied by a chemical adjustment starting from the former magnesite-HMC interface initiating two new reaction fronts adjusting the magnesite composition, i.e., replacing Ca by Mg and the recrystallization of HMC by a VHMC phase with X_{Mg} of 0.5 representing a dolomite stoichiometry. EBSD analysis reveal that the recrystallization of the inner part of the reaction rim is accompanied by the formation of subgrain boundaries and rotation of c-axis during grain coarsening.

This study highlights the importance to quantitatively understand the link between reaction progress, fluid composition, fluid transport and the evolution of fluid pathways to describe and model reaction front propagation in reactive transport models.

Jonas L, Müller T, Dohmen R, Baumgartner L, Putlitz B (2015): Transport-controlled hydrothermal replacement of calcite by Mg-carbonates. - *Geol* 43, 779-782, doi: <https://doi.org/10.1130/G36934.1>

Jonas L, Müller T, Dohmen R, Immenhauser A, Putlitz B (2017): Hydrothermal replacement of biogenic and abiogenic aragonite by Mg-carbonates: Relation between textural control on effective element fluxes and resulting carbonate phase. - *Geochim Cosmochim Acta* 196, 289-306, doi: <https://doi.org/10.1016/j.gca.2016.09.034>

Gem spinel in the Imperial Crown of the Holy Roman Empire: Evidence for very early gemstone heating?

L. Nasdala¹, T. Lamers², H.A. Gilg³, C. Chanmuang N.¹, M. Griesser²,
F. Kirchweiger², A. Erlacher¹, M. Böhmler⁴, G. Giester¹

¹Institut für Mineralogie und Kristallographie, Universität Wien, 1090 Vienna, Austria

²Kunsthistorisches Museum Wien, 1010 Vienna, Austria

³School of Engineering and Design, Technische Universität München, 80333 Munich, Germany

⁴WITec Wissenschaftliche Instrumente und Technologie GmbH, 89081 Ulm, Germany

e-mail: chutimun.chanmuang@univie.ac.at

The Imperial Crown of the Holy Roman Empire, part of the Imperial Regalia, is the key exhibit in Vienna's Imperial Treasury. It is currently investigated within the three-year interdisciplinary project 'Crown' (www.projekt-reichskrone.at) led by Kunsthistorisches Museum Vienna. The research aims, among others, at issues regarding the Imperial Crown's materials, manufacturing technology and time, as well as its state of preservation. During the first measurement campaign in Spring 2022, we had the task to determine conclusively – and, if possible, to characterise further – all 172 (inorganic) gemstones in the crown, whereas studies of the pearls were planned for the second measurement campaign (2023).



Figure 1. The front plate of the Imperial Crown of the Holy Roman Empire (size 11.2 cm × 14.9 cm) contains two spinels, a pink stone (#A3) in the upper row, left side, and a large red stone (#A25) in the centre of the third row. Photo © KHM-Museumsverband (Christian Mendez); reproduced with permission.

Non-destructive spectroscopic analyses were done on site, using a fibre-coupled WITec confocal Raman probe system equipped with an alpha300 controller. Photoluminescence (PL) and Raman spectra were excited with a 457 nm diode laser (0.05–8.5 mW measured behind the objective). An Olympus 20× objective (free working distance 25 mm) was used.

Besides 71 blue sapphires, 50 garnets, 20 emeralds, 13 amethysts, four chalcedonies and 11 glass imitates, there are three spinels in the Imperial Crown, two in the front plate (Fig. 1) and one in the central cross (Nasdala et al. 2023). The analytical identification of spinel in the

Imperial Crown is of art-historical interest. So far the first appearance of gem spinel in European jewellery was known for the thirteenth century (e.g., Ogden 2021) whereas the central, large spinel in the front plate (#A25) seems to be original; that is, set into the Imperial Crown about 1000 years ago already. This stone hence represents one of the very earliest uses of spinel in jewellery. Furthermore, the stone has two drill holes that indicate an even older use.

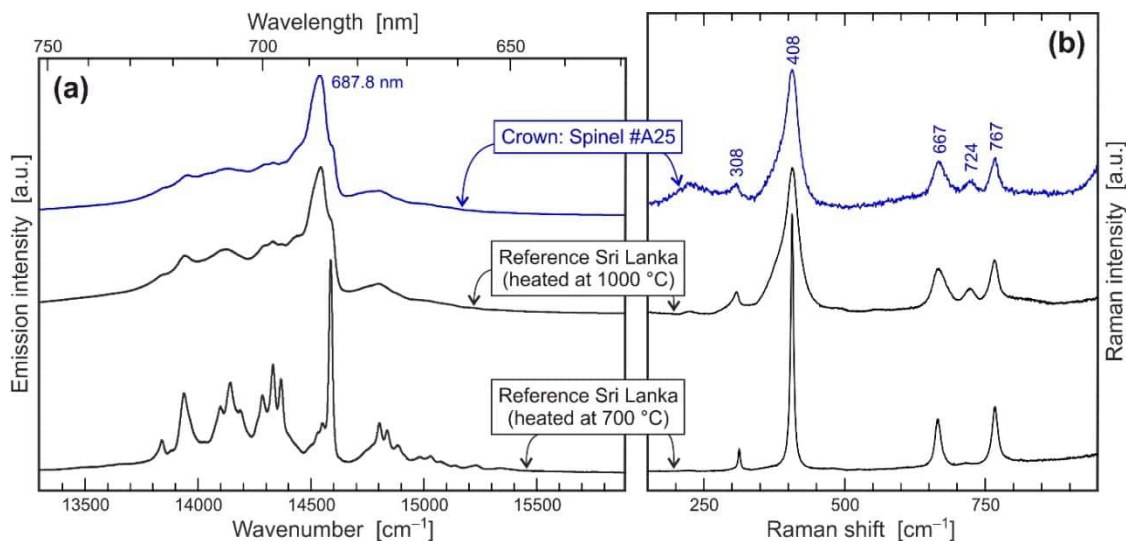


Figure 2. PL spectrum (a) and Raman spectrum (b) of spinel #A25 (blue graphs), shown in comparison with reference spectra (black graphs) obtained from a gem-quality spinel from Sri Lanka that was heat-treated in air.

The central spinel in the front plate (stone #A25) turned out to be of particular scientific interest, as it did not yield PL and Raman spectra that are typical of MgAl_2O_4 with (close to) normal occupation of cation sites. Instead, the PL spectrum (Fig. 2a) is characterised by loss of fine structure. Such spectra are obtained from natural Mg-Al spinel only after being heat-treated (Widmer et al. 2015; Liu et al. 2022). Similarly, heat-treatment results in significant broadening and asymmetry of Raman bands (Fig. 2b). These spectroscopic phenomena are assigned to heating-induced cation disorder; that is, increase of partial inversion of the cation occupation, according to $^{[4]}\text{Mg}^{[6]}\text{Al}_2\text{O}_4 \rightarrow ^{[4]}(\text{Mg}_{1-x}\text{Al}_x)^{[6]}(\text{Al}_{2-x}\text{Mg}_x)\text{O}_4$ (with $x > 0.2$) (Widmer et al., 2015; Ma et al., 2022). The spectra obtained from spinel #A25 hence give strong indication that this stone was heated to close to 1000 °C. This is supported also by the presence of a multitude of healed fractures, ‘lily pad’ inclusions, and melted sulphides at the surface.

Heating of red ‘yāqūt’ to enhance colour and transparency is known back to the ninth century (e.g., Troupeau 1998). ‘Yāqūt’ (an Arabian term) has generally be assumed to refer to gem corundum, but the possibility cannot be eliminated that it – and hence also the early heating – may have included spinel as well. Our spectroscopic results indicate that, as early as about 1000 years ago, spinel #A25 may have been subjected to heat-treatment.

- Liu Y, Qi L, Schwarz D, Zhou Z (2022): Color mechanism and spectroscopic thermal variation of pink spinel reportedly from Kuh-i-Lal, Tajikistan. - *Gems Gemol* 58, 338-353
- Ma Y, Bao X, Sui Z, Zhao X, Liu X (2022): Quantifying Mg–Al cation distribution in MgAl_2O_4 -spinel using Raman spectroscopy: An experimental calibration. - *Solid Earth Sci* 7, 60-71
- Nasdala L, Lamers T, Gilg HA, Chanmuang N C, Griesser M, Kirchweiger F, Erlacher A, Böhmeler M, Giester G (2023): The Imperial Crown of the Holy Roman Empire, part I: Photoluminescence and Raman spectroscopic study of the gemstones. - *J Gemmol* 38(5), 448
- Ogden JM (2021): Gem knowledge in the thirteenth century: The St Albans jewels. - *J Gemmol* 37(8), 816
- Troupeau G (1998): Le premier traité arabe de minéralogie: Le livre de Yūḥannā Ibn Māsawayh sur les pierres précieuses. - *Ann Islamologiques* 32(6), 219
- Widmer R, Malsy A-K, Armbruster T (2015): Effects of heat treatment on red gemstone spinel: Single-crystal X-ray, Raman, and photoluminescence study. - *Phys Chem Miner* 42(4), 251

Determination of the electronic polarizabilities of bromine in bromates, perbromates, and bromides

S. Nezamabadi¹, P. Fuzon², F. Kraus², R.D. Shannon³, I. Spieß¹, R.X. Fischer¹

¹ FB 5 Geowissenschaften, Universität Bremen, Klagenfurter Straße, D-28359 Bremen, Germany

²FB Chemie, Philipps-Universität Marburg, Hans-Meerwein-Str. 4, D-35032 Marburg, Germany

³Geological Sciences/ CIRES, University of Colorado, Boulder, Colorado 80309, USA

e-mail: rfischer@uni-bremen.de

Empirical electronic polarizabilities of Br^{5+} , Br^{7+} , and Br^- were determined to predict refractive indices of bromates, perbromates, and bromides, respectively, at $\lambda = 589.3$ nm. Polarizabilities of the bromine ions were derived from the total electronic polarizabilities of compounds containing Br calculated from the mean refractive indices using the Anderson-Eggleton relationship (Anderson, 1975; Eggleton, 1991; Shannon and Fischer, 2016). Refractive indices (RI) of bromates and bromides are taken from literature data and from measurements on potassium bromate (KBrO_3) and potassium bromide (KBr), respectively. Because of the lack of literature data on perbromates, we have done RI measurements on sodium perbromate monohydrate ($\text{NaBrO}_4 \cdot \text{H}_2\text{O}$).

Structure analyses were performed using single-crystal X-ray diffraction data of KBrO_3 , KBr , and $\text{NaBrO}_4 \cdot \text{H}_2\text{O}$. Refractive indices were determined using the immersion method with a micro-refractometer spindle stage at $\lambda = 589.3$ nm as described by Medenbach (1985), yielding $n_e = 1.538$ and $n_o = 1.677$ ($\langle n \rangle = 1.6307$) for optically uniaxial KBrO_3 (Figure 1), and $n_x = 1.470$, $n_y = 1.491$, $n_z = 1.492$ ($\langle n \rangle = 1.4843$) for an optically biaxial $\text{NaBrO}_4 \cdot \text{H}_2\text{O}$ crystal (Figure 2).



Figure 1: (a) KBrO_3 crystal mounted on the spindle stage of the polarization microscope. (b) orientation of the crystal to determine $n_e = 1.538$. (c) orientation of the crystal to determine $n_o = 1.677$. Due to the equality of the refractive indices of the sample and the immersion oil, the sample is not visible in (b) and (c).

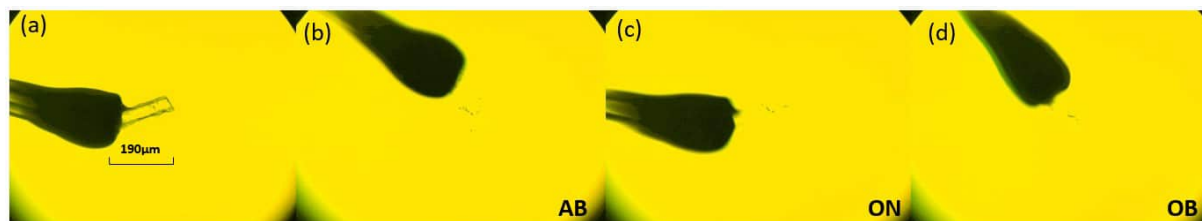


Figure 2: (a) $\text{NaBrO}_4 \cdot \text{H}_2\text{O}$ crystal mounted on the spindle stage of the polarization microscope. (b) orientation of the crystal to determine $n_x = 1.470$. (c) orientation of the crystal to determine $n_y = 1.677$. (d) orientation of the crystal to determine $n_z = 1.492$. Since the refractive index of the sample matches that of the oil, the sample is not visible in (b), (c), and (d).

Analyzing 18 compounds with established refractive indices containing Br^{5+} , along with data from this study, the polarizability of $^{131}\text{Br}^{5+}$ was determined by calculating the difference between the total polarizabilities of the respective compounds and the sum of polarizabilities of their ions omitting Br with values for the ions taken from Shannon and Fischer (2016). The individual electronic polarizability of $^{131}\text{Br}^{5+}$ was found to be 2.20 ± 0.34 [\AA^3].

The determination of the refractive indices of $\text{NaBrO}_4 \cdot \text{H}_2\text{O}$ with four-coordinated Br^{7+} yielded an electronic polarizability value of 1.086 [\AA^3] for Br^{7+} . Using this value now enables the prediction of refractive indices of perbromates with polarizability values from Shannon & Fischer (2016) as listed in Fehler: Verweis nicht gefunden Table 1.

Table 1: Predicted mean refractive indices of compounds containing tetrahedrally coordinated Br^{7+} . Crystal data are from the ICSD database. V_m is the molar volume of the compound, α_{tot} is the total electronic polarizability of the compound and $\langle n \rangle$ is the mean refractive index.

Compound	Space group	V_m [\AA^3]	α_{tot} [\AA^3]	$\langle n \rangle$ (± 0.025)
KBrO_4	$P n m a$	98.98	8.949	1.541
CsBrO_4	$I 4_1/a m d$	122.5475	10.680	1.522
$\text{NH}_4(\text{BrO}_4)$	$P n m a$	107.73	9.785	1.544
$\text{LiBrO}_4 \cdot \text{H}_2\text{O}$	$C 1 2/c 1$	100.4775	9.349	1.557
$\text{LiBrO}_4 \cdot 3\text{H}_2\text{O}$	$P 6_3 m c$	147.565	12.630	1.513
$\text{Ba}(\text{BrO}_4)_2 \cdot 3\text{H}_2\text{O}$	$P 6_3/m$	237.185	22.955	1.580
$\text{Ca}(\text{BrO}_4)_2 \cdot 4\text{H}_2\text{O}$	$P \bar{1}$	266.25	23.190	1.522
$\text{Co}(\text{BrO}_4)_2 \cdot 6\text{H}_2\text{O}$	$P \bar{3} m 1$	305.34	26.543	1.521
$\text{Ni}(\text{BrO}_4)_2 \cdot 6\text{H}_2\text{O}$	$P \bar{3}$	291.18	26.467	1.544

For the anion Br^- the two parameters α^o and N_o were determined describing the anion polarizability α^- of Br^- according to $\alpha^- = \alpha^o \cdot 10^{-N_o/V}$ with $V = V_{\text{an}}^{1.2}$ where V_{an} is the anion volume (see Shannon & Fischer, 2016).

Anderson OL (1975): Optical properties of rock-forming minerals derived from atomic properties. - Fortschr Miner 52, 611–629

Eggleton RA (1991): Gladstone-Dale constants for the major elements in silicates: Coordination number, polarizability, and the Lorentz-Lorentz relation. - Canad Miner 29, 525–532

Medenbach O (1985): A new microrefractometer spindle-stage and its application. - Fortschr Miner 63, 111-133

Shannon RD, Fischer RX (2016): Empirical electronic polarizabilities of ions for the prediction and interpretation of refractive indices: oxides and oxyalts. - Amer Mineral 101, 2288–2300

Mirdita ophiolites, Albania: Refertilization of spinel-plagioclase-peridotites in the shallow Mantle Lithosphere

T. Ntaflos¹, P. Koutsovitis², K. Onuzi³, C. Hauzenberger⁴

¹Department of Lithospheric Research, University of Vienna, Josef-Holaubek-Platz 2, 1090 Vienna, Austria

²Department of Geology, University of Patras, Greece

³Instituti i Gjeoshkencave, Rr. "Don Bosko", Nr.60, Tirane, Albania

⁴Department of Earth Sciences – NAWI Graz Geocenter, University Graz Universitaetsplatz 2, Austria
e-mail: theodoros.ntaflos@univie.ac.at

The Albanian ophiolites are located between the Dinarides (N. Macedonia and Serbia) in the east and the Hellenides in the west. The Mirdita Ophiolites in Albania are divided into two units namely the western ophiolitic unit with MORB geochemical affinity and the eastern ophiolitic unit with SSZ affinity. The western unit consists of the Krabbi, Puka, Comsique and Skenderbeu massifs where intrusives and dykes are present as well. All massifs represent upper mantle, variably serpentinized spinel and plagioclase peridotites.

The Krabbi massif with a diameter of 30 km is a piece of upper mantle ultramafic body consisting of spinel-plagioclase lherzolites and harzburgites with bulk-rock Mg# ranging from 89.5 to 91.8 and Ca/Al ratio varying from 1.13, that is slightly higher than the Primitive Mantle ratio of 1.1, to 1.26 indicating an excess of Ca in the studied samples. Minor and trace elements trends such as Ni, V and Yb versus Mg# are very similar to those of the orogenic peridotites. The chondrite normalized REE abundances have convex upward patterns where the majority of the samples show that the Yb_N is slightly higher compared to La_N suggesting moderate metasomatic events affecting the LREE.

Besides the rock forming mineral olivine, orthopyroxene, clinopyroxene and spinel there are also disseminated plagioclases and kaersutites. Strongly tectonized samples show secondary protogranular and porphyroclastic textures. Rounded spinel occurs mainly as inclusion in olivine and orthopyroxene whereas holly-leaf shaped spinel is interstitial.

The plagioclase neither coexists nor surrounds spinel, which precludes any subsolidus transition from spinel- to plagioclase-peridotite stability field. However, the clinopyroxene, as can be inferred from their negative Eu-anomaly in the chondrite normalized REE patterns, appears to be in equilibrium with coexisting plagioclase. Apparently, the plagioclase-rich residual melt affected the peridotites in the spinel-peridotite field but crystallized and equilibrated with clinopyroxene at shallow depths.

A striking textural feature is the frequent replacement of olivine grains by orthopyroxene with simultaneous formation of Ti-rich diopside and Al-rich spinel, suggesting metasomatic infiltration of a melt with tholeiitic composition. This feature has been observed in the samples with Mg# = 89.5, Al₂O₃ = 4.3 wt% and CaO = 3.77 wt% similar to the composition of the Primitive Mantle.

The existence of fertile peridotites with similar to the Primitive Mantle composition suggests that the otherwise strongly depleted oceanic lithospheric mantle has been refertilized after metasomatic introduction of melts with tholeiitic composition.

Fahlore analyses from a prehistoric work and settlement site in Kundl, Tyrol

L. Oettel¹, P. Tropper¹, L.M. Eß²

¹University of Innsbruck, Institute of Mineralogy and Petrography

²University of Innsbruck, Institute of Archaeology

e-mail: lena.oettel@uibk.ac.at

Between 2018 and 2019, the largest prehistoric area excavation in North Tyrol to date took place in Kundl (district of Kufstein). On an area of about 11,600 m² in the Wimpissinger gravel pit, horizons from the 1st millennium BC were uncovered.

The excavated work area offers a unique large-scale insight into the work stages between mining and metal production. The phases of use of this work area extend from the Early Bronze Age to the late Iron Age.

During the excavations, in addition to hundreds of slag remains from the Early and Late Bronze Age, three storage vessels were excavated, which can also be assigned to the Late Bronze Age (Eß, unpublished). Around one of the storage vessels fahlore ore lumps were draped and examined in the context of an origin determination of the smelted ores.



Figure 1. Storage vessel with fahlore wreath (picture: Talpa GnbR 2019)

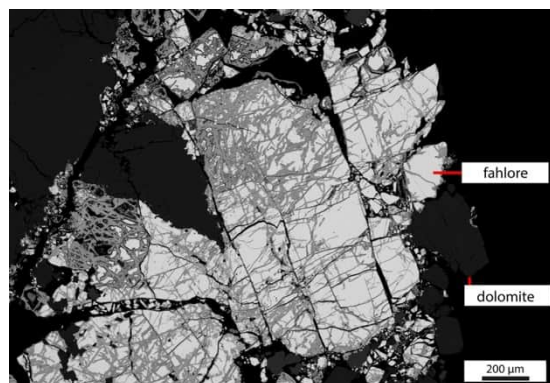


Figure 2. BSE picture of an analysed stone, which was draped around the storage vessel (picture: L. Oettel 2020)

Electron probe microanalysis of these fahlore minerals were undertaken for putting possible provenance constraints on the ores. Since this examination did not yield a satisfying match within the HiMAT mineral chemical database, the source of the smelted fahlores could yet not be determined. For this reason, additional 37 samples of fahlores were taken from a wide variety of localities/tectonic units (e.g. Northern Limestone Alps, Engadin Window) and examined by electron beam microprobe to increase the chemical database considerably.

Micro-CT analyses from a prehistoric work and settlement site in Kundl, Tyrol

L. Oettel¹, P. Tropper¹, G. Degenhart²

¹University of Innsbruck, Institute of Mineralogy and Petrography

²Core facility μ CT at the Medical University Innsbruck

e-mail: lena.oettel@uibk.ac.at

Prehistoric mining and production sites for copper are known from the Eastern Alps, reaching back to the beginning of the Early Iron Age, but the further processing of the copper products (bronze foundries etc.) could so far only be localized indirectly.

A key site for the production step between mining and metal processing, which has hardly been investigated so far, is offered by the Late Bronze and Iron Age workshop area of Kundl in the Tyrolean Lower Inn Valley, which was used over a long period of time, from the late 11th century BC, with an interruption in the 8th/7th century, until the 1st century BC. In Kundl (district of Kufstein), the largest archaeological excavation in North Tyrol to date was carried out in 2018 and 2019, during which nearly 31,000 finds were recovered. The excavation area of around 11,000 m² in the area of the Wimpissinger gravel pit is located directly next to the Iron Age burial ground of the Fritzens-Sanzeno culture discovered in the 1970s.

During the more recent excavations, Late Bronze Age as well as Iron Age use horizons were discovered, which were separated from each other by meter-thick gravel layers, resulting in an excellent preservation of the finds and features (Staudt et al. 2021).



Figure 1. Oven battery with roasting bed (picture: Talpa GnbR, 2019)

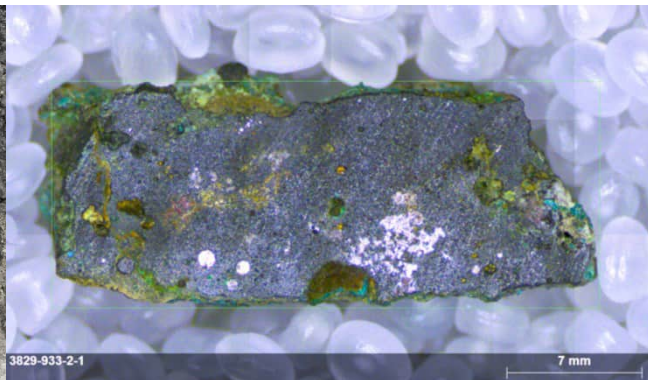


Figure 2. Heterogenous slag from early bronze age horizon (picture: L. Oettel, 2021)

Due to the temporal diversity of the slag finds (Bronze Age to Iron Age), the Kundl site is an ideal pilot project for slag investigations using microcomputed tomography, as this allows to visualize the improvement of the production process of copper to be traced as a function of time. Early as well as Middle and Late Bronze Age slag finds were excavated from various horizons. Furthermore, within the horizons there are samples of all slag categories (heterogeneous slag, plate slag, slag sand and furnace slag), which have preserved the different working steps.

Staudt M, Bader M, Eß LM, Lueger D, Oettel LS, Tropper P, Trebsche P (2021): Eine Werksiedlung aus der Bronze- und Eisenzeit bei Kundl (Nordtirol). - Vorbericht über die Ausgrabungen 2018–2019 in der Schottergrube Wimpissinger. In: *Archaeol Austr* 105, 249-282

Phosphorus in the deep Earth: An experimental investigation of Ca-phosphates at upper- to lower-mantle P-T conditions

T. Pausch¹, B. Joachim-Mrosko¹, A.C. Withers², T. Ludwig³, J. Vazhakuttiyakam¹,
J. Konzett¹

¹*Institute for Mineralogy and Petrography, University of Innsbruck*

²*Bayerisches Geoinstitut, Universität Bayreuth*

³*Institute of Earth Sciences, Heidelberg University*

e-mail: tristan.pausch@uibk.ac.at

During subduction and dehydration of oceanic crust, P can be transported into the mantle wedge by fluids or melts, and either enters silicate phases, in particular garnet and olivine, or, if bulk P concentrations are sufficiently high, forms apatite. This P-enriched peridotite will then be dragged down with the subducted slab into the deep mantle. When apatite reaches its upper pressure stability limit, the anhydrous Ca-phosphate tuite will form. While the role of Ca-phosphates in the global P-cycle is well understood for the crust and shallow upper mantle, this is not the case for the deep silicate Earth near and below 660 km depth.

In this study we investigated the *P-T* stability, phase relations, and compositional evolution of tuite in a peridotitic bulk composition at *P-T* conditions of the upper- to lower-mantle transition. For this purpose, multianvil experiments were performed at 15 to 25 GPa and 1600 to 1800 °C. A synthetic peridotite, based on the composition of a moderately fertile spinel lherzolite, was used as starting material. This peridotite was doped with 3% synthetic β -Ca₃(PO₄)₂, 1% of a trace element mix containing a range of HFSE, LILE and REEs, and approx. 2200 µg/g of Br and Cl each.

The coexisting phases stable within the studied *P-T* range include tuite, majoritic garnet, ringwoodite, forsterite, clinoenstatite, bridgmanite, davemaoite, ferropericlasite, and melt. Tuite breaks down between 1700 and 1750 °C at 20 to 25 GPa and between 1750 and 1800 °C at 15 GPa, which yields a negative slope for the tuite-out reaction.

Beyond the *P*-stability of apatite, tuite and/or garnet are the main P carriers in a typical peridotite dependent upon the bulk P content. With increasing depth, the modal amount of Ca-phosphates decreases due to a progressive phosphate-to-silicate P transfer, leading to P contents of up to 4.8 wt% P₂O₅ in majoritic garnet at 1600 °C and 20 GPa. However, as soon as garnet reaches its stability limit, tuite is very likely the most important P-carrying phase at subsolidus conditions while bridgmanite and davemaoite contain small to negligible P (< 60 µg/g and <380 µg/g respectively) even when buffered by tuite.

NanoExtrem-NanoExtrem2: Nano-focus end-station for experiments at ID27 at ESRF

**L. Pennacchioni¹, M. Mezouar², C. L. Sahle², W. Morgenroth¹, S. Jahn³, M. Herrmann³,
M. Schulze³, A. Pakhomova², B. Wehinger², G. Garbarino², S. Bauchau², K. Martel², F. Gerbon²,
D. Andrault⁴, M. Wilke¹**

¹University Potsdam, Potsdam, Germany

²European Synchrotron Facility, ESRF, Grenoble, France

³University of Cologne, Cologne, Germany

⁴Université Clermont Auvergne, Clermont-Ferrand, France

e-mail: lea.pennacchioni@uni-potsdam.de

Research groups from the Universities of Potsdam and Cologne contributed to the construction and improvement of an end station for nano-focused X-ray diffraction (XRD), fluorescence (XRF), and imaging (XRI) at the ID27 high-pressure beamline at the ESRF, Grenoble, in a BMBF project ‘Nanoextrem’. A second BMBF project, ‘Nanoextrem2’, was funded to expand the experimental possibilities with the addition of a high-resolution X-ray emission (XES) spectrometer and pulsed laser heating to the beamline.

An end station for in situ XRD, XRF, XRI and XES at extreme conditions will allow to investigate samples in the field of high-pressure materials and solid state physics in an unprecedented manner.

The end station allows for different focusing schemes by Kirkpatrick-Baez (KB) mirror systems (covering an energy range of 15 to 60 keV) arranged to serve either a nano focus setup, a laser-heating setup, a micro focus arrangement for spatial flexibility and heavy load setups. A Soller slit system was developed and implemented to reduce the Compton scattering of complex sample environments.

Highlights of the setup that have been already characterized : (i) the focusing of the nano-beam (available in the energy range between 15 and 25 keV) to 300×300 nm; (ii) the gain of a factor 70 in flux obtained using a submicron-focused pink beam compared to the monochromatized microbeam (FWHM for pink and monochromatic beam is $0.8 \mu\text{m} \times 0.8 \mu\text{m}$ at $0.3738 \text{ \AA} / 33.17 \text{ keV}$).

As an example, preliminary results on high-pressure XRD experiments on hydrous and anhydrous SiO₂ glasses up to 40 GPa will be presented, as well as performance parameters. In particular, pressure induced structural changes in the SiO₂-H₂O system will be discussed and the first results of a laser-heating experiment up to 4000 K to study the structures of the respective melts will be shown.

Discerning different nucleation mechanisms in synthetic trachybasalts: example from three Titanomagnetite populations in single experiments

S. Peres¹, T.A. Griffiths¹, F. Colle², S. Iannini Lelarge³, M. Masotta^{3,4}, A. Pontesilli⁵, L. Mancini⁶

¹Department of Lithospheric Research, University of Vienna, Josef-Holaubek-Platz 2, 1090 Wien, Austria

²Dipartimento di Scienze Chimiche, della Vita e della Sostenibilità Ambientale, Università di Parma, Campus Universitario, Parco Area delle Scienze 157A, 43124, Parma, Italy

³Dipartimento di Scienze della Terra, University of Pisa, Via Santa Maria 53, 56126 Pisa, Italy

⁴CISUP, Centro per l'Integrazione della Strumentazione Università di Pisa, Lungarno Pacinotti 43, 56125 Pisa, Italy

⁵Istituto Nazionale di Geofisica e Vulcanologia, Via di Vigna Murata 605, 00143 Roma, Italy

⁶ZAG - Slovenian National Building and Civil Engineering Institute,

Dimičeva ulica 12, 1000 Ljubljana, Slovenia

e-mail: stefano.peres@univie.ac.at

Heterogeneous nucleation, i.e. nucleation on a pre-existing surface, is energetically more favourable than homogeneous nucleation because it requires overcoming a lower energetic barrier in order to form a critical nucleus. In most natural and experimental crystallizing magmas, heterogeneous nucleation is suggested to be the main nucleation mechanism, but robust criteria to prove the heterogeneous nucleation origin of a given crystal or phase in natural rocks and ex-situ samples are lacking.

Here we apply multiple analytical methods in order to assess the nucleation mechanism of titanomagnetite (Tmt) crystals that crystallized in the proximity of clinopyroxene (Cpx) crystals in a synthetic trachybasaltic melt (with 2 wt.% added H₂O) in crystallisation experiments carried out in a piston-cylinder apparatus at a constant pressure of 4 kbar. After 30 minutes of superheating at 1300 °C, the samples were cooled at a rate of 80°C / min to the final resting temperatures of 1150 °C and 1100 °C. These temperatures correspond to a respective undercooling (ΔT expressed as $T_{\text{liquidus}} - T_{\text{experiment}}$) of 30° and 80°. The dwell times at these temperatures were 30 minutes and 8 hours, respectively.

3D image processing and 3D image analysis of high-resolution synchrotron X-ray computed microtomography (SR μ CT) data resulted in a precise phase segmentation of Cpx, Tmt, glass and bubbles. Moreover, it was possible to discriminate three main Tmt populations spatially distributed alongside Cpx crystals but morphologically different to each other: a) Tmt grains > 100 μ m in size, skeletal in shape, and mostly isolated in the melt (population 1); b) Tmt grains between up to 100 μ m in size, anhedral to partially skeletal in shape, and always decorating Cpx grains edges and tips (population 2); c) needle-to-flattened Tmt grains almost completely enclosed within Cpx grains (population 3).

The pair correlation function $g(r)$, i.e. a measure of the frequency of an interpoint distance (of r), has been evaluated for the 3D point pattern composed by the centroids of each Tmt population, extracted from several VOIs inside 3D scans of the samples. Tmt grains of population 1 have an unclear 3D point pattern characterized by $g(r)$ near 1, a possible sign of a randomly distributed point pattern. Populations 2 and 3 show clear clustered 3D point patterns, characterized by $g(r) > 1$ and interpoint distances r up to 200 μ m.

Electron backscatter diffraction (EBSD) analysis enables us to clarify the crystallographic orientation relationships (CORs) between Cpx and Tmt crystals which share boundaries. Less than 60 % of the total shared Cpx-Tmt boundary length of population 1 Tmt crystals is characterized by the presence of CORs. Individual crystals of this population show no CORs between the two crystal phases at all, or boundary misorientations dispersed around known specific CORs. In contrast, more than 85% of the total shared Cpx-Tmt boundary length in Tmt populations 2 and 3 follows a COR. Locally, clusters of multiple Tmt decorating single Cpx crystals show more than 95% of the cumulative shared length characterized by the presence of CORs.

Considering the skeletal-to-euhedral shape, the unclear 3D point pattern distribution and the lack of CORs in some Cpx-Tmt pairs classified as Population 1, we suggest that the isolated single grains from this class are most likely formed by homogeneous nucleation. Individual large grains of this same population showing CORs may represent unusually large heterogeneously nucleated Tmt grains, Cpx grains heterogeneously grown on a pre-existing Tmt crystal, or potentially Tmt-Cpx interaction after nucleation apart.

Considering the anhedral or acicular shape, the highly clustered point pattern, and the ubiquitous presence of CORs, we interpret Population 2 and 3 Tmt grains to have formed by heterogeneous nucleation on top of pre-existing Cpx crystals.

In conclusion, multiple Tmt morphologies and distributions coupled with different COR systematics imply different nucleation mechanisms and growth histories for the three populations. Notably, the different Tmt nucleation mechanisms occurred during or right after a single cooling event. Multiple microstructural populations of crystals in natural magmas should be carefully assessed before inferring the existence of complex thermal (or other) histories. A multi-methodological approach which combines 3D SR μ CT data with 2D crystallographic one is indispensable to confidently discern between homogeneous and heterogenous nucleation mechanisms.

Funded by the Austrian Science Fund (FWF): P 33227-N

Mineral reactions in thermally treated calcareous clays for brick production

P.R. Pesek¹, C.L. Lengauer¹, R. Abart², A. Kurka³, G. Früh⁴, W. Gaggl⁴

¹University of Vienna, Department of Mineralogy and Crystallography,
Josef-Holaubek-Platz 2, 1090 Vienna, Austria

²University of Vienna, Department of Lithospheric Research, Josef-Holaubek-Platz 2, 1090 Vienna, Austria

³Wienerberger AG, Wienerbergerplatz 1, 1100 Vienna, Austria

⁴Wienerberger AG, Hauptstraße 4, 2332 Hengersdorf, Austria
e-mail: patrick.pesek@univie.ac.at

The commercial production of bricks usually requires firing temperatures in the range of 800-1000 °C. Some raw materials for brick production may contain up to several wt% carbonates. These carbonates thermally decompose in the range of 600-900 °C and subsequently induce the formation of new mineral phases and microporosity. This allows the production of high thermal insulating clay blocks which contribute for an energy efficient building stock, however, the additional release of CO₂ is an unfavorable side effect regarding the overall carbon footprint. Strongly supporting the European Green Deal, Wienerberger AG is striving to find solutions for a reduction of these raw material related process emissions. Therefore, an approach was targeted to find and evaluate additives, which allow lower firing temperatures in the range of decomposition temperatures of carbonates concurrently keeping the physico-technical parameters of the fired products comparable to available products. In this context, it is particularly important that the pure clay-type raw material and its thermal behavior is foremost characterized so that comparisons with clay-additive mixtures can later be made.

Test specimens were extruded, dried, and fired at 620 °C, 700 °C, 760 °C and 880 °C. The mineral phases, chemical composition and thermal behavior of the green body and the fired sherds were determined using PXRD, XRF and TA, respectively. SEM-EDX and EPMA were used for high-resolution images of microstructures and phase identification as well as for identifying mineral reactions.

The results revealed a multitude of processes occurring during the firing process of the investigated calcareous clay. A selection of relevant mineral reactions is listed below:

(i) Individual clay minerals were dehydroxylated at 620 °C, while the matrix was visibly molten at a firing temperature of 880 °C (Fig. 1A). Within the reduction core, a higher level of melting was present than at the rim, possibly due to FeO that rather acts as a fluxing agent than Fe₂O₃ (Fischer 1987).

(ii) The beginning of decomposition of carbonates was observed at 620 °C. Decomposing carbonates can react with clay minerals, which leads to a densification of sherds at 600 °C (Fischer 1987). Small dolomite grains displayed an advanced level of decomposition at 700 °C with grains exhibiting a dolomite-type core surrounded by MgO and a Ca-rich shell. This degree of decomposition was also visible within larger dolomite grains at 760 °C. Calcite was also partially decomposed and consisted of a calcite-type core surrounded by a Ca-rich shell. At 880 °C almost all of the carbonate grains had vanished. Remaining MgO or pores with or without carbonate residues were surrounded by a rim of Ca-Mg-Al-silicates due to significant diffusion of Ca and Mg into the matrix (Fig. 1B). PXRD exhibited newly formed gehlenite and akermanite at this temperature.

(iii) Pyrite thermally decomposed between 300-600 °C, gaseous SO₂-SO₃ was formed (c.f. Schmidt, 1968) and confirmed by evolved gas analysis. The SO₂-SO₃ gas, however, stayed at most in the sherds and reacted with MgO and CaO of the decomposing carbonates thus forming sulfates (Schmidt 1968). Low concentrations of S were detected in carbonates at 700 °C. The amount of detected S increased with increasing firing temperature. Domains with elevated S contents were formed along the rims of the remaining carbonate grains at 760 °C. At a firing temperature of 880 °C, S could be found in the residues of former carbonates and in the Ca-Mg-Al-silicate reaction rims (Fig. 1B).

(iv) Some Na-rich feldspars exhibited a K-enriched rim at 880 °C (Fig. 1C) due to an exchange of Na⁺ for K⁺ (Riccardi et al. 1999). Collapsed clay minerals (Riccardi et al. 1999) and partially collapsed muscovite (Ionescu & Hoeck 2011) can be considered as sources of K⁺.

(v) Some quartz grains were characterized by a rim enriched in Al, Na, K and Fe at 880 °C (Fig. 1C). The interaction of these foreign elements indicates a softening or partially melting of quartz grains (Ionescu & Hoeck 2011).

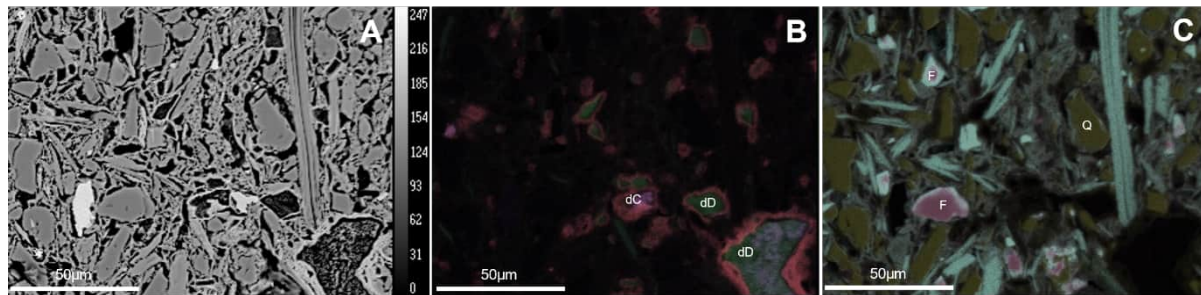


Figure 1. (A) BSE-image of a calcareous clay fired at 880 °C; (B) Stacked element maps of Mg (green), Ca (red) and S (purple); (C) Stacked element maps of Si (yellow), Na (magenta) and K (cyan). Abbreviations: dC decomposed calcite, dD decomposed dolomite, F feldspar, Q quartz.

The outlined observations made are an important basis for firing experiments of clay-additive mixtures. Various mineral reactions were identified, and observations reported in literature were confirmed. The two most significant processes observed in detail are the gradual decomposition of carbonates starting from 620 °C and the melting of the matrix between 760-880 °C. Especially, the role of sulfur during the decomposition of carbonates provides important information for brick producing processes, since the formation of water-soluble sulfates causes severe efflorescence (Schmidt 1961).

Fischer P (1987): Die Bildung des grobkeramischen Scherbens beim Brennen, Teil II. – ZI-Jahrbuch 88, 96

Ionescu C, Hoeck V (2011): Firing-induced transformations in Copper Age ceramics from NE Romania – Eur J Miner 23, 937-958

Riccardi MP, Messiga B, Duminuco P (1999): An approach to the dynamics of clay firing – Appl Clay Sci 15, 393-409

Schmidt E (1961): Ausblühungen. – Die Ziegelindustrie 5, 132

Schmidt E (1968): Die physikalischen und chemischen Veränderungen beim Ziegelbrand – ZI-Jahrbuch 68, 208

Coherent lamellar intergrowth from exsolution of alkali feldspar

E. Petrishcheva, D. Heuser, R. Abart

*Department of Lithospheric Research, University of Vienna
e-mail: elena.petrishcheva@univie.ac.at*

We investigate coherent lamellar intergrowth resulting from exsolution in alkali feldspar. This structure forms when an initially homogeneous alkali feldspar of intermediate composition enters the miscibility gap during cooling below about 550°C and separates into lamellae of more Na-rich and lamellae of more K-rich composition. As the lattice parameters of alkali feldspar are strongly compositional dependent, formation of these lamellae induces strains and stresses within the structure. In coherent intergrowth the elastic and chemical strains interact in such a way that coherent boundaries are maintained between the lamellae.

The presence of elastic deformation affects the system's free energy and consequently influences its equilibrium phase relations such as binodal points and the miscibility gap. In earlier papers, due to the problem of having fewer equations than unknown variables, certain simplifying assumptions were made regarding the strains. In particular, the strains lying in the plane parallel to the lamellar interfaces were assumed to be zero, which we deem unphysical. Instead, we take advantage of the principle that the system tends towards the state with the minimum energy among all possible equilibrium states.

To determine the elastic stresses and strains and their impact on the system's free energy, we calculate and minimize the overall elastic energy of the lamellar structure. The elastic energy acts against the separation of Na-rich and K-rich lamellae, leading to binodal points deviating from the expectations based solely on chemical equilibrium in an unstrained state. By accounting for the elastic energy, we obtain both the corrected binodal points and the miscibility gap as represented by the so-called *coherent solvus*, which now is not unique and depends on the composition of the homogeneous precursor feldspar.

The main mathematical challenge lies in the fact that calculation of the elastic energy requires knowledge of the binodal points, the latter in turn, are determined by the total free energy of the system. To overcome this challenge, we employ a method of successive approximations. Observed lamellar orientations agree well with our calculations. These results represent a significant improvement and generalization of earlier work by Robin (1974).

Micro-CT and micro-XRF investigations of an Early Bronze-Age smelting crucible fragment

M. Piccolruaz¹, P. Tropper¹, G. Degenhart²

¹University of Innsbruck, Institute of Mineralogy and Petrography, 6020 Innsbruck, Austria

²Medical University of Innsbruck, Institute of Radiology, 6020 Innsbruck, Austria
e-mail: peter.tropper@uibk.ac.at

In this investigation, a fragment of an early Bronze Age smelting crucible fragment with an adherent slag crust was examined. Together with ore fragments, raw copper and copper objects this fragment documents the evidence of small-scale smelting activity at the early Bronze Age site Buchberg near Wiesing in the Inn valley.

The sample was analyzed by electron microprobe analysis as well as micro-XRF. Mineralogically and chemically three different areas can be distinguished. The first area (Bereich A) away from the slag crust is unmelted and consists mainly of clay minerals and different temper components (orthogneiss, quartz, plagioclase, K-feldspar, muscovite). The second area (Bereich B) closer to the slag crust shows melting and thus consists mainly of a glass matrix with occasional inclusions of covellite (CuS). The third area (Bereich C) represents the slag crust and contains clinopyroxenes in a glass matrix, and also small amounts of acanthite (Ag₂S). Furthermore, abundant Cu-Sb-Fe-Zn-O phases (possibly the alteration phase theisite, Cu₅Zn₅(AsO₄,SbO₄)₂(OH)₁₄) and chalcosine (Cu₂S) occur. The glass in area C contains high concentrations of phosphorus, arsenic and antimony and the SiO₂ content decreases strongly in the glass from area B to area C.

The crucible fragment was scanned using a micro-CT, which resulted in a three-dimensional image illustrating the distribution of high-density phases in the crucible fragment and the slag crust. Quantitative evaluation of the CT results of the slag crust yielded in very little pore space of 3 vol.%, whereas the amount of the high-density phases (Cu-Sb-Fe-Zn-O phases) is 43 vol.% and thus is clearly concentrated in the slag crust.

Finally, the results show that the ores used for copper smelting in the Early Bronze Age were As-rich tetradrites deriving most likely either from the Devonian Schwaz Dolomite or the carbonates of the Schwaz Triassic (the occurrence of acanthite points towards it). The high phosphorous contents in the slag can either be interpreted as resulting from firing plant materials (wood) or the possible addition of bone apatite to the smelting process.

STOE Diffractometers empowering Mineralogical Crystallography

T. Pippinger¹

*¹STOE & Cie GmbH, Darmstadt, Germany
e-mail: pippinger@stoe.com*

STOE, established in 1887, manufacturing equipment for the optical examination of crystals, has been at the forefront of powder and single crystal X-ray diffraction since the 1960s. STOE invented and patented the transmission geometry technique for Powder XRD and additionally, they developed the first pixel detector XRD system with an open Eulerian cradle for single crystals.

Headquartered in Darmstadt, Germany, STOE maintains complete in-house capabilities for research and development, software programming, electrical and mechanical engineering, and production. This integrated approach enables STOE to offer both standard and customized solutions to its customers. Whenever it comes to quality, STOE accepts no compromises.

STOE's latest instruments facilitate precise profile and Rietveld analyses, as well as ultrafast single crystal diffraction experiments on even the tiniest crystals. Furthermore, high-temperature and high-pressure accessories are available, which can be seamlessly integrated in the hardware and software, allowing for the convenient simulation of non - ambient inner earth conditions.

These solutions tailored to Mineralogical Crystallography and more will be discussed in the presentation.

Clays from the Westerwald area as a source for high reactive main cement constituent

C. J. Piribauer¹, R. Diedel¹, H. Knapp¹, W. Heuser¹, M. Schellhorn¹

¹Stephan Schmidt Group,
e-mail: christoph.piribauer@stephan-schmidt.group

The cement and concrete industry are currently in a state of transition due to high CO₂ emissions. According to a study of the vdz (Deutscher Verband der Zementindustrie), there are three main levers to lower the emissions: alternative fuels, CCS / CCU and clinker reduced cements. As most of the emissions are so called process emissions and the potential for CCS / CCU is limited in a close range to the cement producers, there is a strong focus on the development and usage of clinker reduced cements. Calcined clays play an important role here as a substitute for the cement clinker made from limestone. To meet the decarbonisation targets of the German cement industry, 6.8 to 7.5 million tonnes/a of clay will be needed by 2030 (Basten, 2022). In order to cover this very high demands for clays, waste clays from treatment processes, such as filter cakes and clays from sludge ponds, are considered in addition to conventionally mined clays. As these secondary raw materials occur only in relatively small quantities with strongly varying compositions, they are likely to play only a minor role in the future due to the strong influence of the mineralogical-chemical composition on the calcination conditions and therefore on the resulting reactivities and technological properties.



Figure 1. Mine Wimpsfeld 3, white kaolinitic-illitic clays with an overburden of bentonites and basalt. – Picture: Stephan Schmidt Group

Stephan Schmidt KG operates 20 open-cast clay mining operations in Germany, 16 in the Westerwald area. From these deposits, more than 100 clays were selected for a screening process not only focussing on their basic suitability for calcination, but also with regards to a long-time availability for a constant material supply of a calciner. In a first screening step, the carbonate content (< 5 mass-%), the sulphide concentration (< 1.5 mass-%) and the clay mineral/quartz ratio (> 50 %) were assessed. Clays that met these requirements were calcined at 750 °C and subjected to a test for pozzolanic properties. The Surana method (Surana and Joshi, 1990) was chosen to determine the pozzolanicity. By chemically treating the calcinates after Surana, the available reactive Si and Al ions could be determined via ICP-OES. At a concentration $>80,000$ ppm (Al+Si), suitability as a clinker substitute is ensured, comparable to the performance of blast furnace slag and fly ash (Schulze and Rickert, 2019). Next to this information, also the influence of the calcined clays on the early strength can be estimated, as a higher Al content leads to the formation of CA phases. The final step in the evaluation of calcined clays involves the testing of CEM I cements (activity index/EN 450-1; water demand/EN 196-3; compressive strength/EN 196-1), in which 25 % of the cement clinker phase is replaced by calcined clays.

Based on this knowledge, 2 main supply areas have been identified. While the raw material mixture from Arbon/Wimpfeld 3 (Fig. 1) has a high smectite content, the Sedan mixture is kaolinitic-illitic dominated. Each site allows the delivery of 250,000 t clay/a, which corresponds to the production of 200,000 t/a of calcinate.

Basten M (2022): Die Nachfrage nach Primär- und Sekundärrohstoffen der Steine-und-Erden-Industrie bis 2040 in Deutschland. - Bundesverband Baustoffe Steine und Erden e.V. Berlin

Surana M, Joshi S (1990): Estimating reactivity of pozzolanic materials by a spectrophotometric method. - Advances in Cement Research 3, 81-83

Schulze S, Rickert J (2019): Suitability of natural calcined clays as supplementary cementitious material. - Cement and Concrete Composites 1, 92-97

An uncommon terrestrial rock that was believed to be a meteorite

L. Pittarello^{1,2}, S. Chernonozhkin³, H. Downes⁴, O. Marchhart², S. Merchel², A. Wieser²,
F. Vanhacke⁵, J. Villeneuve⁶, S. Goderis⁷

¹Naturhistorisches Museum, Vienna, Austria

²University of Vienna, Austria

³Montanuniversität Leoben, Austria

⁴Birkbeck University of London, United Kingdom

⁵Ghent University, Belgium

⁶CRPG, Université de Lorraine, Vandœuvre les Nancy, France

⁷AMGC, Vrije Universiteit Brussel, Belgium

e-mail: lidia.pittarello@nhm.at

Ureilites are achondrite meteorites, which can be associated to mantle restites, but containing up to 8 wt% carbon and which have experienced melting, smelting, and shock (e.g., Goodrich 1992; Goodrich et al. 2007). In the framework of a research project on isotopic zoning across olivine grains from selected ureilites (Chernonozhkin et al. *subm.*), a chip from Dyalpur was loaned from the Natural History Museum London (sample BM.51185). Petrographic and geochemical analysis of this sample revealed some features, which are not consistent with the previous characterization of Dyalpur and ureilites in general. However, as clasts with peculiar characteristics are not uncommon among ureilites (e.g., clast ALM-A with a trachyandesitic composition; Bischoff et al. 2014), we decided for further investigations. Oxygen isotopic ratios are close to the terrestrial fraction line, but this can also indicate mixing of different components by impact on the parent body (e.g., for angrites, Rider-Stokes et al. 2023). However, cosmogenic radionuclide measurements by accelerator mass spectrometry (Lachner et al. 2021) finally confirm a terrestrial origin of the sample. The (yet preliminary) upper limit of $^{26}\text{Al}/^{27}\text{Al}$ 4.4×10^{-12} corresponding to 0.3 dpm/kg (^{26}Al) measured is >60 times lower than the one of true Dyalpur sample, and also far lower than literature values for ureilites including Dyalpur (e.g., Aylmer et al. 1990).

The typically terrestrial features, including the occurrence of pargasite-hornblende amphibole and hazlewoodite (a Ni-sulfide), both never described before in ureilites, are associated with other features, which are quite uncommon for terrestrial rocks, such as the presence of carbon-rich veins inducing chemical reduction along their margin, and a Fo₉₁ groundmass, embedding sub-rounded amphibole clasts. Geothermobarometric estimates (e.g., Hammarstrom & Zen 1986; Ridolfi & Renzulli 2012; etc.) on amphibole resulted in pressure estimate of 6-7 kbar and temperature estimate of 790-840 °C.

Terrestrial rocks presenting similar features are rare, mostly consisting of metasomatized peridotite-xenoliths in basalts recording breakdown of amphibole due to heating and decompression during transport (e.g., Ban et al. 2005; Kaeser et al. 2007). Further studies are planned to identify the nature of the sample and to reconstruct the case leading to its classification as Dyalpur ureilite in the collection of the NHM London.

- Aylmer D, Vogt D, Herzog GF, Klein J, Fink D, Middleton R. (1990): Low ^{10}Be and ^{26}Al contents of ureilites: Production at meteoroid surfaces. - *Cosmochim Acta* 54, 1775-1784
- Ban M, Witt-Eickschen G, Klein M, Seck HA. (2005): The origin of glasses in hydrous mantle xenoliths from the West Eifel, Germany: incongruent break down of amphibole. - *Contrib Mineral Petrol* 148, 511-523
- Bischoff A, Horstmann M, Alix Barrat J-A, Chaussidon M, Pack A, Herwartz D, Ward D, Vollmer C, Decker S (2014): Trachyandesitic volcanism in the early Solar System. - *P Natl Acad Sci USA* 111, 12689 -12692
- Chernozhukhin SM et al. (subm.): Early differentiation and core formation on the ureilite parent body recorded in the stable isotopic signatures of Fe, Zn and Mg.
- Goodrich CA (1992): Ureilites. A critical review. - *Meteoritics* 27, 327-352
- Goodrich CA, Orman vanJA, Wilson L (2007): Fractional melting and smelting on the ureilite parent body. - *Geochim Cosmochim Acta* 71, 2876
- Hammarstrom JM, Zen E (1986): Aluminum in hornblende: An empirical igneous geobarometer. - *Amer Mineral* 71, 2876-2895
- Kaesler B, Kalt A, Pettke T (2007): Crystallization and breakdown of metasomatic phases in graphite-bearing peridotite xenoliths from Marsabit (Kenya). - *J Petrol* 48, 1725-1760
- Lachner J, Martschini M, Kalb A, Kern M, Marchhart O, Plasser F, Priller A, Steier P, Wieser A, Golser R (2021): Highly sensitive ^{26}Al measurements by Ion-Laser-InterAction Mass Spectrometry. - *Int J Mass Spectrom* 465, 116576
- Rider-Stokes BG, Greenwood RC, Anand M, White LF, Franchi IA, Debaille V, Goderis S, Pittarello L, Yamaguchi A, Mikouchi Z, Claeys P (2023): Impact mixing among rocky planetesimals in the early Solar System from angrite oxygen isotopes. - *Nat Astron* (2023). <https://doi.org/10.1038/s41550-023-01968-0>
- Ridolfi F, Ranzulli A (2012): Calcic amphiboles in calc-alkaline and alkaline magmas: thermobarometric and chemometric empirical equations valid up to 1,130°C and 2.2 GPa. - *Contrib Mineral Petrol* 163, 877-895

U-Pb garnet, zircon, and rutile petrochronology of eclogite xenoliths from the Navajo Volcanic Field (USA)

J.E. Pohlner¹, R. Albert¹, S. Aulbach¹, S. Hao¹, A. Gerdes¹, J.B. Walters¹, D.J. Schulze², H. Helmstaedt³

¹*Institut für Geowissenschaften and Frankfurt Isotope and Element Research Center (FIERCE),
Goethe-Universität Frankfurt*

²*Department of Earth Sciences and Department of Chemical and Physical Sciences, University of Toronto,
Mississauga, Canada*

³*Department of Geological Sciences and Geological Engineering, Queen's University, Kingston, Canada
e-mail: pohlner@em.uni-frankfurt.de*

Complementary insights from multiple mineral geochronometers are often indispensable to disentangle the complex multi-stage history of subduction-related rocks. Previous geochronological work on eclogite xenoliths of the Navajo Volcanic Field (NVF) sparked controversies about their origin, especially whether they are derived from oceanic crust of the Farallon plate, or from older continental lithosphere, based on occasional Proterozoic zircon U-Pb ages. We present new LA-ICP-MS U-Pb data from garnet, zircon, and rutile alongside geochemical and geothermobarometric data to test models for the origin and evolution of the NVF xenoliths.

The NVF comprises intrusions of serpentinized ultramafic microbreccia (SUM) which intruded the Colorado Plateau at ~30 Ma. Eclogite xenoliths from this SUM are mineralogically unusual, strongly resembling orogenic rather than typically biminerally kimberlite-borne equivalents. Besides ubiquitous rutile, many contain zoisite pseudomorphs after lawsonite (with rare lawsonite relics), matrix monazite, and/or abundant pyrite along with rare coesite. Previous studies obtained peak P-T conditions around 4 GPa and 600°C. Chemically, some of the eclogites resemble mid-ocean ridge basalts, whereas most experienced varying degrees of multi-stage metasomatism. Zoned omphacite with Na-rich rims accompanied by an increase of whole-rock Na₂O contents (up to 11 wt%) and omphacite modes (sometimes >90%) reflects interaction with a siliceous fluid. Mg-rich garnet rims with mantle-like δ¹⁸O are interpreted to reflect a massive hydration event just prior to entrainment in the SUM. The latter is also thought to have caused the crystallization of monazite with published ~30 Ma ages.

The various xenoliths yield variable garnet U-Pb dates, indicating garnet growth at different stages, but exclusively from the Cretaceous to shortly before SUM formation. The non-uniform garnet data may suggest that the NVF eclogite xenolith suite was assembled from rocks that entered the eclogite facies diachronously over tens of Myr. Metamorphic zircon ages cover a range similar to the garnet ages. Various stages of potential interaction with internally-derived (from lawsonite dehydration) and externally-derived (metasomatic) fluids may have induced (re)crystallization and/or partial re-setting of geochronometer minerals over a considerable time span.

There is currently no evidence for pre-Mesozoic metamorphism in the eclogites. By contrast, the hypothesis of a Proterozoic protolith origin is still under consideration, and can only be tested by dating rare igneous zircon cores. A zircon and rutile U-Pb dating campaign planned for the near future will reveal how the resultant ages relate to those obtained from garnet.

Blue- and green-spotted "K2 gneiss" from the Goldberggruppe, Austria

J. Portenkirchner¹, E. Libowitzky²

¹Department of Lithospheric Research, University of Vienna

²Department of Mineralogy and Crystallography, University of Vienna

e-mail: eugen.libowitzky@univie.ac.at

"K2 gneiss" or "K2 granite" is a grey to white (meta)granite with cm-sized round blue (and sometimes green) spots stained by fine-grained azurite (and sometimes malachite). Due to its attractive appearance it has been carved to various stone artefacts and traded world-wide. Although this rock-type has been known exclusively from the slopes of the K2 in the Himalaya Mountains (hence the name), a second occurrence has been found in the Goldberggruppe in Austria some two years ago.

This special gneiss (Fig. 1) from the N wall of Hoher Sonnblick, Rauris Valley, Salzburg, has never been described in previous literature, although the mapping of the area has been done in great detail (Exner 1962, 1964). Extended field trips during the past years were not successful to confirm "K2 gneiss" in the neighboring areas SW - NW of Hoher Sonnblick peak. Only a special rock with similar appearance has been known from the "Weiße Wand" at Stanziwurten, Möll Valley, Carinthia, some 6 km SSW of Hoher Sonnblick. However, this rock shows a matrix of barite, calcite and quartz with blue and green spots of azurite and malachite.

Besides of normal petrographic investigations with the polarizing microscope (i.e. quartz, feldspar, muscovite, calcite), the blue and green spots were probed with micro-Raman spectroscopy. By comparison with reference spectra from the RRUFF data base (Downs 2006) azurite (Fig. 2) and malachite were unambiguously identified in all samples.

While the barite rocks from "Weiße Wand" contain also tiny chalcopyrite and tennantite grains as obvious primary source of copper, "K2 gneiss" from Hoher Sonnblick lacks any primary copper sulfides; only tiny striated cubes of pyrite have been observed (note the relics of tiny brown spots of limonite in the center of Fig.1).

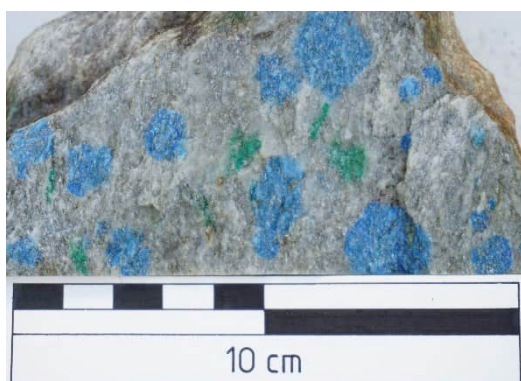


Figure 1. "K2 gneiss" from the Goldberggruppe with spots of azurite (blue) and malachite (green)

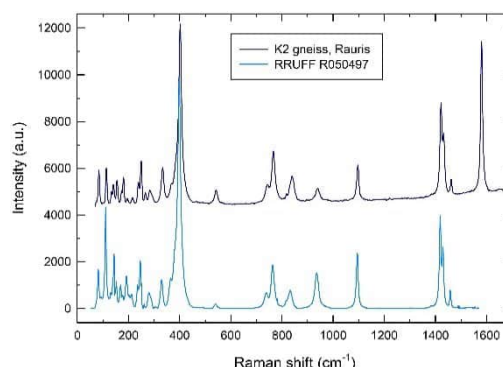


Figure 2. Micro-Raman spectra of azurite from "K2 gneiss" compared to an azurite reference from the RRUFF data base (Downs 2006).

Downs RT (2006): The RRUFF Project: an integrated study of the chemistry, crystallography, Raman and infrared spectroscopy of minerals. – Progr Abstr 19th General Meeting IMA, Kobe, Japan, O03-13

EXNER C (1962): Geologische Karte der Sonnblickgruppe, 1:50000. – Verlag der Geologischen Bundesanstalt, Wien

EXNER C (1964): Erläuterungen zur Geologischen Karte der Sonnblickgruppe, 1:50000. – Verlag der Geologischen Bundesanstalt, Wien

Electron Diffraction – Structure Elucidation of Nano-Crystalline Materials

A. Portieri¹, P. Simoncic¹

¹*Eldico Scientific, Badenerstraße 790, 8048 Zurich-Altstetten, Switzerland
e-mail: simoncic@eldico.ch*

Electron diffraction (known also as ED, 3D ED or microED) performing nano-crystallography on crystals smaller than 1 μm is increasingly gaining momentum in science and industry. Complementary to neutron-, powder-, and single-crystal X-ray diffraction, the disruptive technology of electron diffraction opens up fascinating new perspectives for a wide variety of compounds in the fields of chemical, pharmaceutical, and advanced materials research. The recent introduction of dedicated instrumentation to perform ED experiments is a key aspect of the continued growth and success of this technology. ELDICO Scientific presents the electron diffractometer ED-1, a smart combination of a 5-axis nanometer-precise goniometer, a large sample chamber, radically simplified electron optics, and an ultra-high-speed hybrid-pixel Dectris Quadro® camera for diffraction data acquisition. Several examples of data collected on ELDICO ED-1 are showcased to demonstrate the potential and advantages of a dedicated electron diffractometer, covering selected applications and challenges of electron diffraction: 1) polymorphism, 2) crystal mapping and extrapolation to powder XRD, and 3) structure elucidation of energy storage materials as well as zeolites and minerals.

Thracian marbles from Archaic to Roman Times – Imports or local production?

W. Prochaska, S. Ladstätter, V. Anevlavi

*Austrian Archaeological Institute, Austrian Academy of Sciences, Franz Klein-Gasse 1, 1190 Vienna, Austria
e-mail walter.prochaska@oeaw.ac.at*

Marble use and trade in the region of Thracia took place extensively already before it became Roman province in 46 AD. Within this territory some of the most prominent and renowned marble sources of antiquity are located (e.g., Prokonnesos or Thasos). The coastal regions at the Aegean, Marmara, and Black Sea, as well as the islands, were shaped by Greek culture and these marbles were widely exported throughout the empire. Accordingly, the marble trade in these coastal or island regions was always connected to the international commerce. Recent extensive studies in the course of the project “Fingerprinting White Marbles - Quarries and Cities of Roman Thrace, 1st-3rd century AD” (Austrian Science Fund) revealed that these marbles also were extensively used not only in the coastal areas but also in the larger inland cities of Thrace. In contrast to these renowned international marbles, the numerous marble deposits in the interior, in particular in today's Bulgaria, have received far less attention, however, as will be shown in this paper, they were of considerable economic importance.

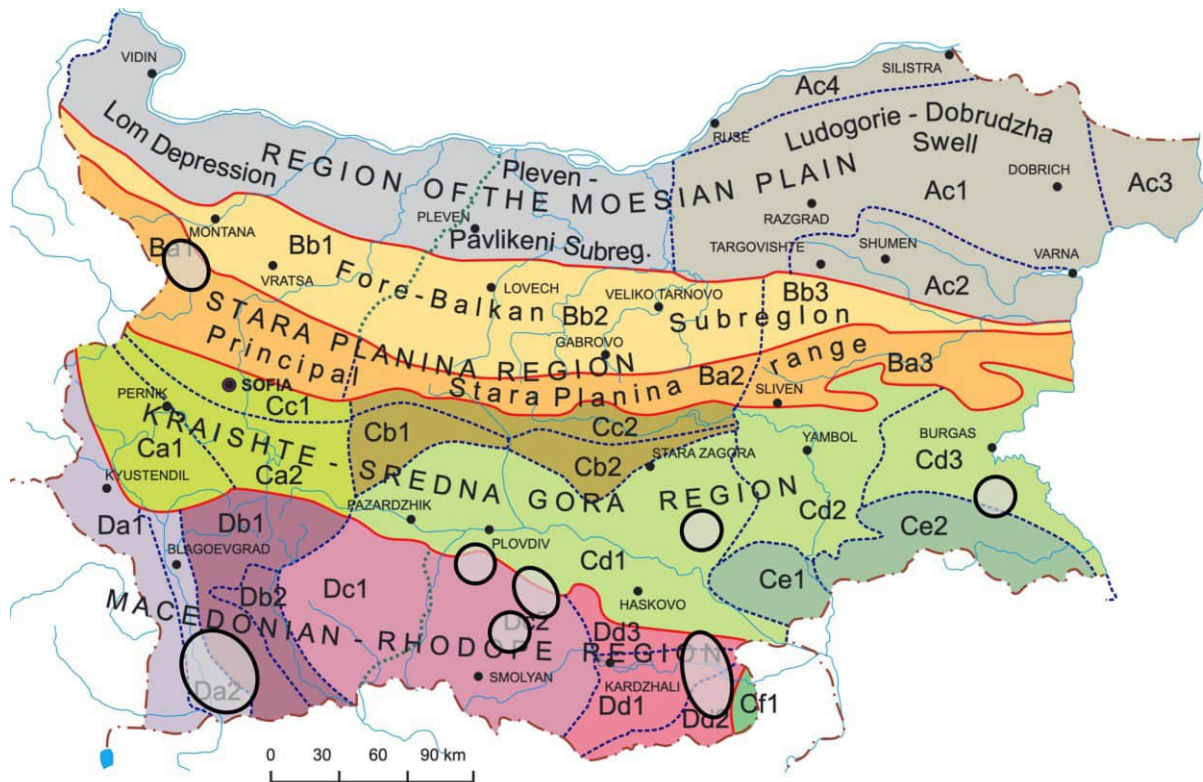


Figure 1. Geologic/geomorphological zonation of Bulgaria (Zagorchev 2009) with the marble producing areas.

The integration of the territory into the Roman Empire was followed by urbanisation and the extension of the infrastructure. Evidence of Roman marble production in the inland territory of Thrace is known in different areas: The most important geologic unit for economic marble production are the Rhodope Mountains with high-grade marble deposits. In the eastern parts of the Sredna Gora region further marble deposits occur with different metamorphic grades. Furthermore, in greenschist facies series of the NW Balkan Mountains near the town of Berkovitsa fine-grained marbles occur. Initial analyses indicate that these marbles were not only employed in the province itself, but were also exported. On the other hand, architecture and sculpture in the province of Thrace reveal striking connections to Asia Minor. By means of a sampling of the Thracian quarries on one hand and of Roman artefacts throughout the province on the other hand, the question regarding marble trade as well as the cultural and technological transfer will be discussed in the presentation. One example of far distant trade of the marble of that region is the “boarhunt” found during excavations in 2010 in Felix Romuliana in today’s Serbia sculptured from Berkovitsa marble.



Figure. 2: The sculpture “boarhunt” made of marble from Berkovitsa SW of the town of Montana in today’s Bulgaria. The sculpture or its marble was transported along a distance of more than 100 km in beeline.

More than 1400 samples from ancient quarries in Thrace and samples from artefacts in the museums all over the region were analysed in order to assign the marble of a given artefact to a corresponding quarry or quarry area. To achieve reliable results a multi method approach was applied using stable isotope analysis (O- and C-isotopes), trace element analysis by ICP-MS and petrographic investigations. Naturally, this large number of variables analysed has to be evaluated by statistical means. We used the programme packages STATISTICA and SPSS. On this basis the different marbles of Thracia can be told apart, and a very precise correlation of the artefacts to the corresponding sources can be achieved.

Zagorchev I (2009): Geomorphological zonation of Bulgaria. Principles and state of the art. - Proceedings of the Bulgarian Academy of Sciences 628(8), 981-992.

Prochaska W Zivic M (2018): The marbles of the sculptures of Felix Romuliana in Serbia. in Proceedings of the XI ASMOSIA Conference (Split May 2015) pp 301-311

Modern non-ambient X-ray diffraction for the investigation of minerals, metals and industrial materials of any type

B. Puhr¹, A.O.F. Jones¹, B. Schrode¹, M. Kremer¹, P. Vir¹, A. Paiva¹

¹Anton Paar GmbH, Graz, Austria
e-mail: barbara.puhr@anton-paar.com

Modern powder X-ray diffraction (XRD) systems must nowadays be able to meet the challenges faced by multi-user and multi-application facilities. Instruments must be capable not only of routine XRD measurements, but also have to offer advanced capabilities such as measurements under non-ambient conditions (varying temperature, pressure, gas atmosphere, humidity, ...) which can drastically change material properties.

The recently launched XRDynamic 500 automated multipurpose powder X-ray diffractometer from Anton Paar (Fig. 1) has set new standards in terms of data quality, automation and efficiency for laboratory powder diffractometers. The core of XRDynamic 500 is the TruBeam™ concept that comprises a large goniometer radius and evacuated optics units, automatic change of the beam geometry and all optics components, and automated instrument and sample alignment routines. All of these features combine to deliver outstanding data quality that can be measured with high efficiency in a straight-forward manner. The high level of automation means that you can perform measurements on one or many samples with different geometries and instrument configurations in one batch with no user intervention needed.

XRDynamic 500 can also be equipped with different non-ambient attachments to perform measurements under non-ambient conditions. These attachments are perfectly integrated into the hard- and software (plug-and play mode, integrated control unit, built-in connections) and guarantee best-in-class convenience for your non-ambient XRD studies.

To highlight the potential of XRDynamic 500, we will present key instrument features and benefits in addition to recent application data on non-ambient diffraction. Examples include in-situ structural changes of bentonite samples and materials used for technical applications (Fig. 2), how salt mineral compositions change under the influence of gas and humidity, and the study of the tempering temperature on the properties of steel.



Figure 1. The XRDynamic 500 automated multipurpose powder X-ray diffractometer from Anton Paar.

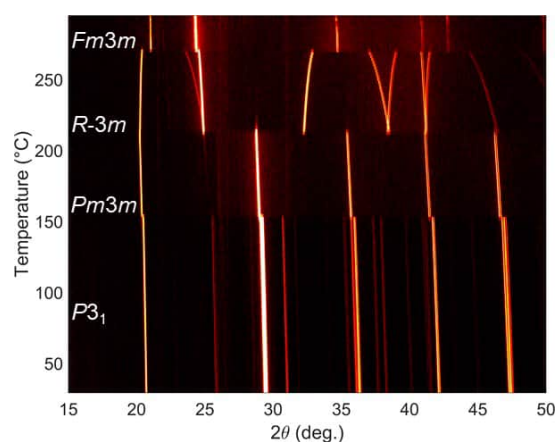


Figure 2. Temperature-induced phase transitions of RbNO₃ (Weidenthaler & Ternieden, 2022).

Machine learning-assisted pyrite indicator mineral approach in mineral exploration

S. Raič¹, F. Molnár², N. Cook³, P. Nikkola⁴, K. Szentpéteri⁴, H. O'Brien⁴,
A. Taivalkoski⁵, J.-P. Ranta⁵

¹*Institute of Applied Geosciences, University of Technology, Graz, Austria*

²*Department of Mineralogy, Institute of Geography and Earth Sciences, Eötvös Loránd University, Budapest, Hungary*

³*Sustainable Minerals Institute, University of Queensland, Indooroopilly, Queensland, Australia*

⁴*Geological Survey of Finland, Espoo, Finland*

⁵*Oulu Mining School, University of Oulu, Oulu, Finland*

e-mail: sara.raic@tugraz.at

Discovering new ore deposits that supply and satisfy the growing industrial demand for green transition metals is becoming more important than ever for transitioning into a non-fossil fuel future. This task however, appears to be unprecedented, when considering the required amount of technology metals. It becomes therefore highly relevant to develop and implement innovative and sustainable, but time- and cost-efficient exploration methods for deeply buried, undiscovered mineral deposits. A way to tackle this challenge is by using known European mineral deposits as testing grounds for new exploration technologies. For this purpose, the domestic mineral resources in northern Finland provide an ideal ecosystem and diversity of profitable green transition metals such as nickel, copper, cobalt and gold. The glaciated terranes in which these mineral systems occur, however, require special exploration methods such as the indicator mineral approach. Indicator minerals (e.g. sulfides, oxides and native gold) are recovered from glacial sedimentary samples and their individual grains are used for trace element analysis by LA-ICP-MS, which ideally could provide key information on the character of their source bedrocks, type of mineralization, as well as the glacial transport direction.

In this study we have tested the indicator mineral approach in the Rompas-Rajapalot Au-Co project areas in the Paleoproterozoic Peräpohja belt in northern Finland, by analyzing and comparing the trace element geochemistry of pyrite grains from bedrock and till samples. A machine learning-based approach was implemented using unsupervised self-organizing maps (SOM) and k-means clustering for mineralization-related pattern recognition. The obtained results show that pyrite grains recovered from till can be discriminated and clustered based on their compositions, and further correlated with pyrite from two hydrothermal deposit types within the study area: (i) the Au-Co mineral system at Rajapalot, and (ii) the vein-style Au system at Rompas. Mapping of recognized patterns, in accordance with ice flow directions, assists in (i) the localization of potential target-areas, (ii) and improves our understanding of similar mineral systems.

Tungsten mineralization in East Tyrol – repeated recycling of W in the crust?

J. G. Raith¹, F. Altenberger¹, F. Hutter², J. Weilbold³, C. Auer³

¹Montanuniversität Leoben, Leoben

²GeoSphere Austria, Vienna

³geo.zt gmbh, Hall in Tirol

e-mail: johann.raith@unileoben.ac.at

Geochemical tungsten anomalies and occurrences were discovered in the Lienz area in the 1980-ies during regional W prospecting campaigns (e.g., Neinavaie & Ronge 1985) and are summarized as "Polymetallic skarn district Drauzug-Gurktal nappe system Lienz-Hochstein" in the IRIS data base. Low- to medium grade metamorphic Austroalpine units were intruded by a pluton west of Lienz in the Oligocene (Edenwald intrusion, ≈30 Ma). A km-sized contact metamorphic aureole with metapelitic hornfels developed around the composite intrusion especially at its western to southern contacts (Linner et al. 2013).

Three types of scheelite mineralization are distinguished in the region: (1) Strata-bound scheelite in low-grade metamorphic metabasites in the Early Palaeozoic Thurntal Quartzphyllite (disseminations, stringers, deformed quartz veinlets; e.g., Tafinalpe). The association of W-As (arsenopyrite) is specific for this type (Portugaller 2010); (2) Sulfide-scheelite skarn mineralization (disseminations, veins; e.g., Edenwald). Massive sulfides (pyrrhotite, chalcopyrite etc.) are associated with thin intercalations of marble and calc-silicate rocks (Ca amphiboles, calcian plagioclase, grossular, diopside-hedenbergite, vesuvianite, wollastonite) (Hutter 2022). This type is interpreted as a reduced magmatogenic skarn, a mineralization style very rare in the Eastern Alps. (3) Scheelite in quartz veins and clefts within the intrusive rocks. This pure scheelite mineralization is controlled by brittle division surfaces in the intrusive rocks.

The Oligocene plutonic rocks span a wide petrographic composition from metaluminous (gabbro)diorite, tonalite, to more evolved peraluminous granodiorite/granite. They are magnesian showing calc-alkaline magma characteristics. The high W bulk values (up to hundreds of ppm W) to are due to post-magmatic (type 3) hydrothermal processes.

LA-ICP-MS trace element analyses of scheelite allow to discriminate these different mineralization styles. We present combined micro-textural features (obtained from CL imaging) and trace element data of scheelite in their geological/petrographic context, we discuss the possible applications for exploration and propose that tungsten has undergone several stages of crustal recycling.

Hutter F (2022): Wolframvererzungen und Intrusionsgesteine am Lienzer Schlossberg, Osttirol. - Masterarbeit, Montanuniversität Leoben

Linner M, Reitner JM, Pavlik W (2013) Geologische Karte 179, Lienz 1:50.000.- Geologischen Bundesanstalt, Wien

Neinavaie MH, Ronge W (1985): Wolframprospektion 1984 in Teilen Osttirols, Kärntens, Niederösterreichs und der Steiermark sowie petrographische Untersuchungen an neu aufgefundenen Wolframvererzungen im Arbeitsgebiet. - Unveröffentlichter Ber VOEST-ALPINE, Eisenerz

Portugaller T (2010): Scheelitvererzungen im Thurntaler Quarzphyllitkomplex, Osttirol: Petrographische und chemische Untersuchungen an Nebengesteinen und Bachsedimenten. - Masterarbeit, Montanuniversität Leoben

Expanding the magmatic and metamorphic geochronological record of the Isua supracrustal belt

A. Ramírez-Salazar^{1,2}, D. Sorger³, T. Müller³, S. Piazzolo¹

¹ School of Earth and Environment, University of Leeds, Leeds

² Instituto de Geología, Universidad Nacional Autónoma de México, Ciudad Universitaria 04510, Mexico City, Mexico

³ Geoscience Centre, University of Göttingen, Goldschmidtstraße 1, Göttingen, Germany
e-mail: r.s.anthonyy@gmail.com

The emplacement history of the protoliths of the Isua supracrustal belt (ISB), southwestern Greenland, goes back to the Eoarchean and is often interpreted to preserve one of the oldest metamorphic records on Earth. Thus, in many studies the metamorphic characteristics of this belt are used to advance our understanding of Archean tectonics. However, the age of its main tectonometamorphic event(s) remains debated with main arguments derived from cross-cutting relationships while direct dating of metamorphic minerals is sparse. Recent microstructural and quantitative P-T analyses (Ramírez-Salazar et al., 2021; Zuo et al., 2021) showed that the ISB experienced a syn-tectonic amphibolite facies event at 550–600 °C and 0.5–0.7 GPa (M₁), followed by a relatively static (lower) amphibolite facies episode at <540 °C and <0.5 GPa (M₂), both later overprinted by greenschist facies fluid-related metamorphism (M₃). In order to constrain the timing of different tectonometamorphic, as well as magmatic, events of the ISB, we combine microstructural and P-T analyses with several geochronometers (Sm-Nd and Lu-Hf in garnet, and U-Pb in rutile and titanite). Our results expand the history of the ISB and reveal new events occurring in its associated rock formation.

Local metamorphism at 650–675 °C and 0.4–0.6 GPa associated with the emplacement of a tonalite-trondhjemite-granodiorite (TTG) body occurring at ≈3,660 Ma is recorded in hornblendite enclaves adjacent to the ISB. Additional information on the magmatic history is provided by an intrusive, garnet-bearing granitoid showing potentially igneous garnet crystallization at ≈3,550 Ma. Sm-Nd and Lu-Hf dates derived from metamorphic garnets within ISB supracrustal rocks show no evidence of a regional, major tectonometamorphic event (M₁) prior to ≈3,400 Ma. Instead, the analysis of syn-tectonic garnets suggests that M₁ most likely occurred at ≈2700 Ma. Moreover, new U-Pb data of post-tectonic titanite suggest that static post-tectonic metamorphism (M₂) occurred during the Neoproterozoic (≈2,700–2,600 Ma), whereas late retrogression event(s) are most likely Paleoproterozoic (<2,200 Ma) in age.

Our findings highlight that the observed main regional ISB metamorphism and concomitant deformation did not occur in the Eoarchean. While results of this study cannot fully discriminate between different geodynamic interpretations, our results suggest that the main tectonometamorphic event forming the current structures of the ISB are not related to pre 3,400 Ma Early Earth, but rather to late Archean geodynamics.

Ramírez-Salazar A, Müller T, Piazzolo S, Webb AAG, Hauzenberger C, Zuo J, Haproff P, Harvey J, Wong TK, Charlton C (2021): Tectonics of the Isua Supracrustal Belt 1: P-T-X-d constraints of a poly-metamorphic terrane. - *Tectonics* 40, doi:10.1029/2020TC006516

Zuo J, Webb AAG, Piazzolo S, Wang Q, Müller T, Ramírez-Salazar A, Haproff PJ (2021): Tectonics of the Isua Supracrustal Belt 2: Microstructures reveal distributed strain in the absence of major fault structures: *Tectonics* 40, doi:10.1029/2020TC006514

Pressure prediction in a poly-metamorphic terrain based on μ -EDXRF. An example from the Archean Vumba Schist Belt, Botswana

D. Rammlmair¹

¹Leibniz University Hannover, Germany
e-mail: d.rammlmair@mineralogie.uni-hannover.de

The Archean Vumba Schist Belt in the NE of Botswana comprises komatiitic successions, bimodal volcanics, sediments, Archean soils, banded iron formation, rodingites, and is intruded by several generations of granitoids, late pyroxenite and dolerite dykes. The belt experienced three metamorphic events, where due to strong uplift and tilting a shift of metamorphic centers from high grade in the NW to medium grade in the center and low grade in the SE can be observed. Shear zone and quartz vein hosted gold deposits are related to the late low grade metamorphic impact.

Several hundred rock slices were mapped by the μ EDXRF M4 Tornado, Bruker nano. The measurement was performed in 20 μ m steps, 2msec acquisition time using a Rh-tube at 50kV and 600 μ A, a poly-capillary beam guide, no filters, two silicon drift detectors arranged in 180°, 90° to the tube with 51° take off or incidence angle, respectively.

The mapping provided bulk area chemical information and phase distribution for the very same area. Phase distribution was obtained by supervised endmember-based classification using the spectral angle mapper (SAM) algorithm of the hyperspectral software ENVI for 165 spectral regions of interest. The minimum per channel per pixel was obtained for both detectors to widely omit diffraction signals of individual grains. Both, area chemistry and modality were used to select samples of similar chemistry along strike from NW to SE to compare the metamorphic impact. A series of mafic rocks was selected and investigated in detail putting focus on the amphibole chemistry by masking all other phases and applying a second SAM classification based on amphibole solid solution endmembers only. The amphibole endmembers were derived from EPMA analyses and amphibole classification by Li et al. (2022) following the classification scheme of Hawthorne et al. (2012). This second classification is the key to differentiate the impact of individual metamorphic events within individual mafic rock slices by visualizing amphiboles classified according to chemistry representative for different PT environments. The pressure estimation provided by Li et al. (2022), referring to the method of Hollister et al. (1987), was used for pressure prediction of amphiboles in individual samples across the belt. The dominant pressure is around 8.9 kb, but relics indicate values of >10 kb, and retrograde alteration shows values of > 4 kb.

Automated mineralogy applied to μ EDXRF, provided a detailed endmember data base exists, is a fast and easy to apply method, despite obscuring effects such as grain boundaries, grain size, shape as well as orientation-based diffraction. Information on rock and mineral chemistry, modality, and mineral sub-classes can be obtained for large sample numbers for preselection of most adequate samples for polished thin sections and EPMA investigations.

Li X, Zhang C, Behrens H, Holtz F (2020): Calculating amphibole formula from electron microprobe analysis data using a machine learning method based on principal components regression. - *Lithos* 362-363, 105469, 10.1016/j.lithos.2020.105469.

Hawthorne FC, Oberti R, Harlow GE, Maresch WV, Martin RF, Schumacher JC, Welch MD (2012): Nomenclature of the amphibole supergroup. - *Amer Mineral* 97, 2031–2048

Hollister LS, Grissom GC, Peters EK, Stowell HH, Sisson VB (1987): Confirmation of the empirical correlation of Al in hornblende with pressure of solidification of calc-alkaline plutons. - *Amer Mineral* 72, 231–239

Diabases are petrologists best friends: quantitative *P-T* constraints on the Eoalpine metamorphic gradient in the Ötztal Complex using diabase dikes

G. Raso¹, P. Tropper¹, D. Rammlmair²

¹University of Innsbruck, Institute of Mineralogy and Petrography, A-6020 Innsbruck, Austria

²Institute of Mineralogy, Leibniz University, Hannover, Germany

e-mail: peter.tropper@uibk.ac.at

The Ötztal Complex (ÖC) is a large crystalline complex in the western part of the Austroalpine units. The ÖC consists of quartzofelspathic and metapelitic metasediments with various intercalations of orthogneisses, amphibolites and rare metacarbonates. The oldest metamorphic event is Ordovician in age (460 – 490 Ma), leading to the formation of orthogneisses and scattered occurrences of migmatites. The Variscan metamorphic overprint ranges from 390 – 295 Ma and the first stage of the Variscan event was a high-pressure metamorphism around 373 – 359 Ma, leading to the formation of eclogites in the central part of the ÖC. The conditions of the eclogite-facies metamorphism were estimated to be 650 – 750 °C and 20 – 28 kbar. The dominant Variscan amphibolite-facies metamorphism occurred around 330 – 350 Ma with estimated *P-T* conditions of 570 – 640 °C and 5.8 – 7.5 kbar for the northwestern part of the ÖC. Subsequently after Variscan amphibolite-facies metamorphism diabase dikes intruded into the polymetamorphic basement. The youngest metamorphic event in this Austroalpine basement occurred during the Cretaceous Eo-Alpine orogeny (100 – 73 Ma). The intensity of the Eo-Alpine overprint varies within the ÖC and increases from NW (lower greenschist-facies) to SE (epidote-amphibolite facies) and reaches 550 - 600°C and ≥ 11 kbar in the Schneeberg Complex. Unfortunately, so far, no quantitative data concerning the *P-T* conditions of the Eoalpine metamorphic overprint in the NW of the ÖC exist. This is where the post-Variscan diabase dikes come in.

The importance of these diabase dikes lies in the fact that field- and textural investigations revealed a post-Variscan emplacement since these dikes only show Eoalpine metamorphism and deformation. The mineral assemblage of these dikes is amphibole + plagioclase + epidote + biotite + muscovite + titanite + quartz +/- garnet. Changes in plagioclase and amphibole chemistry are concordant with a prograde metamorphic evolution. Plagioclase changes from almost pure albite ($X_{An} < 0.1$) to intermediate plagioclase with $X_{An} = 0.3-0.4$. Amphiboles show a strong increase in Al^6 and Al^4 as well as Na^B and Na^A from NW to SE. This is qualitatively indicative of increasing *P-T* conditions. The *P-T* calculations were done using the programs Thermocalc v.3.21 and v.3.33 and mode-2 calculations (only using linearly independent reactions and statistical evaluation). The increase in *T* is from 400°C in the NW to almost 600 °C in the SE at the Timmelsjoch. Similarly *P* increases from 6-7 kbar in the NW to almost 12 kbar in the SE using Thermocalc v.3.33. Calculations using Thermocalc v.3.21 yielded slightly different *P-T* conditions from 300 °C and 3 kbar in the NW to 600 °C and 9 kbar in the SW. These differences are due to the use of different activity models for amphibole solid solutions, which has a profound impact on the calculations. Nonetheless these data represent the first quantitative *P-T* estimates for the Eoalpine metamorphic gradient north above the chloritoid isograd.

Recycling of Mineral Waste Materials by Geopolymerization – First Results

**B. Ratz¹, T. Sattler¹, F. Steindl², S. Raič², I. Zögl², S. Radinger², O. Rudić³,
F. Mittermayr³, C. Grengg²**

*¹Montanuniversitaet Leoben, Chair of Waste Processing Technology and Waste Management,
Franz-Josef-Straße 18, 8700 Leoben, Austria*

²Institute of Applied Geosciences, Graz University of Technology, Rechbauerstraße 12, 8010 Graz, Austria

*³Institute of Technology and Testing of Construction Materials, Graz University of Technology,
Inffeldgasse 24, 8010 Graz, Austria
e-mail: bettina.ratz@unileoben.ac.at*

The building and construction industry is responsible for 40 % of the anthropogenic CO₂ emissions and consumes enormous amounts of resources. In recent decades, there has been a significant increase in the production of waste, of which mineral waste is the largest stream in Austria, accounting for 76 % of the total waste. It is currently mostly disposed in landfills. To counteract the negative environmental impact of building and construction and to reduce the amount of landfilled waste, a Christian Doppler Laboratory for waste-based geopolymer construction materials in the CO₂-neutral circular economy (GECCO₂) was launched at Graz University of Technology. The goal is to produce environmentally friendly, highly resilient and Portland-cement-free geopolymer construction materials, also known as alkali-activated materials, from currently unexploited mineral waste materials. These geopolymers are then to be used in, for example, the environment of biochemically aggressive waste systems, such as sewer manholes, tanks and basins, or biowaste treatment facilities. Tasks of the Chair of Waste Processing Technology and Waste Management at the Montanuniversitaet Leoben, include the identification and selection of relevant mineral waste streams and the mineralogical, chemical and environmental characterization of selected waste materials, and elaboration of potential pretreatment strategies. With the obtained results, a material portfolio of suitable Austrian waste materials and industrial by-products will be created. First results will be presented regarding the mineralogical and chemical characterization of the selected waste materials.

Preliminary EBSD analysis and interpretation of Spinel-Olivine-Plagioclase pseudomorphs in skarnoid xenoliths from Southern Slovakia

L. Reato¹, M. Huraiová¹, T. Griffiths², G. Habler², R. Abart², V. Hurai³, P. Konečný⁴

¹Comenius University, Faculty of Natural Sciences, Department of Mineralogy, Petrology and Economic Geology, Ilkovičova 6, 842 15 Bratislava, Slovakia

²University of Vienna, Department of Lithospheric Research, Josef-Holaubek-Platz 2, 1090, Vienna

³Slovak Academy of Sciences, Institute of Earth Sciences, Dúbravská Cesta 9, 840 05 Bratislava, Slovakia

⁴State Geological Institute of Dionýz Štúr, Department of Special Laboratories, Mlynská Dolina 1, 817 04 Bratislava, Slovakia

e-mail: reato1@uniba.sk

Calc-silicate skarnoid xenoliths, with dimensions of up to 20 cm in diameter, were collected from Pleistocene alkali basalts of Southern Slovakia. Their general mineralogy and petrology have been described in Reato et al. (2022). They are composed of layers of relict augitic diopside, skeletal olivine and interstitial ternary feldspar (An₅₇₋₈₆), alternating with layers of anorthite (An₉₅₋₁₀₀) ± high Al, Fe³⁺ clinopyroxenes [Ca(Al,Fe³⁺)AlSiO₆] ± melilite inclusions. Such a mineral assemblage is indicative of thermal metamorphism in a high *f*O₂ environment and can be found in skarn or paralava (Foit et al. 1987; Pascal et al., 2005). Occasional pockets and veins of calcite ± aragonite can be present in both layers. Most of the xenoliths contain pseudomorphs comprising olivine (Ol), spinel (Spl), and ternary feldspar with an integrated average composition resembling tschermakitic amphibole. The pseudomorphs are characterised by very fine grained (1-100 μm²) skeletal to dendritic olivine and spinel, surrounded by interstitial ternary feldspar. The interstitial ternary feldspar within the pseudomorphs (An₅₃₋₉₆) has compositions similar to the one in the diopside + olivine layer (An₅₇₋₈₆). A sharp chemical boundary between the pseudomorphs and the anorthite layer is present. The olivine within the pseudomorphs is richer in Mg and has a more restricted composition (Fo₈₅₋₈₈) compared to olivine outside the pseudomorphs (Fo₆₆₋₈₈), which is characterised by much bigger (>100 μm) crystals, growing perpendicular to the elongation direction of the pseudomorphs.

The sample's lineation and foliation were determined by X-ray micro-computed tomography using an industrial v|tome|x L 240 tomograph from the Institute of Earth Sciences - SAS in Banská Bystrica, and thin sections were cut parallel to the lineation and perpendicular to the foliation. Locations with interesting micro-structural features were selected through transmitted light microscopy. The mineralogy of the selected areas was quantified through EMPA at the State Geological Survey of Slovakia in Bratislava, using a CAMECA SX-100 electron microprobe. EBSD analysis, together with EDS maps, were produced at the Laboratory for Field-Emission Scanning Electron Microscopy and Focused Ion Beam Applications at the University of Vienna, using the FEI Quanta™ 3D FEG instrument. After this, data were re-indexed and processed using EDAX OIM Analysis™ at the University of Vienna, and the Matlab™ toolbox MTEX (Bachmann et al. 2010).

A region containing a pseudomorph at the contact between the anorthite layer and the diopside + olivine layer was selected to determine the microstructural characteristics of the three different domains and their interactions. Both anorthite and ternary feldspar outside the pseudomorph keep the same crystal orientation inside the pseudomorph, despite their change in composition. The grain boundary misorientation angle distribution between olivine and spinel inside the pseudomorph shows a peak at 56°. When only the Spl-Ol boundary segments in the range 55°-57° misorientation angle are considered, a very strong misorientation axis

peak, suggestive of a near-specific crystallographic orientation relationship (COR), was observed. This was confirmed by plotting Spl directions with respect to Ol for the selected boundaries, revealing alignment of one of the $\{111\}$ Spl planes with the (100)Ol plane and one of the $\{110\}$ Spl planes with (001)Ol, with minor dispersion (generally $<5^\circ$) around the perfect relationship.

The observed COR between spinel and olivine implies an interaction between the two lattices, most likely during simultaneous growth. Similar plane relationships have been found in experimental petrology studies and were related to the exsolution of spinel from olivine occurring in the mantle transition zone (Hamaya & Akimoto 1982; Green, 1984). However, the xenoliths' protolith was formed and transformed within the crust (Reato et al. 2022), implying a different simultaneous growth process is responsible for the COR in this case. Concerning the behaviour of plagioclase within the pseudomorph, we can conclude that it has likely grown after olivine and spinel, using the plagioclase crystals from outside the pseudomorphs as a template for its growth within them, analogous to the formation of myrmekites (Phillips and Evans, 1980; Yuguchi & Nishiyama 2008). This feature is typical of rapid cooling systems, which is in accordance with the geological context and history of the xenoliths, which are thought to have undergone high-T thermal metamorphism before being collected by the host alkali basalt (Reato et al. 2022).

- Bachmann F, Hielscher R, Schaeben H (2010): Texture Analysis with MTEX – Free and Open-Source Software Toolbox. *Sol. St. Phen* 160, 63–68
- Foit FF, Hooper RL, Rosenberg PE (1987): An unusual pyroxene, melilite, and iron oxide mineral assemblage in a coal-fire buchite from Buffalo, Wyoming. - *Amer Mineral* 72, 137-147
- Hamaya N, Akimoto SI (1982): On the mechanism of the olivine-spinel phase transformation. - *Phys Earth Plan In* 29, 6-11
- Green HW (1984): How and why does olivine transform to spinel? - *Geophys Res Lett* 11, 817-820
- Phillips ER (1980): On polygenetic myrmekite. - *Geol Mag* 117, 29-36
- Pascal M, Katona I, Fonteilles M, Verkaeren J (2005): Relics of high-temperature clinopyroxene on the join Di–CaTs with up to 72 mol.% $\text{Ca}(\text{Al},\text{Fe}^{3+})\text{AlSiO}_6$ in the skarns of Ciclova and Magureaua Vatei, Carpathians, Romania. - *Can Mineral* 43, 857–881
- Reato L, Huraiová M, Konečný P, Marko F, Hurai V (2022): Formation of esseneite and kushiroite in tschermakite-bearing calc-silicate xenoliths ejected in alkali basalt. - *Minerals* 12, 156
- Yuguchi T, Nishiyama T (2008): The mechanism of myrmekite formation deduced from steady-diffusion modeling based on petrography: Case study of the Okueyama granitic body, Kyushu, Japan. - *Lithos* 106, 237-260

Metamorphism induced strength inversion at high-pressure conditions

A. Rogowitz^{1,2}, S. Schorn¹, B. Huet³, L. Menegon⁴, B. Grasemann²

¹*Institute of Earth Sciences, University of Graz, Austria*

²*Department of Geology, University of Vienna, Austria*

³*GeoSphere Austria, Vienna, Austria*

⁴*Njord Centre, University of Oslo, Norway*

e-mail: anna.rogowitz@uni-graz.at

We present structural, microstructural and petrographical data from an eclogite-facies shear zone of the Hohl locality (Koralpe, Eastern Alps, Austria). The shear zone spans over about 6 meter in thickness and shows a pronounced foliation (average: 047/63) characterized by alternating layers of proto- to ultramylonitic eclogite with different mineralogical content. Two stretching lineations have been identified: (1) a penetrative NW-SE striking mineral lineation (average: 122/27) defined by the shape and orientation of prismatic minerals and (2) a N-S striking stretching lineation (average: 354/20) which occurrence is limited to ultramylonitic layers. The latter appears to cross-cut the NW-SE striking lineation and is therefore considered as younger. The shear zone bears rocks with two distinct eclogite facies mineral assemblages of which one is dominated by clinozoisite, amphibole and garnet. This lithology occurs as foliated sigmoidal lenses hosted by typical eclogite containing omphacite, garnet, clinozoisite, amphibole, quartz, kyanite and rutile.

Both lithologies derived from NMORB gabbro which intruded during Permian rifting. Whole rock geochemical data shows that the lenses are enriched in Al and depleted in Mg and Fe when compared to the eclogite matrix. Protolith assemblage calculations suggest that lenses have originally been plagioclase-rich cumulates within a clinopyroxene-plagioclase gabbro matrix. Considering experimentally derived flow-laws on clinopyroxene-plagioclase aggregates (Dimanov & Dresen, 2005) indicates that lenses were less competent than the gabbro. However, the sigmoidal shape of lenses surrounded by ultramylonitic eclogite suggests that the lenses were stronger during shear zone development.

Microstructural investigations reveal an ultramylonitic fabric dominated by fine-grained (~50 µm) euhedral clinopyroxene within the host eclogite. Triple- and quadro-junctions, open grain boundaries and a lack of intracrystalline strain suggest that eclogite dominantly deformed by fluid supported grain boundary sliding. On the other hand, the microstructure of lenses is dominated by coarse-grained elongated clinozoisite (~300 µm) and amphibole aggregates (~2 mm). Amphibole aggregates are sigmoidal and characterized by a coarse-grained highly strained clast and strain free slightly elongated crystals in strain shadows. These observations indicate that lenses deformed by combined dislocation and dissolution-reprecipitation creep.

Our data shows how mineral replacement resulted in a strength inversion whereas the lenses, initially weaker than their host, are stronger than the surrounding eclogite after metamorphism at eclogite-facies conditions (720 ± 20 °C, 21 ± 3 kbar). The switch in strength caused stress concentration at the lithological contacts and subsequent strain localization in the weaker eclogitic mineral assemblage. Activation of fluid assisted grain boundary sliding in eclogite ultramylonites is assumed to have further weakened the eclogite, causing drastic strain partitioning. Later N-S-directed deformation subsequently solely localized within the weaker ultramylonitic eclogite.

Structural peculiarities in $(1-x)\text{Na}_{0.5}\text{Ba}_{0.5}\text{TiO}_3-x\text{BaTiO}_3$ at the morphotropic phase boundary studied by high-pressure XRD and Raman spectroscopy

C. Rösche¹, T. Boffa-Ballaran², T. Malcherek¹, C. Paulmann¹,
R. J. Angel³, B. Mihailova¹

¹*FB Erdsystemwissenschaften, Universität Hamburg, Germany*

²*Bayerisches Geoinstitut, Universität Bayreuth, Germany*

³*Istituto di Geoscienze e Georisorse, CNR, Padova, Italy*

e-mail: constanze.roesche@uni-hamburg.de

Perovskite-type (ABO_3) ferroelectric solid solutions are widely used functional materials, whose properties are utilized, for example, in sensors and actuators. The currently market-leading ferroelectric ceramics $\text{Pb}_{1-x}\text{Zr}_x\text{TiO}_3$ contain lead, which is undesirable from an environmental point of view. The solid solution $\text{Na}_{0.5}\text{Bi}_{0.5}\text{TiO}_3-x\text{BaTiO}_3$ (NBT- x BT) is one of the promising lead-free alternatives, however, its properties still need to be accurately constrained. Compositional variations may change the symmetry of the ferroelectric phase and shape the nanoscale structure, allowing to tune the properties by chemical substitutions. At the morphotropic phase boundary (MPB) with $x = 0.05 - 0.06$ for NBT- x BT the dielectric permittivity, piezoelectric coefficient, and electromechanical coupling factor are enhanced (Ge et al. 2011) due to an increased structural flexibility (de la Flor et al. 2019), making such compositions a good starting point for improvement by additional chemical doping. For an effective modification of the material, better understanding of the relation between the chemical composition and the nanoscale structural features in NBT- x BT is needed.

In this study, we have analyzed the response of the structure of NBT-0.048BT to external hydrostatic stress by performing high-pressure single-crystal X-ray diffraction (XRD) and Raman spectroscopic experiments up to 9 GPa, using the diamond-anvil-cell technique. It is known that in the case of Pb-based relaxor ferroelectrics pressure suppresses the polar order, while it enhances the antiferrodistortive order. Thus, the complementary high-pressure analyses of Bragg scattering, informative of long-range order, X-ray diffuse scattering (XDS), indicative of intermediate-range order and Raman scattering, sensitive to the intermediate-/short-range order can help to reveal subtle structural features, which are hard to detect at ambient pressure (Mihailova et al. 2011). The combination of different experimental methods allows us to obtain a comprehensive picture of the pressure-induced structural transformations ranging from the local to the long-range scale. At ambient and low pressure the deviations from the average pseudo-cubic perovskite structure produce strong diffuse scattering, which evolves into sharp Bragg peaks with increasing pressure [see Fig. 1 (a) and (c)]. The appearance of additional Bragg peaks indicates a phase transition between 4.4 and 5.5 GPa. The Raman data [Fig. 1 (b) and (d)] resolve the multistep local scale structural changes that lead to the change in symmetry. First a reduction of the Ba-induced local BO_6 anisotropy is taking place at 0.5 - 0.9 GPa, followed by decoupling of adjacent A- and B-site dipoles near 1.2 GPa. This allows for development of antipolar order of A-cation off-center displacements starting above 1.9 GPa, similar as it has been observed by Kreisel et al. (2003) in pure NBT at lower pressures. Furthermore, there is a strong amplification and increase in correlation length of octahedral tilts above 2.7 GPa and a change in the tilt pattern at 4 - 4.5 GPa.

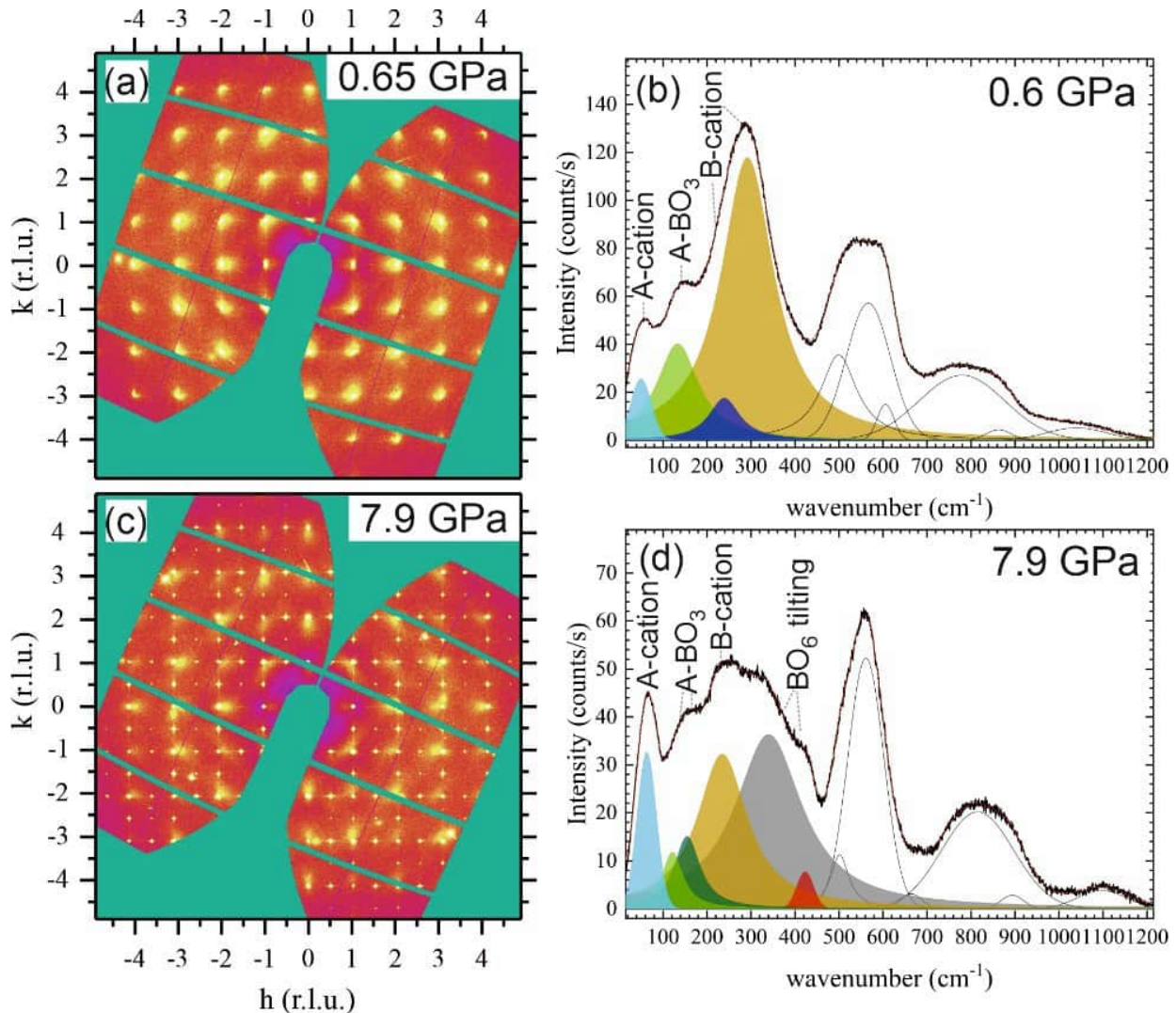


Figure 1. X-ray diffraction pattern in $hk0$ plane (a) and (c) and Raman scattering (b) and (d) of NBT-0.048BT at ~ 0.6 GPa and 7.9 GPa. The colored peaks in (b) and (d) are associated with A-cation off-centering vibrations (light blue), A- BO_3 translations (light and dark green), B-cation off centering vibrations (dark blue and orange) and BO_6 tilting vibrations (grey and red).

Ge W, Cao H, DeVreugd C, Li J, Viehland D, Zhang Q, Luo H (2011): Influence of BaTiO_3 content on the structure and properties of $\text{Na}_{0.5}\text{Bi}_{0.5}\text{TiO}_3$ crystals. - J Amer Ceram Soc 94, 3084-3087

De La Flor G, Gorfman S, Mihailova B (2019): Local-scale structural response of $(1-x)\text{Na}_{0.5}\text{Bi}_{0.5}\text{TiO}_3-x\text{BaTiO}_3$ to external electric fields. - Appl Phys Lett 114, 42901

Mihailova B, Angel RJ, Maier BJ, Welsch AM, Zhao J, Gospodinov M, Bismayer U (2011): The structural state of lead-based relaxor ferroelectrics under pressure. - IEEE Trans Ultrason Ferroelectr Freq Control 58, 1905-1913

Kreisel J, Bouvier P, Dkhil B, Thomas PA, Glazer AM, Welberry TR, Chaabane B, Mezouar M (2003): High-pressure x-ray scattering of oxides with a nanoscale local structure: Application to $\text{Na}_{1/2}\text{Bi}_{1/2}\text{TiO}_3$. - Phys Rev B68, 14113

**Turning toolboxes into an ecosystem:
How to make research software interoperable?
Moderator**

Thomas Rose^{1,2}

¹*Goethe-Universität Frankfurt, Institut für Geowissenschaften, Frankfurt, Germany*

²*Forschungsbereich Archäometallurgie, Leibniz-Forschungsmuseum für Georessourcen /
Deutsches Bergbau-Museum Bochum, Bochum, Germany
e-mail: thomas.rose@em.uni.frankfurt.de*

I am an archaeologist and geochemist by training, currently working in the German National Research Infrastructure consortium for the Earth System Sciences (*NFDI4Earth*). The aim of the consortium is to provide a central access point for all resources related to research data management and data science in the Earth System Sciences. In addition, I am a core team member of *GlobaLID*, the Global Lead Isotope Database. *GlobaLID* aims to become an infrastructure for the publication, curation and access of lead isotope data in archaeology. Moreover, *GlobaLID* further aims to bring the lead isotope community closer together, to create collaboration opportunities for researchers from less wealthy countries, and to provide training materials for the lead isotope method. In addition, I am author of the R package *ChronochRt*.

At the heart of all these endeavours lies my strong belief, that high-quality research can only be maintained in the future when its transparency is increased and hurdles (e.g. financial, infrastructural) are lowered. Besides making research data FAIR – findable, accessible, interoperable, reusable –, research software is a key component to turn this vision into reality. However, it won't be enough to have lots of tools at hand, as efficient and user friendly they may be. A crucial aspect is to design them, and the structure of the data processed by them, in a way that allows seamless passing of data between different software and, ideally, enable different software to directly communicate with each other. Consequently, not only the data but also the software must become interoperable.

Currently, there seems to be little coordination between the different groups working on research software in mineralogy, geochemistry, and neighbouring fields. However, aligning our efforts towards a common vision would be beneficial for all people involved in the development of such software and the community in general.

Hydrothermal pyritization of nano-magnetite and the record of biominerals in ancient sulfide systems

E.A. Runge^{1,2}, T.H. Chiu³, M. Mansor³, A. Kappler^{3,4}, J.-P. Duda^{1,2}

¹*Geobiology, Geoscience Center, University of Goettingen, Germany,*

²*Sedimentology & Organic Geochemistry, University of Tuebingen, Germany*

³*Geomicrobiology, University of Tuebingen, Germany*

⁴*Cluster of Excellence EXC 2124, Controlling Microbes to Fight Infection, University of Tuebingen, Germany*
e-mail: eric.runge@uni-tuebingen.de

The microbial formation of magnetite nanoparticles in hydrothermal environments can be driven by enzymatically controlled reactions or occur as a by-product of microbial Fe cycling. The resulting biogenic magnetite has characteristic traits that distinguish it from its abiotic counterpart, which makes it a potential biosignature. Furthermore, the precipitates may preserve chemical and isotopic information that provide valuable insights into conditions during their formation; hence, they might be used as environmental proxies. However, sulfidic diagenesis driven by hydrothermal fluids and microbial S cycling may cause the rapid transformation of microbial magnetite to Fe sulfide minerals, potentially altering or erasing biosignatures and proxies encoded in the primary precipitates. Thus, understanding the mechanisms, and characterizing the products of such sulfidation reactions is crucial for reading the record of biominerals in ancient hydrothermal sulfide deposits. Here, we present sulfidation experiments with synthetic and biogenic magnetite at physical and chemical conditions relevant to microbial niches in hydrothermal environments (<121 °C, excess S/Fe). By integrating multiple analytical techniques (e.g., scanning electron microscopy, sequential Fe extraction, Raman spectroscopy), we demonstrate a potential taphonomic bias against biogenic magnetite in hydrothermal environments and a strong influence of diagenetic fluid-mineral interactions on magnetite preservation. We further suggest that a portion of Fe sulfide minerals in hydrothermal deposits may be secondary products of magnetite sulfidation, highlighting the importance of understanding their diagenetic history for (bio)geochemical analyses. Our approach will aid the identification of biominerals and their transformation products in ancient rocks and pave the way for a more robust reconstruction of microbial evolution and environmental change through geological time.

Highly siderophile element and Re-Os isotope compositions of the 3.5 Ga Tomka Iron Formation, Daitari Greenstone Belt, India

A. Salzmann¹, T. Schulz¹, S. Viehmann², J. Jodder³, A. Hofmann⁴, C. Koeberl¹

¹*Department für Lithosphärenforschung, Universität Wien, Österreich*

²*Institut für Mineralogie, Leibniz Universität Hannover, Deutschland*

³*Evolutionary Studies Institute, University of the Witwatersrand, South Africa*

⁴*Department of Geology, University of Johannesburg, South Africa*

e-mail: a01610854@unet.univie.ac.at

Banded iron formations (BIFs) are Precambrian sedimentary rocks that are the product of chemical precipitation from seawater diagenetic, and metamorphic processes. Their abundance reach a maximum at around 2.4 Ga and appear to correlate with the Paleoproterozoic rise of atmospheric oxygen (Great Oxidation Event) with the subsequent change from anoxic to oxic conditions in the shallow parts of the ancient oceans. BIFs may thus represent robust archives, traced by rare earth elements and Yttrium (REY) and the Sm-Nd isotope system (Viehmann et al. 2015b) for the physico-chemical evolution of early Earth's atmosphere and oceans.

Following earlier studies that applied the redox-sensitive highly siderophile element (HSE) abundances and the Re-Os isotopes system to the Neoproterozoic Temagami BIF (Schulz et al. 2021) and the Neoproterozoic Urucum BIF (Prost 2023), we investigate the application of these geochemical tools to a BIF of the Paleoproterozoic Daitari Greenstone Belt, Singhbhum Craton, India. This multiproxy approach has the potential to record the influence of different source contributions to the BIF forming seawater column (i.e., continental vs. hydrothermal vs. possibly meteoritic). Analyses were conducted using the laboratory and thermal ionization mass spectrometry facilities at the GeoIsotope Core Facility of the Department of Lithospheric Research at the University of Vienna and (for isotope dilution concentration measurements of selected HSEs) in cooperation with the mass spectrometry facilities at the Freie Universität Berlin.

The Tomka, as well as any other, BIF can only serve as a geochemical seawater archive if devoid of detrital contamination and pristine (i.e., devoid of diagenetic, metamorphic, and hydrothermal overprints). The Tomka BIF is a promising candidate to preserve primary seawater signatures, because it was only subjected to greenschist-facies metamorphism, whereas other old iron formations (e.g., Isua BIF) almost exclusively underwent higher grade metamorphism (Nutman et al. 2017; Jodder et al. 2023).

A comparison between literature data for immobile elements such as Zr, and fluid mobile elements, such as Sr (Bau & Möller, 1993; Kamber et al. 2004; Viehmann et al. 2015a, 2016), in combination with the $^{187}\text{Os}/^{188}\text{Os}$ ratios reported in this study for the Daitari BIF layers (chert-, magnetite- and mineralogically mixed layers) might indicate only minor syn- and postdepositional disturbances. Accordingly, most of the analyzed samples have a weak linear correlation in the $^{187}\text{Os}/^{188}\text{Os}$ vs. $^{187}\text{Re}/^{188}\text{Os}$ diagram and scatter around a ~ 3.5 Ga reference isochron. The $^{187}\text{Os}/^{188}\text{Os}$ ratios range from mantle-like values of ~ 0.14 to more radiogenic values up to ~ 0.41 (which is still significantly less radiogenic than the present-day upper continental crust with a value of ~ 1.4 ; Peucker-Ehrenbrink & Jahn 2001). Iridium

contents of the analyzed samples are exclusively crust-like at ~0.03 ppb, thus excluding any extraterrestrial component, while Os concentrations (mostly ranging between 0.1 and 0.3 ppb) can be as high as 1 ppb. More data, including Pt, Ru and Pd concentrations, will be presented at the conference.

- Bau M, Möller P (1993): Rare earth element systematics of the chemically precipitated component in early precambrian iron formations and the evolution of the terrestrial atmosphere-hydrosphere-lithosphere system. - *Geochim Cosmochim Acta* 57, 2239–2249, doi:10.1016/0016-7037(93)90566-F
- Jodder J, Hofmann A, Xie H, Elburg MA, Wilson A (2023): Geochronology of the Daitari Greenstone Belt, Singhbhum Craton, India. - *Precamb Res* 388, 106997, doi:10.1016/j.precamres.2023.106997
- Kamber BS, Bolhar R, Webb GE (2004): Geochemistry of late Archaean stromatolites from Zimbabwe: evidence for microbial life in restricted epicontinental seas. - *Precamb Res* 132, 379–399, doi:10.1016/j.precamres.2004.03.006
- Nutman AP, Bennett VC, Friend CRL (2017): Seeing through the magnetite: Reassessing Eoarchean atmosphere composition from Isua (Greenland) ≥ 3.7 Ga banded iron formations. - *Geosci Front* 8, 1233–1240, doi:10.1016/j.gsf.2017.02.008
- Peucker-Ehrenbrink B, Jahn B (2001): Rhenium-osmium isotope systematics and platinum group element concentrations: Loess and the upper continental crust. - *Geochem Geophys, Geosystems* 2, paper no. 2001GC0001172, 22pp, doi:10.1029/2001GC000172
- Prost T (2023): Direct radiometric dating of a Neoproterozoic iron formation – Rhenium-Os and highly siderophile element systematics of the Urucum Iron Formation, Brazil. - Master's thesis, Univ Vienna, 113 pp
- Schulz T, Viehmann S, Hezel DC, Koeberl C, Bau M (2021): Highly siderophile elements and coupled Fe-Os isotope signatures in the Temagami Iron Formation, Canada: Possible signatures of Neoproterozoic seawater chemistry and Earth's oxygenation history. - *Astrobiology* 21, 924–939, doi:10.1089/ast.2020.2311
- Viehmann S, Bau M, Böhn B, Dantas EL, Andrade FRD, Walde DHG (2016): Geochemical characterisation of Neoproterozoic marine habitats: Evidence from trace elements and Nd isotopes in the Urucum iron and manganese formations, Brazil. - *Precamb Res* 282, 74–96, doi:10.1016/j.precamres.2016.07.006
- Viehmann S, Bau M, Hoffmann JE, Münker C (2015a): Geochemistry of the Krivoy Rog Banded Iron Formation, Ukraine, and the impact of peak episodes of increased global magmatic activity on the trace element composition of Precambrian seawater. - *Precamb Res* 270, 165–180, doi:10.1016/j.precamres.2015.09.015
- Viehmann S, Bau M, Smith AJB, Beukes NJ, Dantas EL, Böhn B (2015b): The reliability of ~2.9 Ga old Witwatersrand banded iron formations (South Africa) as archives for Mesoarchean seawater: Evidence from REE and Nd isotope systematics: *J African Earth Sci* 111, 322–334, doi:10.1016/j.jafrearsci.2015.08.013.

Hydrogen induced changes in the mineralogical phase composition of downhole cements: fundamentals research within the context of Underground Hydrogen Storage

T. Sammer¹, K. Ravi², J. G. Raith¹

¹Chair of Resource Mineralogy, Montanuniversität Leoben

²Chair of Drilling and Completion Engineering, Montanuniversität Leoben
e-mail: thomas.sammer@unileoben.ac.at

Hydrogen is nowadays commonly considered a promising way of storing energy from renewable energy sources, hence increasing the efficiency of renewable energy sources. However, to store large volumes of hydrogen on a seasonal (e.g., winter – summer) time scale fast storage volumes are needed (Reitenbach et. al. 2015). Underground hydrogen storage (UHS, e.g., the idea of using natural geological reservoirs like depleted gas fields) promises exactly that. To make UHS a feasible process, fundamentals research investigating not just the integrity of reservoir and cap rocks, but also the interaction of hydrogen with downhole materials (e.g., cement) used in boreholes is essential. Boreholes provide access to geological reservoirs but are also the bottleneck of any production or storage operation. In general, boreholes are lined with downhole materials, consisting of a steel casing surrounded by cement. The cement acts as a bonding between the steel casing and the wallrock, providing mechanical stability and tightness for the hole. However, the effect that hydrogen might have on the mineralogical phase composition and subsequently on physical and mechanical parameters of downhole cement is still very scarcely known (Reitenbach et. al. 2015). This project, which is part of a PhD programme on H₂ production and storage at Montanuniversität Leoben, Austria aims to contribute to a better understanding of this issue.

The mineralogical phase composition of a cement class G, a standard type portland cement used in the petroleum industry, before and after hydrogen treatment was investigated and the influence was evaluated that potential reactions might have on the physical and mechanical properties.

The mineralogical methods applied were: XRD, FE-SEM, EPMA. Physical parameters such as porosity, pore size distribution and permeability were measured using Hg-porosimetry, N₂ sorption and nitrogen permeation, respectively. The mechanical properties were characterized by determining compressive and tensile strength. Additionally Young's modulus was determined from the stress-strain curves obtained during compressive strength testing.

Additionally, thermodynamic modelling using Gibbs Energy Minimization Software (GEMS) was carried out. The modelling indicates that certain redox-sensitive phases within hardened cement pastes are susceptible to hydrogen alteration caused by the strong reducing character of hydrogen. Especially ferric iron and sulphate bearing phases like brownmillerite, monosulfoaluminate (AFm) and ettringite (AFt) are altered, resulting in the formation of native iron, magnetite, and iron sulphides.

Partial melting of hornblende–epidote eclogite at the pressure maximum (eclogite type-locality, Eastern Alps, Austria)

S. Schorn¹, A. Rogowitz^{1,2}, C. Hauzenberger¹

¹*Institute of Earth Sciences, NAWI Graz Geocenter, University of Graz, Universitätsplatz 2, 8010 Graz, Austria*

²*Department of Geology, University of Vienna, Josef Holaubek-Platz 2, 1090 Vienna, Austria*

e-mail: simon.schorn@uni-graz.at

Pristine hornblende–epidote eclogite from within the eclogite type-locality (Hohl, Koralpe) of the Eastern Alps in Austria preserves cm-thick, concordant leucocratic segregations of coarse-grained euhedral hornblende–epidote–quartz and fine-grained disseminated garnet–omphacite–rutile. Petrographic- and mineral chemical data and phase diagram modelling are interpreted in terms of limited melting at or close to the well-established pressure maximum (21 ± 3 kbar and 680–740 °C) followed by melt crystallization near these conditions. Plagioclase \pm amphibole/ clinopyroxene films formed at sub-eclogite facies conditions from final melt vestiges. Natural variability in rock composition and bulk oxidation state leads to variable mineral modes and calculated high-pressure solidus temperatures for compositional endmembers sampled at Hohl. Oxidized conditions ($X_{\text{Fe}^{3+}} \sim 0.5$) favour hydrous but refractory amphibole–epidote-rich assemblages with a fluid-present solidus temperature of ~ 740 °C at 20 kbar, whereas more reduced rocks ($X_{\text{Fe}^{3+}} \sim 0.2$) are fertile ‘true’ eclogites (>70 vol. % garnet + omphacite) that commence melting at ~ 720 °C. The interlayering of such eclogites constitutes a fluid source–sink couple at appropriate (pressure–)temperature conditions, favouring fluid transfer from neighbouring dehydrating layers to melt-bearing ones down gradients in chemical potential of H₂O ($\mu_{\text{H}_2\text{O}}$). Moderate degrees of fluid-fluxed melting (<10 %) would not alter the peak assemblage provided the resulting melts are removed from the source rock. We suggest that eclogites with a comparable composition and metamorphic history are however unlikely to produce voluminous melts, thus not significantly contributing to adakite magmatism and crustal differentiation in collisional settings.

Thermoelastic properties and phase transition of natural pollucite

J. Schreuer¹, M. Münchhalfen¹, E. Hartman¹

¹*Ruhr-Universität Bochum, Institut für Geologie, Mineralogie und Geophysik,
Universitätsstraße 150, Bochum, 44801, Germany
e-mail: schreuer@rub.de*

Pollucite $(\text{Cs,Na})\text{AlSi}_2\text{O}_6 \cdot y\text{H}_2\text{O}$, a cesium-bearing zeolite belonging to the analcim group characterized by ANA topology of its tetrahedral framework, has long been considered to be a suitable material for use in fixation and deposition of radioactive Cs isotopes in high-level nuclear waste. Particularly favorable properties are the stability and low thermal expansion at high temperatures, the capability to host large amounts of Cs, and the low leaching rate of Cs. However, below about 500 K, the three-dimensional framework gradually changes from an "expanded form" to a "collapsed form" which is accompanied by a significant shrinkage of the unit cell volume without a change of symmetry (e.g., Kobayashi et al. 1997). Phase transformations from the cubic phase to a low-temperature tetragonal phase are also known (e.g., Kobayashi et al. 2006). Both processes can negatively affect the mechanical integrity of pollucite crystals and ceramics. The aim of our work is, therefore, to investigate the thermoelastic behavior of pollucite between 100 K and 673 K using dilatometry and resonant ultrasound spectroscopy.

The elastic properties of our pollucite samples at room temperature are in reasonable agreement with values reported by Sanchez-Valle et al. (2010). The temperature coefficients of the three independent elastic stiffnesses are uncharacteristically positive for stable materials. In the course of the framework "collapse", the longitudinal stiffness c_{11} and the shear resistance c_{44} soften between 673 K and 133 K by nearly 50% and 35%, respectively. At the same time, the deviations from the Cauchy-relations take on negative values, indicating the increasing importance of directional interactions.

Sanchez-Valle C, Chio C-H, Gatta, GD (2010): Single-crystal elastic properties of $(\text{Cs,Na})\text{AlSi}_2\text{O}_6 \cdot \text{H}_2\text{O}$ pollucite: A zeolite with potential use for long-term storage of Cs radioisotopes. - J Appl Phys 108, 093509

Kobayashi H, Yanase I, Mitamura T (1997): A new model for the pollucite thermal expansion mechanism. - J Am Ceram Soc 80, 2161-2164

Kobayashi H, Sumino S, Tamai S, Yanase I (2006): Phase transition and lattice thermal expansion of Cs-deficient pollucite, $\text{Cs}_{1-x}\text{Al}_{1-x}\text{Si}_{2+x}\text{O}_6$ ($x \leq 0.25$). - J Am Ceram Soc 89, 3157-3161

Chemical composition and crystal structure of oxy-dravite from the Beluga occurrence, Nunavut Territory, Canada

L. Skřápková¹, J. Cempírek¹

¹*Departement of Geological Sciences, Faculty of Science, Masaryk University, Kotlářská 2, 602 00 Brno
e-mail: lenka.skrapkova@gmail.com*

A new occurrence of oxy-dravite was found in a composition near its ideal end-member at the Beluga occurrence, Nunavut territory, Canada. Oxy-dravite belongs to the sodic group of the tourmaline supergroup with dominant ^WO, and commonly forms a solid solution with foitite, schorl, and oxy-schorl. Since its original description (Bosi & Skogby 2013) from the quartz-muscovite schist from Osarara (Narok district, Kenya), the mineral has been found at several localities worldwide, typically in metamorphic environments, and typically in solid solution with other species (Čopjaková et al. 2012; Cempírek et al. 2013; Pieczka et al. 2018).

The contribution provides new information about the occurrence, chemical composition, physical and structural properties of the oxy-dravite with a near-endmember composition from the Beluga occurrence. These data improve characterization of physical properties of oxy-dravite, allow examination of oxy-dravite solid solutions with respect to other species, improve the interpretation of Al–Mg disorder among the Y- and Z-sites, and discuss its petrogenetic importance.

The Beluga property is located in the southern part of Baffin Island, Nunavut territory, Canada. The locality is known largely due to the occurrence of sapphire-bearing calc-silicate pods. These pods are hosted in a shelf sequence of clastic rocks and carbonates along with garnet-bearing metasediments of the Lake Harbour Group, Trans-Hudson orogeny (St-Onge et al. 2007).

The tourmaline sample has a relatively homogenous composition, with only minor change from the crystal core to its rims. The X-site is predominantly occupied by Na (up to 0.91 apfu), its Ca content is low (max. 0.12 apfu) and vacancies are minimal. The octahedral Y-site is dominated by Al and Mg (2.77–2.81 apfu), Fe content is low (max. 0.18 apfu); Li content measured using LA-ICP-MS is negligible. The octahedral Z-site is similarly to Y-site also occupied by Al with minor Mg. The T-site is dominated by Si (up to 5.95 apfu), substituted by inconsiderable amount of Al. The V- and W-sites are characterised by high OH (2.92–3.00 apfu) and O contents (0.80–0.95 apfu), with minor F (0.12–0.17 apfu) only.

The crystal structure of the oxy-dravite sample was refined from single-crystal X-ray diffraction data. The refinements were performed using the SHELXTL crystallographic software package (Sheldrick 2008, 2015) of Bruker AXS. Scattering factors for neutral atoms were employed for the cations and ionic factors for O²⁻ were used for oxygen (Hovestreydt 1983). The structure of dravite after Foit and Rosenberg (1979) was introduced as an initial model for refinement that was processed (by refining occupancy of Na at X-site, and Mg Fe vs. Al at the Y and Z sites) to a final R index of ~ 1.45 % for an anisotropic displacement model. The H3-atom site was located in residual electron density maps whereas the H1 site was impossible to locate. The H3-site isotropic displacement parameter was constrained to be equal to 1.2 times of that of the O3-site. The distance of the H3 from the donor oxygen atom was not constrained, and the structure refinement provided O3–H3 = 0.949 Å. The mean bond-lengths of the individual sites are: <X–O> ~ 2.673 Å, <Y–O> ~ 1.999 Å, <Z–O> ~ 1.928 Å, <T–O> ~ 1.621 Å, and <B–O> ~ 1.375 Å.

The Beluga oxy-dravite has trigonal symmetry, space group $R3m$ with $a = 15.9121(2)$ Å, $c = 7.1788(10)$ Å, $V = 1574.12(5)$ Å³ and $Z = 3$. The crystal structure was refined to $R1 = 1.45$ using 1613 unique reflections. The oxy-dravite is optically uniaxial negative, with $\omega = 1.6453(5)$ and $\varepsilon = 1.6074(18)$ and strongly pleochroic – light yellowish-brown colour in the omega direction and colourless in the epsilon direction; its calculated density is 3.069 g.cm⁻³ with a compatibility index 0.016 (superior category).

The Beluga oxy-dravite, ideally $\text{Na}(\text{Al}_2\text{Mg})(\text{Al}_5\text{Mg})(\text{Si}_6\text{O}_{18})(\text{BO}_3)_3(\text{OH})_3(\text{O})$, has similarly to the holotype (Bosi & Skogby 2013) disorder between Y- and Z-site. However, the final form of Mg-disorder between the octahedral sites heads towards $(\text{Mg}_2\text{Al})(\text{Al}_6)$ rather than $(\text{Al}_2\text{Mg})(\text{Al}_5\text{Mg})$. This is the evidence that the oxy-dravite structure has more stable configurations and it is not necessary to divide Mg in ratio of 1:1 between the octahedral sites.

In comparison with other Mg-dominant end-members (oxy-dravite, dravite, fluor-dravite, uvite a Mg-foitite a Mg-lucchesiite), the Beluga oxy-dravite has lower density and comparable to lower values of refractive indexes ω and ε . Similarly, the Beluga oxy-dravite has lower unit cell volume and calculated density, the only exception is magnesiofoitite with the lowest values.

The main petrogenetic environments of oxy-dravites are aluminous metapelites and metapsammites, low-Ca ultramafics and (Cr,V)-rich metasediments (Pieczka et al. 2018). The oxy-dravite holotype was described by Bosi & Skogby (2013) from a quartz-muscovite schist in the Osarara locality. Čopjaková et al. (2012) found oxy-dravite in tourmalinites associated with mica-schist of the Krkonoše-Jizera Crystalline Massif, whereas Pieczka et al. (2018) reported a further occurrence of oxy-dravite from a quartz vein cutting granitic gneisses of the Kowary Unit. Oxy-dravite was also described by Ertl et al. (2003) from a primitive pegmatite vein cutting a gneiss of the Gföhl Unit. Oxy-dravite was also formed in amphibolite (Şek et al. 2022) or in the metaevaporite layers within dolomitic marbles (Krmíček et al. 2021). The Beluga oxy-dravite occurs in calc-silicate pods in association with dolomitic marbles (Belley et al. 2017); the necessary conditions for its crystallization (besides high B₂O₃ content) are increased content of Al and Na, and low content of F in the Mg-rich system.

- Belley PM, Dzikowski TJ, Fagan A, Cempírek J, Groat LA, Mortensen JK, Fayek M, Giuliani G, Fallick AE, Gertzbein P (2017): Origin of scapolite-hosted sapphire (corundum) near Kimmirut, Baffin Island, Nunavut, Canada. - *Can Mineral* 55, 669
- Bosi F, Skogby H (2013): Oxy-dravite, $\text{Na}(\text{Al}_2\text{Mg})(\text{Al}_5\text{Mg})(\text{Si}_6\text{O}_{18})(\text{BO}_3)_3(\text{OH})_3\text{O}$, a new mineral species of the tourmaline supergroup. - *Am Min* 98, 1442-1448
- Cempírek J, Houzar S, Novák M, Groat LA, Selway JB, Šrein V (2013): Crystal structure and compositional evolution of vanadium-rich oxy dravite from graphite quartzite at Bitovánky, Czech Republic. - *J Geosci* 58, 149-162
- Čopjaková R, Škoda R, Vašinová-Galiová M (2012): „Oxy-dravit“ z turmalinitů krkonošsko-jizerského krystalinika. - *Bulletin Min-Pet Odd NM Praha* 20, 37
- Ertl A, Hughes JM, Brandstätter F, Dyar MD, Prasad PSR (2003): Disordered Mg-bearing olenite from a granitic pegmatite at Goslarn, Austria: A chemical, structural, and infrared spectroscopic study. - *Can Mineral* 41, 1363-1370
- Foit FF, Rosenberg PE (1979): The structure of vanadium-bearing tourmaline and its implications regarding tourmaline solid solutions. - *Am Min* 64, 788-798
- Hovestreydt E (1983). On the atomic scattering factor for O²⁻. - *Acta Crystallogr* A39, 268-269
- Krmíček L, Novák M, Trumbull RB, Cempírek J, Houzar S (2021): Boron isotopic variations in tourmaline from metacarbonates and associated calc-silicate rocks from the Bohemian Massif: Constraints on boron recycling in the Variscan orogen. - *Geosci Front* 12, 219-230
- Pieczka A, Ertl A, Sek MP, Twardak D, Zelek S, Szeleg E, Giester G (2018): Oxy-dravite from Wolowa Góra Mountain, Karkonosze massif, SW Poland: Crystallochemical and structural studies. - *Mineral Mag* 82, 913-928

- Sęk MP, Włodek A, Stachowitz M, Woźniak K, Pieczka A (2022): Magnesio-lucchesiite from the Kowary vicinity, Karkonosze Mountains, SW Poland: the third occurrence worldwide. - *Mineral Mag* 87, 60-68
- Sheldrick GM (2008): A short history of SHELX. - *Acta Crystallogr A* 64, 112-122
- Sheldrick GM (2015): Crystal structure refinement with SHELXL. - *Acta Crystallogr C* 71, 3-8
- St-Onge MR, Wodicka N, Ijewliw O (2007): Polymetamorphic evolution of the Trans-Hudson Orogen, Baffin Island, Canada: Integration of petrological, structural, and geochronological data. - *J Petrol* 48, 271-302

Monazite fission-track dating of a heavy mineral sand, NE Sri Lanka

E. Skrzypek¹, S. Jones², B. Kohn², L. Chung², A. Gleadow²

¹*Institute of Earth Sciences, University of Graz*

²*School of Geography, Earth and Atmospheric Sciences, The University of Melbourne
e-mail: etienne.skrzypek@uni-graz.at*

Monazite fission-track (MFT) analysis appears to have potential for ultra-low temperature thermochronology. Recent experiments suggest that the nominal MFT closure temperature is ~25-45 °C (Jones et al., 2021). However, monazite commonly shows a wide range of compositions, so that it is crucial to assess the influence of compositional variations on fission-track systematics. For that, a MFT study of monazite grains from a heavy mineral beach sand (Polmuddai, NE Sri Lanka) was undertaken.

Electron microprobe analyses of 84 grains show significant variations in SiO₂ (0.12 - 2.63 wt.%), CaO (0.13 - 2.03 wt.%), ThO₂ (1.30 - 13.38 wt.%), UO₂ (0.07 - 1.28 wt.%) or Ce₂O₃ (23.94 - 34.31.03 wt.%). The analyses show that actinides were incorporated in monazite through the cheralite and/or huttonite substitutions. Eighty grains statistically define a main age population with a weighted mean Th-U-total Pb age of 502 ± 5 Ma (MSWD=1.3), while four other grains show older dates (ca. 1600 - 1900 Ma).

Spontaneous fission tracks were revealed by etching polished monazite mounts in a H₂O:HCl (1:1 by volume) solution at 90 °C. Due to the variability of monazite compositions, step-etching at five-minute intervals was performed to avoid under-/over-etching and limit surface damage. The majority of grains were well-etched after 10 - 15 minutes, whereas a few required up to 60 minutes. Fission tracks were manually counted using both reflected- and transmitted-light images.

The different monazite grains or domains yield individual MFT dates ranging from 3.90 to 0.25 Ma. It is recommended to use electron microprobe analyses to approximate the density of monazite domains, as it can noticeably influence the MFT age calculation. Only Si appears to show a fair correlation with MFT date, suggesting that higher Si content (SiO₂ = 1.5-2.0 wt.%) slows down FT annealing. This finding is supported by a tendency for Si-richer monazite grains to show longer confined track lengths (> 9 µm) than Si-poor ones (< 9 µm). A remaining question for further investigation is whether FT formation and annealing could also have an impact on U-Th dating of monazite, especially on radiogenic Pb loss.

Jones S, Gleadow A, Kohn B (2021): Thermal annealing of implanted ²⁵²Cf fission tracks in monazite: Geochronology 3, 89–102

Formation of reaction textures in aluminous paragneisses during near-isothermal exhumation

D. Sorger^{1,2}, C.A. Hauzenberger², F. Finger³, M. Linner⁴, E. Skrzypek², S. Schorn²

¹*Geoscience Center, Georg-August-University Göttingen, Goldschmidtstraße 1, Göttingen 37077, Germany*

²*NAWI Graz Geocenter, University of Graz, Universitätsplatz 2, Graz 8010, Austria*

³*Department of Geography and Geology, University of Salzburg, Hellbrunnerstraße 34, Salzburg 5020, Austria*

⁴*Department of Hard Rock Geology, Geological Survey of Austria, Neulinggasse 38, Vienna, 1030, Austria
e-mail: dominik.sorger@uni-goettingen.de*

Two different types of aluminous paragneiss found in the Loosdorf complex in NE Austria, were studied to investigate the post-peak history of the Gföhl unit in the southern Bohemian Massif. Both paragneiss types contain coarse-grained granulite assemblages and retrograde reaction textures. The peak metamorphic conditions, estimated using phase equilibrium modelling, indicate that the Loosdorf complex experienced metamorphism at 0.9-1.1 GPa and 780-820°C. The dominant mineral assemblage during this peak metamorphism includes garnet-biotite-sillimanite-plagioclase-K-feldspar-quartz-granitic melt ± kyanite ± ilmenite ± rutile.

The first type of paragneiss, called Ysper paragneiss, exhibits cordierite moats around garnet and cordierite-spinel or cordierite-quartz symplectites at former garnet-sillimanite interfaces. These textures suggest a post-peak near-isothermal decompression path reaching around 0.4 GPa. The second type, Pielach paragneiss, shows only intermittent cordierite coronae around garnet porphyroblasts and lacks symplectites. The presence of cordierite suggests near-isothermal decompression to 0.4-0.5 GPa and 750-800 °C. This relatively high-temperature decompression path is attributed to the simultaneous exhumation of a large high-pressure-ultrahigh-temperature (HP-UHT) granulite body.

The timing of regional metamorphism in the granulites and the southern Bohemian Massif is well constrained and peaked around 340 Ma. Monazite from the Loosdorf paragneiss samples yield a slightly younger age of approximately 335 Ma. Although these ages overlap within the error, they are interpreted as reflecting near-isothermal decompression and exhumation, which led to the formation of the observed reaction textures.

Tl-retention by jarosite-group minerals in technosoils from the central part of the Allchar deposit, North Macedonia

F. Stadler¹, T. Đorđević^{2,1}, A. Vaněk³, M. Mihaljevič⁴, T. Serafimovski⁵, G. Tasev⁵, I. Boev⁵, B. Boev⁵

¹*Institut für Mineralogie und Kristallographie, Universität Wien, Josef-Holaubek-Platz 2, 1090 Wien, Austria*

²*University Service Centre for TEM, Technische Universität Wien,*

Wiedner Hauptstraße 8-10, 1040 Vienna, Austria

³*Department of Soil Science and Soil Protection, Faculty of Agrobiological Sciences, Czech University of Life Sciences Prague, Kamýcká 129, 165 00, Prague 6, Czech Republic*

⁴*Institute of Geochemistry, Mineralogy and Mineral Resources, Faculty of Science, Charles University, Albertov 6, 128 43, Prague 2, Czech Republic*

⁵*Faculty of Natural Sciences, University "Goce Delčev"-Štip, Goce Delčev 89, 2000 Štip, North Macedonia
e-mail: stadlerfiona63@gmail.com*

Areas naturally enriched in thallium (Tl) represent a severe threat to surrounding ecosystems as the bioavailability of this highly toxic heavy metal strongly depends on its retention by the weathering-induced formation of secondary Tl-minerals. Estimations on the remediation potential of such areas therefore require a detailed mineralogical characterization of included Tl-bearing secondary minerals. This study focusses on the Allchar Sb-As-Tl-Au deposit in the southern part of North Macedonia, as its mineralogical composition is a rarity in the world. It contains remarkable concentrations of Tl, estimated to be around 1,000 tons of metal. In this study, stockpile material from abandoned, surface-exposed mining wastes and surrounding soils of the Sb-rich central part of the Allchar deposit was examined for the presence of secondary Tl-minerals. A combination of optical microscopy, powder X-ray diffraction (PXRD) and scanning electron microscopy with energy dispersive spectroscopy (SEM-EDS) was performed to determine the speciation of Tl in heavily weathered technosoils. The chemical composition of the soils measured by inductively coupled plasma mass spectrometry (ICP-MS) showed Tl-concentrations in the range of 480 to 4600 ppm. The main constituents of the examined samples could be identified as quartz, gypsum, sheet silicates, iron oxides and iron oxyhydroxides, followed by the presence of heavily weathered pyrite, marcasite and realgar, as well as traces of arsenopyrite and stibnite. Further weathering products comprise arsenates such as scorodite, alumopharmacosiderite, arseniosiderite, Ca-antimonates of the roméite-group, tripuhyite and sulfates of the jarosite group. Minor contents of Ce-monazite, apatite, zirkon, rutile, baryte, sphalerite and native gold could also be encountered. This paragenesis is suggesting acidic weathering conditions with pH-values ranging from 2-3. During weathering, dissolved Tl was mainly incorporated in an incomplete solid-solution between jarosite and dorallcharite with Tl concentrations up to 2.2 at%, which consequently represent the main host minerals of Tl. However, Tl could also be encountered in iron oxyhydroxides (up to 0.5 at%) and sheet silicates (up to 0.2 at%). Based on our results, Tl-jarosites are important secondary host phases for Tl in the central part of Allchar. Yet, the instability of jarosite at near-neutral pH conditions also characterizes it as a possible source of soluble Tl. Consequently, it is essential to further examine the role of jarosite-group minerals in Tl-retention under various environmental conditions.

This work was supported by the Austrian Science Fund (FWF) [grant number P 36828-N to T. Đorđević].

The "Schaudepot" for minerals and rocks of the Krauhuletz-Gesellschaft in Eggenburg, Lower Austria

F. F. Steininger¹, A. Rauscher²

¹Neue Gasse 7, 3730 Eggenburg, Austria

²Hofwiesenstrasse 46, 3511 Furth-Aigen, Austria

e-mail: Fritz.Steininger@senckenberg.de

The Krauhuletz-Gesellschaft in Eggenburg, Lower Austria, operates a local but internationally much noticed museum. The three-story main building in the city centre hosts the permanent exhibition accompanied by special presentations mostly with a regional focus which change regularly. The entire area in the north-western part of Lower Austria is noticeable rich in prehistoric and early history besides folklore. But not only remains from the early settlers can be found here. The region belongs to the Bohemian Massif with its very complex geological setting. The exhibits in the museum belonging to Earth's history range from mineralogy to geology and palaeontology. The collection is that large and the number of display items is still growing. Hence two further buildings were provided by the city of Eggenburg. They serve as depots for the extensive scientific collections:

Depot 1 is a former cinema (named "Lichtspielhaus") hosting the extensive paleontological collections. They focus on the many regional geological units (e.g., from the Carboniferous of Zöbing and the Lower Miocene of Eggenburg). Also prehistoric and early historical objects that cannot be shown in the main building are stored here. Worthy to note is the large library compiling Earth science topics besides descriptions of the flora and fauna of the area. It hosts a large collection of offprints, scientific journals, and geological maps. This depot is named in honour of the long-serving governor of Lower Austria "Dr. Erwin Pröll Study Collection".

Depot 2 is a two-storey building used earlier as the production site by a furniture factory, it is known as the "MöFa". It is, besides other objects, dedicated to Geosciences. It combines an exhibition of minerals, rocks, and some fossils from the area in showcases besides the storage of samples for scientific investigations in the future. As the area is heavily forested, outcrops are short-lived. Minerals and rocks originating from sites that will not be accessible without great effort in future (e.g., road constructions, building pits, progress in quarry mining) are preserved. These samples are maintained in the depot's racks. From these two purposes result the name "Schaudepot" that means "look and store".

On the ground floor of the building there is the new two-track exhibition and storage area for minerals and rocks. It includes five rooms with a total area of 183 m². In the entire collection are only mineral specimens and rock samples from the Austrian part of the Bohemian Massif - Waldviertel, the Dunkelsteiner Wald (located south of the Danube between Melk and Krems), and the Mühlviertel (located to the west and belongs already to Upper Austria). The samples were donated by finds and private donations from collectors of this area. So far, there are in total about 7,700 mineral specimens and about 1,500 rock samples stored. The exhibition area comprise five rooms that are briefly characterized here.

Showroom 1 (23 m², 5 showcases) exhibits minerals and rock from some quarries: Among them is Amstall (about 20 km west of Krems), a graphit deposit well known for reddish corundum or xenotime. It is the type locality for Amstallite (a rare Ca-Al-silicate). The Eibenstein quarry (close to the border to the Slovakia) is located in the "Bunte Serie"

(metamorphic rocks including biotite- and hornblende gneisses, amphibolites, calcisilicate rocks, marbles) and exhibits rarely pegmatite veins. The Loya quarry (a few steps north from the Danube and close to Ybbs-Persenbeug) is well known for wollastonite and thulite (a pink variety of zoisite). Pegmatite veins are located in the entire Waldviertel including the Southern Dunkelsteiner Wald and in the Western Mühlviertel. Famous mineral samples found in these pegmatites are smoky quartz (var. morion from Brunn near Fratres), opal (from Waldkirchen), or quartz (cutted samples from Langau).

Also some fossils from the Eggenburg area (Loibersdorf, Eggenburgian, Lower Miocene) are shown here; remarkable is a giant “Herzmuschel“ (Larvicardium kübecki).

Showroom 2 (10 m²) is dedicated to the large variety of rocks occurring in the Waldviertel. The rocks are stored on shelves and might be touched. Slices of Chalcedony and Garnet Pyroxenites are illuminated from the reverse; also these samples are from the Waldviertel.

The **Collection & showroom 3** (Fig. 1) is the largest room and captures nearly half of the entire area (80 m², 16 cabinets). To enable an easy access, samples are stored according to location in an alphabetical order (from Aggsbach-village to Zissersdorf). In one cabinet samples from the southern Lower Austria and the Mühlviertel are stored. Others contain a systematic collection of silicates from the Waldviertel, private collections were handed over in a grateful manner. In some show cases minerals of the Waldviertel are arranged according to their tectonic units. Series of quartz crystals (from Äpfelgschwendt, Loiwein, and Felling), pegmatite minerals (from Wanzenau, Horn, and the Königsalm), opals (from Waldkirchen) are on display.

Despite the large exhibition area, also the window niches are used to store large samples and a hardness scale according to Mohs and Rosiwal. Also a rock cleft is rebuilt.



Fig. 1 View to the main storage (room 3).

The relatively small display **Showroom 4** (10 m²) is dedicated exclusively to the Amethysts from the Waldviertel. Most of them are from Maissau, a small village about 10 km south of Eggenburg. A long time ago farmers when tilling the fields and mineral collectors became aware of Amethyst specimens often with an astonishing bright violet colour and sometimes large in size. The outcrop was excavated by the Krahuletz-Society in 1986 and 1988. The amethyst bearing quartz vein was rich in wonderful samples up to a size of some 0.2 m. Crystals (partly multiple zoned and exhibiting distinct varieties) are shown besides cut slices and polished specimens. Furthermore, finds from other localities in the Waldviertel are on display, among them are samples from Eggenburg, Grafenberg, Maigen, or Kautzen. Spectacular are amethyst sections in transmitted light. Two tubular showcases exhibit polished amethysts from Maissau and Eggenburg, respectively.



Fig. 2: The storage of minerals and rocks (room 5)

The collection **showroom 5** (**Fig. 2**) (60 m²) hosts mineral and rock samples from the Waldviertel that came from former scientific investigations or result from new finds during constructions of roads or other buildings. They are exclusively reserved for scientific investigations in future. The samples stored here reflect the variety of minerals and rocks that can be found in the entire area. The rocksamples range from plutonites to sediments and metamorphites. Cuttings and mineral samples are stored in a systematic order in pull-out cabinets and drawer units. Furthermore, a working area for microscopic investigations, a stone cutting device and a storage of reference literature can be found here.

Opening hours: every 1st Saturday a month (10 am to 4 pm). Information: www.krahuletzmuseum.at. Contact: A. Rauscher (+43 66473571480). Steininger (Fritz.Steininger@senckenberg)

Rauscher A, Steininger F (2023): Kurzfürer durch das Schaudapot für Mineralien und Gesteine der Krahuletz-Gesellschaft – 3730 Eggenburg, Museumsgasse 6. – Pub. Krahuletz-Ges. 2023/1: 29 S., 26 Abb., Raumplan, Verkehrsspinne.- Eggenburg (Krahuletz-Gesellschaft)

Inorganic crystal structure database

A. Steudel¹, S. Rühl¹, S. Rehme¹

¹FIZ Karlsruhe – Leibniz-Institute for Information Infrastructure,
Hermann-von-Helmholtz-Platz 1, 76344 Eggenstein-Leopoldshafen, Germany
e-mail: annett.steudel@fiz-karlsruhe.de

ICSD (Inorganic Crystal Structure Database) is the world's largest database for fully determined inorganic crystal structures. It is made available to the scientific community and industry by FIZ Karlsruhe. ICSD contains the crystallographic data of published crystalline inorganic structures, including atom coordinates, dating back to 1913. Organometallic and theoretical structures have been added within the past years. The ICSD data are of excellent quality. Only data that have passed thorough quality checks are included.

The ICSD database now contains more than 280,000 crystal structures. Around 12,000 new structures are added every year. Through our continuous quality assurance, existing content is modified, supplemented or duplicates removed. As a result, and by filling gaps from previous years, even the older content is not static.

Highlights of ICSD:

- All important crystal structure data are available, including unit cell, space group, complete atomic parameters, site occupation factors, Wyckoff sequence, molecular formula and weight, ANX formula, mineral group, etc.
- 80 % of the structures are allocated to about 10,000 structure types. This allows for searches for substance classes.
- Continuous selection and evaluation of theoretical structures. They can serve as a basis for developing new materials through data mining processes.
- Keywords to describe to physical and chemical properties are provided.
- Abstracts for a quick grasp of the article content are available.
- Simulation of Powder Diffraction Data

Last year the revision of the mineral names took place, which included a standardization of the mineral names. The standardization of the mineral names was done following the International Mineralogical Association (IMA) and this enabled us to link mineral entries to the two mineral databases "webmineral.com" and "mindat.org", so that further information about the minerals can be retrieved.

For a large part of the minerals, we have also included the hierarchical classification. This makes it easier to find minerals in the same hierarchical level (or below) and thus can also be used in teaching for improved understanding.

Since the last update of ICSD, topological information is included in the database for about half of the inorganic structures in ICSD. As a first step, this information can be used to search for the coordination of a central atom. This coordination can then also be represented visually. The topological data provide much more information which will be made available in future updates.

Crystal chemistry and structural transformations in Fe²⁺-bearing talc studied by Raman spectroscopy

L. Stoeck¹, S. Aspiotis^{1,2}, B. Mihailova¹

¹Department of Earth Sciences, University of Hamburg, Grindelallee 48, Hamburg, 20146, Germany

²Centre for the Study of Manuscript Cultures (CSMC), Cluster of Excellence 'Understanding Written Artefacts', University of Hamburg, Warburgstrasse 28, Hamburg, 20354, Germany
e-mail: lennard.stoeck@studium.uni-hamburg.de

High temperature behaviour of Fe²⁺-bearing hydrous silicates have recently gained much attention, because they are important reservoirs of water and can contribute into volatile cycling as well as into redox processes in the vicinity of subduction zones (Spandler et al. 2007; Bernardini et al. 2023), especially after the discovery of thermally induced reversible Fe²⁺ ↔ Fe³⁺ oxidation in Fe²⁺-bearing double-chain silicates, resulting in the activation of delocalized e⁻ and H⁺ with anisotropic mobility (Mihailova et al. 2021; Rösche et al. 2022). Therefore, Fe-bearing hydrous silicates with a strong anisotropic structure, such as amphiboles, can be an important factor to explain the occurrence of anisotropic conductivity anomalies in the lithosphere.

Talc (Mg₃Si₄O₁₀(OH)₂) is another rock-forming mineral with a highly anisotropic structure and significant implications in several fields, including petrology, geophysics and environmental science (Spandler et al. 2007). Besides talc is among the most important industrial minerals, because of its properties, such as chemical inertness, affinity for organic chemicals and hydrophobicity. These characteristics allow its use in several applications including paper coating, paint, cosmetics and polymer industries, for which the knowledge of the stability field of talc is critical (Ulian et al. 2014). So far temperature-induced changes in the structure and properties of talc have mostly been analyzed via X-ray diffraction, Fourier-transform infrared spectroscopy and thermogravimetry-differential scanning calorimetry (Liu et al. 2014).

In this contribution, we present (i) a new approach to quantify minor amounts of elements such as Fe and Mn in the octahedral sheets of talc using Raman spectroscopy (ii) results analyzing the temperature-induced changes in talc to gain further insight into the oxidation processes at high temperatures and structural transformations on an atomic level scale.

We analyzed a Fe²⁺-bearing sample from Zillertal in Austria, whose exact chemical formula (Mg_{2.93}Fe²⁺_{0.08}Ni_{0.01}Si_{4.04}OH_{1.81}O_{0.19}) was determined by electron microprobe analysis (Aspiotis et al., 2023). Spectra have been collected in two different sample orientations within the temperature range 150K-1400K in ranges from 15-1215cm⁻¹ and 3370-3770cm⁻¹.

We show that the Mg²⁺ (and Fe²⁺+ Mn²⁺) contents can be quantified by fractional intensities of the OH-stretching peaks assigned to various *M1M2M2* local configurations as well as by the wavenumber of the MO₆-vibrational mode near 360 cm⁻¹ (Aspiotis et al., 2023). Heating/cooling experiments demonstrate that the Raman peak at 3660cm⁻¹ associated with the OH-Fe²⁺MgMg stretching mode vanishes at 1250K but recovers when cooling down to room temperature. This clearly indicates the occurrence of reversible oxidation mechanisms at least at 1250K, and the existence of delocalized charge carriers (e⁻ and H⁺). Upon further heating up to 1400K talc undergoes a structural breakdown, decomposing into clinoenstatite

(Wesołowski, 1984). Therefore, we prove the existence of the “oxo-state” for talc between 1250K and 1400K, where Fe^{2+} is oxidized into Fe^{3+} , without a structural breakdown.

The trends for Fe^{2+} -bearing talc will be compared to pure-Mg talc, which is currently being analyzed by in situ-temperature Raman spectroscopy.

Acknowledgements: The research for this study was funded by the Deutsche Forschungsgemeinschaft (DFG, German Research Foundation) under Germany’s Excellence Strategy – EXC 2176 ‘Understanding Written Artefacts: Material, Interaction and Transmission in Manuscript Cultures’, project no. 390893796. The research was conducted within the scope of the Centre for the Study of Manuscript Cultures (CSMC) at Universität Hamburg. We thank Stefanie Heidrich and Peter Stutz, Universität Hamburg, to help with WD-EMPA measurements and sample preparation. We are very grateful to the Mineralogical Museum, Hamburg for kindly providing the talc crystals.

- Aspiotis S et al. (2023) Raman spectroscopy for crystallochemical analysis of Mg-rich layered silicates: serpentine and talc. - to be submitted to J Raman Spectr
- Bernardini S, Della Ventura G, Schlüter J, Mihailova B (2023): Thermally-activated electron hopping in Fe-rich amphiboles: Implications for the high-conductivity anomalies in subduction zones. - *Geochem* 83, 125942
- Liu X, Liu X, Hu Y (2014): Investigation of the thermal decomposition of talc. - *Clays Clay Miner* 62, 137-144
- Mihailova B, Della Ventura G, Waesermann N, Xu W, Schlüter J, Galdenzi F, Marcelli A, Redhammer GJ, Boiocchi M, Oberti R (2021): Atomistic insight into lithospheric conductivity revealed by phonon–electron excitations in hydrous iron-bearing silicates. - *Commun Mater* 2, 57
- Rösche C, Waesermann N, Petrova M, Malcherek T, Schlüter J, Mihailov B (2022): Oxidation processes and thermal stability of actinolite. - *Phys Chem Miner* 49, 47.
- Spandler C, Hermann J, Faure K, Mavrogenes JA, Arculus RL (2008): The importance of talc and chlorite “hybrid” rocks for volatile recycling through subduction zones; evidence from the high-pressure subduction mélange of New Caledonia. - *Contr Mineral Petrol* 155, 181-198
- Ulian G, Tosoni S, Valdrè CG (2014): The compressional behaviour and the mechanical properties of talc $[\text{Mg}_3\text{Si}_4\text{O}_{10}(\text{OH})_2]$: a density functional theory investigation. - *Phys Chem Miner* 41, 639-650
- Wesołowski M (1984): Thermal decomposition of talc: a review. - *Thermochim Acta* 78, 395-421

**Micromorphology meets micro-XRF:
A case study from the Iron Age site of Haselbach (Lower Austria)**

F. Stuffer¹, S. Cereda², P. Tropper¹, P. Trebsche²

¹University of Innsbruck, Institute of Mineralogy and Petrography, 6020 Innsbruck, Austria

²University of Innsbruck, Institute of Archaeologies, 6020 Innsbruck, Austria

e-mail: peter.tropper@uibk.ac.at

In the context of this investigation a chemical characterization of archaeological sediments from Haselbach (Lower Austria) was carried out on six uncovered thin sections by means of micro-XRF analysis. The elemental mapping was carried out with a Bruker M4 Tornado. The analysed thin sections were collected at the boundary between the loess substrate and the fill (cultural layer) of different structures: five come from pit houses and one from a pit. Samples were first examined with a polarization microscope and, subsequently, “objects” of interest were selected to clarify their chemical composition.

The results of the micro-XRF analysis show the exact spatial distribution of the detected elements in thin section: aluminum (Al_2O_3), silicon (SiO_2), magnesium (MgO), calcium (CaO), iron (FeO), phosphorus (P_2O_5), potassium (K_2O), titanium (TiO_2), sulfur (SO_3), and manganese (MnO). False colour maps were also produced to enhance the relative concentration of the aforementioned elements. Furthermore, the objects found in the thin sections could be quickly identified, by combining their morphological characteristics with their elemental composition. They consist of: bone and pottery fragments, aggregates of trampled debris, charcoal, faecal remains, ashes and different types of pedofeatures.

Thanks to the elemental analysis it was also possible to determine that, in all six thin sections, the in-situ loess is mainly composed of the elements Al, Fe, K, Mn, Si, and Ti, while the fill deposits show increasing contents of the elements Ca, P and S. Both microscopic and chemical results show that organic matter occurs in the cultural layer, indicating the influence of humans and animals in the formation of these deposits. The loessy substrate, on the other hand, has remained largely untouched by human and animal activity. Specific archaeological questions, such as the actual use of the pit houses and the pit, could not be answered on the basis of these results alone. Further analyses (i.e., micromorphological and archaeological) are thus required for a comprehensive understanding of these built features.

In-situ $^{40}\text{Ar}/^{39}\text{Ar}$ dating of phenocrysts in the phonolite from Late Quaternary East Eifel Olbrück volcano

M. Sudo¹, U. Altenberger¹, C. Günter¹

¹University of Potsdam, Institute of Geosciences, Potsdam, Germany
e-mail: msudo@geo.uni-potsdam.de

Since 2002, University of Potsdam has started the $^{40}\text{Ar}/^{39}\text{Ar}$ dating laboratory with a CO_2 continuous laser and a pulsed Nd-YAG UV laser, then the in-situ $^{40}\text{Ar}/^{39}\text{Ar}$ dating has been applied to metamorphic rocks with 400-10 Ma ages. However, it was not well known to what extent in-situ $^{40}\text{Ar}/^{39}\text{Ar}$ dating was available to younger samples. In order to investigate the applicability of $^{40}\text{Ar}/^{39}\text{Ar}$ dating to very young samples, we used phonolite from Olbrück volcano, a late Quaternary monogenetic volcano group in the East Eifel, where Lippolt et al. (1990) had reported the presence of excess ^{40}Ar in nosean or hauyne in the phonolites. Sudo et al. (2014) reported for Ar isotopic ratio measurements on natural samples and also preliminary dating results of the first $^{40}\text{Ar}/^{39}\text{Ar}$ dating including assumptions, because the analyses were done more than one year after the neutron irradiation. Since then, three more neutron irradiations and $^{40}\text{Ar}/^{39}\text{Ar}$ dating have been done so far, then those results of the $^{40}\text{Ar}/^{39}\text{Ar}$ dating have been accumulated and are reported here.

For the samples for Ar isotope analyses, thick rock sections with a thickness of about 0.5 mm and a long diameter of up to 12 mm were prepared, then their surfaces were examined in detail by SEM-EDS. Then they are irradiated with fast neutrons for 4 h at the CLICIT facility of the OSTR nuclear reactor at the University of Oregon, USA. In-situ spot analysis of the sample surfaces was then carried out at the University of Potsdam using a UV pulse laser at a wavelength of 266 nm to determine the Ar isotope ratios. In most cases, one spot did not yield enough gas for targets of sanidine, leucite, nosean or groundmass parts, and in the case of nosean, up to 5-6 spots of 200 microns diameter laser irradiation was conducted for a single measurement.

The results of the dating by weighted averaged when they agree within error, as follows; sanidine: 0.42 ± 0.29 Ma (N = 3, error 1sigma), leucite: 0.08 ± 0.16 Ma (N = 3), groundmass 0.71 ± 0.17 Ma (N = 2). These ages agree with the Ar/Ar age of 0.41 ± 0.01 Ma by Lippolt within 2 sigma error from sanidine and leucite. In contrast, the nosean, in which the excess ^{40}Ar has been reported, yielded two results, done in two separate irradiations, as 3.14 ± 0.45 Ma (N = 8), 31.06 ± 4.1 Ma (N = 5) and one outlier 154.5 ± 11.2 Ma. The nosean ages by Lippolt et al. (1990) were 11.2-12.2 Ma, suggesting that the excess ^{40}Ar in nosean is heterogeneously distributed. Sudo et al. (2014) reported the existence of melt inclusions in the nosean and the concentration of Cl in them. This time the correlation was also observed between the excess ^{40}Ar and Cl-derived ^{38}Ar in nosean.

Lippolt HJ, Troesch M, Hess JC (1990): Excess argon and dating of Quaternary Eifel volcanism, IV. Common argon with high and lower-than atmospheric $^{40}\text{Ar}/^{36}\text{Ar}$ ratios in phonolitic rocks, East Eifel, F.R.G. - Earth Planet Sci Lett 101, 19-33

Sudo M, Altenberger U, Günter C (2014): In-situ Ar isotope, $^{40}\text{Ar}/^{39}\text{Ar}$ analysis and mineral chemistry of nosean in the phonolite from Olbrück volcano, East Eifel volcanic field, Germany: Implication for the source of excess ^{40}Ar . – Geophysical Research Abstracts, EGU General Assembly 2014

Digital Microscopy Solutions: Practical Analysis for different applications

A.R. Szalai¹

¹KEYENCE VHX 7000
e-mail: r.szalai@keyence.eu

Due to the high depth of field and depth composition, the system offers fully sharp images within seconds. With tilting and rotating stage, it is possible to inspect the crystals in all angles, giving the user an all-around view of the sample. The 4K resolution provides high quality for a detailed analysis. Keyence VHX lenses can be used with all lightning options such as brightfield, darkfield, transmitted light, diffuser, polarisation, DIC, mix light, and shadow effect mode for the surface analysis. Intuitive software design and a steering console secure comfortable usability for the operator, which makes an experience to microscope.

Next to 2D and 3D measurement, profile- and area measurement are available for perform analysis. Automatic report functions shorten the process of documentation.

Unravelling the true nature of Martian ‘lh’-kieserite

D. Talla¹, M. Wildner¹

¹*Institut für Mineralogie und Kristallographie, Josef-Holaubek-Platz 2, 1090 Wien, Österreich
e-mail: dominik.talla@univie.ac.at*

The confirmed presence of hydrous sulfates on celestial bodies in our solar system such as Mars or the icy moons of Jupiter and Saturn has been a hotly debated topic for several decades (recently e.g., Clark et al. 2005; Bishop et al. 2009; Noel et al. 2010). Especially Mg-sulfate hydrates, with the ability to change their hydration state based on local humidity and temperature, are regarded as one of the key components governing the water budget at equatorial latitudes on Mars (Milliken et al. 2007).

Furthermore, these and other sulfate compounds are supposed to play an important role on the icy moons of Jupiter and Saturn, where their presence, possibly along with pressure-induced structural changes (e.g., Meusburger et al. 2020), influences thermodynamic equilibria leading to the presence of subsurface oceans, potentially even supporting life (Solomonidou et al. 2009).

Especially kieserite, $\text{MgSO}_4 \cdot \text{H}_2\text{O}$, given its broad field of stability compared to the other hydrates, is also believed to form on the surface of the icy moons via decomposition of higher Mg-sulfate hydrates by cosmic rays and UV radiation, with the stability of the sulfate monohydrate strongly enhanced by the surrounding vacuum (Zolotov & Shock 2001).

A still unsolved enigma is the structural and spectroscopic character of the so-called ‘lh’-kieserite polytype (where ‘lh’ stands for ‘low-humidity’), which, according to dehydration experiments under simulated Martian conditions performed by Wang et al. (2009), is presumed to be the dominant variant of monoclinic kieserite on the surface of Mars. Until now, however, no thorough investigation of this new ‘polytype’ has been conducted.

Comparing the powder patterns of ‘lh’-kieserite as documented by Wang et al. (2009) to other sulfate species, we observed a striking resemblance between this enigmatic compound and the tetragonal Mg-hydroxide sulfate hydrate (‘MHSH’) mineral caminite. To date, the latter was found on Earth in an entirely different environment compared to that on the surface of Mars – namely in black smokers on oceanic rift zones, reflecting its experimentally confirmed reverse solubility (e.g., Hochella et al. 1983). An entire range of such MHSH compounds is anticipated, where the cell metrics are dictated by variable occupancy of the Mg and H sites.

Taking the reverse solubility of the MHSH mineral group into account, we designed a novel autoclave prototype, allowing venting of the aqueous solvent at maximum temperature, preventing re-dissolution of the high-temperature phase assemblage upon cooling. Indeed, we were already able to synthesize several representatives of the said tetragonal compounds as single crystals with the expected variability in the Mg- and H-site occupancy, proving the existence of an (at least partial) MHSH solid solution series, with tetragonal ‘MHS’ (Mg-hydroxide sulfate, $c = 12.885 \text{ \AA}$; Fleet & Knipe 1997) and monoclinic kieserite ($2d_{001} = 13.499 \text{ \AA}$; Bechtold & Wildner 2016) as theoretical endmembers. As the Mg-site occupancy decreases in favour of the H content, the tetragonal c -lattice parameter lengthens, conversely to the a axis.

The comparison of powder patterns of 'lh'-kieserite and MSHH shown in Fig. 1 (using CuK α radiation) is quite conclusive: the prominent reflection doublet at 26.5 and 28° 2 θ , along with the characteristic pair at ~55° 2 θ present in both phases, strongly indicates that both compounds are indeed one and the same substance.

This leaves the question as to why the MSHH group has not been previously considered as 'lh'-kieserite. Firstly, naturally occurring minerals belonging to this series are scarce, with only the aforementioned caminite found in nature to date. Secondly, both IR and Raman spectra of kieserite and MSHH bear striking resemblance (Fig. 2), making a spectroscopic discrimination rather ambiguous, more so taking into account the limited signal-to-noise ratio of remote measurements from orbiter instruments.

Our contribution aims to corroborate the existence and properties of the MSHH mineral group, which seems, in light of the newest findings, to represent an important constituent of sulfate assemblages present on celestial bodies in our solar system.

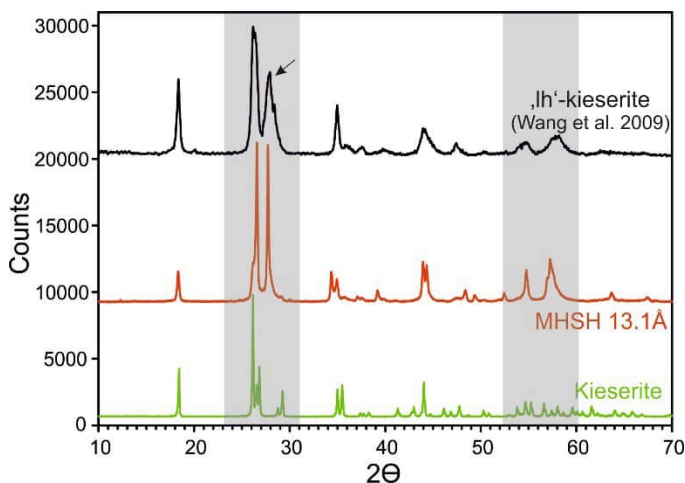


Figure 1. Comparison of the powder pattern of 'lh'-kieserite, MSHH and kieserite. Note the close match between Bragg reflections in 'lh'-kieserite and the MSHH variant with the *c*-cell parameter equal to 13.1 Å (highlighted in grey).

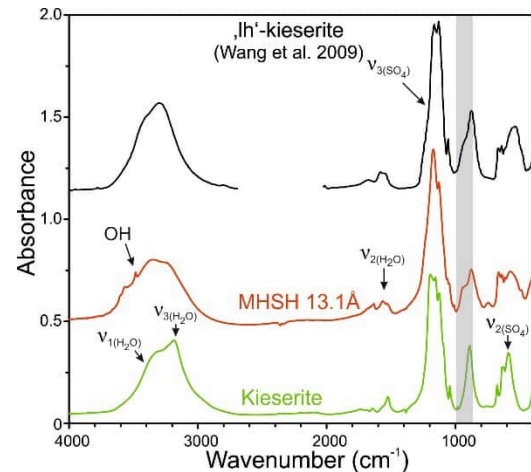


Figure 2. Close resemblance between IR spectra of 'lh'-kieserite, MSHH and kieserite. Apart from a shoulder at ~950 cm⁻¹, diagnostic for MSHH, the spectral envelopes are quite similar.

We gratefully acknowledge financial support of this work by the FWF grant-in-aid P34227-N.

Bechtold A, Wildner M (2016): Crystal chemistry of the kieserite–cobaltkieserite solid solution, Mg_{1-x}Co_x(SO₄)·H₂O: well behaved oddities. - Eur J Miner 28, 43-52

Bishop JL, Parente M, Weitz CM, Noe Dobrea EZ, Roach LH, Murchie LS, McGuire PC, McKeown NK, Rossi CM, Brown AJ, Calvin WM, Milliken R, Mustard JF(2009): Mineralogy of Juventae Chasma: Sulfates in the light-toned mounds, mafic minerals in the bedrock, and hydrated silica and hydroxylated ferric sulfate on the plateau. - J Geophys Res 114, E00D09

Clark BC, Morris RV, McLennan SM, Gellert R, Jolliff B, Knoll AH, Squyres SW, Lowenstein TK, Ming DW, Tosca NJ, Yen A, Christensen PR, Gorevan S, Brückner J, Calvin W, Dreibus G, Farrand W, Klingelhofer G, Waenke H, Zipfel J, Bell III JF, Grotzinger J, McSween, HY, Rieder R (2005): Chemistry and mineralogy of outcrops at Meridiani Planum. - Earth Planet Sci Lett 240, 73-94

Fleet ME, Knipe SW (1997): Structure of magnesium hydroxide sulfate, [2MgSO₄·Mg(OH)₂] and solid solution in magnesium hydroxide sulfate hydrate and caminite. - Acta Cryst B53, 358-363

- Hochella MF, Keefer KD, deJong BHWS (1983): The crystal chemistry of a naturally occurring magnesium hydroxide sulfate hydrate, a precipitate of heated seawater. - *Geochim Cosmochim Acta* 47, 2053-2058
- Meusburger JM, Ende M, Matzinger P, Talla D, Miletich R, Wildner M (2020): Polymorphism of monohydrate sulfate kieserite under pressure and its occurrence on giant icy Jovian satellites. - *Icarus* 336, 113459
- Milliken RE, Mustard JF, Poulet F, Jouglet D, Bibring J-P, Gondet B, Langevin Y (2007): Hydration state of the Martian surface as seen by Mars Express OMEGA: 2. H₂O content of the surface. - *J Geophys Res* 112, E08S07
- Noel A, Bishop JL, Al-Samir M, Gross C, Flahaut J, McGuire PC, Weitz CM, Seelos F, Murchie S (2015): Mineralogy, morphology and stratigraphy of the light-toned interior layered deposits at Juventae Chasma. - *Icarus* 251, 315-331
- Solomonidou A, Coustenis A, Bampasidis G, Kyriakopoulos K, Moussas X, Bratsolis E, Hirtzig M (2011): Water oceans of Europa and other moons: implications for life in other solar systems. - *J Cosmol* 13, 4191-4211
- Wang A, Freeman JJ, Jolliff BL (2009): Phase transition pathways of the hydrates of magnesium sulfate in the temperature range 50°C to 5°C: Implication for sulfates on Mars. - *J Geophys Res* 114, E04010
- Zolotov MY, Shock EL (2001): Composition and stability of salts on the surface of Europa and their oceanic origin. - *J Geophys Res* 106, 32815-32827

An extensible, open, and web-based research environment to understand geochemical data

T. Tamanna¹, D.C. Hezel¹

*Institute of Geosciences, Goethe University, Frankfurt, Altenhöferallee 1, 60438 Frankfurt am Main, Germany
e-mail: tamanna@uni-frankfurt.de*

Introduction: The application of Data Science in Geochemistry and Cosmochemistry is becoming increasingly important and relevant to handle and work with the exponentially growing number of geo- and cosmochemical data over the last few decades. Exploring large databases provides the opportunity to research huge datasets to better understand the Earth's dynamics (Jiao et al. 2018). In the last 20-30 years, geochemical data and standards have been collected in databases such as GeoROC, EarthChem, MetBase, or AusGeochem.

The objective of this project is to create methods to work with databases such as, organising and cleaning of data, visualising data on different kinds of plots, statistical analyses of the geochemical data, detection and checking the influence of outliers, integrate these with existing tools such as pyrolite, IsoplotR, GeoPyTool and implement these tools in a modular, open, and web-based research environment. The overall goal is to combine geochemical data and software, which will enable new routes of research and possibly a new area of original scientific discoveries (Ma 2023).

Methods: The web application was developed using python and deployed through streamlit. The python source codes are publicly available on GitHub.

Results and Discussion: We developed a web page with which geochemical database data can be visualized on a map or various types of plots such as scatter plots (bivariate plots), category plots which show the normalised concentrations with respect to e.g., chondrite, or primitive mantle versus a list of user-defined elements and ternary plots. For this we used GEOROC data as an example. The entire database was initially organized by choosing a subset of required elements needed to complete the various web application components. The nan values were replaced by 0 and the columns with no information were dropped. Boxplots were used to identify the outliers. Those outliers, which might be a result of typing errors, were dropped.

Jiao et al. (2018): Progress and challenges of big data research on petrology and geochemistry. - Solid Earth Sci 3, 105-114

Ma X (2023): Data science for geoscience: Recent progress and future trends from the perspective of a data life cycle. - Geol Soc Amer, Special Paper 558



You are cordially invited to attend

MinWien2023

17 to 21 September 2023

A joint meeting of the three Mineralogical Societies



Topics: Mineralogical, Petrological,
Geochemical Sciences, deposits &
related disciplines
(basic, applied & industrial topics)

Programme

Sunday, 17 September 2023

Mineralogy for the public

Young Scientists meet each other

Opening Ceremony

After Party

Pre-conference

Male K...

16-17 S...

Guides: P. Bačik I. Bros...

Abstracts, A - G

Thursday,

September 2023

Scientific sessions

Poster presentations

Industrial exhibition

Conference dinner

Wednesday 20 September 2023

Festival Hall, Vienna's City Hall

Half-day tours

18-21 September, 2023

Poster Prizes for young scientists

DMG - General Assembly

Public lecture



Conference Site: Alma Mater Rudolphina - University of Vienna
Geozentrum - UZAI, Josef-Holaubek-Platz 2, 1090 Vienna

Organisation: Institut für Mineralogie und Kristallographie

Further information: <https://minwien2023.univie.ac.at>

e-mail: minwien2023.mineralogie@univie.ac.at



You are cordially invited to attend

MinWien2023

17 to 21 September 2023

A joint meeting of the three Mineralogical Societies



Topics: Mineralogical, Petrological,
Geochemical Sciences, deposits &
related disciplines
(basic, applied & industrial topics)

Programme

Sunday, 17 September 2023

Mineralogy for the public

Young Scientists meet each other

Opening Ceremony

Together Party

Pre-conference

Male K...

16-17 S...

Guides: P. Bačik I. Bros...

Abstracts, H - N

Thursday,

September 2023

Scientific sessions

Poster presentations

Industrial exhibition

Conference dinner

Wednesday 20 September 2023

Festival Hall, Vienna's City Hall

Half-day tours

18-21 September, 2023

Poster Prizes for young scientists

DMG - General Assembly

Public lecture



Conference Site: Alma Mater Rudolphina - University of Vienna

Geozentrum - UZAI, Josef-Holaubek-Platz 2, 1090 Vienna

Organisation: Institut für Mineralogie und Kristallographie

Further information: <https://minwien2023.univie.ac.at>

e-mail: minwien2023.mineralogie@univie.ac.at



You are cordially invited to attend

MinWien2023

17 to 21 September 2023

A joint meeting of the three Mineralogical Societies



Topics: Mineralogical, Petrological,
Geochemical Sciences, deposits &
related disciplines
(basic, applied & industrial topics)

Programme

Sunday, 17 September 2023

Mineralogy for the public

Young Scientists meet each other

Opening Ceremony

After Party

Pre-conference

Male K...

16-17 S...

Guides: P. Bačík I. Bros...

Abstracts, O - Sch

Thursday,

September 2023

Scientific sessions

Poster presentations

Industrial exhibition

Conference dinner

Wednesday 20 September 2023

Festival Hall, Vienna's City Hall

Half-day tours

18-21 September, 2023

Poster Prizes for young scientists

DMG - General Assembly

Public lecture



Conference Site: Alma Mater Rudolphina - University of Vienna

Geozentrum - UZAI, Josef-Holaubek-Platz 2, 1090 Vienna

Organisation: Institut für Mineralogie und Kristallographie

Further information: <https://minwien2023.univie.ac.at>

e-mail: minwien2023.mineralogie@univie.ac.at



You are cordially invited to attend

MinWien2023

17 to 21 September 2023

A joint meeting of the three Mineralogical Societies



Topics: Mineralogical, Petrological,
Geochemical Sciences, deposits &
related disciplines
(basic, applied & industrial topics)

Programme

Sunday, 17 September 2023

Mineralogy for the public

Young Scientists meet each other

Opening Ceremony

After Party

Pre-conference

Male K...

16-17 S...

Guides: P. Bačík I. Bros...

Abstracts, Sci - Z

Thursday,

September 2023

Scientific sessions

Poster presentations

Industrial exhibition

Conference dinner

Wednesday 20 September 2023

Festival Hall, Vienna's City Hall

Half-day tours

18-21 September, 2023

Poster Prizes for young scientists

DMG - General Assembly

Public lecture



Conference Site: Alma Mater Rudolphina - University of Vienna
Geozentrum - UZAI, Josef-Holaubek-Platz 2, 1090 Vienna

Organisation: Institut für Mineralogie und Kristallographie

Further information: <https://minwien2023.univie.ac.at>

e-mail: minwien2023.mineralogie@univie.ac.at

Defect adamantines: potential materials for photovoltaic applications

Y. Tomm¹, G. Gurieva¹, D. M. Többens¹, S. Schorr^{1,2}

¹Helmholtz-Zentrum Berlin für Materialien und Energie

²Institute of Geological Sciences, Freie Universität Berlin

e-mail: susan.schorr@helmholtz-berlin.de

Compounds of the Adamantine family includes kesterite ($\text{Cu}_2\text{ZnSnS}_4$), currently the most promising material for fully inorganic thin film photovoltaic technology that is free of critical raw-materials and thus provides sustainable solutions.

Ternary adamantines like the chalcopyrites can be transferred by chemical substitution to a quaternary adamantine such as $\text{A}^{\text{I}}_2\text{B}^{\text{II}}\text{C}^{\text{IV}}\text{X}^{\text{VI}}_4$ (e.g., $\text{Cu}_2\text{ZnSnS}_4$) and $\text{A}^{\text{I}}\square\text{B}^{\text{III}}\text{C}^{\text{IV}}\text{X}^{\text{VI}}_4$ compounds, the latter are called defect adamantines (Pamplin 1981).

Defect adamantines like $\text{Cu}\square\text{GaGeS}_4$ and $\text{Cu}\square\text{GaSnS}_4$ can be seen as a compound within the solid solution between gallite – radvaniceite (Sejkora et al. 2022), $(\text{CuGaS}_2)_{1-x}(\text{GeS}_2)_x$ and gallite – berndtite $(\text{CuGaS}_2)_{1-x}(\text{SnS}_2)_x$, at $x = 0.5$, respectively.

Single crystals of these defect adamantines were grown by chemical vapor transport using iodine as transport agent. Aiming for chemical compositions according to the defect adamantine, chemical analysis of the grown crystals by X-ray fluorescence (XRF) has shown, that crystals in the system $(\text{CuGaS}_2)_{1-x}(\text{GeS}_2)_x$ show $\text{Cu}/(\text{Ga}+\text{Ge})$ ratios between 0.45 and 0.9 as well as $\text{Ge}/(\text{Ga}+\text{Ge})$ ratios between 0.15 and 0.6. Thus the single crystals show a quite strong deviation from the stoichiometric composition ($\text{Cu}/(\text{Ga}+\text{Ge}) = \text{Ge}/(\text{Ga}+\text{Ge}) = 0.5$). We explain this behavior by the flexibility of the crystal structure of the end members and the defect adamantine. Their crystal structures are based on a corner-sharing network of tetrahedra (CuS_4 , GaS_4 , GeS_4 or $\square\text{S}_4$). By multiple energy anomalous synchrotron X-ray diffraction (MEAD) it was shown, that $\text{Cu}\square\text{GaGeS}_4$ crystallizes in the tetragonal chalcopyrite-type structure. It compares to the crystal structure of gallite, but with a higher fraction of vacancies.

The single crystals grown aiming for $\text{Cu}\square\text{GaSnS}_4$ adopt the chalcopyrite-type structure and the $\text{Cu}/(\text{Ga}+\text{Sn})$ values are close to 1. Thus there is only a very limited solubility in the $(\text{CuGaS}_2)_{1-x}(\text{SnS}_2)_x$ system. Berndtit (SnS_2) crystallizes in a trigonal structure type where the Sn^{4+} cations are coordinated by 8 sulfur anions. The very limited solubility between Gallite and Berndtite may be explained by the different coordination of the four-valent cation.

The band gap energy (determined by UV-Vis spectroscopy) of the mixed crystals in the $(\text{CuGaS}_2)_{1-x}(\text{GeS}_2)_x$ system cover a range of 2.1 to 2.4 eV, showing a strong bowing behavior in the dependency on the chemical composition parameter x . The crystals obtained in the system $(\text{CuGaS}_2)_{1-x}(\text{SnS}_2)_x$ have band gap energies within 1.7 and 2.0 eV. Thus, such defect adamantines are interesting materials for photovoltaic applications.



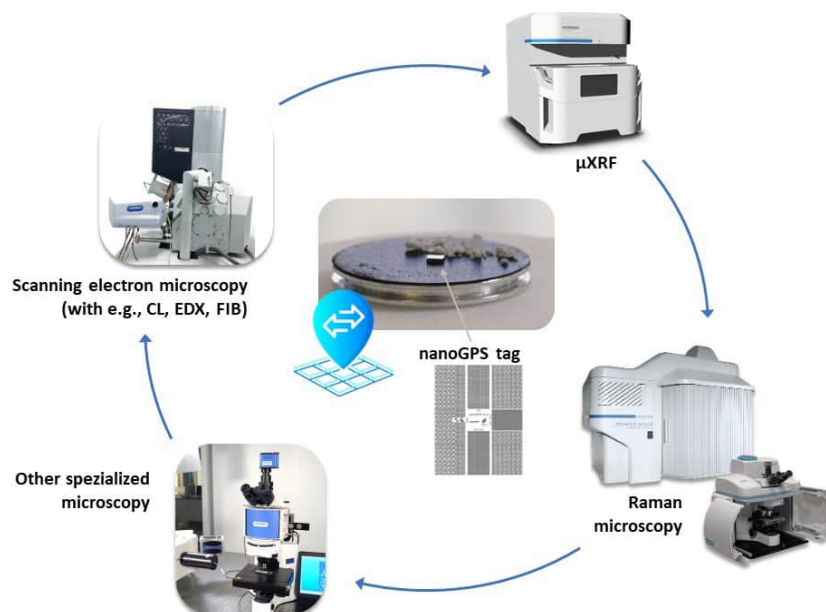
Figure 1. Single crystals of off-stoichiometric $\text{Cu}\square\text{GaGeS}_4$ (left) and $\text{Cu}\square\text{GaSnS}_4$ (right).

nanoGPS navYX™ – HORIBAs collaborative and inter-instrumental solution for correlative microscopy

M. Trapp¹, C. Lenz¹

¹HORIBA Jobin Yvon GmbH, Oberursel, Germany
e-mail: christoph.lenz@horiba.com

A comprehensive characterization of geological or mineralogical samples requires the application of more than one method to combine their complementary strengths. For example, the synergetic combination of μ -XRF (or SEM-EDX) with Raman microscopy provides information on both, the element composition as well as phase and structural properties of a specimen. However, relocation of points of interest (POI) on a μ m-scale is one of the most tedious and time-consuming issue if the specimen is transferred between various instruments, especially if the imaging technique strongly differs (e.g., SEM vs. light microscopic image). Here, we present HORIBAs nanoGPS navYX™ technology that provides a unique solution to this problem and is independent from the respective instrument or manufacturer (Acher et al. 2021). Typical requirements to successfully apply this technique include the option for microscopic sample imaging or visualization (min. 2x to 5x magnification) and software-controlled, motorized sample stage positioning. Nearly all types of microscopy techniques, such as SEM, μ -XRF, AFM, Raman or light microscopy, hence, may be correlated using nanoGPS navYX™. To do so, a small relocation tag with a patented reading pattern is attached to the sample. This tag defines a virtual coordination system that is read by the dedicated navYX™ software and saves all points and measurement sites of interest. On every calibrated instrument, the saved POIs may be easily relocated independently of sample positioning or rotation via direct conversion of the virtual nanoGPS coordinates into the instrument's stage coordinates.



Acher O, Nguyễn T L, Podzorov A, Leroy M., Carles P A, Legendre S (2021): An efficient solution for correlative microscopy and co-localized observations based on multiscale multimodal machine-readable nanoGPS tags. - Meas Sci Technol 32(4) 045402

Visible and invisible complexities in rocks: mineralogical and petrological constraints on the Variscan metamorphic gradient in the Southalpine metamorphic basement (Brixen quartzphyllites)

P. Tropper¹, T. Klotz², A. Wzietek¹, H. Pomella²

¹University of Innsbruck, Institute of Mineralogy and Petrography, 6020 Innsbruck, Austria

²University of Innsbruck, Institute of Geology, 6020 Innsbruck, Austria

e-mail: peter.tropper@uibk.ac.at

The basement of the Southern Alps is represented by the Brixner Quartzphyllite whose Variscan *P-T* conditions correspond to a greenschist-facies metamorphic overprint. This metamorphic basement shows a metamorphic gradient ranging from the lower greenschist-facies in the S to the amphibolite-facies in the N. This metamorphic gradient reached peak metamorphic conditions in the Brixen area and decreases in a southern direction. Due to the emplacement of Permian intrusions into this basement, locally a Permian contact metamorphic overprint can be observed. The aim of this study was to provide mineralogical and mineral-chemical constraints of major mineral phases as well as accessories such as apatite on this gradient and if possible obtain *P-T* conditions along a profile from north to south.

The quartzphyllite samples were collected along a traverse from Reccoaro (TKP054) in the S to Brixen (TKP022) in the N. Petrographic investigations revealed that the metapelites contain quite a complex polyphase mineral assemblage. The mineral assemblage in the S is represented by chlorite + muscovite + albite + quartz. Towards the center of the traverse, biotite occurs in the mineral assemblage, which has subsequently been replaced by chlorite. Samples in the vicinity of the Permian Cima d'Asta intrusion show petrographic evidence for contact metamorphism since K-feldspar, chloritoid and andalusite occur. In the N the mineral assemblage is chlorite + muscovite + plagioclase + quartz + garnet. Therefore, the metapelitic zones of chlorite, biotite and garnet could be observed along the traverse.

Mineral chemical investigations revealed further complexities. The chemical compositions of muscovite, chlorite and plagioclase vary continuously with increasing *P-T* conditions from S to N. Si in muscovite decreases (from 3.3 to 3.1 apfu) with increasing Al⁶ (from 2.4 to 2.7 apfu). Muscovite also shows an increase in the paragonite component from 4% to 13%. Similarly chlorite changes its composition also showing a decrease in Si and an increase in Al⁶. Plagioclase changes from pure albite to anorthite contents of 30%. The data also revealed that the southernmost sample (TKP054) shows evidence for a later *T*-accentuated overprint (Permian?) texturally not visible. Also, the second southern sample (TKP056) from the traverse shows two plagioclase generations, which are also likely due to a later overprint.

The chemical composition of apatite also changes continuously from S to N with slightly increasing F contents. F increases from 3.6 wt.% in the S to 3.8 wt.% in the N. A contemporaneous increase in FeO, Y₂O₃, and Cl has also been observed. Geothermobarometry yielded so far *P-T* conditions of 554 ± 11 °C and 6.49 ± 1.3 kbar in the northernmost sample TKP022. Currently it is planned to apply muscovite-chlorite-quartz geothermobarometry to the rest of the samples of the traverse to obtain more quantitative data on the *P-T* gradient from the southern samples. This study clearly shows that quartzphyllites indeed are able to record complex metamorphic histories hidden in petrographic and mineral chemical data.

Don't drink that stuff: mineralogical constraints on the Ni-anomaly in waters from rock glaciers in the Ötztal Complex

P. Tropper¹, K. Krainer², G. Winkler³, G. Bertolotti², V. Schmit²

¹University of Innsbruck, Institute of Mineralogy and Petrography, 6020 Innsbruck, Austria

²University of Innsbruck, Institute of Geology, 6020 Innsbruck, Austria

³University of Graz, Institute of Earth Sciences, 8010 Graz, Austria

e-mail: peter.tropper@uibk.ac.at

The hydrology of intact rock glaciers is complex and mainly controlled by climatic factors (weather), bedrock composition, size, composition and internal structure. Rock glaciers may serve as aquifers, storing and releasing water over different timescales and thus are of increasing interest as reservoirs for drinking water supply. However, still little is known on the quality (chemistry) of water released from permafrost springs.

Increasing concentrations of ions and heavy metals were detected in two high Alpine lakes, which are impacted by meltwater from rock glaciers. During the last years, abnormally high Ni concentrations (and high concentrations of other elements such as Cu, Co Zn) high above the upper limit for drinking water were recorded from a number of springs released from intact rock glaciers and permafrost-related springs in the Ötztal Alps. High concentrations of Ni, Co, Zn, Mn, Fe and Al were recently recorded from permafrost ice of a core drilled on rock glacier Lazaun. It has previously been shown that creeks and high alpine lakes derived from intact rock glaciers and characterized by low water temperatures, high EC, high sulfate, Mg and Ca, and partly high metal concentrations display a significantly lower biodiversity compared to high alpine creeks and lakes that are not influenced by water derived from permafrost.

In this contribution, we concentrate on nickel because: (1) Ni in drinking water is a toxic heavy metal; (2) Ni occurs in concentrations high above the upper limit for drinking water that is at 0.02 mg/L according to the Drinking Water Regulation (Trinkwasserverordnung – TWV 2023) of the Austrian Government; and (3) Ni-minerals are so far unknown from the rocks of the Ötztal Complex.

In the course of this study, thin sections of paragneiss and amphibolite rock samples from the rock glaciers Krummgampen, Wannekar and Lazaun were prepared and the minerals were analyzed using the electron probe microanalysis, with respect to their Ni contents. Petrographic investigations show that the mineral assemblage (silicates and sulfides) is heavily altered. Sulfides for instance are almost completely replaced by goethite and silicates such as garnet, biotite and staurolite show replacement by chlorite. The results show that the sulfides, namely pyrrhotite contain Ni contents of up to 1.2 wt.% NiO, chalcopyrite on the other hand contains much lower Ni contents of up to 0.2 wt.% NiO. Silicate minerals contain Ni concentrations below 0.1 wt.% NiO. With respect to additional heavy elements (Mn, Zn) present in the waters, garnet contains up to 10 wt.% MnO and staurolite contains up to 1.7 wt.% ZnO. These data show that in the absence of evidence for other heavy element sources, the altered mineral assemblage in the rocks from the rock glaciers are the most obvious source of these elements.

Non-ideal, but how non-ideal? Low-temperature calorimetry of the Al-F-titanite – titanite solid solution

P. Tropper¹, E. Dachs², U. Troitzsch³

¹University of Innsbruck, Institute of Mineralogy and Petrography, 6020 Innsbruck, Austria

²University of Salzburg, Chemie und Physik der Materialien, 5020 Salzburg, Austria

³Research School of Physics, Australian National University, Canberra, Australia

e-mail: peter.tropper@uibk.ac.at

Al-rich titanite [Ca(Ti,Al)(O,F,OH)SiO₄] has been the focus of many previous mineralogical studies, because Al is one of the most common and abundant substituents for Ti in natural titanite. Moreover, the substitution appeared to be pressure and temperature dependent and thus could be of interest for geothermobarometry. The two coupled substitution reactions that account for the formation of Al-bearing titanite are: $\text{Ti}^{4+} + \text{O}^{2-} = \text{Al}^{3+} + \text{F}^-$ and $\text{Ti}^{4+} + \text{O}^{2-} = \text{Al}^{3+} + \text{OH}^-$. Hence Al-rich titanite is made up of the three end-members CaTiOSiO₄ [titanite], CaAlFSiO₄, and CaAlOHSiO₄ (vuagnatite).

Tropper et al. (2018) measured the heat capacity (C_P) data of Al-F-bearing titanite that yielded the standard entropy S°_{298} of F-Al-titanite CaAlFSiO₄ (FAT). C_P of synthetic FAT was measured with relaxation calorimetry and differential scanning calorimetry between 5 and 764 K. The results yielded $S^\circ_{298.15}$ to be 115.4 ± 2.0 J/(mol·K) and subsequently the standard Gibbs free energy of formation from the elements, $\Delta_f G^\circ$, of CaAlSiO₄F to be between -2583 ± 3.0 and -2588 ± 3.0 kJ/mol, and the standard enthalpy of formation from the elements, $\Delta_f H^\circ$, to lie between -2728 ± 3.0 and -2733 ± 3.0 kJ/mol, depending on the thermodynamic data retrieval approach.

This study focusses on the determination of the entropy of mixing along the F-Al-titanite – titanite join. The following compositions (X_{Ti}) were measured: 0.18, 0.33, 0.63, 0.77, 0.82, 0.91. The corresponding values of $S^\circ_{298.15}$ are: 120.2, 127.27, 126.66, 128.43, 127.55, and 130.84 J/(mol·K) \pm 1.6-1.8 J/(mol·K) (2σ). Calculation of the excess entropy S^{ex} yielded a positive deviation from ideality. Due to the scatter of the data and the relatively large errors in S^{ex} , it is possible to use a symmetrical as well as an asymmetrical fit through the data. For simplicity, a regular model was fit through the data in accordance with the regular activity model proposed by Tropper et al. (2002). The corresponding values of the entropic Margules parameter W_S is 28 ± 16 J/(mol·K). In conjunction with data on W_V and estimates on W_H , this value will be another step closer to the comprehensive formulation of a non-ideal activity model for the system Al-F titanite – titanite.

Tropper P, Troitzsch U, Dachs E Benisek A (2018): Heat capacity measurements of CaAlSiO₄F from 5 to 850 K and its standard entropy. - Amer Miner 103, 1165-1168

Geochemical insights into one of the earliest marine habitats on Earth – the reliability of 3.5-billion-year-old jaspillites from the Dresser Fm., Australia

S. Viehmann¹, D. Krämer², C. Koeberl³, S.V. Hohl⁴, M.J. van Kranendonk⁵

¹University of Hannover, Institute of Mineralogy, Hannover, Germany

²Federal Institute of Geosciences and Natural Resources (BGR), Hannover, Germany

³University of Vienna, Department of Lithospheric Research, Vienna, Austria

⁴State Key Laboratory of Marine Geology, Tongji University, Shanghai, P.R. China

⁵University of New South Wales Sydney, Australian Centre for Astrobiology, Sydney, Australia
e-mail: s.viehmann@mineralogie.uni-hannover.de

The ca. 3.5 billion-year-old Dresser Formation in the Pilbara Craton, Western Australia, is famous for its traces of early life in the form of microfossil assemblages and stromatolites. These unique rock types provide fascinating windows into habitats of microbial life and the state of the ambient atmosphere-hydrosphere system. Among several pioneering studies targeting interdisciplinary fields of geo(micro)biology and geochemistry, trace elements in combination with Fe isotopes of jaspillites from different units within the Dresser Formation have recently been reported to reconstruct ancient paleo-environments (Johnson et al. 2022). This geochemical study targeted jaspillites, i.e., chemical sediments that are proposed to directly reflect ancient fluid chemistry from which the jaspillites formed, from four consecutive horizons of the Dresser Formation. They propose severe and fluctuating paleo-environmental changes during the deposition of these units in combination with changing nutrient availability and limitation during land-sea transitions based on Rare Earth's and yttrium (REY) and Fe isotope systematics. While this study provides a crucial milestone in understanding the earliest microbial habitats on Earth, the source of elements providing nutrients among other elements in the ancient Dresser aqueous environments remains still incompletely understood.

To determine the sources affecting water chemistry in the Dresser Formation, we obtained trace element and radiogenic Nd isotope compositions of high pressure-high temperature digestions of jaspilitic cherts directly overlying the famous “candelabra”-stromatolites from a terrestrial hot spring deposit (Djokic et al. 2017). The trace element data corroborate the endmembers (Johnson et al. 2022): endmember I shows seawater-like shale-normalized (subscript SN) REY_{SN} patterns with positive La_{SN}, Gd_{SN} anomalies, heavy REY_{SN} over light REY_{SN} enrichment, and super-chondritic Y/Ho ratios. In contrast, the endmember II is characterized by the lack of typical seawater-like anomalies, sub-chondritic Y/Ho ratios, and light REY_{SN} over heavy REY_{SN}. Positive Eu_{SN} anomalies representing REY contributions from high-temperature, hydrothermal fluids in the ancient Dresser depositional environment are present in both endmembers. Radiogenic Nd isotope compositions, commonly used to determine the local sources of REY in modern and ancient seawater due to the short residence time of Nd, show a significant impact of post-depositional alteration and a reset of the Sm-Nd isotope system in the Dresser Formation jaspillites. A best-fit isochron calculation yields a Sm-Nd age of 2260 Ga ± 180 Ma that overlaps with thermo-tectonic events in Pilbara Craton between 2430 to 2400 Ma and 2215 to 2145 Ma (Rasmussen et al. 2005), respectively, suggesting that Nd isotope of the Dresser Formation jaspillites are unreliable geochemical proxies to reconstruct sources in Dresser fluids 3.5 Ga ago. We – however- strongly emphasize that overall REY distributions and Fe isotope compositions must not necessarily be affected by these events, although the Nd isotope compositions in the Dresser jaspillites show significant disturbances.

- Djokic T, Van Kranendonk MJ, Campbell KA, Walter MR, Ward CR (2017): Earliest signs of life on land preserved in ca. 3.5 Ga hot spring deposits. - *Nat Comm* 8, 15263
- Johnson CM, Zheng X-Y, Djokic T, Van Kranendonk MJ, Czaja AD, Roden EE, Beard BL (2022): Early Archean biogeochemical iron cycling and nutrient availability: New insights from a 3.5 Ga land-sea transition. - *Earth Sci Rev* 103992
- Rasmussen B, Fletcher IR, Sheppard S (2005): Isotopic dating of the migration of a low-grade metamorphic front during orogenesis. - *Geology*, 33, 773-776

Analysis of Vickers indentation tests by means of Atomic Force Microscopy (AFM)

P. Vivanco-Chávez¹, M. Klichowicz², H. Lieberwirth², F. Mertens¹, O. Popov², G. Heide³

¹Institute for Physical Chemistry, Technische Universität Bergakademie Freiberg

²Institute for Mineral Processing Machines and Recycling Systems Technology, Technische Universität Bergakademie Freiberg

³Institute for Minealogy, Technische Universität Bergakademie Freiberg
e-mail: Patricia-Ilein.Vivanco-Chavez@chemie.tu-freiberg.de

The study of the mechanical properties of materials such as fracture toughness (K_{IC}) and Vickers hardness (VH), at micro/nanometric scales is scarce and at the same time a challenge to determine them. Therefore, this research shows a new methodology of analysis and insight in detail regarding the elastic/plastic behaviour of investigated materials with Vickers indenters. In this research five samples were analysed: a fused silica as reference material, a synthetic quartz crystal (SQ \square and SQ \times) and finally quartz grains from granite and granodiorite. A possible tool for the verification of the recorded indentation depths is Atomic Force Microscopy (AFM). Using an AFM allows to measure with great accuracy such as the length of the cracks (l), the depth of residual indentation (h_f) and the indentation marks (d), allowing to determine K_{IC} and HV with greater accuracy, i.e. at the nanoscale.

Keywords: Microhardness; Vickers Indentation; Quartz; Atomic Force Microscopy, Radial Cracks; Cone Crack; Palmqvist Cracks

Background: The importance of realistic modelling of the mechanic behaviour of mineral materials has increased due to its demand and contributions to mineral processing optimization and mining. These models rely on the accurate characterisation of mechanical properties, e.g. fracture toughness (K_{IC}) which characterises the resistance to unstable crack propagation under the crack opening. Since the theory and application of this parameter are described in standard textbooks like Anderson (2017) and Gross & Seelig (2018), the focus is set on the properties which are relevant for minerals, as well as the characterisation of different types of crack morphology that was first observed and analysed by Cook & Pharr (1990).




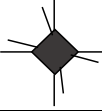




In contrast to macroscopic measurement approaches, the microscopic fracture toughness is calculated from the size of the cracks, which can be observed as a result of indentation hardness testing with a Vickers pyramid (for details see Roebuck et al. 2008 and ISO 28079:2009). To date, this method has been applied to hard metals (Palmqvist, 1957), technical non-metallic materials like glasses and ceramics (Cook & Pharr, 1990; Moradkhani et al. 2013), and rocks and minerals (Swain & Lawn, 1976; Whitney et al. 2007; Han et al. 2020).

However, this approach presents some challenges as the measurement quality of this parameter is affected by the difficulty of implementing this method on natural minerals, i.e. not all minerals show regular cracks after indentation (Whitney et al. 2007), the type of crack can often only be assumed based on literature references since different crack systems (Glandus et al. 1991), and the crack length measurements via microscope have low accuracy. Therefore, in this study, AFM is used to analyze with high precision the indentation marks and cracks caused by micro indentation tests with a Vickers indenter, thus, increasing the accuracy of mechanical property (K_{IC}) calculation.

Methods: The investigation of microhardness and fracture toughness of mineral phases was carried out using a Shimadzu HMV-G21DT Micro Vickers Hardness Tester, in which each sample underwent 30 indentation tests with a maximum load of $F = 980.7 \text{ mN}$ and a 15-second holding time. Subsequently, the indentation marks were analyzed with Park NX10 AFM to scan the sample surfaces, where the indentation diagonals (d_i) and crack length (l) are determined, and the final depth of the residual hardness impression (h_f) measured on scales ranging from micrometres to a few nanometers.

Results: The following is a synthesis of the crack morphologies found in this study (Table 1) and a summary comparison of the fracture toughness (K_{IC}) of this study with other authors (Figure 1).

Table 1. Summary classification of the different morphologies in the indented samples (30 indentations for each sample).

Sample	Cracks Morphology							
								
	No cracks	PRC	SRC	PRC + SRC	PCC	PCC + SRC	PRC + SCC	PRC + SRC + SCC
FS	5 (16.6%)	-	2 (6.6%)	-	3 (10%)	4 (13.3%)	10 (33.3%)	6 (20%)
SQ _{//}	-	25 (83.3%)	-	5 (16.6%)	-	-	-	-
SQ _⊥	-	5 (16.6%)	-	25 (83.3%)	-	-	-	-
Q-Gr	-	10 (33.3%)	-	20 (66.6%)	-	-	-	-
Q-Bg	-	3 (10%)	7 (23.3%)	20 (66.6%)	-	-	-	-

PRC = Primary Radial Cracks; SRC = Secondary Radial Cracks; PCC = Primary Cone Cracks; SCC = Secondary Cone Cracks

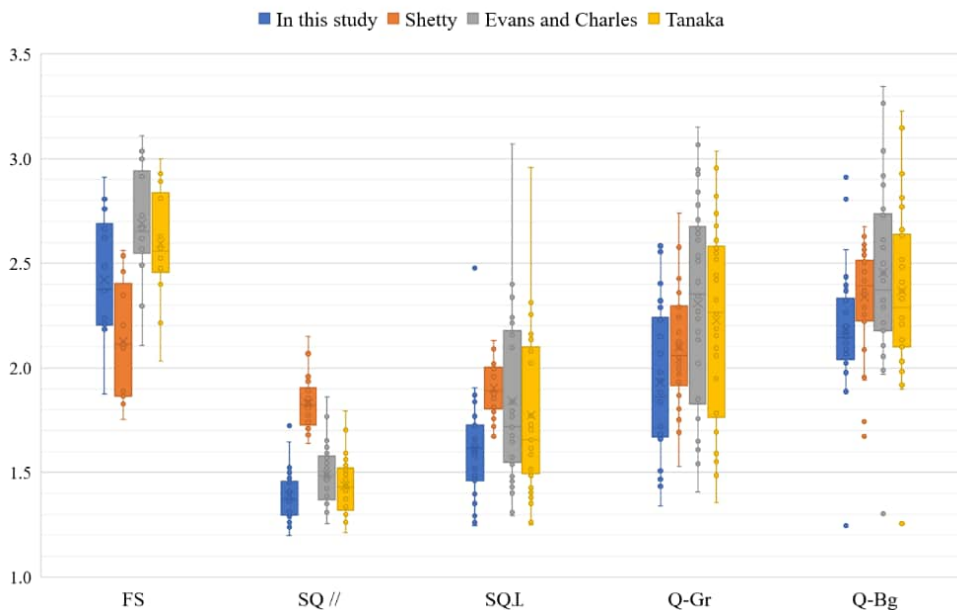


Figure 1. Comparison boxplot between the different K_{IC} values of the authors Deschamps et al. (2013), Tanaka (1987), Evans & Charles (1976) and this present study.

Conclusions:

- In this study, the characterization of the types of crack morphologies are both quantitatively and qualitatively determined (Table 1) and are consistent with models based on the literature review.
- Reconstruction of an indentation profile of the tested material based on the parameters of h_f and h_{max} is established, which is important to explain the elastic/plastic behaviour of the indented minerals.
- The fracture toughness (K_{IC}) values from this study agrees with the models of other authors (Figure 1), and this parameter is inversely proportional to the Vickers hardness (VH).

- Anderson TL (2017): Fracture mechanics: Fundamentals and applications. - Fourth ed, CRC Press Taylor & Francis Group: Boca Raton, Fla., London, New York, ISBN 9781498728133
- Roebuck B, Bennett E, Lay L, Morrell R (2008): Measurement good practice guide No. 9. - Palmqvist Toughness for Hard and Brittle Materials; Teddington, Middlesex, UK, TW11 0LW, ISBN 1368-6550
- Cook RF, Pharr GM (1990): Direct observation and analysis of indentation cracking in glasses and ceramics. - J Amer Ceram Soc 73, 787–817, doi:10.1111/j.1151-2916.1990.tb05119.x
- Evans AG, Charles EA (1976): Fracture toughness determinations by indentation. - J Amer Ceram Soc 59, 371–372, doi:10.1111/j.1151-2916.1976.tb10991.x
- Glandus JC, Rouxel T, Tai Q (1991). Study of the Y-TZP toughness by an indentation method. - Ceram Internat 17, 129–135, doi:10.1016/0272-8842(91)90041-W
- Gross D, Seelig T (2018): Fracture mechanics: With an introduction to micromechanics. - 3rd ed., Springer Internat Publ, Cham, ISBN 9783319710907.
- Han Q, Qu Z, Wang P, Bi G, Qu G (2020): Applications of micro-indentation technology to estimate fracture toughness of shale. - Materials (Basel) 13, doi:10.3390/ma13184208.
- International Organization for Standardization. ISO 28079 (2009): Hardmetals - Palmqvist toughness test (28079)
- Moradkhani A, Baharvandi H, Tajdari M, Latifi H, Martikainen J (2013): Determination of fracture toughness using the area of micro-crack tracks left in brittle materials by Vickers indentation test. - J Adv Ceram 2, 87–102, doi:10.1007/s40145-013-0047-z
- Palmqvist S (1957): Method att Bestamma Segheten hos Spread Material, Sarskit Hardmettaler. - Jernkontorets Annaler 141, 300–307
- Shetty DK, Wright IG, Mincer PN, Clauer AH(1985): Indentation fracture of WC-Co Cermets. - J Mater Sci 20, 1873–1882, doi: 10.1007/BF00555296
- Swain MV, Lawn BR (1976): Indentation fracture in brittle rocks and glasses. - Int J Rock Mech Mining Sci Geomech Abstr 13, 311–319, doi:10.1016/0148-9062(76)91830-1
- Tanaka K (1987): Elastic/plastic indentation hardness and indentation fracture toughness: the inclusion core model. - J Mater Sci 22, 1501–1508. doi: 10.1007/BF01233154
- Whitney DL, Broz M, Cook RF (2007): Hardness, toughness, and modulus of some common metamorphic minerals. - Amer Mineral 92, 281–288, doi:10.2138/am.2007.2212

Tracking transformation processes in the Mg phosphate mineral system – A mineralogical study for environmental applications

R. Volkmann^{1,2}, R. Blukis³, C. Schmidt¹, L. G. Benning^{1,2}

¹German Research Centre for Geosciences Potsdam

²Freie Universität Berlin

³Leibniz-Institut für Kristallzüchtung Berlin

e-mail: rebeccav@gfz-potsdam.de

Phosphorous is an essential component of all living beings and is an important component in fertilizers. It is a scarce element on Earth and mining of phosphorous deposits is environmentally harmful (Manning, 2008). Therefore, recent research is focusing on P-recovery from anthropogenic sources, e.g., from wastewaters. The mineral struvite ($\text{MgNH}_4\text{PO}_4 \cdot 6\text{H}_2\text{O}$) is recovered from wastewater and reutilized as a slow-release nitrogen and phosphorus fertilizer (Le Corre et al. 2009). However, struvite is unstable under atmospheric conditions, leading to its decomposition and transformation into other phosphate phases (Tansel et al. 2018). This subaerial transformation has not yet been characterized and kinetic parameters for the transformation reactions are unknown.

In this study, the decomposition and transformation of struvite was investigated by altering synthetic μm - and mm -sized crystals at different temperatures (22–60 °C) in open and closed systems for up to 10 months. Phase transformations were monitored by optical microscopy and Raman spectroscopy and transformation kinetic parameters were quantified by powder X-ray diffraction (XRD) and Rietveld analysis.

Struvite transformed to different products following different mechanisms. In open systems, and at 22 °C, struvite transformed to newberyite ($\text{Mg}(\text{PO}_3\text{OH}) \cdot 3\text{H}_2\text{O}$) by losing its ammonia and three of its water molecules. However, struvite remained fairly stable and at 22 °C this transformation proceeded only by 15 % even after 10 months. In contrary, at 37 and 60 °C, struvite transformed faster and primarily to another phase - dittmarite ($\text{MgNH}_4\text{PO}_4 \cdot \text{H}_2\text{O}$) which retained its ammonia but lost five out of six water molecules; newberyite occurred only as a minor product (< 5 wt.-%). In the open system, the phase formation proceeded about 35 % faster at 37 °C and 100 % faster at 60 °C compared to 22 °C. In contrast, in the closed system even after 10 months at 60 °C struvite remained stable and the transformation barely started (< 2 wt.-%). The XRD data showed that after about 8 months at 37 °C and after 2 months at 60 °C in the open system amorphization of struvite occurs through the complete loss of ammonia and water.

Microscopic imaging revealed that both newberyite and dittmarite were characterized by pseudomorphic overgrowth after struvite, while showing similar optical properties. Yet, the kinetic data indicates different formation mechanisms for the two phases. The partial pressure of water and ammonia in the reacting atmosphere, which was documented by the differences in open and closed kinetic rates, as well as differences in the crystal structures were the main drivers for the breakdown of struvite to the two other magnesium phosphate phases.

As struvite is used as a slow-release fertilizer in agriculture, our results document that its transformation to newberyite leads to the loss of ammonia, which has important implications for fertilizer storage. Even at 22 °C, after 10 months 15 % of the ammonia is lost. Although at higher temperatures (≥ 37 °C) the transformation leads to the retaining of ammonia in the

dittmarite structure, such a temperature requires a higher energy demand for storage. Therefore, our study indicates that struvite fertilizer should not be stored at ambient conditions, but at temperatures below 22 °C and in closed containers.

Manning DAC (2008): Phosphate minerals, environmental pollution and sustainable agriculture. – Elements 4, 105-108

Le Corre KS, Valsami-Jones E, Hobbs P, Parsons SA (2009): Phosphorus recovery from wastewater by struvite crystallization: A review. - Crit Rev Environ Sci Technol 39, 433-477

Tansel B, Lunn G, Monje O (2018): Struvite formation and decomposition characteristics for ammonia and phosphorus recovery: A review of magnesium-ammonia-phosphate interactions. – Chemosphere 194, 504-514

Provenance studies on raw garnets from the Zillertal (Tyrol), Ahrntal (South Tyrol), and Radenthein (Carinthia)

S. Wagner¹, B. Zerobin², R. Köchl³, P. Tropper¹, G. Goldenberg²

¹*Institute of Mineralogy and Petrography, University of Innsbruck*

²*Department of Archaeologies, University of Innsbruck*

³*Department of History and European Ethnology, University of Innsbruck*

e-mail: simon.wagner@uibk.ac.at

There is evidence of the use of the mineral garnet as a gemstone in jewellery since the early Middle Ages. In the Alps, too, garnet is still used today in the form of traditional costume jewellery, especially the garnet variety almandine. From the middle of the 19th century, garnet mining began in the Zillertal, Ahrntal and Radenthein, of which all three remained important sites until the early 20th century. However, due to the export to the gemstone-cutting factories in the Czech Republic at the time, the raw garnets lost their actual origin and were henceforth traded as "Bohemian garnets". Nevertheless, a chemical differentiation and determination of origin is possible even in this state with suitable analytical methods (EPMA, micro-XRF, etc.). On a macroscopic level, it is not possible to distinguish visually between the different garnet deposits. The most significant features are the size and colour of cut garnets, since the true Bohemian garnets often only measure a few millimetres and show a more intense red colour than alpine garnets. A further criterion for distinguishing between the different alpine deposits can be achieved via the individual inclusion pattern, which can be attributed to the different conditions of garnet formation and differing host rock composition. Typical inclusions of Zillertal and Ahrntal garnet are, for example, chlorite, apatite, zircon, quartz, ilmenite, and epidote. In contrast, garnets from Radenthein show oriented growth, which is typically seen with the ilmenite and rutile inclusions. The clearest differences are due to chemical differences in the composition of the garnets, which can also be attributed to different formation conditions (P-T-X). Typically, these chemical differences can be clearly visualized by plotting certain oxides against each other. This method has proven to be very effective in distinguishing garnet deposits on a global scale and therefore forms the basic discrimination method in provenance studies (e.g. Then-Obłuska et al. 2021). On a local scale apparent chemical differences are only visible to a limited extent. However, the use of compositional data analysis allows a clearer distinction between the different alpine garnet deposits. In the case of chemical composition, certain conditions must be met to achieve a successful evaluation of discrimination features. With the help of software like *CoDaPack 2.0* (Comas-Cufi & Henestroza 2011), these analyses can be carried easier and allow therefore a better differentiation between the different garnet deposits within Austria. Applying PCA on this big dataset, consisting of samples directly from the deposits and the former warehouse in Zell am Ziller, clearly shows that the biggest variance in the data set is produced by the three oxides MgO, MnO and CaO. By plotting these in a ternary diagram five different groups can be identified.

Petrological investigations on garnet-chlorite-mica shists of the Rosstrugg and Hornkees (Zemmgrund, Zillertal)

S. Wagner¹, B. Zerobin², R. Köchl³, P. Tropper¹, G. Goldenberg²

¹*Institute of Mineralogy and Petrography, University of Innsbruck*

²*Department of Archaeologies, University of Innsbruck*

³*Department of History and European Ethnology, University of Innsbruck*
e-mail: simon.wagner@uibk.ac.at

Geologically, the Zemmgrund (Zillertal) is part of the Tauern Window and belongs tectonostratigraphically to the Venediger Duplex (Subpenninic Nappes). The garnet deposits occur locally on the Rosstrugg and around the Hornkees glacier within ductile shear zones within the “Zentralgneisse”. Similar shear zones can be observed in other parts of the innermost Zillertal, for example, the Stilluptal. The garnet-bearing host-rocks can be described as chlorite-mica-shist, which formed during the alpine orogeny (Selverstone et al. 1991). Especially at the Rosstrugg and Hornkees these garnets can reach sizes of several millimetres and are usually of good quality (few inclusions, beautiful red colour, etc.), which is why they were also used to produce garnet jewellery and are also very popular among mineral collectors.

The samples of the garnet-bearing chlorite-mica-shist have been taken directly from the historic mining site at the Rosstrugg and the mineral site close to the Hornkees glacier. Both host rocks are mainly composed of Bt+Chl+Qz and show minor amounts of Fsp+Ms±Rt±Zrn±Ap±opaque phases. The garnets in this matrix show different sizes, often reaching several millimeters. Crack formation can also be observed depending on the thin section. The inclusion pattern of the garnets varies as well; typically, however, Chl+Ap+Zrn+Qz+Rt+Ilm can be found.

Regarding their geochemical composition, garnets have been analysed with the help of μ -XRF, EPMA and LA-ICP-MS. Continuous zoning can be observed in all garnet samples, with the almandine component showing the largest proportions from 60 mol% (core) to 73 mol% (rim). The trace element distribution of Co, Zn, or Zr, for example, correlates with the pattern of the almandine component, whereas e.g., Ti shows a decreasing concentration from the core to the rim. The same can be observed for Y, whose distribution is already clearly visible in the distribution images generated with μ -XRF. HREEs, such as Yb or Lu, follow the same trend.

The pressure and temperature of garnet formation have been calculated using *Thermocalc v.3.45* and the extension *TC_Comb* (Dolivo-Dobrovolsky 2023). The AveragePT calculations resulted in $T = 613 \pm 10$ °C and $P = 8.2 \pm 0.4$ kbar. Calculation of garnet isopleths using the program *Perplex* yielded garnet growth with decreasing pressures (approx. 8.9 kbar in the core and 7.7 kbar in the rim) and increasing temperatures (560 °C in the core and 590 °C in the rim). Additionally, pseudosection modelling [P-T, P-a(H₂O)] was done using *THERIAK-DOMINO* and the most current database *td-d62-mp50-05* (Tinkham 2022). The combination of geothermobarometry and thermodynamic modelling clearly shows that a (H₂O) greater than 0.6 must have been predominant. The obtained garnet ages (Lu-Hf-geochronology) of 32.5 Ma agree with the existing age data of the Alpine metamorphic event and correspond with the “Tauernkristallisation”.

Dolivo-Dobrovolsky D (2023): TC_Comb software

Silverstone J, Morteani G, Staude J-M (1991): Fluid channelling during ductile shearing: transformation of granodiorite into aluminous schist in the Tauern Window, Eastern Alps. - J Metamorph Geol 9, 419–431

Tinkham DK (2022): td-ds62-mp50-05 database

Anhydrite formation in planetary surface environments – The case of the Atacama Desert

N. Wehmann¹, C. Lenting¹, T.M. Stawski², L. Agudo Jácome², S. Jahn¹

¹*Institut für Geologie und Mineralogie, Universität zu Köln, Zùlpicher Straße 49b, 50674 Köln, Germany*

²*Bundesanstalt für Materialforschung und -prüfung (BAM), Department for Materials Engineering,
Unter den Eichen 87, 12205 Berlin, Germany
e-mail: n.wehmann@uni-koeln.de*

Gypsum ($\text{CaSO}_4 \cdot 2\text{H}_2\text{O}$), bassanite ($\text{CaSO}_4 \cdot 0.5\text{H}_2\text{O}$), and anhydrite (CaSO_4) are essential evaporite minerals for the evolution of hyper-arid surface environments on Earth and Mars (Voigt et al. 2019; Vaniman et al. 2018). The formation mechanism of especially anhydrite has been a matter of scientific debate for more than a century (van't Hoff et al. 1903). To date, there exists no model that can reliably predict anhydrite formation at earth's surface conditions. While thermodynamics favor its formation, it is hardly achieved on laboratory time scales at conditions fitting either the Atacama Desert on Earth, or the surface of Mars (Wehmann et al. 2023, *subm.*). In light of most recent developments (e.g. Stawski et al. 2016), that advocate for a complex, non-classical nucleation mechanism for all calcium sulphates, we present an analysis of natural samples from the Atacama Desert to identify key features that promote the nucleation and growth of anhydrite under planetary surface conditions. Our analyses reveal at least three distinct anhydrite facies, with differing mineralogy and micro- to nano-structures. The facies are (1) aeolian deposits with sub- μm grain sizes, (2) (sub-)surface nodules that formed from aeolian deposits and (3) selenites with secondary anhydrite rims. Possible mechanisms of their formation will be discussed.

Hoff JVT, Armstrong EF, Hinrichsen W, Weigert F Just G (1903). Gips und Anhydrit. - Z Phys Chem 45(1), 257-306

Stawski TM, Van Driessche AE, Ossorio M, Diego Rodriguez-Blanco J, Besselink R, Benning LG (2016): Formation of calcium sulfate through the aggregation of sub-3 nanometre primary species. - Nature Comm 7, 11177

Vaniman DT, Martínez GM, Rampe EB, Bristow TF, Blake DF, Yen AS, Sumner DY (2018): Gypsum, bassanite, and anhydrite at Gale crater, Mars. - Amer Miner 103, 1011-1020

Voigt C, Klipsch S, Herwartz D, Chong G, Staubwasser M (2020): The spatial distribution of soluble salts in the surface soil of the Atacama Desert and their relationship to hyperaridity. - Global and Planetary Change 184, 103077

Wehmann N, Lenting C, Jahn S (2023): Calcium sulfates in planetary surface environments. - Available at SSRN 4479259

Crystallography in energy applications

C. Weidenthaler

*¹Max-Planck-Institut für Kohlenforschung, Mülheim an der Ruhr, Germany
e-mail: weidenthaler@mpi-muelheim.mpg.de*

The energy transition requires the implementation of sustainable energy carriers. Hydrogen is one of these options, but the storage is still a challenge. Ammonia, NH₃, is intensively investigated as a suitable candidate as an H₂ storage medium and is already used for heavy-duty transportation systems. The efficient splitting of NH₃ into H₂ and N₂ for fuel cell applications requires the development of catalysts where supported transition metals are one amongst others.

To understand the function of a catalyst, it is inevitable to use in situ/operando techniques in addition to ex-situ analytics. This contribution presents a combination of different in situ techniques that were used to investigate structure-property relationships of several types of Co- and Ni-based catalysts supported on different oxides such as La₂O₃, Al₂O₃, and MgO. In addition to in situ X-ray diffraction experiments, X-ray total scattering and X-ray absorption methods reveal structure changes of the catalysts and the supports on different lengths scales from bulk to the atomic scale. In addition to the results obtained from structure studies, the reduction behaviour, surface chemistry, and catalytic activities will be included to the overall discussion.

For Co-based catalysts supported on Al₂O₃, it could be shown that a significant fraction of the Co catalysts reacts with Al₂O₃ and forms catalytically inactive CoAl₂O₄ (Weidenthaler et al. 2022). The Co content in the spinel cannot be compensated by higher metal loadings. Alumina is known to prevent sintering and a re-dispersion of metallic Co after the reaction was observed. However, the disadvantage of its tendency to form inactive cobalt aluminates predominates.

The second system, Co on basic La₂O₃ support, forms in situ during NH₃ cracking from a LaCoO₃ pre-catalyst. The structural transformation from LaCoO₃ to the catalysts via several intermediate phases was monitored by means of operando X-ray diffraction experiments. The catalytically active metallic Co neither reacts with La₂O₃ nor re-disperses after the reaction. The conversion for Co on La₂O₃ is comparable to the most active Co on Al₂O₃ catalyst, despite having multiple higher Co-loading.

The third system involves Ni on MgO, which shows a clear dependence of the catalytic conversion on the activation process and the associated structural changes.

Weidenthaler C, Schmidt W, Leiting S, Ternieden J, Kostis A, Ulucan TH, Budiyo E (2022): In-situ investigations of Co@Al₂O₃ ammonia decomposition catalysts: The interaction between support and catalyst. - Chem Cat Chem 14, e202200688

Confocal μ -XANES as a tool to analyse Fe oxidation state in heterogeneous samples: The case of melt inclusions in olivine from Hekla volcano

M. Wilke¹, R. Botcharnikov², J. Garrevoet³, M. Portnyagin⁴, K. Klimm⁵,
S. Krashenninikov^{1,6}, R. Almeev⁶, S. Moune⁷, G. Falkenberg³

¹*Institut für Geowissenschaften, Universität Potsdam, Germany*

²*Institut für Geowissenschaften, Johannes-Gutenberg Universität Mainz, Germany*

³*Deutsches Elektronen-Synchrotron, DESY, Hamburg, Germany*

⁴*GEOMAR Helmholtz-Zentrum für Ozeanforschung, Kiel, Germany*

⁵*Institut für Geowissenschaften, Goethe Universität Frankfurt, Germany*

⁶*Institut für Mineralogie, Leibniz Universität Hannover, Germany*

⁷*Observatoire de Physique du Globe de Clermont-Ferrand, Université Clermont Auvergne, France*

e-mail: wilkem@uni-potsdam.de

Here we present a confocal Fe K-edge μ -XANES method for the analysis of Fe oxidation state in melt inclusions of one-side polished samples, potentially applicable to any heterogeneous sample. The new technique allows for an analysis of small volumes with high spatial 3D resolution of $<100 \mu\text{m}^3$. Using a confocal setup, the probed volume is restricted to that just beneath the surface of the exposed object. This protocol avoids contamination of the signal by the host mineral and minimizes self-absorption effects. This technique has been calibrated and tested on a set of experimental glasses with a wide range of $\text{Fe}^{3+}/\sum\text{Fe}$ ratios. The method was applied to the analysis of natural melt inclusions trapped in forsteritic to fayalitic olivine crystals of the Hekla volcano, Iceland. Our measurements reveal changes in $\text{Fe}^{3+}/\sum\text{Fe}$ from 0.17 in basaltic up to 0.45 in dacitic melts, whereas magnetite-ilmenite equilibrium testifies redox conditions with $\text{Fe}^{3+}/\sum\text{Fe} \leq 0.20$ (close to FMQ, Fayalite-Magnetite-Quartz redox equilibrium) along the entire range of Hekla melt compositions. This discrepancy indicates that the oxidized nature of glasses in the melt inclusions could be related to post-entrapment process of diffusive hydrogen loss from inclusions and associated oxidation of Fe in the melt. The $\text{Fe}^{3+}/\sum\text{Fe}$ ratio in silicic melts is particularly susceptible to this process due to their low FeO content and it should be critically evaluated before petrological interpretation.

Investigating the metal sources of the Early Nordic Bronze Age through a multi-proxy approach

A. Wittke¹, B. Cornelis¹, D. Berger¹

¹*Curt-Engelhorn-Zentrum Archäometrie, Mannheim, Germany
e-mail: andreas.wittke@ceza.de*

The Early Nordic Bronze Age (NBA Period IB, 1600–1500 BC) is characterized by huge amounts of metal products reaching northern Germany and Scandinavia for the first time, demonstrated by the appearance of a refined repertoire of bronze products (Nørgaard et al, 2019). Examples for these products are the blades of swords and daggers of the Sögel and Wohlde district, which suddenly appear as highly sophisticated metal artefacts without local precursors. Both blade types have hilt-plates with four or five rivets, while Sögel blades have a rounded and Wohlde plates have a trapezoidal formed hilt-plate. One of the great desiderates of archaeologists is determining the origin of archaeological bronzes and their metal sources (copper and tin). To reconstruct the provenance of the source materials isotope and elemental compositions of metals have since become important tools. This work pursues a multi-isotope approach combining Pb, Cu and Sn isotopes with trace element composition (Berger et al. 2022) of about 300 blades of the Sögel and Wohlde type from the Early NBA to investigate the origin of the raw material sources and of the blades. Additionally, we search for evidence of source mixing and/or recycling to gain a better insight into the manufacturing practices and to validate the provenance analysis. For this, the blades are isotopically and chemically analysed and compared with ores and typologically related blades from other regions in Central and Southern Europe. This may help to reconstruct relationships between artefacts of different origins and to reveal cultural and trade networks. Moreover, a critical evaluation of the data will be undertaken against the background of potential metal/ore mixing and recycling.

First results of 49 blades from the Early NBA indicate the Alpine Mitterberg as a potential source region for the copper based on Pb and Cu isotope composition, and trace element patterns. The majority of the blades consists of low-impurity copper of chalcopyrite quality typical for the Mitterberg. However, some blades were likely produced from Slovakian copper ores and there could even be indications of mixing both copper sources. Regarding tin, the Erzgebirge would be a very likely supplier, but some regions of Cornwall are also possible because of matching Sn isotope values. Based on the isotopic data of a single blade (Pb, Cu, Sn), we are able to comprehend the manufacturing steps of the object and their meaning for the choice of source materials. In future research, more artefacts from the NBA and Central and Southern Europe, as well as copper ores of the Mitterberg and the Slovakian Ore Mountains will be studied to conduct statistical analysis and to check for mixing practices.

Berger D, Brüggemann G, Bunnefeld J-H, Pernicka E (2022): Identifying mixtures of metals by multi-isotope analysis: Disentangling the relationships of the Early Bronze Age swords of the Apa–Hajdúsámson type and associated objects. - *Archaeometry* 64, 44–74, <https://doi.org/10.1111/arc.12714>

Nørgaard HW, Pernicka E, Vandkilde H (2019): On the trail of Scandinavia's early metallurgy: Provenance, transfer and mixing. *PLoS ONE* 14, 1-32, <https://doi.org/10.1371/journal.pone.0219574>

Study of natural As_2S_3 glass

T. Witzke¹, G. Nénert¹, M. Gateshki¹

¹Malvern Panalytical B. V., Lelyweg 1, 7602 EA, Almelo, The Netherlands,
e-mail: thomas.witzke@malvernpanalytical.com

At the burning mine dump of the Lichtenberg open cast, Ronneburg, Thuringia, Germany (mined for uranium-bearing alum shale) and the burning mine dump of the Katerina coal mine, Radvanice, Czech Republic, orange-red to red glassy crusts and droplets with the composition As_2S_3 were found. The material was solidified from a melt, which was probably a sublimation product from a gas phase. X-ray diffraction showed that the material is amorphous. No peaks, but just a flat, very broad hump around $d = 5 \text{ \AA}$ were observed in the diffraction patterns.

To be able to characterize structurally this amorphous mineral, Pair Distribution Function (PDF) analysis has been carried out. Similarly, to previous studies on the synthetic materials (Georgiev et al., 2003), the PDF data show that this mineral is intrinsically phase separated into small As-rich (As_4S_4) and large S-rich clusters. We show in Fig. 1 the PDF fit of the as-collected data using the previously reported model. This result suggests that this new mineral is closely related to the synthetic As_2S_3 glass.

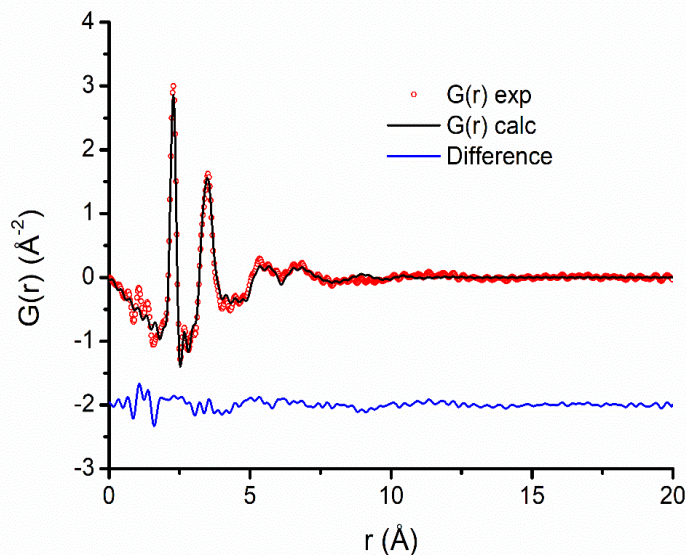


Figure 1: PDF fit of the experimental data using a phase separation model made of As_4S_4 and Sulfur cluster

Retrograde serpentinization and low-pressure metamorphic characteristics in the 3.8 Ga Isua Supracrustal belt, Greenland

J. Wolf¹, D. Sorger¹, S. Piazzolo², A.A.G. Webb³, T. Müller¹

¹*Geoscience Center Göttingen, Georg-August-University, Germany*

²*School of Earth and Environment, The University of Leeds, United Kingdom*

³*Division of Earth and Planetary Science and Laboratory for Space Research, University of Hong Kong, Hong Kong, China*

e-mail: j.wolf@stud.uni-goettingen.de

The Eoarchean Isua Supracrustal Belt (ISB) in West Greenland exposes one of the oldest rock records on Earth. Its tectonic setting is still subject of debate with interpretations ranging from plate tectonics to environments that are dominated by vertical tectonics. A first order question is the presence or absence of a metamorphic gradient within the belt. To that end, phase equilibria modeling combined with multiple geothermobarometric data convincingly suggested a homogeneous distribution of peak metamorphic conditions (550-600 °C; 0.8 - 1.0 GPa) (Ramírez-Salazar et al. 2021). However, recent studies of a dunite lens from the ISB suggested different metamorphic conditions varying from ultra-high pressure (Nutman et al. 2021) to low pressure deserpentinization (Guotana et al. 2022). In this study, we re-examine the petrography, mineral assemblages, reaction textures as well as the role of CO₂ in the metamorphism affecting ultramafic rocks from the specified lens B in the northwestern limb of the ISB. The texture of four different samples were analyzed using polarization microscopy, BSE imaging and EBSD measurements. Element x-ray maps and major element composition of major and accessory humite phases have been determined using EPMA. Phase equilibria modeling was done using the software package PerpleX to evaluate the role of CO₂.

Our petrographic observations show mineral assemblages of antigorite, olivine, magnesite, Ti-rich-humites and Fe-oxides. Antigorite (XMg = 0.99), magnesite, and Fe-oxide result from the breakdown reaction of olivine (XMg = 0.96). High forsterite content is interpreted to be the result of a hotter Archean mantle rather than deserpentinization. While the presence of accessory Ti-phases has been used as indicator for decompression through the breakdown reaction of Ti-chondrodite to form Ti-clinohumite, we present textural evidence of Ti-clinohumite being replaced by Ti-chondrodite pointing to a different reaction along a cooling path at lower pressures. The presence of carbonate instead of brucite highlights the role of CO₂ and its necessity to accurately describe phase relations for the metamorphic evolution of ultramafic rocks. Here, we present evidence from phase equilibria modeling, equally pointing to a simple cooling path at intermediate pressure conditions in agreement with metamorphic conditions obtained for the rest of the belt, rather than isothermal decompression from pressures higher than 2.0 GPa. The resulting lack of evidence for higher pressure conditions experienced by these mafic lenses thus removes a strong argument for the ISB to exhibit a metamorphic gradient, confirming the record of homogeneous metamorphic conditions within the belt.

- Guotana JM, Morishita T, Nishio I, Tamura A, Mizukami T, Tani K, Harigane Y, Szilas K, Pearson DG (2022): Deserpentinization and high-pressure (eclogite-facies) metamorphic features in the Eoarchean ultramafic body from Isua, Greenland. - *Geosci Front* 13, 101298, <https://doi.org/10.1016/j.gsf.2021.101298>
- Nutman AP, Scicchitano MR, Friend CRL, Bennett VC, Chivas AR (2021): Isua (Greenland) ~3700 Ma meta-serpentinite olivine Mg# and $\delta^{18}\text{O}$ signatures show connection between the early mantle and hydrosphere: Geodynamic implications. - *Precambrian Res.* 361, 106249, <https://doi.org/10.1016/j.precamres.2021.106249>
- Ramírez-Salazar A, Müller T, Piazzolo S, Webb AAG, Hauzenberger C, Zuo J, Haproff P, Harvey J, Wong TK, Charlton C (2021): Tectonics of the Isua Supracrustal Belt 1: P-T-X-d Constraints of a Poly-Metamorphic Terrane. - *Tectonics* 40, e2020TC006516. <https://doi.org/10.1029/2020TC006516>

Cement analysis by X-ray diffraction and X-ray fluorescence

S. Wollstadt¹, T. Füllmann¹, E. Hartmann¹

¹Rigaku Europe SE, Hugenottenallee 167, 63263 Neu-Isenburg, Germany
e-mail: elmar.hartmann@rigaku.com

Cement is one of the most important materials for construction and reacts with water to form hydrates, which gradually condense and harden. This hardening is caused when the formed hydrates coat cement particles and bind them together. A detailed understanding of the hydrate formation process is expected to lead to the elucidation of the mechanism of condensation and hardening. X-ray diffraction (XRD) techniques can identify crystalline hydrates such as ettringite and monocarbonate in cement. We report on the observation of changes in the crystalline phase of ordinary Portland cement over time with a water/cement ratio of 25% using a liquid sample holder which can prevent the sample from drying in an ambient environment by covering the sample surface with a film. Fig. 1 exemplifies changes in the XRD pattern of cement during a hydration reaction.

In addition, X-ray fluorescence (XRF) techniques are used to control the chemical composition of cement products and interim products. Since the fusion method can eliminate sample heterogeneity problems, such as grain size and mineralogical effects, it is possible to obtain high accuracy for cement samples and to establish calibrations using a variety of materials. ASTM C114-18 covers chemical analysis of hydraulic cements. In this standard, mainly procedures of wet chemical analysis are described and XRF spectrometry is mentioned as an example of “Rapid Test Methods”. In practice, XRF spectrometry has been used for chemical composition analysis of cement owing to its simple sample preparation and high precision. We will show quantitative analysis for Portland cements by the fusion method according to ASTM C114-18, as displayed in Table 1, using a multi-channel simultaneous wavelength dispersive XRF (WDXRF) spectrometer, which enables the simultaneous measurement of all the elements in the sample under investigation. The counting time of the measurement was 40 seconds for twelve elements in cement.

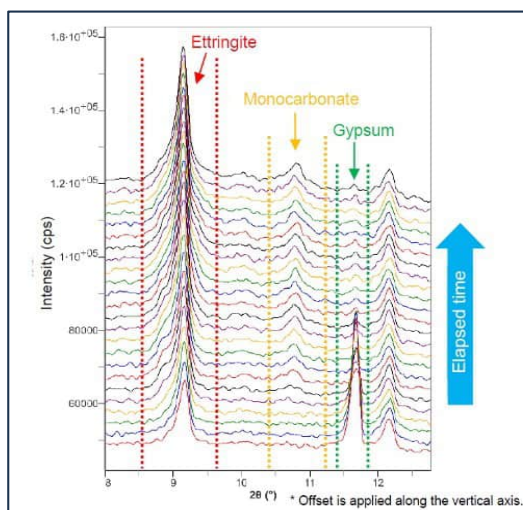


Figure 1. Overlaid X-ray diffraction patterns of hydrated cement.

Analysis component	Analysis range	Difference between duplicates		Qualified
		Limit (ASTM)	Maximum difference	
SiO ₂	18.637 – 22.38	0.16	0.05	✓
Al ₂ O ₃	3.875 – 7.06	0.20	0.01	✓
Fe ₂ O ₃	0.152 – 3.09	0.10	0.003	✓
CaO	57.58 – 67.87	0.20	0.14	✓
MgO	0.814 – 4.475	0.16	0.01	✓
SO ₃	2.086 – 4.622	0.10	0.01	✓
Na ₂ O	0.021 – 1.068	0.03	0.006	✓
K ₂ O	0.093 – 1.228	0.03	0.004	✓
TiO ₂	0.084 – 0.3663	0.02	0.003	✓
P ₂ O ₅	0.022 – 0.306	0.03	0.001	✓
ZnO	0.0048 – 0.107	0.03	0.0004	✓
Mn ₂ O ₃	0.0073 – 0.2588	0.03	0.001	✓

Table 1. Qualification test results (unit: mass%)

Stable tungsten (W) isotope behavior during the early diagenesis in the Gulf of California

R. Yang^{1,2}, M. Gutjahr², F. Scholz², F. Kurzweil¹, S. Eroglu³, C. Münker¹

¹*Institute of Geology und Mineralogy, University of Cologne, Zùlpicher Straße 49b, 50674 Cologne, Germany*

²*GEOMAR Helmholtz Centre for Ocean Research Kiel, Wischhofstraße 1-3, 24148 Kiel, Germany*

³*Institute of Geology and Paleontology, Westfälische Wilhelms Universität,*

Correns Straße 24, 48149 Münster, Germany

e-mail: ryang2@uni-koeln.de

The stable W isotope system has recently emerged as a promising redox indicator, but its modern oceanic budget is not yet fully understood. Specifically, the mechanisms of W delivery to the sediments and its behavior during early diagenesis remain unknown.

In this study, three sediment cores in the gulf of California were thoroughly analyzed. Our findings indicate that W in marginal sediments is a combination of authigenic and detrital W components, with varying contributions at different depths. Authigenic W is likely bound to Mn oxides and released into the pore water in the Mn reduction zone. The delivery of W is primarily associated with Mn shuttling. Light W is adsorbed and released upon reductive dissolution of Mn oxides.

The sub-surface conditions in all the three cores are anoxic, leading to limited enrichment of W in sediments. Despite being geochemical twin elements, W and Mo display contrasting behaviors in sulfidic environments. Consequently, the distinctive behavior of W makes it a valuable indicator for identifying the cycling of Mn, an essential element for biological processes, and for tracing the oxidation history of the early Earth's oceans.

Unravelling the formation history of the Maronia Skarn, NE Greece: Insights from melilite group minerals

M. Zeug¹, A. Repstock², P. Voudouris³, H. Gevorgyan⁴, H. Schleicher⁵

¹ Landesamt für Geologie und Bergwesen Sachsen-Anhalt,
Fliederwegkaserne 13, 06130 Halle, Saale, Germany

² Geological Survey and Geophysics, Sächsisches Landesamt für Umwelt,
Landwirtschaft und Geologie, Pillnitzer Platz 3, 01326 Dresden, Germany

³ Department of Mineralogy and Petrology, National and Kapodistrian University of Athens,
University Campus-Zografou, 15784, Athens, Greece

⁴ Institute for Mineralogy, TU Bergakademie Freiberg, Brennhausgasse 4, 09599 Freiberg

⁵ Mineralogisch-Petrographisches Institut, Universität Hamburg, Grindelallee 48, 20146 Hamburg, Germany
e-mail: manuela.zeug@sachsen-anhalt.de / manuela.zeug@univie.ac.at

The Maronia skarn is situated in the northern region of the Aegean Sea, approximately 25 km west of Alexandroupolis in northeastern Greece. During the Oligocene (29.8 Ma) the Maronia pluton (monzonite, quartz monzonite, monzogabbro) intruded into Mesozoic metasediments of the Circum Rhodope Belt (Schaarschmidt et al. 2021). This intrusive event led to the development of a remarkable skarn mineralisation within the western metamorphic aureole caused by the contact between the pluton and the adjacent marbles. The western contact aureole extends 3km in length and up to 100m in width.

Skarn zones between the pluton and the marble were identified based on mineral assemblages and the chemical composition of granditic garnet, which is present in each skarn zone. Garnet crystals of the western contact aureole of the Maronia skarn correspond to the grossular-andradite solid solution series. The Maronia skarn contains a variety of unusual and remarkable mineralisation, including (i) Ti-Zr-Cr-rich garnet crystals, which occurrence is possibly unique worldwide (Voudouris & Katerinopoulos 2004, Katerinopoulou et al. 2009), (ii) predominantly Ti-rich dark brown andradite crystals (2–6 wt% TiO₂) that contain subhedral to euhedral titanite crystals [CaTi(SiO₄)O] in the core, and (iii) andradite-rich garnet (2–8 wt% TiO₂) within a melilitic skarn that contain perovskite (CaTiO₃) in the core. The skarn mineral assemblages (e.g. Ti-rich garnet, melilite, perovskite) in both the endoskarn and the exoskarn indicate a development in a silica-undersaturated magmatic environment (cf. Russel et al. 1999).

Melilite group minerals are restricted to the exoskarn and refer to gehlenite (Ca₂Al[AlSiO₇]-åkermanite (Ca₂Mg[Si₂O₇]) solid solution series. Various stages of skarn formation can be identified based on the appearance of the melilite solid solutions, which are reflected in four different zones in the Maronia exoskarn. The first zone is fine-grained consisting of clinopyroxene, interstitial melilite, and andradite-rich garnet, which may contain perovskite cores. This fine-grained zone is assumed to be closest to the pluton. The adjacent zone consists of almost tabular, slightly rounded cube-shaped crystals associated with interstitial andradite-rich garnet (2–8 wt% TiO₂) with or without perovskite-cores (Fig. 1). These melilite crystals are closer in composition to gehlenite suggesting a formation of a high-temperature skarn (Deer et al. 1992; Katona et al. 2003; Marinacea et al. 2011, and references therein) at a formation temperature exceeding 900°C in the prograde stage of skarn formation (cf. Mposkos & Doryphoros 1993). In the following zone melilite crystals show zoning with a gehlenitic core and an åkermanitic rim indicating the initial retrograde stage (cf. Reverdatto et al. 1979). Next to the latter zone, melilite solid solutions are completely replaced by vesuvianite representing a late retrograde stage during the cooling down at temperatures below melilite stability (~ 675 °C, Mposkos & Doryphoros 1993). Results of the

present study show that melilite crystals can be used to reveal the different stages of Maronia skarn evolution.

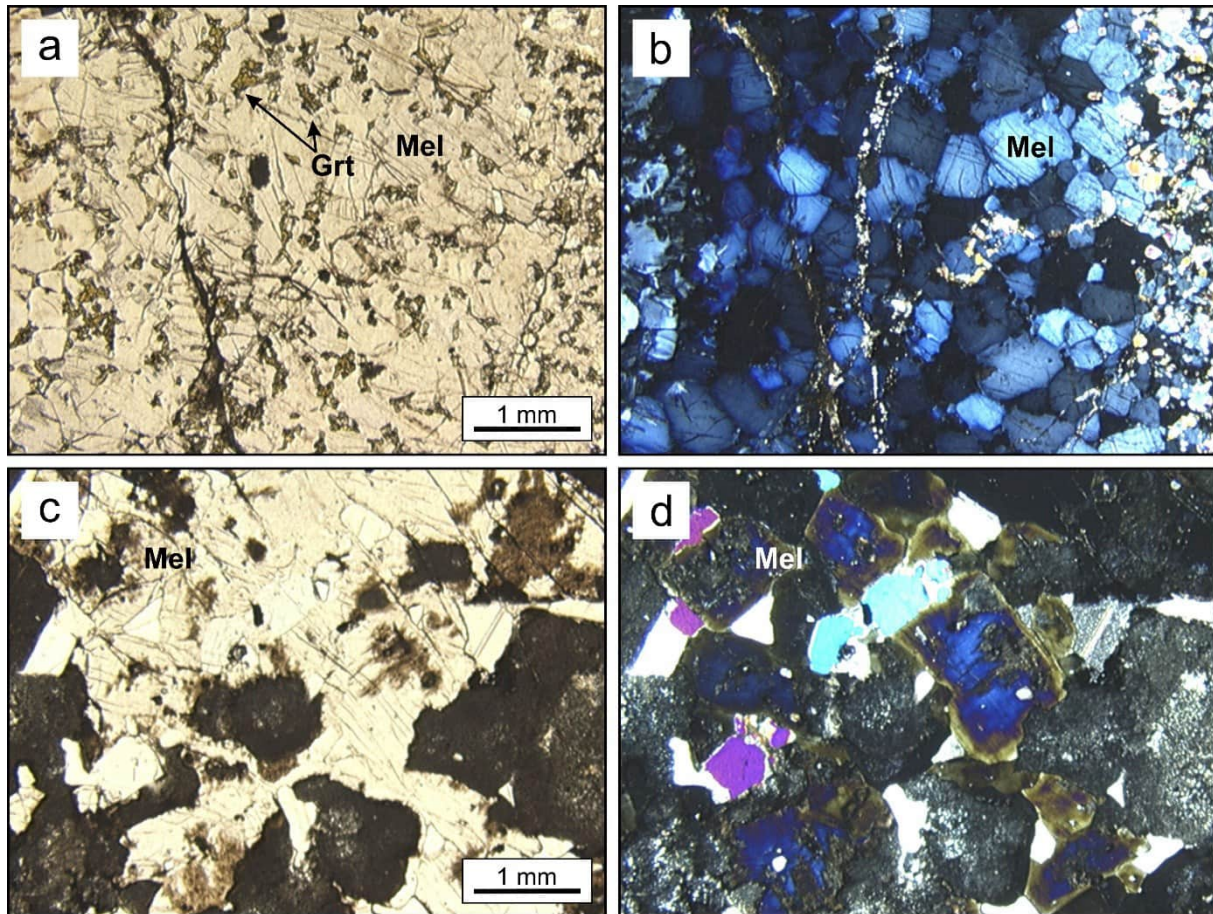


Figure 1. Plane-polarised (a and c) and cross-polarised (b and d) transmitted light photomicrographs of melilite zones in the Maronia skarn. The melilite in a and b is closer to the gehlenite endmember, suggesting a formation in the prograde stage. The melilite in c and d shows clear zonation of a gehlenite-rich core surrounded by an åkermanite-rich rim, which indicates an initial retrograde stage of skarn formation. Foto: M. Zeug

- Deer WA, Howie RA, Zussman J (1992): *An Introduction to the Rock-Forming Minerals* (second ed.). Longman, Hong Kong
- Katerinopoulou A, Katerinopoulos A, Voudouris P, Bieniok A, Musso M, Amthauer G (2009): A multi-analytical study of the crystal structure of unusual Ti–Zr–Cr-rich Andradite from the Maronia skarn, Rhodope massif, western Thrace, Greece. - *Miner Petrol* 95, 113–124
- Katona I, Pascal M-L, Fonteilles M, Verkaeren J (2003): The melilite (Gh50) skarns at Oravița, Banat, Romania: transition to gehlenite (Gh85) and to vesuvianite. *Can. Mineral.* 41, 1255–1270
- Marincea S, Dumitraș D-G, Ghineț C (2011) Gehlenite from three occurrences of high-temperature skarns, Romania: New mineralogical data
- Mposkos E, Doryphoros K (1993): High temperature skarns in the Maronia area (NE Greece). - *Bull Geol Soc Greece*, 23–35
- Reverdatto VV, Pertsev NN, Korolyuk VN (1979): P-T-Evolution and origin of zoning in melilite during the regressive stage of contact metamorphism in carbonate-bearing rocks. *Contrib Miner Petr* 70, 203–208
- Russell JK, Dipple GM, Lang JR, Lueck B (1999): Major-element discrimination of titanian andradite from magmatic and hydrothermal environments: an example from the Canadian Cordillera. *Europ J Miner* 11, 919–935
- Schaarschmidt A, Klemd R, Regelous M, Voudouris PC, Melfos V, Haase KM (2021) The formation of shoshonitic magma and its relationship to porphyry-type mineralisation: the Maronia pluton in NE Greece. *Lithos* 380–381, 105911
- Voudouris P, Katerinopoulos A (2004): New occurrences of mineral megacrysts in Tertiary magmatic-hydrothermal and epithermal environments in Greece. *Documenta Naturae* 151, 1–21

How to predict strength and optimum mix-designs of mineral-waste-based geopolymers

I. Zögl¹, O.Rudić², C. Grengg¹, F. Steindl¹, D. Etehad¹, M. Dietzel¹, S. Raič¹

¹*Institute of Applied Geoscience, Graz University of Technology*

²*Institute of Technology and Testing of Construction Material, Graz University of Technology*
e-mail: iris.zoegl@tugraz.at

Reducing the carbon footprint of building material production (*ca.* 9 % of anthropogenic CO₂) in the short term is essential to achieve global climate targets. In this regard, mineral wastes and industrial secondary raw materials show large potential as a low-CO₂ alternative to traditional carbonate-based binder systems. In order to promote and establish the use of mineral waste based binders as strong future competitors in the construction industry, optimal combinations of solid and liquid binder components have to be developed in so-called mix designs to meet material requirements. In this context, the desired material properties, such as adequate workability, high strength, improved chemical resistance and minimal shrinkage strongly depend on elemental ratios (*e.g.* Si/Al, Al/K) within the mix design. These are multi-variable challenges that are conventionally solved by changing one variable of the mix design at a time, until the desired results are achieved. In order to ensure a more time- and cost-efficient strategy, and to generate optimum experimental conditions, we are applying the Design of Experiment (DoE) and Response Surface Methodology (RSM) approaches to alkali-activated waste-based binder systems. DoE is a widely used procedure that seeks to predict a desired outcome (*e.g.* compressive strength, elemental ratios), which is then systematically optimized by a set of statistical techniques (RSM). In the current study, we evaluated the most desirable relative contents of the mix design components metakaolin, mineral wastes and aqueous potassium silicates (waterglass as alkaline activator) under the conditions of (i) maximizing the content of mineral wastes and (ii) achieving the desired material properties (*e.g.*, compressive strength). Preliminary results demonstrate how a minimum number of experimental runs and samples enables a refinement of possible mix-ratio-combinations. Re-iterations of these experimental procedures allow to accurately predict relevant material properties such as mechanical performance of the hardened mineral-waste-based binder material. Additionally, economic and ecological decisions could be already made during early stages of experimental approaches by including manufacturing costs and CO₂ emissions to the existing DoE models.